The design and manufacture of multi-layered hydrogel-based constructs for articular cartilage/osteochondral reconstruction

Thesis submitted in accordance with the requirements of

The University of Liverpool for the degree of

Doctor of Philosophy by

Yunjie Hao

February 2022

Acknowledgements

At the beginning, I would like to thank my primary supervisor Dr. Jude Curran of the University of Liverpool (UK), and Professor Fangang Tseng of National Tsing Hua University (Taiwan), for their trust and guidance throughout all my PhD journey.

Then I want to thank all my secondary supervisors from both Universities, including Dr. James R. Henstock, Professor John A. Hunt, Professor Yu-Chuan Su, and their students for the support, encouragement and inspiration during my studies at both Universities.

Many thanks to Dr. Raechelle D'Sa and all the past and present members of her lab in UK, such as Dr. Man Li and Dr. Jenny Aveyard, and thanks to previous and current students of Professor Fangang's lab, especially Mr. Wu Chuan-Yung, as well as Miss Kuo Mei-Ling a personal assistant of Professor Fangang from NTHU, for your always support and all collaborative works during my time spent in both labs.

I would also like to thank the University of Liverpool and National Tsing Hua University for establishment and sponsoring the joint dual PhD program, giving me the chance to achieve a PhD degree in my favourite subject.

Finally, I appreciate my parents and all family members, without your unconditional support, I would not be able to finish this study.

List of conferences attended during PhD Study

Yunjie Hao, Manohar Prasad Koduri, Fan Gang Tseng, James, Henstock, John A. Hunt, Jude Curran, 'Viability test of a novel nanosensor for 3D multilayer tissue reconstruction', The UK Society for Biomaterials Annual Conference 2018 (UKSB 2018), 2018, Bath, UK.

Yunjie Hao, Manohar Prasad Koduri, Fan Gang Tseng, James, Henstock, John A. Hunt, Jude Curran, 'A novel oxygen nanosensor for *in vitro* microenvironment monitoring in mesenchymal stem cell culture', The 23rd International Conference on Miniaturized Systems for Chemistry and Life Sciences (μTAS 2019), 2019, Basel, Switzerland.

Yunjie Hao, Manohar Prasad Koduri, Fan Gang Tseng, James, Henstock, John A. Hunt, Jude Curran, 'The design and development of a novel oxygen nanosensor for use in *in vitro* Mesenchymal stem cell culture', 2019 International Conference on Smart Sensors and 22nd Nano Engineering and Microsystem Technology Conference, 2019, Hsinchu, Taiwan.

Chuan-Yung Wu, **Yun-Jie Hao**, Yu-Chuan Su and Fan-Gang Tseng, 'Digital Light Processing-Based 3D Printed Hydrogel Scaffolds for Articular Cartilage Tissue Engineering' The 24th International Conference on Miniaturized Systems for Chemistry and Life Sciences (μTAS 2020), 2020, Online.

Chuan-Yung Wu, **Yun-Jie Hao**, Yu-Chuan Su and Fan-Gang Tseng, 'Self-assembly hydrogel scaffolds 3D-printed for cartilage reparation' The 25th International Conference on Miniaturized Systems for Chemistry and Life Sciences (μTAS 2021), 2021, Palm Springs, California, USA

Structure of Thesis

This study is part of a joint project in the dual PhD program between the University of Liverpool (UK) and National Tsing Hua University (Taiwan). There are six chapters included in this thesis:

Chapter one is the **Introduction** chapter. In this chapter, motivations of the whole project, aims, objectives and hypothesis of this study were introduced.

Chapter two is the **Literature review** chapter. In this chapter, the structure, constituent components, specific microenvironment and the physiological function of the target tissue were reviewed at the beginning. Then the chondral/osteochondral lesions, recommended grading systems, available clinical treatments and tissue engineering strategies were concisely introduced. Finally, the inhomogeneous microenvironment of the target tissue and a few 3D fabrication strategies toward reconstruction of the inhomogeneous articular cartilage/osteochondral tissue were discussed.

Chapter three described **the design and manufacture of 3D-printed PEGDA scaffold for reconstructing the deep zone of the articular cartilage/osteochondral tissue *in vitro*.**

Chapter four demonstrated **the design and manufacture of alginate-based 3D tissue culture system for reconstructing the middle layer of the articular cartilage/osteochondral tissue *in vitro***.

Chapter five illustrated the **characterisations of a novel fluorescent oxygen nanosensor for cell-based tissue culture *in vitro*.**

Chapter six drew some **conclusions and future works suggested** for this project.

The works presented in chapter three and four were finished at NTHU while those from chapter five were completed at the University of Liverpool.

Abstract

Specific physiological characteristics and anatomical position of the hyaline cartilage/osteochondral tissue in the synovial joint determine its ineffective self-restoration after injuries. However, a majority of medical treatments for chondral/osteochondral defects are palliative or reparative. Tissue engineering working on regenerating tissue or organ in the aspect of biophysical structure, biochemical components and physiological function, by making use of seeding cells, biomaterial scaffolds, bioactive agents and assisting facilities, provide an alternative option for patients and a platform to study biological tissue development, materials science and engineering technologies. In this study, 3D printing technology and hydrogel materials were employed to design and manufacture two distinctive layers of the multi-layered inhomogeneous articular cartilage/osteochondral tissue, toward building up the entire soft tissue by hydrogel-based 3D tissue culture systems in a layer-by layer manner *in vitro*. By using classic cell viability and proliferation screening assays, a novel oxygen nanosensor, regarding the size and concentration, was evaluated in cell culture system *in vitro*, before being incorporated into the 3D hydrogel-based tissue layers established in this study.

In chapter three, a photopolymerised hydrogel scaffold with hexagonal shape and uniformed hole arrays (100-200 μm in diameter and space) to simulate the perpendicularly arranged chondrogenic extracellular microenvironment of the deep zone in the articular cartilage/osteochondral tissue, was fabricated, where seeding cells delivered by type I collagen gel were successfully engrafted and survived. The miniaturised scaffold suspending in viscous solution, was confirmed a self-assembly property after being injected into an area simulating the small chondral lesion, providing a hope to be developed into an injectable strategy to support the scaffold-assisted autologous chondrocyte

implantation in future clinical applications.

In chapter four, the ion-crosslinked alginate hydrogel with simulated size of the middle zone in the articular cartilage tissue, were fabricated successfully with the support of 3D-printed mould. With additional fibrous materials, the mechanical property and printability of alginate materials could be both improved. The alginate-based hydrogel system under 0.05M $SrCl_2$ condition was biocompatible for chondrocytes to be cultured in both 2D monolayer and 3D encapsulation, but bioinert alginate material is insufficient for cell adherence in 2D in the long run. Low-concentration (2 and 4%) alginate with additional nanocellulose fibres might be suitable to be developed into bio-inks for extrusion-based 3D printing in future 3D fabrications.

In chapter five, three sizes (390, 520, 890nm) of nanosensors with a series of concentrations (25, 50, 100, 500, 1000, 2000 μg/mL) were characterised the cytotoxicity and fluorescent performances in cell culture system *in vitro*. No toxic effect of the nanosensor on the viability and proliferation of living cells in culture were observed, except for nanosensor with larger size at higher concentrations. After evaluating the effect of nanosensors with two smaller sizes (390 and 520nm) and three concentrations (25, 500, 1000 μg/ml) on the viability, proliferation and differentiations of living cells *in vitro*, and the fluorescent intensity in culture, 520nm size around 500μg/ml were selected as the optimised regime of the nanosensor for subsequent investigations.

This study revealed that by 3D printing and hydrogel materials, individual 3D soft cartilaginous tissue layer with and without pattern, with different sizes, could be designed and manufactured *in vitro*, contributing to reconstruction of the multi-layered articular cartilage/osteochondral tissue in a layer-by-layer manner. By applying classic biocompatible examinations, nanoparticle-based fluorescent sensor, regarding the size and concentration, could be evaluated its impact on the

viability, proliferation and differentiation of seeding cells, contributing to further development and optimisation of the nanosensor for its application in 3D tissue development *in vitro* and the underlying mechanisms regarding interactions between microenvironmental factors and seeding cell behaviours in 3D *in vitro*.

List of Abbreviations and Acronyms

2/3/4 D	2/3/4 dimensions or two/three/four dimensional
AC	Articular cartilage
ACI or periosteal-ACI	Autologous chondrocyte implantation (First generation of ACI)
ADAM	A disintegrin and metalloproteinase domain-containing protein
AD-MSCs	Adipose tissue-derived MSCs
ALP	Alkaline phosphatase
AMIC®	Autologous Matrix Induced Chondrogenesis®
BARX	A protein encoded by Barx gene, a member of the Bar subclass of homeobox transcription factors.
Barx2	BARX Homeobox 2 gene
b-FGF	basic Fibroblast growth factor
BG	Bioactive glass
bioMEMS	biomedical (or biological) Microelectromechanical systems, a subset of MEMS
BMAC	Bone marrow aspirate concentrate
BMI	Body mass index
BM-MSCs	Bone marrow-derived MSCs
BMP	Bone morphogenic protein
BMS	Bone marrow stimulation
BMU	Basic multicellular unit
C-ACI	Collagen-assisted ACI
CAD	Computer-aided design
CAL	Computed axial lithography
CaP	Calcium phosphate
CaReS-1S®	Collagen type I gel developed scaffold product
CD	Cluster of differentiation
Chm-1	Chondromodulin-1
CLIP	Continuous liquid interface production
c-Myc	A member of Myc oncogene family, a transcription factor (sometimes refers to as MYC, the cellular homolog of the retroviral v-myc oncogene.)
COL1A1	Collagen Type I Alpha 1 Chain
COL1A2	Collagen Type I Alpha 2 Chain
CPs	Chondroprotective agents
CS	Chondroitin sulphate
CT	Computer tomography
CUPE	Elastic urethane-doped polyester materials
dECM	decellularized Extracellular matrix
DHF	Denatured human fibrinogen
DIW	Direct ink writing
DLP	Digital light processing

DMD	Digital micromirror device
DNA	Deoxyribonucleic acid
ECM	Extracellular matrix
EDTA	Ethylenediaminetetraacetic acid
EHD	Electrohydrodynamic
EHDP	Electrohydrodynamic direct printing
EMA	European Medicines Agency
ER	Endoplasmic reticulum
ESCs	Embryonic stem cells
FACIT	Fibril associated collagen with interrupted triple helices
FDA or US FDA	(U.S.) Food and Drug Administration
FDM	Fused deposition modelling
FFF	Fused filament fabrication
FSA	French Society of arthroscopy systems
FT-NIR	Fourier transformed near infrared
G	α-L-guluronic acid
GA	Glutaraldehyde
GA	Glycolic acid
GAG	Glycosaminoglycan
GelMA	Gelatin methacrylamide
GelNB	Photo-crosslinked gelatin norbornene
Gly	Glycine
GP	Glycerol phosphate
H&E staining	Haematoxylin and Eosin staining
HA	Hyaluronic acid/hyaluronate/hyaluronan
HAM cells	Human amniotic mesenchymal cells
HAP	Hyaluronic acid protein
hESCs	human Embryonic stem cells
HLA	Human leukocyte antigen (the MHC class II antigen)
HLA-DR	Human Leukocyte Antigen-DR isotype (an MHC class II cell surface receptor encoded by the human leukocyte antigen complex)
HPL	Human platelet lysate
hTeRT gene	human Telomerase reverse transcriptase gene
Hypro	Hydroxyproline
ICM	Inner cell mass
ICRS	International Cartilage Repair Society
IGF-1	Insulin-like growth factor 1
IL-1	Interleukin-1
IL-1 Ra	IL-1 receptor antagonist
IPN	Interpenetrating polymeric hydrogel
iPSCs	induced Pluripotent stem cells
ISCT	International Society of Cellular Therapy
ITS	Insulin-transferrin-selenium
KGN-100	Kartogenin-100

Klf4	Kruppel like factor 4 gene
KS	Keratin sulphate
Lin28	Lin-28 Homolog A gene, encoding an RNA-binding protein
M	β-D-mannuronic acid
M-ACI or MACI	Matrix-induced or matrix-assisted ACI (Second generation of ACI)
MACI®	Matrix-induced autologous chondrocyte implantation technique, developed by Sanofi Biosurgery Inc.
MACT	Matrix-assisted autologous chondrocyte transplantation
MA-MFX	Matrix-assisted bone marrow stimulation procedures
MEMS	Microelectromechanical systems
MF	Microfracture
Mg-HA	Magnesium-enriched HA
MHC	Major histocompatibility complex in humans
micro-CT	micro-Computed tomography
microRNAs	a class of small non-coding RNAs of about 22 nucleotides in length
MMPs	Matrix metalloproteinases
MRI	Magnetic resonance imaging
MSC	Mesenchymal stem cell
Nanog	Nanog Homeobox
NSAIDs	Nonsteroidal anti-inflammatory drugs
OA	Osteoarthritis
OARSI	Osteoarthritis Research Society International
OAT	Osteochondral autograft transfer
OC	Osteochondral
OCA	Osteochondral allograft implantation
OCD	Osteochondrosis dissecans
OCT	Optical coherence tomography
Oct4	Octamer-binding transcription factor 4
OP-1	Osteogenic protein 1
PA	Phloretic acid
PC	Pericellular capsule
PCL	Poly(ε-caprolactone)
PCM	Pericellular matrix
PD-GE	Platelet-derived growth factor
PDLLA/PEG/HA	(PLA-PEG-PLA/HA)
PEG	Polyethylene glycol
PEG(SH)2	Poly (ethylene glycol) dithiol
PEGDA	Polyethylene glycol diacrylate
PGA	Poly (glycolic acid)
PGS	Poly (glycerol sebacate)
PLA	Poly-L-lactic acid
PLA	Poly (lactic acid)
PLGA	Polylactic-co-glycolic acid
PLGA	Poly (lactic-co-glycolic acid) copolymer

PLM	Polarized light microscopy
pNIPAAm	poly (N-isopropylacrylamide) (or abbreviated as PNIPA, PNIPAAm, NIPA, PNIPAA, PNIPAm)
POSS	Polyhedral oligomeric silsesquioxane
PPS	Propylene sebacate
Pro	Proline
PRP	Platelet-rich-plasma (PRP)
PUU	Poly(urea-urethane) polymer
PVA	Poly (vinyl alcohol)
RA	Rheumatoid arthritis
RFE	Radiofrequency energy
rhFGF	Recombinant human fibroblast growth factor
RP	Rapid prototyping
RUNX2	Runt-related transcription factor2
SB	Subchondral bone
sCNC	sulphated Cellulous nanocrystal
SEM	Scanning electron microscopy
SHG	Second harmonic generation
SLS	Selective laser sintering
SMAD	Referring to the homologies to the Caenorhabditis elegans SMA ('small' worm phenotype) and MAD family ('Mothers Against Decapentaplegic') of genes in *Drosophila*, containing a group of signal transducers for receptors of the TGF-β superfamily.
Smad3	SMAD family member 3 gene
Sox	SRY-box transcription factor
SR	Synchrotron radiation
SRY-box	Sex determining region Y-box
Supartz®	Sterilised non-pyogenic viscoelastic HA solution
SZP	Superficial zone protein
β-TCP	β-calcium phosphate composite
PDS	Polydiaxanone or poly (p-dioxanone)
TE	Tissue engineering
TEM	Transmission electron microscopy
TGF-β	Transforming growth factor-beta
TM	Territorial matrix
TNF-α	Tumour necrosis factor-α
TPEF	Two-photon-excited fluorescence
TPP	Two-photon or multiple photons-based polymerisation
UV	Ultraviolet

List of Contents

Chapter one: Introduction

In this chapter, motivations and outline of the joint project, aims, objectives and hypothesis of this study will be introduced.

1.1 Motivations

Countless people are enduring joint diseases due to tissue failure of wear and tear along with ageing, sports injuries, accidental impacts, skeletal ailments, and chronic conditions of arthritis, leading to a reduced quality of life with unhappiness, continuous pain and risk of disability [1]. The initially damaged soft cartilage part, due to its avascular feature and absences of nerve and lymph, is often related to insufficient knowledges of the cause and process of these defects, lagging diagnoses and inadequate drug delivery by traditional vasculature-based approach, and ineffective to self-rehabilitate through normal regenerative process [2, 3]. Careless management and repetitive injuries in the cartilage typically result in the osteochondral (OC) defect involving both cartilage and adjacent bone, which may progress from localised area to arthritis affecting the entire joint. Arthritis including osteoarthritis (OA) and rheumatoid arthritis (RA), is one major pathological cause of the OC defect over time, frequently occurring in the knee joint. It was estimated that, over half a hundred million of adults (about a quarter of all adults over 18 years old) in US would suffer from the diagnosed arthritis by 2040 [4]. Across UK with varied incidence and prevalence of the musculoskeletal joint problems, adults aged over 50 presented a high prevalence of age-dependent OA, leading to increases in patients consulting chondral/OC treatments and consequently raising concerns of losing millions of working days and reducing productivity. Whereas among young people, in about 15-29 per 100,000 population the osteochondral lesions could occur from

childhood (10-20 years old) through their adult life, which are often developed from traumatic micro-injury or osteochondritis dissecans [5]. In many countries, the chondral/osteochondral defects and the associated morbidity/comorbidity possess big personal and socioeconomic impacts [6]. Most chondral/osteochondral defects need clinical interventions such as physiotherapy, medications and surgical treatments including micro-drilling, microfracture, osteotomy, debridement, autologous chondrocyte implantation (ACL)/matrix-induced ACI (M-ACI), osteochondral grafts transplantation or metallic implantations, and even the total joint replacement, depending on the severity diagnosed in clinics [3, 7-12]. However, most of current options are either palliatives to relieve the pain temporarily, or invasive, reparative solutions with great potential to cause complications, side effects or problems after surgeries, such as donor site morbidity, tissue fibrosis, immunological rejection, repetitive operations, long recovery time, limited implantation grafts available from donors and usually short-term, unsatisfied or failed outcomes post-operationally for patients, few of which are truly restorative, effective and long term strategies [7, 13-16].

Tissue engineering (TE) strategy offers a promising substitute for current surgical and orthopaedic therapies to treat chondral/osteochondral defects, by which bioactive synthetic constructs are designed and manufactured to repair, replace and regenerate damaged tissues, and challenges regarding the use of autograft or allograft could be prevented [17-19]. A TE design generally refers to the assembly of seeding cells and biomaterials by fabrication techniques and incubation under controlled microenvironments, which could not only produce the target tissue substitute for potential clinical applications, but also fill blanks between developmental biology and artificial tissue regeneration methodology [20-23]. Cell-based TE plans require proper tissue culture system

to expand and/or differentiate seeding cells within biomimetic microenvironment which is essential though incomplete area of knowledge [20]. Accumulated studies have illustrated that conventional 2D culture system is insufficient and sometimes provides contradictive information of the real tissue target during development [24-27]. It is necessary to design and develop appropriate 3D tissue culture system to simulate as much as possible the natural microenvironment of the target tissue, after all, the majority of living tissues or organs are complex and in 3D, involving mixed types of cells and pre-defined microenvironments such as highly organised architecture of extracellular matrix (ECM), and dynamic interactions between cell and surroundings (cell-cell, cell-ECM and cell-bioactive molecules etc.,) [28]. Hence, this study is firstly motivated by the urgent need of a biomimetic 3D tissue culture system to simulate and fabricate the target multi-layered articular cartilage/osteochondral tissue, *in vitro*.

As the development of materials science, and manufacturing techniques, it was found that hydrogel materials featuring with high volume of water and hydrophilic polymer, possessed a relatively similar physiological environment as the natural extracellular microenvironment especially for the soft tissue [29-33]. Various 3D fabrication techniques such as the microfluidics involved bioMEMS [34], electrospinning and force spinning techniques [35], versatile additive manufacturing (AM) approaches mainly the 3D (bio) printings and smart-materials supported 4D printing [36-41], have been also broadly incorporated into TE designs to fabricate scaffolds and substrates with biomimetic microenvironments to support seeding cells to engraft, survive and function [42, 43]. The second motivation of this study is to apply hydrogel material and 3D printing technology for multi-layered articular cartilage/osteochondral tissue reconstruction *in vitro*.

In addition, to fabricate the target tissue, it is essential to understand comprehensively about the

3D microenvironment throughout the tissue development, to assist improvements in biomimetic designs of TE strategies and precise controls of the complex 3D culture system, to finally simulate the target tissue successfully *in vitro* [44-46]. The articular cartilage/OC tissue has depth-dependent zonal structure [47]. Chondrocytes in the cartilaginous tissue live in a hypoxic microenvironment [48, 49], where throughout the whole tissue thickness, there is a depth-related gradient of oxygen concentrations [50-52]. Several studies have revealed that the formation and maintenance of the unique phenotype of zonal chondrocytes in cartilaginous tissue are highly correlated with the depth-dependent oxygen microenvironment [53]. Hence the third motivation of this study is to develop nanoparticle-based sensors (e.g., oxygen nanosensor) to be finally incorporated into 3D tissue culture system established in this study to monitor and investigate essential microenvironmental factors (oxygen consumption and level) during tissue development in 3D *in vitro*, providing information to improve future TE design and real time control of the microenvironmental factors for 3D tissue culture practices.

1.2 Outline of the joint project

The overall project contains mainly two parts. The first part is to design and develop a type of nanoparticle-based sensor for real-time monitoring environmental factors during 3D tissue development *in vitro*. The oxygen-sensitive fluorescent nanosensor was preliminarily developed in another study in NTHU [54]. This study focused on the design and manufacture of 3D tissue construct for the multi-layered articular cartilage/osteochondral tissue reconstruction *in vitro*. The whole project was planned to apply the nanosensor developed in the first study, to monitor and study the microenvironmental cue during the target articular cartilage/osteochondral tissue

development *in vitro* in the 3D tissue culture system established in the second study.

1.3 Aims of this study

- To develop 3D hydrogel-based tissue culture systems for the multi-layered articular cartilage/osteochondral tissue reconstruction *in vitro*.
- Oxygen is an important factor for living cells to survive, proliferate and differentiate in both 2D and 3D tissue culture microenvironments. Different from 2D culture system, the oxygen consumption and requirement in a 3D structure are seeding cell-dependent (cell type) and depth-related (distance of diffusion). Throughout the natural articular cartilage/osteochondral tissue, there is a depth-dependent anisotropic microenvironment including the oxygen level, architecture and components of ECMs, water content, and mechanical properties, highly correlated with the depth-dependent morphology and density of local chondrocytes. Local chondrocytes in each layer contribute to the formation of the microenvironment in the specific tissue layer and different layer in the articular cartilage tissue part provides a specific microenvironment including the balanced oxygen profile for local chondrocytes to live with. To better simulate the natural inhomogeneous multi-layered articular cartilage/osteochondral tissue *in vitro*, those depth-dependent factors in the tissue-specific microenvironment such as the oxygen level in each layer are required to be monitored and studied during the tissue development in 3D. Therefore, to design and develop a nanoparticle-based sensor (oxygen nanosensor) for monitoring these environmental factors such as the oxygen profile during 3D tissue development, and to develop appropriate tissue culture systems for applying the nanosensor during 3D tissue development *in vitro* are both required. Recently, a novel

fluorescent oxygen-sensitive nanosensor [54] was designed and developed in another study of this joint project. Another aim of this study, is to characterise the design and development of this type of nanoparticle-based sensor in cell culture system *in vitro*, before applying the nanosensor for further tissue culture applications in complex microenvironment.

1.4 Objectives of this study

- Design and fabrication of 3D moulds for alginate-based material to be used in 3D culture by Phrozen™ Sonic XL 4K 3D printer. 3D tissue layer fabrication by alginate-based materials would be performed to simulate the middle zone of the articular cartilage/OC tissue.
- Design and fabrication of PEGDA hydrogel scaffold with optimised geometrical and topographical features by customised DLP 3D printer. 3D tissue layer fabrication based on the patterned scaffold would be performed to simulate the deep zone of the articular cartilage/OC tissue.
- Characterisation of a novel oxygen nanosensor designed for tissue culture applications *in vitro*.

1.5 Hypothesis of this study

- By 3D printing and hydrogel materials, 3D soft cartilaginous tissue layers with and without pattern could be designed and fabricated *in vitro*, toward the multi-layered articular cartilage/OC tissue reconstruction.
- Alginate-based materials assisted by 3D-printed mould could be used to fabricate the middle layer of the articular cartilage/OC tissue *in vitro*.
- Photocurable PEGDA hydrogel materials could be designed and printed with patterns by DLP 3D printer as scaffold to simulate the deep layer of the articular cartilage/OC tissue *in vitro*.

- By applying biocompatible examinations such as the MTT assay and LDH assay, to evaluate impacts of nanosensor on the viability, proliferation and differentiation of both fibroblasts and MSCs *in vitro* and the fluorescent intensity of the nanosensor in culture, the oxygen nanosensor applied in cell culture system *in vitro*, in terms of the size and concentration, could be characterised and optimised for further study.

References

[1] Waldron T. Chapter 20: Joint disease. in Buikstra, Jane (3rd Ed.) Ortner's identification of pathological conditions in human skeletal remains. Elsevier;. 2019:719-48.

[2] Krishnan Y, Grodzinsky AJ. Cartilage diseases. Matrix Biol. 2018;71-72:51-69.

[3] Broom ND, Thambyah A. The Soft Hard Tissue Junction: Structure, Mechanics and Function. Cambridge: Cambridge University Press; 2018.

[4] Hootman JM, Helmick CG, Barbour KE, Theis KA, Boring MA. Updated projected prevalence of self-reported doctor-diagnosed arthritis and arthritis-attributable activity limitation among US adults, 2015–2040. Arthritis & rheumatology. 2016;68:1582-7.

[5] Andriolo L, Crawford DC, Reale D, Zaffagnini S, Candrian C, Cavicchioli A, et al. Osteochondritis dissecans of the knee: etiology and pathogenetic mechanisms. A systematic review. Cartilage. 2020;11:273-90.

[6] Lynch M, Bucknall M, Jagger C, Wilkie R. Healthy working life expectancy at age 50 for people with and without osteoarthritis in local and national English populations. Scientific reports. 2022;12:1-13.

[7] Richter DL, Schenck Jr RC, Wascher DC, Treme G. Knee articular cartilage repair and restoration techniques: a review of the literature. Sports health. 2016;8:153-60.

[8] Gracitelli GC, Moraes VY, Franciozi CE, Luzo MV, Belloti JC. Surgical interventions (microfracture, drilling, mosaicplasty, and allograft transplantation) for treating isolated cartilage defects of the knee in adults. Cochrane Database Syst Rev. 2016;9:CD010675.

[9] Oliveira JM, Pina S, Reis RL, San Roman J, (Ed.). Osteochondral tissue engineering: challenges, current strategies, and technological advances: Springer; 2018 (Vol.1059).

[10] Outerbridge RE. The etiology of chondromalacia patellae. J Bone Joint Surg Br. 1961;43-B:752-7.

[11] Cavalcanti Filho MMdC, Doca D, Cohen M, Ferretti M. Updating on diagnosis and treatment of chondral lesion of the knee. Revista Brasileira de Ortopedia. 2012;47:12-20.

[12] Brittberg M, Winalski CS. Evaluation of cartilage injuries and repair. JBJS. 2003;85:58-69.

[13] Fu L, Yang Z, Gao C, Li H, Yuan Z, Wang F, et al. Advances and prospects in biomimetic multilayered scaffolds for articular cartilage regeneration. Regenerative biomaterials. 2020;7:527-42.

[14] Demoor M, Ollitrault D, Gomez-Leduc T, Bouyoucef M, Hervieu M, Fabre H, et al. Cartilage tissue engineering: molecular control of chondrocyte differentiation for proper cartilage matrix reconstruction. Biochimica et Biophysica Acta (BBA)-General Subjects. 2014;1840:2414-40.

[15] Mitchell ME, Giza E, Sullivan MR. Cartilage transplantation techniques for talar cartilage lesions. JAAOS-Journal of the American Academy of Orthopaedic Surgeons. 2009;17:407-14.

[16] Erickson B, Fillingham Y, Hellman M, Parekh SG, Gross CE. Surgical management of large talar osteochondral defects using autologous chondrocyte implantation. Foot and Ankle Surgery. 2018;24:131-6.

[17] Panseri S, Russo A, Cunha C, Bondi A, Di Martino A, Patella S, et al. Osteochondral tissue engineering approaches for articular cartilage and subchondral bone regeneration. Knee Surgery, Sports Traumatology, Arthroscopy. 2012;20:1182-91.

[18] Nukavarapu SP, Dorcemus DL. Osteochondral tissue engineering: current strategies and challenges. Biotechnology advances. 2013;31:706-21.

[19] Tamaddon M, Wang L, Liu Z, Liu C. Osteochondral tissue repair in osteoarthritic joints: clinical challenges and opportunities in tissue engineering. Bio-design and Manufacturing. 2018;1:101-14.

[20] Ingber DE, Mow VC, Butler D, Niklason L, Huard J, Mao J, et al. Tissue engineering and developmental biology: going biomimetic. Tissue engineering. 2006;12:3265-83.
[21] Chung C, Burdick JA. Engineering cartilage tissue. Advanced drug delivery reviews. 2008;60:243-62.
[22] Schuurman W, Harimulyo E, Gawlitta D, Woodfield T, Dhert WJ, van Weeren PR, et al. Three-dimensional assembly of tissue-engineered cartilage constructs results in cartilaginous tissue formation without retainment of zonal characteristics. Journal of tissue engineering and regenerative medicine. 2016;10:315-24.
[23] Campos Y, Almirall A, Fuentes G, Bloem HL, Kaijzel EL, Cruz LJ. Tissue engineering: an alternative to repair cartilage. Tissue Engineering Part B: Reviews. 2019;25:357-73.
[24] Skardal A, Murphy SV, Devarasetty M, Mead I, Kang H-W, Seol Y-J, et al. Multi-tissue interactions in an integrated three-tissue organ-on-a-chip platform. Scientific reports. 2017;7:1-16.
[25] Georges PC, Janmey PA. Cell type-specific response to growth on soft materials. Journal of applied physiology. 2005;98:1547-53.
[26] Bougault C, Paumier A, Aubert-Foucher E, Mallein-Gerin F. Molecular analysis of chondrocytes cultured in agarose in response to dynamic compression. BMC biotechnology. 2008;8:1-10.
[27] Barlič A, Drobnič M, Maličev E, Kregar-Velikonja N. Quantitative analysis of gene expression in human articular chondrocytes assigned for autologous implantation. Journal of orthopaedic research. 2008;26:847-53.
[28] Lund AW, Yener B, Stegemann JP, Plopper GE. The natural and engineered 3D microenvironment as a regulatory cue during stem cell fate determination. Tissue Engineering Part B: Reviews. 2009;15:371-80.
[29] Griffith LG, Swartz MA. Capturing complex 3D tissue physiology in vitro. Nature reviews Molecular cell biology. 2006;7:211-24.
[30] Graham N. Hydrogels: their future, Part I. Medical device technology. 1998;9:18-22.
[31] Graham N. Hydrogels: their future, Part II. Medical device technology. 1998;9:22-5.
[32] Nguyen KT, West JL. Photopolymerizable hydrogels for tissue engineering applications. Biomaterials. 2002;23:4307-14.
[33] Lee KY, Mooney DJ. Hydrogels for tissue engineering. Chemical reviews. 2001;101:1869-80.
[34] Bettinger CJ, Weinberg EJ, Kulig KM, Vacanti JP, Wang Y, Borenstein JT, et al. Three-dimensional microfluidic tissue-engineering scaffolds using a flexible biodegradable polymer. Advanced materials. 2006;18:165-9.
[35] Sarkar K, Gomez C, Zambrano S, Ramirez M, de Hoyos E, Vasquez H, et al. Electrospinning to forcespinning™. Materials today. 2010;13:12-4.
[36] Fu Q, Saiz E, Tomsia AP. Direct ink writing of highly porous and strong glass scaffolds for load-bearing bone defects repair and regeneration. Acta biomaterialia. 2011;7:3547-54.
[37] Masood SH, Alamara K. Development of scaffold building units and assembly for tissue engineering using fused deposition modelling. Advanced Materials Research: Trans Tech Publ; 2010,83. p. 269-74.
[38] Vijayavenkataraman S, Zhang S, Lu WF, Fuh JYH. Electrohydrodynamic-jetting (EHD-jet) 3D-printed functionally graded scaffolds for tissue engineering applications. Journal of Materials Research. 2018;33:1999-2011.
[39] Morris VB, Nimbalkar S, Younesi M, McClellan P, Akkus O. Mechanical properties, cytocompatibility and manufacturability of chitosan: PEGDA hybrid-gel scaffolds by stereolithography.

Annals of biomedical engineering. 2017;45:286-96.
[40] Schoonraad SA, Fischenich KM, Eckstein KN, Crespo-Cuevas V, Savard LM, Muralidharan A, et al. Biomimetic and mechanically supportive 3D printed scaffolds for cartilage and osteochondral tissue engineering using photopolymers and digital light processing. Biofabrication. 2021;13:044106.
[41] Langford T, Mohammed A, Essa K, Elshaer A, Hassanin H. 4D printing of origami structures for minimally invasive surgeries using functional scaffold. Applied Sciences. 2021;11:332.
[42] Tayebi L, Rasoulianboroujeni M, Moharamzadeh K, Almela TK, Cui Z, Ye H. 3D-printed membrane for guided tissue regeneration. Materials Science and Engineering: C. 2018;84:148-58.
[43] Do AV, Khorsand B, Geary SM, Salem AK. 3D Printing of Scaffolds for Tissue Regeneration Applications. Adv Healthc Mater. 2015;4:1742-62.
[44] Hattori K, Sugiura S, Kanamori T. Microenvironment array chip for cell culture environment screening. Lab on a Chip. 2011;11:212-4.
[45] Metallo CM, Mohr JC, Detzel CJ, de Pablo JJ, Van Wie BJ, Palecek SP. Engineering the stem cell microenvironment. Biotechnology Progress. 2007;23:18-23.
[46] Rivron NC, Rouwkema J, Truckenmüller R, Karperien M, De Boer J, Van Blitterswijk CA. Tissue assembly and organization: developmental mechanisms in microfabricated tissues. Biomaterials. 2009;30:4851-8.
[47] Ng HY, Lee KA, Shen Y-F. Articular cartilage: structure, composition, injuries and repair. JSM Bone Joint Dis. 2017;1:1010.
[48] Murphy CL, Thoms BL, Vaghjiani RJ, Lafont JE. Hypoxia. HIF-mediated articular chondrocyte function: prospects for cartilage repair. Arthritis research & therapy. 2009;11:1-7.
[49] Pfander D, Gelse K. Hypoxia and osteoarthritis: how chondrocytes survive hypoxic environments. Current opinion in rheumatology. 2007;19:457-62.
[50] Zhou S, Cui Z, Urban JP. Factors influencing the oxygen concentration gradient from the synovial surface of articular cartilage to the cartilage–bone interface: a modeling study. Arthritis & Rheumatism. 2004;50:3915-24.
[51] Fermor B, Christensen S, Youn I, Cernanec J, Davies C, Weinberg J. Oxygen, nitric oxide and articular cartilage. Eur Cell Mater. 2007;13:56-65.
[52] Kellner K, Liebsch G, Klimant I, Wolfbeis OS, Blunk T, Schulz MB, et al. Determination of oxygen gradients in engineered tissue using a fluorescent sensor. Biotechnology and bioengineering. 2002;80:73-83.
[53] Obradovic B, Meldon JH, Freed LE, Vunjak-Novakovic G. Glycosaminoglycan deposition in engineered cartilage: experiments and mathematical model. AIChE Journal. 2000;46:1860-71.
[54] Koduri MP, S. Goudar V, Shao Y-W, Hunt JA, Henstock JR, Curran J, et al. Fluorescence-based nano-oxygen particles for spatiometric monitoring of cell physiological conditions. ACS applied materials & interfaces. 2018;10:30163-71.

Chapter two: Literature review

2.1 Introduction

Tissue engineering (TE) is bringing the 3D tissue fabrication technology into clinical applications. Before fabrication, understandings of the structure, component and function of the target tissue and current available fabrication techniques are essential. The target tissue in this study is the multi-layered inhomogeneous articular cartilage/osteochondral (OC) tissue unit in the synovial joint. There are three types of joints in vertebrate, including synarthroses or fibrous joints, amphiarthroses or cartilaginous joints, and diarthrodial or synovial joints, with different ability to perform motion. Fibrous joints such as connections between bones in the skull are not able to move, whereas joints in the intervertebral disk and in the spine having less or no ability to move, belong to cartilaginous joint. Elements such as the wrist, elbow, shoulder, hip, knee, ankle and talus, having relatively large capability to move, are classified into synovial joints [1-3]. The articular cartilage and synovial fluid are two essential parts in the synovial joint. Synovial fluid could be seen as a mixture of dialysate or concentrated solution of blood plasma and hyaluronic acid protein (HAP) complex, containing water, small molecules and macromolecules which are secreted by the membrane of articular capsule (synovium) and kept in the supportive cavity extended from the articular cartilage matrix [2-5]. Articular cartilage (AC) predominantly is the type of hyaline cartilage (Figure 2.1), covering the surface of both ends of epiphyses at synovial joint where trabecular hard bones are connected [4, 6]. The transitional interface between soft cartilage and hard bone in the joint area is the complex load-bearing junction namely the osteochondral (OC) tissue [7].

In this chapter, the structural characteristics, biochemical constituents, and physiological function

of the target tissue will be reviewed at the beginning. Chondral/osteochondral lesions, recommended grading systems, available clinical treatments and TE strategies will then be concisely introduced. Finally, to better simulate biological objects *in vitro*, the inhomogeneous microenvironment throughout the entire tissue and potential 3D fabrication strategies toward reconstruction of the inhomogeneous target tissue will be discussed. Due to the overlap in structure, function and lesion classification, articular cartilage tissue, chondral lesions and relevant topics will be generally reviewed along with OC tissues in a broader range in this chapter.

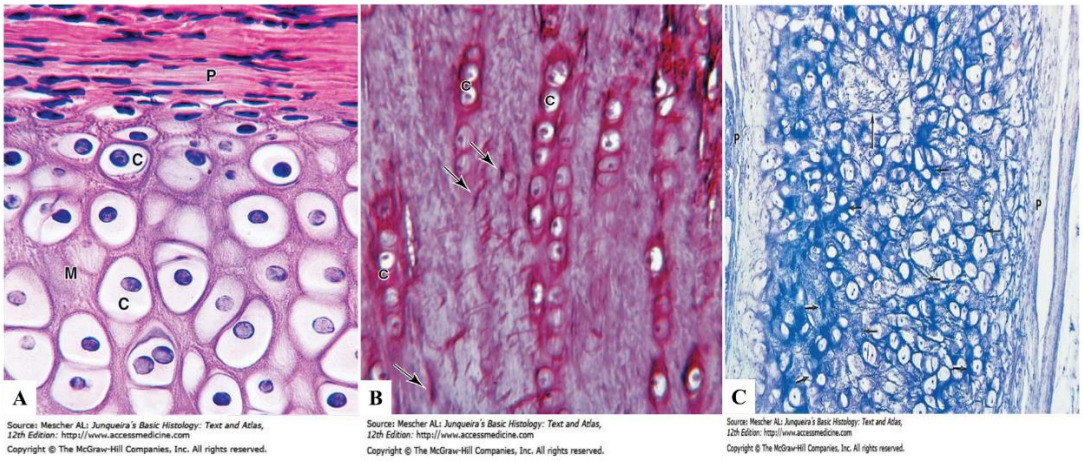

Figure 2.1 Images of three types of cartilage in human skeleton after staining by light microscope. A: Hyaline cartilage; P indicates the perichondrium on one side consisting of type I collagen, fibroblastic cells and MSCs. C indicates the larger and rounded chondroblasts and chondrocytes. M indicates the matrix around cells locating in the lacunae. (X200, H&E: hematoxylin and eosin) B: Fibrocartilage; C indicates the axially arranged isogenous aggregates of chondrocytes in columnar lacunae. Around the columnar lacunae, there are type I collagen fibres secreted by chondrocytes in basophilic matrix. Arrow indicates scattered fibroblasts with elongated nuclei. Acidophilic matrix indicates containment of a large number of type I collagen fibres in bundles, around chondrocytes and type II collagen fibre matrix. (X250, Picrosirius-hematoxlin) C: Elastic cartilage; P indicates perichondrium (P) on both surfaces. Arrow indicates the elastic fibres filled in the matrix. Cell size and distribution in elastic cartilage is very similar to that of hyaline cartilage. (X100. Weigert resorcin-fuscin.) Images were adapted from reference [8].

2.2 Structural characteristics, biochemical constituents, and physiological function of the articular cartilage/OC tissue

In general, the whole OC tissue in adult contains the overlying mature articulate cartilage (AC),

the underlying subchondral bone (SB) and the middle chondroid interface interconnecting the cartilage with the bone. The superficial hyaline cartilage tissue in the synovial joint is soft, deformable under pressure and recoverable after pressure removal. Immature hyaline cartilage is usually translucent and bluish-white, yet becomes opaque and yellowish after maturation. Mature AC is featured with absences of blood vessel, nerve and lymph and is made up of simply one type of resident cells (chondrocytes) embedded in abundant chondrogenic extracellular matrix (ECM) [9-11]. Immature AC covering the bone serves as the osseous anlage during body development, while mature AC contributes to forming a healthy, smooth and lubricating 'contact area' for synovial joint, supports the musculoskeletal structure and attenuates mechanical forces passing through the joint due to regular body motions and other external impacts [4]. The AC matrix in combination with the synovial membrane forms the double diffusion system for nutrients and gases (in particular the oxygen and carbon dioxide) from synovial fluid, metabolites generated by resident cells and turnovers of cellular matrix, to convectively pass through [12, 13]. The intermediate chondroid interface is difficult to define precisely due to variable thickness of the OC tissue in different species, and under different physiological (e.g., development, aging, anatomical site) and pathological (e.g., congenital monstrosity, inflammation) circumstances. This interfacial area with transitional properties from soft non-mineralised cartilage to stiff mineralised bone, often involves the tidemark line and calcified cartilage being considered as the ending area of AC [14]. In healthy OC tissue, this structure supports the transmission of mechanical force across areas between AC and SB in the joint but impedes the potential diffusions from SB to AC partially by the penetrated end-capped non-looped blood vessels [15]. The SB part in the OC unit is a place from which the structure and components of osseous tissue could initially be observed and it

naturally attaches to the underlying real trabecular and cortical bones. The relatively stiff and dense SB area in the OC unit, contributes to managing highly impacted forces and tensile stresses/strains delivered from both the 'contact area' via overlying cartilage matrix, and the interior area of the loaded incongruous joint [15, 16], and to assisting with diffusions of nutrients and gases from bone marrow [17] through extended vasculatures during dynamic modelling and remodelling process of long bones.

2.2.1 Structural characteristics, varied thickness and proportional volume

The OC tissue in structure was basically seen as biphasic (cartilage-bone). However, from the schematic image (Figure 2.2), the OC tissue in a typical synovial joint (e.g., in the knee), actually presents a multi-layered architecture with five distinctive zones, which are superficial zone on the top surface, middle zone (transitional zone), deep zone (radical zone), calcified zone and subchondral bone area (subchondral bone plate and subarticular spongiosa) on the bottom, manifesting a transition from soft compliant cartilage to hard stiff bone in a depth-related order. Sometimes this tissue could also be described as a triphasic structure including articular cartilage, calcified cartilage bordered by tidemark line and cement line, and subchondral bone part [9, 18]. More reports from immunochemical and immunohistochemical staining, biochemical examination in combination with certain advanced technologies such as Polarized light microscopy (PLM), Scanning electron microscopy (SEM), Transmission electron microscopy (TEM), Fourier transformed near infrared (FT-NIR) spectroscopy, Optical coherence tomography (OCT), Second harmonic generation (SHG), Two-photon-excited fluorescence (TPEF) and Raman spectroscopy, have suggested us the possible existence of more elaborated zonal arrangement and depth-

dependent constitution in the whole tissue [19-21], remaining further studies to clarify.

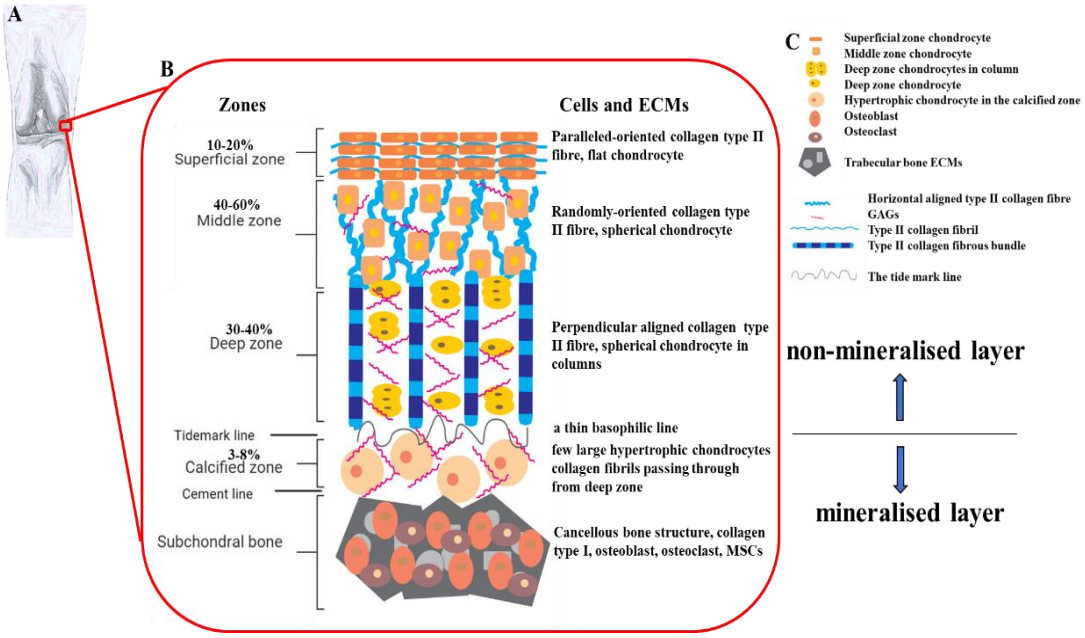

Figure 2.2 Schematic image of the ultrastructure of the healthy osteochondral tissue in knee joint A: Schematic image of the anatomical model of a knee joint B: Schematic image of the longitudinal section view of the ultrastructure of the healthy osteochondral tissue in the knee joint C: Illustrations of the signs within image B. Images were adapted from reference[9].

As specialised connective tissue the AC part totally is a thin layer about 2 to 7 mm thick, but larger than the interface area and SB part in the OC tissue [22-24]. Accumulated studies have revealed that variations in the thickness of them anatomically depend on the joint such as the site of the joint in the body and the joint congruency [15], the physiological status of the body and the type of species of the sample [22, 24]. Therefore, usually proportional volume was used to describe the thickness of each distinctive ultrastructure in the OC tissue. In the superficial zone, its volume accounts for 10 to 20% of the cartilaginous part and it is occupied by flat chondrocytes within condensed thin collagen fibres which are in the form of packed bundles paralleling to each other. Although existence of vertically arranged collagen fibres was also observed, chondrocytes in this zone are mainly oriented by these horizontal aligned bundles of fine fibrils which also form the special lamina splendens structure representing the articular surface, covering the superficial zone

[14, 19]. In the middle zone, its volume is about 2-3 times larger than that of the superficial zone, accounting for 40-60% of the cartilaginous part and it is filled with rounded chondrocytes enclosed by randomly oriented type II collagen fibres. In the deep zone, its volume accounts for 30-40% of the cartilaginous part and it is packaged with spherical chondrocytes alongside perpendicularly aligned large bundles of type II collagen fibres [14]. In the calcified zone, its volume accounts for 3-8% of the cartilaginous part [25, 26] regardless of varied sites of tested samples and irregular contours, and it has a few large hypertrophic chondrocytes sporadically being surrounded by some type II collagen fibres penetrating from the deep zone and anchoring in the calcified matrix and underlying subchondral bone area. The resident chondrocytes of calcified zone are located in the uncalcified lacunae area [14], with similar features of growth plate chondrocytes, staying quiescent rather than activated [26]. The subchondral bone (SB) area has varied anatomical features of density, thickness, contour and components depending on the site of joint as well, but generally its structure is about a few-millimetre thin containing two mineralised layers which are named the subchondral bone plate and subarticular spongiosa, with different thickness and density of honeycomb-like lamellar structure and narrow intervening space [14, 15]. The bony lamellar sheet in the SB area is composed of mainly the paralleled type I collagen fibrils, hosting osteocytes, osteoblasts, osteoclasts, other progenitor cells and migrated mesenchymal stem cells (MSCs) [9]. In the SB area, the trabeculae-like lamellar structure has thicker plates, narrower interval spaces, and deflected a few angles in the direction below the perpendicular articular surface, comparing to the real trabeculae of underlying hard bone [14, 15, 26, 27]. This area is adjacent to the beneath cancellous bone in both trabecular structure and vasculature, however, being separated from calcified zone by the cement line, occasionally, small vascular canals might be connected at the

area between calcified zone and SB area in the OC tissue where collagen fibres are not continuously penetrated [14, 15].

As mentioned, there is a thin wavy line of irregular boundary called tidemark line resulting from the dynamic mineralisation process within the chondroid interface where some biomolecules (protein, lipid but proteoglycan) could be accumulated discontinuously [26], finally separating the below mineralised parts (calcified zone and subchondral bone) from above non-mineralised parts (superficial, middle and deep zones). It could be seen as an ultrastructural group of collagen fibrils with small space of channels in between the deep zone and calcified zone. The various contours and irregularity of tidemark line may be correlated with the degenerative condition and the weight-bearing location of the synovial joint [14]. Correspondingly, on the other side of the calcified zone, there is another line of boundary separating calcified zone from subchondral bone as well, which is termed cement line [28].

Classically, by histological staining [6], the zonal arrangement of tissue specific ECM and the organisation of cells within the OC tissue could be observed and qualified. For example, the whole OC unit could be stained by toluidine blue [7]. Whereas it is the fast green but safranin-O dye that could be used to stain the superficial zone, consisting of fine collagen fibres on the surface and elongated chondrocytes with tangential orientation [6]. The safranin-O dye could be applied to stain other zones, such as the middle, deep and calcified zones, to display the random distribution of rounded cells, spherical cells in column and sporadically distributed large hypertrophic cells respectively [6]. Apart from afront mentioned dyes, Alcian blue staining for GAGs, Picrosirius red or Masson trichrome staining for collagen fibres of the connective tissue are also used to discriminate the zonal structure of the OC tissue in the musculoskeletal system [20, 29]. The

tidemark line is a visible border line between the deep zone and calcified zone [6], having basophilic affinity that could be stained easily by basic dyes, for instance, the toluidine blue [10], Haematoxylin and Eosin staining (H&E staining) [16] and by dyes having affinity with non-proteoglycan protein and lipid [10]. The cement line separating the calcified zone from subchondral bone area could be observed by Safranin-O/Fast green staining, in contrast the tidemark line might not be visualised by this way. However, by von Kossa staining, the calcified zone in black could be distinguished from above hyaline cartilage in salmon pink and underneath subchondral bone in colourless, where the two interfaces (tidemark and cement line) could be shaped, consistent with SEM images [28].

2.2.2 Biochemical constituents and major components

From previous histological studies of explants and cadaveric samples, not only the approximate range of thickness and proportional volume of each zone, but also the biochemical composition, especially those major components of the OC tissue have been identified.

In the AC part, it is found that about 65-80% of its wet weight is water [10], other non-cell components are mainly proteins secreted by chondrocytes to form ECMs, such as the collagen family, proteoglycan family and many others [22]. Although more than 90% of collagen fibres within the AC part are type II (10-20% of the wet weight of the AC part), other members of the collagen family are existed, such as type III (about 10% of all types of collagen fibres), type VI (less than 1%), type IX (1%) and type XI collagen (3%) [9] in non-mineralised AC; type I, II and X are found in the transitional part and in particular type X could be found in deep zone, calcified zone [7], and in growth plate [30]. Except the collagen family, another abundant protein family

within chondrogenic ECM is proteoglycans (having glycosaminoglycan (GAG) chains) (10-20% of the wet weight of the AC) including versican, the hyaluronan-GAGs keratin sulphate-chondroitin sulphate protein complex, small leucine-rich repeat proteoglycan family, perlecan, lubricin (superficial zone protein SZP) and the cartilage-specific aggrecan (4-7% of the wet weight of the AC) [6, 31]. Besides, other non-collagenous and non-proteoglycan proteins which could be divided into two groups, are as follows: thrombosondin-1, -3, and -5 (cartilage oligomeric matrix protein), matrilin-1 (cartilage matrix protein, fibronectin) and matrilin-3, fibronectin and tenascin-C, belong to the structural protein group; the others belonging to the regulatory protein group include matrix Gla protein, chondromodulin-I and II, gp-39/YKL-40, cartilage-derived retinoic acid-sensitive protein and some important growth factors like the bone morphogenic protein (BMP) family and transforming growth factor-β (TGF-β) [6].

In the SB part, the water content would be greatly reduced from about 60% at birth to 15-25% after birth a few months as the tissue maturing and mineralising, and due to its direct connection with underlying hard bone and interactive mass exchange, the predominant collagen fibre is type I secreted by osteoblasts and mineralised with osteocalcin to form the mineralised ECM of osseous tissue. Another protein secreted in bony area is osteonectin which forms the non-mineralised ECM together with type I collagen fibres [7] within osseous tissue.

2.2.3 Physiological functions of the articular cartilage/OC tissue and mechanical forces

The specialised structure and constituent components determine the physiological function of the OC tissue which is allocated to be performed individually or synergically. Generally, joints are applied on forces by activities, movements or accidental impacts, leading to occurrences of the

sliding motion of the ‘contact area’ in between the joint surfaces, where in combination with the synovial fluid, the AC in healthy OC tissue functionally provide the lubricative low-friction interface over the ‘contact area’ at bone-bone junctions and deals with various mechanical forces, such as static/dynamic loading impacts, loading absorption and attenuation, loading distribution and transformation, and loading transfer within the body environments sometimes in a magnitude ranging from zero to very high or conversely in a very short time of period [32].

In a loaded joint, at least five types of forces could be generated and distributed though in a zone-related differential manner throughout the entire OC tissue, including tensile strain, compressive/shear strain and stress, fluid flow and hydrostatic pressure covering both the solid and liquid phases in the tissue [32, 33]. Different part of the tissue presents different biomechanical behaviours in response to allocated forces.

For example, AC has been characterised as a viscoelastic material in the joint, presenting a creep and stress-relaxation reaction to constant loading or deformation forces in a time-dependent manner [34]. In AC part, cyclic joint pressures are generated when intermittent or imported forces are loaded by joint cartilages of both sides of diarthrodial joints periodically over the ‘contact area’ during physical activities, resulting in a cyclic compressive stress in the solid phase of chondrogenic ECMs and a heavy cyclic hydrostatic pressure in the liquid phase of the interstitial fluid in the superficial zone where a relatively higher content of water is contained than the other AC zones. Once the solid ECMs are compressed locally by forces across the zone, the gel-like interfibrillar water will be pressurised against the water flow being squeezed out of the ECMs with the low fluid permeability resulting from the electrostatic repulsive forces between the negatively charged proteoglycan aggregates and the trapped interfibrillar water. This kind of restriction to the

interstitial fluid flow mainly happens in the superficial zone where the solid ECMs consisting of lacunal collagen fibres consolidate as fluid is exuding, leading to a very high compressive pressure to deform local chondrocytes. Due to the exudation and consolidation in superficial zone a physical seal is formed to prevent underlying zones from fluid inflow and to drain the fluid strictly out of the superficial zone toward the 'contact area'. In addition, collagen fibres of the solid ECMs also contribute to resisting the tensile strain and shear stress in superficial zone because of the molecular motions in both solid (collagen-proteoglycan ECM) and liquid phases (flow-dependent frictional drag) of ECMs. As the fluid flow in superficial zone is sealed and the water content is decreased, reduced exudation and consolidation occur in the middle zone where the tissue layer generally contains hydrostatic pressure and a low fluid flow, leading to a moderate compressive strain experienced by local chondrocytes. Besides, randomly arranged collagen fibrils and precisely organised intra and intermolecular crosslinks in the collagen network of ECMs in the middle zone, contribute to the local tensile strength to resist and stabilise any occurring tensile force or stretching-related shear stress. The interstitial fluid flow is very less likely to be observed in the deep zone and below, due to progressive consolidations of those collagen fibrils in above superficial and middle zones, and restrictions by the impermeable subchondral bone and neighbouring cartilaginous tissues. Hence, in the deep zone, there is little fluid flow and less compressive strain, where local chondrocytes mainly experience fluid pressures. Some collagen fibrils could pass through the 3D tidemark line from non-mineralised cartilage part to the calcified cartilage zone. The formation, appearance and dynamic changes of the tidemark line also reflect the dynamic microenvironment and distribution of biomechanical forces across the tissue especially the interfacial regions between non-calcified and calcified cartilages [15]. Below the

tidemark line within the mineralised area of the OC tissue, there is no fluid flow and no flow-dependent compressive strain, local cells primarily endure hydrostatic pressures and interface shear strains [32, 33].

Previous studies revealed that under dynamic impacts, the SB part was less compliant and much stiffer than the AC part, but was relatively flexible and deformable under pressures to be able to contribute to attenuating peak forces even more than the AC part [15, 35], really depending on its thickness, structure and the amount of strain applied [27]. Hence, the AC may contribute to the distribution and attenuation of loadings to reduce the transmitted peak loads toward underlying SB, to some extent, the SB is responsible for preventing the underlying cancellous bone from damages due to transmitted excessive biomechanical loadings.

In summary, the physiological function of the articular cartilage/OC tissue determined by its structure and components, is to deal with force and provide lubrication. The mechanical property of the AC is featured with softness, compliance and deformability, whose mechanical behaviour is often described by the biphasic model and viscoelastic model, depending on the application. In the commonly employed biphasic model, pressurised interstitial fluid flow happens throughout the whole viscoelastic cartilaginous tissue under the ‘contact area’ after loading, contributing to reducing surface friction and stress toward the solid ECMs, which ultimately endue the AC with the ability to hold a majority of loadings even more exceeding the weight of body. The fibrous collagen network in the solid ECMs contributes to resisting any occurring tensile strain, shear stress and hydrostatic compressive stress-induced strains [32, 36]. Comparing to the AC, the mechanical property of the SB relates to the stiffness regarding its compact condensed subchondral cortical plate, and viscoelasticity referring to its subchondral trabecular components. Physiological

function of the SB is to biomechanically support the overlying cartilage and to attenuate or absorb forces to protect underlying bone tissue, also determined by its type I collagenous components and mineralisation. Although appropriate loading is important to keep the homeostasis of both cartilage and bone, to retain the shape of hard bone and to remain the congruent morphology of the joint [15, 36, 37], imbalanced distributions of mechanical forces in the joint, due to reasons such as the abnormal structure, excessive loading, degeneration and wear and tear, would directly lead to cracks, injuries and subsequent inflammations in joint areas.

2.3 Chondral/OC defects, grading systems, current clinical options and TE strategies

As the musculoskeletal trauma, defects or injuries in the multi-layered chondral/OC tissue of synovial joints, could be resulted from numerous original or derivate reasons such as genetical disorder and deformation, degeneration with aging, wear and tear, mechanical trauma, inflammations, tumour, metabolic abnormality, and autoimmune disorders such as the rheumarthritis (RA), in which the osteoarthritis (OA) is one of the most diagnosed degenerative diseases in orthopaedics and traumatology, having impacts on almost every part of the synovial joint in the musculoskeletal system [38, 39].

Previous studies found that same as other tissues, a series of events would occur in the damaged articular cartilage including an increased water content, chondrogenic ECM disruption and degradation, local cell apoptosis or necrosis, loosing and losing constituent components within the joint, and inflammations [11]. Symptoms of chondral/osteochondral lesions commonly involve pain, swelling, joint locking, catching, stiffness and grinding sensation [40, 41], whereas no symptoms or no significant disability could be also reported by patients whose lesion and

degenerative changes were mild and small at earlier time [40, 42]. Degree of chondral/osteochondral defects was defined mainly by patient factors such as age, sex and medical history, symptoms, experience of doctor and tactile feedbacks in early studies [40]. In order to reliably describe and diagnose these defects, and to provide suitable treatments and better prognosis in clinics, uniformed or compatible grading systems for classification and criteria are necessary. The description and classification of chondral/osteochondral defects in patients have been established and developed along with the classification criteria and grading systems.

2.3.1 Chondral/osteochondral defects and grading systems

As increasing knowledges of investigations about the failure of OC tissue *in vivo* and potential mechanisms to explain the observed structural splits or fractures in OC samples *in situ* or *ex vivo*, research studies focused on the pattern of external forces and subsequent changes in local structure, in which the grade of mineralisation, the level of maturity and the degenerating stages in the period of growth and development (e.g. early or late) of samples were confirmed to have critical roles in explaining relevant mechanisms and in describing chondral/osteochondral failures which were related to some major mechanical forces (direct or indirect, compressive or shear stress) [43]. For example, it was found that sudden mechanical forces such as the tangential shear stress from activities between bone and muscle might cause the cartilage part splitting off the connected bone [44]. Various splits around the fragile tidemark line in the interfacial region might be resulted from direct or combined mechanical forces, such as rotational and compressive forces together. The immature OC tissue with no or less tidemark line structure due to inadequate calcification, might be the reason why OC lesions are more commonly seen in young people [45, 46], whereas in adult joint with mature OC tissue containing fully developed non-mineralised cartilage, calcified

cartilage zone, subchondral bone plate and subarticular spongiosa, to form gradients of compliance and stiffness within a large range, chondral defects such as cartilage tissue damage and delamination of the AC around the tidemark line, are more likely to happen, where the tissue configuration determines its vulnerability to direct shear stress or compressive and tractive/tensile forces derived from transformed shear stress [15, 43, 47-49]. By various impact loading tests and simulations from schematic, theoretical, mathematical models, various descriptions and assessments of the chondral/OC failures emerged, but results may vary from the applied tests, tools, specific regimes and mechanical forces involved, and the anatomy of samples (e.g. the degree of maturity and degeneration) [43].

Clinical studies on patterns of chondral/osteochondral injuries, were often based on knowledges of anatomies of musculoskeletal system, biomechanical properties of synovial joint samples, histological staining and advanced imaging techniques. Potential mechanism and classification system were developed and applied to carefully discriminate the clinical samples of surgical lesions from nonsurgical lesions [50]. For example, OC injury can be roughly divided into two clinical patterns which are chronic type, often called osteochondrosis dissecans (OCD), in young people whose joint usually experiences a low-level pain resulting from relatively normal but repetitive, chronic loadings; and acute type, referring to osteochondral fractures, in mature adult having internal dislocation or derangement in joint tissue dealing with abnormal loadings such as strong axial force, combination of force and torsion, shearing stress, particularly in the AC part [51].

It was said that many grading systems in clinic were developed from the one described by Berndt and Harty in 1959 based on the radiographic images of reproduced OC injuries in cadaver, in which those injuries were classified into four grades according to those obtained images (Figure 2.3).

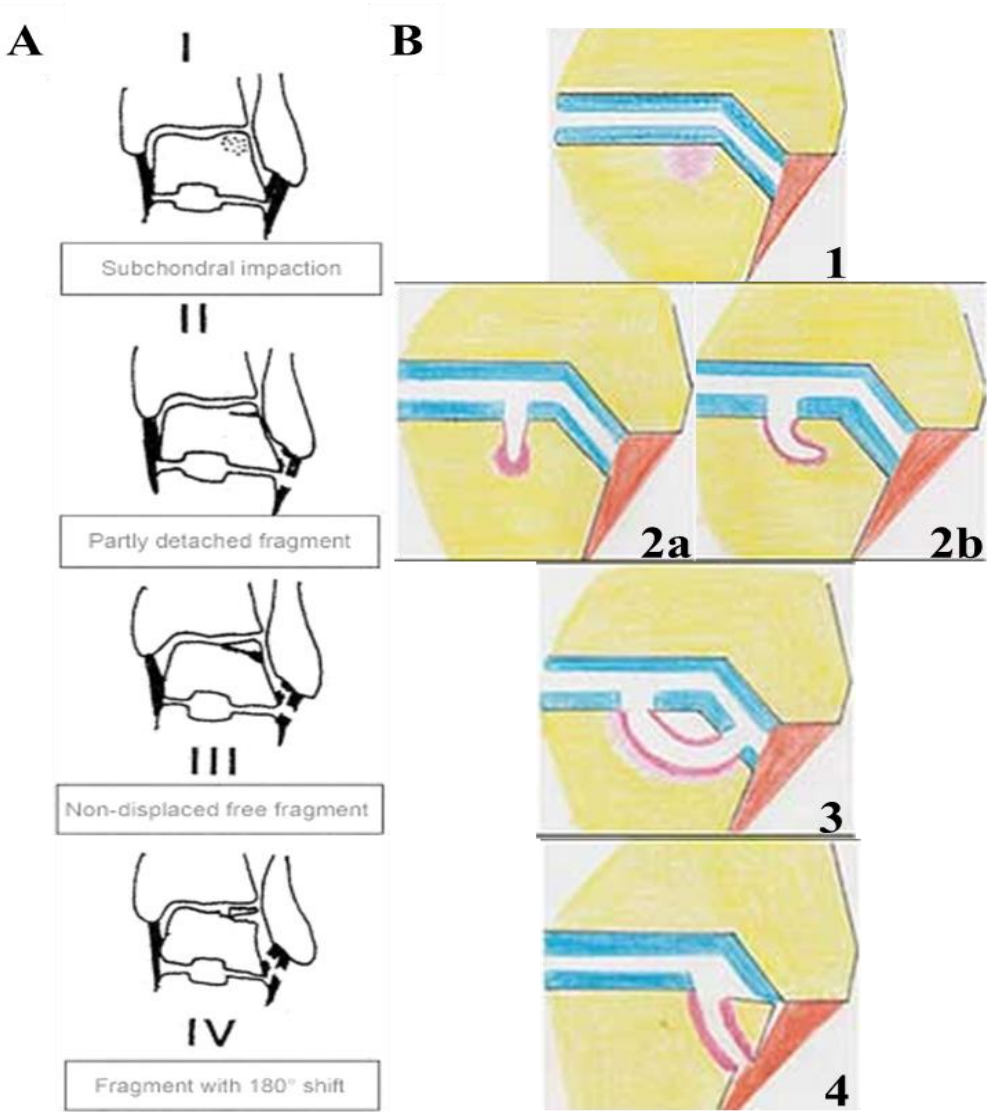

Figure 2.3 Schematic images illustrating different grades of osteochondral defects of the talus by the Berndt & Harty classification and the one proposed by Anderson and Crichton.

A: Illustration of the Berndt & Harty Classification. I: Stage 1 lesion of a subchondral impaction. II: Stage 2 lesion of a partly detached fragment defect. IIIC: Stage 3 lesion of a non-displaced free fragment. IV: Stage 4 lesion of a fragment with 180° shift defect. B: Schematic images illustrating the classification proposed by Anderson and Crichton, based on Magnetic Resonance Imaging (MRI). B-1: Stage 1 lesion of a trabecular compression in subchondral area. Plain radiographs show normal but bone scan shows positive and MRI shows bone marrow edema (BME). B-2a: Stage 2a lesion of a subchondral cyst, surrounding the BME. B-2b: Stage 2b lesion of the incomplete separation of a fragment, non-detached, surrounding the BME. 3: Stage 3 lesion of a completely detached, non-displaced fragment, in the presence of synovial fluid around the fragment, surrounding the BME. 4: Stage 4 lesion of a displaced fragment with adjacent BME. Images were adapted from references [50, 52-54].

In brief, stage one defect was generally a subchondral fracture (sclerosis) due to compressive force but AC part was not damaged; stage two injury was a partially attached fragment with detached

fragment within the OC unit; stage three damage was the broken OC unit having a detached and displaceable fragment remained; stage four lesion was the broken OC unit with the displaced fragment being extruded out of the OC area [50, 51]. As the development of imaging technologies to directly visualise clinical samples, more advanced tools such as the plain film radiography, or radiography with arthrography together, scintigraphy, ultrasonography, computer tomography (CT), and magnetic resonance imaging (MRI), have been incorporated in grading systems to manage diagnosis, prognosis and assessment of clinical samples with chondral/osteochondral injuries [51]. Considering images with more details obtained by CT, MRI, in combination with arthroscopy, and validations and correlations among them, the four-stage grading system was further modified [51, 55-57] and applied to describe site-specific lesions directly, such as the Beck and Konan system for hip joint, modified Collin and French Society of arthroscopy (FSA) systems for knee joint [57-61], and grading system from Mintz for talus joint [62].

Despite limitations and advanced imaging challenges on the criteria of this kind of macroscopic grading systems still require further modification and validation to finally achieve consistent and reliable classification systems to support different patients for education purposes, medical studies, therapeutic regimen planning and disease prognosis [58], the Outerbridge Classification System (Figure 2.4) with simplified five grades of common chondral/osteochondral defects in the joints, without considering the depth of lesions, remains the most widely employed reference in clinic [63]. Based on this system, a few currently well-accepted and used other types of classification systems could be developed [64]. Those five grades of lesions from 0 to 4 in the **Outerbridge Classification System** are briefly described as follows [18, 42, 58, 65]:

The No. 0 grade: This should be a normal cartilage in the OC unit.

The No. 1 grade: This cartilaginous part of the OC unit has swelling and/or soften features.

The No. 2 grade: The cartilaginous part of the OC unit has reduced thickness with chondral defects such as fissures on the surface but not reaching to the subchondral bone part and the size of the injured area in diameter is less than 1.5 cm.

The No. 3 grade: The cartilaginous part of the OC unit has full-thickness chondral defects such as fissures reaching to the subchondral bone area and/or the injured size in diameter is larger than 1.5 cm.

The No. 4 grade: The injured area in the OC unit is deeply involving the subchondral bone part.

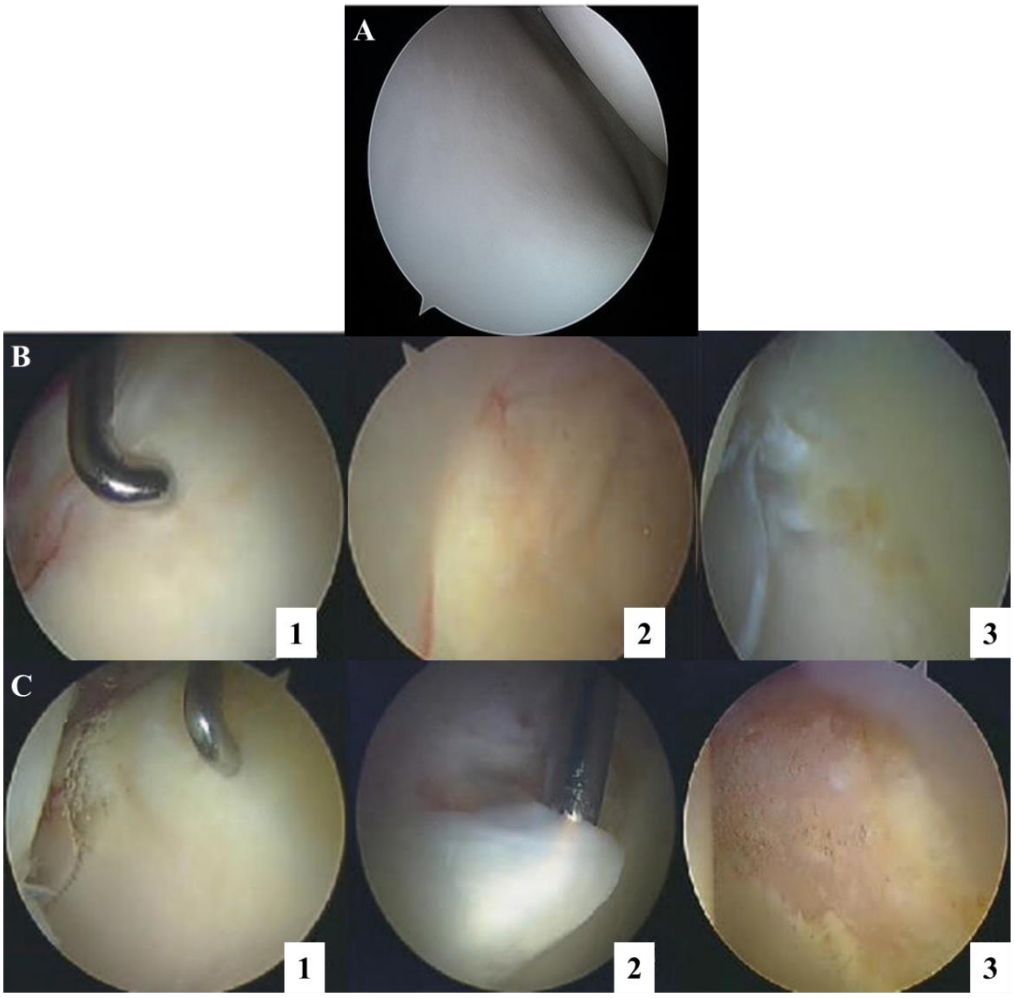

Figure 2.4 A healthy articular cartilage in the tibiofemoral joint and chondral lesions from slight to severe types in the hip joint categorised by the Outerbridge classification system in arthroscopic view.
A: A healthy articular cartilage (Grade 0). B: Four grades of lesion classified by the Outerbridge classification

system; B-1: Grade 1; B-2: Grade 2; B-3: Grade 3. C: Three different patterns identified in Grade 4 lesions. C-1: Wave sign; C-2: Carpet; C-3: Global degeneration. Images were adapted from references [66, 67].

Some early clinical studies of chondral lesions which were mainly focusing on the OA, also developed various scoring systems based on histopathological staining to assess the degree of disease and quality of treatments, even if their samples were limited to biopsies, animal models and staining techniques, and most results were impractical and non-reproducible [11, 12, 38, 68, 69]. Then a visual histological scoring system and recommendations from the Histological Endpoint Committee of the International Cartilage Repair Society (ICRS), the corrected Histological/Histochemical Grading System (HHGS) and the Osteoarthritis Research Society International and the Cartilage Histopathology Assessment system (OARSI histological score) based on histological scoring of biopsy specimens were finally established aiming to provide relatively standard criteria to reliably compare and validate results acquired by different observers, methodologies and technologies [11, 18, 70-76]. Details about these scoring systems and amendments based on histological images can be found in many reviews [11, 18, 71, 73], here the well-accepted and commonly employed basic criteria and classification system recommended by the ICRS are briefly described below [11].

The criteria recommended by the ICRS:

About the surface: the normal joint should have a smooth, continuous and slippery surface. About the matrix: the hyaline articular cartilage should have tissue-specific components (type of collagen and proteoglycan) and viscoelasticity. About the cell distribution: in the normal mature cartilaginous part, resident cells should be organised in columns in the middle and lower zones; abnormal mature cartilaginous tissue presents disrupted arrangement of those columnised resident cells. About the viability of cell population: cell population and matrix turnover should be viable

to observe. About the subchondral bone: the geometry and loading pattern of the joint could be observed by the presence and property of the subchondral bone area. About the mineralisation: the mineralised area (calcified cartilage) in the cartilaginous part could be seen as a pathological sign to indicate the impaired function of the cartilage.

Based on the depth and involvement of the subchondral bone of lesions, and developed from the Outerbridge system, **the classification system from the ICRS** [64] (Figure 2.5) is generally described as follows:

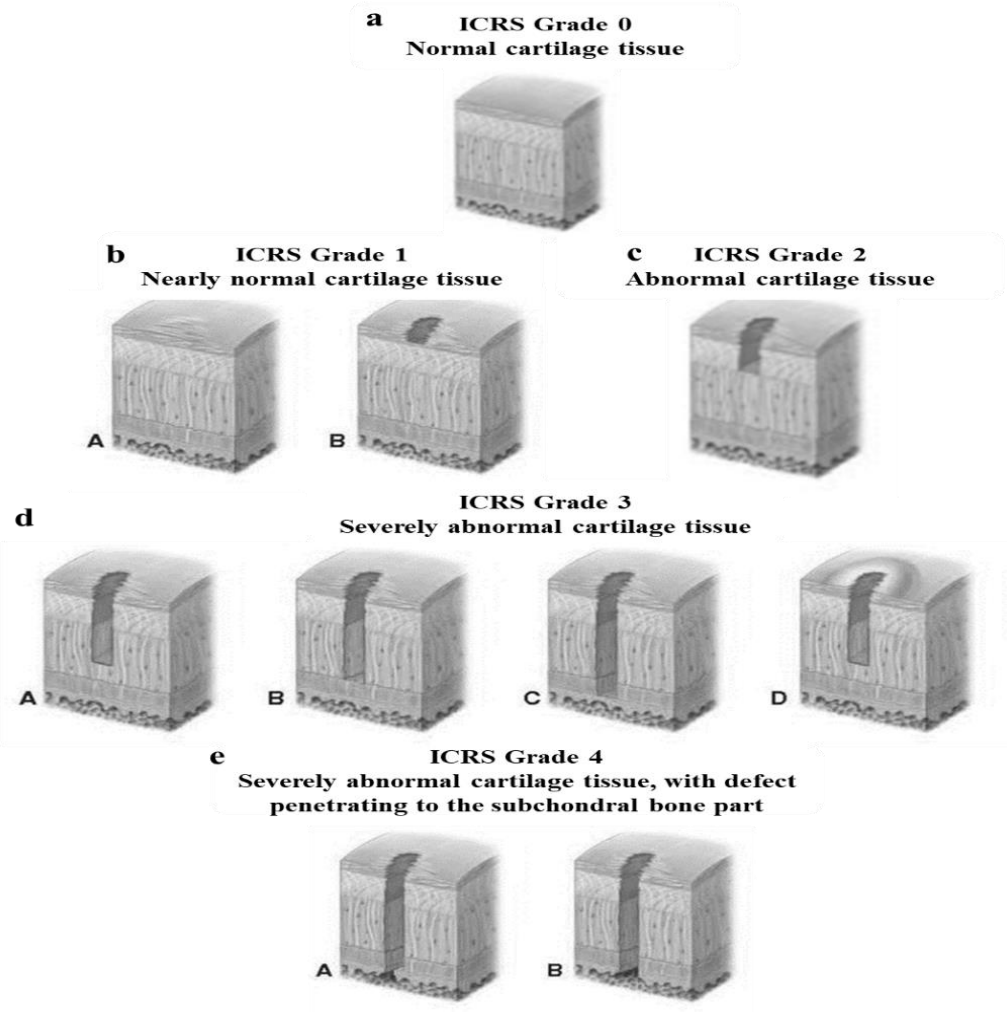

Figure 2.5 Schematic images of the ICRS classification.

a: ICRS Grade 0 lesion. b: ICRS Grade 1 lesion; b-A: Subtype A lesion. b-B: Subtype B lesion. c: ICRS Grade 2 lesion. d: ICRS Grade 3 lesion; d-A: Subtype A lesion. d-B: Subtype B lesion. d-C: Subtype C lesion. d-D: Subtype D lesion. e: ICRS Grade 4 lesion; e-A: Subtype A lesion; e-B: Subtype B lesion. Images were adapted from reference [66].

Grade 0 lesion: This tissue is normal cartilage tissue. Grade 1 lesion: This tissue is nearly normal, having superficial fissure. Subtype A: This tissue has soft indentation. Subtype B: This tissue has fissures and cracks on the superficial area. Grade 2 lesion: This tissue has abnormal cartilage, featuring with the depth of lesion down to less than half of the depth of the cartilage part. Grade 3 lesion: This cartilage tissue has severe abnormality, belonging to cartilage defect. Subtype A: the depth of lesion down to more than half of the depth of the cartilage part. Subtype B: the depth of lesion down to the calcified layer of the cartilage. Subtype C: the depth of lesion down to the subchondral bone area but not passing through the subchondral bone area. Subtype D: This tissue shows blisters within the cartilage part. Grade 4 lesion: This cartilage tissue has severely abnormality and the defect penetrates to subchondral bone part. Subtype A: The penetrated defect in subchondral bone part is not in a full diameter size. Subtype B: The penetrated defect in subchondral bone part is in a full diameter size.

2.3.2 Current clinical options and challenges

Based on the standard criteria and grading system, patients with a variety of chondral/OC problems (Figure 2.6) would be assessed and grouped to be processed for appropriate treatment. Mostly, mechanical force-induced lesions initiate in the soft cartilaginous part, or in the cartilage-bone interface such as the tidemark line fissures [14], leading to small or moderate chondral lesions. Whereas considering situations such as the late stage of severe OA, the penetration of chondral lesion from AC to SB area, SB fractures and the full-thickness OC defect, there would be more correlated to severe chondral/osteochondral lesions. Therefore, medical treatments primarily would be selected on the basis of the severity of these chondral/osteochondral lesions, being

described, assessed and usually scored after clinical inspections (direct imaging) or among surgeries (biopsy) under above mentioned criteria by those scoring/grading systems, regarding the anatomical site, shape, size and depth of the lesion. Other necessary factors such as symptoms, patient demands, demographic features including age, sex, body mass index (BMI), life style, and medical history of patients would be also considered in making decisions of subsequent plans for treatment and rehabilitation [35].

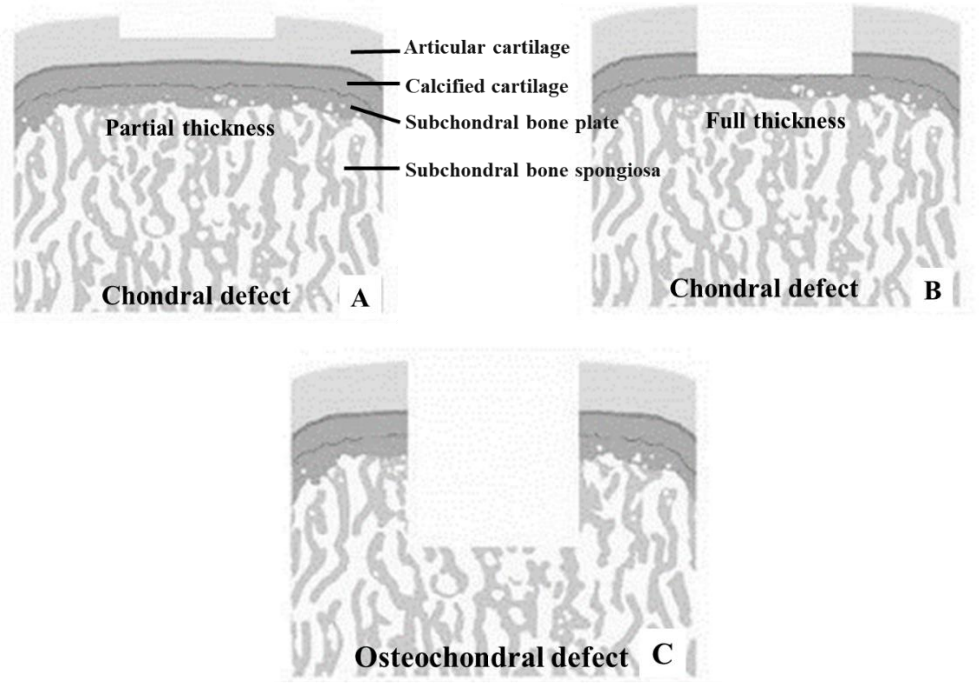

Figure 2.6 Schematic images indicating the general classification of chondral/osteochondral defects. A-B: Chondral defects involve only the cartilage tissue layer. A: Partial thickness chondral defect; B: Full thickness chondral defect. C: Osteochondral defects contain the chondral defect extending from the cartilage through the subchondral bone plate into the subchondral bone. Images were adapted from reference [77].

2.3.2.1 Current clinical options

Nowadays people have various choices in clinic, ranging from non-operative options such as pharmacotherapy, physical therapy, orthotics, patient educations, activity modification and life style management [42], to operative options including the cell-free therapies for moderate degenerative joint diseases (e.g. larger-size legions, grade III lesions) and limited OC lesions of

some specific locations (other than femur, patella, tibia etc.,), such as micro-drilling, abrasion arthroplasty, microfracture, lavage, debridement, and the cell-related techniques such as autologous chondrocyte implantation (ACI) and matrix-induced ACI techniques, bone marrow stimulation techniques (e.g., arthroscopic marrow stimulations, bone marrow aspirate concentrate), osteochondral autograft transfer (or mosaicplasty) technique and osteochondral allograft transplantation. For some end-stage patients or patients with severe joint diseases, prosthetic element, metallic implant or the total joint replacement would be provided [18, 78-82].

Non-operative treatments are often indicated to patients without symptoms having less requirement for surgery or those who want to delay or avoid surgeries [83]. For those patients with existing symptoms, this type of strategy is insufficient, but still could be used to temporarily alleviate stress and anxiety. In clinic, these prescribed options may include physical therapies focusing on enhancing muscle and flexibility of hamstring, with/without supportive tools or devices; knee sleeves or unloader braces to unload the diseased cartilage or to improve patient proprioception; nonsteroidal anti-inflammatory drugs (NSAIDs) such as ibuprofen, naproxen, celecoxib and high-dose aspirin; corticosteroid injections on judicious applications; and injectable or oral chondroprotective agents (CPs) such as nutrition supplements (calcium, vitamins, omega-3, glucosamine, chondroitin phosphate), nutraceuticals (glucosamine or chondroitin sulphate), intraarticular steroids, and intraarticular viscosupplements (hyaluronic acid or hyaluronate based solutions) [42, 63, 83].

For severe damages, in most cases, **orthopaedic operations or surgical interventions** will be required. Several surgical interventions are available currently, which according to the anticipated outcomes after treatments, could be roughly classified into three types [13, 18, 42] as follows: The

palliative options such as arthroscopic lavage, and chondroplasty (debridement of cartilage); The reparative options include bone marrow-stimulating techniques, such as micro-drilling, abrasion arthroplasty, and microfracture; The restorative options contain ACI, ACI-based techniques such as the matrix-induced ACI, and osteochondral graft implantations.

For patients who have fewer physical requirements and their lesions are less than 2 cm^2, palliative procedures would be suitable. For patients who do have more physical needs such as young people, then reparative or restorative options might be selected [64]. Comprehensive descriptions and detailed procedures of these techniques have been reviewed extensively everywhere [13, 24, 81, 84-89]. Some frequently-applied strategies are briefly introduced below.

A) Palliative strategies (Figure 2.7)

a) Arthroscopic lavage: Arthroscopy supported by inserted arthroscope (a small camera) during surgery could precisely provide an intra-articular examination and visualisation inside the joint space and cavity [24]. Arthroscopic lavage was mentioned firstly in 1935. Its aim mainly is to clean the damaged synovial joint by moving inflammatory tissues, some loose parts and debris out of the defected cartilage part to reduce symptoms such as joint pain [63]. It is used to deal with small chondral lesions.

b) Chondroplasty: This technique is also mentioned as the debridement of cartilage or arthroscopic joint debridement, dealing with small chondral lesions (smaller than $1cm^2$) engaging in arthroscopic examination [24]. With the purpose of recovering a smooth chondral surface with a stable border, its procedure may involve tissue eliminations such as meniscus resection, loose, inflamed or excessive parts removal, synovectomy and lavage, by performing curettage, a mechanical shaver or (thermal, ablation or laser) radiofrequency (RFE) wand [63, 94]. Comparing

to non-operative treatments, this way could help significantly relieve pains from certain patients such as those who had acute degenerative defect or early stage of knee osteoarthritis [64].

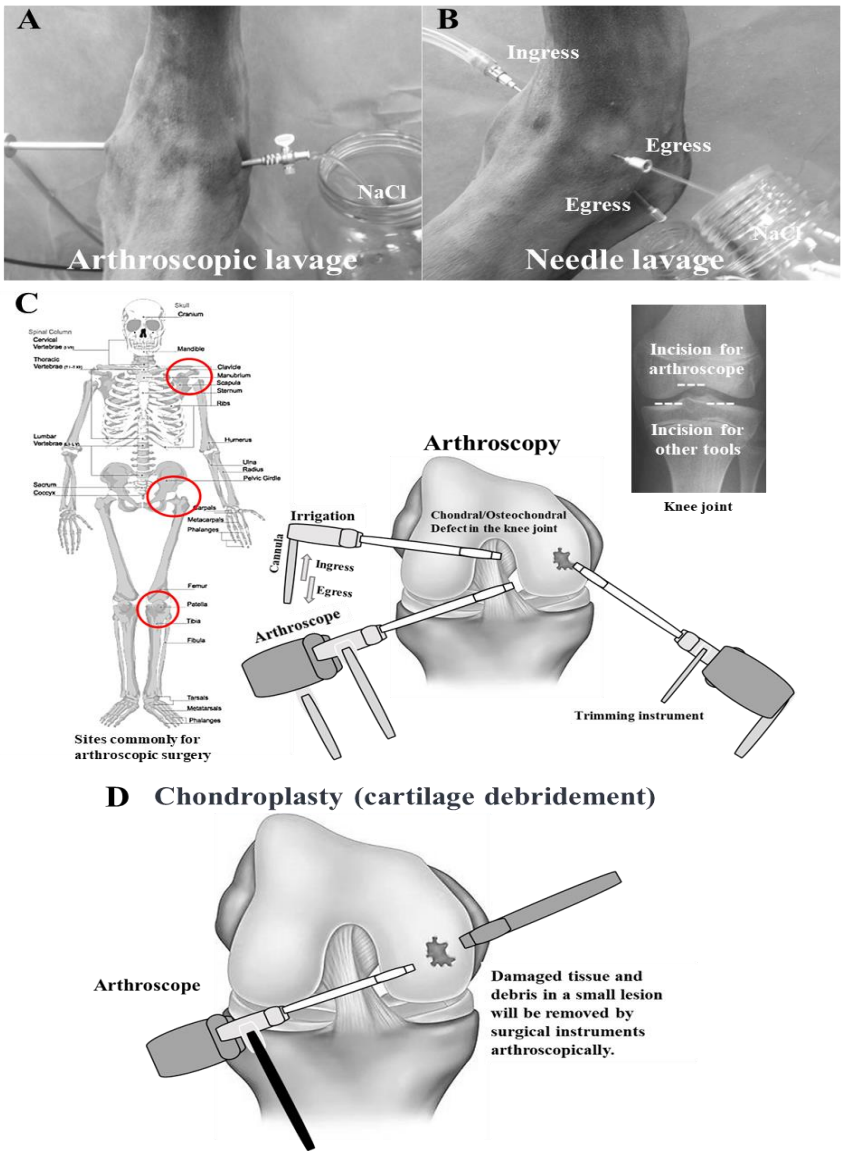

Figure 2.7 Schematic images illustrating arthroscopic lavage, needle lavage, arthroscopy and chondroplasty.

A: Image showing the tarsocrural joint of a horse treated by the arthroscopic lavage. B: Image showing the tarsocrural joint of a horse treated by the needle lavage. C: Schematic images of common sites, and the arthroscopy in knee joint. D: Schematic image of chondroplasty or cartilage debridement. Images were adapted from references [90-93].

B) Reparative strategies

Debridement refers to the wound management of removing the contaminated, damaged, or necrotic tissue, bacteria, and debris from the wound, through standard processes and specific devices or

tools depending on the technique involved, in surgery by professionals to assist healing or prepare the wound bed for subsequent treatments [95]. It is a conventional treatment for chondral lesion in the knee, which was also mentioned as chondroplasty, or arthroscopic debridement [96]. In earlier studies, this technique was reported promisingly reparative results in patients, but due to inconsistent and controversial results in recent decades, it has been confirmed to temporarily relieve pain in selected patients, and inappropriate for some patients with osteoarthritis, certain injuries and malalignment [96].

Bone marrow stimulation-related techniques aim to introduce a stimulation to induce pluripotent stem cells, progenitor cells and other reparative factors from marrow to penetrate into the defect area by haemorrhage [88], often referring to micro-drilling, abrasion arthroplasty, and microfracture.

a) Micro-drilling: This type of treatment is also mentioned as subchondral drilling or arthroscopic drilling, first used in the late 1950s [63, 97]. Usually, the subchondral bone would be drilled after surface lesion debridement, subsequently causing expected bleeding from bone marrow to inburst to the defect area. Potential repairment could proceed along with the formation of blood clots.

b) Abrasion arthroplasty: This technique was first performed by Johnson in 1981 [97] on patients with severe chondral lesions at femoral condyle and the procedure was extended from that of micro-drilling with additional removal of the surface of the subchondral bone about one to three millimetres. There were disagreements on the size and depth of the breached subchondral bone area by these marrow-stimulating techniques in clinic, due to many inconsistent and complicated post-operative findings reported in clinical studies [97]. At present, this procedure would be suggested to certain patients who have low locomotive demands and whose diseases are not

femorotibial malalignment, but probably the one related to sclerotic degenerative arthritis [63]. The purpose of this procedure is also to remove excessive and damaged parts in the articular cartilage to allow the influx of blood from bone marrow after breaching the subchondral bone to introduce progenitor cells and factors to the defect area to repair. However, most clinical outcomes of this treatment are varied, inconsistent, unsuccessful and even worse [98].

c) Microfracture (MF): This technique was introduced thereafter, around late 1980s, with improvements in managing the process of perforating the surface of subchondral bone by the arthroscope-supported surgical awl, to induce reparative elements (cells and factors) to flow into the lesion [64, 99, 100], but avoid thermal osteonecrosis due to drillings [63, 98]. Usually, its first step is to perform arthroscopic debridement to remove all damaged tissues and scars including the calcified area, in order to provide the remaining area with trimmed and well-shaped contour between the defect site and surrounding cartilage tissue. This allows the remaining area to be a microenvironment with reduced biomechanical forces (compressive and shear forces) where holes with controlled size, depth, interval space and place, would then be made by a surgical awl and confirmed by arthroscopic examinations on the efflux and influx of fluids from those holes. The last step is to follow the rehabilitative protocol in combination with guidance post-operatively for a period of time depending on the size, anatomical site, depth of the lesion, patient factors such as the age, sex, and BMI, and auxiliary steps after surgery [64], to relieve symptoms and gradually achieve a fully weight-bearing function as well as many other expectations.

Bone marrow stimulation strategies (Figure 2.8) featured with relative cost-effectiveness, easy process, improved symptom relief and potential rehabilitation outcomes from follow-up studies, have been suggested to patients with small and moderate lesions (1-5 cm^2), expressing less

demands of physical motions, where the microfracture technique has been considered as a gold standard treatment to deal with chondral lesions by FDA (U.S. Food and Drug Administration) and a lot of clinicians [100]. However, essential limitations including limited applications for specific type and degree of lesions, a repaired heterogeneous tissue with insufficient mechanical property due to the major growth of fibrocartilage with type I collagen instead of hyaline cartilage with type II collagen, reported complications such as the osteophytes and tissue malalignments, successful outcome requiring strict post-operative protocol, and a potential reason leading to failures of other secondary treatments (e.g., ACI after MF), do exist and make this strategy remain a short-term reparative but curative option, motivating investigations of restorative and really regenerative strategies to handle chondral/osteochondral lesions in clinic [83, 88, 94, 99].

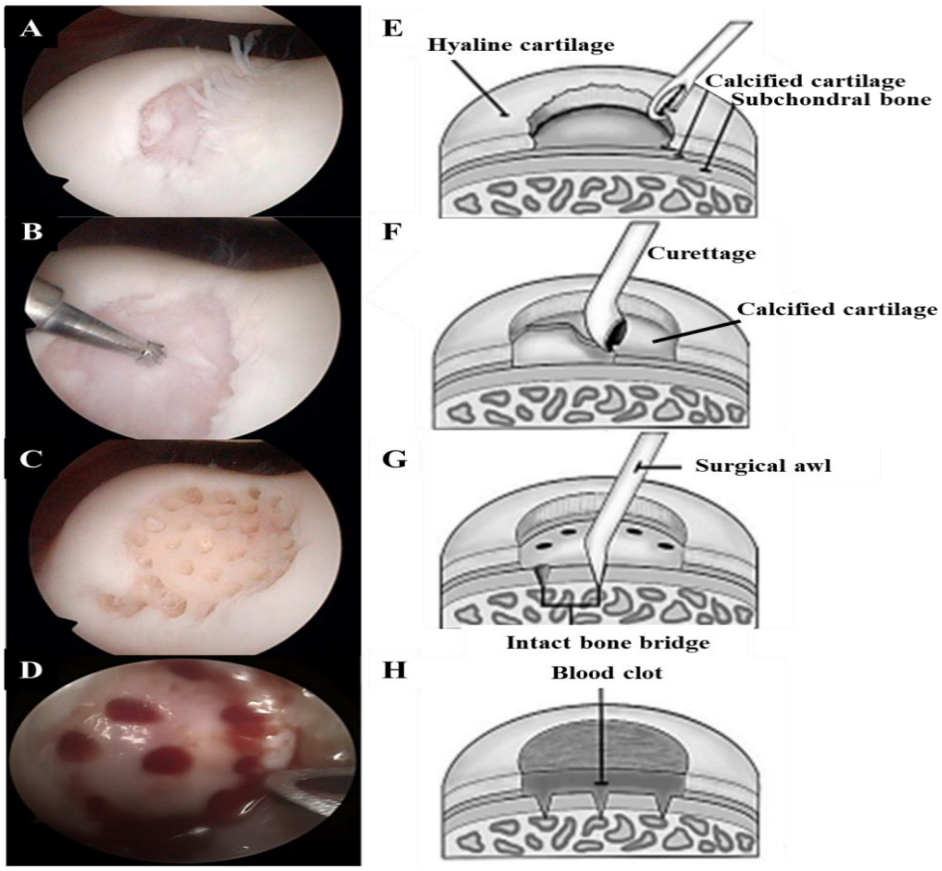

Figure 2.8 Arthroscopic photographs and schematic images illustrating the bone marrow stimulation technique. A-D: Arthroscopic photographs of micro-drilling/microfracture technique. A: A chondral tear on a knee joint. B: Surface debridement of the damaged cartilage tissue and scar. C: A view of drilled holes or fractures after

drilling or microfracture. D: Blood containing marrow elements was flowing out of fractures after tourniquet release, and clotted. E-H: Schematic images showing steps of microfracture surgery. E: Small defect is debrided to create a stable cartilage margin. F: Curettage on the calcified cartilage layer. G: Microfractures by an awl were formed to penetrate to the subchondral bone, which are separated by intact bone bridge, to communicate with bone marrow. H: Well-anchored blood clots containing reparative elements are formed finally. Photos and images were adapted from references [101-103].

C) Restorative strategies

a) Autologous chondrocyte implantation (ACI) techniques: In late 1980s [88], end-differentiated chondrocytes expanded *in vitro* before being transplanted to repair chondral lesions of joint diseases was emerged and continuously developed to form the early ACI technique and subsequent advanced versions [89].

The whole procedure of ACI technique originally contains two surgeries and three stages including isolation, expansion and transplantation (Figure 2.9). Chondrocytes are usually harvested from biopsies of non- or low-weight bearing places in the knee (e.g., the lateral edge of the intercondylar notch, the superomedial edge of the trochlea) at the first surgery after arthroscopic examination and evaluation, and then proliferated *in vitro* for a few weeks to reach enough number of cells required by the following transplantation at the second surgery. The transplanted defect area is often covered by a periosteum obtained from the surface of patient autologous ipsilateral upper tibial shaft or femur for many purposes such as immobilisation of the subsequently injected grafts and to be a patch to seal the place to protect the healing process. The solution containing millions of concentrated autologous chondrocytes will be injected into the place under the covering patch which is sewn and sealed as an envelope. After injection, the patch will be tightly closed by fibrin glue and suture [64]. Potential benefits from covering a periosteal patch on the transplant in the debrided and trimmed cartilaginous area, were also considered as having positive impacts on providing autogenous cells and humoral microenvironments for new hyaline-like tissue formation

[64].

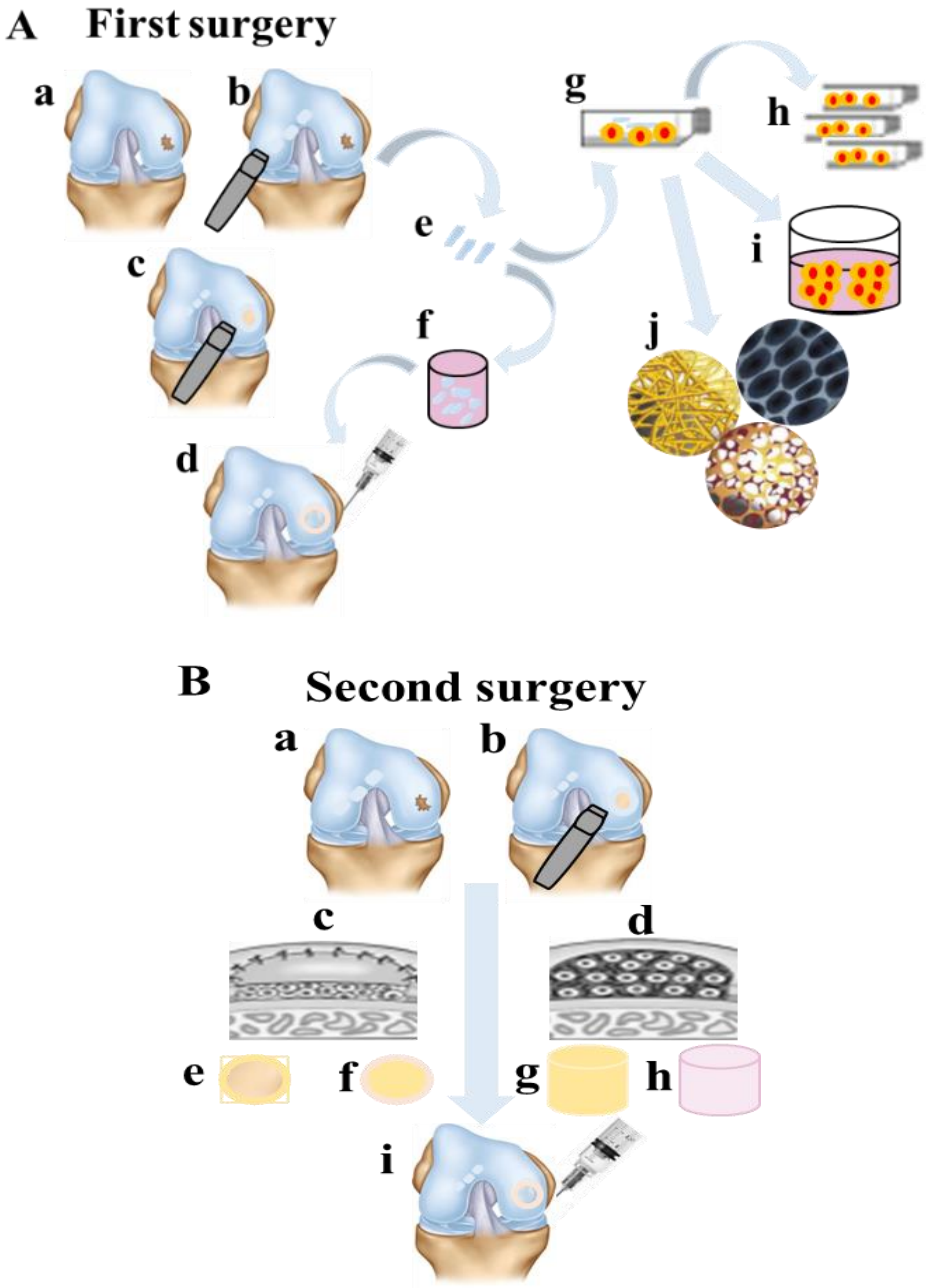

Figure 2.9 Schematic images show autologous chondrocyte implantation (ACI) technique and ACI derivates. In the first arthroscopic surgery (A), cartilage biopsies are harvested from lower weight-bearing area separate from chondral defect area. Biopsy tissue is processed to release chondrocytes. Then chondrocytes are expanded in vitro, either in 2D system, or in 3D system with/without scaffold. In this case, an injectable strategy could be provided, in which minced cartilage biopsies would be mixed with appropriate biomaterial solution and injected back to debrided and trimmed defect area, in the same surgery. No second surgery is required, ideally. In the second open surgery (B), the defect area is debrided. For the first and second generations of ACI technique, expanded chondrocytes in high density will be injected under a patch composing of periosteum or collagen sewn over the defect. For the third generation of ACI or the matrix-associated autologous chondrocyte transplantation (MACT), expanded chondrocytes (or chondrocyte-containing seeding cells) are cultured in collagen to be

injected in defect area, followed by the fibrin glue fixation. No suture is required in MACT. For the fourth generation of ACI, various seeding cells with biomaterial scaffolds under bioactive culture condition will be applied to fit for the defect area. A-a: A knee joint with chondral defect. A-b: Cartilage biopsy is harvested by surgical curettage. A-c: The defect area is debrided and trimmed by surgical instrument. A-d: Trimmed defect is administrated with injectable reparative substances. A-e: cartilage biopsies. A-f: Minced cartilage biopsies are mixed with injectable solution. A-g: Chondrocyte isolation from cartilage biopsies in vitro. A-h: Chondrocytes are expanded in 2D system. A-i: Chondrocytes are expanded in 3D system without scaffold. A-j: Chondrocytes are expanded in 3D scaffold culture system. B-a: The chondral defect in a knee joint after first surgery. B-b: Debrided and trimmed chondral defect in a knee joint. B-c: Schematical image showing the chondral defect with injected chondrocytes under a patch. B-d: Schematical image showing the chondral defect filled with reparative substances. B-e: Schematical image of the periosteal patch applied in the first generation ACI. B-f: Schematical image of the collagen-based patch applied in the second generation ACI. B-g: Schematical image of the chondrocyte-laden matrix applied in the third generation ACI or MACT. B-h: Schematical image of the seeding cell-laden scaffold applied in the fourth generation ACI. Images were adapted from references [13, 91, 101, 107].

Pain relief in patients with large lesion, relatively high proportion of successful treatments with expected outcomes for more than 10 years duration after surgery, and many other advantages documented by clinical practices, make ACI as one of the most valuable restorative strategies, being recommended to selected patients such as those who are young (age 15-50) having moderate to high demand of physical activities, whose chondral lesions (subchondral bone beds should be intact) are classified in large sizes (2-10 cm^2) with moderate symptoms, and whose first treatments are failed [63, 104]. In addition, rehabilitation protocol and specific guidance after surgical operations are indispensable patient care post-operationally in ACI-involved therapeutic plans. However, the two-stage procedure of ACI techniques, a long recovery time after ACI and long durations prior to implantation for preparing differentiated chondrocytes and optimising background factors, should be specified to patients. Contraindications of using ACI technique including OA-related degenerative damage in cartilages, subchondral bone-involved osteochondral lesion (confirmed by advanced imaging techniques), malalignment-related abnormality of weight distribution in the joint area, concomitant ligamentous instability in the joint area, and bipolar lesions within the same knee compartment, have also been increasingly clarified in clinical studies

[94, 104]. As well as challenges regarding the hypertrophic tissue formation, relatively thin and fragile autogenous periosteum found in some patients, donor site morbidity, high risk in the failure of lesions with larger size and lesions involved subchondral bone in particular in patients whose medical history involved in marrow stimulation strategy, and the potential total joint failure due to progressive degeneration in other overloaded unaffected compartment of the joint in the long term, are requiring further studies to improve [99, 104].

Improved versions of ACI technique have been continuously developed since 1980s when both promising outcomes and limitations of ACI technique to deal with chondral lesions were gradually elucidated in clinical studies [89, 105]. In the second generation of ACI, autogenous periosteum patch for injecting liquid cell solution was replaced by a type of xenograft membranes which are mainly collagen-based membranes (e.g., collagen type I/III bilayer) as well as other bioengineered analogous membranes, and depending on the membrane patch, procedures of the second surgery of implantation could be simplified. The open arthroscopic implantation process was also modified by applying mini-open method to debride lesion sites prior to implantations. As the development and participation of tissue engineering, biological science, tissue culture technology and materials science, the third generation of ACI technique employing well-designed scaffolds instead of previous membranes, has been evolving from the matrix-assisted ACI technique [89, 105], in which scaffolds designed with bioinspiration, controlled biodegradation, non-cytotoxicity, appropriate biological properties (biomechanical strength and compliance), and even the seeding cell-laden scaffolds, are presenting promising futures in cartilage regeneration and in optimising procedures of regenerative surgeries [89, 104-106].

Currently, based on components, these in-developing scaffolds could be classified into

carbohydrate-related type (crosslinked polymers such as chitosan, agarose and hyaluronan), protein-based type (e.g. collagen, fibrin, gelatin), synthesised polymer-formed type (polylactic acid , polycaprolactone, polyglycolic acid, carbon fibre, hydroxyapatite, tricalcium phosphate etc) and composite type (mixture of the other three types) [89], which are not only bringing their specific strengths and weaknesses in the designed scaffolds, but also requiring more studies to illustrate, validate and improve in both research and medical practices [89, 105].

b) Osteochondral grafts (autograft and allograft): Patients with osteochondral defects, involving subchondral bone area, would be suggested by orthopaedic surgeons to apply osteochondral grafts (Figure 2.10). However, it has been noticed that osteochondral grafts may have higher effectiveness on managing focal defects and worse outcomes for dealing with degenerative defects [106]. It is now often suggested to selected patients who have symptoms, within 50 years old, whose lesions are around 1-2 cm^2 and unipolar, in the distal femoral condyle of a non-degenerative joint within properly aligned limb. In some cases, patients with stable ligaments, without deficient or with corrected meniscal competence should be considered and prepared, to protect transplanted grafts from premature wears. Usually chondral/osteochondral lesions are examined and debrided to outline the shape and size of autografts required. Profile of osteochondral autografts is similar to a plug with round cylindrical shape, consisting of the whole osteochondral tissue, where the cartilage should be in full thickness but subchondral bone could be in a few thicknesses. The autograft plugs should be carefully collected arthroscopically or through arthrotomy, from none or low weight-bearing parts of the donor, where the distal lateral or medial trochlea, and the femoral intercondylar notch within the patient joint are preferred candidate sites according to many medical practices [83, 88]. Usually, single stage surgery will be performed and

commercial gadgets with uniformed size and shape will be used to harvest these plugs from donor sites and to press-fit these plugs into recipient places. Appropriate guidelines and rehabilitation protocols post-operatively for patients to recover with better outcomes within reasonable time are also highly recommended [64, 88, 94]. Challenges and limitations in using autografts, such as donor site selections and potential morbidity, inadequate availability, some technical difficulties regarding the plug selection and contour matching to the receiving sites, integration after press-fitting the plug, subsidence of the surface of transplanted graft, subchondral cyst formation, fibrocartilage formation between the transplanted graft and surrounding tissues, and other risks in tissue collapses after surgery, made people to consider alternatives such as allografts [98].

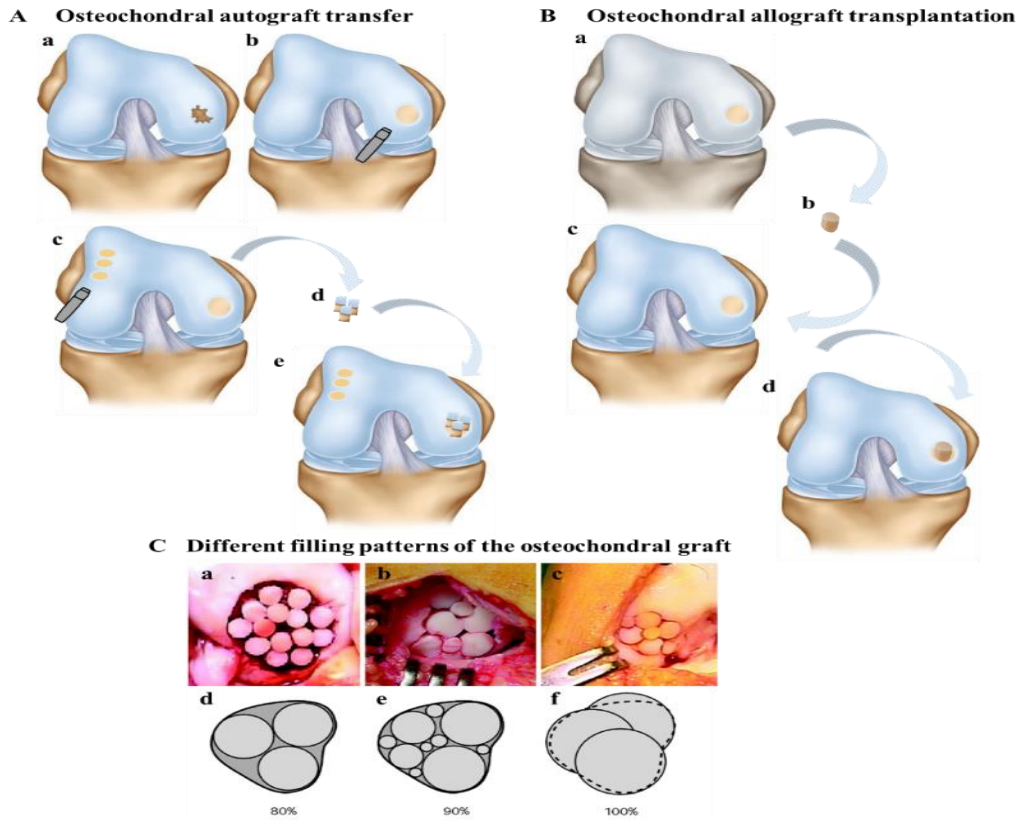

Figure 2.10 Schematic images illustrating the osteochondral graft techniques.

A: Schematic images illustrating the Osteochondral autograft transfer (OAT) technique. A-a: A knee joint with osteochondral defect. A-b: The defect is debrided, trimmed and outlined the shape and size of autograft required. A-c: Osteochondral autografts are collected arthroscopically from the none or low weight-bearing parts of the donor sites of the patient. A-d: Schematic images of the harvested osteochondral autograft plugs. A-e: Osteochondral autografts are transferred to fill in the defect area. B: Schematic images illustrating the

Osteochondral allograft transplantation (OCA) technique. B-a: The shape and size of allograft are outlined in the donor sites of other joint matching the defect area of the patient. B-b: Schematic image of the harvested osteochondral allograft plug. B-c: The defect area of the receiver is debrided, trimmed and outlined. B-d: The osteochondral allograft plug is transplanted into the receiving site. C: Intraoperative images (a-c) and illustration (d-f) showing 80% (a,d), 90% (b,e), and 100% (c,f) coverage by different filling patterns of osteochondral grafts for a complex defect. Images were adapted from references [91, 108].

In osteochondral allograft transplantation (OCA), procedures of surgery and post-operative rehabilitation protocols and guidance are typically same as those of osteochondral autograft transfer (OAT), with the main exception of which the graft plugs are often taken from other individual than the associated patient, such as a cadaver, offering a source of grafts potentially matching to the anatomic site, size, and numbers expected, and requiring more steps in preparation, cleaning and preservation of allografts. Comparing to OAT which is often indicated for younger patients with smaller size lesions (1-2 cm^2), osteochondritis dissecans (OCD) or isolated traumatic lesion, OCA transplantation could be provided to older patients with larger size lesions (larger than 2 cm^2) [94]. Even if with advantages about avoiding some challenges when using OAT such as the availability of autografts and donor site morbidity, concerns about using allografts such as “fresh tissue graft” preparation and preservation techniques (e.g. body dead within 12hrs, plug extracted within 14 days and transplanted within 28 days), graft storage (prefer not deep-frozen storage, stored within antibiotic solution) and cost issues, donor site specificities (weight-bearing or not, curvature and topographic features), viable mature chondrocytes availability and chondrocyte survival after implantation, some technical difficulties similar to that of using OAT, and additional risks in disease transmission and immunogenicity due to the use of allografts, should also be stressed on and are remaining future studies to improve [64, 88, 94, 98].

In brief summary, if the chondral lesion is smaller than 2 cm^2, surgical procedures often involve MF and OAT; if the lesion area is in the range between 2 and 4 cm^2, procedures usually consider

OAT and ACI; if the area is more than 4 cm^2 and in some cases involving the subchondral bone part, then OCA and ACI would be selected [82]. Accumulated studies have also revealed that these approaches would benefit patients from improved quality of life and pain relief in short term (2-5 years) [109], while combination of two or more techniques such as MACI combined with MF, and OAT in combination with ACI, may present improved outcomes or less failures in long term (10 years), comparing to single approach treatment such as using MF alone [110]. ACI followed by MF, OCA, or OAT, have become frequently employed approaches with better outcomes to treat chondral/OC lesions in joints [84]. And to some extent, the outcome of certain treatment might be greatly related to the size of lesion, the sex, age and previous surgical experiences of the individual patient as well [13, 111], suggesting that more considerations of patient factors before designing therapeutic plans, more relevant pre-operational tests, more long-term follow-up studies and proper scoring systems for describing tissue repairs after surgical procedures, are crucial to improve expected outcomes and knowledges for future effective clinical recommendations, evaluations and prognosis [13, 74, 82].

2.3.2.2 Challenges

For small-size or low-grade chondral defects without subchondral bone involvement, some traditional surgical operations might not be cost-effective and ideal. Palliative, and most reparative methods in clinic are primarily aiming at relieving symptoms, or emphasising on removal of damaged tissues followed by filling with something relatively bioinspired but poorly regenerative. Although improved outcomes and minimal invasion of those strategies could be achieved as benefits, long-term efficacies (10, 15, 20 years) after operation and method-associated specific

disadvantages or side effects are inescapable and controversially varied from case to case, due to selected patients and inconsistent methodologies of data report and analyses in different studies [110, 112]. In fact, none of those methods serve as truly restorative treatment except ACI-based techniques, especially the scaffold-supported advanced MACI [18].

However, even if ACI-based techniques have been introduced and developed for a few decades and several FDA approved products are available in medical fields [86], disadvantages and limitations, such as the patient selection, multi-step procedure (comparing to the MF using one-step procedure), periosteal patch/flap/membrane (periosteum) or struts/matrix (depending on the generation of ACI) induced side effects (hypertrophy of chondrocytes, necrosis etc), low cost-effectiveness regarding chondrocytes expansion, higher risks in early failure or reoperation (in comparison with MF), frequency of radiographic osteoarthritis, ratio of survived mature hyaline cartilage tissue after ACI operation *in vivo* (comparing to native cartilage tissue), long and delayed post-operation time for patients to rehabilitate and return to normal work, different regional regulations for the availability of the medical treatment delivered to different patients (approval, research, insurance reimbursement, off-label indications, concomitant procedures etc), and controversial results of some meta-analysed data about clinical outcomes between ACI and others, remain to be solved and optimised in the future [86, 113].

Besides, considering certain extreme conditions, such as degenerative joint diseases in particular the OA, and severe macro-fractures, for the sake of breaking up the joint congruency and normal patterns of biomechanical loading input, to result in higher-ranking OC defects to have to require OC grafts and even replace the total joint, therapeutic plan should focus on the OC tissue reconstruction by using simulated substitutes regarding the anatomical structure, physiological

function, and better integrations with surrounding tissues without causing immunologic reaction and inflammation. At present, there is not a secure method validated clinically to faithfully regenerate the whole OC tissue in both structure and function, with a long-term stability *in vivo*, although for small or partial OC defect, the OC grafting/plug, is able to regenerate the superficial mature hyaline cartilage in physiological structure *in vivo* for a relatively longer time after surgery and to progressively integrate with surrounding tissues of the implant in particular the SB part [85, 114], demonstrating superior advantages over ACI-based and marrow-stimulating approaches. However, different approach might fit for different condition. As mentioned, OC graft treatment is often indicated to defined scope of applications, having specific limitations and challenges as well. Apart from limitations and considerations of using ACI-based techniques and OC graft transplantations in clinical application, other challenges of applying current available clinical options may involve the varied features of clinical samples, the limited availabilities of appropriate biomedical materials to be applied, and reliable strategies to obtain suitable substitutes. Moreover, on the one hand, more practices are still staying in research area (*in vitro* tissue culture model and *in vivo* animal model evaluation), requiring further developments and evaluations; on the other hand, biopsy evaluation from human patients remains difficult, postoperative outcomes from recorded clinical studies, were mostly scored very low in the long-term follow-ups, and sometimes method-specific complications were still unavoidable [74, 115, 116].

2.3.3 Tissue engineering-based regenerative strategies

As the increasing knowledges and developments of science and technology in areas of biology, material and engineering, TE approaches referring to biomaterial scaffold-free methods,

biomaterial-inspired scaffold/substrate-supported strategies, and approaches involving seeding cells in combination with biomaterial scaffolds and environmental factors, with the aid of delicate bioreactors or functionalised devices, have been gradually established and explored to regenerate complicated anisotropic tissues including the multi-layered articular cartilage/OC tissue, providing an alternative option to conventional medical approaches. Clinical options using scaffold-based advanced MACI techniques and artificial chondral/osteochondral graft implantations, have been seen as using TE strategies to deal with chondral/osteochondral defects. Various TE-based strategies incorporating with special engineering designs, fabrication technologies, and environmental factors including biochemical, biophysical, bioelectrical and magnetic stimuli, with/without auxiliary bioreactor/device, have emerged, bringing hopes to overcome current challenges in articular cartilage/OC tissue regenerations.

In the following sections, fundamental elements in TE strategy toward articular cartilage/OC tissue regeneration, will be discussed, involving commonly-applied seeding cells, biomaterials, and 3D fabrication techniques, which have evolved and benefited from advancements of areas such as cell and developmental biology, materials science, nanotechnology, and additive manufacturing technologies since recent decades [117].

2.3.3.1 Seeding cells for articular cartilage/OC tissue engineering

Since the successful application of end-differentiated chondrocytes in ACI techniques for articular cartilage tissue reparation, chondrocytes, stem cells (mesenchymal stem cells (MSCs), induced pluripotent stem cells (iPSCs)), and gene-modified cells have gradually become popularised seeding cells for cell-based articular cartilage/OC tissue reconstructions [118]. Here chondrocytes

and BM-MSCs as candidate seeding cells of this study will be briefly introduced.

2.3.3.1.1 Chondrocytes

The small proportion of chondrocytes along with a large volume of chondrogenic ECMs contribute to the formation and maintenance of cartilaginous tissue, throughout the tissue development and maturation. Chondrocytes typically have an ovoid shape which could be varied with different layers of the articular cartilage, displaying a range of diameters from 10 to 30 μm [119, 120]. In cytoplasm, the granular endoplasmic reticulum (ER) and the Golgi complex are two predominant organelles, related to the generation and secretion of chondrogenic proteins such as collagen fibres and proteoglycans. Lysosomes in chondrocyte are responsible for cellular metabolism and the turnover of chondrogenic ECMs. The feature of mitochondria in chondrocyte are highly associated with the developmental status, activity and tissue location. It was reported that the number of mitochondria in immature tissue was more than that in adult tissue, as well as the different shape and some characteristics between those two tissues were observed, reflecting distinct respiratory activity and oxygen demand. Degenerated chondrocytes usually contain larger filament in cytoplasm than that of normal chondrocytes and the cellular glycogens might contribute to the calcification by providing organic phosphates [121]. The natural microenvironment of chondrocytes in articular cartilage is hypoxic where mature cells can survive and endure a low-oxygen condition [121]. However, from studies, both low and high oxygen pressures would have negative impacts on the proliferation and anabolism of chondrocytes. Throughout the entire multi-layered articular cartilage/OC tissue, there is actually a gradient of the balanced oxygen concentration in each layer, ranging from a relatively high oxygen pressure in superficial layer

down to very low in the calcified layer [121]. A three-zone ultrastructure of chondrogenic matrices around chondrocytes inside cartilaginous tissue have also been identified by histological staining and advanced microscopic imaging techniques [10], in which the combination of chondrocyte with certain extension of surroundings has been termed “chondron” [122], serving as a functional unit playing a critical role in regulating the biomechanical and biochemical microenvironment of chondrocytes locally, relevant to cellular deformation and metabolic activity, responsive to the local stress-strain, micro-mechano-transduction via solid phase of ECMs, swelling behaviour, osmotic pressure and fluid flow in microenvironment, and even the electrical fields around chondrocytes [123-126]. Therefore, chondrocytes naturally live in a complex 3D microenvironment *in vivo*.

After being employed in ACI technique to deal with chondral lesion in OA patients successfully, and subsequently approved by FDA to be used in clinic, autologous mature chondrocytes were increasingly studied in cell-based therapies, where such as in the ACI/MACI techniques, outcomes were greatly relied on seeding cell populations, requiring massive expansion of chondrocytes with enough quantity and high quality *in vitro* before implantations. However, in practice, challenges such as the dedifferentiation phenomenon in passaged chondrocyte culture along with the associated cellular changes in morphology and gene expression, and the dysfunction of chondrocytes expanded under static 2D monolayer culture system [127, 128], as well as improvements on the proliferation, chondrogenesis and functional cartilaginous tissue regeneration by applying carefully designed biomimetic tissue culture systems such as additional growth factors, bioactive scaffold/substrate, extra biophysical stimuli, different oxygen condition, and a preferred 3D rather 2D microenvironment were gradually observed [128-131], demonstrating the sensitivity

and responsiveness of chondrocytes to surroundings. Factors such as 3D microenvironment, specific biochemical and biophysical signals, and oxygen concentrations would induce responsive alterations in gene expression, signalling, and cytoskeletal arrangements of chondrocytes which participate in cell fate and behaviours, confirming the importance of environmental stimuli in the *in vitro* chondrocyte expansion system [132, 133], and resulting in more topics to be investigated and considered while culturing chondrocytes *in vitro*.

Recent decades, such topics as scaffold-free approaches to prepare chondrocyte sheet/aggregate, scaffold-based 3D chondrocyte cultural systems, assorted dynamic perfusion systems and customised bioreactors/devices incorporated with various stimuli to provide well-controlled microenvironments for cell growth and tissue development *in vitro*, have emerged to explore potential mechanisms and to overcome challenges on culturing chondrocytes, such as to maintain the differentiated phenotype and function of primary/passaged chondrocytes in culture, to improve the proliferation and anabolism of matured chondrocytes in preparation for ACI, and to fabricate larger functional tissue substitutes to satisfy clinical requirements in dealing with larger or severer chondral/osteochondral lesions such as the OA-induced partial thickness defect of articular cartilage and full-thickness cartilaginous defect [134-144].

For example, by using surface-modified culture devices [145], layers of scaffold-free chondrocyte sheets could be fabricated *in vitro* for treating chondral defect in animal models [146]. As compared to defects without treating allograft, chondrocyte sheet-grafted partial thickness chondral defect of the medial femoral condyle in animal models presented chondrogenic matrix maintenance, proper integration with surrounding tissues, tissue function recovery, preventions from tissue degeneration, and higher scores examined by the ICRS histological grading system of biopsies after treatments

for a few weeks, suggesting the potential of applying cell aggregates to regenerate articular cartilage in clinic [147]. The cell-sheet based strategy was further confirmed in more animal models and improved to treat selected human patients with OA of the knee in pre-clinical studies [148]. Microtissue implants made up of scaffold-free autologous chondrocyte aggregates (3D spheroids), were further developed and confirmed similar outcomes in animal models [149] (Figure 2.11).

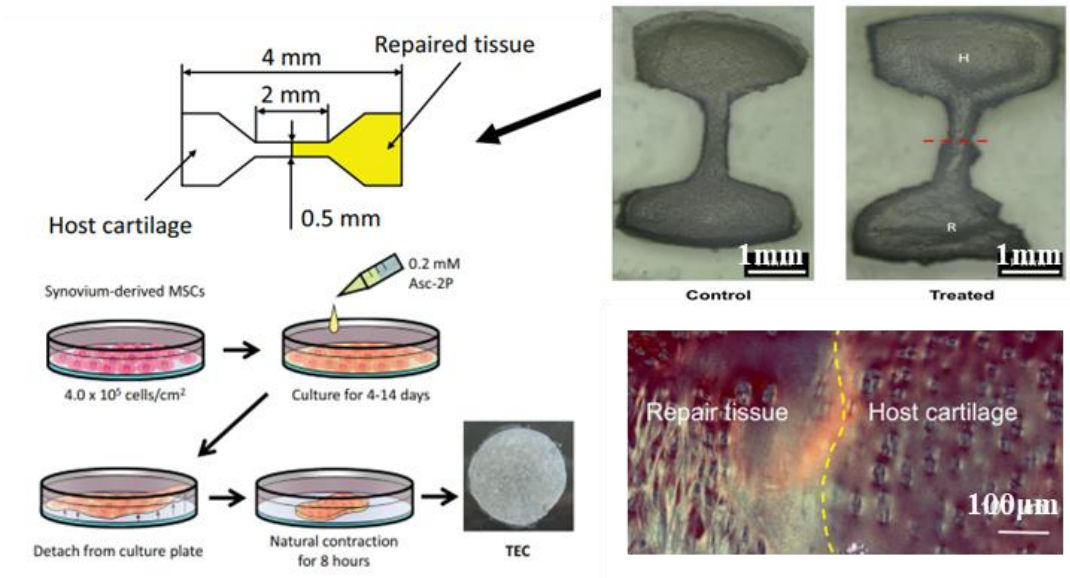

Figure 2.11 Schematic images illustrating the scaffold-free 3D cartilage tissue engineering. The tissue engineered construct (TEC) used for implantation into animal model with cartilage defects, was designed, prepared and histologically assessed after implantation. Images were adapted from reference [150].

To date, **scaffold-free TE strategies** using assembled building units (2D cell sheet/3D microtissue/spheroid/strand), have been applied to reconstruct various types of tissues and organs [149, 151-165], in preclinical and clinical tests [166]. This bottom-up approach allows complex, hierarchical tissues to be built up by functional blocks in a layer-by-layer manner. To meet requirements for transplantation, a large amount of seeding cells is commonly associated with the engineered tissue by scaffold-free approach, in which the process is trying to simulate a series of stages in natural tissue growth and development, often involving the condensation, proliferation, differentiation, ECM generation and maturation of the target tissue. Cell sheet, aggregate, and self-assembly microtissue through scaffold-free approaches have been employed in cartilaginous TE

[167].

Limitations on the availability of autologous chondrocytes, risks and challenges due to the use of allogeneic and xenogeneic chondrocytes, demands to improve the maturation of chondrocytes and engineered tissue constructs *in vitro*, organisations of building blocks assembly and 3D fusions of the engineered tissue with surrounding native tissue after implantation, could all benefit from the involvement of exogenous factors, such as additional biochemical and/or biomechanical stimuli, employment of advanced device/bioreactor, functionalised biomaterials, and specific fabrication strategies, in the process of cell adhesion, proliferation, migration, organisation, maturation, metabolism and fusion, during chondrocyte expansion *in vitro* and cartilage tissue regeneration *in vivo* [167, 168].

For example, conventional scaffold-free cell sheets/aggregates are fragile, and insufficient to grow larger and simulate the natural 3D architecture and orientation of complex tissues, often requiring specific mould/confinement and cultural enhancement strategies [167]. By using the biodegradable elastic urethane-doped polyester materials (CUPE), the single thin sheet featuring with strong, elastic and porous properties was developed to fabricate cell sheet in a long-time culture *in vitro* for soft tissue reparation [169]. Novel protocols and tools, such as the microwell mesh platform and microfluidic devices [170, 171], were designed and developed to fabricate chondrogenic microtissue efficiently and functionally. Necessities of supplementary growth factors were observed, such as the TGF-ß in long-term culture to maintain the function of expanded chondrocytes *in vitro* [172], and additional basic fibroblast growth factor (b-FGF) in the expansion medium to improve the proliferation and chondrogenic ECM production of passaged porcine articular chondrocytes *in vitro* [173]. Other bio-inspired factors such as the human serum, human

platelet lysate (HPL), platelet-derived growth factor (PD-GF), insulin-like growth factor 1 (IGF-1), insulin-transferrin-selenium (ITS), and L-ascorbic acid were also observed the ability to improve the proliferation of chondrocyte and to maintain chondrogenic characters in culture *in vitro* [168, 172-176]. In terms of these supplements and substitutes for animal ingredients in culture medium, preclinical evaluations on the tumorigenicity and genetic instability should be considered carefully before using [177].

Specific tissue culture system/device and advanced bioreactors have also been designed and developed to improve the expansion of articular chondrocytes and to engineer the scaffold-free tissue construct *in vitro* [137, 178-183]. By a rotational culture system and a mould, primary rabbit chondrocytes, produced more chondrogenic GAGs, developed less cellular apoptosis in the centre of the tissue-engineered scaffold-free tissue *in vitro*, and formed the qualified and quantified tissue blocks with organised shape for clinical surgery in a relatively shorter time [178]. In the presence of both mechanical stimulation and biochemical supplements, the scaffold-free cartilaginous tissue fabricated by passaged sheep articular chondrocytes in a mould, displayed an improved mechanical property and larger size than a standard expectation [143].The improvement of well-designed advanced bioreactors with additional stimuli (biochemical and biomechanical signals) on the formation of larger and thicker neocartilage tissue without scaffold, and on the chondrogenesis of primary/passaged articular chondrocytes *in vitro*, has been further confirmed by accumulated studies, pointing out a future trend in scaffold-free TE strategies for tissue fabrications [137, 179-183].

Scaffold-free strategies struggle with acquiring enough number of functional chondrocytes and large size of building blocks for the following TE applications, whereas these challenges might be

addressed by making use of biomaterials and scaffolds, shedding light on potential successes in future strategies of using the combination of both approaches [167]. Although **biomaterial scaffold-based approaches** remain several limitations to be considered before using and to be solved by future developments, such as the risk of toxic products degraded from the biomaterial scaffold/substrate, impacts of the degradability and resorption of biomaterial scaffold/substrate on tissue remodelling, integrations of engineered tissues with surrounding tissues *in vivo*, and potential interactions between seeding cells with biomaterial scaffold/substrate, a great many studies have been investigating, where a few successful designs have been commercialised [184].

For example, decellularized extracellular matrix (dECM) (Figure 2.12) retaining the natural architecture, similar components and biomechanical features of the original tissue specific ECM, has been seen as the natural bioactive scaffold to support seeding cells to attach, proliferate, migrate, and differentiate [166]. In addition to the immunological inertia of pure ECM components but the immunological activity of immune cells and cell membrane proteins, xenogeneic sources of dECM could also be considered, providing an ideal type of natural biomaterial scaffold in TE [166, 185, 186]. It was reported that, 3D hyaluronic dECM scaffolds derived from both human and animal tissues, in the shape of non-woven mesh, or featured with large pores and soft sponge-like structure, were successfully fabricated. After seeding with autogenic, allogenic, or xenogenic cells *in vitro* or further being implanted in animal models *in vivo*, cell attachment, proliferation, migration, neogenesis of hyaline cartilaginous tissue with porous structure and chondrogenic components, and seamless integrations of the neo-regenerated tissue with surrounding cartilaginous tissues and smooth cartilage surfaces were observed, confirming the biocompatibility, stability and potential applications for transplantation or ACI-based clinical applications [187-189].

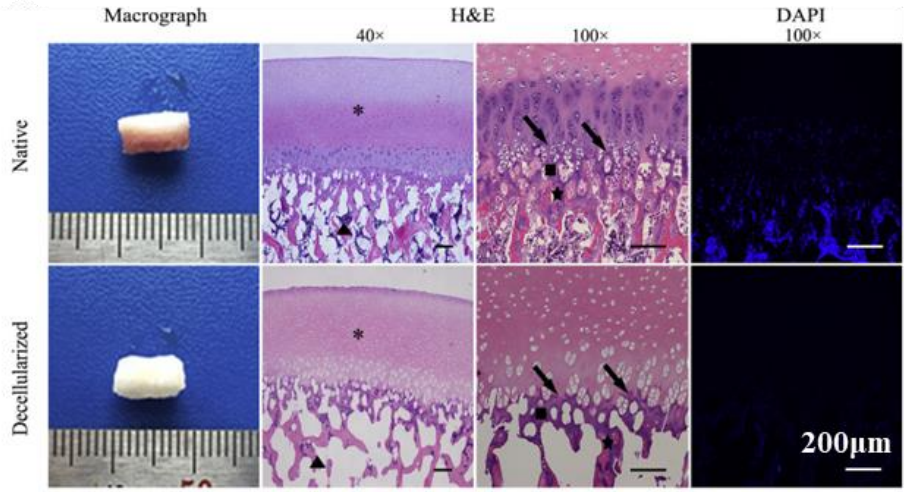

Figure 2.12 Schematic images illustrating the decellularized osteochondral ECM scaffold. ***A decellularized osteochondral extracellular matrix (ECM) scaffold was prepared by completely removing cellular components to reduce immunogenicity and preserve natural stratified structure. In H&E staining images, *, Cartilage; arrow, tidemark; ■, calcified cartilage; ★, subchondral bone; and ▲, zone of spongy bone [190]. Images were adapted from reference [190].***

Biomaterial scaffold has been the fundamental element in TE since 1980s when TE technology was proposed in reconstruction surgery and organ transplantation [166, 191]. Comparing to cell-free scaffold approach focusing on modifying or bio-functionalising substrates/matrices to recruit or promote autologous reparative factors moving toward the defect area, scaffold-based TE strategies that employ seeding cells combined with biomaterial scaffolds, offering broader range of possibilities and creative options, are more frequently investigated [166, 192]. Scaffolds either consisting of chondrogenic ECM components or molecules, or made up of various biocompatible, biodegradable, biomaterials (natural, synthetic or composite), were evaluated, in particular to favour the matrix-assisted ACI techniques in clinical applications and graft-based transplantations [193, 194].

For example, homologous chondrocytes-laden natural fibrin gel and fibrin gel-delivered perichondral graft, were implanted in animal model and human patient with chondral lesions [195, 196], while natural collagen material and collagen-based 3D (sponge) composite scaffold were

applied to deal with full-thickness osteochondral defect [197, 198]. 3D scaffolds in the shape of fibre mesh, non-woven mesh, sponge sheet or semisolid, produced by synthesised biodegradable polymer/co-polymers were successfully designed to deliver seeding cells to regenerate cartilaginous tissue in animal models [199-201]. Composite scaffolds were also fabricated by natural biomaterials modified with chondrogenic ECM molecules such as chondroitin-sulphate-A and GAG-analogue [202]. Comparing to cell-free scaffold-alone group, chondrocytes delivered by scaffold into the full-thickness OC lesion in knee joints of animal models, not only regenerated the cartilaginous tissue, but also presented better post-operative outcomes such as smooth tissue surface, organised chondrocytes in columns, uniformly distributed tissue-specific GAGs, subchondral bone reconstruction and integration with surrounding bone tissue [203]. A study investigating four groups of allogeneic implants including chondrocytes-dECM composite scaffold, cell-free scaffold alone, chondrocytes alone scaffold-free solution, and control/background solution group (free of both scaffold and chondrocytes), further confirmed that, comparing to cell-free groups where only fibrous tissues were detected, transplants containing chondrocytes (with/without scaffold) presented neo-cartilaginous tissue regenerations, where in chondrocytes-loaded groups, qualified and quantified tissue constructs were only observed in transplants of cell-scaffold composites, along with detections of the preimplantation mass volume and higher biomechanical properties [204].

Biomaterial-based scaffolds/matrices-supported cell expansion/delivery systems, could contribute to determining the structure and function of the final engineered tissue construct [202], some validated and approved products to deal with chondral/osteochondral defects, have been commercialised [205-207], which are varied from areas due to different regulation and requirement,

availability and category of these commodities from different country [208] (Appendix A-C).

Challenges of cost-effectively expanding viable and functional chondrocytes *in vitro*, impede the adoption of current cell-based therapy in clinic, such as the ACI and graft-dependent implantations/transplantations. Although applying chondrocytes in combination with scaffolds remain the most applied approaches in both research and practice, cell-free substrate/scaffold-alone cartilage treatments are increasingly investigated, some of which presented promising results, such as the human serum-treated PGA-HA scaffold implantation after MF perforation [209, 210], platelet-rich-plasma (PRP)-treated PGA-HA scaffold implantation following BMS treatment (drilling) [211], and other bioactive material-developed or bio-functionalised cell-free scaffolds including human amniotic mesenchymal cells (HAM)-derived ECM-coated polylactic-co-glycolic acid scaffold [212], poly (1,3-propylene sebacate)-poly (glycerol sebacate)-bioactive kartogenin-100 (PPS/PGS/KGN-100) scaffold [213], collagen type I gel developed scaffold (CaReS-1S®) [214], polyethylene glycol diacrylate-denatured human fibrinogen composite scaffold (GerlrinC®) [215]. Several other types of modified composite scaffolds [213, 216-218] were also confirmed their positive impacts on the neo-cartilaginous tissue regeneration in animal models and/or pre-clinical/clinical practices, providing an additional option to treat chondral/osteochondral lesions toward best outcomes and to prevent from challenges in handling cells and associated regulations [192].

To conclude, scaffold-free strategy in cartilage TE, using pre-fabricated cell aggregates as building blocks, to address challenges on the seeding cell expansion *in vitro* and later fusion *in vivo*, to some extent, could support ACI and graft-based approaches to deal with chondral lesions of small to middle sizes. For large-size, or severe defects, biomaterials and supportive tools would be required.

Scaffold-based strategy in cartilage TE, highly relies on the biomimetic design, appropriate functional biomaterials to be used and fabrication technologies. This is a complicated but fascinating subject, although an ideal robust biodegradable, biocompatible and bioactive 3D scaffold is still at the fore of the way. To apply a scaffold or not, or to select a synergic strategy considering both, should be carefully taken into account [219].

2.3.3.1.2 Stem cells

Since the realisation and description of the self-renewal and differentiation flexibility of human embryonic stem cells (hESCs) in late 1990s, stem cell research, biotechnology and cell-based therapy have experienced a fast-growing period, bringing in challenges such as ethical issues regarding the use of ESCs generated from human embryonic tissues. Other sources of cells with various "stemness" were then discovered and studied genetically, confirming the existence of the unspecialised population of cells in both adult and embryo [220, 221]. Stem cells could be defined as unspecialised cells with the ability to self-renew and differentiate into other type of cells in an organism. Regarding the origin, stem cells could be roughly grouped into embryonic stem cells, non-embryonic (adult) stem cells, cloning (somatic cell nuclear transfer) stem cells and induced pluripotent stem cells (iPSCs) [221]. While considering the hierarchy of various potentials resulting from the spatiotemporal and genetic specialisations during development, stem cells could be classified into five categories [220-222], as follows:

1) The totipotential stem cells, able to generate the embryo and trophoblasts of the placenta, denoting that they can differentiate into all type of cells in the living organism, such as the cells from the zygote and those few cells firstly divided by zygote.

2) The pluripotential stem cells, able to differentiate into almost all type of cells in three germ layers but not the embryo and the placenta, such as the ESCs from the inner cell mass.

3) The multipotential stem cells, able to produce restricted types of cell lineages, such as the central nervous system-derived stem cells (potential to differentiate tri-lineages of neuron, oligodendrocyte and astrocyte), the hematopoietic stem cells (potential to generate blood cells and platelet), and the mesenchymal stem cells (MSCs).

4) The oligopotential stem cells, able to generate more limited types of cell lineages, such as the adult lymphoid stem cells and myeloid stem cells.

5) The unipotential stem cells, able to produce the least types of cells which is the only one specific type of their own, such as the adult muscle stem cells, and dermatocytes.

In clinic, based on the cell source of transplant, stem cells could also be divided into: autologous stem cells (collected from the same patient), allogeneic stem cells (collected from another donor of the same species of the patient), syngeneic stem cells (collected from the identical twin of the patient) and xenogeneic stem cells (collected from another donor of the different species of the patient) [221]. **A) Embryonic stem cells (ESCs)** from the inner cell mass (ICM) of the blastocytes, contribute to the generation and development of the foetus and epiblasts, having the pluripotency to generate all types of cells responsible for the formation and maintenance of organs and tissues in the future developed organism, which were considered as an ideal source of cells in TE. However, accumulated studies further demonstrated many challenges in legally applying ESCs as candidate seeding cells from bench to bed, including the standard isolation and identification protocols, establishment of autologous ESCs by somatic nuclear transfer technology, genetic and epigenetic problems during ESC culture *in vitro*, shortage of appropriate culture system and cell lines for

clinical requirement, risks in its immunogenicity and tumorigenicity, difficulties in controlled differentiations, the disputable ethical issues and various regulations regarding the medical use of human ESCs [223].

B) Induced pluripotent stem cells (iPSCs): As the increase in knowledges of ESCs, and advancement of biotechnologies, the reprogramming technique was established, by which a group of essential factors (Sox2, Nanog, Oct4, c-Myc, Lin28, Klf4 etc) in regulating stem cell behaviour and function, could be transferred into somatic cells to generate iPSCs [224, 225]. This brought in a promising future to provide personalised stem cells with unlimited proliferation ability and pluripotency *in vitro*, for stem cell-based therapy and transplantation, although refinement and optimisation on this technique to improve the reprogramming efficiency, to reduce the underlying risks in performing gene manipulation such as tumorigenicity, genetic and epigenetic abnormalities, and to avoid contaminations and potential safety issues regarding the use of animal products, remained challenges [224].

C) MSCs as multipotent stem cells, have been isolated from many organs and tissues including bone marrow stroma, adipose tissue, muscle, skin, umbilical cord, dental pulp, brain, heart, liver, being characterised by the expression of specific surface antigens (profiles of positive/negative MSC phenotypes and cluster of differentiation (CD) markers: CD34, CD45, Stro-1, CD105, CD106, CD73, CD90, CD31, etc.), and capabilities of adherence, colonial formation and multi-lineage differentiation (at least osteogenesis, adipogenesis and chondrogenesis) in culture *in vitro* [221, 226, 227]. With similar functions as those of ESCs (stemness, differentiation, homing, immunomodulation, trophic impacts of paracrine and autocrine bio-factors etc.) but more feasibilities (more sources to harvest, anti-inflammation, mobilisation, etc.) and less associated

ethical/legal problems, MSCs have been increasingly investigated as seeding cells in cell-based TE, regenerative medicine, drug delivery and cell therapy [228-230]. In articular cartilage/osteochondral TE, MSCs from different origins, have been studied. Here a few of them are introduced below including bone marrow-derived MSCs (BM-MSCs), adipose tissue derived MSCs (AD-MSCs), and synovial MSCs.

a) BM-MSCs: Multipotent stem cell populations in bone marrow were described in 1970s, where a heterogeneous group of precursor cells of stromal mechanocytes were highly adhesive, fibroblast-like morphology in culture, could form colony in monolayer culture, proliferated *in vitro* slowly, different from hemopoietic stem cells and immune cells, radiosensitive, sensitive to hypoxia, and having varied differentiation potency under inducers [231]. After isolation and demonstration from subsequent studies, BM-MSCs were finally identified in the 2000s, along with the clarification of the term 'mesenchymal stem cell (MSC)' [232]. At first, MSC-containing populations were isolated from bone marrow aspirates by the adhesive property, then many methods were developed to extract the homogeneous group of BM-MSCs from the cultured heterogenous group of progenitor cells, such as the 70% gradient of Percoll® [233], and a density gradient of 1.073g/ml solutions [234], followed by the characterisation of specific surface antigens by flow cytometry. These MSC-markers have been accumulated, such as CD29, CD 44, CD73, CD90, CD105, CD166, Stro-1 and many others [232, 235, 236]. Although specific and common MSC surface markers are still controversial topics at present, the minimal criteria for MSC studies to follow regarding the definition and characterisation of MSCs, have been established by the International Society of Cellular Therapy (ISCT), which are briefly introduced as follows [235, 237, 238]:

1) Under the standard cell culture condition, MSCs should present adherence to the plastic tissue culture flasks.

2) A series of specific surface markers could be considered to identify the phenotype of MSCs isolated and cultured *in vitro*, including the more than 95% positive markers of CD105, CD73 and CD90, and the less than 2% negative markers of CD34, CD45, CD14/CD11b, CD79a/CD19 and HLA-DR (Human Leukocyte Antigen-DR isotype).

3) MSCs should at least differentiate into osteoblasts, adipocytes and chondroblasts *in vitro*, characterised by staining protocols.

About identifying homogeneous group of MSCs by surface markers, a great many studies have been working on this topic, by which our knowledges of MSCs could be improved and many new MSCs from new origin and subpopulations of stem cells could be discovered [239-244]. Regarding the stemness of stem cells, differences between common and specific phenotypes of MSCs derived from various origins, and biological functions and spatiotemporal changes of markers between MSCs cultured *in vitro* and those corresponding ones stayed originally *in vivo*, numerous studies have explored, leading to more unknown knowledges to be investigated [232, 239-241, 245-250].

BM-MSCs are one of the most frequently studied and used MSCs, although there are challenges regarding the invasive process of obtaining autologous BM-MSCs and site morbidity in donors, relatively rare cell population in bone marrow, a low expansion rate, ageing and decreasing abilities of differentiations *in vitro* in culture as increasing cell passage number, and donor-related cell qualities [251].

In clinical applications, marrow stimulation techniques, have taken advantages of recruiting autologous MSCs from bone marrow along with bleeding and ‘superclot’ formation, to participate

in cartilage/osteochondral tissue reparation, since 1950s [252-255], however, this approach is restricted to deal with small to medium lesions in selective patients for a short term, clinical results are often inconsistent, and the regenerated fibrocartilage or mixture of fibrocartilage and hyaline cartilage tissue would lead to the post-operative failure in the long-term assessment [221, 252]. Various biomaterial substrates/matrices were then designed and developed as bio-functionalised cell-free fillings and/or supplemental covers to improve this *in situ* regenerative approach, either to stabilise the fragile 'superclot', or to provide bioactivated microenvironments for MSCs to migrate, proliferate, differentiate and avoid apoptosis in the defect area, some of which were commercialised [205-208, 219, 256, 257], such as the AMIC® (Appendix A, B). Both scaffold-free and scaffold-supported stem cell-based TE approaches and platforms/bioreactors to support the engineered tissue fabrication and culture have been extensively studied.

For example, an implant formed by autologous whole blood clot with chitosan-glycerol phosphate (GP) to fill in the full-thickness chondral lesion of animal sheep model after microfracture, was observed better adhesion within one hour after the surgery, and an improved cartilaginous tissue regeneration in both biochemical components and structure, after six months[258]. Further studies on this implant applied in conjunction with marrow stimulation techniques, suggested that, removal of calcified cartilage tissue and the remaining porous subchondral bone with blood vessel to supply nutrition and reparative factors, would correlate with better regenerative results such as the formation of hyaline cartilage tissue and structural integration with surrounding tissues [259]. With additional thrombin to accelerate the solidification of the chitosan-GP/blood implant in the defect area, more durable tissues could be regenerated for long-term focal cartilage defect recovery [260]. Due to the insufficient autologous MSCs would normally be supplied by bone marrow [252],

implants made up of scaffold/substrate and pre-loaded MSCs were developed. This allowed TE to bring more sources of seeding cells and encouraged the advancement of biomaterial-scaffold/substrate. For example, a study found that human BM-MSCs seeded in the biodegradable 3D hydrogel scaffold, and cultured with additional growth factor (TGF-beta) for about 21 days, could successfully differentiate into chondrocytes to regenerate cartilaginous tissue *in vitro* [261]. A biomimetic scaffold made up of 3D fibrous poly(ε-caprolactone) (PCL), HA and bioactive factors, was also successfully supported the recruitment, proliferation and chondrogenesis of cultured primary human BM-MSCs *in vitro* [262]. After implanting an autologous BM-MSC-laden freeze-dried PGA-HA scaffold in full-thickness articular cartilage lesions in animal rabbit models about a months, regenerated chondrogenic tissues with distributed round chondrocytes and structural integration with the bone were detected [263]. Human BM-MSCs were also successfully engrafted and differentiated in a PGA-HA scaffold *in vitro* [264], which was then approved in clinical trials and commercialised (Chondrotissue®). It was further found that additional treatments/supplements such as the autologous platelet-rich plasma (PRP), bone marrow aspirates/concentrates from surgery and autologous (human) serum to the HA or PGA-HA scaffolds, would improve the hyaline cartilaginous tissue regeneration and post-surgery outcomes from patients [265-268], demonstrating important roles played by the microenvironment during tissue regeneration.

The biomaterial substrates/scaffolds with appropriate biochemical components and/or architecture were increasingly developed, along with the accumulated knowledges of various factors engaging in the recruitment, attachment, proliferation, migration and differentiation of stem cells during tissue development and maintenance, such as chemokines, growth factors, cytokine, porosity,

geometry, topographical property and biomechanical features [269-293]. Some products were applied as cell-free approaches in tissue regeneration [213, 269, 294], others were designed as injectable cell-laden scaffolds/systems to deliver stem cells for treatments and/or for implantations [295-300]. Still more others were developed to supportive scaffold-based approaches, in which except for those bioactivated, artificial or xenogenous substrates/scaffolds, positive effects on stem cells-associated functional neo-cartilaginous tissue regeneration were also observed in substrates/scaffolds developed from or incorporated with dECM components and/or chondrogenic ECM molecules. By these approaches, challenges of anisotropic tissue structure, natural biophysical properties, inflammation, disease transmission, immunogenicity and potential ethical problems in medical practices would be possibly solved [269, 301-307].

As the development of sciences and technologies, novel bioactive substrates/scaffolds for stem cells-based TE and therapy [308], supportive bioreactors to provide biomimetic stimuli and to control the microenvironment of stem cells in culture [309], as well as some promising MSCs derived from other origins, have been continuously studied in articular cartilage/OC TE [251].

For example, by a low-cost microfluidic approach, hBM-MSCs could be encapsulated rapidly in microgels, which presented high-efficient chondrogenesis, while cultured in chondrogenic inducing medium, comparing to those cultured in bulk hydrogel and those in pellet culture [310].

A cell-free silk fibroin-chitosan blending hydrogel system incorporated with stromal cell-derived factor-1 to attract local MSCs to migrate, and microsphere loaded with kartogenin (a small bioactive molecule) to induce MSC differentiation, was developed and tested both *in vitro* and *in vivo*, to be an injectable cell-free solution to improve the recruitment of endogenous MSCs and chondrogenesis of MSCs by spatiotemporal release of bio-functional compounds [311].

3D platforms such as the microwell-mesh made up of biocompatible material PDMS, 3D microgel system formed by crosslinked hydrogel polymers, and various fabrication techniques to aggregate MSCs followed by performing chondrogenesis under controlled 3D microenvironment to produce condensation-like engineered building blocks in articular cartilage TE were emerged [312-315]. A broad range of biomaterials (both natural and synthetic) especially hydrogel polymers such as PEG, alginate, chitosan, HA-based, by plenty of novel/traditional polymerisation techniques [315, 316], and fabrication techniques such as electro-spraying, force-extrusion, sol-gel, emulsion templating and microfluidic process [317-323], were employed in cell-based articular cartilage/OC TE. In addition to use BM-MSCs, AD-MSCs and synovial MSCs as other endogenous seeding cells were investigated in articular cartilage/OC TE as well.

b) AD-MSCs, featuring with abundant tissue sources containing more cell numbers, easy and low invasive process to harvest, rapid expansion *in vitro*, and stable status of intact undifferentiation, comparing to BM-MSCs, as an alternative seeding cell, were first isolated in early 2000s [324], which have emerged in dealing with cartilage/OC tissue defects [325]. Being classified into MSCs, AD-MSCs cultured in monolayer under chondrogenic induction would be able to differentiate into chondrocytes *in vitro* [326], although insufficient potential of chondrogenesis was sometimes reported in AD-MSCs studies, along with common limitations such as decreased viability and differentiation abilities of MSCs cultured *in vitro* for a long term and after cryopreservation [251, 327]. Studies focusing on promoting the expansion, adhesion, chondrogenesis *in vitro* and *in vivo*, by biomaterial scaffolds/substrate and many other novel strategies to regenerate cartilage/OC tissues, and the underlying mechanisms have been extensively reviewed [251, 325, 327, 328].

c) Synovial MSCs, firstly identified in early 2000s [329], could be isolated from both synovial

fluid and synovial membrane of the synovium in synovial joint, where hyaline cartilage is naturally formed during joint tissue development [3, 330, 331]. Previous studies have found that synovial MSCs present a higher proliferation rate than other types of MSCs *in vitro* and *in vivo* regardless of the age of the donor, more stable differentiation properties than that of BM-MSCs and AD-MSCs even under a low seeding density, more relevant gene profile than that of BM-MSCs to chondrocytes, different protein profile from that of BM-MSCs and AD-MSCs, and low immunogenicity with additional capability of suppressing the proliferation of immune cells (T cells), suggesting the superiority of applying synovial MSCs as seeding cells in articular cartilage/OC tissue engineering application and the promising use in clinic [329, 332-334].

Apart from these, MSCs and chondroprogenitor cells from healthy or OA articular cartilage tissues, have also been identified by a few studies, in which the cell population, *in vitro* expansion rate, specific surface markers and chondrogenic differentiation capability were preliminarily explored, improving our knowledges of tissue specific MSCs, the underlying mechanisms of developmental and pathological process of the articular cartilage/OC tissue in joints, and potential roles played by these subpopulations of resident cells [335-339].

Thus it can be seen that, different type of seeding cells may have different strengths and weaknesses to be applied in articular cartilage/OC TE applications (Appendix D), requiring more future investigations to know the underlying mechanisms, to get consistent and valid results, and to facilitate future cell-based therapy and TE strategies for articular cartilage/OC regeneration [118].

2.3.3.2 Biomaterials for articular cartilage/OC tissue engineering

The application of biomaterials in medical area increased as the growing knowledge of biology

and various sterilising techniques. More biocompatible materials were then required to support the implant surgery and other clinical applications [340]. Biomaterial as an important element in TE, could be categorised by the type of ingredient, such as the metallic, ceramic, polymeric, biological (generated by a biological system) and composite biomaterials. Based on features such as the biodegradability, biomaterials could also be classified into biodegradable and non-biodegradable materials [340]. The choice of a biomaterial to be used, should be determined by the designing criteria for the final application purpose [341]. In terms of the biomaterial applied in TE strategy for medical applications, it provides a complicated microenvironment with physical, chemical, and biological cues to have impacts on the cell-based tissue regeneration, including roughness, topographical and geometrical patterns, porosity, the whole architecture, mechanical stiffness, viscoelasticity, surface chemistry, biomolecules, bioactive groups, which have been extensively reviewed [342], indicating future trends that biomaterials should be worthy of being modified precisely and specifically to facilitate the controlled microenvironment. Apart from the biodegradability, the stability, absorbability, cytotoxicity, immunogenicity, and the responsibility for inflammation, of the candidate biomaterial should also be considered in selecting appropriate biomaterials for TE.

In articular cartilage/OC TE, various biomaterials have been investigated, either to form a platform (scaffold/substrate) to assist or help deliver reparative factors (seeding cells, bioactive compounds). Here a few attractive and popularised hydrogel polymers will be briefly introduced.

Hydrogel belongs to polymeric materials, consisting of hydrophilic polymers and a lot of water absorbed by functional groups within the structure. Monomers of the hydrogel polymer could be physically (light, pressure, sound, temperature, electric field, and magnetic field) or chemically

(ionic strength, pH value, molecular species and solvent composition) crosslinked into 3D network of polymeric chains by proper crosslinkers or crosslinking conditions, leading to the retention of water and the formation of gel-like (sometimes colloidal gels) products. Hydrogel could be made from the original form of monomer, chemical prepolymers or existing parts of final polymer by three different methods of polymerisation, and the final property of hydrogel highly relates to the preparation process and building units [343, 344].

Hydrogels could be classified by different features. For examples, based on the composition and components, there could be homo-polymeric hydrogel (from one single form of monomer), copolymeric hydrogel (from two or more different monomers) and multipolymer hydrogel such as the interpenetrating polymeric hydrogel (IPN) (two or more independently crosslinked polymers contained in one polymeric network); based on the structural configuration, there could be amorphous hydrogel without crystalline, semi-crystalline hydrogel containing amorphous phase mixed with crystalline portion, and crystalline hydrogel; based on the crosslinking mechanism, there could be hydrogel network crosslinked permanently by chemical way, and hydrogel network formed temporarily by physical ways such as ionic bond, hydrogen bond, and hydrophobic interaction; based on the physical structures, there could be hydrogel film, hydrogel sphere and 3D hydrogel matrix; based on the surface charge of polymeric chain, there would be ionic hydrogel, non-ionic hydrogel, ampholytic hydrogel and zwitterionic hydrogel; and simply based on the origin of ingredient, there would be natural polymer hydrogel, and synthetic polymer hydrogel [344, 345].

Because of the soft, flexible and viscoelastic features, large volume of water content and high hydrophilicity, and the variety in hydrogel types and polymerisation processes, hydrogel materials have been employed in many areas, including the biomedical and TE fields. For TE applications,

biocompatible hydrogel materials are usually investigated to develop scaffolds/substrate to support seeding cell engraftment, to simulate the 3D ECM network of soft tissues, and to deliver bioactive components to regenerate the target tissue.

2.3.3.2.1 Natural hydrogel materials

Natural hydrogel materials, such as collagen, collagen derived gelatine, fibrin, hyaluronic acid (HA) or hyaluronate, alginate, and chitosan, have natural origins. As candidate materials in this study, collagen and alginate will be stressed below.

A) Collagens are a family of proteins with many types. It has been found that there are around 46 polypeptide chains involved in the formation of at least 28 different types of collagens and some other proteins have the collagenous domain, however, the polypeptide sequences of collagens among different species and tissues keep remaining conservative. All of their structures contain a typical triple helix wound by three polypeptide chains (alpha chains) full of glycine and proline [346, 347]. The major molecular sequence of a mature collagen is split from that of the procollagen containing a collagenous domain (the major triple helix) in between two non-collagenous domains (N-and C-propeptides). Three different N-propeptide structures had been identified in human collagen type I to III, type V and type XI. The molecular sequence of the collagenous domain determines the left-handed alpha helix structure of its polypeptide chain which is also called the alpha chain. Three parallel alpha chains identical or not, intertwine to form the typical right-handed triple helix structure of collagen protein [348-350].

Collagens can be grouped into fibrillar collagen (e.g. type I,II,II, V and XI collagen), beaded filament collagen (type VI collagen), basement membrane collagen (e.g. type IV collagen), short

chain collagen (type VIII and X collagen), transmembrane collagen (membrane-associated collagen with interrupted triple helices)(e.g. type XIII, XVII collagen), fibril associated collagen with interrupted triple helices (FACIT) (e.g. type IX,XII and XIV collagen), FACIT like collagen, collagen with multiple triple-helix domains and interruptions, and other unclassified collagen [350, 351]. The most abundant collagen in animal organisms belongs to the fibrillar collagen group where the most common and best studied collagen protein is the type I collagen. Fibrillar collagen proteins contribute to assemble into striated collagen fibrils followed by the formation of larger collagen fibres with hierarchical structure. The highly-organised collagen fibres and the heterogeneous glycoprotein family compose the ECM network [350] in tissues such as the bone, tendon, blood vessel, nerve, cartilage, skin and other connective tissues [351]. Except in the articular cartilage where the type II collage is the major collagen type, type I collagen fibres are the fundamental components of almost all other tissues.

The molecular structure of type I collagen protein in most cases contains two alpha 1 (COL1A1) chains and one alpha 2 chain (COL1A2), forming the heterotrimeric alpha chain. Hydroxylation of specific amino acid residues of the polypeptide chain of collagen is an essential posttranslational modification process of collagen proteins and critical for type I collagen fibre to keep its structure stable and to have competent biomechanical property [349]. After the cleavage of peptide or pro-peptide bonds at certain sites by enzymes such as the matrix metalloproteinases (MMPs) or other factors, the released lysine and/or hydroxylysine at some sites could be crosslinked covalently, resulting in the change of fibrous network and mechanical property of the collagen materials [349]. It is a self-assembly process for the collagen fibril monomers to form macromolecular collagen fibres, involving in the two-step fibrillogenesis of collagen protein which are the nucleation and

growth of fibres.

Collagen-based materials could be crosslinked by both physical and chemical approaches under optimised conditions (concentrations of reagent, pH, temperature etc.), involving various chemical reagents (aldehyde, isocyanate, imidoester, carbodiimide, alkyl and aryl halide, acylating compounds, N-substituted maleimides, diisocyanate, cyanamide, diamines, acyl azide, and glutaraldehyde (GA)), and some physical treatments (short-wave ultraviolet (UV) irradiation, gamma ray). Under a few other conditions such as severe dehydration, treatments of some acids (tannic acid), collagens could also be crosslinked [352-354]. The underlying mechanisms of these collagen crosslinking techniques refer to the responsive linkage between specific side chains of amino acids of neighbouring polypeptide chains activated by those reactive factors (active group/radical energy). After the inter/intramolecular crosslinking, the mechanical properties (elasticity, shear etc.), stability, anti-protease property, swelling ratio and biocompatibility of crosslinked collagens will become different from those of the non-crosslinked, and may vary from different crosslinking techniques, suggesting a careful consideration of the crosslinking technique to be used for collagen materials in medical applications [352, 353, 355, 356].

The crosslinked fibrillar collagens contain the non-interrupted triple helix structure, leading to their resistance to most proteolytic enzymes at normal physiological conditions (pH, temperature etc.), while denatured structure will greatly improve the sensitivity and susceptibility of collagen fibres to more proteinases [357]. It has been found that only a few proteinases could work on the cleavage of collagen fibres and *in vivo*, this represents the degradation and remodelling process of collagen, highly relevant to the physiological and pathological statuses of the body, such as tissue development, ageing, morphogenesis, wound healing, arthritis, arteriosclerosis, periodontitis,

asthma, periodontal diseases and cancer metastasis [357, 358]. The matrix metalloproteinases (MMPs) family, some serine proteinases and a few cathepsins, released from inflammatory cells and fibroblasts, could degrade collagen fibres under appropriate pH conditions, and different enzyme may work on different cleavage site of the polypeptide chain of different collagen type through different process [359]. The syntheses and secretion of these enzymes could be induced under some pathological conditions and details about these proteinases, degradation and resorption of various collagen proteins have been extensively reviewed by many studies [357-360].

Currently, commercial collagen materials are mainly purified from animal tissues processed by enzyme, salt and acid [361, 362], whereas recombinant/synthetic collagen products have also merged and been investigated to overcome the challenges resulting from animal-derived collagen materials [350]. In biomedical and TE area, as natural polymeric hydrogel biomaterial, with viscoelasticity, biocompatibility, low antigenicity, mild inflammatory response, and abundant sources, collagen (type I) has been extensively studied and applied [363]. For articular cartilage/OC TE practices, collagen membrane designed for ACI and MACI, collagen material-based injectable cell/drug (e.g., gene) delivery system/matrices, and collagen-contained 3D scaffold/substrate for implantation/transplantation, have been designed and explored (some of which are mentioned).

For example, injectable collagen systems were designed for delivering small molecular compounds/genes/proteins, including collagen fibre suspension, viscous non-collagen fibre solution, and collagen-laden aqueous solutions, however, the open system of collagen solution is easy to incorporate but difficult to control the release of small compounds/ bio-macromolecules, requiring complicated design of the hydrogel system [363]. Collagen gel-involved substrates/scaffolds are often fabricated into solid forms such as meshwork, pellet, membrane, plug

and sponge, by thermo or irradiation powers, to increase the rigidity and prevent collagen scaffold/substrate from contraction. To strengthen and improve collagen gel for TE, functionalisation and modification of the active groups of collagen sequences, such as the carboxyl, amino acid, as well as designs of composite materials have also been investigated [363].

B) Alginate is a type of polysaccharide biomaterial, consisting of α-L-guluronic acid (G) and β-D-mannuronic acid (M) combined in a linear structure. Some bacteria and brown algae (*Phaeophyceae*) [364, 365], are natural and typical sources of alginate, determining the sequence arrangement and proportions of M and G blocks, from which varied the physical and chemical characters of alginates. Generally, three arrangements of G and M blocks, have been found in alginates, including consecutive GG block, MM block, and GM or MG block.

Alginic acid is insoluble, but alginate (the monovalent salt) and esterified alginate are soluble in water solution which is stable and viscous. In the water solution, because of those carboxylic groups on the backbone structure formed by G and M units, the alginate becomes anionic and could be crosslinked physically by divalent cations (carboxyl group) such as the calcium, strontium and barium. In alginate solution, there are hydrogel bonds between hydroxyl groups and carboxyl groups, contributing to the solubility and viscosity of the solution [366]. The crosslinking and gelation process is selective and dependent on the length, distribution and proportion of the G unit in the whole structure of alginate materials. An increase in the content of G block may lead to an increase in the mechanical properties of the alginate materials such as the rigidity, compressive and tensile strengths and flexibility [367]. The crosslinking process is also kinetic and relevant to the concentration, source and type of cations. Higher concentration of cations refers to a faster crosslinking process, and the speed and quality of the crosslinking vary from different cations and

associated anions as well [368]. Alginate hydrogels crosslinked by cations of different ionic strength, type and source, also present different mechanical properties. Besides, alginate hydrogel formed by the cation-mediated crosslinking is not stable and will degrade gradually as the ion leaching out of the hydrogel structure to aqueous solutions. Hence, the alginate hydrogel resulted from counterions-mediated crosslinking is reversible, and will degrade in solutions containing more monovalent cations (e.g. sodium) or chelators (EDTA, sodium citrate, sodium oxalate etc.) [367].

Molecular weight of the alginate is another factor having impact on its degradation and subsequently the mechanical properties. It has been found that, high molecular weight alginate hydrogel is associated with less numbers of hydrolytic positions, leading to decreased degradation speed, and the molar mass of alginate influences the stiffness of crosslinked alginate and the viscosity of soluble alginate [367]. Stable alginate hydrogels now could be formed covalently by many compounds such as some peptides or small amino acid sequences, polyethylene glycol diamine, adipic dihydrazide [345, 369], and after those free hydroxyl or carboxyl groups on the backbone sequences being modified with some chemicals [365, 370-380], such as the methacrylate, boronic acid, hydrophobic groups, cyclodextrin and poly (N-isopropylacrylamide) (pNIPAAm), alginate hydrogel derivatives with specific features could be developed, such as the ability to be photocrosslinked or self-assembly or temperature-sensitive, controlled swelling and mechanical properties, adjustable degradation, improved adhesions to certain type of protein or cells, and/or targeted cell types [364, 365]. More details about the molecular structure, potential chemical modifications and derivates of alginate materials have been extensively reviewed [365, 367, 381-384].

As natural biomaterials with favourable advantages including biocompatibility, biodegradability, non-immunogenicity, non-cytotoxicity, convenient to obtain from many sources, and approved by the U.S. FDA, alginate materials have been applied in many biomedical and pharmaceutical areas such as drug delivery, wound healing and tissue engineering [385]. Various forms and derivates have been developed to facilitate these biomedical applications. In articular cartilage/OC TE, alginate-involved composite, and alginate-based scaffold for 3D culture and modified/functionalised designs to improve the attachment, proliferation, organisation and differentiation have been extensively investigated [282, 384].

For example, disk-shaped tissue constructs containing primary chondrocytes blended with alginate solution were fabricated in the presence of calcium chloride *in vitro* and implanted subcutaneously into nude mice. After 12 weeks, new-cartilaginous tissue was regenerated [366] *in vivo*. And it was found that within the alginate hydrogel, chondrocytes could distribute homogenously retaining the differentiated morphology and be immobilised as gel polymerisation. Alginate scaffold/carrier could be degraded by enzymatic hydrolysis and the remaining products were non-inflammatory although they were not absorbable by the organism [386]. Injectable alginate material-based systems for delivering growth factor genes, autologous seeding cells, and specific or bioactive hydrogel scaffolds into animal models for articular cartilage regeneration were also investigated, which results were positive and promising [387-390]. An absorbable PGA-PLA-alginate scaffold was developed and seeded with chondrocytes to form an implant. After implantation in animal model with full-thickness OC defect for months, cells were successfully engrafted and delivered to the defect area. Neo-articular cartilaginous tissues were then observed and better clinical outcomes were assessed, comparing to those without alginate or using alginate alone [391]. A study

of MSC-laden alginate system with hydrophobic modification showed that the modified alginate material could be crosslinked rapidly and homogeneously without cations, and the hydrogel system was biocompatible and stable for primary MSC culture and differentiation *in vitro* [392]. From another study, alginate materials were covalently functionalised with collagen, to develop a biomimetic 3D shape-memorable scaffolds with aligned pores. Adipose-derived MSCs were successfully seeded and differentiated into chondrocytes after chondrogenic induction in this scaffold. The engineered tissue construct presented aligned cell distribution within the scaffold and an improved mechanical property [393]. Human adipose-derived MSCs which were encapsulated in 3D low-viscosity alginate hydrogel by the mould-casting way under the ion strength of 102 mM calcium chloride, and cultured statically with chondrogenic inducing medium up to 28 days, could differentiate into chondrocytes with spherical morphology in 3D hydrogel and produced more sulphate GAGs and type II collagen, correlating with the observation of increased mechanical properties [394]. By using microfluidic device, a 3D alginate scaffold with organised porous structure was also developed and successfully support the proliferation and differentiation of primary chondrocytes cultured *in vitro* [395].

Apart from these, chlorogenic acid modified alginate scaffold to improve the chondrogenesis of chondrocyte-engrafted implant *in vivo*, alginate hydrogel-based MSC-chondrocyte co-culture system, alginate hydrogel with a series of pore sizes to simulate the zonal structure of articular cartilage tissue, functionalised alginate to develop durable, high-strength or photocurable alginate-based materials, PCL-alginate composite for 3D bioprinting the chondrocyte-laden construct, and many other studies to develop novel alginate-involved materials for articular cartilage tissue regeneration have been explored widely [396-401], demonstrating the attractiveness and popularity

of alginate materials.

In summary, natural biomaterials such as collagen, alginate, hyaluronic acid, gelatine and fibrin, usually possess favourable features such as biosafety, natural biocompatibility, biodegradability, non-immunogenicity and non-inflammatory activity in homologous species, however, common challenges are insufficient mechanical properties, source-dependent physical and/or chemical characters, potential antigenicity or disease transfer between donor and receiver of different species.

2.3.3.2.2 Synthesised polymer materials

Synthesised polymer materials are developed to complement disadvantages of natural materials such as the poor mechanical property and rapid degradation. Comparing to scaffolds/matrices made up of natural hydrogel materials, the fabrication process and modification are more controllable while using synthetic materials. In articular cartilage/OC TE applications, here are some frequently used synthesised biomaterials to be briefly introduced.

A) Poly (vinyl alcohol) hydrogel (PVA) is a hydrophilic polymer synthesised from vinyl alcohol monomers. Vinyl acetates are polymerised in alcoholic solutions, by the induction of free radicals, to become poly (vinyl acetate) which will be partially hydrolysed to form PVA. PVA with different degree of hydrolysis could be prepared by managing the step of hydrolysis, having impact on the solubility, crystallinity, polymer behaviour and chemistry of the material [402].

PVA as synthesised biomaterial with many advantages including the controlled water solubility and biodegradability, biocompatibility, less toxicity, and adhesion has been applied in both industrial and biomedical areas. PVA materials with low degree of hydrolysis is more soluble than that of high degree of hydrolysis at low temperature, because the hydrophobic acetate residues

could reduce the potential formations of hydrogen bonds between hydroxyls in intra and inter molecules. PVA materials having high degree of hydrolysis should be dissolved in water solution at temperatures higher than 70°C. The acetate residues also contribute to the crystallisation of PVA at high temperature. PVA materials with low degree of hydrolysis could be crystallised easier than those of high degree of hydrolysis. It was found that the tacticity, molecular weight and regioselectivity of PVA materials all depend on the degree of hydrolysis of PVA. Co-polymerisation process was then developed to improve the preparation of PVA-based materials [402, 403].

In biomedical and TE area, PVA hydrogel materials are usually prepared by two technical steps containing crosslinking and processing. In the former step, physical, chemical and irradiative techniques could be used. Physical crosslinking approaches include the formation of strong hydrogen bonds to crystallise the PVA materials through freeze-thaw repeating circles. This process is controllable and the PVA hydrogel formed by this way could present many attracting features including biodegradability, tissue-mimicking viscoelasticity, good room temperature stability, swelling behaviour, and improved mechanical properties. Disadvantages of PVA hydrogel formed by this physical crosslinking may refer to the varied structure, mechanical stability and morphology of the crosslinked materials, from different temperature, time and numbers of circles of the repeating freeze-thaw process, and the polymer sources. Chemical crosslinking process involves the formation of covalent bonds between those hydroxyl groups in PVA materials, through various crosslinkers such as the glyoxal, glutaraldehyde, borate, monoaldehyde, along with other compounds such as the acetic acid, sulphuric acid and methanol. Chemical crosslinking provides a stable polymerisation of the PVA hydrogel but also brings toxic remains and by-products which

are difficult to eliminate to meet further biomedical requirements. It was found that PVA materials crosslinked by irradiations such as the electron beam, gamma ray, were non-toxic and presented improved cell attachments. However, it is an expensive technique, comparing to the other crosslinking methods, leading to the use of combined techniques to synthesise this material. For the latter processing step, various fabrication techniques have been studied, such as the freeze-drying, cast-drying, solution blowing, coagulation, electrospinning, emulsion, sol-gel transformation, and rapid prototyping, which details could be found in many literatures [402].

PVA-related hydrogel materials have been employed in many biomedical applications including wound healing, drug delivery, artificial tissue fabrication and tissue regeneration [403]. However, there are some challenges of using pure PVA materials reported regarding certain biomedical practices, such as the limited elasticity, rigid structure, insufficient hydrophilicity, potential interactions with living tissue and body fluids, poor permeability of highly crosslinked PVA materials, weak stability in water solution and problems on fixation and deswelling have been also observed from applications of commercialised PVA hydrogel products [404], resulting in the design and development of composite PVA materials to improve those characters. Many other materials such as cellulose, chitosan, HA, starch, and aspartic acid, have been investigated to co-polymerise with PVA to form composite materials for better performances [402, 403].

B) Synthetic biopolymer group of poly-alpha-hydroxy acids (PLA, PGA and PLGA)

a) Poly (lactic acid) (PLA) polymer is formed by polymerised lactic acid monomers which are mostly produced by fermenting renewable sources (sugarcane, corn). Alternatively, lactic acid can be synthesised by chemical hydrolysis of the lactonitrile. PLA could also be recycled by hydrolysis back into lactic acids. Lactic acid monomers could form dimers, trimers and oligomers during

fabrications and the lactide is a cyclic dimer in the form of a ring. PLA commercially could be formed from lactic acid solution in a direct condensation polymerisation manner or from lactide in a process called the ring-opening polymerisation, where the concentration, impurity, residual component, and optical purity of raw materials (lactic acid or lactide) will have effect on the quality of productions of lactide and PLA [405]. Novel methods such as direct polycondensation in combination with chain extension of lactic acid, enzyme-related biosynthesis, and metabolic engineering-involved synthesis, have been investigated with specific advantages and disadvantages [406].

PLA materials with high molecular weight are colourless, rigid, glossy, thermoplastic material, having similar characters as polystyrene materials [406]. The physical and chemical features of PLA, such as the molar mass, molecular structure, optical purity, rheology, microstructure, conformation, residues, impurity, and degradation half-life, are determined by the polymerisation process, which will have impacts on further applications of PLA [405]. As aliphatic polyesters approved by FDA and European regulatory authorities for food application and drug releasing materials, PLA biomaterials with advantages of renewable, eco-friendly, biodegradable, biocompatible, processable at high temperature and energy-saving features, have been extensively used in textile, food industry and biomedical areas. However, disadvantages regarding some applications remain concerns, such as the extremely slow degradation rates (months to several years), fragile and weak mechanical property of pure PLA materials, strong hydrophobicity, poor cell compatibility and affinity, potential activity to induce inflammation, and permeability of gas [406]. Fortunately, chemical and physical modifications have been established to improve PLA materials, such as polymer blending, plasticisation with different plasticisers, co-polymerisation

with other polymers, composition with fibrous materials, crosslinking through electron beam, gamma irradiation and chemical treatments, surface coating, plasma treatment, and various chemical modifications with other compounds, which details available in many literatures could be looked over [406-409].

b) Poly (glycolic acid) (PGA) is a biopolymer whose glass-transition temperature is around 37°C, and melting point is around 220°C. PGA could be synthesised by glycolic acid monomer and glycolide by a series of methods, including glycolic acid-initiated polymerisations (direct polycondensation, oligomerisation of glycolic acid and chain extension polymerisation, azeotropic condensation polycondensation), ring opening polycondensation process from glycolides (melt/bulk polycondensation, solution polymerisation of glycolide, cationic and anionic polymerisation, suspension/emulsion polycondensation), solid-state polycondensation of halogenoacetates, acid or enzyme-catalysed polymerisations [410]. The synthesising methods and catalysts applied, determine the structural properties of PGA products, such as the molecular weight, molecular form of glycolic acids, molar mass distribution and the structure of the polymerised chain, which subsequently regulate the physicochemical characters of PGA materials, including the mechanical properties (Young's modulus, elongation-at-break point, tensile strength), the thermal features (melting point, glass transition temperature, crystallisation), and the polymer density [410].

It has been found that highly polymerised PGA materials are mainly insoluble except in some fluorinated solvents, having rapid degradation rate and stronger mechanical properties than PLA materials. PGAs with high molecular weight are unstable and degraded faster than PLA. The degradation of PGA materials is generally regulated by the degree of polymerisation and

amorphous phase structure [410-412]. PGA with higher molecular weight has slower degradation rate and the degraded glycolic acid of PGA is the natural products of metabolism. Higher molecular weight and degree of polymerisation also lead to more stable mechanical strength of PGA materials [410].

As synthesised biomaterials with attractive mechanical properties, biodegradability, and inert immunogenicity, PGA has many applications in particular in the biomedical field. It has been applied to fabricate biodegradable scaffolds/implants, drug delivery system, polymer-based barrier membrane, biodegradable stent, and absorbable sutures for surgical purposes [413]. PGA-based commercial sutures have been approved by FDA since 1960s. However, the expensiveness of high molecular weight PGA material limits its applications, and inflammatory responses induced by hydrolysed products of PGA *in vivo* require further studies to understand more about the associated inflammatory responses and complement inhibition approaches regarding PGA-based materials for medical applications [410]. Modification and composite materials of PGA are being investigated, to address out current limitations on its biomedical applications [413, 414].

c) Poly (lactic-co-glycolic acid) (PLGA) is copolymerised product by lactic acid and glycolic acid monomers, in an amorphous and linear structure. Based on the ratio between the two monomers, the form of the polymerised PLGA could be defined. Same as other synthetic biopolymers, the methods and procedures of the synthesis have great impacts on the physical and chemical properties of the produced PLGA, such as the structure of the polymer sequences, the ratio of two monomers, boiling point, molecular weight and purity. More alternative approaches and novel catalysts were developed to optimise and simplify the polymerisation processes and the associated costs. It was found that PLGA is soluble in many solvents such as the acetone, tetrahydrofuran and

chlorinated solvents, to be fabricated into the designed size and shape, and to encapsulate molecules and drugs. The structural information of PLGA determines its degradation rate playing an important role in the following medical applications such as the drug delivery system. From literatures, higher molecular weight of PLGA may cost longer time to degrade; more lactic acid monomers in PLGA structure usually present more hydrophobic features, reducing the degradation rate; end group with modification causes longer degradation time; additional acids and plenty of water, could increase the degradation rate [415]. Hydrolysed PLGA will experience four stages including the hydration (water penetration to break the hydrogen bonds and van der Waals force), initial degradation (break up the covalent bonds and molecular weight decreases), constant degradation (autocatalysis, cleavage of covalent bonds in the backbone and reduced integrity) and the solubilisation (further cleavage of fragments to become soluble molecules). The mechanical properties of the PLGA materials are varied from the fabrication process, resultant structure, molecular weight and ratio of monomers, usually very rigid. The glass transition temperature of PLGA is around 37°C and related to the content of lactic acid monomers and molecular wight [415-418].

Similarly, PLGA materials have been applied in many areas including biomedical fields in the forms of fibre, film, microsphere, hydrogel, 3D porous scaffold, and composite materials, to deliver biomolecules, pharmaceutical drugs, bioactive factors, and to be fabricated into tissue culture scaffolds for tissue regeneration, which could be discovered in many literatures [415, 419, 420]. For the future trends, modification and functionalisation of PLGA materials and PLGA-based composite materials, to improve the mechanical properties for certain application, to enhance the affinity, and to reduce the potential cytotoxicity for bio-applications are worth efforts to study [415,

418, 420].

C) Polyethylene glycol (PEG) is the linear polyether containing a series of repeated ethylene glycols. PEG can be formed by the direct polymerisation of ethylene oxide with hydroxyl group of other compounds such as the water molecules, another ethylene glycols and diols. PEG can also be synthesised by the ring-opening polymerisation of epoxyethane. Functional groups on the PEG structure contribute to the various PEG-based derivatives which could be provided commercially now and usually named by molecular weight. Process of the modification and conjugation of PEG is often termed as the PEGylation, which details could be found in many literatures [421]. Briefly, PEG could be modified by the ε-amino group of lysine in proteins at non-specific site. Modification of PEG at specific sites by PEGylations (N-terminal PEGylation, bridging PEGylation, thiol PEGylation and C-terminal PEGylation) and catalyst-initiated PEGylations have also been reported. PEG molecules could be used to modify other polymers due to active groups on the terminals of PEG, by such techniques as salinisation and Click chemistry, which processes are varied from different functional groups and methodologies. Apart from those, physical PEGylation of PEG with other polymers by adsorptions, hydrophobic interactions and electrostatic adsorption between PEG and other hydrophobic groups/sequences, and bonding between PEG with metal or chelate have been also discovered.

PEG materials are flexible, biocompatible, amphiphilic, and capable of hydration, which have been approved by FDA as inert materials for human oral, dermal and intravenous applications. In biological circumstances, PEG materials present poor stimulation and adhesion to cells, weak protein adsorptions, low cellular internalisation and no obvious inflammatory activities. In room temperature, low molecular weight PEGs are liquid; PEGs with medium molecular weight (1000-

2000) are soft solid, while high molecular weight PEGs (more than 2000), are crystallised hard solid whose melting temperature is about 63℃. The polarisation of PEG polymers is related to their hydrophilicity, permeation and solubility. Hydrophobic materials modified by PEG molecules could be improved their hydrophilicities.

PEG is thermosensitive material which could be degraded at high temperature, depending on the molecular weight. It was found that the glass transition and melting temperatures could be changed by mixing or polymerising PEGs of different molecular weights. By this kind of manipulation, the mechanical properties and chemical stability of PEG materials would be altered. The molecular weight of PEG regulates the absorbability and half-life of PEG material in body and by oxidation of the alcohol group, PEG materials could be further degraded by specific enzymes of metabolism. As relatively biosafe ingredients [422, 423], PEG-based materials have been extensively applied in biomedical and pharmaceutical areas, as plasticiser, solubilising factor (solubiliser), permeation enhancing factor, anti-fouling factor for medical device, supporting factor for long-time circulating treatment, drug-releasing modifier, therapeutic approach, and tissue engineering scaffold materials, as well as used in many other industries [421].

Among various PEG derivatives, **poly (ethylene glycol) diacrylate (PEGDA)** with the photocurable character to form hydrogel polymer in the presence of photoinitiator by light radiations, has been paid a great many attentions and applied in many biomedical fields. PEGDA monomer could be synthesised by catalyst-induced esterification of the hydroxy group of PEGs and acryloyl group of compounds such as acryloyl chloride at room temperature under the condition of nitrogen. The physical and chemical properties, the degradation rate, molecular weight and structure are determined by the raw material of PEG molecules, and due to the esterified

terminal groups (functional groups) on the PEG backbones, hydrolysis rate of PEGDA hydrogel is relatively slow [424].

Previous studies have observed many favourable advantages of PEGDA hydrogel, such as bio-inert and biocompatible features, fouling-resistance, adjustable mechanical properties and swelling ratio regarding the molecular weight and concentration. However, as PEG-based materials, unsatisfactory features of PEGDA materials have also been reported, such as relatively inactive surface feature of the polymer for cells to adhere and attach to, specific photoinitiators with cost-effectiveness and low cytotoxicity for biomedical practices, unsatisfied protein adsorption and diffusivity, degradation and remodelling related failures of PEGDA hydrogel-based scaffolds and delivery systems [424-426], requiring further modification, functionalisation and conjugation with other materials or compounds to improve, and requiring novel PEG-based materials to be developed.

Different types of synthesised biomaterials have different advantages and limitations regarding varied applications in practices. In terms of biomedical and tissue engineering applications, the ideal scaffold/delivery system may be from **the composite materials** of natural and synthetic materials, with both advantages incorporated but limitations prevented, such as improved biocompatibility, cell adherence and affinity, controlled mechanical and degradation properties. Various composite products have been investigated for articular cartilage/OC tissue regeneration applications.

For example, chitosan and gelatine modified by thermosensitive materials were developed into an injectable water-soluble co-polymer solution, by which MSCs and chondrocytes were delivered into animal models to survive and successfully regenerated the hyaline-like cartilaginous tissue *in*

vivo [427, 428] . In combination with dECM component and growth factor, the biocompatibility of PEGDA scaffold was improved for MSCs to distribute homogenously, and to keep their phenotypes during proliferation and differentiation [429]. Bioactive materials such as collagen, collagen analogue, fibrin gel, also provide a better microenvironment to improve the engraftment, homogenous distribution, proliferation and differentiation of seeding cells (MSCs and chondrocytes) in scaffolds made up of synthesised biomaterials such as the PLGA, PEG, after incubation [430, 431] [432]. A study of the HA-PEG-albumin gel matrix found that the modification could even provide an environment to support articular chondrocytes rather endothelial cells to survive, proliferate and differentiate in scaffolds *in vitro* and *in vivo* [433]. Alginate microspheres blended PVA hydrogel to fabricate porous composite scaffold could deliver chondrogenic cells. The mechanical property of the scaffold could be tuned to simulate that of the articular cartilage, by changing the proportion of PVA, and hydrogel microspheres could encapsulate and release gradually growth factors, to mimick the biochemical environment for chondrocytes to migrate and grow, indicating a promising use of this kind of scaffold in dealing with chondral defects [434]. Similar results were also observed in another study where a porous PLA scaffold was treated with growth factors before being seeded by alginate-encapsulated BM-MSCs [261].

Hence, scaffolds fabricated by well-prepared composite materials might benefit from individual features of ingredient materials and specific designs, to offer an effective delivery system/tissue engineering implement to have synergically positive impacts on the engraftment, survival, migration, proliferation and differentiation of seeding cells [419].

To conclude, composite materials which could be synthesised with controlled composition,

required properties and desired versatility to be able to meet varied applications, offer a great prospect to substitute conventional synthetic material or pure natural material, to be utilised in future wound healing and tissue engineering applications [435].

2.3.3.3 Biomaterial scaffold fabrication techniques in tissue engineering

Biomaterial scaffold fabrication is a technological element in tissue engineering strategy. Most tissues and organs are spatiotemporally developed into 3D complex architectures with various patterns of ECM which could be simulated in designing the tissue specific scaffold for scaffold-based tissue engineering. Based on the biomaterials and intended scheme of the scaffold, methodology to process the fabrication could be varied and versatile. In TE, hydrogel polymers with advantageous features have become the ideal biomaterial to fabricate 3D scaffold/substrate to simulate the 3D ECM of especially soft tissues, and 3D porous scaffold is such a typical design that could provide appropriate microenvironment for seeding cells to engraft, survive and form the target tissue/organ. Considering the abundancy, availability and importance of hydrogel polymers, many techniques were developed to fabricate hydrogel materials, which could be divided into non-designed techniques, such as the emulsion freeze-drying, melt moulding, solvent casting/salt leaching, phase separation, gas foaming, electrospinning, and designed techniques, including rapid prototyping of solid materials and additive manufacturing [436, 437]. Details of those techniques could be found from many reviews and here the 3D printing technique for 3D fabrication of hydrogel materials to be applied in this study that will be introduced below.

Evolved from rapid prototyping (RP) technique, 3D printing or additive manufacturing technique is similarly a bottom-up approach to build up the 3D product layer by layer based on information

from the professional modelling software, image scanning, mathematical equation processed by computer-aided design (CAD). Different from the RP technique, which is focusing on using solid materials to be processed at high temperature by expensive machines, 3D printing technique with fascinating features such as controllable, flexible, usage of various materials, fast speed processing, relatively inexpensive, and versatile, nowadays has been developed into various types and could be applied in multiple industries, multidisciplinary projects, and collaborations with other techniques [438, 439]. According to the types of building materials to be used, 3D printing processes could be classified into solid-based, liquid-based, powder-based and paper sheet based. Based on different fabricating methodologies, there could be direct 3D printings such as the extrusion-based, laser-based, jet droplet-based, fuse deposition-based, stereolithography-based 3D printings, and indirect 3D printings such as the wax printing [438-441]. In biomedical and tissue engineering areas, there could be bio-printings based on bio-ink containing living cells as building materials, and non-bio-printings focusing on scaffold/substrate fabrications. For 3D fabrication of biocompatible, biodegradable and porous scaffold/substrate for tissue engineering applications, various materials have been employed in 3D printing, such as metal, polymer, ceramic and hybrid composite [438], in which hydrogel soft polymer-based 3D printing to directly fabricate scaffold/substrate to simulate the ECM architecture has gained increasing attention. Here some 3D printing techniques for fabricating scaffolds based on the hydrogel polymer materials will be introduced, including extrusion-based 3D printing, inkjet 3D printing and digital light processing-based 3D printing.

A) Extrusion-based 3D printings: In this technology, materials are extruded from nozzles and become continuous filament forms to be deposited selectively to generate the 3D structure on the

platform. This platform could move along with XYZ three directions, which in combination with various nozzles and curing tools, compose an extrusion 3D printer. Fuse deposition modelling (FDM) or fused filament fabrication (FFF) methodology was its original basis, in which thermoplastic materials with balanced mechanical and rheological properties, and heated nozzles are usually applied [442]. Properties of the melt polymer determine the size of nozzle, resolution of printed product and the speed of printing process. For hydrogel materials with printability (appropriate viscoelasticity), direct ink writing (DIW) 3D printing is an alternative choice. In DIW printer, the air pressure-driven piston or screw is used to extrude the viscoelastic material, and additional curing steps related to the printing materials, are often required to stabilise the printed structure after material deposition. The rheological features of the ink (printing material) determine its printability and the success or failure of this printing, usually containing the shear thinning property, yield point and recoverability of the ink. Additional devices to support viscoelastic changes of the materials under transient shears during and after extrusion by mechanical forces, could broaden the range of candidate inks, such as UV sensitive, thermo-responsive, ion/chemical curable hydrogel materials and composite materials which have been developed to be the ink for DIW 3D printing. DIW printing could benefit from the broad range of candidate polymer material inks, in which the poorly printable materials could become printable by tuning their rheological properties via methods such as two-step curing, embedded printing, rheological modifications [443]. The challenge of DIW printing refers to the post-printing curing, the shape fidelity, supportive and sacrificial materials required to fabricate complex 3D structures, low speed, and limited resolution, remaining optimisation and improvement of the printer device and printing processes [444, 445]. With additional electric fields, electrohydrodynamic direct printing (EHDP)

is derived from DIW printing. In the setup of EHDP, the distance between substrate platform and nozzle is very close usually below 1 cm, allowing the precise and controllable deposition of materials. Due to the electrical stretching to the ink, printing resolution could be greatly improved to nanoscale. EHDP also benefits from a large variety of materials, but the electrostatic repulsion determines the limited height of the printed structures [446-448].

B) Inkjet 3D printings: In this technology, materials with low viscosity, are shaped into droplet to be deposited selectively to fabricate the 3D structure. The printer often is made up of three dimensionally (XYZ) movable platform, jetting head, and supportive curing device. Liquid materials could be jetted out of the head in the shape of droplet, to reach to the movable platform and be deposited and cured exactly at the planned position. Based on the jetting style, two types of inkjet printer have been developed, which are continuous inkjet printer and drop-on-demand inkjet printer, with different printing speed, nozzle size, droplet size and resolution. From the continuous printer, liquid inks are pushed out continuously of the head, to form a droplet stream before being deposited. Each droplet is charged and selected by controlling the charge of the deflector and irrelevant droplets are then removed and recycled, remaining the relevant droplets cured at the correct position. From the drop-on-demand printer, material droplet is only generated from the liquid material ink by the pressure force as requirement inside the nozzle and pushed out when the force becomes stronger than the threshold. From literatures, the force could be generated by heating and piezoelectric transducer. The configuration of the printer and the property of the printing materials, are responsible for the generation of the ink droplet, the printing speed, and resolution. Liquid materials with high concentration, bigger size solute, and non-phase-change feature, may be unsuitable for this printing, reducing the variety of candidate inks. In addition, supportive

materials with high density are often required for the liquid droplet materials to build 3D structure, increasing the cost value of using this printing to fabricate. To date, many efforts have been made to improve and optimise this technique, and novel designs such as the jetting heads with multiple nozzles for high resolution, fast, direct 3D structure printing with multi-materials, have been developed, as a state-of-the-art powerful technique for many applications [448, 449].

C) Vat photopolymerisation 3D printing (Digital light processing (DLP)/digital projection lithography 3D printing): In this technology, optical sources with specific wavelengths are used to cure the photocurable polymer selectively, in the vat container in a layer-by-layer manner, to fabricate the 3D structure. The whole process is similar as that of the conventional stereolithography (SLA) technique. So far, many types of vat photopolymerisation-3D printing with desired printing speed and resolutions, have been developed, such as the DLP-3D printing, two-photon or multiple photons-based polymerisation (TPP), continuous liquid interface production (CLIP) and computed axial lithography (CAL).

With similar fabrication process as SLA and selective laser sintering (SLS) techniques, DLP-3D printing uses different state of materials, configuration setup and light source [448]. Generally, the setup of the printer contains a connected computer, a vat having a transparent bottom and filled with the photocurable materials, a z-axial direction movable building platform controlled by a motor, a special digital light projector screen as the light source, and the digital micromirror device (DMD) as the heart of this printing technique to control the light beams by the binary pulse-duration modulation technique [450]. During printing, light of a specific wavelength is emitted from the light source passing through the transparent bottom of the vat to cure the inner photosensitive materials at the designed places of the building plate, where thin layers of

photopolymerised materials will be piled up to form the 3D structure layer by layer from the bottom layer to the top layer as the building plate moving up. The 3D pattern, thickness of one layer, speed and distance of the moving plate for individual layer printing could be designed and set up in the connected computer. Different configuration of the 3D printer, light source (screen) and directional motion of the building plate may vary. The building plate will move up and down in the process of printing one layer, and continuously repeat the movement till all layers of the total structure have been printed.

Comparing to the SLA using the movable point light source, DLP applying the digital micromirror device as dynamic mask to form the whole pattern of an individual layer at a time rather than a voxel of the pattern layer, improve the speed of the printing process [448]. However, during the printing process, due to the motion of building platform and the photo-crosslinking mechanism, the light-driven polymerisation at certain place will be inhibited by the oxygen gas in the liquid material, forming the dead area in the pattern and causing a slow non-continuous printing process. In addition, the material ink should be photocurable and in low-viscosity liquid form, limiting the range of available source and quality of materials. In order to improve the resolution and printing speed, updated devices, such as the CLIP with additional oxygen inhibitor, TPP replacing light source with ultrashort two-photon laser pulse, and the CAL equipped with a rotational stage to send lights in a series of 2D arrays, have been developed, and various additives such as the diluent to reduce viscosity of liquid material, the radical inhibitor to impede the unwanted advanced crosslink, and the light absorber to control the depth of the polymerisation and light intensity, have been utilised in combination with photocurable materials and initiators, to enhance and control the quality of printing. Novel photocurable materials, multi-material printing and composite materials

for vat photopolymerisation-3D printing have also been paid increasing attentions, bringing hopes to overcome challenges of the printability and quality of materials in the future [444, 448, 450, 451]. Various common 3D-printing technologies are summarised in Figure 2.13.

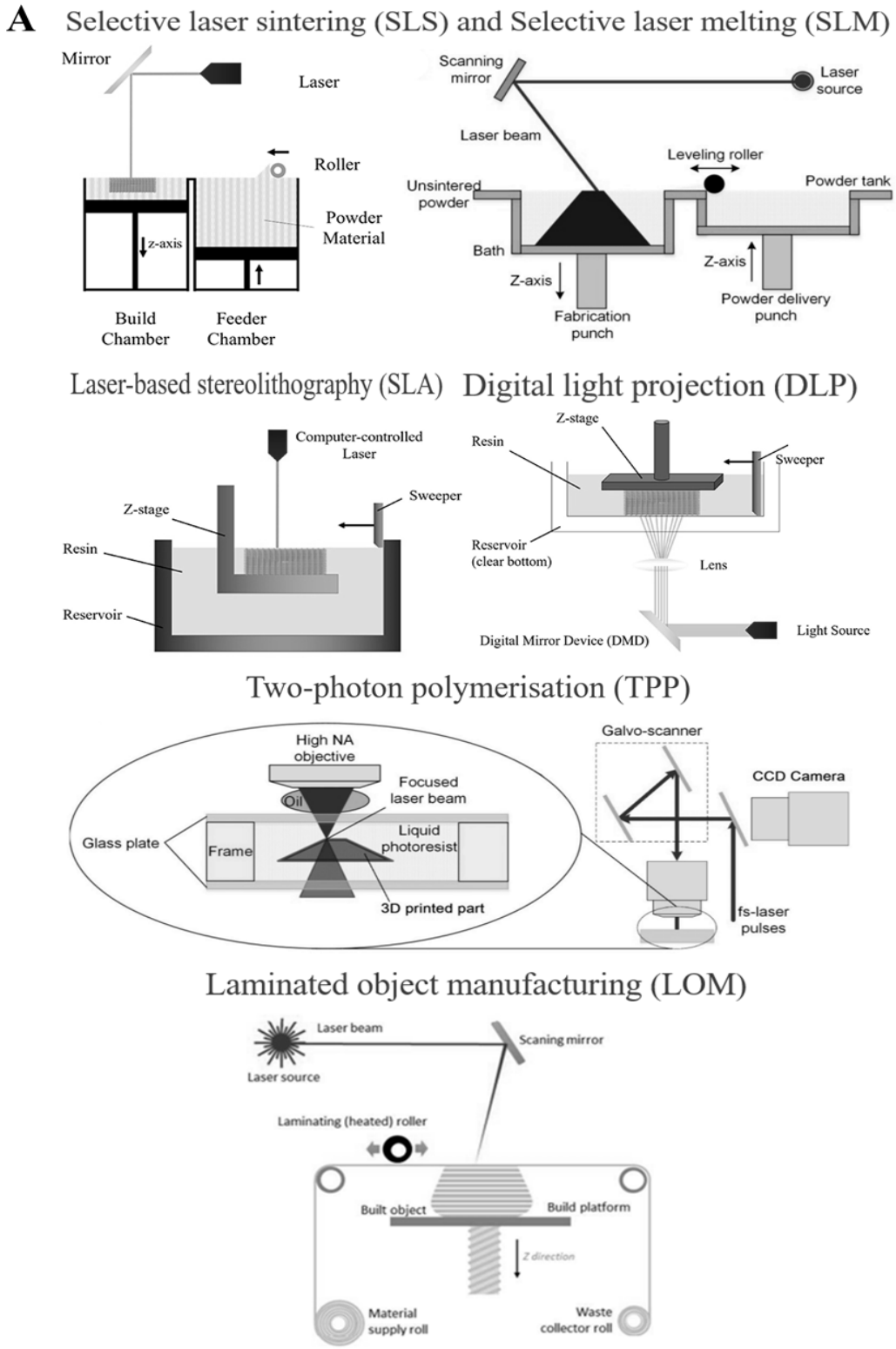

B Fused deposition modeling (FDM)

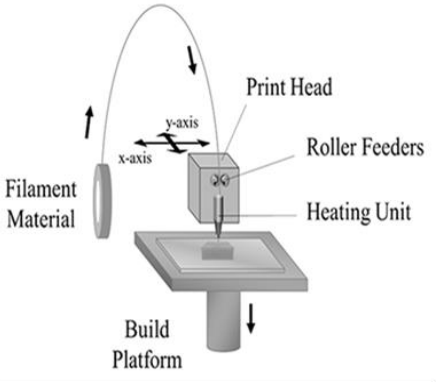

Direct ink writing (DIW)

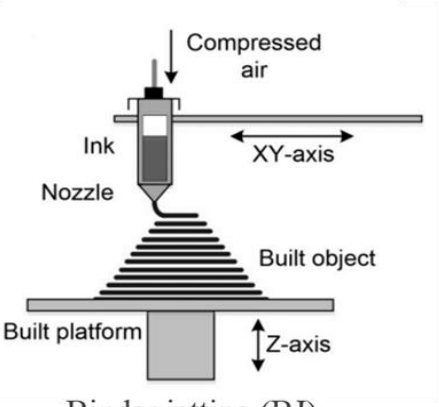

Electronic beam melting (EMB)

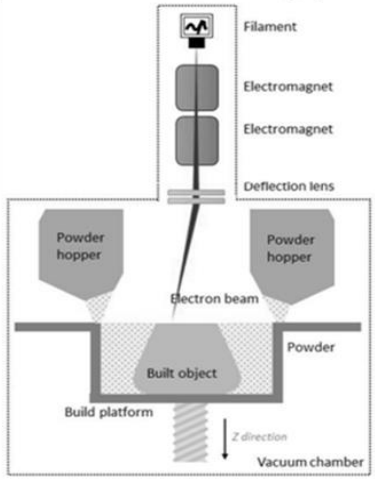

Binder jetting (BJ)

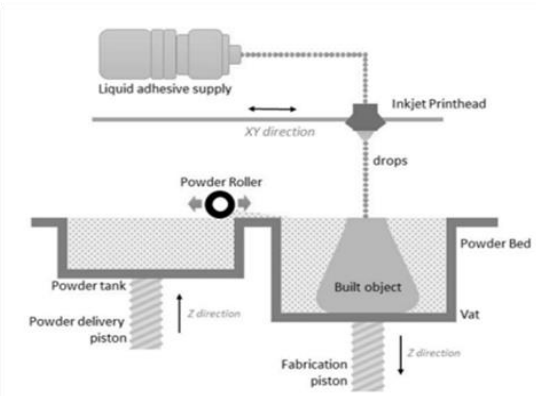

C Electrohydrodynamic printing (EHDP)

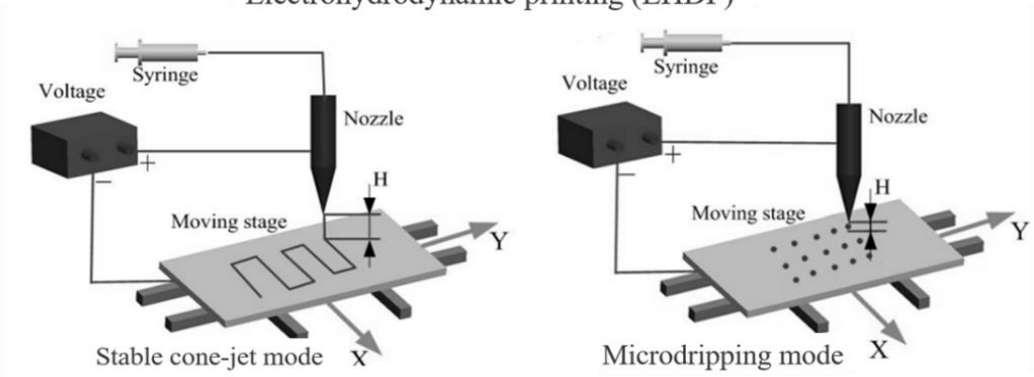

Inkjet printing

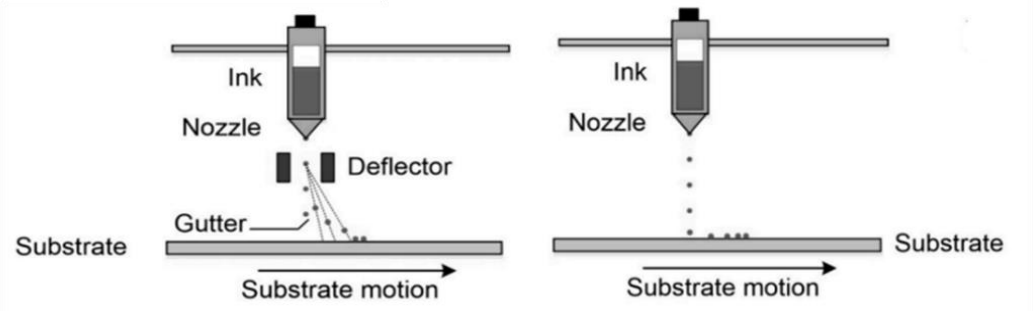

Continuous inkjet mode (CIJ)

Drop-on-demand mode (DOD)

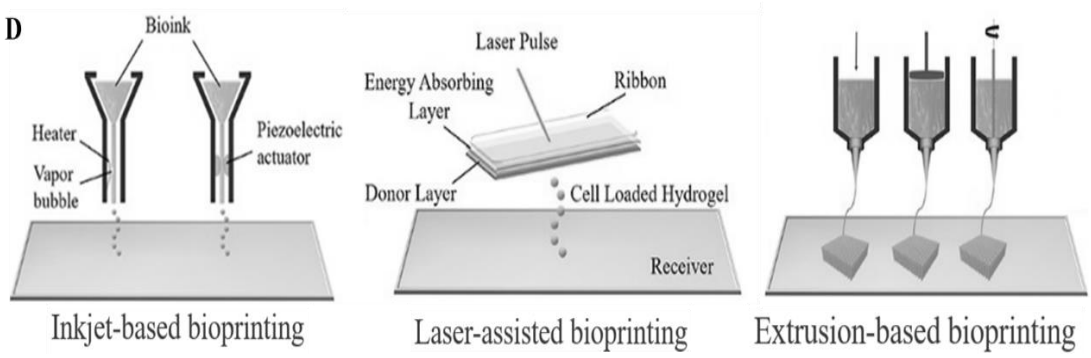

Figure 2.13 Schematic images of common additive manufacturing (AM)/3D printing technologies A: Laser/light assisted printing systems including selective laser sintering/melting (SLS/SLM), laser-based stereolithography (SLA), digital light projection (DLP), two-photon polymerisation (TPP), laminated object manufacturing (LOM) technologies. B: Extrusion-based systems using solid/semi-solid ink, including fused deposition modelling (FDM), direct ink writing (DIW), electronic beam melting (EMB), binder jetting (BJ) technologies. C: Electrohydrodynamic printing (EHDP) and inkjet printing technologies with two printing modes. D: Mainly applied bio-printing technologies, including inkjet-based, laser-assisted and extrusion-based bioprinting. Images were adapted from references [456-461].

Recent developments in 3D printing technology, hydrogel materials, bioactive factors, contribute to the rapid emergency of 3D bioprinting approaches for biomedical and TE applications, by which seeding cells carried by hydrogel materials could be fabricated into the target tissue with specific architecture directly. Extrusion, inkjet, DLP and FDM 3D printings, natural/synthesised hydrogel polymers and chondrocytes/MSCs have been successfully applied to bio-print cartilaginous tissue constructs *in vitro*. Regarding technology, hydrogel material and seeding cells, there are still unavoidable limitations and requirements. For the future prospects, combination of multiple printing techniques, novel and smart biomaterials to perform '4D printing', would be very promising and interesting areas for multidisciplinary researchers to study, practice and collaborate [418, 452-455].

2.4 Inhomogeneous articular cartilage/OC tissue and associated tissue engineering fabrication strategies

Previous studies have observed and confirmed that the articular cartilage/OC tissue naturally

present an anisotropic multi-layered architecture, where the inhomogeneity makes its inherent microenvironment unique, complicated and distinguishable. Some well-accepted inhomogeneous features inside the tissue will be stressed below, followed by discussions on fabricating this complex tissue by specific TE strategies.

2.4.1 Inhomogeneous multi-layered articular cartilage/OC tissue

In terms of the type, shape, size and density of resident cells, the morphology, distribution and organisation of major ECM components, and the average mechanical properties of each layer, there are depth-related zonal differences, some of which display gradients (Figure 2.14).

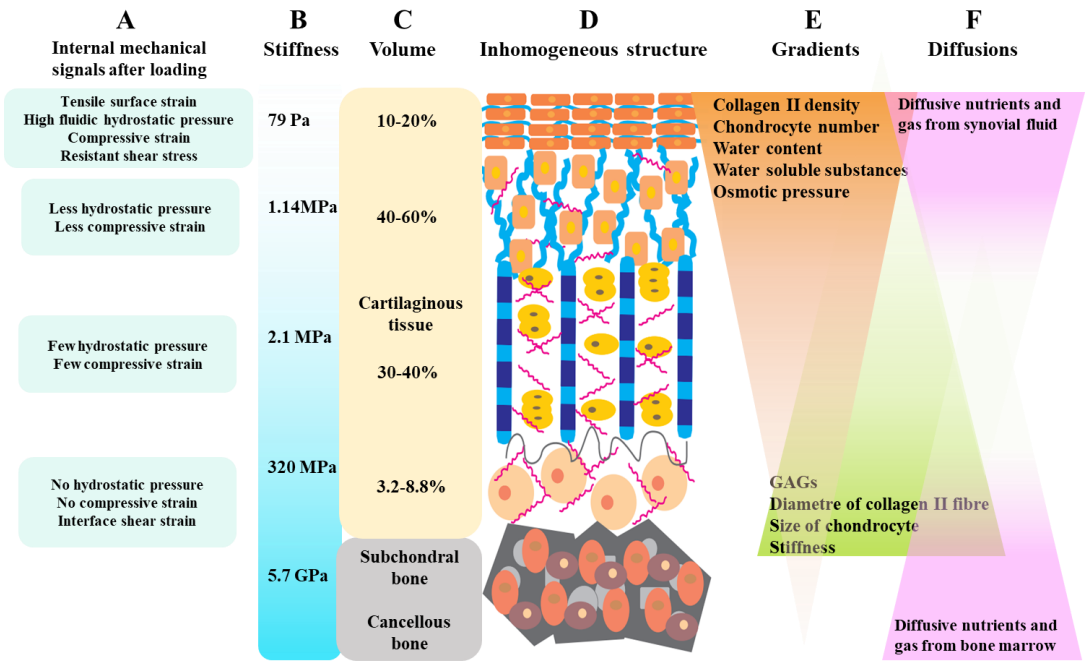

Figure 2.14 Illustrations of the inherent inhomogeneity inside the articular cartilage/osteochondral tissue A: List of internal mechanical signals inside the inhomogeneous tissue after joint loading. B: Approximate stiffness reported from literatures. C: Schematic image of the inhomogeneous articular cartilage/osteochondral tissue structure. D: Inherent gradients inside the tissue. E: Two-side diffusions of nutrients and gas inside the tissue. (Images were adapted from reference[9].)

Generally, for the type of major resident cells inside the OC tissue, there are chondrocytes in the articular cartilage part, hypertrophic chondrocytes in the calcified cartilage part, and osteocytes in

the subchondral bone part. Inside the OC tissue, there are rising gradients regarding the size of chondrocytes, diameters of type II collagen fibres, concentrations of GAGs inside the chondrogenic ECMs, and the zone-dependent mechanical properties. Correspondingly, there are decreasing gradients regarding the numbers of chondrocytes (cell density), concentrations of type II collagen fibres inside the ECM components, the water content and the associated water-soluble molecules [462]. Regarding these inhomogeneities, specific details will be stressed below.

2.4.1.1 The depth-dependent inhomogeneity of major components inside the OC tissue

Previous studies found that compositions of the articular cartilage/OC tissue are varied from diverse species and independent on the thickness of the cartilage of the species, but related to the unique characteristics of that species [463]. In the same species, as major components inside the multi-layered OC tissue, resident cells and surroundings are distinctively inhomogeneous in each layer and throughout the entire tissue, from the composition to arrangement, and the content of resident cells is not in proportion to that of their surroundings.

A) Chondrocytes as the main resident cells in the cartilaginous part, only possess 1-5% volume and 5% of the wet weight of the articular cartilage tissue, but are in charge of the establishment, development and maintenance of the major mass of the whole chondral part in the OC tissue. Chondrocytes produce, embed in and interact with the chondrogenic ECMs consisting of the type II collagen, proteoglycans, water and other substances, which in total account for 95-99% of the volume of the cartilaginous tissue [462]. Confirmed by staining images, the size and morphology of different zonal chondrocyte are varied with depth. There are small flat chondrocytes in the superficial layer, while in the middle layer, chondrocytes become round and bigger. In the deep

layer, larger spherical chondrocytes with lacunae, are often clustered in columns [22].The cellular density in adult human cartilage has been found on average about 23,500 cells in the cross-sectional area of 1 mm^2, which is corresponding to 2.35 million cells per cm^2, depending on locations of the samples [464], and from the superficial, middle to deep zones, the depth-dependent densities of local cells are approximately 3:2:1 [465], displaying a gradient. Although it has also been found that the location and distribution of the nuclei of chondrocytes could remain uniform, the cellularity of chondrocytes in the articular cartilage is depth-dependent and age-related [466, 467].Varied zonal chondrocytes present different biosynthetic capability and cellularity, contributing to the formation of depth-related zonal structure in the articular cartilage/OC tissue.

B) Collagen fibres: The type II collagen secreted by chondrocytes, contribute to 10-20% of the wet weight of the articular cartilage and account for 90-95% of all types of collagens in cartilaginous tissues [10, 22]. In the crosslinked type II collagenous ECM network, the interconnection between collagens and proteoglycan inside is mediated by the short type IX collagen and the diameter of type II collagen fibril is regulated by the copolymerised type XI collagen fibrils during assembly [22]. Type IX and XI collagens are also cartilaginous tissue specific, playing important roles in organising and stabilising the collagenous networks in chondrogenic ECMs [468]. In the subchondral bone part**,** osteoblasts, migrated BM-MSCs and osteoclasts, are located, producing the ECM network and contributing to the modelling and remodelling of this bony structure inside the OC tissue. The osteoid ECMs are made up of type I collagen fibres which are secreted by osteoblasts and mineralised with the osteocalcin. Except for mineralised ECMs, there are also unmineralised ECMs inside the osteoid ECMs, which are formed by the type I collagen fibres with osteonectin [7].Type I and XI collagens have similar molecular

chains and polymerised fibrillar forms as type II collagen [468].

Throughout the OC tissue, collagen fibres are organised into an anisotropic depth-related supportive framework, in the form of 3D continuous microfibrillar architecture to arrange local resident cells, immobilise water, and structurally provide tensile strength to the whole tissue [469]. Whereas individual layer inside the OC tissue presents depth-specific features regarding the composition and arrangement of collagen components [22, 462, 467, 469]. A wide variety of the diameters of the type II collagen fibril in the OC tissue has been observed, ranging from less than 20 nm in immature tissue to more than 100 nm in adult mature tissue. For example, the 'lamina splendens' structure, representing the most superficial layer of the articular cartilage, is formed by the horizontally oriented fine collagen fibres [470, 471]. Bundled collagen fibres from the middle zone passing through the deep zone to the calcified zone is on an average of 55 μm in diameter, different from individual collagen fibril bundles observed in the trabecular bone, which is about 70 nm in diameter [469].

Although between weight-bearing and less-weight bearing areas, healthy and diseased area, or different ages of samples, there are differences in the zone/depth dependent features of the volumes, densities of cells, matrix volume per cell, diameters of collagen fibres, and the thickness/volume of the articular cartilage/OC tissue [465], the depth-dependent inhomogeneity of major components inside the articular cartilage/OC tissue has been well-accepted. Taken together, in the superficial zone, small chondrocytes with flattened morphology are arranged in parallel alignment to the articular surface, in a very high and compact density. The small nuclei are located in the central area of cytoplasm. Collagen fibres (mainly type II and minor type IX) in this zone are thin, with small diameter (20-50 nm), and highly condensed in the organisation of flat layers or broad leaves,

in parallel to the joint surface. In the middle zone, chondrocytes are round shape with a reduced density, randomly oriented inside the thickest ECMs. The numbers (density) of the type II collagen fibres are reduced but their diameters are increased (60-80 nm). The randomly distributed type II collagen fibres in this zone are organised obliquely (the upper 1/3 length) to the joint surface and formed the interconnected network enclosing the chondrocytes with slightly increased volume. In the deep zone, chondrocytes are spherical, lower density with again increased volume. The distribution of chondrocytes in this zone is either singular or clustered, vertically piled up in columns perpendicular to the articular surface. The type II collagen fibres are similarly, oriented vertically to the joint surface (connecting the lower 2/3 length of the fibre in the middle zone), with again reduced numbers (density) but increased individual fibril diameters (40-100 nm). In the transitional calcified zone, resident chondrocytes are hypertrophic chondrocytes with the largest volume but the lowest cell density, sporadically being enclosed and supported by the fewest amount (density) of isotropic collagen fibres. These bundled type II collagen fibrils have the largest diameter (100-110 nm), which are extended from the deep zone and passing through the tidemark line to anchor in this zone. Type X collagen is specifically synthesised by hypertrophic chondrocytes, and detected in the hypertrophic zone of the growth plate tissue in the immature cartilage, in the calcified zone of a healthy cartilage, and in the OA cartilage. The length of this molecule is around 138 nm about the half of that of those typical fibrillar collagens (type I, II, III and V). The reducing density of the type II collagen from the top to the bottom layer of the articular cartilage was found in accordance with increasing impacts of other types of collagens observed in the middle, deep (the type VI collagen in the interterritorial and pericellular matrix) [472] and calcified zones (type X collagen) [6], on regulating the size and crosslinking of the ECM network

and on interacting with other biological molecules [462]. In the subchondral bone part, resident cells are osteoblasts and the major type of collagen fibre is produced by osteoblasts to form the osteogenic ECMs containing mainly the type I collagen fibre (more than 95% of the dry weight) and tiny amounts of other isoforms. In this part, no chondrocytes and type II collagen fibres were observed [473].

2.4.1.2 The depth-dependent inhomogeneity of other components inside the OC tissue

A) Gradients of other biocomponents of chondrogenic ECMs: Apart from the collagen family, another necessary component in chondrogenic ECMs is the proteoglycan protein family accounting for about 10-20% wet weight of the cartilaginous tissue and structurally providing compressive strength [10]. Proteoglycans are protein polysaccharide molecules in which the aggrecan monomer is the largest and most abundant member, in combination with other minorities which have smaller size than aggrecan and secreted by chondrocytes, such as biglycan, decorin and fibromodulin, to contribute to immobilising chondrocytes (type VI collagen in PCM) and other molecules, to connect and fill intervals of the fibrillar network, and to stabilise the solid phase (type II collagen) of chondrogenic ECMs [22].

Glycosaminoglycan (GAG) is the type of carbohydrate with repeated disaccharide molecules, which enable the GAG chain to bind proteins by sugar bonds. The keratin sulphate (KS) and chondroitin sulphate (SC), are two common subtypes of GAGs in the articular cartilage, in addition to others such as heparan sulphate, dermatan sulphate, and hyaluronan or HA. GAG molecules have negative charge, resulting in attractions to water and cations, and repellents to those having negative charges (each other) [6]. Proteoglycans consist of a protein in the middle, and one or more

attached GAGs in surrounding areas. Aggrecan monomers are often formed into a complex which is further greatly glycosylated with approximately 90% carbohydrate in components. It is found that one aggrecan molecule can covalently connect with highly negatively charged sulphate GAG chains containing about 60 KS and 100 CS to form the repeating disaccharide units in about one sulphate group per disaccharide manner. And at the N-terminal of aggrecan molecule, there is a globular protein which has great affinity with hyaluronan (or HA) molecules and link proteins (glycoprotein). The structure of HA molecules is a polysaccharide chain with no branch. HA is responsible for integrating many aggrecan monomers into large aggregates, whereas the function of link proteins is to stabilise the connected HA backbone with GAG chains of large aggrecan aggregates [10, 22].

Concentrations of proteoglycan and GAG in chondrogenic ECMs, also have depth-related gradients inside the whole OC tissue. In the superficial zone, they have the lowest concentrations which are progressively increasing to the highest amount in the calcified zone [10]. In addition, due to the interweaving proteoglycans which are covalently aggregated by aggrecans with negatively charged GAGs, there are negatively charged microenvironment within the chondrogenic ECM network. Therefore, those attracted cations could increase the osmotic pressure for water which would be subsequently attracted and trapped to reduce the osmosis. It was reported that the osmotic pressure within articular cartilage is about 350 to 450 mOsm, higher than that of the other tissue part where the pressure is about 280 mOsm [22]. The entrapped water is then confined by the collagen fibrillar ECM network due to electrostatic forces to form the liquid phase of chondrogenic ECMs and consequently restrained by the integrated solid phase of chondrogenic ECM network, thus leading to the Donnan effect, in which involves the generation of the osmotic

pressure by water absorption, tissue swelling, counteracting forces to prevent tissue swelling and fluid flowing, and consequently the high tensile stress within the chondral part of the whole OC tissue [22].

B) Gradients of water content and water-soluble substances: As mentioned that water content accounts for up to 75-80% of the weight of the articular cartilage [22], 30% of which is trapped in the intrafibrillar space by collagen fibres, another smaller amount is located in the intracellular space and the rest resides in the porous matrix [33]. Water trapped by collagen fibres is found in a gel form displaying a similar gradient as that of type II collagen fibres inside the OC tissue. For instance, the water content is about 80% in the superficial zone but decreases progressively down to 65% in the deep zone and becomes almost zero in the SB area inside the OC tissue [33]. Water kept in the AC part provides a media to disperse nutrients to feed chondrocytes and contributes to establishing the low-friction interface between the surface of the AC and the synovium within the contact area of the synovial joint [33]. The depth-related gradient of water also contributes to the interior zone-related hydrostatic pressure for each zone to respond to and resist internally distributed loadings.

The SB part, together with the calcified zone divided by the tidemark line, are mineralised areas reflecting transitive constituents and functions inside the OC tissue, where the hypertrophic chondrocytes contribute to deposit minerals, produce other type of collagen (type X collagen) to form the calcified zone [474], assist, and may be able to transdifferentiate into osteoblasts in company with other recruited osteocytes and migrated MSCs to compose the SB part and deposit bony matrix [22]. Taken together, the SB part, comparing to the AC part, has the lowest water content, the fewest components related to chondrogenic ECM and the lowest elasticity, but

strongest stiffness and highest grade of mineralisation.

Water content throughout the OC tissue, displays a depth-related gradient, hence it is reasonable that balanced concentrations of water-soluble molecules and substances present a similar gradient inside the tissue, such as small soluble inorganic ions (sodium, calcium, potassium and chloride), systemic hormones, dissolved regulatory peptides, and local growth factors (TGF-β, IL-1, tumour necrosis factor-α, insulin-like growth factors) by autocrine [22, 33], which are able to dissolve and transported to and from chondrocytes by the osmotic pressure in the liquid phase of chondrogenic ECMs and by interstitial fluid flow responding to intermittent mechanical forces [22].

C) Diffusions throughout zones: As connective tissue, chondrocytes located in non-mineralised AC zones of the OC tissue, partially obtain nutrients and gases by passive diffusion mainly from the synovial fluid [22]. Whereas the SB connecting to the bone marrow of a hard bone, whose modelling and remodelling during development and diseases, is fed by those extended blood vessels delivering the requested nutrients and gases [475]. In the calcified transitional part, hypertrophic chondrocytes endure and prefer the hypoxic microenvironment. Although there were found both invasions of uncapped open blood vessels in the growth plate and penetrations of capped non-looped capillaries in calcified zone [26], nutrients in the calcified zone, are predominantly diffused from the SB part which is fed by bone marrows via few invaded vessels during tissue development. Dynamic variations of the thickness of the calcified zone, and the age and anatomical site dependent location of the tidemark line, suggest their movements against the invasion and extension of open-end blood vessels, therefore, the mineralised part could be physically separated from the unmineralised part without any direct contact, any effective diffusion of nutrition, and any potential invasion of vascular system [26]. As a result, inside the synovial

joint, throughout the whole OC tissue there are diffusions from both synovial fluid and bone marrow, where these supplied contents of nutrients and gases (oxygen) present depth-dependent inhomogeneities [15].

D) Ultrastructure inside chondrogenic ECMs: Evidences from histological staining, labelling and microscopic technologies like confocal microscopy, transmission electron microscopy (TEM) or Raman spectrum microscopy confirmed an existence of a three-zone ultrastructure of chondrogenic matrices around chondrocytes in cartilaginous tissue, including the pericellular matrix (PCM) zone, territorial matrix (TM) zone and inter-territorial matrix zone [10] (Figure 2.15). The inter-territorial matrix known as the chondrogenic bulk ECMs accounts for the most volume which is mainly made up of the type II collagen fibres and organised differently among each specific zone. The TM zone contains the surrounding area of chondrocytes and their PCMs where the chondrocytes could stay individually or in a cluster or in a column [10]. The most important PCM zone consists of chondrocyte and its PCM which is a narrow rim (2 μm wide) of tissue closely contacting with the membrane of chondrocyte [10, 122]. The chondrocyte with surrounded PCM is termed “chondron” [122], which is rich in proteins such as the laminins, some cell membrane-associated molecules (anchorin CII, nidogens, biglycan, βig-h3), TGF-β induced protein, latent-TGF-β-binding protein-2, ADAM28, triosephosphate isomerase, peroxiredoxin-4, proteoglycans (aggrecan, hyaluronan, decorin and abundant perlecan), fibronectin, collagen (type II, IX and abundant VI) and von Willebrand factor A domain-related proteins which bind the type VI collagen and perlecan [10, 124, 476, 477]. By virtual of micropipette aspiration, enzymatic isolation and other techniques including *in situ* imaging, immunofluorescence-guided atomic force microscopy, computational modelling, mathematical modelling and finite element modelling, especially from

the 3D reconstructed images, the morphology and arrangement of chondrocytes were determined to be consistent with that of chondrons in each zone of the articular cartilage tissue, contributing to the depth-related local architecture inside the chondrogenic matrix, inter-territorially [122].

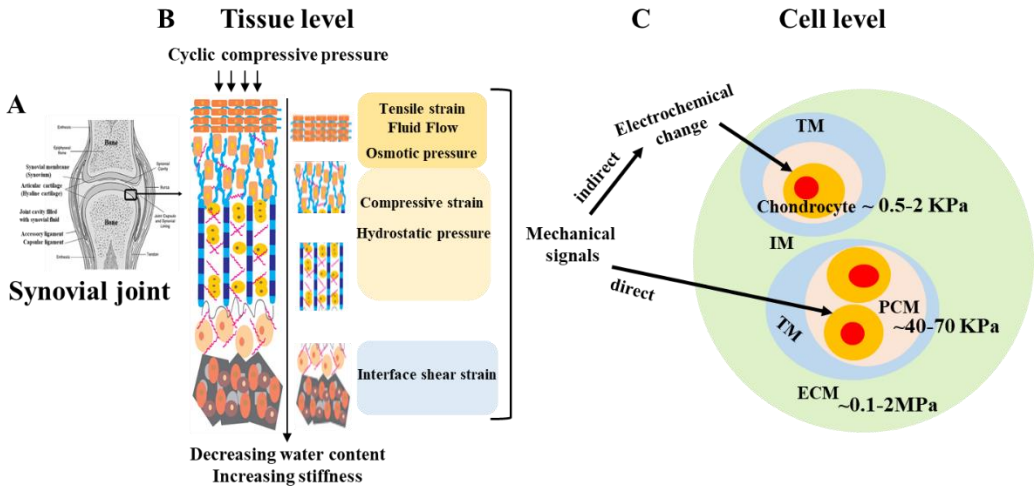

Figure 2.15 Schematic images of mechanical forces throughout the entire osteochondral tissue of a typical synovial knee joint after loading and mechanical signals transmitting chondrocytes.

A: Anatomic image of a typical synovial knee joint. B: Common mechanical forces throughout the osteochondral tissue after joint loading. C: Images illustrating two ways of mechanical signals transmitting to local cells inside ECMs and the elastic modulus gradient outward from chondrocyte, to the PCM and ECM. TM: the territorial matrix. PCM: the pericellular matrix. IM: the inter-territorial matrix. ECM: the extracellular matrix. Images were adapted from references [90, 478, 479].

Moreover, in contrast with chondrogenic bulk ECMs, it was found that although chondrogenic PCMs in isolated chondrons, have similar zone-related variation as ECMs, they possess distinctive components immunohistochemically featured by type VI collagen and perlecan [476], and intermediated biomechanical properties (about 1/3 weaker than that of ECMs but stiffer than that of the chondrocyte) [479]. Despite the mechanism is not fully understood, chondron has been considered as a functional unit playing a critical role in regulating the biophysical and biochemical microenvironments of chondrocytes locally inside the chondrogenic ECMs of the articular cartilage of the OC tissue [124, 480], involving cellular deformation and metabolic activity responsive to the local stress-strain, micro-mechano-transduction via solid phase of ECMs,

swelling behaviour, osmotic and fluid flow in microenvironment, and electrochemical potentials around chondrocytes [32, 123, 124, 126].

2.4.1.3 The depth-dependent inhomogeneity of biomechanical properties inside the OC tissue

As mentioned, a piece of AC tissue is confined by neighbouring tissues inside the OC tissue which are either pressurised and limited in liquid permeability or impermeable. Hence the actual fluid flow is often restricted in limited zones and as a large amount of water is tended to be exuded, the solid ECMs reduce inner porosity which further decrease the local permeability and possibility of the remaining fluid flow to deeper zones (deep zone and calcified zone), but significantly increase the local compressive strain (consolidation) resulting in a potentially local deformation and loads transfer inside the chondrogenic ECMs around chondrocytes [32, 36]. According to some studies, the distribution of compressive strains in response to the high hydrostatic compressive stress created by the fluid flow, being measured throughout the AC, displayed a zone-dependent gradient which is more than 50% located in the superficial zone, 10 to 20% in the middle zone and 0 to 5% in the deeper zones (deep and calcified zones), consistent with the confining trends of pressurised fluid flow caused by joint loading in the AC part.

As a stratified complex tissue dealing with forces, biomechanical properties of the OC tissue have been investigated both individually and integrally. Due to the zonal structure and depth-dependent biochemical components, specifically the water content of liquid ECMs, the size and density of type II collagen fibres throughout zones, and the organisation of the solid ECM network, biomechanical properties of individual zones are varied with depth. Due to the stiffness of articular cartilage tissue, would increase as the applied strain increases, and the modulus is time-dependent,

it is currently not described by a single Young's modulus, but the calculated equilibrium modulus after mechanical testing, where a series of known strains were employed, and the force-stress values at equilibrium were recorded to draw the stress-strain curve [33]. Although the studied equilibrium properties of tissue samples including Young's modulus/aggregate modulus and Poisson's ratio may be varied from the techniques used (values measured by indentation test were found higher than those from compression test and were highly related to the size of indenter [481, 482]), the characterised theoretical model (biphasic isotropic or anisotropic samples) and the sites or species of the sample [481], according to previous studies the approximate equilibrium modulus of articular cartilage tissue in knee joint, was about 0.5~0.9MPa [483], while individually, it was increased from the superficial layer at 0.079MPa, 1.14 MPa of the middle layer, to 2.1 MPa of the deep layer [484]. Whereas the elastic modulus of the human SB in the knee on average were around 1.15~2.3 GPa, higher than that of the calcified cartilage which was measured around 0.32 GPa [485, 486], and lower than those of the cancellous bone and cortical bone which were measured about 1.3~7.8 and 12~20 GPa, respectively [35, 473, 486].

The equilibrium modulus reflecting the stiffness of the cartilage, increases from the superficial zone (0.079 MPa) to the deep zone (2.1MPa) [7, 484, 487]. In contrast, the measured tensile modulus decreases from the superficial zone (25MPa) to the deep zone (15MPa) [484, 488, 489]. As the mineral deposition increases throughout OC zones, biomechanical properties within the OC tissue from the AC to the SB are varied by several orders of magnitude, offering an anisotropic biomechanical microenvironment for zone-specific resident cells to survive and function.

Thus, it can be seen that, there is an inhomogeneous anisotropic microenvironment inside the multi-layered OC tissue, from the zonal structure and arrangement of major components, ultrastructure

inside ECMs, depth-related inhomogeneities of other components, diffusions, to other associated issues (e.g., osmotic pressures, biomechanical properties and responses) [22]. Different from conventional strategies for simple homogeneous tissue regeneration, to design and fabricate appropriate biomaterial scaffolds simulating the anisotropic microenvironment toward successful complex inhomogeneous tissue reconstruction, is more difficult, and full of challenges. A few specific TE strategies toward reconstruction of the inhomogeneous articular cartilage/OC tissue will be discussed below.

2.4.2 TE fabrication strategies toward inhomogeneous articular cartilage/OC tissue reconstruction

Development and maturation of tissues and organs are spatiotemporally regulated processes, which are partially determined by the specific microenvironment with many factors, such as various biochemical and biophysical cues. TE strategy by manipulating its fundamental elements and potential impact factors to provide a biomimetic microenvironment for seeding cells to proliferate and differentiate, allows the fabrication of complicated heterogeneous tissues or organs *in vitro*. For reconstructing the multi-layered articular cartilage/OC tissue with inherent features of inhomogeneities and gradients, various fabrication techniques, tissue culture systems, novel biomaterials and methods have been developed. As mentioned, the multi-layered articular cartilage/OC tissues are nonuniform, having depth-specific local resident cells, 3D stratified zonal structures and zone-specific microenvironments. Here are some discussions on the TE strategies in terms of simulating fundamental TE elements such as seeding cells, biomaterial scaffold and tissue culture system, specifically toward the inhomogeneous articular cartilage/OC tissue reconstruction.

2.4.2.1 Applications of inhomogeneous seeding cells

Seeding cell is a key element in TE strategy to regenerate target tissue. Previous studies have observed that by applying inhomogeneous seeding cells, regarding the seeding density and the type of cells, the inhomogeneous articular cartilage/OC tissue could be engineered *in vitro*.

2.4.2.1.1 Seeding density

Seeding density is important for cells to keep connection and communication in culture, by which cellular phenotypes and genotypes could be maintained and regulated. Previous studies have confirmed that sensitive cells such as stem cells need certain population in culture to keep their stemness, and chondrocytes in culture, require appropriate seeding densities for them to stabilise their specific morphology and differentiation capabilities [490, 491]. By simulating the varied densities of seeding cells, functional cartilaginous tissue might be produced rapidly.

For example, 96 biocompatible and bioresorbable implants consisting of non-woven PGA mesh scaffold and different concentrations of chondrocytes were designed and fabricated. After *in vitro* culture for one week, followed by subcutaneous implantation into animal mice models for months, cell density-related and time-dependent cell viability and neocartilage tissue production were observed, suggesting the possibility of optimising the quantity and quality of the engineered cartilaginous tissue by using varied density of seeding cells [492]. A 3D porous scaffold was seeded with chondrocytes in a series of densities and cultured. After two weeks , differences in the thickness, wet weight, contents of DNA, collagen and GAGs, and different mechanical property (compressive modulus) of the engineered cartilage were observed, displaying a seeding density-dependent manner, suggesting the impact of cell density on the properties of engineered tissue

construct and the potential of fabricating inhomogeneous tissue by varied seeding cell densities [493]. A series of tissue constructs with chondrocytes and type II collagen gel, were fabricated by 3D bioprinting, in which there were three concentrations (high, medium, low) of chondrocytes and two types of distributions (homogeneous, with gradient). The medium concentration of chondrocytes and the gradient of seeding cells were mimicking those in human articular cartilage. After a few weeks in culture *in vitro*, they observed the similar cell density-related chondrogenic ECM generations and chondrogenic ECMs with gradient were developed by the construct with a gradient of seeding cell distributions, suggesting the importance of cell density and pattern of cell distribution for the articular cartilage tissue fabrication *in vitro* [494]. A nonuniform tissue construct composing human articular chondrocytes-laden alginate-PCL composite was also engineered by 3D bioprinting, in which three different densities of seeding cells to simulate the superficial, middle and deep zones of the human articular cartilage tissue, were designed. After 25 days in chondrogenic inducing medium, a high cell viability in construct, density-related chondrogenic ECM productions, and smooth interfaces between zones with different seeding density, were confirmed [495].

2.4.2.1.2 Zonal chondrocytes

Due to the development of imaging techniques and biotechnologies, the zone-specific chondrocytes locating in different layers of the articular cartilage/OC tissue have been observed, isolated and investigated. Apart from their distinct morphologies and sizes, other differences and properties of these subpopulations of articular cartilage chondrocytes have also been found, such as the highly instable phenotype and dedifferentiation *in vitro* (2D and 3D) [496], different

capabilities of chondrogenic ECM synthesis (gene and protein level) and accumulation (3D), varied differentiation states between immature and adult cell sources of zonal chondrocytes, and depth-dependent expressions of specific genes and proteins (e.g. zonal markers such as the superficial zone protein, integrin for migration, motility and integration) [497], ECM component-related functional gene and protein expression profiles and secretion, depth-related cell responses in 3D culture system, and varied biomechanical and biochemical features of the engineered tissue constructs derived from different zonal chondrocytes [498-500], varied metabolism for energy and nutrition (oxygen consumption) [501, 502], and different responses to growth factors in culture (3D) [502].

Apart from seeding density variations, lots of studies also explored the articular cartilage/OC tissue fabrication by seeding varied zonal chondrocytes (Figure 2.16). For example, chondrocytes from the superficial and middle zones could be isolated respectively by sequentially enzymatic digestions, and harvested in 3D alginate bead-based expansion system *in vitro*. Then three different tissue constructs with homogeneous zonal chondrocytes (superficial and middle zones) and combined two-layer chondrocytes (without scaffold/substrate) could be fabricated. After a few weeks in culture *in vitro*, zone-related differences in chondrogenic ECM productions and mechanical properties, between those constructs, were observed, in which highest expression level of superficial zone protein was found in the superficial area within composite constructs and intermediate features were also observed in composite constructs [503]. After seeding chondrocytes isolated from full-thickness articular cartilage tissue, middle-deep zone, and deep zone, individually, on porous substrates made up of ceramic and cultured about two months, differences in the thickness and size of chondrogenic ECMs, and varied ECM component synthesis

were observed, in which the subpopulation of chondrocytes from deep zone developed thicker and larger ECMs, cells from full thickness cartilage produced more type II collagen, and chondrocytes isolated from middle-deep zone, generated more proteoglycans and higher compressive modulus than those from others, showing the possibility to generate inhomogeneous tissue constructs by using subpopulations of cells from different sources [504]. A bilayer articular cartilage tissue construct containing zonal chondrocytes embedded 3D PEGDA hydrogels was fabricated and after three weeks in culture *in vitro*, different ECM productions and mechanical properties of the bilayer construct were confirmed, in which, in particular, chondrocytes from superficial zone generated more ECM components (collagen, GAG) and mechanical properties (compressive and shear modulus) than those from deep zone. The inhomogeneous two-layer tissue construct displayed the highest mechanical properties, comparing to those of single layer constructs [499]. Chawla et al. further confirmed the regenerative capability of implanting this type of inhomogeneous multi-layered tissue construct which was developed *in vitro* by alginates embedded with zonal chondrocytes, into animal pig model with full-thickness chondral defect *in vivo*, for about a short period of time (one week). Cellular interactions between implanted and surrounding cells were also observed [505]. Studies also confirmed that, in 2D expansion, zonal chondrocytes (cells isolated from superficial, middle and deep zones) would lose their abilities to produce their specific zonal markers (e.g. type II, VI, IX, collagens, clusterin, cartilage oligomeric protein), however, in hydrogel-supported 3D culture system *in vitro*, comparing to scaffold-free pellet culture system, zonal chondrocytes could regain their abilities to produce their specific zonal markers (e.g. clusterin and cartilage oligomeric protein) and zone-related functions (e.g. higher production of GAGs by chondrocytes isolated from deep zone, than that from cells derived from superficial zone)

[506, 507], although the generation of superficial zone protein was then found correlation with the concentration of hydrogel materials [507].

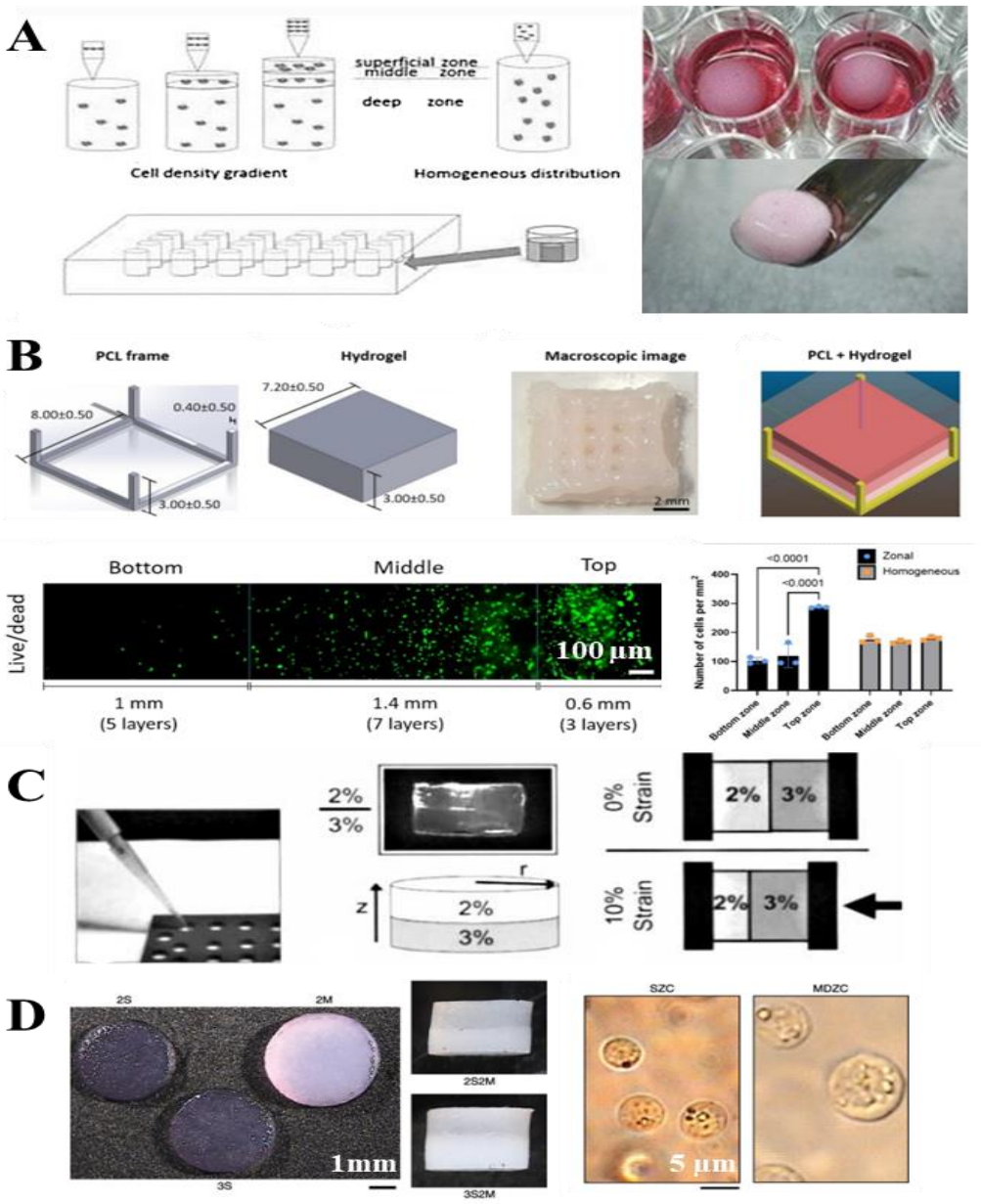

Figure 2.16 Schematic images illustrating applications of inhomogeneous seeding cells in cartilage reconstruction.

A: Zonal cartilage construct was engineered by bio-printed collagen type II hydrogel with biomimetic chondrocyte density gradient from bottom to top, and cultured in a 24-well plate for 3 weeks. B: PCL-reinforced alginate scaffolds with different cell density zones were fabricated by bioprinting. The fluorescent live/dead staining (green: live; red: dead) was applied to show cell distributions in the scaffold with different cell densities mimicking different zone: bottom (5E6 cell/mL), middle (10E6 cells/mL), and top (20E cells/mL). The gradient could be maintained in the scaffold over time. From images based on live/dead staining and bright-field images of H&E staining (matrix: violet; nuclei: dark purple), the cell distribution for the three different zones, bottom, middle, and top, of the zonal and homogeneous control scaffolds were quantified the number of cells (n = 3; p-

values < 0.05 are shown). C: Two concentrations of agarose (2 and 3%), were seeded with chondrocyte both at 60 million cells/ml, and gelled in a customised template to form a bilayer construct. D: Zonal chondrocytes were isolated and seeded in different concentration agarose to construct different single layer. Constructs seeded with MDZCs (2M, 2S2M, 3S2M) were opaque and whitish, similar to native cartilage. The left scale bar is 1 mm. SZCs: superficial zone chondrocytes SZCs); MDZCs: middle-deep zone chondrocytes. The SZC-only constructs are 2S and 3S. Bilayer constructs are 2S2M, and 3S2M. 2S2M construct: 2% agarose SZC/2% agarose MDZC; 3S2M construct: 3% agarose SZC/2% agarose MDZC. Chondrocytes from superficial zone were smaller than those from middle and deep zone. Images were adapted from references [494, 495, 507, 508].

To date, strategies of using zonal chondrocytes to simulate the zonal structure of articular cartilage toward the neo-tissue regeneration are still remained largely in the research field. Few studies have moved into clinical fields, potentially due to some challenges such as the requirement of appropriate and standard protocols to isolate and identify these subpopulation cells from varied tissue samples, and insufficient numbers of these zonal chondrocytes that could be obtained and expanded, remaining further studies [509].

2.4.2.1.3 Co-culture system

Since first studies about co-cultured oocytes for maturation and pre-implantation, co-culture system has become an important approach to study the interactions and communications between cells and cell-environments, the underlying mechanisms, and mutual impacts on cells and their surrounding microenvironments [503]. Many signalling pathways, such as the endocrine, paracrine, autocrine signalling pathways, the synaptic signalling pathways, juxtacrine signalling pathway and intracellular exchange of signals via the gap-junction communications, are involved in various types of cellular communications [503]. Previous studies have found that, in co-culture systems, cellular interaction/communication is mainly regulated by the distance and interactive ability between cells, contributing to the tissue formed by these co-cultured cells *in vitro*. Hence, comprehensive knowledges of these interactions/communications and the underlying mechanisms

are essential and providing a powerful tool for TE studies and associated clinical applications [503]. Differentiation pathways between MSCs and specialised cells (chondrocytes, osteoblasts, adipocytes), dedifferentiation phenomenon between chondrocytes and MSCs, and the trans-differentiation process between chondrocytes and osteoblasts/adipocytes, have been observed and investigated the underlying mechanisms and related impact factors [510-516]. Instead of using single type of seeding cell, co-culture systems (direct/indirect, 2D/3D) in TE strategies, containing multiple types of cells (chondrocyte, osteoblast, synovial fibroblast and MSCs) to regenerate the inhomogeneous articular cartilage/OC tissue *in vitro* and *in vivo*, have been also extensively investigated [247, 503, 517-537]. For example, in direct co-culture system such as micromass/pellet culture or indirect co-culture system such as using Transwell® plate or well-designed biomaterial scaffold/substrate, it was found that, primary chondrocytes mixed (1:5 ratio or mixture of individual micromass) with a series of other types of cells (heterogeneously) such as expanded chondrocytes, fibroblast, mouse feeder cells and ESCs, to form micromass to culture *in vitro*, could all generate cartilaginous tissues, where mainly the primary chondrocyte determined the production of chondrogenic ECMs [518]. To best simulate the cellular environment of articular cartilage *in vivo*, chondrocytes were often co-cultured with MSCs in studies of both intraspecies and interspecies [503, 517]. From both *in vitro* and *in vivo* studies, outstanding positive results have been observed, such as an improved chondrogenesis of MSCs, the increased proliferation and function of chondrocytes, the enhanced engineered neo-tissue in biochemical and biomechanical properties, mutual impacts between co-cultured cells via specific secretions and interactions in co-culture system [247, 519-526] (Figure 2.17).

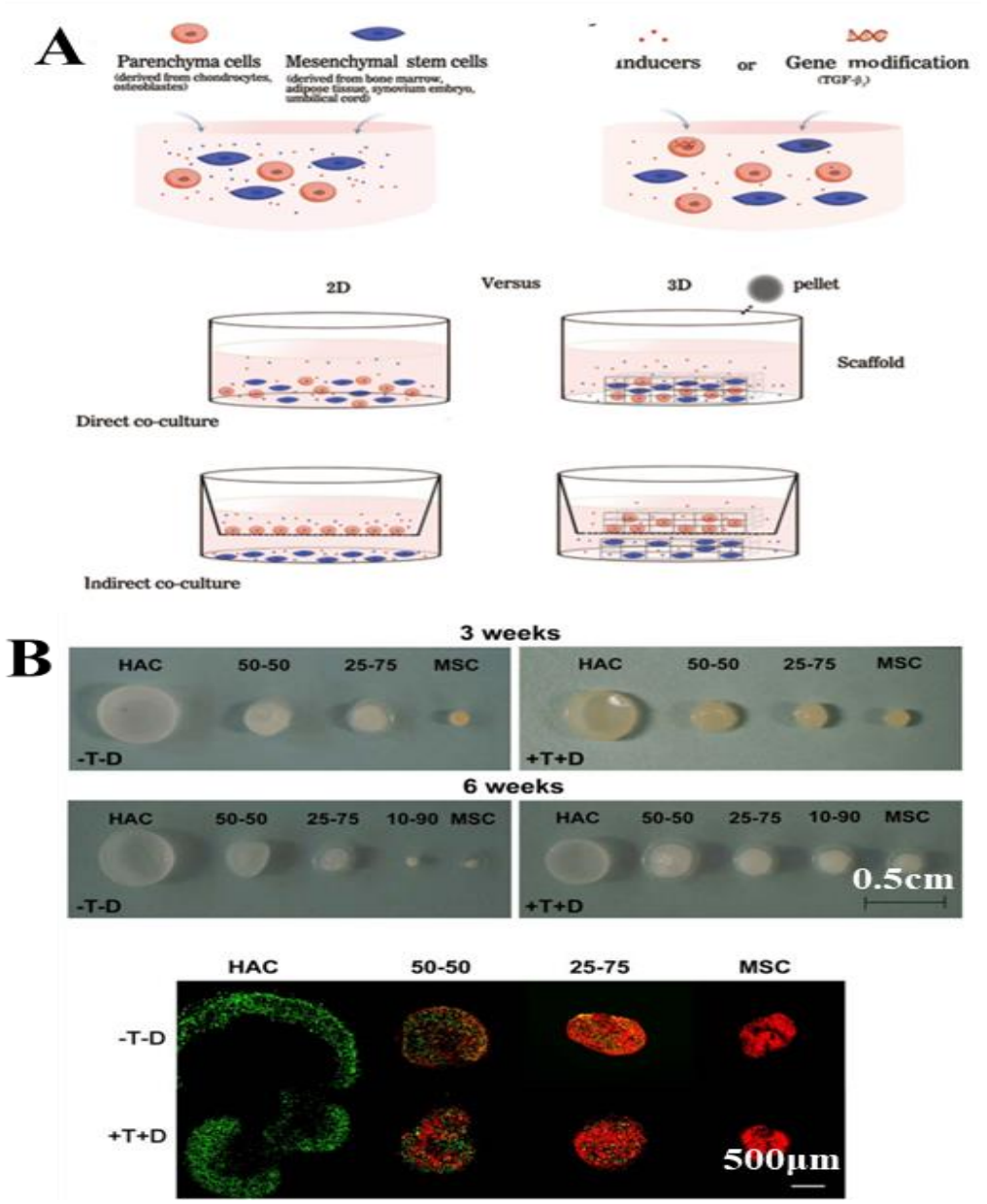

Figure 2.17 Illustrations on the application of co-culture system for cartilage regeneration.

A: Schematic images displaying different co-culture system. B: Images of cell pellets produced by chondrocytes, MSCs alone and combined at different percentage (50:50, 25:75 and 10:90 of HAC:MSC), presenting different shape and random distribution of co-cultured pellets, after incubation for 3 weeks in different condition. With/without chondrogenic inducing factors in medium denote +T+D/-T-D. Images were adapted from references [247, 537].

However, some challenges and problems should be paid more concerns, such as the optimisation of the ratio between different types of cells in co-culture system to get best results, are often required and may be species-related; chondron co-cultured with MSCs could induce generations of fibroblastoid cells and reductions of expressions of cartilage genes and GAGs, requiring more

studies on associated mechanisms; growth factor-induced production of ALP could not be prevented by co-culture system, especially in indirect manner; growth factors may have negative impact on the production of GAGs; production of GAGs and collagen by co-cultured cells are regulated by different mechanisms; morphology and associated cadherin expression in MSCs are different from those in chondrocytes; inconsistent results of improvements by co-culture system were also reported, due to reasons such as varied sample sources, donor variations (age, healthy or diseased, anatomical sites), technologies applied to isolate cells, and some unknown reasons, requiring future more studies to clarify, in particular *in vivo* studies [503, 517, 526, 527].

To regenerate the functional interface between cartilage and bone or the entire inhomogeneous osteochondral tissue, co-cultured chondrocytes with osteoblasts, co-cultured pre-differentiated MSCs with/without the support of biomaterial scaffolds were often applied. For example, by culturing different seeding cells in different biomaterial scaffolds, the cartilage-like construct (chondrocytes cultured in PGA mesh) and bone-mimicking construct (periosteal cells cultured in PLGA-PEG foam) were fabricated separately *in vitro*. Then they were sutured together to form a composite product. After weeks in culture *in vitro*, constant generations of osteogenic markers and increased chondrogenic markers were observed. But a better interfacial integration was found in the composite formed by one-week precultured construct rather than that precultured four weeks, suggesting the possibility of co-culturing chondrocyte with osteocyte to regenerate the OC tissue and requirements of an early interaction between chondrocytes and osteoblasts in the co-culture system [528]. Similar results were observed in another study, where the composite OC construct was made up of chondrocyte-seeded PGA sutured with osteoblast-laden PGA, and co-cultured in a bioreactor with circulating system *in vitro* [533]. The importance and underlying mechanisms of

the interaction between chondrocytes and osteoblasts to modulate the formation of the cartilage-bone interface, were also investigated in direct and indirect co-culture system (2D and 3D), in which the ECM-related and matrix architecture-dependent cellular responses in the morphology, adhesion and migration of chondrocytes within the co-culture system provided great contributions, as well as the paracrine signalling pathways, reciprocal regulations between chondrocytes and osteocytes, and the applied biomaterials also played important roles, suggesting more concerns to be considered in TE designs and more related studies to validate [529-534].

By co-culture system and well-designed biomaterial scaffold, the possibility to fabricate the entire OC tissue is increasing. For instance, a biomimetic PGA-PLA scaffold seeded in co-cultured osteoblasts with chondrocytes, was implanted in animal models. After three months, the regeneration of neo-OC tissue (both bone and connected cartilage tissues) in both structure (shape) and mechanical function (stiffness), was observed, providing the hope to regenerate the entire inhomogeneous OC tissue by the hydrogel-delivered co-cultured composite implant [535]. A biphasic scaffold with different sizes of pores, was made up of biodegradable poly (hydroxyethyl methacrylate) hydrogel, in which the part with small monodispersed pores was coated by hydroxyapatite particles and cultured MSCs to mimick the subchondral bone, while the other part with big pores was coated by HA and cultured with chondrogenic differentiated MSCs to simulate the articular cartilage part. After co-culturing *in vitro* for four weeks under growth medium without additional growth factors, the cell attachment, proliferation and differentiations on both parts and the depositions of both chondrogenic and osteogenic ECMs were observed concurrently in this biphasic tissue construct [536].

As an advanced cell culture technology, co-culture system allows biomimetic microenvironments

with various impact signals to be integrated naturally, providing an appropriate platform for TE studies on complex inhomogeneous tissues/organs such as the articular cartilage/OC tissue. By using co-culture system, problems such as the dedifferentiation of chondrocytes in culture, insufficient number of differentiated mature chondrocytes, hypertrophic differentiation of chondrogenic MSCs in culture could be overcome, and the simultaneous development of the entire OC tissue with distinct components could be achieved. In the future, as the increase in knowledges on the underlying mechanisms about intercellular communications, interactions between different types of cells, cell-cellular niches, and cell-biomaterials, co-culture system will be further improved and optimised to facilitate its application in TE and other biomedical fields [537].

2.4.2.2 Applications of inhomogeneous biomaterial scaffolds

Biomaterial scaffold for TE applications ideally should provide appropriate 3D architecture to support seeding/reparative cells to develop into neo-tissues both *in vitro* and *in vivo*. Scaffold-based TE strategy highly relies on the biomimetic design, appropriate biomaterials and fabrication technologies. A well-designed 3D biomaterial scaffold as another important element in TE strategy, has been greatly developing in pace with rapid advancements in materials science and fabrication technology. The basic criteria for designing 3D biomaterial scaffold, should concern many issues such as the biocompatibility, controllable biodegradability, suitable surface biochemistry for cells to attach, proliferate, migrate and differentiate, sufficient biomechanics to support and maintain the 3D structure and tissue function *in vivo* throughout spatiotemporal changes, biomimetic geometrical/topographical features as guidance for cells, adequate microenvironmental cues such as biological, biochemical, biophysical, bioelectrical and magnetic signals, for cells to survive and

for tissue to develop, and the assistance to form functional ECMs and positive cellular interactions between cells and cell-ECMs [341, 538].

In articular cartilage/OC TE, as the complex zonal character with many gradients throughout the tissue, homogeneous scaffold-developed tissue constructs are usually deficient in reflecting the natural inhomogeneous 3D architecture and physiological functions, partially leading to the dissatisfaction, inadequacy and inconformity of current TE products for both research and clinical applications [453]. To design and fabricate the inhomogeneous tissue construct, in particular contributing to regenerating tissues with inherent gradients in morphology and comparable functions, has increasingly been paid more attentions. State-of-the-art fabrication techniques, novel biomaterials, and ingenious designs, have all been involved, in combination with traditional methods of using conditioned culture media to achieve gradients of biochemical ingredients, and employing well-designed bioreactors/devices to intentionally provide controlled external factors [341, 453, 539].

To date, a few studies have exploited the design and fabrication of heterogenous scaffolds for articular cartilage/OC tissue regenerations, by various materials and techniques to rebuild the natural inhomogeneity in structure and function, generally involving continuous or discrete biomaterials, homogeneous or hybrid materials, modified monophasic, biphasic, triphasic and multi-layered scaffolds (Figure 2.18) [540].

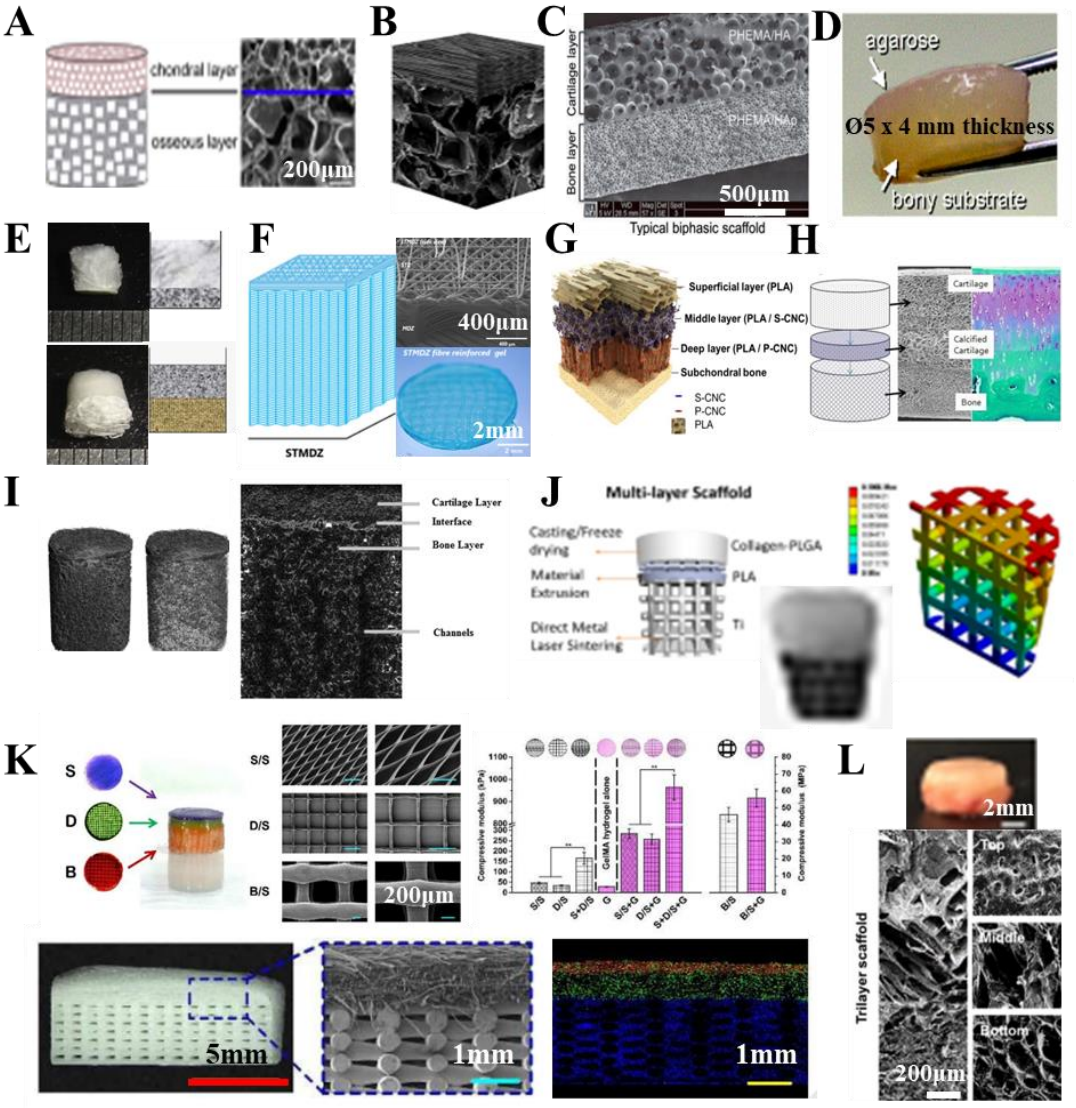

Figure 2.18 Illustrating images of a few 3D design and engineered inhomogeneous scaffold for multi-layered articular cartilage/osteochondral tissue reconstruction.

A: A biphasic scaffold with different porosity. B: 3D design of a biphasic scaffold with a fibre layer on a porous layer. C: A typical biphasic scaffold fabricated by composite materials. D: A scaffold with agarose hydrogel on a bony substrate. E: Freeze-dried by-layered collagen scaffold and a bi-layer microporous scaffold with collagen and electrospun poly-L-lactic acid nanofibers. F: 3D design and illustration of a sophisticated bi-layered scaffold with densely distributed fibre mat, and a uniform hydrogel layer. G: 3D design of a porous multilayer scaffold mimicking the architecture of mature articular cartilage, by employing anisotropic arrangement of PLA and modified cellulose nanocrystal materials. H: A 3D design of the multi-layered scaffold with porous layers mimicking the integrated bone, calcified cartilage and articular cartilage layers for 6mmx6mm osteochondral defect. I: 3D design of a multi-layered scaffold and its micro-CT image. J: The schematic images displaying the 3D design of a multi-layered collagen-Hap scaffold, the fabricated scaffold and the finite element analysis on distributions of deformation and stress throughout the scaffold. K: Images of a tri-layered PCL fibre-reinforced hydrogel scaffold, with different orientation and spacing of the fibre, different growth factor loading and different mechanical property in each layer. L: Image of a cell-laden tri-layered scaffold after implantation for 8 weeks, and the cross-section view of this scaffold. Images were adapted from references [530, 536, 541-550].

For example, different concentrations of agarose hydrogels embedded with chondrocytes were applied to simulate different depth-dependent layers of the cartilaginous tissue [508]. By changing polymer materials and technical parameters while performing the 3D fibre deposition, PEG-based copolymer scaffolds with interconnected inhomogeneous pores [551] and mechanical features [552] could be designed and fabricated. Biphasic PCL scaffolds consisting of porous sheet and uniaxially aligned nanofibres, with/without incorporation of chondroitin sulphate (CS), hyaluronic acid (HA) and hydroxyapatite, were both developed to simulate the inhomogeneous articular cartilage/ OC tissue, in which PCL products with different pattern could be combined by high temperature (over the melting point of PCL polymer) [553] or by electrostatic force [554]. Agarose and PLGA-bioactive glass hybrid microspheres encapsulated with different types of seeding cells (chondrocyte and osteoblast) were employed to fabricate a bioactive triphasic system, to simulate the cartilaginous part, cartilage-bone interface and subchondral bone part of the OC tissue and for co-culturing cells [555]. The multi-layered zonal structure and bioactive microenvironment of the OC tissue were also simulated by a polymeric multi-layered scaffold, containing a porous PLA layer, a sulphated cellulose nanocrystal-embedded PLA layer and a vertically-aligned tubular PLA layer incorporated with phosphate and cellulose nanocrystal [550]. By using a commercial device with two connected chambers, chondrocyte-laden PEG-based solutions containing different concentration of PEG and photoinitiator, were crosslinked continuously by UV light exposure. Determined by the portion of PEG monomers in the hydrogel solutions, an inhomogeneous hydrogel platform with a gradient of mechanical features but continuous chemical components could be formed, which was applied to fabricate the zone-related and stiffness-dependent cartilaginous tissue construct [556]. A series of hybrid scaffolds made up of different polymers

with nanopores and dynamic temperature-responsive stiffness were designed and fabricated by combining 3D printing and phase separation techniques. Based on these novel thermo-responsive scaffolds with stiffness memory (different initial stiffness from stiffness after relaxation), inhomogeneous OC tissue construct could be directly generated by engrafted MSCs cultured with different inducing medium (soft scaffold with chondrogenic inducing medium, stiff scaffold with osteogenic inducing medium) [554, 557]. By using melt-electrowritting and FDM techniques, PCL-PEG hybrid scaffold was successfully fabricated. In combination with photocurable hydrogel-delivered MSCs and PLGA microsphere-loaded growth factors, a triphasic tissue construct was integrated and developed after UV light exposure, in which the top layer with smaller pores, additional TGF-beta and BMP was formed to mimick the superficial layer; the middle layer with medium pores and additional TGF-beta, was produced to mimick the deep layer; the bottom layer with bigger pores and additional BMP, was fabricated to mimick the subchondral bone part. After culturing the inhomogeneous tissue construct three weeks *in vitro*, different differentiations by MSCs in different layers, as well as the layer-specific cellular morphology and ECM productions were observed, comparable to those of native tissue. After implanting the engineered inhomogeneous tissue construct into animal model with OC defect, the regenerated neo-tissue with better lubricating surface on the top area of the scaffold-based implant was obtained, providing a hope to utilise the artificial biomimetic OC tissue construct to deal with OC defects in clinic in the future [547].

Although these inhomogeneous scaffolds presented capabilities for chondrocytes or MSCs to engraft, survive, proliferate, differentiate and for inhomogeneous tissue to be fabricated, most of them were remained in short-term, *in vitro*, small-scale studies, requiring special device, technique,

or having complicated fabrication process, insufficient to support in-depth research and to meet the clinical requirement. Besides, only a few studies explored the fabrication of biomaterial scaffold with gradients of components or properties, immediately developed during process or gradually formed over time after fabrication (Figure 2.19). Based on the established fabrication methods such as the 3D (bio)printing, component redistribution, controlled phase change, post-modification, and combined techniques, new methodology and novel materials are required to be created or discovered to be employed in design and fabrication of the biomimetic scaffold with inhomogeneities for multi-layered complex inhomogeneous tissue reconstruction [453, 558].

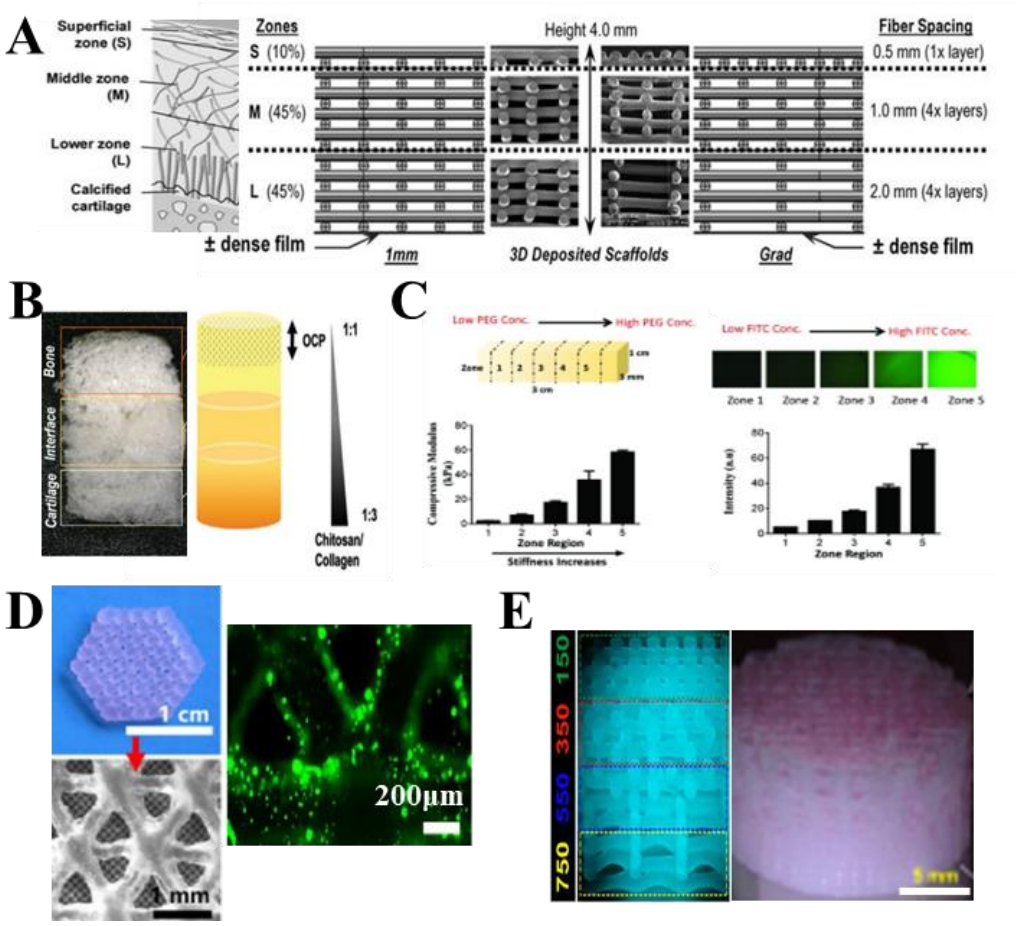

Figure 2.19 Illustrations of inhomogeneous scaffold with gradients and 3D bio-printed tissue constructs A: Schematic images displaying a design of a 3D-deposited scaffold made up of porous poly (ethylene glycol)-terephthalate–poly (butylene terephthalate) (PEGT/PBT) copolymer, containing either a homogeneous fiber spacing (1mm) or an anisotropic gradient of pore size (Grad). B: A macroscopic image illustrating the fabricated multi-layered hydrogel scaffold and its design of composition. C: Schematic images illustrating the fabricated

inhomogeneous multi-layered hydrogel scaffold consisting of 8-arm-poly (ethylene glycol) (PEG)-norbornene (MW 10,000 g/mol), PEG-dithiol (MW 1500 g/mol), and 25% methacrylated chondroitin sulphate (CS-MA), measurements of the compressive modulus and the gradient of FITC-labelled BSA protein molecules from zone 1 to zone 5. BSA, bovine serum albumin; FITC, fluorescein isothiocyanate. D: Images illustrating the 3D-fabicated Li-Mg-Si bioceramics (LMS)-containing gellan gum hydrogel (GAM) scaffold and a bio-printed seeding cell-laden GAM construct after printing examined by live and dead assay. E: Schematic image of a four-layer PCL scaffold with gradient for anisotropic cartilage construction and the bio-printed anisotropic cartilage construct with MSCs and growth factors after transplantation in animal model for weeks. Images were adapted from references [551, 556, 559-561].

2.4.2.3 Applications of inhomogeneous culture systems

Living cells could sense and interact with surroundings, which have been confirmed contributions to the survival and behaviours of cells in culture, such as the adherence, proliferation, migration, differentiation and death [33]. As connective tissue in the load-bearing joint, biomechanical signals are one of the indispensable factors determining the development, homeostasis, maturation, dysfunction and disease of the articular cartilage/OC tissue [32], in terms of the homeostasis of cartilaginous tissue, the threshold of bone strain, the modelling and remodelling behaviours of subchondral bone plate in normal physiological condition and the anatomical shape of the joint [125, 475]. More evidences about the great influence of biomechanical microenvironment on seeding cells cultured *in vitro*, involved studies on mechano-sensing and mechano-transduction processes [32, 123-125], where biomechanical microenvironment could often be controlled by adjusting various mechanical properties of the 2D/3D biomaterial scaffold/substrate, such as the stiffness, elasticity, strength and viscoelasticity, or by adjusting various mechanical stimuli applied with regimes, such as compressive stress, shear stress, and tensile stress, applied with different frequency, amplitude, and strength [562, 563]. In addition, the geometrical and topographical features in 2D/3D microenvironment provided by roughness or patterns of surroundings including the associated scaffold/substrate, ambient materials and neighbouring cells, could also be

interpreted mechanically into the regional strain for seeding cells to manage during interactions [564, 565].

Another key factor during tissue development in culture that should be considered in the tissue culture system is the biochemical signal and the associated signalling pathways. Tissue is developed by a source of cells through a specific differentiation mechanism evolved [566]. The mechanism as the guidance involves a series of spatiotemporal variances in the microenvironment of the initial cells, in which the distribution of biochemical cues via diffusion or specific media (ECM, vesicles etc.) regulate the degree of impact on the recipient cells. Among various biochemical cues, morphogen is the substance providing dose-related positional information to individual cells within an area, resulting in the formation of tissue patterns based on varied responses from cells [567]. For the inhomogeneous tissue with many inherent gradients, its development is sequentially regulated by various biochemical factors such as growth factors, transcriptional factors, and certain metabolic products, some of which are morphogens with gradients. These factors together are responsible for the formation of inhomogeneous articular cartilage/OC tissue containing gradients of zone-specific resident cells developed from homogeneous groups of osteochondro-progenitor cells [539, 566, 567].

Several studies have taken advantages of these potential influences of biochemical and biomechanical signals on seeding cells in culture, to purposefully incorporate these environmental cues into the TE design to form the inhomogeneous culture system for inhomogeneous articular cartilage/OC tissue reconstruction, such as by applying **well-designed devices and functionalised bioreactors** as culture systems to prepare 3D engineered tissue construct *in vitro* (Figure 2.20)**.**

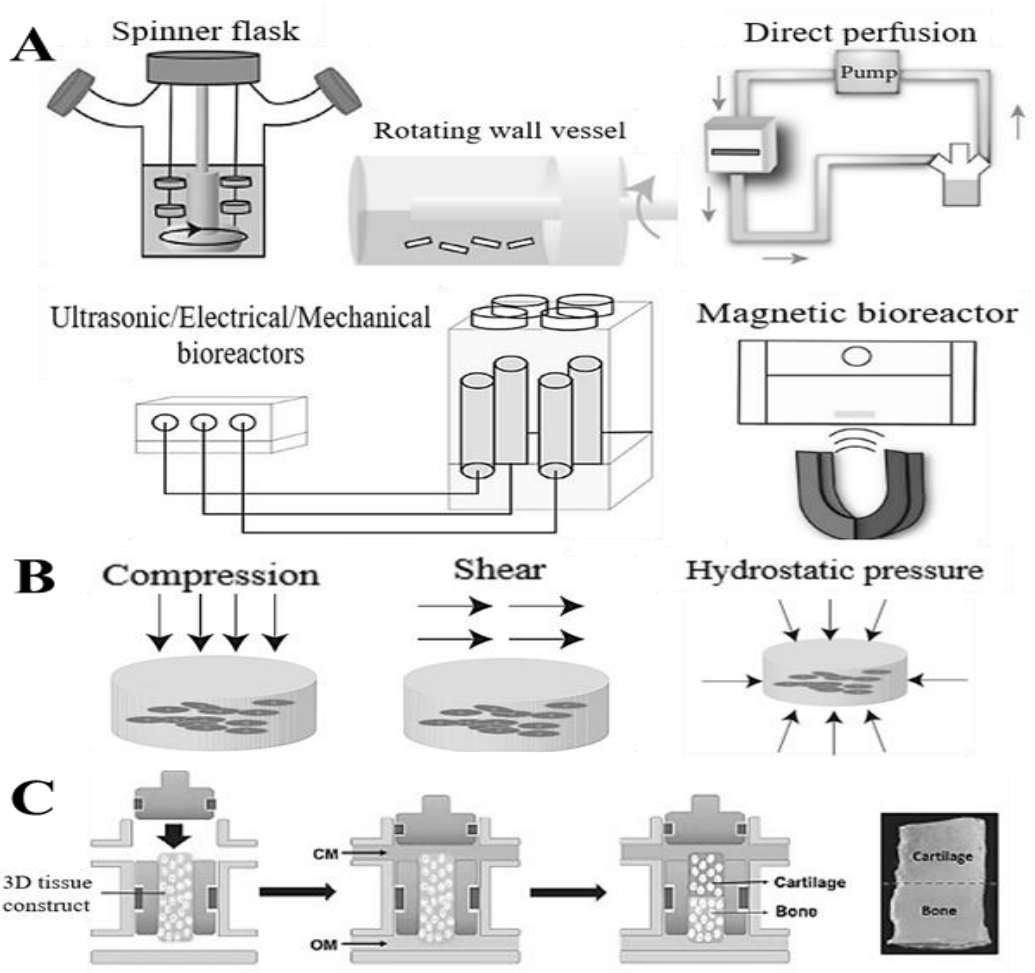

Figure 2.20 Illustrations of bioreactors for tissue engineering applications.

A: A few common bioreactors for tissue engineering. B: Common mechanical forces in engineering articular cartilage/osteochondral tissue. Arrows display the direction of mechanical loads imposing on the engineered tissue. C: Schematic images demonstrating a bioreactor with top and bottom perfusions, respectively, for bi-phasic OC tissue reconstruction. Images were adapted from references [309, 568].

For example, it was found that human BM-MSCs aggregation cultured for a long period of time in the loading chamber of a cell culture device supplying cyclic hydrostatic pressure, could generate more chondrogenic ECMs, comparing to those under short-term training or cultured with non-loading condition [144]. Based on a co-culturing model [569], expanded foetal sheep chondrocytes cultured in a microenvironment containing biochemical compounds (TGF-β1, chondroitinase-ABC, lysyl oxidase-like 2 protein and cytoD), and with proper mechanical confinement provided by directly pressing deadweight, without using any scaffold material just by self-assembly, could be engineered into a relatively large cartilaginous tissue construct with functionally improved

ECMs regarding the contents of ECM components, tensile modulus and inner organisation [570]. In order to co-culture chondrocytes with osteoblasts in a biphasic scaffold, a dynamic culture system with spinner flasks was modified. The resulted two-chamber system contained a magnetic stirrer on the bottom of each chamber to provide the mechanical force to mix the culture medium and to stimulate seeding cells in culture. A gravity-driven siphon-based bioreactor containing a perfusion chamber, modified siphon tubes, and a reservoir bottle with medium, was also designed and modified to culture cell-laden biphasic scaffold. Gravity and siphon process could perfuse the culture system without using other power [571]. Similar multi-chamber bioreactors with perfusing system for co-culturing the cell-laden biphasic scaffold [572], and multiphasic porous scaffold-based tissue construct [573] toward OC tissue regeneration *in vitro*, were also developed. A novel bioreactor combining two-chamber system with mechanical stimulation was developed for inhomogeneous cartilage tissue regeneration, in which two chambers were designed to mimick nutrition supplies from the synovial fluid and subchondral bone, respectively. Hence, graded biochemical compounds such as growth factors and nutrients could be supplied. Along with the incorporation of mechanical loadings, this bioreactor was intended to fabricate the cartilage tissue with zonal structure. Preliminary results from computer models confirmed the function of this bioreactor, remaining further experiments to validate [574]. To induce gradient, a dual-chamber rotational bioreactor was modified with a 3D-printed keratin-based membrane to control the flow. From results of computer modelling and real experiments, this bioreactor was confirmed to provide graded cell numbers to engraft in the scaffold, bringing the hope for inhomogeneous multi-layered tissue reconstruction *in vitro* as well [575].

Well-designed bioreactors/devices serve as flexible and powerful tools to investigate the

underlying mechanism of 3D cell-based tissue culture in controlled microenvironment, and to technically offer the possibility of fabricating quantified and qualified, engineered tissue constructs *in vitro*. As the development of engineering and manufacturing technologies, more cost-effective and novel designs of bioreactors/devices for inhomogeneous tissue reconstructions *in vitro* will be available in the near future [576-579].

In conclusion, articular cartilage/OC tissue is an inhomogeneous complex connective tissue with multiple layers, locating at the synovial joint area to deal with mechanical forces and motions. Due to the lack of vascular, lymphatic and neural systems, defects or injuries in this place are incapable of reparation and regeneration effectively, often requiring exterior interventions. Based on the standard grading system and criteria, chondral/OC defects could be measured and described, resulting in the development and application of relevant clinical treatments. However, most medical strategies currently are not truly restorative, until the involvement of tissue engineering strategies, bringing in the third generation of ACI technique (scaffold-assisted ACI) and engineered tissue grafts for implantation/transplantation. As the rapid advancements of science and technologies, TE strategies have been greatly improved in every fundamental element referring to seeding cells, biomaterial scaffolds, 3D tissue fabrication techniques and supportive devices/tools (Figure 2.21). But most studies are stayed at stages of *in vitro*, short-term and small-scale homogeneous products, incompetent at massive clinical demands and in-depth research requirements. To overcome these limitations and challenges emerging from every aspect of the cell-based scaffold-supported TE strategy, future prospects should be stressed on such things as to continuously acquire comprehensive knowledges of the natural processes of the development and pathogenesis of the target tissues/organs, to develop biomimetic tissue culture models as auxiliary

tools for every aspect of the research, to discover more promising seeding cells and improve the associated culture system, to seek novel biomaterials or composite materials for fabricating functional scaffolds, to continuously design and develop current biomaterial fabrication techniques and instruments for 3D complex inhomogeneous tissue reconstruction in controlled biomimetic microenvironments, and to apply more studies from bench to bed under standardised protocols for therapeutic purposes. It is worth to believe that with improvements and optimisations of developmental biology, biomaterials science, engineering technologies and interdisciplinary cooperation and coordination, current problems occurred and confronted during the development of TE field, will be solved in the process of further developments in the near future.

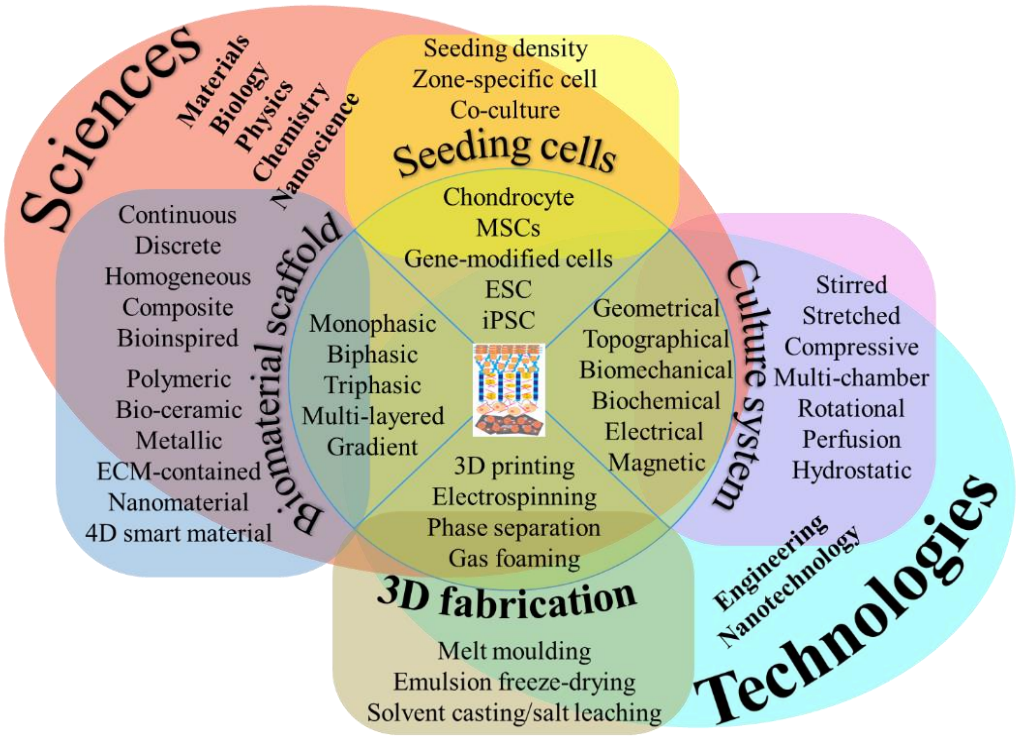

Figure 2.21 A schematic diagram the fundamental elements in inhomogeneous articular cartilage/osteochondral tissue engineering.

The schematic diagram displaying fundamental elements in inhomogeneous articular cartilage/osteochondral tissue engineering including seeding cell management, biomaterial scaffold design from various composition and architecture, 3D fabrication methodology and elaborate culture system (bioreactor, devices) facilitating the control of the complex microenvironment for tissue development in vitro [9, 13, 100, 580, 581].

References

[1] Ogden JA. Anatomy and physiology of skeletal development. Skeletal injury in the child. 2000:1-37.
[2] Johnston SA. Osteoarthritis. Joint anatomy, physiology, and pathobiology. Vet Clin North Am Small Anim Pract. 1997;27:699-723.
[3] Chijimatsu R, Saito T. Mechanisms of synovial joint and articular cartilage development. Cellular and Molecular Life Sciences. 2019;76:3939-52.
[4] Mow VC, Lai WM. Recent developments in synovial joint biomechanics. Siam Review. 1980;22:275-317.
[5] Hui AY, McCarty WJ, Masuda K, Firestein GS, Sah RL. A systems biology approach to synovial joint lubrication in health, injury, and disease. Wiley Interdiscip Rev Syst Biol Med. 2012;4:15-37.
[6] Carballo CB, Nakagawa Y, Sekiya I, Rodeo SA. Basic science of articular cartilage. Clinics in sports medicine. 2017;36:413-25.
[7] Keeney M, Pandit A. The osteochondral junction and its repair via bi-phasic tissue engineering scaffolds. Tissue Engineering Part B: Reviews. 2009;15:55-73.
[8] Mescher AL. Junqueira's basic histology: text and atlas: McGraw-Hill Medical 13th ed. New York; 2013.
[9] Ng HY, Lee KA, Shen Y-F. Articular cartilage: structure, composition, injuries and repair. JSM Bone Joint Dis. 2017;1:1010.
[10] Bhosale AM, Richardson JB. Articular cartilage: structure, injuries and review of management. British medical bulletin. 2008;87:77-95.
[11] Mainil-Varlet P, Aigner T, Brittberg M, Bullough P, Hollander A, Hunziker E, et al. Histological assessment of cartilage repair: a report by the Histology Endpoint Committee of the International Cartilage Repair Society (ICRS). J Bone Joint Surg Am. 2003;85-A Suppl 2:45-57.
[12] O'Driscoll SW, Keeley FW, Salter RB. Durability of regenerated articular cartilage produced by free autogenous periosteal grafts in major full-thickness defects in joint surfaces under the influence of continuous passive motion. A follow-up report at one year. JBJS. 1988;70:595-606.
[13] Davies RL, Kuiper NJ. Regenerative medicine: a review of the evolution of autologous chondrocyte implantation (ACI) therapy. Bioengineering. 2019;6(1):22.
[14] Huber M, Trattnig S, Lintner F. Anatomy, biochemistry, and physiology of articular cartilage. Invest Radiol. 2000;35:573-80.
[15] Madry H, van Dijk CN, Mueller-Gerbl M. The basic science of the subchondral bone. Knee surgery, sports traumatology, arthroscopy. 2010;18:419-33.
[16] Müller-Gerbl M. The subchondral bone plate. Adv Anat Embryol Cell Biol. 1998;141:III-XI, 1-134.
[17] Kawcak CE, McIlwraith CW, Norrdin R, Park R, James S. The role of subchondral bone in joint disease: a review. Equine veterinary journal. 2001;33:120-6.
[18] Nukavarapu SP, Dorcemus DL. Osteochondral tissue engineering: current strategies and challenges. Biotechnology advances. 2013;31:706-21.
[19] Fujioka R, Aoyama T, Takakuwa T. The layered structure of the articular surface. Osteoarthritis Cartilage. 2013;21:1092-8.
[20] Bergholt MS, St-Pierre J-P, Offeddu GS, Parmar PA, Albro MB, Puetzer JL, et al. Raman spectroscopy reveals new insights into the zonal organization of native and tissue-engineered articular

cartilage. ACS central science. 2016;2:885-95.
[21] Palukuru UP, McGoverin CM, Pleshko N. Assessment of hyaline cartilage matrix composition using near infrared spectroscopy. Matrix Biology. 2014;38:3-11.
[22] Ulrich-Vinther M, Maloney MD, Schwarz EM, Rosier R, O'Keefe RJ. Articular cartilage biology. JAAOS-Journal of the American Academy of Orthopaedic Surgeons. 2003;11:421-30.
[23] Goldring MB. Chondrogenesis, chondrocyte differentiation, and articular cartilage metabolism in health and osteoarthritis. Ther Adv Musculoskelet Dis. 2012;4:269-85.
[24] Oliveira JM, Pina S, Reis RL, San Roman J. (Eds.). Osteochondral tissue engineering: challenges, current strategies, and technological advances: Springer; (Vol.1059). 2018.
[25] Muller-Gerbl M, Schulte E, Putz R. The thickness of the calcified layer of articular cartilage: a function of the load supported? J Anat. 1987;154:103-11.
[26] Oegema TR, Jr., Carpenter RJ, Hofmeister F, Thompson RC, Jr. The interaction of the zone of calcified cartilage and subchondral bone in osteoarthritis. Microsc Res Tech. 1997;37:324-32.
[27] Radin EL, Paul IL, Lowy M. A comparison of the dynamic force transmitting properties of subchondral bone and articular cartilage. J Bone Joint Surg Am. 1970;52:444-56.
[28] Wang F, Ying Z, Duan X, Tan H, Yang B, Guo L, et al. Histomorphometric analysis of adult articular calcified cartilage zone. J Struct Biol. 2009;168:359-65.
[29] Tomaszewski R, Wiktor Ł, Gap A. Enhancement of cartilage repair through the addition of growth plate chondrocytes in an immature skeleton animal model. Journal of orthopaedic surgery and research. 2019;14:1-10.
[30] Krishnan Y, Grodzinsky AJ. Cartilage diseases. Matrix Biol. 2018;71-72:51-69.
[31] Correa D, Lietman SA. Articular cartilage repair: Current needs, methods and research directions. Semin Cell Dev Biol. 2017;62:67-77.
[32] Wong M, Carter D. Articular cartilage functional histomorphology and mechanobiology: a research perspective. Bone. 2003;33:1-13.
[33] Sophia Fox AJ, Bedi A, Rodeo SA. The basic science of articular cartilage: structure, composition, and function. Sports health. 2009;1:461-8.
[34] Martinez-Moreno D, Jimenez G, Galvez-Martin P, Rus G, Marchal JA. Cartilage biomechanics: A key factor for osteoarthritis regenerative medicine. Biochim Biophys Acta Mol Basis Dis. 2019;1865:1067-75.
[35] Brown TD, Vrahas MS. The apparent elastic modulus of the juxtaricular subchondral bone of the femoral head. Journal of orthopaedic research. 1984;2:32-8.
[36] McMahon LA, O'Brien FJ, Prendergast PJ. Biomechanics and mechanobiology in osteochondral tissues. Regen Med. 2008;3:743-59.
[37] Mow V, Bachrach N, Setton L, Guilak F. Stress, strain, pressure and flow fields in articular cartilage and chondrocytes. Cell mechanics and cellular engineering: Springer; 1994. p. 345-79.
[38] Mankin HJ, Lippiello L. Biochemical and metabolic abnormalities in articular cartilage from osteo-arthritic human hips. J Bone Joint Surg Am. 1970;52:424-34.
[39] Sangha O. Epidemiology of rheumatic diseases. Rheumatology. 2000;39:3-12.
[40] Simon TM, Jackson DW. Articular cartilage: injury pathways and treatment options. Sports Med Arthrosc Rev. 2006;14:146-54.
[41] Barber-Westin S, Noyes FR. Assessment of sports participation levels following knee injuries. Sports medicine. 1999;28:1-10.
[42] Lasanianos NG, Kanakaris NK. Chondral lesions. Trauma and Orthopaedic Classifications:

Springer; 2015. p. 501-4.
[43] Broom ND, Thambyah A. The Soft Hard Tissue Junction: Structure, Mechanics and Function. Cambridge: Cambridge University Press; 2018.
[44] Milgram J. Tangential osteochondral fracture of the patella. JBJS. 1943;25:271-80.
[45] Meachim G, Bentley G. Horizontal splitting in patellar articular cartilage. Arthritis Rheum. 1978;21:669-74.
[46] Bennett GA, Waine H, Bauer W. Changes in the knee joint at various ages: with particular reference to the nature and development of degenerative joint disease. Physical Therapy. 1943;23:95.
[47] Landells J. The reactions of injured human articular cartilage. The Journal of Bone and Joint Surgery British volume. 1957;39:548-62.
[48] ROSENBERG NJ. Osteochondral fractures of the lateral femoral condyle. JBJS. 1964;46:1013-26.
[49] Kennedy JC, Grainger RW, McGraw RW. Osteochondral fractures of the femoral condyles. The Journal of Bone and Joint Surgery British volume. 1966;48:436-40.
[50] Berndt AL, Harty M. Transchondral fractures (osteochondritis dissecans) of the talus. J Bone Joint Surg Am. 1959;41-A:988-1020.
[51] Sanders RK, Crim JR. Osteochondral injuries. Seminars in Ultrasound, CT and MRI: Elsevier; 2001. p. 352-70.
[52] Anderson IF, Crichton KJ, Grattan-Smith T, Cooper RA, Brazier D. Osteochondral fractures of the dome of the talus. J Bone Joint Surg Am. 1989;71:1143-52.
[53] Laffenêtre O. Osteochondral lesions of the talus: current concept. Orthopaedics & Traumatology: Surgery & Research. 2010;96:554-66.
[54] Posadzy M, Desimpel J, Vanhoenacker F. Staging of osteochondral lesions of the talus: MRI and cone beam CT. Journal of the Belgian Society of Radiology. 2017;101:1.
[55] Hepple S, Winson IG, Glew D. Osteochondral lesions of the talus: a revised classification. Foot Ankle Int. 1999;20:789-93.
[56] Stoller DW. Magnetic resonance imaging in orthopaedics and sports medicine. 3rd Edition ed: Lippincott Williams & Wilkins; 2007.
[57] Noyes FR, Stabler CL. A system for grading articular cartilage lesions at arthroscopy. The American journal of sports medicine. 1989;17:505-13.
[58] Slattery C, Kweon CY. Classifications in Brief: Outerbridge Classification of Chondral Lesions. Clin Orthop Relat Res. 2018;476:2101-4.
[59] Beck M, Kalhor M, Leunig M, Ganz R. Hip morphology influences the pattern of damage to the acetabular cartilage: femoroacetabular impingement as a cause of early osteoarthritis of the hip. The Journal of bone and joint surgery British volume. 2005;87:1012-8.
[60] Collins DH. The pathology of articular and spinal diseases. London: Edward Arnold; 1949.
[61] Konan S, Rayan F, Meermans G, Witt J, Haddad F. Validation of the classification system for acetabular chondral lesions identified at arthroscopy in patients with femoroacetabular impingement. The Journal of Bone and Joint Surgery British volume. 2011;93:332-6.
[62] Mintz DN, Tashjian GS, Connell DA, Deland JT, O'Malley M, Potter HG. Osteochondral lesions of the talus: a new magnetic resonance grading system with arthroscopic correlation. Arthroscopy. 2003;19:353-9.
[63] Falah M, Nierenberg G, Soudry M, Hayden M, Volpin G. Treatment of articular cartilage lesions of the knee. International orthopaedics. 2010;34:621-30.
[64] Tetteh ES, Bajaj S, Ghodadra NS. Basic science and surgical treatment options for articular

cartilage injuries of the knee. J Orthop Sports Phys Ther. 2012;42:243-53.
[65] Outerbridge RE. The etiology of chondromalacia patellae. J Bone Joint Surg Br. 1961;43-B:752-7.
[66] Cassar-Gheiti AJ, Burke NG, Cassar-Gheiti TM, Mulhall KJ. Chondral Lesion in the Hip Joint and Current Chondral Repair Techniques. Cartilage Repair and Regeneration2018. p. 103.
[67] Karpiński R, Krakowski P, Jonak J, Machrowska A, Maciejewski M, Nogalski A. Diagnostics of Articular Cartilage Damage Based on Generated Acoustic Signals Using ANN—Part I: Femoral-Tibial Joint. Sensors. 2022;22:2176.
[68] Caplan AI, Elyaderani M, Mochizuki Y, Wakitani S, Goldberg VM. Principles of cartilage repair and regeneration. Clin Orthop Relat Res. 1997:254-69.
[69] Salter RB, Harris WR. Injuries involving the epiphyseal plate. J Bone Joint Surg Am. 1963;45:587-622.
[70] Acebes C, Roman-Blas J, Delgado-Baeza E, Palacios I, Herrero-Beaumont G. Correlation between arthroscopic and histopathological grading systems of articular cartilage lesions in knee osteoarthritis. Osteoarthritis and Cartilage. 2009;17:205-12.
[71] Custers RJ, Creemers LB, Verbout AJ, van Rijen MH, Dhert WJ, Saris DB. Reliability, reproducibility and variability of the traditional Histologic/Histochemical Grading System vs the new OARSI Osteoarthritis Cartilage Histopathology Assessment System. Osteoarthritis Cartilage. 2007;15:1241-8.
[72] Widuchowski W, Widuchowski J, Trzaska T. Articular cartilage defects: study of 25,124 knee arthroscopies. Knee. 2007;14:177-82.
[73] Hurtig MB, Buschmann MD, Fortier LA, Hoemann CD, Hunziker EB, Jurvelin JS, et al. Preclinical Studies for Cartilage Repair: Recommendations from the International Cartilage Repair Society. Cartilage. 2011;2:137-52.
[74] Hoemann C, Kandel R, Roberts S, Saris DB, Creemers L, Mainil-Varlet P, et al. International Cartilage Repair Society (ICRS) recommended guidelines for histological endpoints for cartilage repair studies in animal models and clinical trials. Cartilage. 2011;2:153-72.
[75] Dwyer T, Martin CR, Kendra R, Sermer C, Chahal J, Ogilvie-Harris D, et al. Reliability and Validity of the Arthroscopic International Cartilage Repair Society Classification System: Correlation With Histological Assessment of Depth. Arthroscopy. 2017;33:1219-24.
[76] Moskowitz RW. Osteoarthritis cartilage histopathology: grading and staging. Osteoarthritis Cartilage. 2006;14:1-2.
[77] Madry H, Ochi M, Cucchiarini M, Pape D, Seil R. Large animal models in experimental knee sports surgery: focus on clinical translation. Journal of experimental orthopaedics. 2015;2:1-12.
[78] Chahla J, Cinque ME, Shon JM, Liechti DJ, Matheny LM, LaPrade RF, et al. Bone marrow aspirate concentrate for the treatment of osteochondral lesions of the talus: a systematic review of outcomes. J Exp Orthop. 2016;3:33.
[79] Erickson B, Fillingham Y, Hellman M, Parekh SG, Gross CE. Surgical management of large talar osteochondral defects using autologous chondrocyte implantation. Foot and Ankle Surgery. 2018;24:131-6.
[80] Hannon CP, Murawski CD, Fansa AM, Smyth NA, Do H, Kennedy JG. Microfracture for osteochondral lesions of the talus: a systematic review of reporting of outcome data. Am J Sports Med. 2013;41:689-95.
[81] Gracitelli GC, Moraes VY, Franciozi CE, Luzo MV, Belloti JC. Surgical interventions (microfracture, drilling, mosaicplasty, and allograft transplantation) for treating isolated cartilage

defects of the knee in adults. Cochrane Database Syst Rev. 2016;9:CD010675.
[82] Richter DL, Schenck Jr RC, Wascher DC, Treme G. Knee articular cartilage repair and restoration techniques: a review of the literature. Sports health. 2016;8:153-60.
[83] Detterline AJ, Goldberg S, Bach Jr BR, Cole BJ. Treatment options for articular cartilage defects of the knee. Orthopaedic Nursing. 2005;24:361-6.
[84] Jones KJ, Sheppard WL, Arshi A, Hinckel BB, Sherman SL. Articular cartilage lesion characteristic reporting is highly variable in clinical outcomes studies of the knee. Cartilage. 2019;10:299-304.
[85] Vannini F, Buda R, Pagliazzi G, Ruffilli A, Cavallo M, Giannini S. Osteochondral allografts in the ankle joint: state of the art. Cartilage. 2013;4:204-13.
[86] Krill M, Early N, Everhart JS, Flanigan DC. Autologous Chondrocyte Implantation (ACI) for Knee Cartilage Defects: A Review of Indications, Technique, and Outcomes. JBJS Rev. 2018;6:e5.
[87] Inderhaug E, Solheim E. Osteochondral Autograft Transplant (Mosaicplasty) for Knee Articular Cartilage Defects. Sports Med. 2018;46 (4).
[88] Simon TM, Jackson DW. Articular Cartilage: Injury Pathways and Treatment Options. Sports Med Arthrosc Rev. 2018;26:31-9.
[89] Welch T, Mandelbaum B, Tom M. Autologous Chondrocyte Implantation: Past, Present, and Future. Sports Med Arthrosc Rev. 2016;24:85-91.
[90] Wilkin D, Brainard J. Human Biology. CK12 flexbook. CK12 Foundation; 2015. Saatavilla: https://textbookequity.org/Textbooks/HumanBiologyCK12.pdf
[91] Mosier B, Minas T, Gomoll AH. Cartilage Defects, Osteochondritis, and Osteonecrosis. Principles of Orthopedic Practice for Primary Care Providers: Springer; 2018. p. 279-90.
[92] Qadeer A, Paddock M. Intra-articular displacement of an avulsed medial (internal) epicondyle ossification centre in the paediatric elbow: a radiographic finding not to be missed. BMJ Case Reports CP. 2019;12 (11):e231635.
[93] Loftin PG, Beard WL, Guyan ME, White BJ. Comparison of arthroscopic lavage and needle lavage techniques, and lavage volume on the recovery of colored microspheres from the tarsocrural joints of cadaver horses. Veterinary Surgery. 2016;45 (2):240-5.
[94] Lewis PB, McCarty LP, 3rd, Kang RW, Cole BJ. Basic science and treatment options for articular cartilage injuries. J Orthop Sports Phys Ther. 2006;36:717-27.
[95] Bhatia S, Hsu A, Lin EC, Chalmers P, Ellman M, Cole BJ, et al. Surgical treatment options for the young and active middle-aged patient with glenohumeral arthritis. Advances in Orthopedics. 2012;2012:846843.
[96] Grieshober JA, Stanton M, Gambardella R. Debridement of articular cartilage: The natural course. Sports medicine and arthroscopy review. 2016;24:56-62.
[97] Bert JM. Abrasion arthroplasty. Operative techniques in orthopaedics. 1997;7:294-9.
[98] Willers C, Wood DJ, Zheng MH. A current review on the biology and treatment of articular cartilage defects (part I & part II). Journal of Musculoskeletal Research. 2003;7:157-81.
[99] Panseri S, Russo A, Cunha C, Bondi A, Di Martino A, Patella S, et al. Osteochondral tissue engineering approaches for articular cartilage and subchondral bone regeneration. Knee Surgery, Sports Traumatology, Arthroscopy. 2012;20:1182-91.
[100] Makris EA, Gomoll AH, Malizos KN, Hu JC, Athanasiou KA. Repair and tissue engineering techniques for articular cartilage. Nat Rev Rheumatol. 2015;11:21-34.
[101] Guermazi A, Roemer FW, Alizai H, Winalski CS, Welsch G, Brittberg M, et al. State of the art: MR imaging after knee cartilage repair surgery. Radiology. 2015;277:23-43.

[102] Saw K-Y, Anz A, Merican S, Tay Y-G, Ragavanaidu K, Jee CS, et al. Articular cartilage regeneration with autologous peripheral blood progenitor cells and hyaluronic acid after arthroscopic subchondral drilling: a report of 5 cases with histology. Arthroscopy: The Journal of Arthroscopic & Related Surgery. 2011;27:493-506.
[103] Wang KC, Frank RM, Cotter EJ, Christian DR, Cole BJ. Arthroscopic management of isolated tibial plateau defect with microfracture and micronized allogeneic cartilage–platelet-rich plasma adjunct. Arthroscopy techniques. 2017;6:e1613-e8.
[104] Minas T, Von Keudell A, Bryant T, Gomoll AH. The John Insall Award: A minimum 10-year outcome study of autologous chondrocyte implantation. Clin Orthop Relat Res. 2014;472:41-51.
[105] Kon E, Filardo G, Di Martino A, Marcacci M. ACI and MACI. The Journal of Knee Surgery. 2012;25:017-22.
[106] Bartlett W, Skinner JA, Gooding CR, Carrington RW, Flanagan AM, Briggs TW, et al. Autologous chondrocyte implantation versus matrix-induced autologous chondrocyte implantation for osteochondral defects of the knee: a prospective, randomised study. J Bone Joint Surg Br. 2005;87:640-5.
[107] Tverdokhlebov S, Bolbasov E, Shesterikov E. Scaffold materials based on fluorocarbon composites modified with RF magnetron sputtering. Osteogenesis/ed Y Lin Rijeka: InTech. 2012:83-116.
[108] Hangody L, Ráthonyi GK, Duska Z, Vásárhelyi G, Füles P, Módis L. Autologous osteochondral mosaicplasty: surgical technique. JBJS. 2004;86:65-72.
[109] Gou GH, Tseng FJ, Wang SH, Chen PJ, Shyu JF, Weng CF, et al. Autologous Chondrocyte Implantation Versus Microfracture in the Knee: A Meta-analysis and Systematic Review. Arthroscopy. 2020;36:289-303.
[110] Devitt BM, Bell SW, Webster KE, Feller JA, Whitehead TS. Surgical treatments of cartilage defects of the knee: systematic review of randomised controlled trials. The Knee. 2017;24:508-17.
[111] Solheim E, Hegna J, Inderhaug E. Early determinants of long-term clinical outcome after cartilage repair surgery in the knee. J Orthop. 2018;15:222-5.
[112] Liberati A, Altman DG, Tetzlaff J, Mulrow C, Gøtzsche PC, Ioannidis JP, et al. The PRISMA statement for reporting systematic reviews and meta-analyses of studies that evaluate health care interventions: explanation and elaboration. Journal of clinical epidemiology. 2009;62:e1-e34.
[113] Xiang Y, Bunpetch V, Zhou W, Ouyang H. Optimization strategies for ACI: A step-chronicle review. J Orthop Translat. 2019;17:3-14.
[114] Lattermann C, Romine SE. Osteochondral allografts: state of the art. Clin Sports Med. 2009;28:285-301, ix.
[115] Swieszkowski W, Tuan BH, Kurzydlowski KJ, Hutmacher DW. Repair and regeneration of osteochondral defects in the articular joints. Biomol Eng. 2007;24:489-95.
[116] Lopa S, Madry H. Bioinspired scaffolds for osteochondral regeneration. Tissue Eng Part A. 2014;20:2052-76.
[117] Lanza R, Langer R, Vacanti JP, Atala A. Principles of tissue engineering: Academic press; 2020.
[118] Liu X, Li T, Zhang D. Research hotspot of seed cell selection in cartilage tissue engineering. Chinese Journal of Tissue Engineering Research. 2021;25:5059.
[119] Phull AR, Eo SH, Abbas Q, Ahmed M, Kim SJ. Applications of Chondrocyte-Based Cartilage Engineering: An Overview. Biomed Res Int. 2016;2016:1879837.
[120] Stockwell RA. Biology of cartilage cells. Cambridge, New York: Cambridge University Press

(CUP) 1979.
[121] Stockwell R. Chondrocytes. Journal of Clinical Pathology Supplement (Royal College of Pathologists). 1978;12:7-13.
[122] Youn I, Choi J, Cao L, Setton L, Guilak F. Zonal variations in the 3D morphology of the chondron measured in situ using serial confocal sections. Osteoarthritis Cartilage. 2006;14:889-97.
[123] Guo H, Torzilli PA. Shape of chondrocytes within articular cartilage affects the solid but not the fluid microenvironment under unconfined compression. Acta biomaterialia. 2016;29:170-9.
[124] Guilak F, Alexopoulos LG, Upton ML, Youn I, Choi JB, Cao L, et al. The pericellular matrix as a transducer of biomechanical and biochemical signals in articular cartilage. Annals of the New York Academy of Sciences. 2006;1068:498-512.
[125] Alexopoulos LG, Setton LA, Guilak F. The biomechanical role of the chondrocyte pericellular matrix in articular cartilage. Acta biomaterialia. 2005;1:317-25.
[126] Likhitpanichkul M, Sun DD, Guo XE, Lai WM, Mow VC. The mechano-electrochemical environment of chondrocytes in articular cartilage explants under unconfined compression: emphasis on the cell matrix interactions. Proceedings of the 2003 Summer Bioengineering Conference, Key Biscayne, FL. 2003.
[127] Schnabel M, Marlovits S, Eckhoff G, Fichtel I, Gotzen L, Vecsei V, et al. Dedifferentiation-associated changes in morphology and gene expression in primary human articular chondrocytes in cell culture. Osteoarthritis Cartilage. 2002;10:62-70.
[128] Caron MM, Emans PJ, Coolsen MM, Voss L, Surtel DA, Cremers A, et al. Redifferentiation of dedifferentiated human articular chondrocytes: comparison of 2D and 3D cultures. Osteoarthritis and cartilage. 2012;20:1170-8.
[129] Lehmann M, Martin F, Mannigel K, Kaltschmidt K, Sack U, Anderer U. Three-dimensional scaffold-free fusion culture: the way to enhanced chondrogenesis of in vitro propagated human articular chondrocytes. European journal of histochemistry: EJH. 2013;57(4):e31.
[130] Grassel S, Ahmed N. Influence of cellular microenvironment and paracrine signals on chondrogenic differentiation. Front Biosci. 2007;12:4946-56.
[131] Tan S, Fang W, Vangsness Jr CT, Han B. Influence of Cellular Microenvironment on Human Articular Chondrocyte Cell Signaling. Cartilage. 2021;13:935S-46S.
[132] Sliogeryte K, Botto L, Lee DA, Knight MM. Chondrocyte dedifferentiation increases cell stiffness by strengthening membrane-actin adhesion. Osteoarthritis Cartilage. 2016;24:912-20.
[133] Darling EM, Athanasiou KA. Articular cartilage bioreactors and bioprocesses. Tissue Eng. 2003;9:9-26.
[134] Georges PC, Janmey PA. Cell type-specific response to growth on soft materials. Journal of applied physiology. 2005;98:1547-53.
[135] Bougault C, Paumier A, Aubert-Foucher E, Mallein-Gerin F. Molecular analysis of chondrocytes cultured in agarose in response to dynamic compression. BMC biotechnology. 2008;8:1-10.
[136] Barlič A, Drobnič M, Maličev E, Kregar-Velikonja N. Quantitative analysis of gene expression in human articular chondrocytes assigned for autologous implantation. Journal of orthopaedic research. 2008;26:847-53.
[137] Tran SC, Cooley AJ, Elder SH. Effect of a mechanical stimulation bioreactor on tissue engineered, scaffold-free cartilage. Biotechnol Bioeng. 2011;108:1421-9.
[138] Parkkinen JJ, Ikonen J, Lammi MJ, Laakkonen J, Tammi M, Helminen HJ. Effects of cyclic hydrostatic pressure on proteoglycan synthesis in cultured chondrocytes and articular cartilage explants.

Arch Biochem Biophys. 1993;300:458-65.
[139] Malaviya P, Nerem RM. Fluid-induced shear stress stimulates chondrocyte proliferation partially mediated via TGF-β 1. Tissue engineering. 2002;8:581-90.
[140] Buschmann MD, Gluzband YA, Grodzinsky AJ, Hunziker EB. Mechanical compression modulates matrix biosynthesis in chondrocyte/agarose culture. Journal of cell science. 1995;108:1497-508.
[141] Smith RL, Donlon BS, Gupta MK, Mohtai M, Das P, Carter DR, et al. Effects of fluid-induced shear on articular chondrocyte morphology and metabolism in vitro. J Orthop Res. 1995;13:824-31.
[142] Huey DJ, Hu JC, Athanasiou KA. Chondrogenically tuned expansion enhances the cartilaginous matrix-forming capabilities of primary, adult, leporine chondrocytes. Cell Transplant. 2013;22:331-40.
[143] Huang BJ, Brown WE, Keown T, Hu JC, Athanasiou KA. Overcoming Challenges in Engineering Large, Scaffold-Free Neocartilage with Functional Properties. Tissue Eng Part A. 2018;24:1652-62.
[144] Saini S, Wick TM. Concentric cylinder bioreactor for production of tissue engineered cartilage: effect of seeding density and hydrodynamic loading on construct development. Biotechnology progress. 2003;19:510-21.
[145] Ebihara G, Sato M, Yamato M, Mitani G, Kutsuna T, Nagai T, et al. Cartilage repair in transplanted scaffold-free chondrocyte sheets using a minipig model. Biomaterials. 2012;33:3846-51.
[146] Okano T, Yamada N, Okuhara M, Sakai H, Sakurai Y. Mechanism of cell detachment from temperature-modulated, hydrophilic-hydrophobic polymer surfaces. Biomaterials. 1995;16:297-303.
[147] Sato M, Yamato M, Hamahashi K, Okano T, Mochida J. Articular cartilage regeneration using cell sheet technology. The Anatomical Record. 2014;297:36-43.
[148] Sato M, Yamato M, Mitani G, Takagaki T, Hamahashi K, Nakamura Y, et al. Combined surgery and chondrocyte cell-sheet transplantation improves clinical and structural outcomes in knee osteoarthritis. NPJ Regen Med. 2019;4:4.
[149] Meyer U, Wiesmann H-P, Libera J, Depprich R, Naujoks C, Handschel J. Cartilage defect regeneration by ex vivo engineered autologous microtissue–preliminary results. in vivo. 2012;26:251-7.
[150] Fujie H, Nansai R, Ando W, Shimomura K, Moriguchi Y, Hart DA, et al. Zone-specific integrated cartilage repair using a scaffold-free tissue engineered construct derived from allogenic synovial mesenchymal stem cells: biomechanical and histological assessments. Journal of Biomechanics. 2015;48:4101-8.
[151] Syed-Picard FN, Du Y, Hertsenberg AJ, Palchesko R, Funderburgh ML, Feinberg AW, et al. Scaffold-free tissue engineering of functional corneal stromal tissue. J Tissue Eng Regen Med. 2018;12:59-69.
[152] Basu A, Rothermund K, Ahmed MN, Syed-Picard FN. Self-assembly of an organized cementum-periodontal ligament-like complex using scaffold-free tissue engineering. Frontiers in Physiology. 2019;10:422.
[153] Stevens K, Kreutziger K, Dupras S, Korte F, Regnier M, Muskheli V, et al. Physiological function and transplantation of scaffold-free and vascularized human cardiac muscle tissue. Proceedings of the National Academy of Sciences. 2009;106:16568-73.
[154] Ma D, Yao H, Tian W, Chen F, Liu Y, Mao T, et al. Enhancing bone formation by transplantation of a scaffold-free tissue-engineered periosteum in a rabbit model. Clinical oral implants research. 2011;22:1193-9.
[155] Stevens KR, Pabon L, Muskheli V, Murry CE. Scaffold-free human cardiac tissue patch created

from embryonic stem cells. Tissue Eng Part A. 2009;15:1211-22.
[156] Toratani T, Nakase J, Numata H, Oshima T, Takata Y, Nakayama K, et al. Scaffold-Free Tissue-Engineered Allogenic Adipose-Derived Stem Cells Promote Meniscus Healing. Arthroscopy. 2017;33:346-54.
[157] Verseijden F, Posthumus-van Sluijs SJ, van Neck JW, Hofer SO, Hovius SE, van Osch GJ. Comparing scaffold-free and fibrin-based adipose-derived stromal cell constructs for adipose tissue engineering: an in vitro and in vivo study. Cell Transplant. 2012;21:2283-97.
[158] Liao HT, Zheng R, Liu W, Zhang WJ, Cao Y, Zhou G. Prefabricated, ear-shaped cartilage tissue engineering by scaffold-free porcine chondrocyte membrane. Plast Reconstr Surg. 2015;135:313e-21e.
[159] Ni M, Rui YF, Tan Q, Liu Y, Xu LL, Chan KM, et al. Engineered scaffold-free tendon tissue produced by tendon-derived stem cells. Biomaterials. 2013;34:2024-37.
[160] Liu Y, Luo H, Wang X, Takemura A, Fang YR, Jin Y, et al. In vitro construction of scaffold-free bilayered tissue-engineered skin containing capillary networks. Biomed Res Int. 2013;2013:561410.
[161] Dissanayaka WL, Zhu L, Hargreaves KM, Jin L, Zhang C. Scaffold-free Prevascularized Microtissue Spheroids for Pulp Regeneration. J Dent Res. 2014;93:1296-303.
[162] Hussain Z, Pei R. Scaffold-free and scaffold-based cellular strategies and opportunities for cornea tissue engineering. Progress in Biomedical Engineering. 2021;3:032003.
[163] Grace D, FannStephen A, YostMichael J. Vascular tissue engineering using scaffold-free prevascular endothelial–fibroblast constructs. BioResearch open access. 2019;8:1-15.
[164] Fujita H, Shimizu K, Yamamoto Y, Ito A, Kamihira M, Nagamori E. Fabrication of scaffold-free contractile skeletal muscle tissue using magnetite-incorporated myogenic C2C12 cells. Journal of Tissue Engineering and Regenerative Medicine. 2010;4:437-43.
[165] Machino R, Matsumoto K, Taniguchi D, Tsuchiya T, Takeoka Y, Taura Y, et al. Replacement of rat tracheas by layered, trachea-like, scaffold-free structures of human cells using a bio-3D printing system. Advanced healthcare materials. 2019;8:1800983.
[166] Ge Y, Gong YY, Xu Z, Lu Y, Fu W. The Application of Sheet Technology in Cartilage Tissue Engineering. Tissue Eng Part B Rev. 2016;22:114-24.
[167] DuRaine GD, Brown WE, Hu JC, Athanasiou KA. Emergence of scaffold-free approaches for tissue engineering musculoskeletal cartilages. Annals of biomedical engineering. 2015;43:543-54.
[168] Anderer U, Libera J. In vitro engineering of human autogenous cartilage. Journal of bone and mineral research. 2002;17:1420-9.
[169] Tran RT, Thevenot P, Zhang Y, Gyawali D, Tang L, Yang J. Scaffold sheet design strategy for soft tissue engineering. Materials. 2010;3:1375-89.
[170] Chang YH, Wu MH. Microbioreactors for Cartilage Tissue Engineering. Methods Mol Biol. 2015;1340:235-44.
[171] Zhang Y, Yu Y, Chen H, Ozbolat IT. Characterization of printable cellular micro-fluidic channels for tissue engineering. Biofabrication. 2013;5:025004.
[172] Tekari A, Luginbuehl R, Hofstetter W, Egli RJ. Transforming growth factor beta signaling is essential for the autonomous formation of cartilage-like tissue by expanded chondrocytes. PLoS One. 2015;10:e0120857.
[173] Jin RL, Park SR, Choi BH, Min B-H. Scaffold-free cartilage fabrication system using passaged porcine chondrocytes and basic fibroblast growth factor. Tissue Engineering Part A. 2009;15:1887-95.
[174] Liau LL, Hassan MNFb, Tang YL, Ng MH, Law JX. Feasibility of human platelet lysate as an alternative to foetal bovine serum for in vitro expansion of chondrocytes. International Journal of

Molecular Sciences. 2021;22:1269.
[175] de Haart M, Marijnissen WJ, van Osch GJ, Verhaar JA. Optimization of chondrocyte expansion in culture: Effect of TGFβ-2, bFGF and L-ascorbic acid on bovine articular chondrocytes. Acta Orthopaedica Scandinavica. 1999;70:55-61.
[176] Ecke A, Lutter A-H, Scholka J, Hansch A, Becker R, Anderer U. Tissue specific differentiation of human chondrocytes depends on cell microenvironment and serum selection. Cells. 2019;8:934.
[177] Al-Masawa ME, Wan Kamarul Zaman WS, Chua KH. Biosafety evaluation of culture-expanded human chondrocytes with growth factor cocktail: a preclinical study. Sci Rep. 2020;10:21583.
[178] Nagai T, Furukawa KS, Sato M, Ushida T, Mochida J. Characteristics of a scaffold-free articular chondrocyte plate grown in rotational culture. Tissue Engineering Part A. 2008;14:1183-93.
[179] Marlovits S, Tichy B, Truppe M, Gruber D, Vécsei V. Chondrogenesis of aged human articular cartilage in a scaffold-free bioreactor. Tissue engineering. 2003;9:1215-26.
[180] Grogan SP, Rieser F, Winkelmann V, Berardi S, Mainil-Varlet P. A static, closed and scaffold-free bioreactor system that permits chondrogenesis in vitro. Osteoarthritis Cartilage. 2003;11:403-11.
[181] Chiu LL, To WT, Lee JM, Waldman SD. Scaffold-free cartilage tissue engineering with a small population of human nasoseptal chondrocytes. The Laryngoscope. 2017;127:E91-E9.
[182] Hossain M, Bergstrom D, Chen X. Computational modelling of the scaffold-free chondrocyte regeneration: a two-way coupling between the cell growth and local fluid flow and nutrient concentration. Biomechanics and modeling in mechanobiology. 2015;14:1217-25.
[183] Li S, Glynne-Jones P, Andriotis OG, Ching KY, Jonnalagadda US, Oreffo RO, et al. Application of an acoustofluidic perfusion bioreactor for cartilage tissue engineering. Lab Chip. 2014;14:4475-85.
[184] Stampoultzis T, Karami P, Pioletti DP. Thoughts on cartilage tissue engineering: A 21st century perspective. Curr Res Transl Med. 2021;69:103299.
[185] Xia C, Mei S, Gu C, Zheng L, Fang C, Shi Y, et al. Decellularized cartilage as a prospective scaffold for cartilage repair. Materials Science and Engineering: C. 2019;101:588-95.
[186] Sutherland AJ, Converse GL, Hopkins RA, Detamore MS. The bioactivity of cartilage extracellular matrix in articular cartilage regeneration. Advanced healthcare materials. 2015;4:29-39.
[187] Brun P, Abatangelo G, Radice M, Zacchi V, Guidolin D, Gordini DD, et al. Chondrocyte aggregation and reorganization into three-dimensional scaffolds. Journal of Biomedical Materials Research: An Official Journal of The Society for Biomaterials, The Japanese Society for Biomaterials, and The Australian Society for Biomaterials and the Korean Society for Biomaterials. 1999;46:337-46.
[188] Schwarz S, Koerber L, Elsaesser AF, Goldberg-Bockhorn E, Seitz AM, Dürselen L, et al. Decellularized cartilage matrix as a novel biomatrix for cartilage tissue-engineering applications. Tissue engineering Part A. 2012;18:2195-209.
[189] Nie X, Chuah YJ, Zhu W, He P, Peck Y, Wang DA. Decellularized tissue engineered hyaline cartilage graft for articular cartilage repair. Biomaterials. 2020;235:119821.
[190] Lin X, Chen J, Qiu P, Zhang Q, Wang S, Su M, et al. Biphasic hierarchical extracellular matrix scaffold for osteochondral defect regeneration. Osteoarthritis and cartilage. 2018;26:433-44.
[191] Vacanti JP. Beyond transplantation. Third annual Samuel Jason Mixter lecture. Arch Surg. 1988;123:545-9.
[192] Kon E, Roffi A, Filardo G, Tesei G, Marcacci M. Scaffold-based cartilage treatments: with or without cells? A systematic review of preclinical and clinical evidence. Arthroscopy: The Journal of Arthroscopic & Related Surgery. 2015;31:767-75.
[193] Grande DA, Halberstadt C, Naughton G, Schwartz R, Manji R. Evaluation of matrix scaffolds for

tissue engineering of articular cartilage grafts. J Biomed Mater Res. 1997;34:211-20.
[194] Moutos FT, Guilak F. Composite scaffolds for cartilage tissue engineering. Biorheology. 2008;45:501-12.
[195] Itay S, Abramovici A, Nevo Z. Use of cultured embryonal chick epiphyseal chondrocytes as grafts for defects in chick articular cartilage. Clinical orthopaedics and related research. 1987:284-303.
[196] Homminga GN, Bulstra SK, Bouwmeester PS, van der Linden AJ. Perichondral grafting for cartilage lesions of the knee. J Bone Joint Surg Br. 1990;72:1003-7.
[197] Wakitani S, Kimura T, Hirooka A, Ochi T, Yoneda M, Yasui N, et al. Repair of rabbit articular surfaces with allograft chondrocytes embedded in collagen gel. J Bone Joint Surg Br. 1989;71:74-80.
[198] Ben-Yishay A, Grande DA, Schwartz RE, Menche D, Pitman MD. Repair of articular cartilage defects with collagen-chondrocyte allografts. Tissue Eng. 1995;1:119-33.
[199] Liu Y, Chen F, Liu W, Cui L, Shang Q, Xia W, et al. Repairing large porcine full-thickness defects of articular cartilage using autologous chondrocyte-engineered cartilage. Tissue engineering. 2002;8:709-21.
[200] Vacanti CA, Langer R, Schloo B, Vacanti JP. Synthetic polymers seeded with chondrocytes provide a template for new cartilage formation. Plast Reconstr Surg. 1991;88:753-9.
[201] Honda M, Yada T, Ueda M, Kimata K. Cartilage formation by cultured chondrocytes in a new scaffold made of poly (L-lactide-ϵ-caprolactone) sponge. Journal of oral and maxillofacial surgery. 2000;58:767-75.
[202] Sechriest VF, Miao YJ, Niyibizi C, Westerhausen-Larson A, Matthew HW, Evans CH, et al. GAG-augmented polysaccharide hydrogel: a novel biocompatible and biodegradable material to support chondrogenesis. J Biomed Mater Res. 2000;49:534-41.
[203] Freed L, Grande D, Lingbin Z, Emmanual J, Marquis J, Langer R. Joint resurfacing using allograft chondrocytes and synthetic biodegradable polymer scaffolds. Journal of biomedical materials research. 1994;28:891-9.
[204] Peretti GM, Randolph MA, Zaporojan V, Bonassar LJ, Xu JW, Fellers JC, et al. A biomechanical analysis of an engineered cell-scaffold implant for cartilage repair. Ann Plast Surg. 2001;46:533-7.
[205] Bicho D, Pina S, Reis RL, Oliveira JM. Commercial Products for Osteochondral Tissue Repair and Regeneration. Adv Exp Med Biol. 2018;1058:415-28.
[206] Cengiz IF, Pereira H, de Girolamo L, Cucchiarini M, Espregueira-Mendes J, Reis RL, et al. Orthopaedic regenerative tissue engineering en route to the holy grail: disequilibrium between the demand and the supply in the operating room. Journal of Experimental Orthopaedics. 2018;5:1-14.
[207] Wasyleczko M, Sikorska W, Chwojnowski A. Review of Synthetic and Hybrid Scaffolds in Cartilage Tissue Engineering. Membranes (Basel). 2020;10:348.
[208] Riff AJ, Davey A, Cole BJ. Emerging technologies in cartilage restoration. Joint Preservation of the knee: Springer; 2019. p. 295-319.
[209] Erggelet C, Neumann K, Endres M, Haberstroh K, Sittinger M, Kaps C. Regeneration of ovine articular cartilage defects by cell-free polymer-based implants. Biomaterials. 2007;28:5570-80.
[210] Erggelet C, Endres M, Neumann K, Morawietz L, Ringe J, Haberstroh K, et al. Formation of cartilage repair tissue in articular cartilage defects pretreated with microfracture and covered with cell-free polymer-based implants. J Orthop Res. 2009;27:1353-60.
[211] Siclari A, Mascaro G, Gentili C, Cancedda R, Boux E. A cell-free scaffold-based cartilage repair provides improved function hyaline-like repair at one year. Clinical Orthopaedics and Related Research®. 2012;470:910-9.

[212] Nogami M, Kimura T, Seki S, Matsui Y, Yoshida T, Koike-Soko C, et al. A Human Amnion-Derived Extracellular Matrix-Coated Cell-Free Scaffold for Cartilage Repair: In Vitro and In Vivo Studies. Tissue Eng Part A. 2016;22:680-8.
[213] Xuan H, Hu H, Geng C, Song J, Shen Y, Lei D, et al. Biofunctionalized chondrogenic shape-memory ternary scaffolds for efficient cell-free cartilage regeneration. Acta Biomaterialia. 2020;105:97-110.
[214] Efe T, Theisen C, Fuchs-Winkelmann S, Stein T, Getgood A, Rominger MB, et al. Cell-free collagen type I matrix for repair of cartilage defects-clinical and magnetic resonance imaging results. Knee Surg Sports Traumatol Arthrosc. 2012;20:1915-22.
[215] Trattnig S, Ohel K, Mlynarik V, Juras V, Zbyn S, Korner A. Morphological and compositional monitoring of a new cell-free cartilage repair hydrogel technology–GelrinC by MR using semi-quantitative MOCART scoring and quantitative T2 index and new zonal T2 index calculation. Osteoarthritis and Cartilage. 2015;23:2224-32.
[216] Zhang S, Chuah SJ, Lai RC, Hui JHP, Lim SK, Toh WS. MSC exosomes mediate cartilage repair by enhancing proliferation, attenuating apoptosis and modulating immune reactivity. Biomaterials. 2018;156:16-27.
[217] Lu J, Shen X, Sun X, Yin H, Yang S, Lu C, et al. Increased recruitment of endogenous stem cells and chondrogenic differentiation by a composite scaffold containing bone marrow homing peptide for cartilage regeneration. Theranostics. 2018;8:5039-58.
[218] Lu Y, Dhanaraj S, Wang Z, Bradley DM, Bowman SM, Cole BJ, et al. Minced cartilage without cell culture serves as an effective intraoperative cell source for cartilage repair. Journal of Orthopaedic Research. 2006;24:1261-70.
[219] Ovsianikov A, Khademhosseini A, Mironov V. The Synergy of Scaffold-Based and Scaffold-Free Tissue Engineering Strategies. Trends Biotechnol. 2018;36:348-57.
[220] Alison MR, Poulsom R, Forbes S, Wright NA. An introduction to stem cells. J Pathol. 2002;197:419-23.
[221] Abofila M, Azab AE, Al Shebani AM, Bshena AN. Stem Cells: Insights into Niche, Classification, Identification, Characterization, Mechanisms of Regeneration by Using Stem Cells, and Applications in Joint Disease Remedy. J Biotech Bioprocess. 2021;2:2766-314.
[222] Ramalho-Santos M, Yoon S, Matsuzaki Y, Mulligan RC, Melton DA. " Stemness": transcriptional profiling of embryonic and adult stem cells. Science. 2002;298:597-600.
[223] Zakrzewski W, Dobrzynski M, Szymonowicz M, Rybak Z. Stem cells: past, present, and future. Stem Cell Res Ther. 2019;10:68.
[224] Lin T, Ambasudhan R, Yuan X, Li W, Hilcove S, Abujarour R, et al. A chemical platform for improved induction of human iPSCs. Nat Methods. 2009;6:805-8.
[225] Inui A, Iwakura T, Reddi AH. Human stem cells and articular cartilage regeneration. Cells. 2012;1:994-1009.
[226] Minguell JJ, Erices A, Conget P. Mesenchymal stem cells. Exp Biol Med (Maywood). 2001;226:507-20.
[227] Caplan AI. Mesenchymal stem cells. J Orthop Res. 1991;9:641-50.
[228] Vasanthan J, Gurusamy N, Rajasingh S, Sigamani V, Kirankumar S, Thomas EL, et al. Role of human mesenchymal stem cells in regenerative therapy. Cells. 2021;10:54.
[229] Stamnitz S, Klimczak A. Mesenchymal stem cells, bioactive factors, and scaffolds in bone repair: from research perspectives to clinical practice. Cells. 2021;10:1925.

[230] Ding D-C, Shyu W-C, Lin S-Z. Mesenchymal stem cells. Cell transplantation. 2011;20:5-14.
[231] Friedenstein AJ. Precursor cells of mechanocytes. International review of cytology. 1976;47:327-59.
[232] Ohishi M, Schipani E. Bone marrow mesenchymal stem cells. J Cell Biochem. 2010;109:277-82.
[233] Haynesworth SE, Baber MA, Caplan AI. Cell surface antigens on human marrow-derived mesenchymal cells are detected by monoclonal antibodies. Bone. 1992;13:69-80.
[234] Pittenger MF, Mackay AM, Beck SC, Jaiswal RK, Douglas R, Mosca JD, et al. Multilineage potential of adult human mesenchymal stem cells. science. 1999;284:143-7.
[235] Lv F-J, Tuan RS, Cheung KM, Leung VY. Concise review: the surface markers and identity of human mesenchymal stem cells. Stem cells. 2014;32:1408-19.
[236] L Ramos T, Sánchez-Abarca LI, Muntión S, Preciado S, Puig N, López-Ruano G, et al. MSC surface markers (CD44, CD73, and CD90) can identify human MSC-derived extracellular vesicles by conventional flow cytometry. Cell Communication and Signaling. 2016;14:1-14.
[237] Dominici M, Le Blanc K, Mueller I, Slaper-Cortenbach I, Marini F, Krause D, et al. Minimal criteria for defining multipotent mesenchymal stromal cells. The International Society for Cellular Therapy position statement. Cytotherapy. 2006;8:315-7.
[238] Horwitz EM, Le Blanc K, Dominici M, Mueller I, Slaper-Cortenbach I, Marini FC, et al. Clarification of the nomenclature for MSC: The International Society for Cellular Therapy position statement. Cytotherapy. 2005;7:393-5.
[239] Zha K, Li X, Yang Z, Tian G, Sun Z, Sui X, et al. Heterogeneity of mesenchymal stem cells in cartilage regeneration: from characterization to application. NPJ Regenerative Medicine. 2021;6:1-15.
[240] Pevsner-Fischer M, Levin S, Zipori D. The origins of mesenchymal stromal cell heterogeneity. Stem Cell Reviews and Reports. 2011;7:560-8.
[241] Rennerfeldt DA, Van Vliet KJ. Concise review: when colonies are not clones: evidence and implications of intracolony heterogeneity in mesenchymal stem cells. Stem cells. 2016;34:1135-41.
[242] Zucherato VS, Penariol LB, Silva LE, Padovan CC, Poli-Neto OB, Rosa-e-Silva JC, et al. Identification of suitable reference genes for mesenchymal stem cells from menstrual blood of women with endometriosis. Scientific reports. 2021;11:1-10.
[243] Al Bahrawy M. Comparison of the Migration Potential through Microperforated Membranes of CD146+ GMSC Population versus Heterogeneous GMSC Population. Stem Cells International. 2021;2021:5583421.
[244] Gang EJ, Bosnakovski D, Figueiredo CA, Visser JW, Perlingeiro RC. SSEA-4 identifies mesenchymal stem cells from bone marrow. Blood. 2007;109:1743-51.
[245] Lee A-Y, Lee J, Kim C-L, Lee KS, Lee S-H, Gu N-Y, et al. Comparative studies on proliferation, molecular markers and differentiation potential of mesenchymal stem cells from various tissues (adipose, bone marrow, ear skin, abdominal skin, and lung) and maintenance of multipotency during serial passages in miniature pig. Research in Veterinary Science. 2015;100:115-24.
[246] Maleki M, Ghanbarvand F, Reza Behvarz M, Ejtemaei M, Ghadirkhomi E. Comparison of mesenchymal stem cell markers in multiple human adult stem cells. Int J Stem Cells. 2014;7:118-26.
[247] Giovannini S, Diaz-Romero J, Aigner T, Heini P, Mainil-Varlet P, Nesic D. Micromass co-culture of human articular chondrocytes and human bone marrow mesenchymal stem cells to investigate stable neocartilage tissue formation in vitro. Eur Cell Mater. 2010;20:59.
[248] Letouzey V, Tan KS, Deane JA, Ulrich D, Gurung S, Ong YR, et al. Isolation and characterisation of mesenchymal stem/stromal cells in the ovine endometrium. PloS one. 2015;10:e0127531.

[249] Akpinar G, Yoneten KK, Kasap M, Karaoz E. Search for novel plasma membrane proteins as potential biomarkers in human mesenchymal stem cells derived from dental pulp, adipose tissue, bone marrow, and hair follicle. The Journal of membrane biology. 2021;254:409-22.
[250] Imboden S, Liu X, Lee BS, Payne MC, Hsieh C-J, Lin NY. Investigating heterogeneities of live mesenchymal stromal cells using AI-based label-free imaging. Scientific reports. 2021;11:1-11.
[251] Fellows CR, Matta C, Zakany R, Khan IM, Mobasheri A. Adipose, Bone Marrow and Synovial Joint-Derived Mesenchymal Stem Cells for Cartilage Repair. Front Genet. 2016;7:213.
[252] Richter W. Mesenchymal stem cells and cartilage in situ regeneration. J Intern Med. 2009;266:390-405.
[253] Filardo G, Madry H, Jelic M, Roffi A, Cucchiarini M, Kon E. Mesenchymal stem cells for the treatment of cartilage lesions: from preclinical findings to clinical application in orthopaedics. Knee surgery, sports traumatology, arthroscopy. 2013;21:1717-29.
[254] Pridie K. A method of resurfacing osteoarthric knee joints. J Bone and Joint Surg41-B. 1959;3:618-9.
[255] Steadman J, Rodkey W, Briggs K, Rodrigo J. The microfracture technic in the management of complete cartilage defects in the knee joint. Der Orthopade. 1999;28:26-32.
[256] McNickle AG, Provencher MT, Cole BJ. Overview of existing cartilage repair technology. Sports medicine and arthroscopy review. 2008;16:196-201.
[257] Yucekul A, Ozdil D, Kutlu NH, Erdemli E, Aydin HM, Doral MN. Tri-layered composite plug for the repair of osteochondral defects: in vivo study in sheep. Journal of Tissue Engineering. 2017;8:1-10.
[258] Hoemann CD, Hurtig M, Rossomacha E, Sun J, Chevrier A, Shive MS, et al. Chitosan-glycerol phosphate/blood implants improve hyaline cartilage repair in ovine microfracture defects. JBJS. 2005;87:2671-86.
[259] Hoemann C, Sun J, McKee M, Chevrier A, Rossomacha E, Rivard G-E, et al. Chitosan–glycerol phosphate/blood implants elicit hyaline cartilage repair integrated with porous subchondral bone in microdrilled rabbit defects. Osteoarthritis and Cartilage. 2007;15:78-89.
[260] Marchand C, Chen G, Tran-Khanh N, Sun J, Chen H, Buschmann MD, et al. Microdrilled cartilage defects treated with thrombin-solidified chitosan/blood implant regenerate a more hyaline, stable, and structurally integrated osteochondral unit compared to drilled controls. Tissue Eng Part A. 2012;18:508-19.
[261] Caterson EJ, Nesti LJ, Li WJ, Danielson KG, Albert TJ, Vaccaro AR, et al. Three-dimensional cartilage formation by bone marrow-derived cells seeded in polylactide/alginate amalgam. Journal of Biomedical Materials Research: An Official Journal of The Society for Biomaterials, The Japanese Society for Biomaterials, and The Australian Society for Biomaterials and the Korean Society for Biomaterials. 2001;57:394-403.
[262] Schagemann J, Paul S, Casper M, Rohwedel J, Kramer J, Kaps C, et al. Chondrogenic differentiation of bone marrow-derived mesenchymal stromal cells via biomimetic and bioactive poly-ε-caprolactone scaffolds. Journal of biomedical materials research Part A. 2013;101:1620-8.
[263] Zhao Q, Wang S, Tian J, Wang L, Dong S, Xia T, et al. Combination of bone marrow concentrate and PGA scaffolds enhance bone marrow stimulation in rabbit articular cartilage repair. Journal of Materials Science: Materials in Medicine. 2013;24:793-801.
[264] Patrascu JM, Krüger JP, Böss HG, Ketzmar AK, Freymann U, Sittinger M, et al. Polyglycolic acid-hyaluronan scaffolds loaded with bone marrow-derived mesenchymal stem cells show chondrogenic differentiation in vitro and cartilage repair in the rabbit model. Journal of Biomedical

Materials Research Part B: Applied Biomaterials. 2013;101:1310-20.
[265] Siclari A, Mascaro G, Kaps C, Boux E. A 5-year follow-up after cartilage repair in the knee using a platelet-rich plasma-immersed polymer-based implant. The Open Orthopaedics Journal. 2014;8:346.
[266] Commins J, Irwin R, Matuska A, Goodale M, Delco M, Fortier L. Biological mechanisms for cartilage repair using a biocartilage scaffold: cellular adhesion/migration and bioactive proteins. Cartilage. 2021;13:984S-92S.
[267] Yin Z, Yang X, Jiang Y, Xing L, Xu Y, Lu Y, et al. Platelet-rich plasma combined with agarose as a bioactive scaffold to enhance cartilage repair: an in vitro study. Journal of biomaterials applications. 2014;28:1039-50.
[268] Lee P, Tran K, Chang W, Shelke NB, Kumbar SG, Yu X. Influence of chondroitin sulfate and hyaluronic acid presence in nanofibers and its alignment on the bone marrow stromal cells: cartilage regeneration. Journal of biomedical nanotechnology. 2014;10:1469-79.
[269] Im GI. Endogenous Cartilage Repair by Recruitment of Stem Cells. Tissue Eng Part B Rev. 2016;22:160-71.
[270] Coburn J, Gibson M, Bandalini PA, Laird C, Mao HQ, Moroni L, et al. Biomimetics of the Extracellular Matrix: An Integrated Three-Dimensional Fiber-Hydrogel Composite for Cartilage Tissue Engineering. Smart Struct Syst. 2011;7:213-22.
[271] Werb Z, Chin JR. Extracellular matrix remodeling during morphogenesis. Ann N Y Acad Sci. 1998;857:110-8.
[272] Lotz M. Cytokines in cartilage injury and repair. Clinical Orthopaedics and Related Research®. 2001;391:S108-S15.
[273] Lee P, Manoukian OS, Zhou G, Wang Y, Chang W, Yu X, et al. Osteochondral scaffold combined with aligned nanofibrous scaffolds for cartilage regeneration. RSC advances. 2016;6:72246-55.
[274] Lee S-H, Shin H. Matrices and scaffolds for delivery of bioactive molecules in bone and cartilage tissue engineering. Advanced drug delivery reviews. 2007;59:339-59.
[275] Fortier LA, Barker JU, Strauss EJ, McCarrel TM, Cole BJ. The role of growth factors in cartilage repair. Clin Orthop Relat Res. 2011;469:2706-15.
[276] Kopesky PW, Vanderploeg EJ, Kisiday JD, Frisbie DD, Sandy JD, Grodzinsky AJ. Controlled delivery of transforming growth factor beta1 by self-assembling peptide hydrogels induces chondrogenesis of bone marrow stromal cells and modulates Smad2/3 signaling. Tissue Eng Part A. 2011;17:83-92.
[277] Zhu W, Castro NJ, Cheng X, Keidar M, Zhang LG. Cold atmospheric plasma modified electrospun scaffolds with embedded microspheres for improved cartilage regeneration. PLoS One. 2015;10:e0134729.
[278] Deng J, She R, Huang W, Dong Z, Mo G, Liu B. A silk fibroin/chitosan scaffold in combination with bone marrow-derived mesenchymal stem cells to repair cartilage defects in the rabbit knee. J Mater Sci Mater Med. 2013;24:2037-46.
[279] Lin D, Cai B, Wang L, Cai L, Wang Z, Xie J, et al. A viscoelastic PEGylated poly(glycerol sebacate)-based bilayer scaffold for cartilage regeneration in full-thickness osteochondral defect. Biomaterials. 2020;253:120095.
[280] Toh WS, Lim TC, Kurisawa M, Spector M. Modulation of mesenchymal stem cell chondrogenesis in a tunable hyaluronic acid hydrogel microenvironment. Biomaterials. 2012;33:3835-45.
[281] Wang T, Lai JH, Yang F. Effects of Hydrogel Stiffness and Extracellular Compositions on Modulating Cartilage Regeneration by Mixed Populations of Stem Cells and Chondrocytes In Vivo.

Tissue Eng Part A. 2016;22:1348-56.
[282] Guo P, Yuan Y, Chi F. Biomimetic alginate/polyacrylamide porous scaffold supports human mesenchymal stem cell proliferation and chondrogenesis. Materials Science and Engineering: C. 2014;42:622-8.
[283] NANSAI R, SUZUKI T, SHIMOMURA K, ANDO W, NAKAMURA N, FUJIE H. Surface morphology and stiffness of cartilage-like tissue repaired with a scaffold-free tissue engineered construct. Journal of Biomechanical Science and Engineering. 2011;6:40-8.
[284] Wu Y, Yang Z, Law JBK, He AY, Abbas AA, Denslin V, et al. The combined effect of substrate stiffness and surface topography on chondrogenic differentiation of mesenchymal stem cells. Tissue Engineering Part A. 2017;23:43-54.
[285] Murphy CM, Matsiko A, Haugh MG, Gleeson JP, O'Brien FJ. Mesenchymal stem cell fate is regulated by the composition and mechanical properties of collagen–glycosaminoglycan scaffolds. Journal of the mechanical behavior of biomedical materials. 2012;11:53-62.
[286] Shanmugasundaram S, Chaudhry H, Arinzeh TL. Microscale versus nanoscale scaffold architecture for mesenchymal stem cell chondrogenesis. Tissue Engineering Part A. 2011;17:831-40.
[287] Nerurkar NL, Sen S, Baker BM, Elliott DM, Mauck RL. Dynamic culture enhances stem cell infiltration and modulates extracellular matrix production on aligned electrospun nanofibrous scaffolds. Acta biomaterialia. 2011;7:485-91.
[288] Schlichting K, Schell H, Kleemann RU, Schill A, Weiler A, Duda GN, et al. Influence of scaffold stiffness on subchondral bone and subsequent cartilage regeneration in an ovine model of osteochondral defect healing. Am J Sports Med. 2008;36:2379-91.
[289] Xing F, Li L, Zhou C, Long C, Wu L, Lei H, et al. Regulation and directing stem cell fate by tissue engineering functional microenvironments: scaffold physical and chemical cues. Stem Cells International. 2019;2019:2180925.
[290] Chen C, Bai X, Ding Y, Lee I-S. Electrical stimulation as a novel tool for regulating cell behavior in tissue engineering. Biomaterials Research. 2019;23:1-12.
[291] Vaca-Gonzalez JJ, Clara-Trujillo S, Guillot-Ferriols M, Rodenas-Rochina J, Sanchis MJ, Ribelles JLG, et al. Effect of electrical stimulation on chondrogenic differentiation of mesenchymal stem cells cultured in hyaluronic acid - Gelatin injectable hydrogels. Bioelectrochemistry. 2020;134:107536.
[292] Balint R, Cassidy NJ, Cartmell SH. Electrical stimulation: a novel tool for tissue engineering. Tissue Engineering Part B: Reviews. 2013;19:48-57.
[293] Lin S, Lee WYW, Feng Q, Xu L, Wang B, Man GCW, et al. Synergistic effects on mesenchymal stem cell-based cartilage regeneration by chondrogenic preconditioning and mechanical stimulation. Stem cell research & therapy. 2017;8:1-12.
[294] Dai Y, Gao Z, Ma L, Wang D, Gao C. Cell-free HA-MA/PLGA scaffolds with radially oriented pores for in situ inductive regeneration of full thickness cartilage defects. Macromolecular Bioscience. 2016;16:1632-42.
[295] Wong KL, Lee KBL, Tai BC, Law P, Lee EH, Hui JH. Injectable cultured bone marrow–derived mesenchymal stem cells in varus knees with cartilage defects undergoing high tibial osteotomy: a prospective, randomized controlled clinical trial with 2 Years' follow-up. Arthroscopy: The Journal of Arthroscopic & Related Surgery. 2013;29:2020-8.
[296] Lee KB, Hui JH, Song IC, Ardany L, Lee EH. Injectable mesenchymal stem cell therapy for large cartilage defects—a porcine model. Stem cells. 2007;25:2964-71.
[297] Elisseeff J. Injectable cartilage tissue engineering. Expert Opin Biol Ther. 2004;4:1849-59.

[298] Roffi A, Nakamura N, Sanchez M, Cucchiarini M, Filardo G. Injectable Systems for Intra-Articular Delivery of Mesenchymal Stromal Cells for Cartilage Treatment: A Systematic Review of Preclinical and Clinical Evidence. Int J Mol Sci. 2018;19:3322.
[299] Marquardt LM, Heilshorn SC. Design of Injectable Materials to Improve Stem Cell Transplantation. Curr Stem Cell Rep. 2016;2:207-20.
[300] Xu J, Feng Q, Lin S, Yuan W, Li R, Li J, et al. Injectable stem cell-laden supramolecular hydrogels enhance in situ osteochondral regeneration via the sustained co-delivery of hydrophilic and hydrophobic chondrogenic molecules. Biomaterials. 2019;210:51-61.
[301] Tang C, Jin C, Du X, Yan C, Min B-H, Xu Y, et al. An autologous bone marrow mesenchymal stem cell–derived extracellular matrix scaffold applied with bone marrow stimulation for cartilage repair. Tissue Engineering Part A. 2014;20:2455-62.
[302] Seong Toh W, Bindzus Foldager C, Hoi Po Hui J, Reino Olsen B, Spector M. Exploiting stem cell-extracellular matrix interactions for cartilage regeneration: a focus on basement membrane molecules. Current Stem Cell Research & Therapy. 2016;11:618-25.
[303] Cheng A, Cain SA, Tian P, Baldwin AK, Uppanan P, Kielty CM, et al. Recombinant extracellular matrix protein fragments support human embryonic stem cell chondrogenesis. Tissue Engineering Part A. 2018;24:968-78.
[304] Li A, Wei Y, Hung C, Vunjak-Novakovic G. Chondrogenic properties of collagen type XI, a component of cartilage extracellular matrix. Biomaterials. 2018;173:47-57.
[305] Kim HD, Heo J, Hwang Y, Kwak S-Y, Park OK, Kim H, et al. Extracellular-matrix-based and Arg-Gly-Asp–modified photopolymerizing hydrogels for cartilage tissue engineering. Tissue Engineering Part A. 2015;21:757-66.
[306] Hastar N, Arslan E, Guler MO, Tekinay AB. Peptide-Based Materials for Cartilage Tissue Regeneration. Adv Exp Med Biol. 2017;1030:155-66.
[307] Kiyotake EA, Beck EC, Detamore MS. Cartilage extracellular matrix as a biomaterial for cartilage regeneration. Annals of the New York Academy of Sciences. 2016;1383:139-59.
[308] Deng C, Zhu H, Li J, Feng C, Yao Q, Wang L, et al. Bioactive scaffolds for regeneration of cartilage and subchondral bone interface. Theranostics. 2018;8:1940.
[309] Fu L, Li P, Li H, Gao C, Yang Z, Zhao T, et al. The application of bioreactors for cartilage tissue engineering: advances, limitations, and future perspectives. Stem Cells International. 2021;2021:6621806.
[310] Li F, Truong VX, Thissen H, Frith JE, Forsythe JS. Microfluidic encapsulation of human mesenchymal stem cells for articular cartilage tissue regeneration. ACS applied materials & interfaces. 2017;9:8589-601.
[311] Dong Y, Liu Y, Chen Y, Sun X, Zhang L, Zhang Z, et al. Spatiotemporal regulation of endogenous MSCs using a functional injectable hydrogel system for cartilage regeneration. NPG Asia Materials. 2021;13:1-17.
[312] Futrega K, Palmer JS, Kinney M, Lott WB, Ungrin MD, Zandstra PW, et al. The microwell-mesh: a novel device and protocol for the high throughput manufacturing of cartilage microtissues. Biomaterials. 2015;62:1-12.
[313] Markway BD, Tan G-K, Brooke G, Hudson JE, Cooper-White JJ, Doran MR. Enhanced chondrogenic differentiation of human bone marrow-derived mesenchymal stem cells in low oxygen environment micropellet cultures. Cell transplantation. 2010;19:29-42.
[314] Yin H, Wang Y, Sun Z, Sun X, Xu Y, Li P, et al. Induction of mesenchymal stem cell chondrogenic

differentiation and functional cartilage microtissue formation for in vivo cartilage regeneration by cartilage extracellular matrix-derived particles. Acta Biomater. 2016;33:96-109.
[315] Millan C, Cavalli E, Groth T, Maniura-Weber K, Zenobi-Wong M. Engineered microtissues formed by schiff base crosslinking restore the chondrogenic potential of aged mesenchymal stem cells. Advanced healthcare materials. 2015;4:1348-58.
[316] Nguyen KT, West JL. Photopolymerizable hydrogels for tissue engineering applications. Biomaterials. 2002;23:4307-14.
[317] Xu Y, Peng J, Richards G, Lu S, Eglin D. Optimization of electrospray fabrication of stem cell–embedded alginate–gelatin microspheres and their assembly in 3D-printed poly (ε-caprolactone) scaffold for cartilage tissue engineering. Journal of orthopaedic translation. 2019;18:128-41.
[318] Yunmin M, Yuanyuan L, Haiping C, Qingxi H. Application and analysis of biological electrospray in tissue engineering. The open biomedical engineering journal. 2015;9:133.
[319] Gerdes S, Ramesh S, Mostafavi A, Tamayol A, Rivero IV, Rao P. Extrusion-based 3D (Bio) Printed Tissue Engineering Scaffolds: Process–Structure–Quality Relationships. ACS Biomaterials Science & Engineering. 2021;7:4694-717.
[320] Kaur G, Pickrell G, Sriranganathan N, Kumar V, Homa D. Review and the state of the art: sol–gel and melt quenched bioactive glasses for tissue engineering. Journal of Biomedical Materials Research Part B: Applied Biomaterials. 2016;104:1248-75.
[321] Aldemir Dikici B, Claeyssens F. Basic principles of emulsion templating and its use as an emerging manufacturing method of tissue engineering scaffolds. Frontiers in Bioengineering and Biotechnology. 2020;8:875.
[322] Choi NW, Cabodi M, Held B, Gleghorn JP, Bonassar LJ, Stroock AD. Microfluidic scaffolds for tissue engineering. Nature materials. 2007;6:908-15.
[323] Inamdar NK, Borenstein JT. Microfluidic cell culture models for tissue engineering. Current opinion in biotechnology. 2011;22:681-9.
[324] Zuk PA, Zhu M, Mizuno H, Huang J, Futrell JW, Katz AJ, et al. Multilineage cells from human adipose tissue: implications for cell-based therapies. Tissue engineering. 2001;7:211-28.
[325] Kasir R, Vernekar VN, Laurencin CT. Regenerative engineering of cartilage using adipose-derived stem cells. Regenerative engineering and translational medicine. 2015;1:42-9.
[326] Kim J-H, Park JS, Yang HN, Woo DG, Jeon SY, Do H-J, et al. The use of biodegradable PLGA nanoparticles to mediate SOX9 gene delivery in human mesenchymal stem cells (hMSCs) and induce chondrogenesis. Biomaterials. 2011;32:268-78.
[327] Veronesi F, Maglio M, Tschon M, Aldini NN, Fini M. Adipose-derived mesenchymal stem cells for cartilage tissue engineering: state-of-the-art in in vivo studies. Journal of biomedical materials research Part A. 2014;102:2448-66.
[328] Vinatier C, Guicheux J. Cartilage tissue engineering: From biomaterials and stem cells to osteoarthritis treatments. Ann Phys Rehabil Med. 2016;59:139-44.
[329] De Bari C, Dell'Accio F, Tylzanowski P, Luyten FP. Multipotent mesenchymal stem cells from adult human synovial membrane. Arthritis & Rheumatism. 2001;44:1928-42.
[330] Harvanová D, Tóthová T, Sarissky M, Amrichová J, Rosocha J. Isolation and characterization of synovial mesenchymal stem cells. Folia Biol (Praha). 2011;57:119-24.
[331] Pacifici M, Koyama E, Shibukawa Y, Wu C, Tamamura Y, ENOMOTO-IWAMOTO M, et al. Cellular and molecular mechanisms of synovial joint and articular cartilage formation. Annals of the New York Academy of Sciences. 2006;1068:74-86.

[332] Pan J-F, Li S, Guo C-A, Xu D-L, Zhang F, Yan Z-Q, et al. Evaluation of synovium-derived mesenchymal stem cells and 3D printed nanocomposite scaffolds for tissue engineering. Science and Technology of Advanced Materials. 2015;16:045001.
[333] Jones BA, Pei M. Synovium-derived stem cells: a tissue-specific stem cell for cartilage engineering and regeneration. Tissue Engineering Part B: Reviews. 2012;18:301-11.
[334] Suzuki S, Muneta T, Tsuji K, Ichinose S, Makino H, Umezawa A, et al. Properties and usefulness of aggregates of synovial mesenchymal stem cells as a source for cartilage regeneration. Arthritis research & therapy. 2012;14:1-13.
[335] Williams R, Khan IM, Richardson K, Nelson L, McCarthy HE, Analbelsi T, et al. Identification and clonal characterisation of a progenitor cell sub-population in normal human articular cartilage. PloS one. 2010;5:e13246.
[336] Pretzel D, Linss S, Rochler S, Endres M, Kaps C, Alsalameh S, et al. Relative percentage and zonal distribution of mesenchymal progenitor cells in human osteoarthritic and normal cartilage. Arthritis research & therapy. 2011;13:1-15.
[337] Nelson L, McCarthy HE, Fairclough J, Williams R, Archer CW. Evidence of a viable pool of stem cells within human osteoarthritic cartilage. Cartilage. 2014;5:203-14.
[338] Huang YZ, Xie HQ, Silini A, Parolini O, Zhang Y, Deng L, et al. Mesenchymal Stem/Progenitor Cells Derived from Articular Cartilage, Synovial Membrane and Synovial Fluid for Cartilage Regeneration: Current Status and Future Perspectives. Stem Cell Rev Rep. 2017;13:575-86.
[339] Frisbie DD, McCarthy HE, Archer CW, Barrett MF, McIlwraith CW. Evaluation of articular cartilage progenitor cells for the repair of articular defects in an equine model. J Bone Joint Surg Am. 2015;97:484-93.
[340] Park JB, Bronzino JD. Biomaterials: principles and applications. 1st Edition ed. Boca Raton: CRC Press; 2002.
[341] Shoichet MS. Polymer scaffolds for biomaterials applications. Macromolecules. 2010;43:581-91.
[342] Kim HS, Kumbar SG, Nukavarapu SP. Biomaterial-directed cell behavior for tissue engineering. Current Opinion in biomedical engineering. 2021;17:100260.
[343] Schacht E. Polymer chemistry and hydrogel systems. Journal of Physics: Conference Series: IOP Publishing; 2004. p. 004.
[344] Ahmed EM. Hydrogel: Preparation, characterization, and applications: A review. Journal of advanced research. 2015;6:105-21.
[345] Zhao W, Jin X, Cong Y, Liu Y, Fu J. Degradable natural polymer hydrogels for articular cartilage tissue engineering. Journal of Chemical Technology & Biotechnology. 2013;88:327-39.
[346] Whu SW, Hung K-C, Hsieh K-H, Chen C-H, Tsai C-L, Hsu S-h. In vitro and in vivo evaluation of chitosan–gelatin scaffolds for cartilage tissue engineering. Materials Science and Engineering: C. 2013;33:2855-63.
[347] Jin R, Teixeira LM, Dijkstra PJ, Karperien M, Van Blitterswijk C, Zhong Z, et al. Injectable chitosan-based hydrogels for cartilage tissue engineering. Biomaterials. 2009;30:2544-51.
[348] Gudmann N, Karsdal M. Type II collagen. Biochemistry of collagens, laminins and elastin: Elsevier; 2016. p. 13-20.
[349] Henriksen K, Karsdal M. Biochemistry of Collagens, Laminins and Elastin. 1st Edition ed: Academic Press Cambridge, MA, USA:; 2016.
[350] Shoulders MD, Raines RT. Collagen structure and stability. Annual review of biochemistry. 2009;78:929-58.

[351] Sherman VR, Yang W, Meyers MA. The materials science of collagen. Journal of the mechanical behavior of biomedical materials. 2015;52:22-50.
[352] Simmons D, Kearney J. Evaluation of collagen cross-linking techniques for the stabilization of tissue matrices. Biotechnology and applied biochemistry. 1993;17:23-9.
[353] Koide T, Daito M. Effects of various collagen crosslinking techniques on mechanical properties of collagen film. Dental materials journal. 1997;16:1-9,109.
[354] Rault I, Frei V, Herbage D, Abdul-Malak N, Huc A. Evaluation of different chemical methods for cros-linking collagen gel, films and sponges. Journal of Materials Science: Materials in Medicine. 1996;7:215-21.
[355] Sheu M-T, Huang J-C, Yeh G-C, Ho H-O. Characterization of collagen gel solutions and collagen matrices for cell culture. Biomaterials. 2001;22:1713-9.
[356] Weadock K, Olson RM, Silver FH. Evaluation of collagen crosslinking techniques. Biomaterials, medical devices, and artificial organs. 1983;11:293-318.
[357] Etherington DJ. Collagen degradation. Annals of the Rheumatic Diseases. 1977;36:14.
[358] Perez-Tamayo R. Pathology of collagen degradation. A review. The American journal of pathology. 1978;92:508.
[359] Song F, Wisithphrom K, Zhou J, Windsor LJ. Matrix metalloproteinase dependent and independent collagen degradation. Front Biosci. 2006;11:3100-20.
[360] Krane SM. Collagenases and collagen degradation. Journal of Investigative Dermatology. 1982;79:83-6.
[361] Exposito J-Y, Valcourt U, Cluzel C, Lethias C. The fibrillar collagen family. International journal of molecular sciences. 2010;11:407-26.
[362] Harrington WF, Von Hippel PH. The structure of collagen and gelatin. Advances in protein chemistry. 1962;16:1-138.
[363] Wallace DG, Rosenblatt J. Collagen gel systems for sustained delivery and tissue engineering. Adv Drug Deliv Rev. 2003;55:1631-49.
[364] Smidsrød O, Skja G. Alginate as immobilization matrix for cells. Trends in biotechnology. 1990;8:71-8.
[365] Lee KY, Mooney DJ. Alginate: properties and biomedical applications. Progress in polymer science. 2012;37:106-26.
[366] Paige KT, Cima LG, Yaremchuk MJ, Schloo BL, Vacanti JP, Vacanti CA. De novo cartilage generation using calcium alginate-chondrocyte constructs. Plastic and reconstructive surgery. 1996;97:168-78; discussion 79.
[367] Rinaudo M. Biomaterials based on a natural polysaccharide: alginate. TIP Revista especializada en ciencias químico-biológicas. 2014;17:92-6.
[368] Santavirta S, Konttinen YT, Saito T, Gronblad M, Partio E, Kemppinen P, et al. Immune response to polyglycolic acid implants. The Journal of Bone and Joint Surgery British volume. 1990;72:597-600.
[369] Lee KY, Rowley JA, Eiselt P, Moy EM, Bouhadir KH, Mooney DJ. Controlling mechanical and swelling properties of alginate hydrogels independently by cross-linker type and cross-linking density. Macromolecules. 2000;33:4291-4.
[370] Rowley JA, Madlambayan G, Mooney DJ. Alginate hydrogels as synthetic extracellular matrix materials. Biomaterials. 1999;20:45-53.
[371] Dhoot NO, Tobias CA, Fischer I, Wheatley MA. Peptide-modified alginate surfaces as a growth permissive substrate for neurite outgrowth. Journal of Biomedical Materials Research Part A: An

Official Journal of The Society for Biomaterials, The Japanese Society for Biomaterials, and The Australian Society for Biomaterials and the Korean Society for Biomaterials. 2004;71:191-200.
[372] Leonard M, De Boisseson MR, Hubert P, Dalencon F, Dellacherie E. Hydrophobically modified alginate hydrogels as protein carriers with specific controlled release properties. Journal of controlled release. 2004;98:395-405.
[373] Lawson M, Barralet J, Wang L, Shelton R, Triffitt JT. Adhesion and growth of bone marrow stromal cells on modified alginate hydrogels. Tissue engineering. 2004;10:1480-91.
[374] Wu Z, Wu J, Zhang R, Yuan S, Lu Q, Yu Y. Colloid properties of hydrophobic modified alginate: Surface tension, ζ-potential, viscosity and emulsification. Carbohydrate polymers. 2018;181:56-62.
[375] Sandvig I, Karstensen K, Rokstad AM, Aachmann FL, Formo K, Sandvig A, et al. RGD-peptide modified alginate by a chemoenzymatic strategy for tissue engineering applications. Journal of biomedical materials research Part A. 2015;103:896-906.
[376] Pettignano A, Grijalvo S, Haering M, Eritja R, Tanchoux N, Quignard F, et al. Boronic acid-modified alginate enables direct formation of injectable, self-healing and multistimuli-responsive hydrogels. Chemical Communications. 2017;53:3350-3.
[377] Choudhary S, Bhatia SR. Rheology and nanostructure of hydrophobically modified alginate (HMA) gels and solutions. Carbohydr Polym. 2012;87:524-30.
[378] Gattás-Asfura KM, Stabler CL. Chemoselective cross-linking and functionalization of alginate via Staudinger ligation. Biomacromolecules. 2009;10:3122-9.
[379] Mahou R, Meier RP, Bühler LH, Wandrey C. Alginate-poly (ethylene glycol) hybrid microspheres for primary cell microencapsulation. Materials. 2014;7:275-86.
[380] Davidovich-Pinhas M, Bianco-Peled H. Alginate–PEGAc: A new mucoadhesive polymer. Acta Biomaterialia. 2011;7:625-33.
[381] Draget KI, Skjak-Braek G, Smidsrod O. Alginate based new materials. Int J Biol Macromol. 1997;21:47-55.
[382] Augst AD, Kong HJ, Mooney DJ. Alginate hydrogels as biomaterials. Macromolecular bioscience. 2006;6:623-33.
[383] Yang J-S, Xie Y-J, He W. Research progress on chemical modification of alginate: A review. Carbohydrate polymers. 2011;84:33-9.
[384] Zhang H, Cheng J, Ao Q. Preparation of alginate-based biomaterials and their applications in biomedicine. Marine Drugs. 2021;19:264.
[385] Sun J, Tan H. Alginate-based biomaterials for regenerative medicine applications. Materials. 2013;6:1285-309.
[386] Marijnissen WJ, van Osch GJ, Aigner J, van der Veen SW, Hollander AP, Verwoerd-Verhoef HL, et al. Alginate as a chondrocyte-delivery substance in combination with a non-woven scaffold for cartilage tissue engineering. Biomaterials. 2002;23:1511-7.
[387] Gonzalez-Fernandez T, Tierney EG, Cunniffe GM, O'Brien FJ, Kelly DJ. Gene delivery of TGF-β3 and BMP2 in an MSC-laden alginate hydrogel for articular cartilage and endochondral bone tissue engineering. Tissue Engineering Part A. 2016;22:776-87.
[388] Yan S, Wang T, Feng L, Zhu J, Zhang K, Chen X, et al. Injectable in situ self-cross-linking hydrogels based on poly (L-glutamic acid) and alginate for cartilage tissue engineering. Biomacromolecules. 2014;15:4495-508.
[389] Chen W, Li C, Peng M, Xie B, Zhang L, Tang X. Autologous nasal chondrocytes delivered by injectable hydrogel for in vivo articular cartilage regeneration. Cell Tissue Bank. 2018;19:35-46.

[390] Shojarazavi N, Mashayekhan S, Pazooki H, Mohsenifard S, Baniasadi H. Alginate/cartilage extracellular matrix-based injectable interpenetrating polymer network hydrogel for cartilage tissue engineering. Journal of Biomaterials Applications. 2021;36:803-17.
[391] Cohen SB, Meirisch CM, Wilson HA, Diduch DR. The use of absorbable co-polymer pads with alginate and cells for articular cartilage repair in rabbits. Biomaterials. 2003;24:2653-60.
[392] Ghahramanpoor MK, Hassani Najafabadi SA, Abdouss M, Bagheri F, Baghaban Eslaminejad M. A hydrophobically-modified alginate gel system: utility in the repair of articular cartilage defects. Journal of Materials Science: Materials in Medicine. 2011;22:2365-75.
[393] Almeida HV, Sathy BN, Dudurych I, Buckley CT, O'Brien FJ, Kelly DJ. Anisotropic shape-memory alginate scaffolds functionalized with either type I or type II collagen for cartilage tissue engineering. Tissue Engineering Part A. 2017;23:55-68.
[394] Awad HA, Wickham MQ, Leddy HA, Gimble JM, Guilak F. Chondrogenic differentiation of adipose-derived adult stem cells in agarose, alginate, and gelatin scaffolds. Biomaterials. 2004;25:3211-22.
[395] Wang C-C, Yang K-C, Lin K-H, Liu H-C, Lin F-H. A highly organized three-dimensional alginate scaffold for cartilage tissue engineering prepared by microfluidic technology. Biomaterials. 2011;32:7118-26.
[396] Cheng X, Li K, Xu S, Li P, Yan Y, Wang G, et al. Applying chlorogenic acid in an alginate scaffold of chondrocytes can improve the repair of damaged articular cartilage. PLoS One. 2018;13:e0195326.
[397] Zhang F, Su K, Fang Y, Sandhya S, Wang DA. A mixed co-culture of mesenchymal stem cells and transgenic chondrocytes in alginate hydrogel for cartilage tissue engineering. Journal of Tissue Engineering and Regenerative Medicine. 2015;9:77-84.
[398] Zeng L, Yao Y, Wang D-a, Chen X. Effect of microcavitary alginate hydrogel with different pore sizes on chondrocyte culture for cartilage tissue engineering. Materials Science and Engineering: C. 2014;34:168-75.
[399] Kundu J, Shim JH, Jang J, Kim SW, Cho DW. An additive manufacturing-based PCL–alginate–chondrocyte bioprinted scaffold for cartilage tissue engineering. Journal of tissue engineering and regenerative medicine. 2015;9:1286-97.
[400] Rouillard AD, Berglund CM, Lee JY, Polacheck WJ, Tsui Y, Bonassar LJ, et al. Methods for photocrosslinking alginate hydrogel scaffolds with high cell viability. Tissue Engineering Part C: Methods. 2011;17:173-9.
[401] Chu Y, Huang L, Hao W, Zhao T, Zhao H, Yang W, et al. Long-term stability, high strength, and 3D printable alginate hydrogel for cartilage tissue engineering application. Biomedical Materials. 2021;16:064102.
[402] Kumar A, Han SS. PVA-based hydrogels for tissue engineering: A review. International journal of polymeric materials and polymeric biomaterials. 2017;66:159-82.
[403] Teodorescu M, Bercea M, Morariu S. Biomaterials of poly (vinyl alcohol) and natural polymers. Polymer Reviews. 2018;58:247-87.
[404] Teodorescu M, Bercea M, Morariu S. Biomaterials of PVA and PVP in medical and pharmaceutical applications: Perspectives and challenges. Biotechnology advances. 2019;37:109-31.
[405] Inkinen S, Hakkarainen M, Albertsson A-C, Södergård A. From lactic acid to poly (lactic acid)(PLA): characterization and analysis of PLA and its precursors. Biomacromolecules. 2011;12:523-32.
[406] Xiao L, Wang B, Yang G, Gauthier M. Poly (lactic acid)-based biomaterials: synthesis,

modification and applications. Biomedical science, engineering and technology. 2012;11:247-82.
[407] Cheng Y, Deng S, Chen P, Ruan R. Polylactic acid (PLA) synthesis and modifications: a review. Frontiers of chemistry in China. 2009;4:259-64.
[408] Pang X, Zhuang X, Tang Z, Chen X. Polylactic acid (PLA): research, development and industrialization. Biotechnology Journal. 2010;5:1125-36.
[409] Lasprilla AJ, Martinez GA, Lunelli BH, Jardini AL, Maciel Filho R. Poly-lactic acid synthesis for application in biomedical devices—A review. Biotechnology advances. 2012;30:321-8.
[410] Budak K, Sogut O, Aydemir Sezer U. A review on synthesis and biomedical applications of polyglycolic acid. Journal of Polymer Research. 2020;27:1-19.
[411] Chu C. Hydrolytic degradation of polyglycolic acid: tensile strength and crystallinity study. Journal of Applied Polymer Science. 1981;26:1727-34.
[412] Shawe S, Buchanan F, Harkin-Jones E, Farrar D. A study on the rate of degradation of the bioabsorbable polymer polyglycolic acid (PGA). Journal of materials science. 2006;41:4832-8.
[413] Göktürk E, Erdal H. Biomedical applications of polyglycolic acid (PGA). Sakarya Üniversitesi Fen Bilimleri Enstitüsü Dergisi. 2017;21:1237-44.
[414] Jem KJ, Tan B. The development and challenges of poly (lactic acid) and poly (glycolic acid). Advanced Industrial and Engineering Polymer Research. 2020;3:60-70.
[415] Gentile P, Chiono V, Carmagnola I, Hatton PV. An overview of poly (lactic-co-glycolic) acid (PLGA)-based biomaterials for bone tissue engineering. International journal of molecular sciences. 2014;15:3640-59.
[416] Passerini N, Craig D. An investigation into the effects of residual water on the glass transition temperature of polylactide microspheres using modulated temperature DSC. Journal of Controlled Release. 2001;73:111-5.
[417] Blasi P, D'Souza SS, Selmin F, DeLuca PP. Plasticizing effect of water on poly (lactide-co-glycolide). Journal of Controlled Release. 2005;108:1-9.
[418] Kopeček J. Hydrogel biomaterials: a smart future? Biomaterials. 2007;28:5185-92.
[419] Raghunath J, Rollo J, Sales KM, Butler PE, Seifalian AM. Biomaterials and scaffold design: key to tissue-engineering cartilage. Biotechnology and applied biochemistry. 2007;46:73-84.
[420] Grigore M. Biomaterials for cartilage tissue engineering. J Tissue Sci Eng. 2017;8:192.
[421] D'souza AA, Shegokar R. Polyethylene glycol (PEG): a versatile polymer for pharmaceutical applications. Expert opinion on drug delivery. 2016;13:1257-75.
[422] Working PK, Newman MS, Johnson J, Cornacoff JB. Safety of poly (ethylene glycol) and poly (ethylene glycol) derivatives. In: Zalipsky JMHaS, editor. Poly (ethylene glycol), Chemistry and Biological Applications. Washington. DC: ACS Publications; 1997. p. 45-57.
[423] Knop K, Hoogenboom R, Fischer D, Schubert US. Poly (ethylene glycol) in drug delivery: pros and cons as well as potential alternatives. Angewandte chemie international edition. 2010;49:6288-308.
[424] Browning MB, Cosgriff-Hernandez E. Development of a biostable replacement for PEGDA hydrogels. Biomacromolecules. 2012;13:779-86.
[425] Zustiak SP, Leach JB. Characterization of protein release from hydrolytically degradable poly (ethylene glycol) hydrogels. Biotechnology and bioengineering. 2011;108:197-206.
[426] Peyton SR, Raub CB, Keschrumrus VP, Putnam AJ. The use of poly (ethylene glycol) hydrogels to investigate the impact of ECM chemistry and mechanics on smooth muscle cells. Biomaterials. 2006;27:4881-93.
[427] Cho JH, Kim S-H, Park KD, Jung MC, Yang WI, Han SW, et al. Chondrogenic differentiation of

human mesenchymal stem cells using a thermosensitive poly (N-isopropylacrylamide) and water-soluble chitosan copolymer. Biomaterials. 2004;25:5743-51.
[428] Ibusuki S, Fujii Y, Iwamoto Y, Matsuda T. Tissue-engineered cartilage using an injectable and in situ gelable thermoresponsive gelatin: fabrication and in vitro performance. Tissue Engineering. 2003;9:371-84.
[429] Lum LY, Cher NL, Williams CG, Elisseeff JH. An extracellular matrix extract for tissue-engineered cartilage. IEEE engineering in medicine and biology magazine. 2003;22:71-6.
[430] Chen G, Liu D, Tadokoro M, Hirochika R, Ohgushi H, Tanaka J, et al. Chondrogenic differentiation of human mesenchymal stem cells cultured in a cobweb-like biodegradable scaffold. Biochemical and Biophysical Research Communications. 2004;322:50-5.
[431] Sha'ban M, Kim SH, Idrus RB, Khang G. Fibrin and poly (lactic-co-glycolic acid) hybrid scaffold promotes early chondrogenesis of articular chondrocytes: an in vitro study. Journal of orthopaedic surgery and research. 2008;3:1-10.
[432] Liu SQ, Tian Q, Hedrick JL, Hui JHP, Ee PLR, Yang YY. Biomimetic hydrogels for chondrogenic differentiation of human mesenchymal stem cells to neocartilage. Biomaterials. 2010;31:7298-307.
[433] Scholz B, Kinzelmann C, Benz K, Mollenhauer J, Wurst H, Schlosshauer B. Suppression of adverse angiogenesis in an albumin-based hydrogel for articular cartilage and intervertebral disc regeneration. Eur Cell Mater. 2010;20:2010.18.
[434] Scholten PM, Ng KW, Joh K, Serino LP, Warren RF, Torzilli PA, et al. A semi-degradable composite scaffold for articular cartilage defects. Journal of biomedical materials research Part A. 2011;97:8-15.
[435] Aslam Khan MU, Abd Razak SI, Al Arjan WS, Nazir S, Sahaya Anand TJ, Mehboob H, et al. Recent advances in biopolymeric composite materials for tissue engineering and regenerative medicines: a review. Molecules. 2021;26:619.
[436] Jian-zhong Z, Jiu-Gen W, Jia-Ju M. Porous structures of natural materials and bionic design. Journal of Zhejiang University-Science A. 2005;6:1095-9.
[437] Sampath UG, Ching YC, Chuah CH, Sabariah JJ, Lin P-C. Fabrication of porous materials from natural/synthetic biopolymers and their composites. Materials. 2016;9:991.
[438] Do AV, Khorsand B, Geary SM, Salem AK. 3D Printing of Scaffolds for Tissue Regeneration Applications. Adv Healthc Mater. 2015;4:1742-62.
[439] Do A-V, Smith R, Acri TM, Geary SM, Salem AK. 3D printing technologies for 3D scaffold engineering. Functional 3D tissue engineering scaffolds: Elsevier; 2018. p. 203-34.
[440] Mota RCdAG, da Silva EO, de Lima FF, de Menezes LR, Thiele ACS. 3D printed scaffolds as a new perspective for bone tissue regeneration: literature review. Materials Sciences and Applications. 2016;7:430-52.
[441] Ramya A, Vanapalli SL. 3D printing technologies in various applications. International Journal of Mechanical Engineering and Technology. 2016;7:396-409.
[442] Placone JK, Engler AJ. Recent advances in extrusion-based 3D printing for biomedical applications. Advanced healthcare materials. 2018;7:1701161.
[443] Choi J-W, Kim H-C. 3D printing technologies-a review. Journal of the Korean Society of Manufacturing Process Engineers. 2015;14:1-8.
[444] Li L, Lin Q, Tang M, Duncan AJ, Ke C. Advanced polymer designs for direct-ink-write 3D printing. Chemistry–A European Journal. 2019;25:10768-81.
[445] Lewis JA. Direct ink writing of 3D functional materials. Advanced Functional Materials.

2006;16:2193-204.
[446] Huang Y, Bu N, Duan Y, Pan Y, Liu H, Yin Z, et al. Electrohydrodynamic direct-writing. Nanoscale. 2013;5:12007-17.
[447] Ahmad Z, Rasekh M, Edirisinghe M. Electrohydrodynamic direct writing of biomedical polymers and composites. Macromolecular Materials and Engineering. 2010;295:315-9.
[448] Zhou LY, Fu J, He Y. A review of 3D printing technologies for soft polymer materials. Advanced Functional Materials. 2020;30:2000187.
[449] Guo Y, Patanwala HS, Bognet B, Ma AW. Inkjet and inkjet-based 3D printing: connecting fluid properties and printing performance. Rapid Prototyping Journal. 2017;23:562-76.
[450] Hornbeck LJ. Digital light processing for high-brightness high-resolution applications. Projection Displays III: International Society for Optics and Photonics; 1997. p. 27-40.
[451] Capel AJ, Rimington RP, Lewis MP, Christie SD. 3D printing for chemical, pharmaceutical and biological applications. Nature Reviews Chemistry. 2018;2:422-36.
[452] Huang J, Xiong J, Wang D, Zhang J, Yang L, Sun S, et al. 3D bioprinting of hydrogels for cartilage tissue engineering. Gels. 2021;7:144.
[453] Li C, Ouyang L, Armstrong JP, Stevens MM. Advances in the fabrication of biomaterials for gradient tissue engineering. Trends in Biotechnology. 2021;39:150-64.
[454] El-Sherbiny IM, Yacoub MH. Hydrogel scaffolds for tissue engineering: Progress and challenges. Global Cardiology Science and Practice. 2013;2013:38.
[455] Amukarimi S, Ramakrishna S, Mozafari M. Smart biomaterials—a proposed definition and overview of the field. Current Opinion in Biomedical Engineering. 2021;19:100311.
[456] Gonçalves AM, Moreira A, Weber A, Williams GR, Costa PF. Osteochondral tissue engineering: The potential of electrospinning and additive manufacturing. Pharmaceutics. 2021;13:983.
[457] Sun D, Chang C, Li S, Lin L. Near-field electrospinning. Nano letters. 2006;6:839-42.
[458] Rossi S, Puglisi A, Benaglia M. Additive manufacturing technologies: 3D printing in organic synthesis. ChemCatChem. 2018;10:1512-25.
[459] Solís Pinargote NW, Smirnov A, Peretyagin N, Seleznev A, Peretyagin P. Direct ink writing technology (3d printing) of graphene-based ceramic nanocomposites: A review. Nanomaterials. 2020;10:1300.
[460] Tamay DG, Dursun Usal T, Alagoz AS, Yucel D, Hasirci N, Hasirci V. 3D and 4D printing of polymers for tissue engineering applications. Frontiers in Bioengineering and Biotechnology. 2019;7:164.
[461] Zhang B, He J, Li X, Xu F, Li D. Micro/nanoscale electrohydrodynamic printing: from 2D to 3D. Nanoscale. 2016;8:15376-88.
[462] Vyas C, Poologasundarampillai G, Hoyland J, Bartolo P. 3D printing of biocomposites for osteochondral tissue engineering. Biomedical Composites: Elsevier; 2017. p. 261-302.
[463] Kamisan N, Naveen SV, Ahmad RE, Tunku K. Chondrocyte density, proteoglycan content and gene expressions from native cartilage are species specific and not dependent on cartilage thickness: a comparative analysis between rat, rabbit and goat. BMC veterinary research. 2013;9:1-9.
[464] Foldager CB, Gomoll AH, Lind M, Spector M. Cell seeding densities in autologous chondrocyte implantation techniques for cartilage repair. Cartilage. 2012;3:108-17.
[465] Eggli PS, Hunzinker EB, Schenk RK. Quantitation of structural features characterizing weight- and less-weight-bearing regions in articular cartilage: A stereological analysis of medical femoral condyles in young adult rabbits. The Anatomical Record. 1988;222:217-27.

[466] Stockwell R. The cell density of human articular and costal cartilage. Journal of anatomy. 1967;101:753.
[467] Jadin KD, Wong BL, Bae WC, Li KW, Williamson AK, Schumacher BL, et al. Depth-varying density and organization of chondrocytes in immature and mature bovine articular cartilage assessed by 3d imaging and analysis. Journal of Histochemistry & Cytochemistry. 2005;53:1109-19.
[468] Eyre D. The collagens of articular cartilage. Seminars in arthritis and rheumatism: Elsevier; 1991. p. 2-11.
[469] Minns R, Steven F. The collagen fibril organization in human articular cartilage. Journal of anatomy. 1977;123:437.
[470] MacConaill M. The movements of bones and joints. The Journal of bone and joint surgery British volume. 1951;33:251-7.
[471] Jeffery A, Blunn G, Archer C, Bentley G. Three-dimensional collagen architecture in bovine articular cartilage. The Journal of bone and joint surgery British volume. 1991;73:795-801.
[472] Pullig O, Weseloh G, Swoboda B. Expression of type VI collagen in normal and osteoarthritic human cartilage. Osteoarthritis and Cartilage. 1999;7:191-202.
[473] Padhi A, Nain AS. ECM in differentiation: a review of matrix structure, composition and mechanical properties. Annals of Biomedical Engineering. 2020;48:1071-89.
[474] Schmid TM, Popp RG, Linsenmayer TF. Hypertrophic Cartilage Matrix: Type X Collagen, Supramolecular Assembly, and Calcification a. Annals of the New York Academy of Sciences. 1990;580:64-73.
[475] Santos MI, Reis RL. Vascularization in bone tissue engineering: physiology, current strategies, major hurdles and future challenges. Macromolecular bioscience. 2010;10:12-27.
[476] Zhang Z. Chondrons and the pericellular matrix of chondrocytes. Tissue Engineering Part B: Reviews. 2015;21:267-77.
[477] Zhang Z, Jin W, Beckett J, Otto T, Moed B. A proteomic approach for identification and localization of the pericellular components of chondrocytes. Histochemistry and cell biology. 2011;136:153-62.
[478] Freudenrich C, Tortora GJ. Visualizing Anatomy and Physiology. New Jersy: John Wiley&Sons. Wiley Global Education; 2011.
[479] Wilusz RE, Sanchez-Adams J, Guilak F. The structure and function of the pericellular matrix of articular cartilage. Matrix Biol. 2014;39:25-32.
[480] Poole CA. Articular cartilage chondrons: form, function and failure. The Journal of Anatomy. 1997;191:1-13.
[481] Korhonen R, Laasanen M, Töyräs J, Rieppo J, Hirvonen J, Helminen H, et al. Comparison of the equilibrium response of articular cartilage in unconfined compression, confined compression and indentation. Journal of biomechanics. 2002;35:903-9.
[482] Miller GJ, Morgan EF. Use of microindentation to characterize the mechanical properties of articular cartilage: comparison of biphasic material properties across length scales. Osteoarthritis and cartilage. 2010;18:1051-7.
[483] Mansour JM. Biomechanics of cartilage. Kinesiology: the mechanics and pathomechanics of human movement. 2003;2:66-79.
[484] Abdulghani S, Morouço PG. Biofabrication for osteochondral tissue regeneration: bioink printability requirements. Journal of Materials Science: Materials in Medicine. 2019;30:1-13.
[485] Mente P, Lewis J. Elastic modulus of calcified cartilage is an order of magnitude less than that of

subchondral bone. Journal of Orthopaedic Research. 1994;12:637-47.
[486] Choi K, Kuhn JL, Ciarelli MJ, Goldstein SA. The elastic moduli of human subchondral, trabecular, and cortical bone tissue and the size-dependency of cortical bone modulus. Journal of biomechanics. 1990;23:1103-13.
[487] Yang PJ, Temenoff JS. Engineering orthopedic tissue interfaces. Tissue Engineering Part B: Reviews. 2009;15:127-41.
[488] Holland TA, Tabata Y, Mikos AG. Dual growth factor delivery from degradable oligo (poly (ethylene glycol) fumarate) hydrogel scaffolds for cartilage tissue engineering. Journal of Controlled Release. 2005;101:111-25.
[489] Harley BA, Lynn AK, Wissner-Gross Z, Bonfield W, Yannas IV, Gibson LJ. Design of a multiphase osteochondral scaffold III: Fabrication of layered scaffolds with continuous interfaces. Journal of Biomedical Materials Research Part A: An Official Journal of The Society for Biomaterials, The Japanese Society for Biomaterials, and The Australian Society for Biomaterials and the Korean Society for Biomaterials. 2010;92:1078-93.
[490] Watt FM. Effect of seeding density on stability of the differentiated phenotype of pig articular chondrocytes in culture. Journal of cell science. 1988;89:373-8.
[491] Kim DS, Lee MW, Lee TH, Sung KW, Koo HH, Yoo KH. Cell culture density affects the stemness gene expression of adipose tissue-derived mesenchymal stem cells. Biomedical Reports. 2017;6:300-6.
[492] Puelacher W, Kim S, Vacanti J, Schloo B, Mooney D, Vacanti C. Tissue-engineered growth of cartilage: the effect of varying the concentration of chondrocytes seeded onto synthetic polymer matrices. International journal of oral and maxillofacial surgery. 1994;23:49-53.
[493] Talukdar S, Nguyen QT, Chen AC, Sah RL, Kundu SC. Effect of initial cell seeding density on 3D-engineered silk fibroin scaffolds for articular cartilage tissue engineering. Biomaterials. 2011;32:8927-37.
[494] Ren X, Wang F, Chen C, Gong X, Yin L, Yang L. Engineering zonal cartilage through bioprinting collagen type II hydrogel constructs with biomimetic chondrocyte density gradient. BMC musculoskeletal disorders. 2016;17:1-10.
[495] Dimaraki A, Díaz-Payno PJ, Minneboo M, Nouri-Goushki M, Hosseini M, Kops N, et al. Bioprinting of a Zonal-Specific Cell Density Scaffold: A Biomimetic Approach for Cartilage Tissue Engineering. Applied Sciences. 2021;11:7821.
[496] Darling EM, Athanasiou KA. Rapid phenotypic changes in passaged articular chondrocyte subpopulations. Journal of orthopaedic research. 2005;23:425-32.
[497] Hidaka C, Cheng C, Alexandre D, Bhargava M, Torzilli PA. Maturational differences in superficial and deep zone articular chondrocytes. Cell and tissue research. 2006;323:127-35.
[498] Hwang NS, Varghese S, Lee HJ, Theprungsirikul P, Canver A, Sharma B, et al. Response of zonal chondrocytes to extracellular matrix-hydrogels. FEBS letters. 2007;581:4172-8.
[499] Sharma B, Williams CG, Kim TK, Sun D, Malik A, Khan M, et al. Designing zonal organization into tissue-engineered cartilage. Tissue engineering. 2007;13:405-14.
[500] Hwang NS, Varghese S, Puleo C, Zhang Z, Elisseeff J. Morphogenetic signals from chondrocytes promote chondrogenic and osteogenic differentiation of mesenchymal stem cells. Journal of cellular physiology. 2007;212:281-4.
[501] Heywood HK, Knight MM, Lee DA. Both superficial and deep zone articular chondrocyte subpopulations exhibit the Crabtree effect but have different basal oxygen consumption rates. Journal of cellular physiology. 2010;223:630-9.

[502] Coates E, Fisher JP. Gene expression of alginate-embedded chondrocyte subpopulations and their response to exogenous IGF-1 delivery. Journal of tissue engineering and regenerative medicine. 2012;6:179-92.
[503] Hendriks J, Riesle J, van Blitterswijk CA. Co-culture in cartilage tissue engineering. Journal of tissue engineering and regenerative medicine. 2007;1:170-8.
[504] Waldman SD, Grynpas MD, Pilliar RM, Kandel RA. The use of specific chondrocyte populations to modulate the properties of tissue-engineered cartilage. Journal of orthopaedic research. 2003;21:132-8.
[505] Chawla K, Klein TJ, Schumacher BL, Jadin KD, Shah BH, Nakagawa K, et al. Short-term retention of labeled chondrocyte subpopulations in stratified tissue-engineered cartilaginous constructs implanted in vivo in mini-pigs. Tissue Engineering. 2007;13:1525-37.
[506] Schuurman W, Gawlitta D, Klein TJ, ten Hoope W, van Rijen MH, Dhert WJ, et al. Zonal chondrocyte subpopulations reacquire zone-specific characteristics during in vitro redifferentiation. The American journal of sports medicine. 2009;37:97-104.
[507] Ng KW, Ateshian GA, Hung CT. Zonal chondrocytes seeded in a layered agarose hydrogel create engineered cartilage with depth-dependent cellular and mechanical inhomogeneity. Tissue Engineering Part A. 2009;15:2315-24.
[508] Ng KW, Wang CCB, Mauck RL, Kelly TAN, Chahine NO, Costa KD, et al. A layered agarose approach to fabricate depth-dependent inhomogeneity in chondrocyte-seeded constructs. Journal of Orthopaedic Research. 2005;23:134-41.
[509] Schuurman W, Klein T, Dhert W, Van Weeren P, Hutmacher D, Malda J. Cartilage regeneration using zonal chondrocyte subpopulations: a promising approach or an overcomplicated strategy? Journal of tissue engineering and regenerative medicine. 2015;9:669-78.
[510] Oh C-D, Chun J-S. Signaling mechanisms leading to the regulation of differentiation and apoptosis of articular chondrocytes by insulin-like growth factor-1. Journal of Biological Chemistry. 2003;278:36563-71.
[511] Ullah M, Stich S, Notter M, Eucker J, Sittinger M, Ringe J. Transdifferentiation of mesenchymal stem cells-derived adipogenic-differentiated cells into osteogenic-or chondrogenic-differentiated cells proceeds via dedifferentiation and have a correlation with cell cycle arresting and driving genes. Differentiation. 2013;85:78-90.
[512] Yao Y, Wang C. Dedifferentiation: Inspiration for devising engineering strategies for regenerative medicine. NPJ Regenerative medicine. 2020;5:1-11.
[513] de Windt TS, Saris DB, Slaper-Cortenbach IC, van Rijen MH, Gawlitta D, Creemers LB, et al. Direct cell–cell contact with chondrocytes is a key mechanism in multipotent mesenchymal stromal cell-mediated chondrogenesis. Tissue Engineering Part A. 2015;21:2536-47.
[514] Huang AH, Motlekar NA, Stein A, Diamond SL, Shore EM, Mauck RL. High-throughput screening for modulators of mesenchymal stem cell chondrogenesis. Annals of biomedical engineering. 2008;36:1909-21.
[515] Cicione C, Díaz-Prado S, Muiños-López E, Hermida-Gómez T, Blanco FJ. Molecular profile and cellular characterization of human bone marrow mesenchymal stem cells: donor influence on chondrogenesis. Differentiation. 2010;80:155-65.
[516] Jikko A, Kato Y, Hiranuma H, Fuchihata H. Inhibition of chondrocyte terminal differentiation and matrix calcification by soluble factors released by articular chondrocytes. Calcified tissue international. 1999;65:276-9.

[517] Nazempour A, Van Wie B. Chondrocytes, mesenchymal stem cells, and their combination in articular cartilage regenerative medicine. Annals of biomedical engineering. 2016;44:1325-54.
[518] Hendriks JA, Miclea RL, Schotel R, de Bruijn E, Moroni L, Karperien M, et al. Primary chondrocytes enhance cartilage tissue formation upon co-culture with a range of cell types. Soft Matter. 2010;6:5080-8.
[519] Tsuchiya K, Chen G, Ushida T, Matsuno T, Tateishi T. The effect of coculture of chondrocytes with mesenchymal stem cells on their cartilaginous phenotype in vitro. Materials science and engineering: C. 2004;24:391-6.
[520] Chen J, Wang C, Lü S, Wu J, Guo X, Duan C, et al. In vivo chondrogenesis of adult bone-marrow-derived autologous mesenchymal stem cells. Cell and tissue research. 2005;319:429-38.
[521] Lübke C, Ringe J, Krenn V, Fernahl G, Pelz S, Kreusch-Brinker R, et al. Growth characterization of neo porcine cartilage pellets and their use in an interactive culture model. Osteoarthritis and cartilage. 2005;13:478-87.
[522] Meretoja VV, Dahlin RL, Kasper FK, Mikos AG. Enhanced chondrogenesis in co-cultures with articular chondrocytes and mesenchymal stem cells. Biomaterials. 2012;33:6362-9.
[523] Zuo Q, Cui W, Liu F, Wang Q, Chen Z, Fan W. Co-cultivated mesenchymal stem cells support chondrocytic differentiation of articular chondrocytes. International orthopaedics. 2013;37:747-52.
[524] Zheng P, Ju L, Jiang B, Chen L, Dong Z, Jiang L, et al. Chondrogenic differentiation of human umbilical cord blood-derived mesenchymal stem cells by co-culture with rabbit chondrocytes. Molecular Medicine Reports. 2013;8:1169-82.
[525] Levorson EJ, Santoro M, Kasper FK, Mikos AG. Direct and indirect co-culture of chondrocytes and mesenchymal stem cells for the generation of polymer/extracellular matrix hybrid constructs. Acta biomaterialia. 2014;10:1824-35.
[526] Marchan J, Wittig O, Diaz-Solano D, Gomez M, Cardier JE. Enhanced chondrogenesis from chondrocytes co-cultured on mesenchymal stromal cells: Implication for cartilage repair. Injury. 2022;53:399-407.
[527] Mo X-t, Guo S-c, Xie H-q, Deng L, Zhi W, Xiang Z, et al. Variations in the ratios of co-cultured mesenchymal stem cells and chondrocytes regulate the expression of cartilaginous and osseous phenotype in alginate constructs. Bone. 2009;45:42-51.
[528] Schaefer D, Martin I, Shastri P, Padera R, Langer R, Freed L, et al. In vitro generation of osteochondral composites. Biomaterials. 2000;21:2599-606.
[529] Spalazzi JP, Dionisio KL, Jiang J, Lu HH. Osteoblast and chondrocyte interactions during coculture on scaffolds. IEEE engineering in medicine and biology magazine. 2003;22:27-34.
[530] Takai E, Lima E, Lu H, Ateshian G, Guo X, Hung C. Natural trabecular bone as a mineralized substrate for osteochondral tissue engineered hydrogel constructs. Trans Orth Res Soc. 2003;49.
[531] Battiston KG, Cheung JW, Jain D, Santerre JP. Biomaterials in co-culture systems: towards optimizing tissue integration and cell signaling within scaffolds. Biomaterials. 2014;35:4465-76.
[532] Burguera E, Vela-Anero A, Blanco F. Modulation of gene expression in human subchondral bone cells co-cultured with human articular chondrocytes. Osteoarthritis and Cartilage. 2012;20:S113-S4.
[533] Mahmoudifar N, Doran PM. Tissue engineering of human cartilage and osteochondral composites using recirculation bioreactors. Biomaterials. 2005;26:7012-24.
[534] Nakaoka R, Hsiong SX, Mooney DJ. Regulation of chondrocyte differentiation level via co-culture with osteoblasts. Tissue Engineering. 2006;12:2425-33.
[535] Weng Y, Cao Y, Arevalo C, Vacanti MP, Vacanti CA. Tissue-engineered composites of bone and

cartilage for mandible condylar reconstruction. Journal of oral and maxillofacial surgery. 2001;59:185-90.
[536] Galperin A, Oldinski RA, Florczyk SJ, Bryers JD, Zhang M, Ratner BD. Integrated bi-layered scaffold for osteochondral tissue engineering. Advanced healthcare materials. 2013;2:872-83.
[537] Zhang Y, Guo W, Wang M, Hao C, Lu L, Gao S, et al. Co-culture systems-based strategies for articular cartilage tissue engineering. Journal of Cellular Physiology. 2018;233:1940-51.
[538] Subia B, Kundu J, Kundu S. Biomaterial scaffold fabrication techniques for potential tissue engineering applications. Tissue engineering. 2010;141:13-8.
[539] Ansari S, Khorshidi S, Karkhaneh A. Engineering of gradient osteochondral tissue: From nature to lab. Acta biomaterialia. 2019;87:41-54.
[540] Zhang B, Huang J, Narayan RJ. Gradient scaffolds for osteochondral tissue engineering and regeneration. Journal of Materials Chemistry B. 2020;8:8149-70.
[541] Steele J, McCullen S, Callanan A, Autefage H, Accardi M, Dini D, et al. Combinatorial scaffold morphologies for zonal articular cartilage engineering. Acta biomaterialia. 2014;10:2065-75.
[542] Atesok K, Doral MN, Karlsson J, Egol KA, Jazrawi LM, Coelho PG, et al. Multilayer scaffolds in orthopaedic tissue engineering. Knee Surgery, Sports Traumatology, Arthroscopy. 2016;24:2365-73.
[543] Tamaddon M, Blunn G, Tan R, Yang P, Sun X, Chen S-M, et al. In vivo evaluation of additively manufactured multi-layered scaffold for the repair of large osteochondral defects. Bio-Design and Manufacturing. 2022:1-16.
[544] Castilho M, Mouser V, Chen M, Malda J, Ito K. Bi-layered micro-fibre reinforced hydrogels for articular cartilage regeneration. Acta biomaterialia. 2019;95:297-306.
[545] Zhang S, Chen L, Jiang Y, Cai Y, Xu G, Tong T, et al. Bi-layer collagen/microporous electrospun nanofiber scaffold improves the osteochondral regeneration. Acta Biomaterialia. 2013;9:7236-47.
[546] Aydin HM. A three-layered osteochondral plug: Structural, mechanical, and in vitro biocompatibility analysis. Advanced Engineering Materials. 2011;13:B511-B7.
[547] Qiao Z, Lian M, Han Y, Sun B, Zhang X, Jiang W, et al. Bioinspired stratified electrowritten fiber-reinforced hydrogel constructs with layer-specific induction capacity for functional osteochondral regeneration. Biomaterials. 2021;266:120385.
[548] Levingstone TJ, Ramesh A, Brady RT, Brama PA, Kearney C, Gleeson JP, et al. Cell-free multi-layered collagen-based scaffolds demonstrate layer specific regeneration of functional osteochondral tissue in caprine joints. Biomaterials. 2016;87:69-81.
[549] Kang H, Zeng Y, Varghese S. Functionally graded multilayer scaffolds for in vivo osteochondral tissue engineering. Acta biomaterialia. 2018;78:365-77.
[550] Camarero-Espinosa S, Rothen-Rutishauser B, Weder C, Foster EJ. Directed cell growth in multi-zonal scaffolds for cartilage tissue engineering. Biomaterials. 2016;74:42-52.
[551] Woodfield T, Blitterswijk CV, Wijn JD, Sims T, Hollander A, Riesle J. Polymer scaffolds fabricated with pore-size gradients as a model for studying the zonal organization within tissue-engineered cartilage constructs. Tissue engineering. 2005;11:1297-311.
[552] Woodfield TB, Malda J, De Wijn J, Peters F, Riesle J, van Blitterswijk CA. Design of porous scaffolds for cartilage tissue engineering using a three-dimensional fiber-deposition technique. Biomaterials. 2004;25:4149-61.
[553] Lee P, Tran K, Zhou G, Bedi A, Shelke NB, Yu X, et al. Guided differentiation of bone marrow stromal cells on co-cultured cartilage and bone scaffolds. Soft matter. 2015;11:7648-55.
[554] Wu L, Virdee J, Maughan E, Darbyshire A, Jell G, Loizidou M, et al. Stiffness memory nanohybrid

scaffolds generated by indirect 3D printing for biologically responsive soft implants. Acta biomaterialia. 2018;80:188-202.
[555] Jiang J, Tang A, Ateshian GA, Guo XE, Hung CT, Lu HH. Bioactive stratified polymer ceramic-hydrogel scaffold for integrative osteochondral repair. Annals of biomedical engineering. 2010;38:2183-96.
[556] Zhu D, Tong X, Trinh P, Yang F. Mimicking cartilage tissue zonal organization by engineering tissue-scale gradient hydrogels as 3D cell niche. Tissue Engineering Part A. 2018;24:1-10.
[557] Wu L, Magaz A, Wang T, Liu C, Darbyshire A, Loizidou M, et al. Stiffness memory of indirectly 3D-printed elastomer nanohybrid regulates chondrogenesis and osteogenesis of human mesenchymal stem cells. Biomaterials. 2018;186:64-79.
[558] Di Luca A, Van Blitterswijk C, Moroni L. The osteochondral interface as a gradient tissue: from development to the fabrication of gradient scaffolds for regenerative medicine. Birth Defects Research Part C: Embryo Today: Reviews. 2015;105:34-52.
[559] Qin C, Ma J, Chen L, Ma H, Zhuang H, Zhang M, et al. 3D bioprinting of multicellular scaffolds for osteochondral regeneration. Materials Today. 2021;49:68-84.
[560] Sun Y, You Y, Jiang W, Wang B, Wu Q, Dai K. 3D bioprinting dual-factor releasing and gradient-structured constructs ready to implant for anisotropic cartilage regeneration. Science Advances. 2020;6:eaay1422.
[561] Amann E, Amirall A, Franco AR, Poh PS, Sola Dueñas FJ, Fuentes Estévez G, et al. A graded, porous composite of natural biopolymers and octacalcium phosphate guides osteochondral differentiation of stem cells. Advanced Healthcare Materials. 2021;10:2001692.
[562] Koh Y-G, Lee J-A, Kim YS, Lee HY, Kim HJ, Kang K-T. Optimal mechanical properties of a scaffold for cartilage regeneration using finite element analysis. Journal of tissue engineering. 2019;10:1-10.
[563] Goetzke R, Sechi A, De Laporte L, Neuss S, Wagner W. Why the impact of mechanical stimuli on stem cells remains a challenge. Cellular and Molecular Life Sciences. 2018;75:3297-312.
[564] Schwerdtner W. Geometric interpretation of regional strain analyses. Tectonophysics. 1977;39:515-31.
[565] Wu H, Kustra S, Gates EM, Bettinger CJ. Topographic substrates as strain relief features in stretchable organic thin film transistors. Organic Electronics. 2013;14:1636-42.
[566] Longobardi L, Li T, Tagliafierro L, Temple JD, Willcockson HH, Ye P, et al. Synovial joints: from development to homeostasis. Current osteoporosis reports. 2015;13:41-51.
[567] Christian JL. Morphogen gradients in development: from form to function. Wiley Interdisciplinary Reviews: Developmental Biology. 2012;1:3-15.
[568] Lin Z, Li Z, Li EN, Li X, Del Duke CJ, Shen H, et al. Osteochondral tissue chip derived from iPSCs: modeling OA pathologies and testing drugs. Frontiers in bioengineering and biotechnology. 2019:411.
[569] Evans ND, Minelli C, Gentleman E, LaPointe V, Patankar SN, Kallivretaki M, et al. Substrate stiffness affects early differentiation events in embryonic stem cells. Journal of European Cells and Materials. 2009;18:1-14.
[570] Nam J, Johnson J, Lannutti JJ, Agarwal S. Modulation of embryonic mesenchymal progenitor cell differentiation via control over pure mechanical modulus in electrospun nanofibers. Acta biomaterialia. 2011;7:1516-24.
[571] Chang C-H, Lin C-C, Chou C-H, Lin F-H, Liu H-C. Novel bioreactors for osteochondral tissue

engineering. Biomedical Engineering: Applications, Basis and Communications. 2005;17:38-43.
[572] Kuiper NJ, Wang QG, Cartmell SH. A perfusion co-culture bioreactor for osteochondral tissue engineered plugs. Journal of Biomaterials and Tissue Engineering. 2014;4:162-71.
[573] O'Dea RD, Waters SL, Byrne HM. A multiphase model for tissue construct growth in a perfusion bioreactor. Mathematical medicine and biology: a journal of the IMA. 2010;27:95-127.
[574] Spitters TW, Leijten JC, Deus FD, Costa IB, van Apeldoorn AA, van Blitterswijk CA, et al. A dual flow bioreactor with controlled mechanical stimulation for cartilage tissue engineering. Tissue Engineering Part C: Methods. 2013;19:774-83.
[575] Navarro J, Swayambunathan J, Janes ME, Santoro M, Mikos AG, Fisher JP. Dual-chambered membrane bioreactor for coculture of stratified cell populations. Biotechnology and bioengineering. 2019;116:3253-68.
[576] Pörtner R, Nagel-Heyer S, Goepfert C, Adamietz P, Meenen NM. Bioreactor design for tissue engineering. Journal of bioscience and bioengineering. 2005;100:235-45.
[577] Freed LE, Guilak F, Guo XE, Gray ML, Tranquillo R, Holmes JW, et al. Advanced tools for tissue engineering: scaffolds, bioreactors, and signaling. Tissue engineering. 2006;12:3285-305.
[578] Zhao J, Griffin M, Cai J, Li S, Bulter PE, Kalaskar DM. Bioreactors for tissue engineering: An update. Biochemical Engineering Journal. 2016;109:268-81.
[579] Selden C, Fuller B. Role of bioreactor technology in tissue engineering for clinical use and therapeutic target design. Bioengineering. 2018;5:32.
[580] Wei W, Dai H. Articular cartilage and osteochondral tissue engineering techniques: Recent advances and challenges. Bioactive Materials. 2021;6:4830-55.
[581] Tomov ML, Gil CJ, Cetnar A, Theus AS, Lima BJ, Nish JE, et al. Engineering functional cardiac tissues for regenerative medicine applications. Current cardiology reports. 2019;21:1-13.

Chapter three: Design and manufacture of 3D-printed PEGDA scaffold for reconstructing the deep zone of the articular cartilage/osteochondral tissue *in vitro*

3.1 Introduction

The articular cartilage/osteochondral tissue consists of five distinctive zones (Figure 3.1), with depth-specific resident cells and ECM arrangement, as mentioned in Chapter two. Above the calcified zone in the transitional and mineralising interface, there is the deep zone containing spherical chondrocytes stacking in columnar proteoglycan-condensed space in between perpendicularly aligned bundles of large type II collagen fibres. The special ultrastructure and components of deep zone participates in sustaining the entire non-mineralised cartilage part by providing the local tensile strength, transient stiffness and compressive strength, against the time and loading dependent distortion and deformation [1-3].

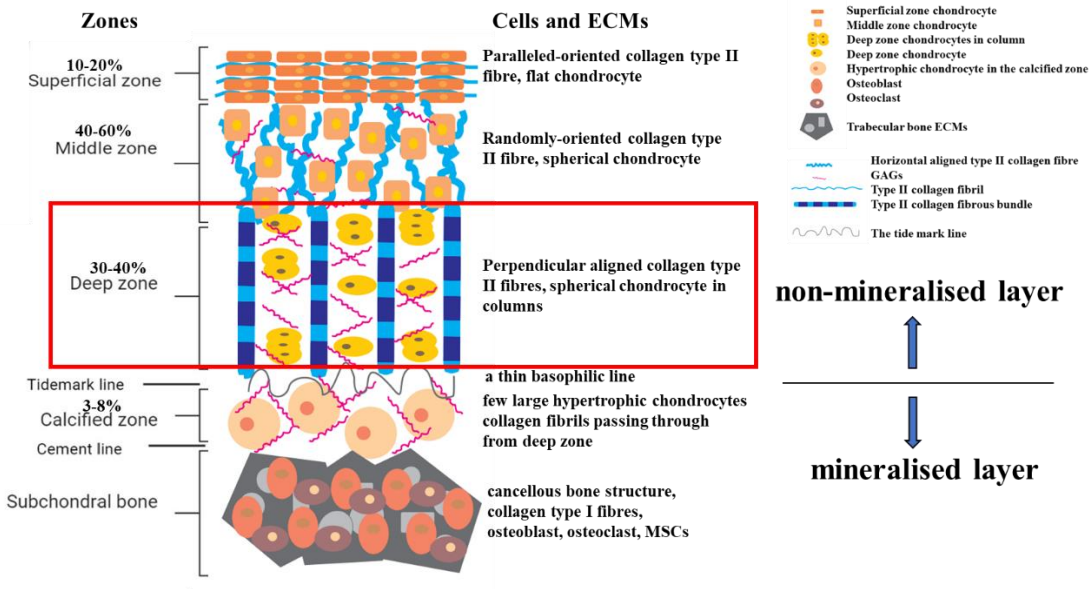

Figure 3.1 Schematic images of the zonal structure of the articular cartilage/osteochondral tissue ***Zonal structure and the specific components of each zone were displayed. In the middle, there is a schematic image of the architecture of the articular cartilage/osteochondral tissue. On the left side of the tissue image, five tissue specific zones, the tidemark line and cement line outlining the transforming interface area were labelled. On the right side of the tissue image, zone-dependent resident cells, ECM components and depth-related arrangement of them were described briefly. The deep zone was highlighted in the tissue image, to stress the***

target tissue layer in this Chapter. Image was reproduced from Figure 2.2.

As mentioned in Chapter two, PEGDA presents many favourable features as biomaterial to fabricate TE scaffold, such as photopolymerisation, biocompatible feature and adjustable mechanical property. DLP-3D printing technology could be applied to manufacture complex 3D structure in a layer-by-layer style, with faster speed and projector-related accuracy. The DLP 3D printer and photocurable PEGDA-based hydrogel have been frequently and successfully used to fabricate specific scaffolds with patterns for tissue engineering applications. Previous studies also found that the mechanical property of PEGDA hydrogels could be selected to match the range of the mechanical property of natural cartilage tissue [4], and PEGDA scaffold have been successfully applied in cell-based cartilage TE as described in Chapter two. Based on the availability of 3D printing technology in NTHU, DLP-3D printer and photocurable PEGDA materials were selected to prove the hypothesis, and to achieve the aim and objectives of this study, which were described in Chapter one.

Hence in this Chapter, the TE scaffold with biomimetic pattern was designed and fabricated by starting with applying photocurable PEGDA hydrogel material and a customised DLP-3D printer. The pattern of the scaffold was designed intending to simulate the cross-sectional arrangement of solid ECM network within the deep zone of the articular cartilage/OC tissue. In favour of an injectable strategy to deal with irregular, small lesions in clinic, the size of the designed scaffold was miniaturised and the shape of the scaffold was optimised to perform a self-assembly property toward future minimal invasive surgical applications. To support the chondrocytes to engraft and differentiate, to regenerate the articular cartilage tissue, collagen type I was utilised to deliver cells. Besides, additional reinforcement by physically blending nanocellulose fibre with PEGDA materials, compressive modulus, swelling capability and biocompatibility of 3D-printed product

were preliminarily investigated. The expected procedure to apply the injectable self-assembly scaffold in surgery to deal with chondral/OC defect, has been schematically described in Figure 3.2.

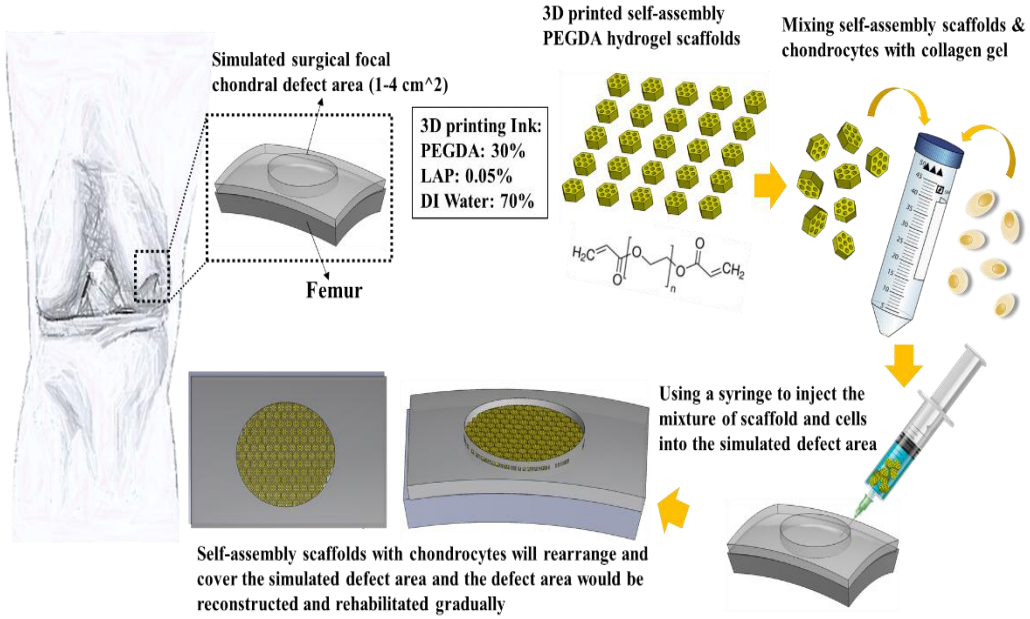

Figure 3.2 A schematic flow chart to describe the procedure of applying the injectable self-assembly PEGDA scaffold to support the articular cartilage tissue reconstruction (Images were adapted with permission from Mr. Wu of NTHU.)

In brief, small lesions in the femoral focal condyle commonly managed in surgical operation are about 1 to 4 cm^2. By DLP 3D printing, the self-assembly scaffolds should be fabricated firstly. Then by mixing scaffolds with reparative cells (chondrocytes or BM-MSCs) and collagen gel carrier into a syringe, the injectable solution would be applied to the defect area in arthroscopic surgery after general debridement. After injection, the miniaturised scaffold will be self-assembled with engrafted cells to cover the defect area to support the neo-cartilage tissue regeneration in situ. By performing this TE-based injectable strategy, patients with chondral/osteochondral defect would be able to tolerate only one surgical operation to get real reparative medical intervention. Inspired and motivated by this potential application in medical area, the self-assembly PEGDA-based scaffold was designed fabricated and preliminarily characterised in this study.

Formulas of photocurable materials examined in this study (Table 3.1) and various designs (Table 3.2) of patterns fabricated in this study were listed below.

Table 3.1 Formulas of photocurable materials tested in this study

Photopolymerisation by UV exposure directly			**Photopolymerisation by DLP-3D printing**			
PEGDA	PEGDA with additional Methyl cellulose (MC)	Characterisations	PEGDA	Characterisations	PEGDA with additional Nanocellulose fibre (NCF)	Characterisations
5%	5%+5%	Compressive test Swelling capability	20%	Compressive test Biocompatibility	30%+0.005%	Compressive test Swelling capability Dehydration rate
7.50%	7.5%+5%		30%	Compressive test	30%+0.01 or 0.02%	
10%	10%+5%				30%+0.2%	

Table 3.2 3D-printed samples and designed size of pattern developed in this study

3D printed samples	**Contour profile**	**Designed size of pattern**
Concave pattern test model for resolution	Hole	500μm in thickness, different diameters (30, 50, 100, 200, 300, 400, 500 μm)
Convex pattern test model for resolution	Cuboid	500μm in thickness, 4:1:1 at length: width: height, different widths (30, 50, 100, 200, 300, 400, 500 μm) with same interval space in between.
Concave pattern test model for shape fidelity	Hole	500 μm in diameter, 500 μm in thickness different space intervals (50, 100, 200, 300 μm)
Concave pattern scaffold	Hole	1cmx1cm area, uniformed hole arrays (100-200 μm in diameter)
Convex pattern scaffold	Rod cylinder Hexagonal cylinder Square cylinder Honeycomb Ridge	aspect ratio 2:5, 300μm in diameter of inscribed circle of different shape, 600-800μm thick
Self-assembly scaffold	Hexagonal shape	uniformed hole arrays (100-200 μm in diameter) a series of diameters of the inscribed circle including 750, 1000, 1250 and 1500 μm, a series of thicknesses including 300, 400, 500 and 600 μm.
	Square shape	uniformed hole arrays (100-200 μm in diameter), 750 μm diameters of the inscribed circle, 300 μm thickness.
	Triangle shape	uniformed hole arrays (100-200 μm in diameter), 1080 μm diameters of the inscribed circle, 300 μm thickness.
Viscosity of liquid solution	0.89cp	Distilled water
	7.5cp	1% Methyl cellulose
	15cp	2% Methyl cellulose
	30cp	4% Methyl cellulose

Notes: P: poise, denoting the unit of the dynamic viscosity of the solution reassured. cP: centipoise, 1cP=0.01P. The intended and finally selected designs or condition were labelled in red.

The DLP-3D printing technique has been described in Chapter two. The photopolymerisation mechanism and the photocurable materials used in this study will be briefly introduced below, followed by a general discussion on the self-assembly phenomenon and the intended pattern of our

design. All works described in this Chapter were finished in NTHU in Taiwan.

3.1.1 Photo-polymerisation and photocurable hydrogel material

Photopolymerisation-based 3D printing techniques including stereolithography-3D printing (SLA), digital light processing-3D printing (DLP) and continuous liquid interface production-3D printing (CLIP), use the photocurable materials (liquid form monomer or oligomer) and photoinitiators (PIs) to do 3D fabrication through the polymerisation process under the exposure of proper light sources [5]. With the advancements in polymer-related material chemistry, and developments of versatile PIs and light sources of different wavelengths, this technique could provide the 3D products with more flexible and controllable options regarding the chemical, mechanical and optical features, and could fabricate the miniaturised 3D complex products with high resolution [5].

Photopolymerisation is also called photocuring or photocrosslinking processes, in which the main components are photocurable monomer/oligomer and PI (or PI system). There are mainly two mechanisms involving in the photopolymerising process, the free radical polymerisation and the cationic polymerisation. In the free radical polymerisation process, it is the free radical that initiates the polymerisation of monomers/oligomers. Photoinitiator molecules belonging to the photosensitizer, will be activated by receiving the energy from light radiations such as the UV light, to immediately generate reactive species such as the free radicals, transferring the energy from light to chemical energy. The reactive species will subsequently react with monomers/oligomers to start chemical reactions to generate the polymer chain or 3D polymer network. There are mainly two types of PIs involved in the free radical polymerisation process. Type I PI is photocleavable. After being activated by the light energy (hv or photon), it will be cleaved into two reactive species

at the area of the weak α-carbon bond. Type II PI will work with co-initiator after receiving the light energy. Co-initiator usually provides the proton or electron for PI to become reactive species [6].

In the cationic polymerisation process, it is the cationic initiator that receives the energy from the light to become excited, forming the cationic species to transfer the charge to a monomer. This monomer then becomes the reactive monomer after receiving the charge, and subsequently reacts with other monomers/oligomers based on the same mechanism to generate the polymer chain or 3D polymer network. In this case, alkene or olefin monomer and heterocyclic monomer are commonly used polymers, possessing the necessary features including the electron-donating substituent and the heterocycle. Many chemicals could be the cationic initiator, such as the classic protic acid, carbenium ion salt, and Lewis acid catalyst compounds ($SnCl_4$, BF_3, $TiCl_4$). Radical-cation pairs derived from the ionizing radiation could also activate a monomer to initiate the polymerisation. But most commonly seen is the Lewis acid-induced reaction, in which the Lewis acid alone or as the co-initiator with other cation sources such as the alcohol, water, ester to provide the cation and usually form a complex to activate monomers to start the following polymerisation. Solutions containing Lewis acid, Bronsted acid and Friedel-Crafts halide, could be able to accept electron (from proton donor) to initiate the polymerisation. Details could be found in many professional reviews [7-11].

Many polymers and compounds have been applied in photopolymerisation-based 3D printing, such as the acrylic or methacrylic based polymers/resins, polymers modified with acrylate groups, epoxy, vinyl ether-related polymers/resins, camphorquinone (CQ), zinc tetraphenylporphyrin (ZnTPP), eosin Y, benzophenone, phenyl bis (2, 4, 6-trimethylbenzonyl) phosphine oxide, 2-Hydroxy-4'-(2-

hydroxyethoxy)-2-methylpropiophenone (Irgaure®2959), diphenyl (2, 3, 6-trimethylbenzoyl) phosphine oxide, and lithium phenyl (2, 4, 6-trimethylbenzoyl) phosphinate (LAP) [12, 13]. In DLP 3D printing, the PEGDA monomer and PEGDA-based derivatives are commonly used to formulate the printing ink, with appropriate PIs, the PEGDA-based hydrogel could be fabricated under a biocompatible condition, contributing to develop the bio-ink consisting of the living cells together with hydrogel materials for 3D bio-printing. PEGDA hydrogel-based tissue engineering scaffolds and bio-inks have been extensively studied, in which the nanocellulose-blended PEGDA materials were also printed successfully, supporting the formula design of using nanocellulose-incorporated PEGDA material as printing ink for 3D TE scaffold fabrication[14].

The photopolymerisation of PEGDA-based material belongs to the free radical initiated polymerisation process, containing the initiation, propagation, and termination reactions. Here is briefly introduced the PEGDA hydrogel polymerisation process [15]:

1) Initiation reaction: After receiving light energy PI is cleaved to radical species, with unpaired electrons having chemical activities to react with monomer forming covalent bond.

$$PI \xrightarrow{UV} R_{A1*} \qquad\qquad R_{A1*} + M \xrightarrow{UV} R_{A1}M\cdot$$

PI: photoinitiator, R_{A1*}: radical species, M: monomer

2) Propagation reaction: Complex of the monomer with radical species receiving the chemical activity, will continue reacting with other monomer to form a longer chain of the polymer.

$$R_{A1}M\cdot + M \xrightarrow{UV} R_{A1}M_2\cdot$$

$$R_{A1}M_2\cdot + M \xrightarrow{UV} R_{A1}M_3\cdot$$

$$\vdots$$

$$R_{A1}M_{(n-1)}\cdot + M \xrightarrow{UV} R_{A1}M_n\cdot$$

3) Termination reaction: The chemical reaction will not stop until two unpaired electrons meet each other and paired.

$$R_{A1}M_n \cdot + R_{A2}M_m \cdot \xrightarrow{UV} R_A M_{n+m} R_{A2}$$

This study was using PEGDA as printing ink containing LAP as photoinitiator to fabricate the 3D scaffold by DLP 3D printer [16].

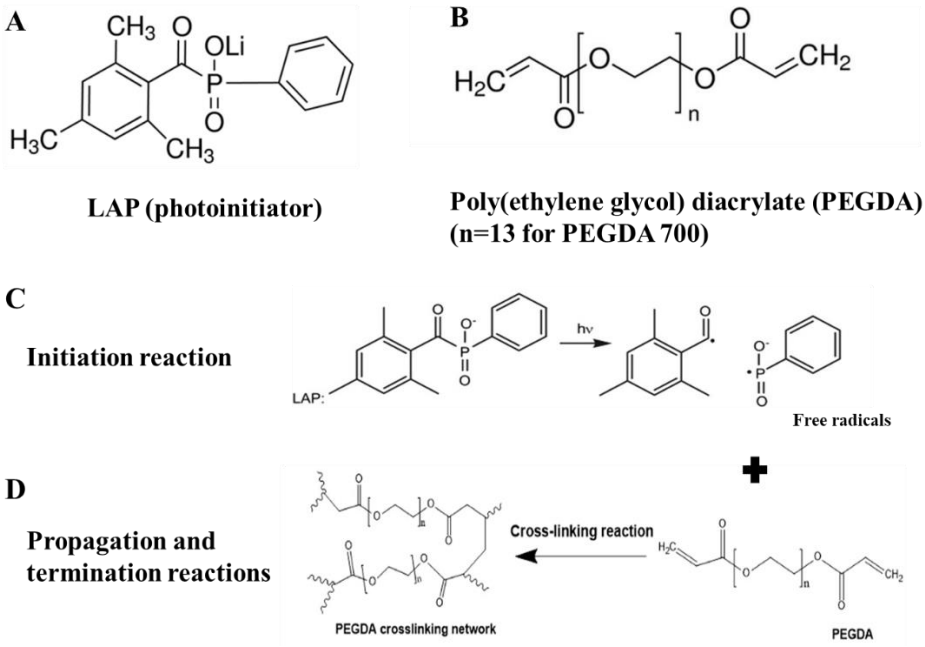

Figure 3.3 Chemical structures of ingredient of the printing ink and associated photopolymerisation process A: Photoinitiator LAP. B: PEGDA monomer. C-D: Schematic images of chemical reactions of the LAP-initiated photopolymerisation process of the PEGDA monomers[16].

3.1.2 Self-assembly process and desired pattern

Self-assembly is an autonomous process by which the disordered system is able to be organised or patterned due to the specific, local interactions among components themselves inside the system [17]. This is a common phenomenon in nature, involving substances at all scales from molecular crystal to the weather system of the earth [17]. Two commonly-seen types of the self-assembly process are the static and dynamic types. In the static self-assembly process, the system is relative equilibrium having no energy dissipated, such as the formation

of molecular crystals, protein folding. In this case, once the structure is formed, no energy will be required and the formation of the structure is stable. In the dynamic self-assembly process, energy in the whole system is dissipating when the components are interacted to form the final organised structure or pattern, such as some chemical reactions requiring either reaction or diffusion, and some events in cells and organisms. It is said that the information requiring for the self-assembly formation of the final structure or pattern has been coded individually and uniformly, leading to the interaction between components [17]. Many studies revealed that the shape, surface chemistry, polarisation, mass of the component might contribute to reflect the underlying information. Hence, to obtain a self-assembly scaffold, shape and pattern have been considered in the design of scaffold. Many patterns have been studied the self-assembly property in 2D array and 3D aggregation from literatures [18, 19], in which based on structure of the target articular cartilage tissue, the hexagonal pattern is chosen as the desired candidate pattern of the scaffold to fabricate and examined the self-assembly property in the miniaturised size (microscale).

3.2 Materials and methods

In this section, all experimental materials regarding chemicals, agents, assay kit, cell lines consumables and instruments, and all experimental methods applied in experiments presented in this chapter, will be described below.

3.2.1 Chemical compounds and solutions

Hydrogel materials, and general chemicals were purchased from Sigma-Aldrich (Merck, UK) directly or by its agent in Taiwan (Echo Chemical Co. Ltd). They were poly (ethylene glycol)

diacrylate (PEGDA, average M.W.=700, CAS No.:26570-48-9), nanocellulose fibre solution (2%), methyl cellulose (M7140), 37% formaldehyde solution (F8775), 25% glutaraldehyde solution (G6257), hydrochloric acid (258148), Thiazolyl Blue Tetrazolium Bromide (M2128) (CAS No.:298-93-1), trypsin-EDTA solution (T4174), penicillin-streptomycin (PS) (P4333), poly-L-lysine solution (P4707).

VECTASHIELD® Mounting Medium for Fluorescence with DAPI was ordered from Vector Laboratories, Inc. Photo-initiator (lithium phenyl-2,4,6-trimethylbenzoylphosphinate or LAP) was ordered directly from Colorado Photopolymer Solutions, LLC. Isopropyl alcohol and ethanol alcohol were ordered from Honeywell (RS components Ltd.). Type I collagen solution (SusGel™ Porcine Collagen Type I) was purchased from Conori Inc.

3.2.2 Medium, agent, assay kit and antibodies

Cell culture medium, balanced salt solutions, growth factors and other additives for cell culture, and differentiations, were purchased from either Corning® or Thermo Scientific Ltd. They are Dulbecco's Modified Eagle medium (DMEM), DMEM and Ham's F-12 medium (DMEM/F12), Phosphate buffered saline (PBS) solution, Dulbecco's phosphate-buffered saline solution (DPBS), 100 mL Penicillin-Streptomycin Solution, 100x (10,000 I.U. Penicillin and 10,000 µg/mL Streptomycin), low viscosity mounting media. Tissue culture serum such as foetal bovine serum (FBS), horse serum (HS), and goat serum (GS), were ordered from Sigma-Aldrich (Merck, UK) and HyClone™ (GE healthcare Life Sciences). CyQUANT™ LDH Cytotoxicity Assay (Invitrogen™), ActinGreen™ 488 Ready Probes™ reagent (AlexaFluor™ 488 phalloidin) for immunostaining and LIVE/DEAD™ Viability/Cytotoxicity Kit, for mammalian cells (L3224),

were purchased from Thermo Scientific Ltd.

3.2.3 Consumables and instruments

Ultrapure water (deionised distilled water, DDW) and distilled water (DW) were produced by lab water purification systems (Merck Millipore Milli-Q™). Three types of centrifuges were used during the study. They are Eppendorf™ 5804 R, Thermo Scientific™ Small Benchtop Centrifuge and Kubota laboratory centrifuges (Japan). Other instruments used in the study, are scanning electron microscopy (SEM) (JSM 7001F FEGSEM; JEOL, Tokyo, Japan), Q150T ES sputter coater, confocal microscope (Zeiss LSM 800), and benchtop normal inverted phase contract light microscopes. Other consumables such as tissue culture flasks, petri dish, microplates, pipette tips, centrifuge tubes, Eppendorf® tubes, beakers, haemocytometer, were provided by suppliers such as the Scientific Laboratory Supplies (SLS) Ltd (UK), Thermo Scientific™ (UK), and Bersing Technology Co., Ltd (Taiwan).

Some accessories of the customised DLP 3D printer were ordered individually, including the light source from NVR UV engine, projector from Young Optics Ltd., single chip microcontroller from Arduino Ltd., and Creation workshop (CW) software to digitally control the projector and motor engine.

3.2.4 Cell lines

Three types of cell lines were used. They are NIH 3t3 fibroblasts (American Type Culture Collection (ATCC)), ATDC5 chondrogenic cell line (European Collection of Authenticated Cell Cultures (ECACC)) and C2C12 myoblasts (ATCC).

3.2.5 Characterisations of biomaterials

For 3D fabrication of PEGDA materials, two methods were applied in this study. The first method was by 3D printing directly, in which PEGDA solution (with/without nanocellulose fibres) containing 0.05% LAP (photo-initiator) was prepared and poured into the vat of 3D printer to print. The 3D product of PEGDA gel was pre-designed in Solidwork® (Dassault Systèmes, SolidWorks Corporation, USA),which file was then transferred to the computer controlling the printer. The printing parameters and setup were optimised before using, based on the resolution and quality of printing. The second method was using UV light to crosslink the solution manually. PEGDA solutions (with/without nanocellulose fibres) containing 0.05% LAP (photoinitiator) were prepared and poured into the 24 well-plate to crosslink under the UV365nm light for 10-20mins. Then the crosslinked PEGDA-based hydrogel was demoulded from the plate and put into another plate containing DDW and kept at 4℃ until further measurement.

3.2.5.1 Compressive modulus

As mentioned in Chapter two, mechanical property is important for hydrogel material to be fabricated into tissue culture scaffold, especially for applications on living cells, different type of seeding cells has different sensitivity and response to the surrounding mechanical microenvironment. Compressive modulus represents the ability of the material to endure changes in the length when subjected to compressive forces, measuring the stiffness of the hydrogel materials. In order to select hydrogel materials to be fabricated as 3D scaffold for cartilage tissue regeneration during a long period of time *in vitro* with appropriate stiffness to keep the patterned scaffold stable and endurable for chondrocytes in the soft cartilage tissue, mechanical property of

the material should be characterised. In this study, due to limitations on time and facilities, compressive modulus of hydrogel materials was examined.

To characterise the compressive modulus of the PEGDA bulk materials, uniformed PEGDA hydrogels of six different formulas were poured into wells of a 24-well microplate and exposed to UV 365nm light directly to crosslink as mentioned above. In this experiment, 5%, 7.5% and 10% PEGDA hydrogel with/without additional 5% cellulose (methyl cellulose, MC) were designed. Then the fabricated 3D hydrogel bulk materials were tested under the unconfined uniaxial compressive forces by the universal machine (ElectroForce 3100, TA instrument). Each condition of the hydrogel has three samples to test and each measurement was repeated three times before statistical analysis. Compressive forces were loaded at a ramp rate of 0.05 mm/s. The slope of the re-plotted stress-strain curve at 10 to 20% strain, was used to calculate the compressive modulus of samples.

To characterise the stability of the crosslinked PEGDA gel in the tissue culture environment, the crosslinked PEGDA-based gels (six formulas listed in Table 3.1) were soaked into the general tissue culture growth medium and put into an incubator. Medium was replaced every two or three days. After 1-, 7-, 14- and 28-days incubations, hydrogels were tested and analysed compressive modulus in same the process mentioned above. Each type of hydrogel contained three samples and each test was repeated three times for statistical analysis.

To characterise the compressive modulus of the 3D-printed PEGDA-based hydrogel, five formulas of PEGDA materials were prepared (listed in Table 3.1), including 20% PEGDA, 30%PEGDA, 30% PEGDA with 0.05% nanocellulose fibres (NCF), 30% PEGDA with 0.01% NCF and 30% PEGDA with 0.2% NCF. Those PEGDA-based hydrogels were printed directly by DLP 3D printer with

uniformed sizes (8mm x 8mm x 6mm) and investigated in the same process mentioned above. Each type of hydrogel contained three samples and each test was repeated three times for statistical analysis.

The compressive modulus (also known as the Young's modulus) representing the stiffness of the crosslinked hydrogel was calculated by the following equations.

For the strain:

$$\boldsymbol{Strain} = \frac{\boldsymbol{the\ compressed\ length}}{\boldsymbol{the\ original\ length}} \quad \boldsymbol{\varepsilon} = \frac{\boldsymbol{\delta}}{\boldsymbol{\iota}} \qquad \textbf{(1)}$$

Where ε is the strain, δ is the compressed length and l is the original length of the sample.

For the stress:

$$\boldsymbol{Stress} = \frac{\boldsymbol{the\ Force\ or\ loading}}{\boldsymbol{the\ area\ of\ the\ sample}} \quad \boldsymbol{\sigma} = \frac{\mathbf{F}}{\mathbf{A}} \qquad \textbf{(2)}$$

Where σ is the stress, F is the applied force and A is the area of the sample.

For the Young's modulus:

$$\boldsymbol{Young's\ Modulus} = \frac{\boldsymbol{Stress}}{\boldsymbol{Strain}} \quad \boldsymbol{E} = \frac{\boldsymbol{\sigma}}{\boldsymbol{\varepsilon}} = \frac{\boldsymbol{F\,l}}{\boldsymbol{A\delta}} \qquad \textbf{(3)}$$

Where E is the compressive modulus, ε is the strain and σ is the stress. In the plotted stress-strain curve, the slope of the linear part at 10-20% strain representing the loading (F) over the length of stretch (δ), was used to calculate the compressive modulus (the Young's modulus) of the sample.

3.2.5.2 Swelling capabilities

Crosslinked bulk PEGDA hydrogel materials were gently wiped the water on the surface and measured the weight by a weighing machine (Sartorius ED2201-CW). After recording the weight (wet weight), samples were freeze-dried overnight by a freeze-drying machine (FD-12N, LAWSON. Co. Ltd). After freeze-drying, each sample was measured the weight by a weighing machine again. After recording the weight (dry weight), samples were soaked into DW for 48hrs to reswell and then gently wiped the water on the surface before the final measurement. Each type

of hydrogel contained three samples and each test was repeated three times.

For 3D-printed PEGDA-based hydrogels, dehydration rate of samples was examined. Photocrosslinked PEGDA-based hydrogels were gently wiped the water on the surface and weighed (wet weight) before being put into an oven to dry. During the drying process, samples were taken out to measure the weight (dry weight) every hour (time point) till the weight was not changed (about 8 hrs). Each group of hydrogel contains three samples and measurement was repeated three times for statistical analysis.

Measurements of weights of the PEGDA-based products, before and after drying, and after reswelling were all recorded and calculated by Microsoft® Excel (Microsoft Corporation, USA). The following equations were used to calculate the weight degree of swelling, water content, swelling ratio and the dehydration rate of the PEGDA-based products.

$$\boldsymbol{Weight\ degree\ of\ swelling} = \frac{\boldsymbol{Weight\ (wet)}}{\boldsymbol{Weight\ (dry)}}\ \boldsymbol{x100\%} \quad \textbf{(4)}$$

$$\boldsymbol{Water\ content} = \frac{\boldsymbol{Weight\ (wet) - Weight(dry)}}{\boldsymbol{Weight\ (wet)}}\ \boldsymbol{x100\%} \quad \textbf{(5)}$$

$$\boldsymbol{Swelling\ ratio} = \frac{\boldsymbol{Weight\ (wet) - Weight(dry)}}{\boldsymbol{Weight\ (dry)}}\ \boldsymbol{x100\%} \quad \textbf{(6)}$$

$$\boldsymbol{Dehydration\ rate\ (time\ point)} = \frac{\boldsymbol{Weight(wet) - Weight(dry)}}{\boldsymbol{Weight(wet)}}\ \boldsymbol{x100\%} \quad \textbf{(7)}$$

Where the Weight (wet) is the measured weight of the wet sample, and the Weight (dry) is the measured weight of the dry sample, at the time point of measurement.

3.2.5.3 Morphology of PEGDA-based hydrogel materials

Crosslinked bulk PEGDA hydrogel materials with/without additional nanocellulose fibres, were freeze-dried by a freeze-drying machine (FD-12N, LAWSON. Co. Ltd) and coated with a thin layer of conductive metals (gold) by a sputter coating machine in a vacuumed chamber, before being

scanned by the SEM (JSM 7001F FEGSEM; JEOL, Tokyo, Japan). SEM images were captured under 10.0 kV.

3.2.6 Cell culture and biocompatibility of PEGDA-based hydrogel materials

General processes regarding cell culture, and cell-based viability and proliferation screening tests applied in this chapter will be introduced below.

3.2.6.1 General cell expansion and passaging process *in vitro*

Cells were cultured and maintained with growth medium (e.g., DMEM supplemented with 10% FBS and 1% PS) in T25/T75 plastic tissue culture flasks and checked the density under a normal inverted phase contrast light microscope every day regularly. Cell medium was replaced every two or three days. When the cell density in flask reached to 80-90% confluences, cell passaging would be performed. Briefly, cells were washed with PBS (1x sterilised) twice and gently drained before adding 0.05% Trypsin-EDTA solution for trypsinisation. After adding trypsin, cells in flask were put into an incubator for about 5-10 mins and checked under an inverted phase contrast microscope. When cells in the flask were going to detach from the bottom of the flask, growth medium was added and pipetted repeatedly to detach cells from the flask. Then cell suspension was pipetted out into a centrifuge tube and centrifugated at 1000 rpm for 5 mins. Supernatant containing trypsin was removed and new growth medium was added to resuspend cells from pellets. Resuspended cells in medium were added into new flasks to culture in a humid incubator at 37℃ 5% CO_2.

For cell-based assays including the viability and cytotoxicity tests or differentiations, detachment of cells from tissue culture flask was same as that mentioned above. After resuspending cells, cell number was counted by the haemocytometer, before subsequently seeding at appropriate cell

density in multi-well plate with or without hydrogel solutions.

3.2.6.2 Cytotoxicity of the photoinitiator for 3D-printed hydrogel product

Experiments and screening assays to evaluate the cytotoxicity of photoinitiator for 3D printer will be described in this section.

3.2.6.2.1 Series number test for appropriate seeding density

Appropriate seeding density of specific type of cell was examined by series cell number test before any cell-involved experiment. Cells cultured in flasks were detached and calculated the total number in the way as mentioned above (3.2.6.1). Then cells were seeded in a series of cell density in a microplate which was then put in an incubator to culture until a certain time point. Cultural medium was replaced every two or three days. There were five groups of seeding densities usually planned and each density group of cells had at least three wells. Each test was repeated three times at least for further statistical analysis.

NIH 3t3 fibroblast, C2C12 myoblast, and ATDC5 chondrogenic cell line were applied in this study. They were all tested in 24-well microplates. The seeding density of NIH3t3 fibroblast in this test were set at 5K,10K, 20K,40K and 80K cells per well. The seeding density of C2C12 myoblast and ATDC5 chondrogenic cell line in this test were both set at 10K, 20K, 50K, 100K and 500K cells per well. All cells were examined by LDH essay after 1-, 4- and 7-days culture.

3.2.6.2.2 MTT assay and LDH assay

For MTT assay to examine the effect on the cell viability (24hr) and proliferation (7 days), after treatments, cultural medium of each well would be replaced by 1mg/mL MTT solution (diluted

from 3mg/mL MTT stock solution by growth medium) and put in an incubator for another 4 hrs. Then the supernatant of each well was gently discarded and replaced by acidic isopropanol solution (aIPA). After shaking the plate to make the purple crystal product dissolved in aIPA, the dissolved solution of each group in tests were transferred into a new 96-well microplate which would be further put into a plate reader (BioTek, Agilent Technologies, Inc., USA) to measure the optical absorption of each well at 570nm wavelength.

For LDH assay, cells were seeded at appropriate density in 24-well microplate and treated the different conditional medium for another 1-, 4- and 7-days culture in an incubator. Culture medium of each well was replaced every two to three days. For seeding density test, after 24hrs or 7 days culture, the supernatant of each well was collected into a tube, fresh growth medium was added into each well after washing once by PBS (1x sterilised). Tubes of supernatant and microplate with cells in growth medium were put into a freezer of -80℃ to freeze and then were thawed at room temperature. The freeze-thawing circle was repeated at least three times to ensure LDH release. In this type of experiment, when cells were seeded in plate, another one million cells from the same source of seeding cells were taken out and put into a 1.5 ml Eppendorf® tubes for analysing the standard curve of cells by LDH assay. These cells in tubes were kept in a freezer of -80℃ and performed the freeze-thawing circle three times together with the experimental plates which were further tested by LDH assay. For cytotoxicity and viability test, after 24hrs seeding in the plate, cell medium was replaced by the conditional medium designed in experimental plan, and then tested after 1-, 4- and 7-days treatment by LDH assay.

The process of LDH assay to examine cell viability and proliferation was performed according to the instruction of the CyQUANT™ LDH kit from the manufacturer. In brief, 50 µl supernatant of

sample was transferred to a new 96-well microplate and then 50 µl substrate was added into wells containing samples. After incubation at room temperature in dark for 30 mins, 50 µl stop solution per well of samples was added to stop the reaction. Finally, absorption at 490nm and reference wavelength at 680nm of samples in the plate were measured by a plate reader (BioTek, Agilent Technologies, Inc., USA). All results were normalised data presenting the cell viability in percentage in figures.

3.2.6.2.3 Cytotoxicity of the photoinitiator on living cells by LDH essay

To examine the cytotoxicity of the photoinitiator LAP applied for fabricating PEGDA-based hydrogels, three cell lines were used to examine the effect of different concentrations of LAP (0.05%,0.1%,0.15%) dissolved in growth medium on the viability and proliferation of three types of living cells cultured in 2D monolayer *in vitro*, including NIH3t3 fibroblast, C2C12 myoblast and chondrogenic cell line ATDC5 cell.

Cells were cultured and seeded in 24-well microplates at their appropriate density which were tested as mentioned (3.2.6.1 and 3.2.6.2.1). After seeding 24 hrs in an incubator, cells in plates were checked for cellular states under an inverted phase contrast microscope. Then growth medium for cells were replaced by conditional medium (growth medium containing different concentrations of LAP) and examined their effects on the cell viability and proliferation by LDH assay after 1-, 4-, and 7-days treatments, respectively. Cultural medium of each well was replaced every two or three days. The concentrations of LAP examined were 0.05%, 0.1% and 0.15%, which would be freshly diluted in growth medium from the stock solutions of 1% LAP prepared in DDW and sterilised by passing through the 0.22 µm filter. Growth medium containing 5% DMSO was

prepared to treat cells as the positive control group. LDH assay was performed as mentioned in 3.2.6.2.2.

3.2.7 Configuration of 3D printers, 3D designs and fabrication of the PEGDA-base scaffolds

Configuration of the customised DLP-3D printer, printing process, 3D designs and fabrication of the PEGDA-based scaffold by the customised DLP-3D printer will be described below.

3.2.7.1 DLP 3D printer and printing process

The customised DLP-3D printer is displayed in Figure 3.4, mainly containing the light sources, a projector, digital micromirror device (DMD) array, a vat with transparent bottom, z-axial movable motor connected to a building platform in a fixed flat orientation. Basic parameters for this 3D printer include 365nm light source from the NVR UV engine, about 34.56mm x 19.44mm working size of the x and y area, and the 1920 x 1080 DMD array. The resolution in X-Y area could reach to 18 μm per pixel and 5 μm minimal thickness of one layer in z direction, respectively.

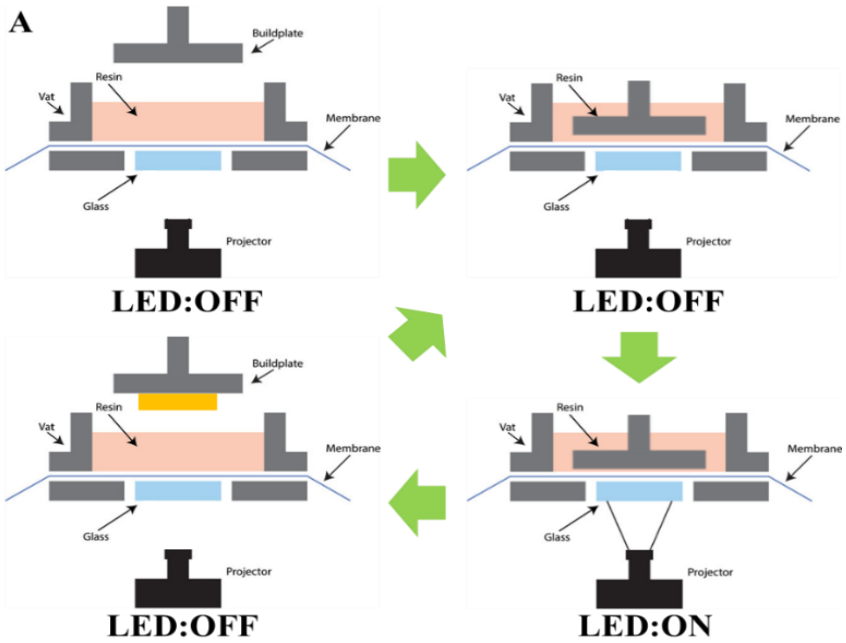

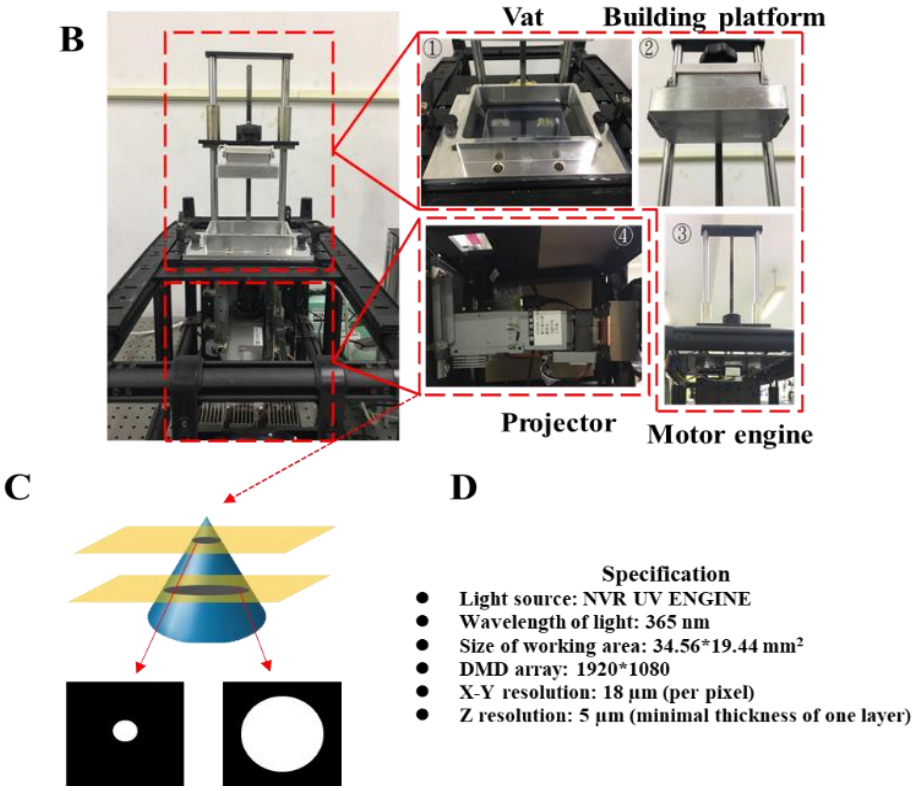

Figure 3.4 The customised digital light processing (DLP) 3D printer and 3D printing process

A: Schematic images of the printing process of the customised DLP 3D printer; B: Image showing the configuration of the customised DLP 3D printer, at least including vat, building platform, motor engine and the projector containing light source and DMD array; C: Schematic images of the sliced patterns reflected by the DMD array (digital masks); D: Specification for the customised DLP 3D printer. (Images were adapted with permission from Prof. Su of NTHU.)

The working process of this printer could be demonstrated simply as follows. The photocurable materials should be poured into the vat on top of a transparent (glass coated with Teflon) screen before printing. The movable building platform is then moving down to the bottom of the vat within the materials after receiving the order from the software installed in the associated computer. After switching on the projector controlled by the software, UV light in the form of beams from the light source will be emitted penetrating through the transparent bottom of the vat to activate the material. By using the DMD array, the sliced 2D patterns of the designed 3D pattern could be transferred and projected to the vat to crosslink the materials between the platform and the transparent screen at the correct position in a layer-by-layer style. Once the former layer of the pattern is built on the

building platform, the projector and light would be switched off. The platform would then be lift off with the crosslinked materials. This printing process will be repeated again and again until the 3D structure of the design is completely printed on the fixed flat building platform. After printing, the 3D product was washed by DDW and taken out of the platform by a knife. Printed samples were then put into a container with small amount of DDW to perform post-printing process. The post-printing process could be done in another device with UV light, or another DLP-3D printer to exposure appropriate light directly for a few seconds (depending on the size and material of sample). In this study, we did the post-printing process in the same DLP-3D printer after printing.

3.2.7.2 3D-printed test models for resolution, aspect ratio and shape fidelity studies

To study the possible resolution of the 3D-printed PEGDA products by this DLP 3D printer, 20% PEGDA solutions containing 0.05% LAP with/without light absorber were prepared to be the inks. A series of concave patterns with the hole having same thickness but different diameters (30, 50, 100, 200, 300, 400, 500 μm), and convex patterns with the cuboid having 4:1:1 of the ratio between length, width and height, and different widths (30, 50, 100, 200, 300, 400, 500 μm) (same as the space in between), were designed. Controlled by a computer, the design with correct format was transferred into the customised software program and printed by the customised DLP 3D printer (Figure 3.4). In the first model, patterns were printed directly in a single layer of PEGDA without additional light absorber to a certain thickness (500μm). In the second model, patterns were fabricated by the PEGDA material containing light absorber to the same thickness (500μm) in a layer-by-layer style (50 layers). The resolutions of concave/convex patterns printed by two different models were then investigated.

To study the possible aspect ratio and shape fidelity of the 3D-printed PEGDA products after printing by this DLP 3D printer, 20% PEGDA solutions with 0.05% LAP and light absorber were prepared to be the ink. A series of convex patterns with fixed sizes (500 μm in diameter and 500 μm in thickness) but different space intervals (50, 100, 200, 300 μm) were designed. Controlled by a computer the design was printed in a layer-by-layer model. Under an inverted light microscope, the top and bottom layer of the 3D pattern were focused and recorded by the connected camera. By using the imaging software of the microscope, differences between measurements from top and bottom layers of a specific pattern could be studied. From the schematic image of the distances measured from top and bottom layers of the same convex pattern, differences between the design and real 3D-printed product could be analysed and described in the form of the angle of the inclination after printing. The aspect ratio and shape fidelity of the convex pattern could be roughly detected by this way.

3.2.7.3 3D designs and fabrications

Here a series 3D designs regarding the self-assembly scaffold, characterisations and optimisation will be described below.

3.2.7.3.1 Design and fabrication of self-assembly scaffold by DLP-based 3D printer

Patterns of the self-assembly scaffold were designed and printed by DLP 3D printer (Figure 3.4). PEGDA hydrogel formula and sizes of the final self-assembly scaffold have been selected after optimisations, which is 20%PEGDA with 0.05% LAP in the formula of hydrogel scaffold, and 0.5-0.6 mm in thickness of a hexagonal shape with organised hole patterns (100-200 μm spaces and diameter) (Figure 3.5).

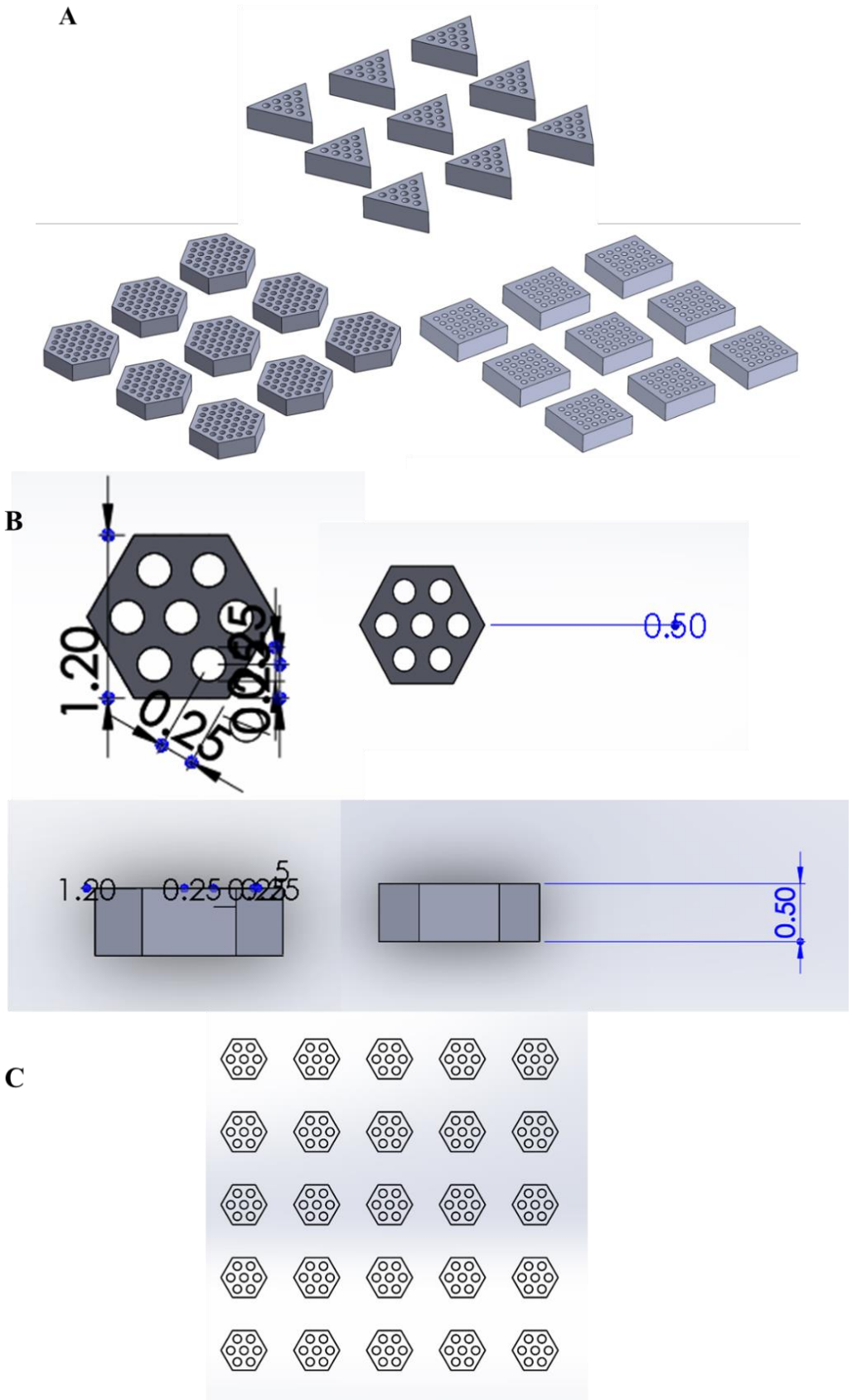

Figure 3.5 Schematic images of the design of the self-assembly scaffold

A: Schematic images of different designs of the self-assembly hydrogel scaffold. Hexagonal shape, square shape and triangle shape of the scaffold with uniformed hole arrays (100-200 μm in diameter). Preliminary designs of

the scaffold contain a series of diameters of the inscribed circle of different shape, including 750, 1000, 1250 and 1500 μm, and a series of thicknesses including 300, 400, 500 and 600 μm. B: Schematic images of the optimised design of the self-assembly hydrogel scaffold (front view and side view) and pattern arrays for 3D printing fabrication. (Images were adapted with permission from Mr. Wu of NTHU.)

3.2.7.3.2 Characterisations of the self-assembly PEGDA scaffold by coverage rate

The self-assembly property of the designed PEGDA scaffold was characterised by the coverage rate after injecting the scaffold-suspended solution into an empty hole simulating the chondral/OC defect area. The process in detail is described as follow. At first, PEGDA scaffolds were designed and printed as mentioned (Figure 3.4 and 3.5). The printed products were checked the morphology and pattern under a normal inverted microscope and kept in DW in centrifuge tubes at 4℃. Secondly, scaffolds within the tube were gently centrifugated to deposit at the bottom of the tube and then the injectable samples were prepared by replacing the supernatant water with carrier solution. After filling the syringe (1 ml) with the prepared samples, they were injected (controlled flow rate) into an empty hole with 1 cm in diameter (2mm in thickness) simulating the size of the chondral/OC defect area of the femoral condyle. The flow rate and velocity of injection were controlled by manually extruding a total 1 ml volume of the suspension within 1 minute (60s). Finally, to measure the self-assembly property of the patterned scaffold after injection, images of the whole area covered with scaffolds were recorded by a camera. By this way (Figure 3.6), each test was repeated at least 10 times. The self-assembly property of the designed pattern after injection was analysed by calculating the coverage rate through image process.

Images after injections of the self-assembly PEGDA scaffolds were taken by the camera and processed by Image J (v1.8.0.112, National Institutes of Health, USA) [20] to become 8-bit black and white images (Figure 3.7).

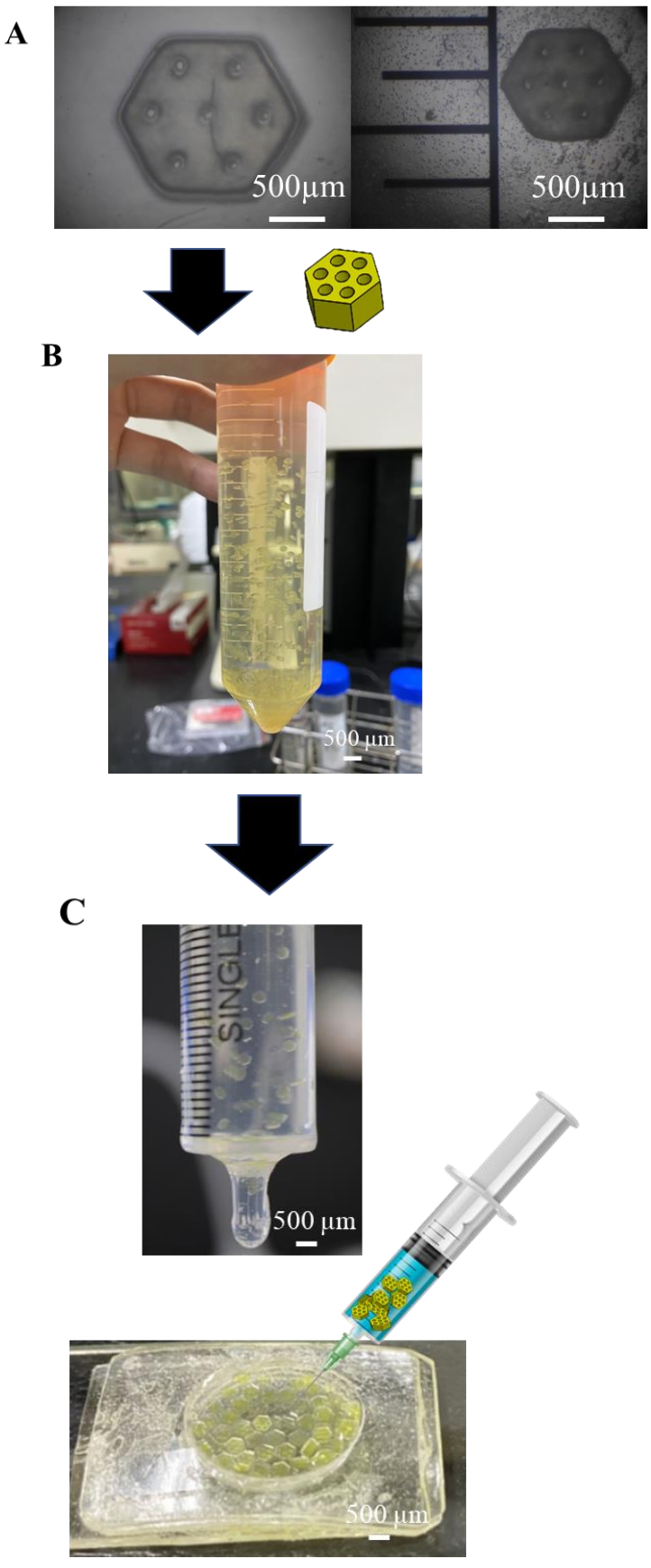
A
500µm
500µm
B
500 µm
C
SINGLE
500 µm
500 µm

Figure 3.6 Schematic images of the characterisation of the self-assembly property of the PEGDA-based scaffold

A: Image of the printed PEGDA scaffold was taken by inverted microscope. The scale bar is 500 µm. The size of holes within the PEGDA scaffolds was fixed at 100-200 µm. B: To perform the self-assembly property in injectable solutions, the PEGDA scaffolds were suspended in liquids such as DW or methyl-cellulose solutions. C: The scaffold-suspended solutions were filled in a syringe and injected into an artificial empty hole (1 cm in diameter) mimicking the chondral/OC defect area, with controlled flow rate. D: After injection and equilibrium, the coverage rate of these scaffolds was measured by analysing images taken by the camera from the bottom of the sample. (Images were adapted with permission from Mr. Wu of NTHU.)

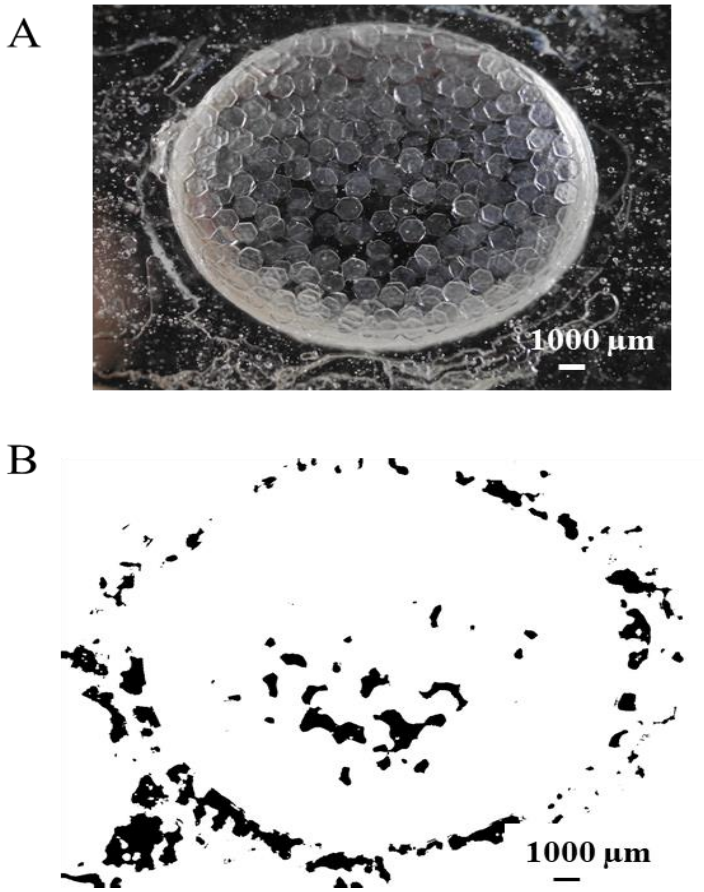

Figure 3.7 Schematic images of the image process to calculate the coverage rate of the injectable sample

A: The original image taken by a camera, showing the area covered by the designed self-assembly scaffold after injection and equilibrium. B: Image after processing, was converted in black and white, indirectly indicating the covered area (white) and uncovered area (black). The scale bar is 1000μm. (Images were adapted with permission from Mr. Wu of NTHU.)

By Image J (v1.8.0.112, National Institutes of Health, USA), the area of black in the experimental area representing indirectly the uncovered area could be calculated. Because the experimental area simulating the chondral/OC defect was designed, the area of the simulated area was fixed, by using the following equation, the coverage rate could be analysed and compared between different experimental groups. By analysing the coverage rate after injecting certain patterns of the designed PEGDA scaffold, the self-assembly property of the specific PEGDA scaffold could be determined.

$$\boldsymbol{Coverage\ rate}\ (\%) = \mathbf{1} - \frac{\boldsymbol{The\ area\ of\ the\ dark\ color\ inside\ simulated\ defect\ area}}{\boldsymbol{The\ area\ of\ the\ simulated\ defect\ area}}\ \boldsymbol{x}\mathbf{100}\% \qquad \textbf{(8)}$$

3.2.7.3.3 Optimisations of the design and self-assembly process of the scaffolds in solutions

To optimise the parameters of sizes, a series of PEGDA scaffolds with uniform hole patterns (100-200 μm) but varied pairs of diameters (0.75,1, 1.35, 1 and 1.5 mm) and thicknesses (0.3, 0.4, 0.55 and 0.6 mm) were designed and printed (Figure 3.8).

To optimise the carrier solution of the injecting process, 4 solutions with various viscosities were prepared to deliver the scaffold as carrier to test the self-assembly property. They are DDW with viscosity of 0.89 cp and methyl-cellulose solutions with three different concentrations (1%, 2% and 4%). The methyl-cellulose compound was commercial products with the tested viscosity (15cp) at 2%. This compound is often used in food industry as thickening material to be added in the formula of products. As the viscosity of polymer will be affected by many factors including the concentration of the polymer, the pH value of the solution, the temperature and the molecular weight of the polymer, in which the viscosity of the solution is in proportionate to the increased

concentration of the polymer, if other conditions are fixed. Hence different concentrations (1%, 2%, and 4%) of methyl cellulose (MC) in DDW were prepared, to approximately simulate the solutions with different viscosities (7.5cp, 15cp and 30cp). Then the tube containing scaffolds were gently centrifugated to deposit at the bottom and the injectable samples were prepared by replacing the supernatant DDW with solutions of varied viscosities.

To validate the self-assembly property of the hexagonal pattern of the PEGDA scaffold, triangle and square patterns were designed and printed (Figure 3.9). By the same process and analysis, the coverage rates of PEGDA scaffolds with three different patterns were examined and compared. The size of the hexagonal pattern of the scaffold is 0.75mm in diameter and 0.3 mm in thickness. The size of the square pattern is 1.08 mm in diameter and 0.3 mm in thickness. The size of the triangle pattern is 0.75 mm in diameter and 0.3 mm in thickness.

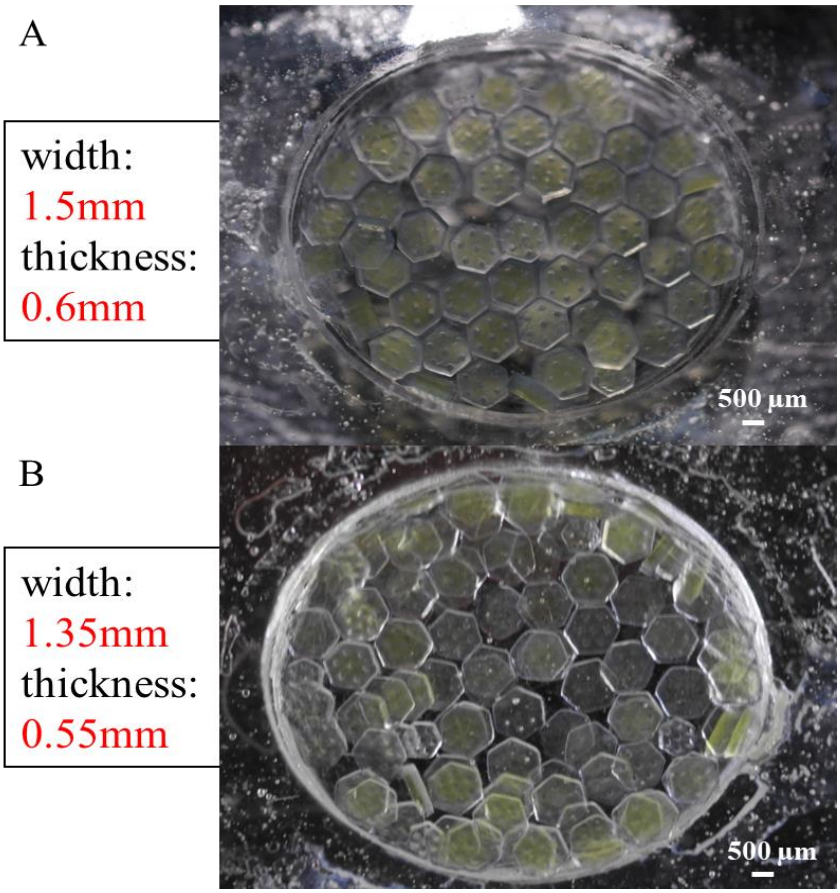

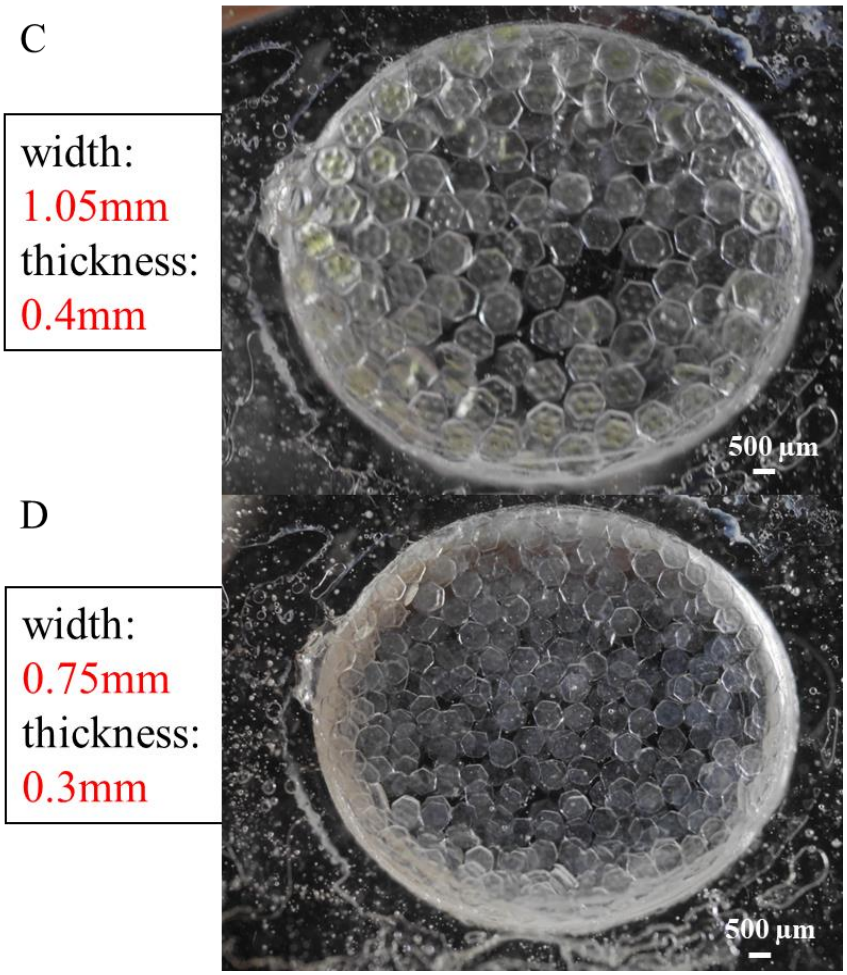

Figure 3.8 Four designs of the patterned scaffold with varied sizes in diameter and thickness

A: PEGDA scaffold with the hexagonal pattern in sizes of 1.5 mm diameter and 0.6 mm thickness; B: PEGDA scaffold with the hexagonal pattern in sizes of 1.35 mm diameter and 0.55 mm thickness; C: PEGDA scaffold with the hexagonal pattern in sizes of 1.05 mm diameter and 0.4 mm thickness; D: PEGDA scaffold with the hexagonal pattern in sizes of 0.75 mm diameter and 0.3 mm thickness. The scale bar is 500 µm. (Images were adapted with permission from Mr. Wu of NTHU.)

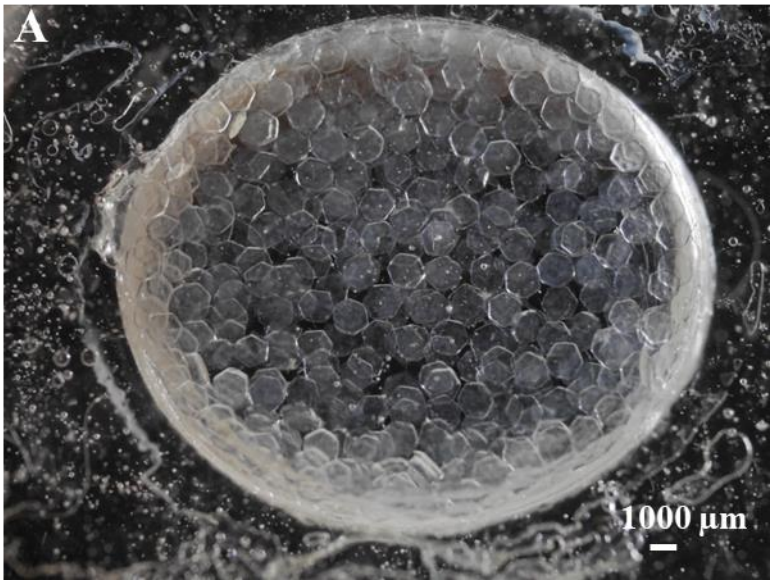

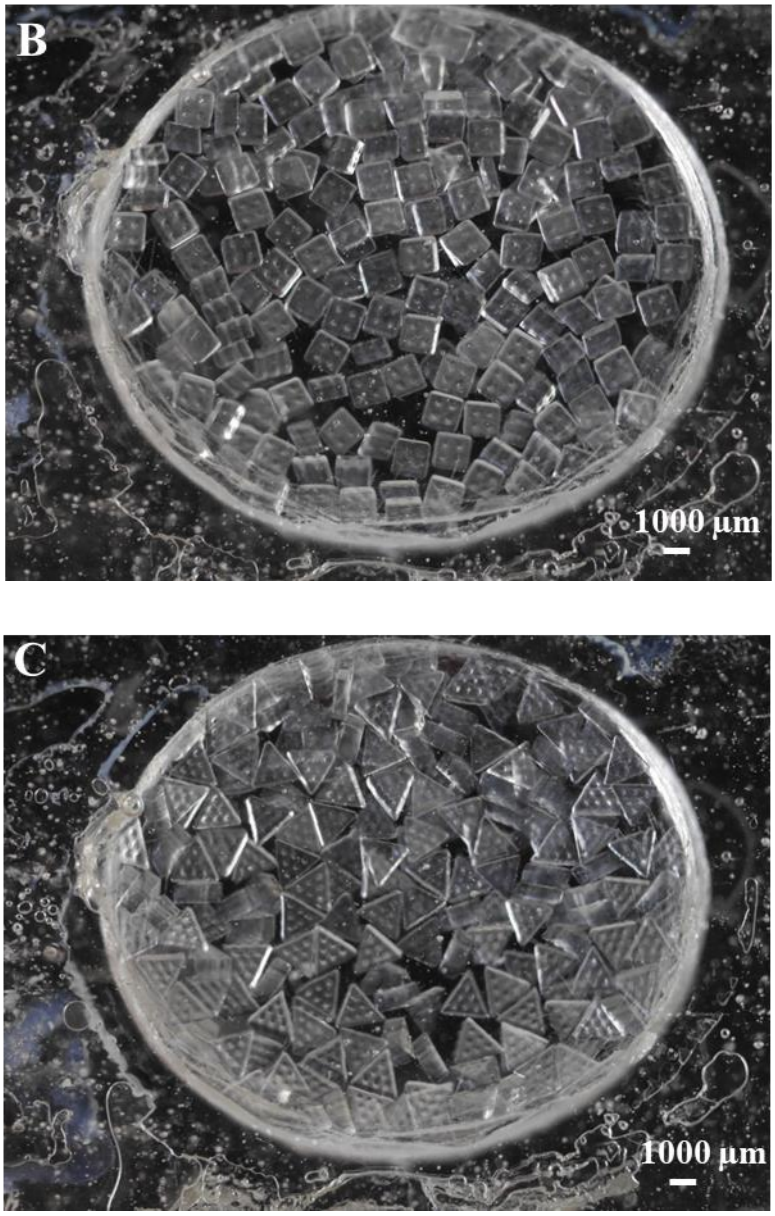

Figure 3.9 Varied pattern of PEGDA scaffold with similar sizes

A: PEGDA scaffold with the hexagonal pattern and sizes of 0.75mm in diameter and 0.3 mm in thickness; B: PEGDA scaffold with the square pattern and sizes of 1.08 mm in diameter and 0.3 mm in thickness; C: PEGDA scaffold with the triangle pattern and sizes of 0.75 mm in diameter and 0.3 mm in thickness. The scale bar is 1000 µm. (Images were adapted with permission from Mr. Wu of NTHU.)

3.2.8 Biocompatibility of the 3D-printed PEGDA scaffold

Evaluations on the biocompatibility of the 3D-printed PEGDA scaffolds, in terms of the leaching test by MTT assay, and the viability of cells cultured with the scaffold in 2.5D and 3D system by Live and Dead assay, will be described in this section.

3.2.8.1 Leaching test of the 3D-printed PEGDA product by MTT assay

The International Organisation for Standards (ISO) contains detailed biocompatibility tests in the ISO 10993 document set, in which a series of national and international standards were compiled into 20 parts, providing specific guidance to perform biological evaluation on medical devices within a risk management process [21, 22]. Considering the intended medical application of the designed TE scaffold, especially the self-assembly hydrogel scaffold in this study, the biocompatibility investigations mentioned in this study such as the MTT assay for the viability and proliferation screening, the cytotoxicity test, and the leaching test of the 3D-printed sample, were referred to the latest version of ISO documents, including the protocol of screening assays (MTT assay in Part 5 Test for *in vitro* cytotoxicity (ISO 10993-5:2017), and the experimental design for examining the leaching of the 3D-printed hydrogel scaffold (Part 12 for sample preparation and reference materials, especially the 10.3 Extraction conditions and methods, and the Table 1 of standard surface areas and extract liquid volumes in the ISO 10993-12:2021 (E) document).

3D-printed PEGDA-based scaffolds were tested for leaching according to the ISO10993-12:2021 (E) document. Based on the guideline from ISO (Table 3.3), experiment for leaching test was designed. In brief, after 3D printing, the PEGDA products were soaked in DMEM (1ml per sample per well) and put into an incubator for three days. Each group of product contains three samples, and DMEM alone in the well was prepared for the black control. Supernatants of the solution after incubating 3D PEGDA products were collected and filtered to sterilise. Then another DMEM medium was added and collected after another 3 days incubation. Three collections were made for one such experiment to test and the experiment was repeated three times. There were four groups involved in the leaching test, including positive control (growth medium with additional DMSO),

blank control (growth medium with the collected DMEM alone solution), negative control (growth medium with same amount of DPBS) and the experimental group (growth medium with collected conditional supernatant DMEM solution) (Figure 3.10). NIH 3t3 fibroblasts were used in the test. In brief, cells were seeded at appropriate density in 24-well microplates and cultured in an incubator (3.2.6.1 and 3.2.6.2.1). After 24 hrs incubation, cells were checked under inverted microscope and the cell medium was replaced with the conditional medium. According to the group of conditional media, cells were classified into different group, including negative control, positive control, blank control, experimental group. Then cells were cultured in an incubator for 1, 4 and 7 days based on the experimental plan. Those conditional media were replaced every two to three days for associated groups. After 1-, 4- and 7-days incubation, samples were examined by MTT assay as mentioned process in 3.2.6.2.2.

Table 3.3 Table of standard surface areas and extract liquid volumes from ISO 10993-12:2021 (E)

Thickness[a] mm	**Extraction ratio** (surface area or mass/volume) ±10 %	**Examples of forms of materials**
<0,5	6 cm^2/ml	film, sheet, tubing wall
0,5 to 1,0	3 cm^2/ml	tubing wall, slab, small moulded items
>1,0	3 cm^2/ml	larger moulded items
irregularly shaped solid devices	0,2 g/ml	powder, pellets, foam, non-absorbent moulded items, porous high-density materials
irregularly shaped porous devices (low-density materials)	0,1 g/ml	membranes, textiles

[a] If the medical device includes multiple tissue contacting components with different thicknesses, the extraction ratio should be justified. One way to do this is to base the ratio on the thinnest material layer of that component.

NOTE While there are no standardized methods available at present for testing solvent absorbing polymer materials (e.g. absorbents and hydrocolloids), a suggested protocol is as follows:

— determine the volume of extraction vehicle that each 0,1 g or 1,0 cm^2 of material absorbs;

— then, in performing the material extraction, add this additional volume to each 0,1 g or 1,0 cm^2 in an extraction mixture.

Note: Information labelled in yellow was referenced in the design of leaching test for the 3D-printed hydrogel in this study.

A

Positive control	Blank Control	Negative control	Test groups
Growth medium with DMSO	50%Growth medium 50% DMEM	50%Growth medium 50% DPBS	50% Growth medium 50% Supernatant

B

C

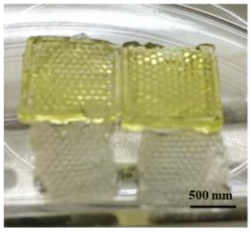

1x1 cm^2
600-800 µm thick

Figure 3.10 Schematic images of the design of leaching test for the 3D-printed PEGDA scaffold
A: Four experimental groups designed; B: Images of the preparations for the experimental groups and black control groups. C: Schematic images of the 3D-printed PEGDA scaffold applied in leaching test.

3.2.8.2 Cell viability on 2.5 D culture evaluated by Live & Dead assay

NIH 3t3 fibroblasts and Chondrogenic cell line ATDC5 cells were used for the 2.5 D viability test. PEGDA-based scaffolds in this test, contains PEGDA with hole patterns, PEGDA thin sheet without pattern and PEGDA thin sheet with additional nanocellulose fibres without pattern. These PEGDA-based scaffolds were printed and soaked into DDW for three days to avoid leaching problems, based on results from the leaching tests (3.2.8.1). Then the scaffolds were further sterilised by 75% alcohol followed by UV light exposure in a biosafety cabinet for 2 hrs before using. For PEGDA thin sheets (with/without additional nanocellulose fibres), 0.1mg/ml type I collagen solution (diluted by 0.01M HCl according to the instruction from manufacturer) were used to coat the material after sterilisation and dried in an incubator for about 1-2 hrs at room temperature.

Cells were cultured and adjusted to the appropriate density (10K cells per well for fibroblasts; 5K cells per well for chondrocytes in 2D in 24-well microplate studies) as mentioned in 3.2.6.1. After

sterilisation and/or coating, 3D-printed scaffolds were transferred carefully by a sterilised tweezer into wells of 24-well microplates, and seeded by the cells at their appropriate density. Then the samples were put into an incubator to culture. Cultural medium was replaced every two to three days. After 7-14 days incubation, Live and Dead assay was applied to evaluate the viability of cells cultured with the 3D-printed PEGDA scaffolds. Staining process was performed according to the instruction from the manufacturer (LIVE/DEAD™ Viability/Cytotoxicity Kit, for mammalian cells (L3224). In brief, samples were taken out of the incubator and checked under normal inverted microscope. Then cultural medium was replaced with staining solution containing green-fluorescent calcein-AM (2μM working solution) and red-fluorescent ethidium homodimer-1 (4 μM working solution) diluted in growth medium. Samples in staining were kept in dark at room temperature for about 30-45 mins and then carefully washed twice with PBS before being transferred gently onto the microscope slides with mounting agent by using a sterilised tweezer for further confocal microscope examination.

3.2.8.3 Cell morphology observation

Cell morphology in the 3D-printed PEGDA scaffolds, was examined by immunofluorescent staining (cytoskeletal F-actin). In this experiment, ATDC5 chondrogenic cell line and type I collagen were used.

3.2.8.3.1 Morphology of cells cultured on PEGDA scaffolds (2.5D)

PEGDA scaffolds with hole and groove patterns were printed and soaked into DDW for up to three days to avoid leaching problems, based on results from the leaching tests (3.2.8.1). Then PEGDA scaffolds were sterilised and coated with 0.1mg/ml type I collagen solution and dried as mentioned

in 3.2.8.2.

Cells were seeded at appropriate density (10K cells per well for fibroblasts; 5K cells per well for chondrocytes) on the coated scaffolds in 24-well microplate and put into an incubator. After 7-14 days incubation, samples were carefully washed by PBS twice and fixed by 4% formaldehyde solution at room temperature for 1-2 hrs. Then samples were washed by DW twice before adding staining solution in which the high-affinity fluorescence-conjugated antibody for cytoskeletal F-actin (AlexaFluor™ 488 phalloidin) was diluted in PBS solution. Samples in staining were kept at room temperature for about 30 mins in dark, and then were washed by PBS twice before examination by confocal microscope or normal fluorescent microscope.

3.2.8.3.2 Morphology of chondrocytes 3D cultured in PEGDA scaffolds

ATDC5 cells were cultured and adjusted to 100000 cells per ml density after resuspension in medium. Then cells were centrifugated again and resuspended with 3 mg/ml type I collagen solution (0.1x diluted by 10x PBS with pH=11 according to the instruction from manufacturer). 3D-printed PEGDA scaffolds (Figure 3.11 A) with the same pattern of the self-assembly scaffold (1mm in diameter, 0.5 mm in thickness) but bigger sizes (1cm in diameter, 0.8 mm in thickness) were prepared as mentioned in 3.2.8.2 and put into wells of 24-well microplates without any coating before seeding (Figure 3.11 B). Then the prepared cell-laden collagen gel was added on the PEGDA scaffolds to cover the scaffold. After 1-2 minutes equilibrium, plates containing samples were put into an incubator to further crosslink about 4-6 hrs. Then growth medium was added into wells containing the crosslinked collagen gel containing both cells and scaffolds. Cultural medium was replaced every two to three days. After 7-10 days incubation, morphology of

the 3D cultured chondrocytes delivered by collagen gel on the PEGDA scaffolds was examined by immunofluorescent staining the cytoskeletal F-actin. The staining process is similar as that mentioned in 3.2.8.3.1.

As a control, the prepared cell-laden collagen gel was also added into a well without PEGDA scaffolds and crosslinked. Instead of morphology, cell viability was examined by Live & Dead assay as mentioned in 3.2.8.2.

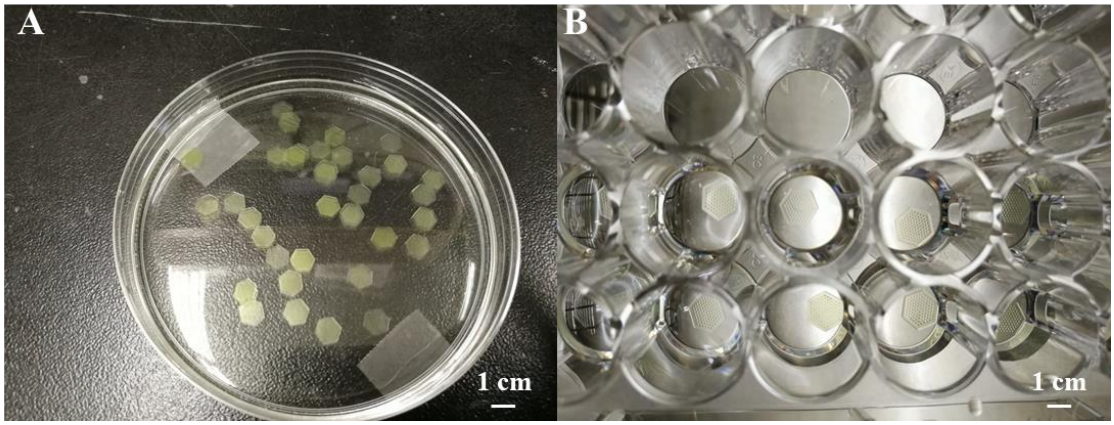

Figure 3.11 Images of 3D-printed self-assembly PEGDA scaffolds with bigger size
A: Images of 3D-printed PEGDA scaffolds kept in DW in a dish. B: PEGDA-based scaffold was prepared in wells of 24-well microplates for cell culture. The scale bar is 1cm.

3.2.9 Statistical analyses

In this section, statistical analysis on data from individual experiment will be described below.

3.2.9.1 Compressive modulus

The PEGDA bulk materials were either designed uniformly or fabricated in the microplate with fixed sizes, where the area of the cross section and the length were determined and recorded, to be analysed the compressive modulus representing the elasticity of the crosslinked hydrogel under compressive forces as mentioned above in 3.2.5.1. Data were all exported to Microsoft® Excel (Microsoft Corporation, USA) to calculate the Young's modulus of the 3D products statistically.

Mean value and standard deviation of samples were used to plot the diagrams, where the differences between groups were analysed by one-way analysis of variance ANOVA (Tukey post hoc test) by Origin2018 (OriginLab®, USA) to compare different groups. The p value less than 0.01 was considered as statistically significant.

3.2.9.2 Swelling degree, water content and dehydration rate

Measurements of weights of crosslinked hydrogels, before and after drying, during dehydration and after reswelling at different time point, were all analysed by Microsoft® Excel (Microsoft Corporation, USA) statistically. Mean value and standard deviation of samples were used to plot diagrams and curves.

3.2.9.3 MTT assay and LDH assay

Absorption data measured by the plate reader (BioTek, Agilent Technologies, Inc., USA) were exposed to Microsoft® Excel (Microsoft Corporation, USA) to compile and analysed statistically by Origin2018 (OriginLab®, USA), where the differences between groups were calculated by one-way analysis of variance ANOVA (Tukey post hoc test) and linear fitting of the cell numbers were also performed. The p value less than 0.05 was considered as statistically significant.

3.2.9.4 Coverage rate

Images taken by the camera were processed by Image J (v1.8.0.112, National Institutes of Health, USA) [20] to become 8-bit black and white images, and calculated the area of black in the image. The designed area simulating the chondral/OC defect was fixed as the area of the simulated defect area to be used to calculate the coverage rate. All data were recorded and analysed by Microsoft®

Excel (Microsoft Corporation, USA). Mean value and the standard deviation were used to plot the diagram, where the differences between groups were analysed by one-way analysis of variance ANOVA (Tukey post hoc test) by Origin2018 (OriginLab®, USA) to compare different groups. The p value less than 0.01 was considered as statistically significant.

3.3 Results and discussions

In this section, all results and discussions will be presented.

3.3.1 Characterisations of the PEGDA material and photocrosslinked PEGDA hydrogel

To characterise the material and 3D-printed hydrogel, morphology of the PEGDA-based material, compressive modulus, swelling capability, dehydration rate and the swelling ratio of crosslinked PEGDA hydrogel were preliminarily evaluated.

3.3.1.1 Morphologies of the PEGDA-based biomaterials

Different concentration of PEGDA solution with/without additional cellulose materials were prepared and crosslinked under the UV light. After freeze-drying, the crosslinked PEGDA-based hydrogels were scanned by the SEM to observe the morphologies (Figure 3.12 A-G). Commercial nanocellulose fibre solution was also prepared to identify the fibrous morphology (Figure 3.12, D and H) by SEM. From images, there were no big differences of the inner structure of the PEGDA gels crosslinked with or without additional cellulose materials. This might be explained by the only 0.2% of the fibrous materials blended into the PEGDA materials and the side of dried samples scanned. In addition, the hydrogel samples containing large amount of water were difficult to be dried thoroughly to be scanned by normal SEM machine. From the SEM image of the commercial

nanocellulose fibre, the fibrous morphology in nanoscale was identified.

A drawback of using hydrogel material to fabricate TE scaffold is the poor mechanical property of the hydrogel scaffold after fabrication. Many fibrous biomaterials have been applied to reinforce hydrogel materials, such as the silk protein fibre, cellulose fibre and other synthesised fibrous materials. In this study, we select the biocompatible cellulose fibre materials to try to improve the mechanical property and biocompatibility of the PEGDA hydrogel scaffold.

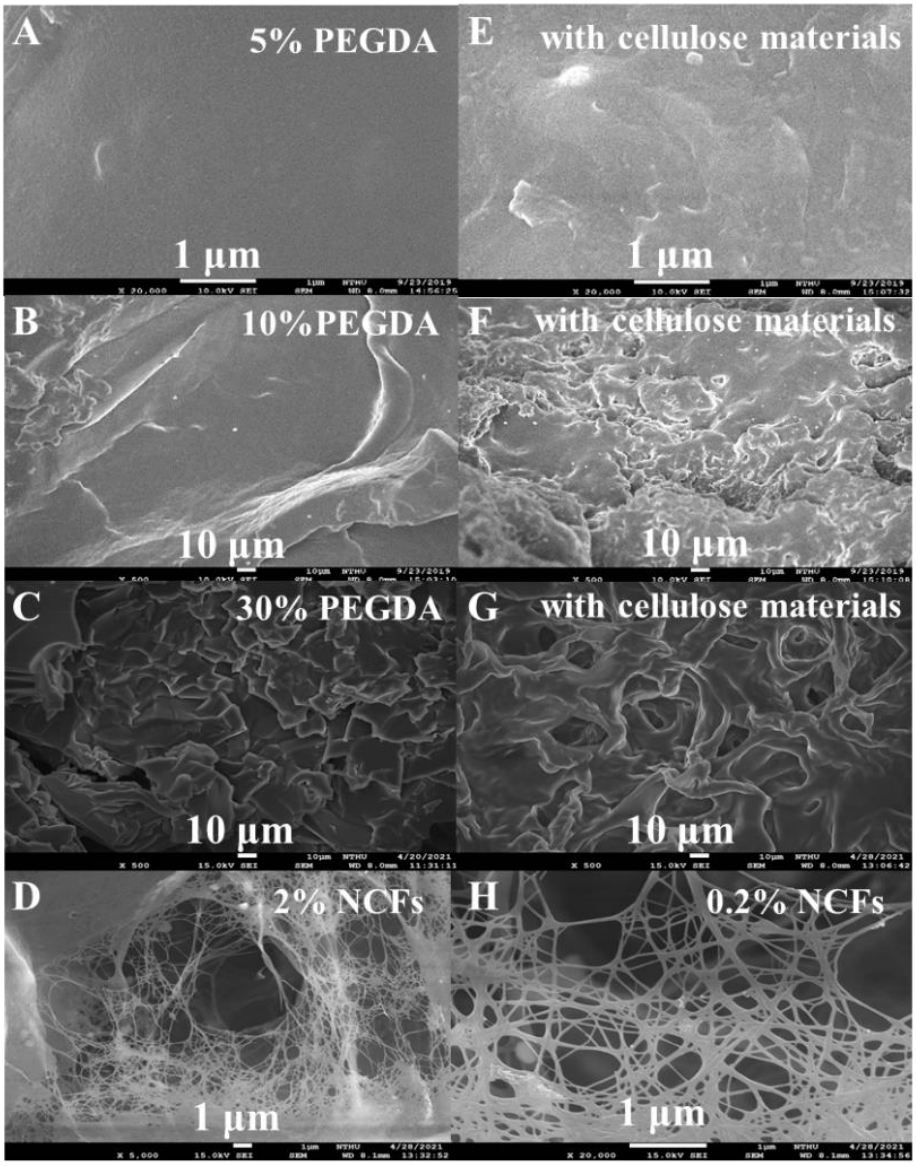

Figure 3.12 Morphologies of the PEGDA-based materials and nanocellulose fibres by SEM

PEGDA-based materials were added into 24-well microplate to crosslink under the UV365nm light for 10-20mins. Demoulded samples were put into 6-well microplate to dry in a freeze dryer overnight. 10 times diluted

(0.2%) and original (2%) nanocellulose fibres (NCFs) solution were dropped into a glass slide and dried in an oven overnight. Then samples were sent to scan the image by the High-Resolution Thermal Field Emission Scanning Electron Microscope (JEOL, JSM-7610F, Japan). A, E: 5% PEGDA with/without additional cellulose material; B, F: 10%PEGDA with/without additional cellulose materials; C, G: 30%PEGDA with/without additional cellulose materials; D, H: Different magnification images of 2% dried nanocellulose fibres. Scale bars were either 1 or 10 μm.

3.3.1.2 Mechanical properties of the PEGDA-based hydrogels

At first, the PEGDA-based hydrogels were crosslinked by exposing to the UV light directly and manually. From results (Figure 3.13), there is a concentration-dependent increase in the mechanical properties of these PEGDA-based hydrogels. The compressive moduli of the hydrogels with additional fibres would be lower a little bit than those without additional fibres, suggesting an improvement of the flexibility of the PEGDA hydrogel after adding fibrous materials. The PEGDA-based materials treated with tissue culture medium, comparing to the one with water, displayed higher compressive modulus value, the concentration-dependent increase in the mechanical property of the PEGDA-based hydrogel did not change. Comparing different days of treatment with culture medium, the compressive modulus of the hydrogels varied in different periods of treatment, but the variation is not very big. Even if there was an increase of the mechanical property in the samples treated with medium from 1 days to 14 days, after 28 days treatment, the compressive moduli of the PEGDA-based hydrogel samples were decreased to the comparable values of those after one day treatment. This result suggested that within around 28 days treatment, the mechanical property of the PEGDA hydrogel could be seen as stable. Due to these hydrogels were manually fabricated, samples in the sample group were not uniform and differences between samples were reflected by the large standard deviation in the plotted figures, especially in high concentration groups. This experiment was performed preliminarily to try to get

used to the photocurable material and the related mechanical test, before the customised DLP-3D printer was ready to use at that time in NTHU (Taiwan).

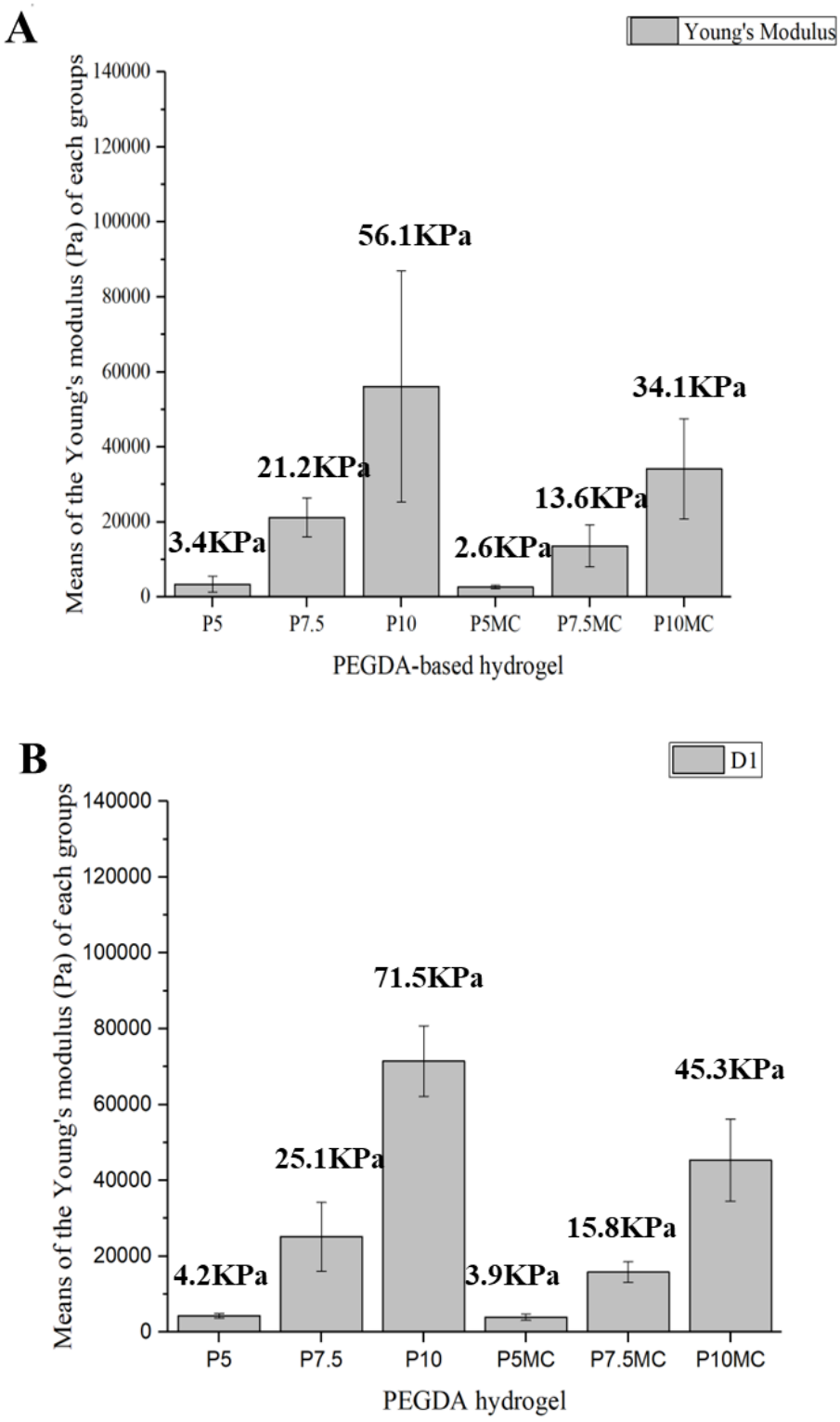

C

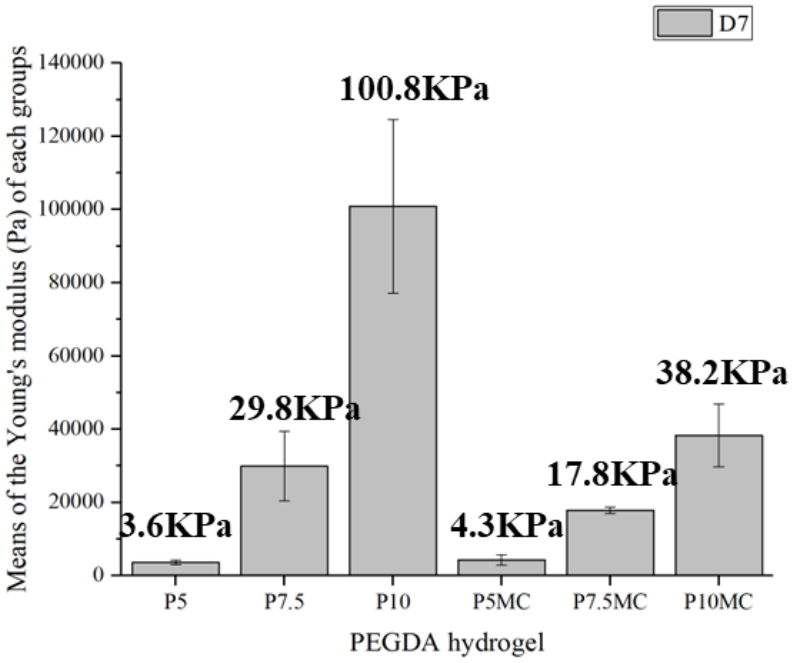
D7
Means of the Young's modulus (Pa) of each groups
140000
120000
100000
80000
60000
40000
20000
0
100.8KPa
38.2KPa
29.8KPa
17.8KPa
3.6KPa
4.3KPa
P5
P7.5
P10
P5MC
P7.5MC
P10MC
PEGDA hydrogel

D

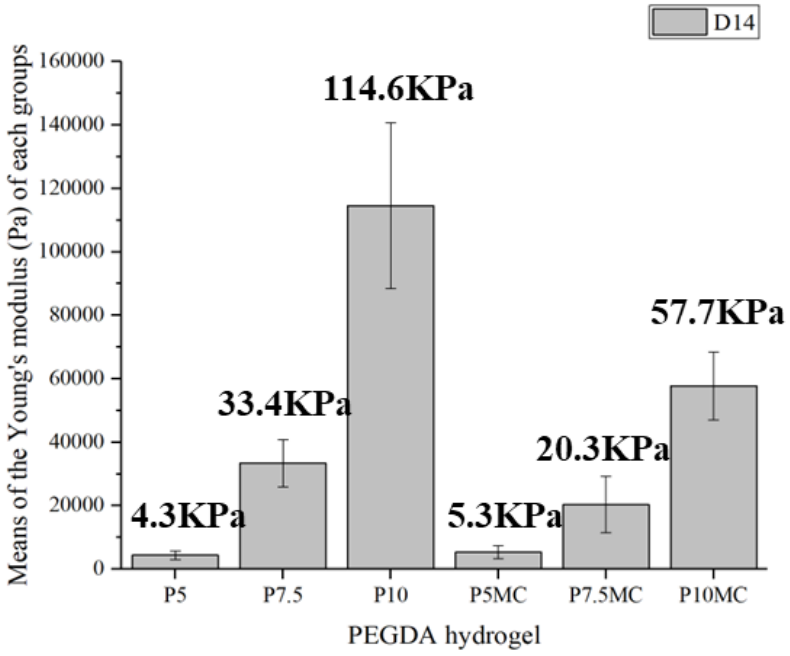
D14
Means of the Young's modulus (Pa) of each groups
160000
140000
120000
100000
80000
60000
40000
20000
0
114.6KPa
57.7KPa
33.4KPa
20.3KPa
4.3KPa
5.3KPa
P5
P7.5
P10
P5MC
P7.5MC
P10MC
PEGDA hydrogel

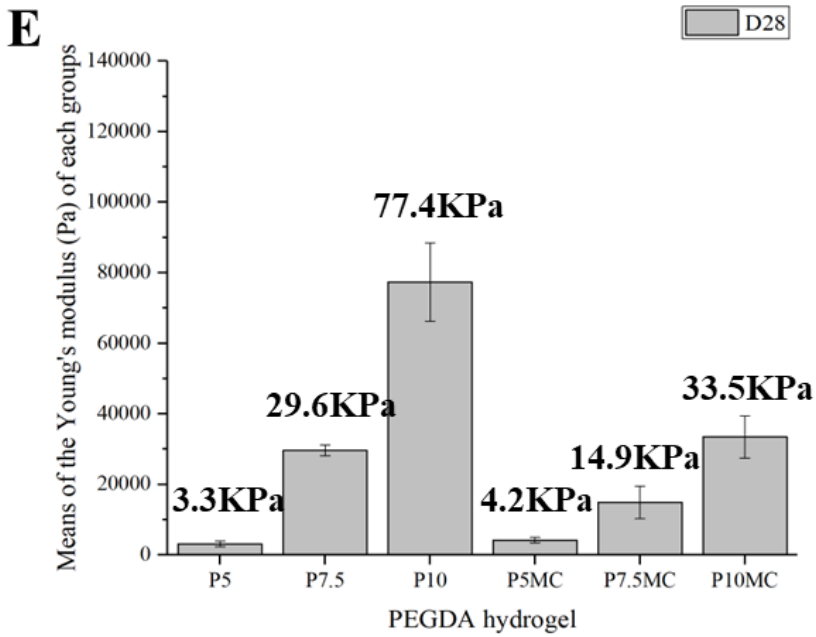

Figure 3.13 Compressive modulus of PEGDA-based hydrogels crosslinked directly by UV light

A: Different concentration of PEGDA hydrogel with/without additional cellulose fibres were crosslinked under UV light directly and measured the compressive modulus. B-E: Individual analysis of the mechanical property of different PEGDA-based hydrogel materials incubated with the tissue culture medium for 1, 7, 14 and 28 days. MC: 5% methyl-cellulose materials in solution.

Then 3D-printed PEGDA-based hydrogels were also performed the compressive test, including the 20% PEGDA, 30% PEGDA and 30%PEGDA with additional nanocellulose fibres (NCFs). From results (Figure 3.14), higher concentration of PEGDA has higher compressive modulus and the additional cellulose fibres would slightly increase the mechanical property of the 3D-printed PEGDA hydrogel. Comparing to the PEGDA-based hydrogel crosslinked directly by UV light, the 3D-printed products have almost one order higher compressive modulus, suggesting effect of the fabrication methods on the mechanical property of the PEGDA-based hydrogel.

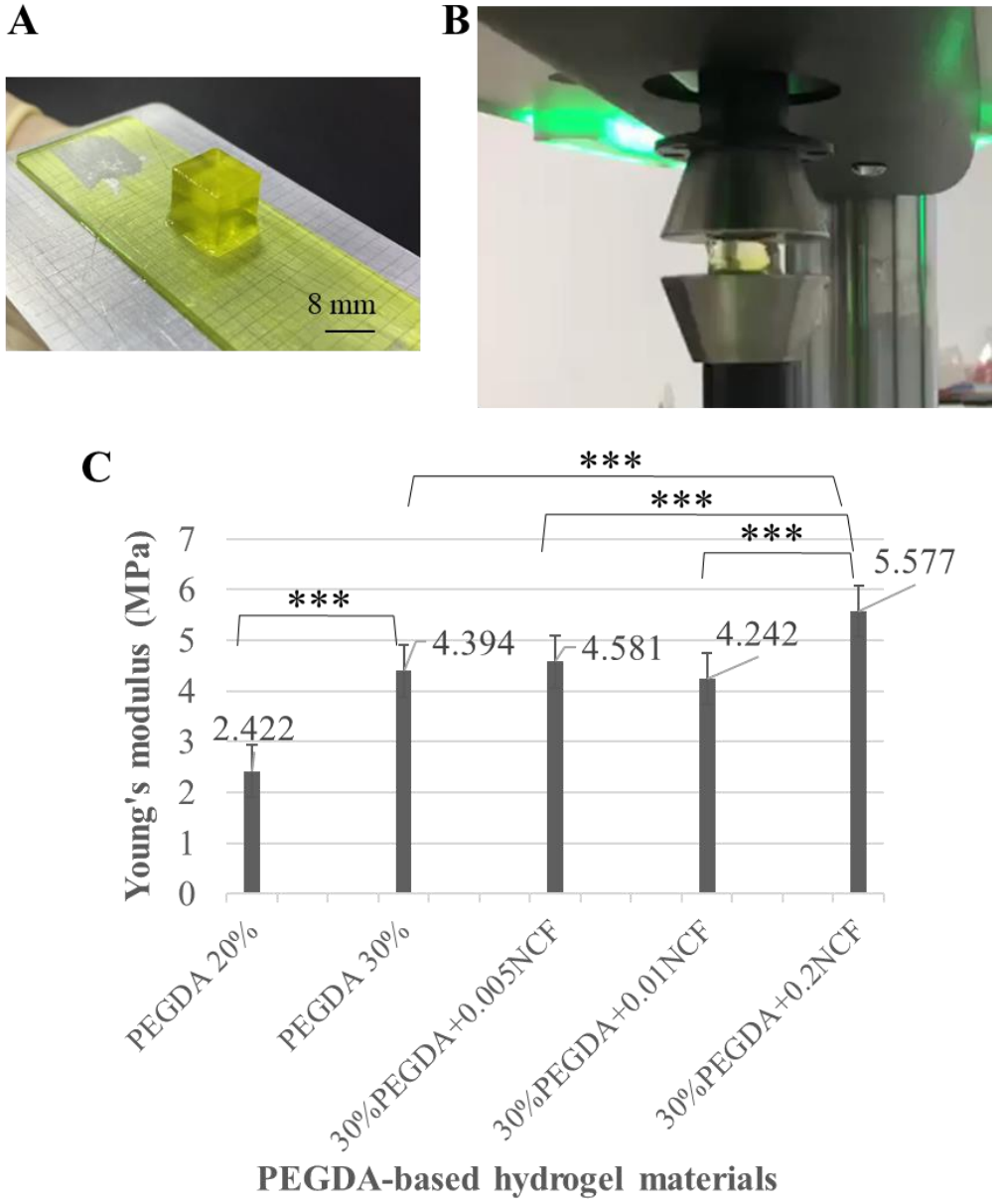

Figure 3.14 Compressive modulus of 3D-printed PEGDA-based hydrogels

A: Schematic image of the 3D-printed PEGDA cuboid for compressive test. B: The PEGDA hydrogel was examining by compressive testing machine. C: Compressive moduli of 3D-printed PEGDA-based hydrogels. Comparisons between experimental group and control group were analysed by ANOVA one way test (Tukey): * P<0.01; * * P<0.001; * * * P<0.0001. (Images were adapted with permission from Mr. Wu of NTHU.)

3.3.1.3 Swelling capabilities of PEGDA-based hydrogels

Equilibrium swelling capability is an important physical character reflecting the network structure and crosslink density of the hydrogel polymer. PEGDA-based hydrogels crosslinked directly by the UV light were examined the weight degree of swelling (Figure 3.15A) and water content

(Figure 3.15B). From the results, PEGDA-based hydrogels have high amount of water (around 90%), similar to those observed in cartilage ECM. Additional cellulose fibre, would not change the water content of the PEGDA-based hydrogel. Higher concentration of PEGDA hydrogel has lower weight degree of swelling and additional cellulose fibres would not change this swelling property of the PEGDA-based hydrogel.

Swelling ratio (Figure 3.16B) and dehydration rate (Figure 3.16A) of the 3D-printed 30% PEGDA-based hydrogels were also examined. From results, with additional nanocellulose fibres in the 30% PEGDA hydrogels, the dehydration rate and swelling ratio were both slightly decreased, suggesting that there would be no obvious effect of the additional nanofibre material on the swelling capabilities of the 3D-printed PEGDA hydrogel, to be used to fabricate TE scaffolds.

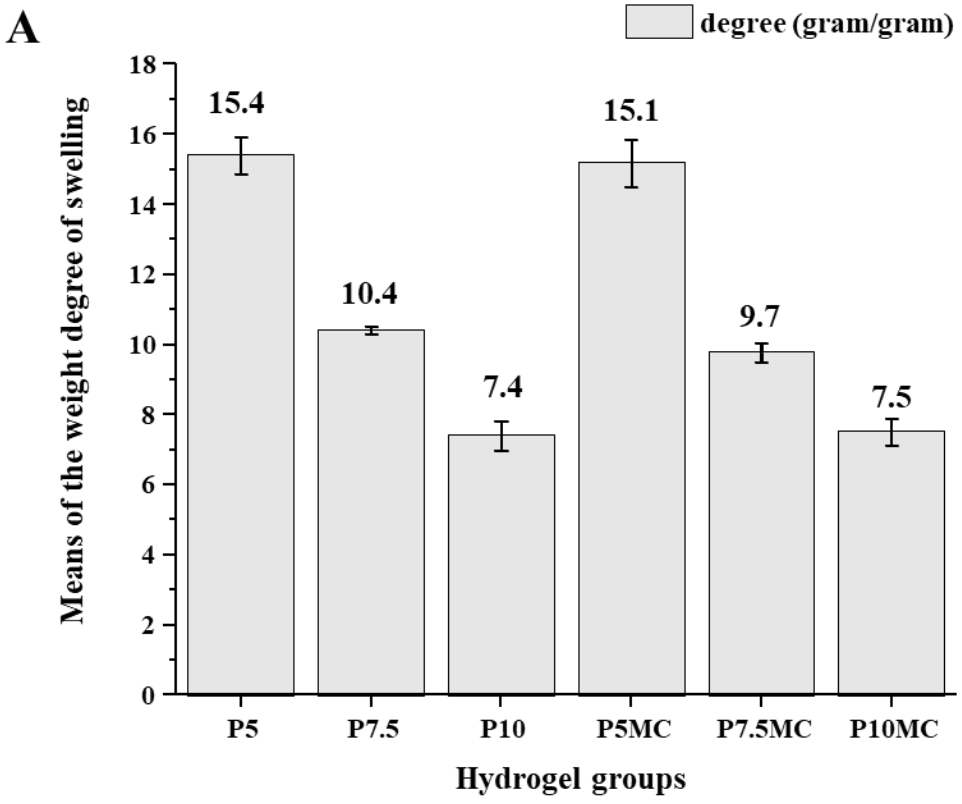

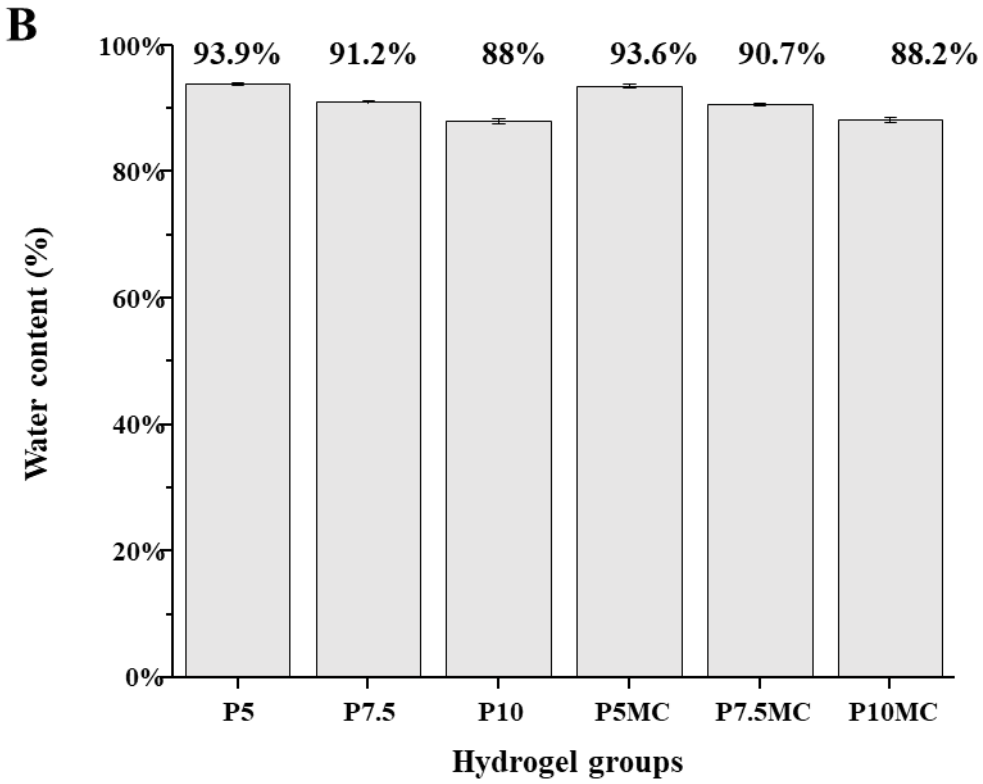

Figure 3.15 Swelling capability after freeze-drying and water content of PEGDA-based hydrogels crosslinked directly by UV light

A: Comparison of the weight degree of swelling of the PEGDA-based hydrogels. B: Comparison of the water content of the PEGDA-based hydrogels. MC: 5% methyl-cellulose materials in solution.

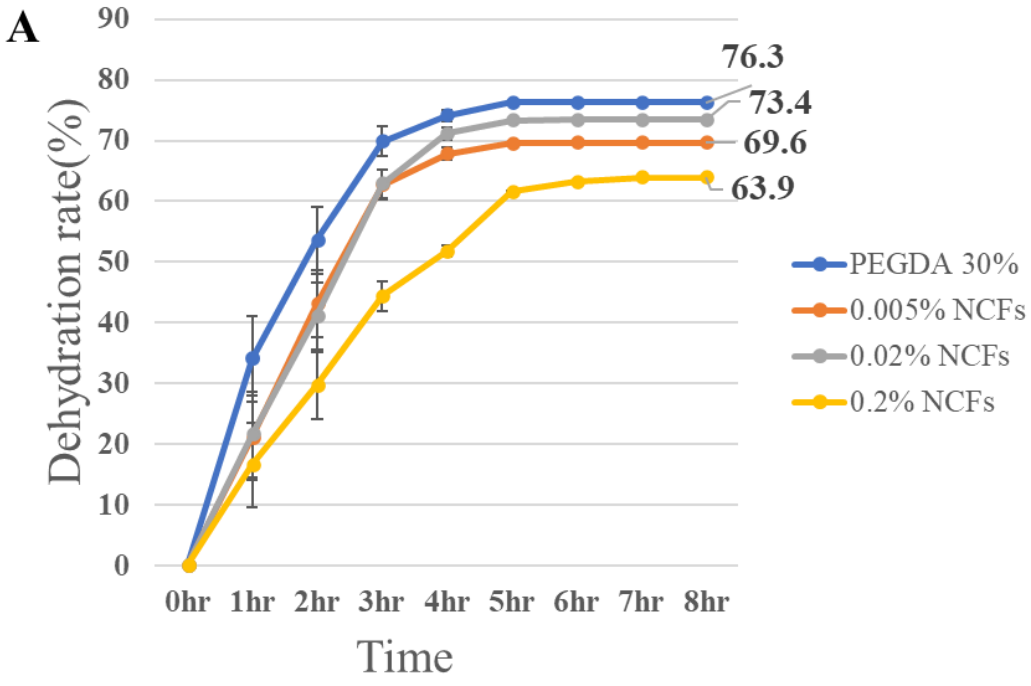

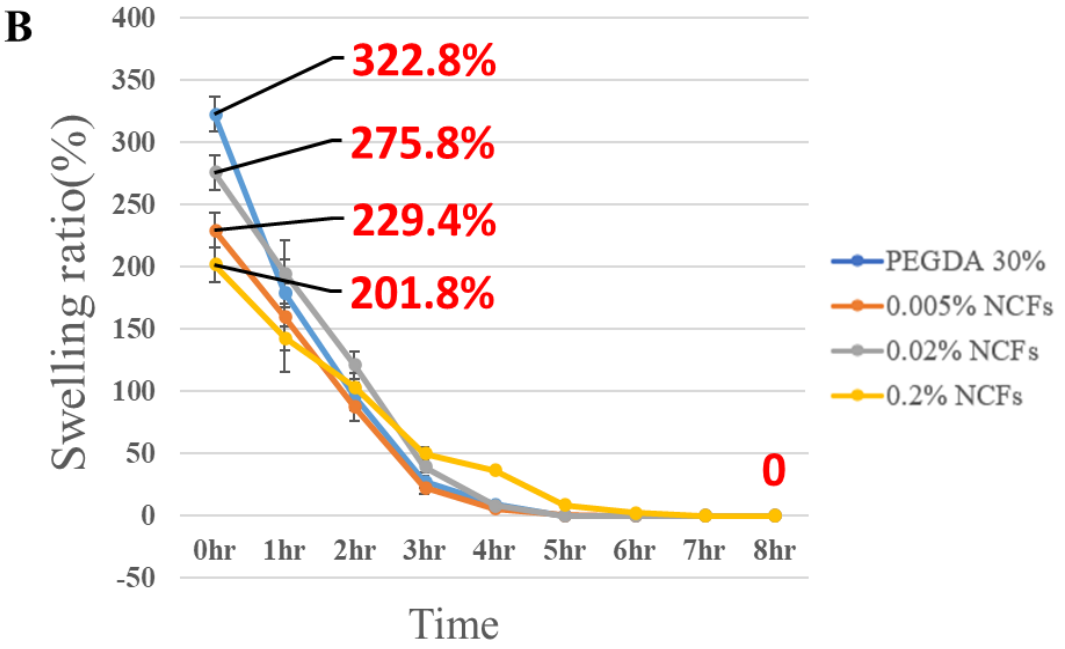

Figure 3.16 Dehydration rate and swelling ratio of 3D-printed PEGDA-based hydrogels

A: Comparison of the dehydration rate of the 3D-printed 30%PEGDA hydrogel with/without additional nanocellulose fibres. B: Comparison of the swelling ratio of the 3D-printed 30%PEGDA hydrogel with/without additional nanocellulose fibres. (Images were adapted with permission from Mr. Wu of NTHU.)

3.3.2 Effect of the photoinitiator LAP on the cell viability and proliferation *in vitro*

Fibroblast NIH 3t3, myoblast C2C12 and chondrogenic cell line ATDC5 cells were tested individually in this study. The results of the seeding cell density test (Figure 3.17 G, H, I) showed that, cell number between 5K to 10K per well in 24-well microplate would be the appropriate seeding density for fibroblasts and around 10K per well would be suitable for myoblasts and chondrocytes. Based on these, cells were seeded at their appropriate density in 24-well microplates and treated with different concentrations of photoinitiators LAP, to examine the cytotoxic effect on living cells *in vitro*. After incubation 1, 4 and 7 days, samples were checked by performing LDH assay. From the results, there was a concentration-related toxic effect of the LAP on living cells and higher concentration of LAP was more toxic on cells in culture. There was a short time-related

effect, in which results from 4-day treatments displayed less viability than those from only one day treatment. Variations of results of the 7-day treatment were observed in all three cell lines, in which after 7 days treatments, the cell viabilities increased rather than decreased as expected. This could be explained by the medium replacement. Every two to three days, cell medium was replaced, in this test, fresh growth medium without LAP was used. Since the LAP is water-soluble, after replacement, the amount of LAP left in the cell culture medium was reduced. And it was reported by other studies that the low cytotoxic feature, hence results after 7-day treatment, showing a slightly increase in the cell viability were due to its low toxicity and the reduced amount left in the cell culture microenvironment.

In our studies, for fibroblast, comparing to control groups, all experimental groups were more than 70% cell living, displaying low toxicity. For myoblast, comparing to control groups, all experimental groups remained more than 60% cell living and comparing to 0.1% and 0.15%, 0.05% LAP presented the lowest toxicity. For chondrocytes, comparing to control groups, all experimental groups remained more than 60% cell viabilities and comparing to 0.1% and 0.15%, 0.05% LAP had the lowest toxicity. Different cell line displayed different sensitivity to this low toxic photoinitiator LAP, suggesting the requirement of different amount of it to be prepared in the formula of 3D printing ink. In addition, although the cytotoxicity of LAP is low, the enhanced effect due to the accumulation of this compound should not be neglected.

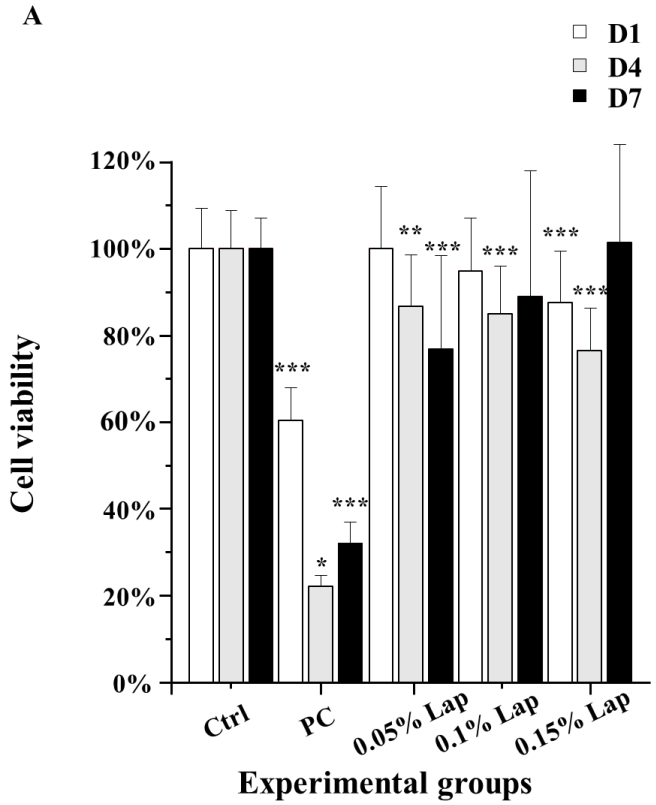
A
D1
D4
D7
Cell viability
120%
100%
80%
60%
40%
20%
0%
***
*
***
**
***
***
***
***
Ctrl
PC
0.05% Lap
0.1% Lap
0.15% Lap
Experimental groups

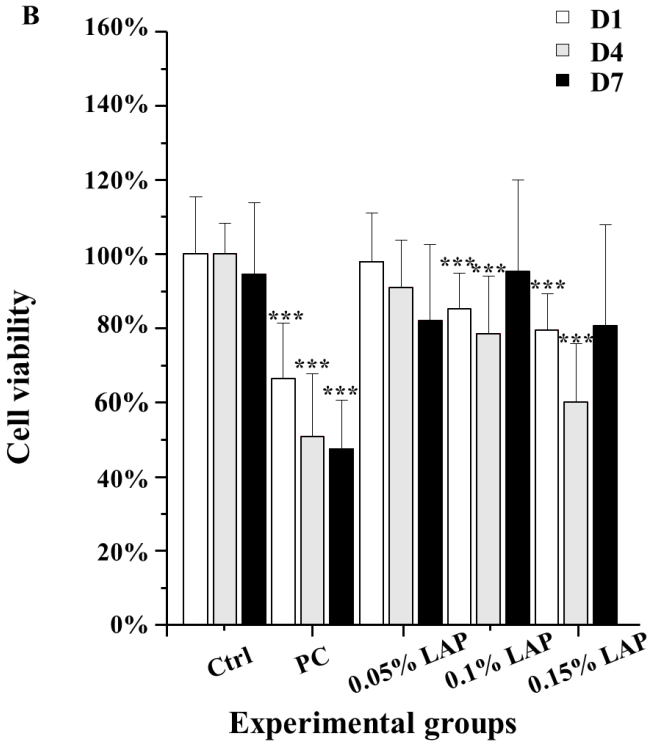
B
D1
D4
D7
Cell viability
160%
140%
120%
100%
80%
60%
40%
20%
0%
***
***
***
***
***
***
***
Ctrl
PC
0.05% LAP
0.1% LAP
0.15% LAP
Experimental groups

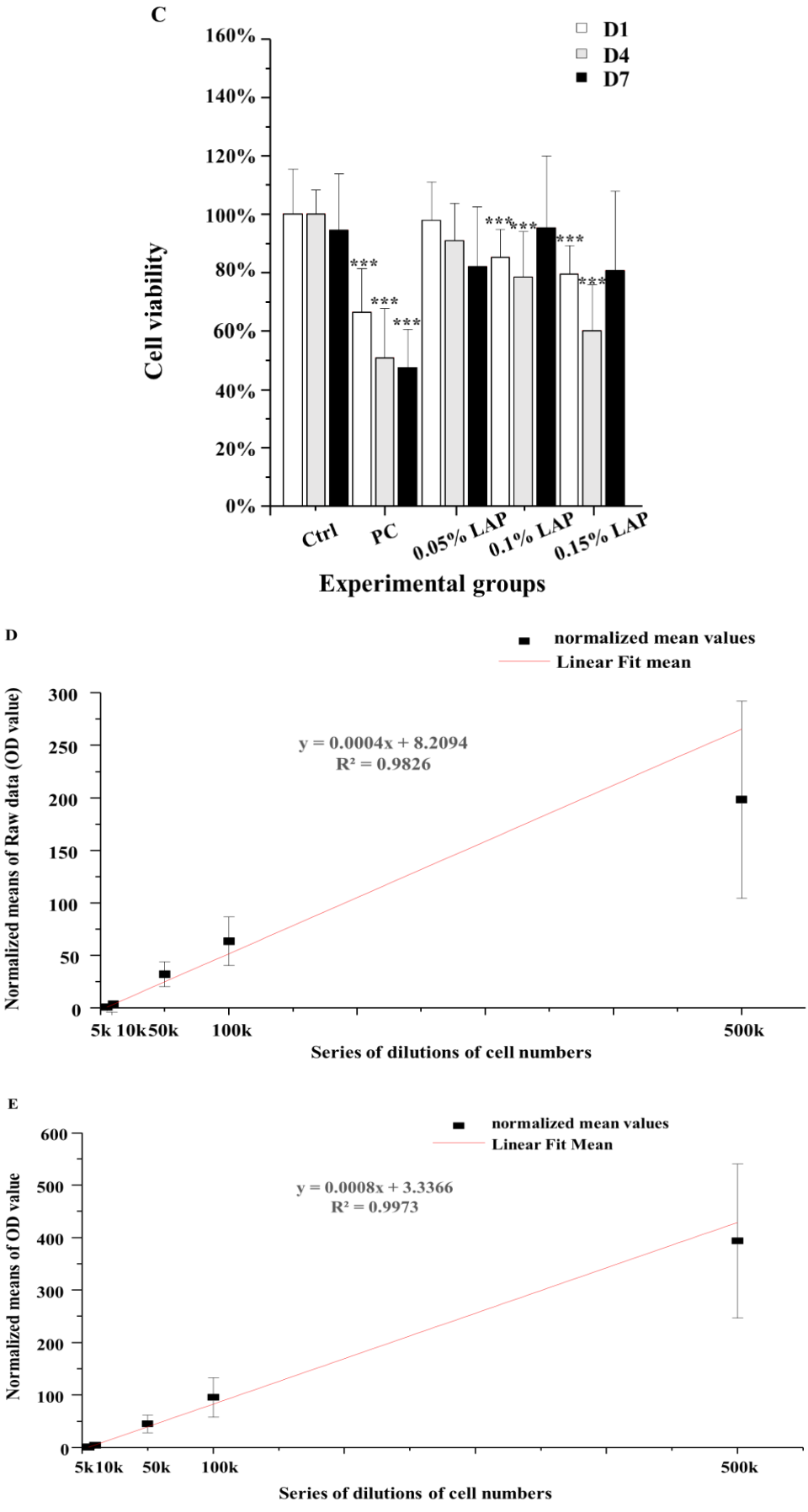
C
D1
D4
D7
160%
140%
120%
100%
80%
60%
40%
20%
0%
Cell viability
***
***
***
***
***
***
Ctrl
PC
0.05% LAP
0.1% LAP
0.15% LAP
Experimental groups
D
normalized mean values
Linear Fit mean
y = 0.0004x + 8.2094
R² = 0.9826
Normalized means of Raw data (OD value)
300
250
200
150
100
50
0
5k
10k
50k
100k
500k
Series of dilutions of cell numbers
E
normalized mean values
Linear Fit Mean
y = 0.0008x + 3.3366
R² = 0.9973
Normalized means of OD value
600
500
400
300
200
100
0
5k
10k
50k
100k
500k
Series of dilutions of cell numbers

F

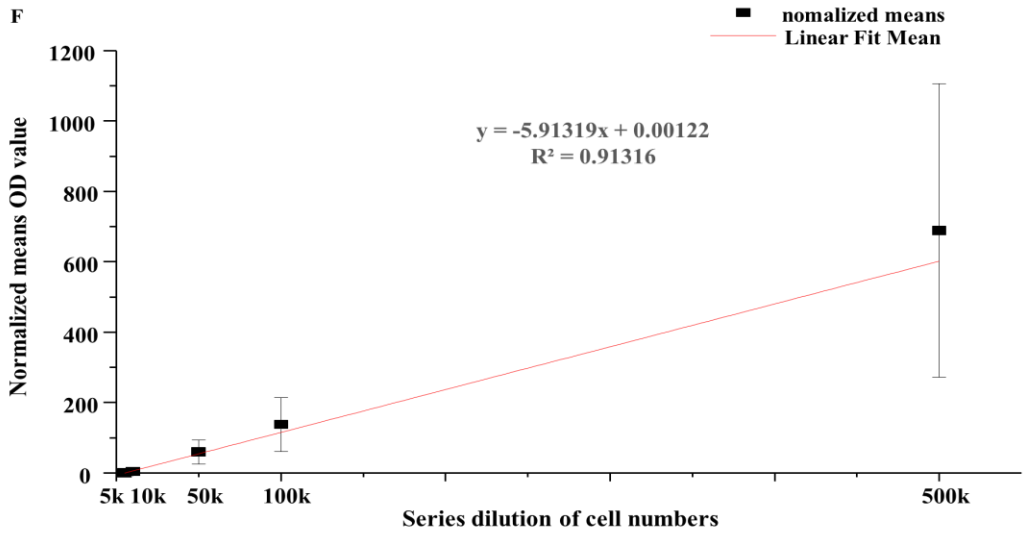
nomalized means
Linear Fit Mean
y = -5.91319x + 0.00122
R² = 0.91316
Normalized means OD value
1200
1000
800
600
400
200
0
5k 10k
50k
100k
500k
Series dilution of cell numbers

G

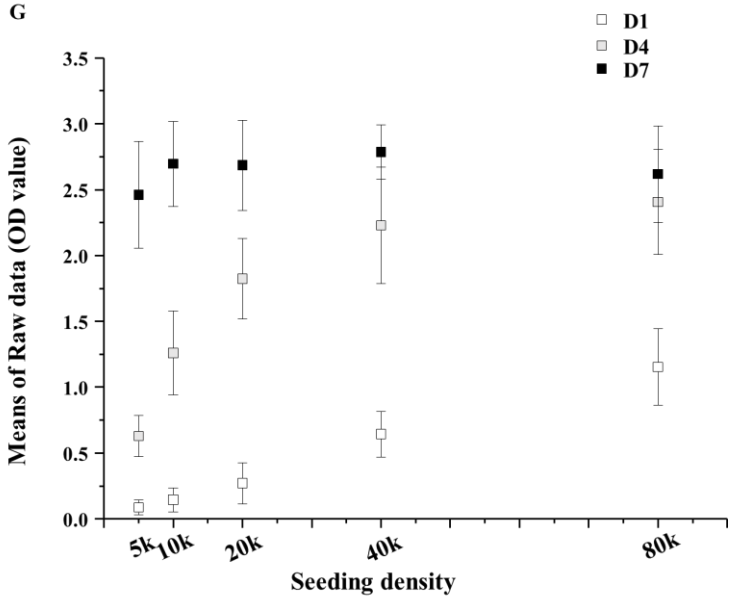
D1
D4
D7
Means of Raw data (OD value)
3.5
3.0
2.5
2.0
1.5
1.0
0.5
0.0
5k
10k
20k
40k
80k
Seeding density

H

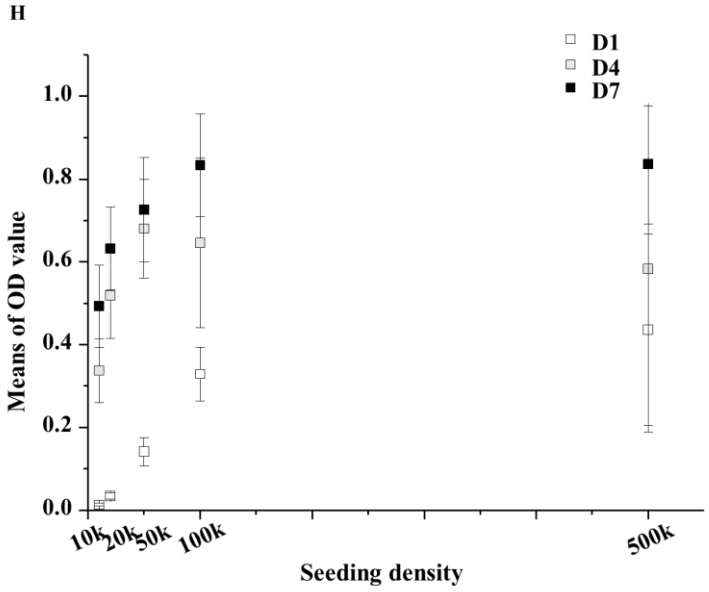
D1
D4
D7
Means of OD value
1.0
0.8
0.6
0.4
0.2
0.0
10k
20k
50k
100k
500k
Seeding density

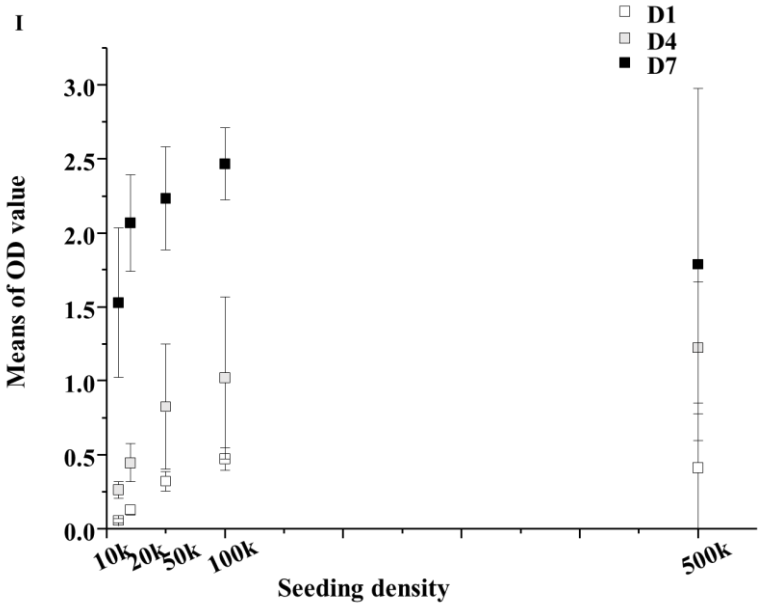

Figure 3.17 Cytotoxic effect of different concentration of LAP on the viability and proliferation of living cells in vitro

Three cell lines were involved in this test, including NIH3t3 fibroblasts (A, D, G), myoblasts C2C12 (B, E, H) and chondrogenic cell line ATDC5 (C, F, I). Before viability tests (A, B, C), cells were examined the seeding density test (G, H, I). Standard curve (D, E, F) for the cell seeding process was performed accompanying with the cell viability test. In brief, cells were cultured at a series of cell densities (e.g., 5K, 10K, 20K, 40K and 80K per well for fibroblasts) in a 24-well microplate and cultured for one, four, and seven days to be examined, respectively by CyQUANT™ LDH Cytotoxicity Assay. Results of experimental groups were presented in raw data or normalized by control group where the cells were only treated with normal growth medium. Comparisons between experimental group and control group were analysed by ANOVA one way test (Tukey): * P<0.05; * * P<0.01; * * * P<0.001. For series number test of fibroblasts, seeding densities were 5K, 10K, 20K, 40K and 80K per well, and N=4, n=12; for series number test of myoblasts, seeding densities were 10K, 20K, 50K, 100K and 500K per well, and N=3, n=9; for series number test of chondrocytes, seeding densities were 10K, 20K, 50K, 100K and 500K per well, and N=3, n=9. For cell viability test of fibroblasts, seeding density was 5K cells per well and N=4, n=12; for cell viability test of myoblasts, seeding density was 5K cells per well and N=3, n=9; for cell viability test of chondrocytes, seeding density was 5K cells per well and N=3, n=9.

3.3.3 Resolution and aspect ratio of PEGDA hydrogels printed by the DLP 3D printer

To establish the resolution, aspect ratio and the printing quality of the concave pattern, a test model in the thickness of 500μm with a series of holes (Figure 3.18 A) was designed and printed by the DLP 3D printer. In the single layer printing model, the ink did not contain the light absorber. From results (Figure 3.18 B), 200 μm was the minimal diameter of the holes that could be printed clearly.

While with additional light absorber in the ink, under the layer-by-layer printing model, and printing parameters setup, 300 μm was the minimal diameter of holes that could be printed clearly. This could be explained by the problem of the accumulated energy from light, especially on bottom layers. The more layers the design contains, the more thickness of the pattern there will be built on the plate, so less light would be penetrated and longer time would be required to expose the bottom layers. Even with additional light absorber in the ink to try to improve the energy from light, this problem of this 3D printer should be concerned. Hence, the aspect ratio of concave model printed in the layer-by-layer model was around 3:5.

To investigate the convex pattern, a test model with a series of cuboids (Figure 3.19 A) was designed and printed by DLP 3D printer. In the single layer printing model, the ink did not add the light absorber. From results (Figure 3.19 B), 100 μm was the minimal width of cuboids that could be printed clearly, by both printing models. Hence, the aspect ratio of convex model printed in the layer-by-layer model was around 1:5. These results suggested that the problem of the accumulated energy from light during printing on the 3D products with convex pattern was not serious, comparing to those with concave pattern. This should be considered in the 3D design and 3D printing.

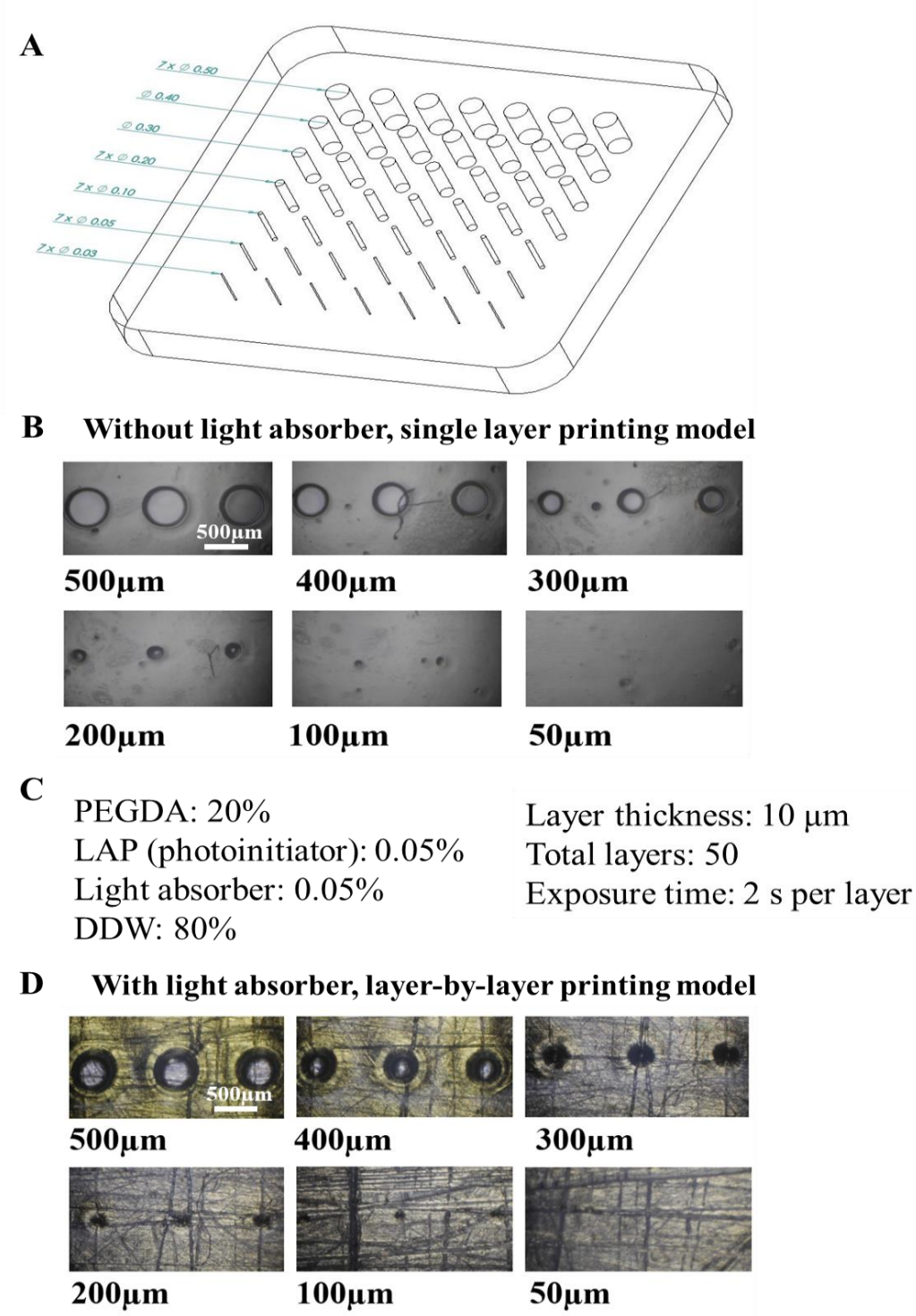

Figure 3.18 Resolution tests of the PEGDA hydrogel with concave patterns printed by two 3D printing models A: 3D design of the concave pattern of PEGDA test model, with 500µm in thickness and a series of varied diameters including 30, 50, 100, 200, 300, 400 and 500 µm. B: 3D-printed PEGDA test model using the printing ink without additional light absorber, by a single layer printing model. Scale bar is 500µm. C: 3D printing ink formula and the key printing parameters in layer-by-layer printing model. D: 3D-printed PEGDA test model using the printing ink with additional light absorber, by the layer-by-layer printing model. Scale bar is 500µm. (Images were adapted with permission from Mr. Wu of NTHU.)

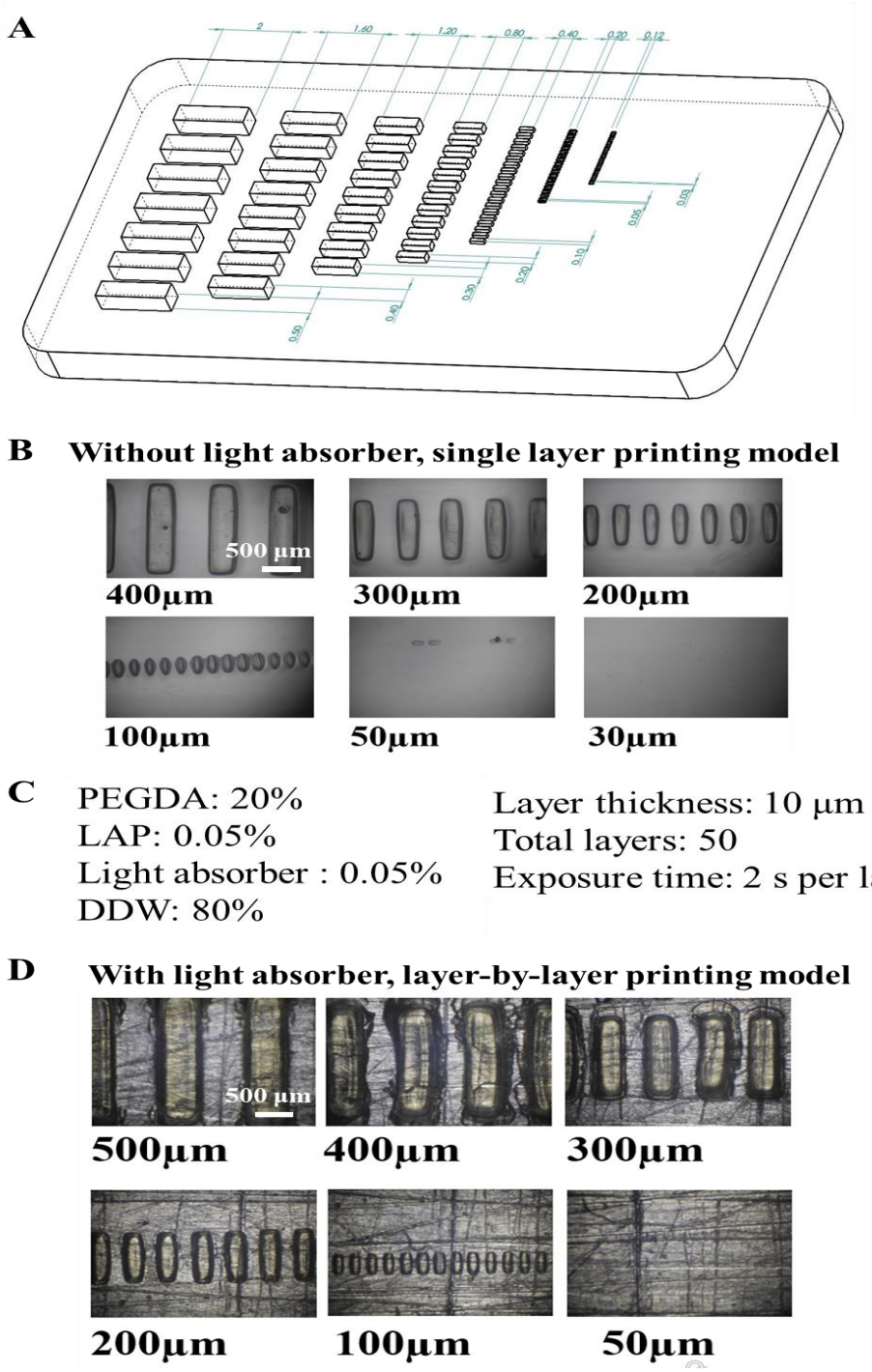

Figure 3.19 Resolution tests of the PEGDA hydrogel with convex patterns printed by two 3D printing models A: 3D design of the convex pattern of PEGDA test model, in which there are cuboids with 4:1:1 in length: width: thickness and a series of varied width (same as their space intervals) including 30, 50, 100, 200, 300, 400 and 500 µm. B: 3D-printed PEGDA test model using the printing ink without additional light absorber, by a single layer printing model. Scale bar is 500µm. C: 3D printing ink formula and the key printing parameters in layer-by-layer printing model. D: 3D-printed PEGDA test model using the printing ink with additional light absorber, by the layer-by-layer printing model. Scale bar is 500µm. (Images were adapted with permission from Mr. Wu of NTHU.)

3.3.4 Shape fidelity of PEGDA hydrogel printed by DLP 3D printer

To access the shape fidelity of the 3D-printed PEGDA hydrogel by this DLP 3D printer, another test model with convex pattern array was designed and printed, in which there were a series of space intervals (50, 100, 200 and 300 μm) between rod patterns with the same size (Figure 3.20 C). With additional light absorber in the 20% PEGDA hydrogel formula ink (Figure 3.20 A), and the key printing parameter setup (Figure 3.20 E), test patterns were printed by the DLP 3D printer in the layer-by-layer model. Under the normal inverted phase contract light microscope, images of patterns with different focused layers (top and bottom) were obtained and measured by the associated imaging software. From results, the measurements of space intervals under two different focused layers (Figure 3.20 F and G) were as follows: for 300 μm design of the space interval, they were 270 μm when focusing on the top layer and 260 μm when focusing on the bottom layer; for 200 μm design of the space interval, they were 160 μm when focusing on the top layer and 120 μm when focusing on the bottom layer; for 100 μm design of the space interval, they were 60 μm when focusing on the top layer and 30 μm when focusing on the bottom layer; for 50 μm design of the space interval, they were 30 μm when focusing on the top layer and 0 μm when focusing on the bottom layer. By analysing these measurement, differences of the 3D-printed convex patterns from the original designs could be detected and visualised by the calculated angle of inclination (Figure 3.20 C), reflecting the shape fidelity of the 3D-printed convex pattern by this DLP 3D printer. From results of these printed test model, there might be a small angle (~2°) for the vertical structure after printing, depending on the distance between two neighbouring convex patterns. For the convex pattern, the farther distance of the space interval there is, the smaller differences (angle of inclination) after 3D printing there would be. This should be considered in the design of PEGDA

scaffold.

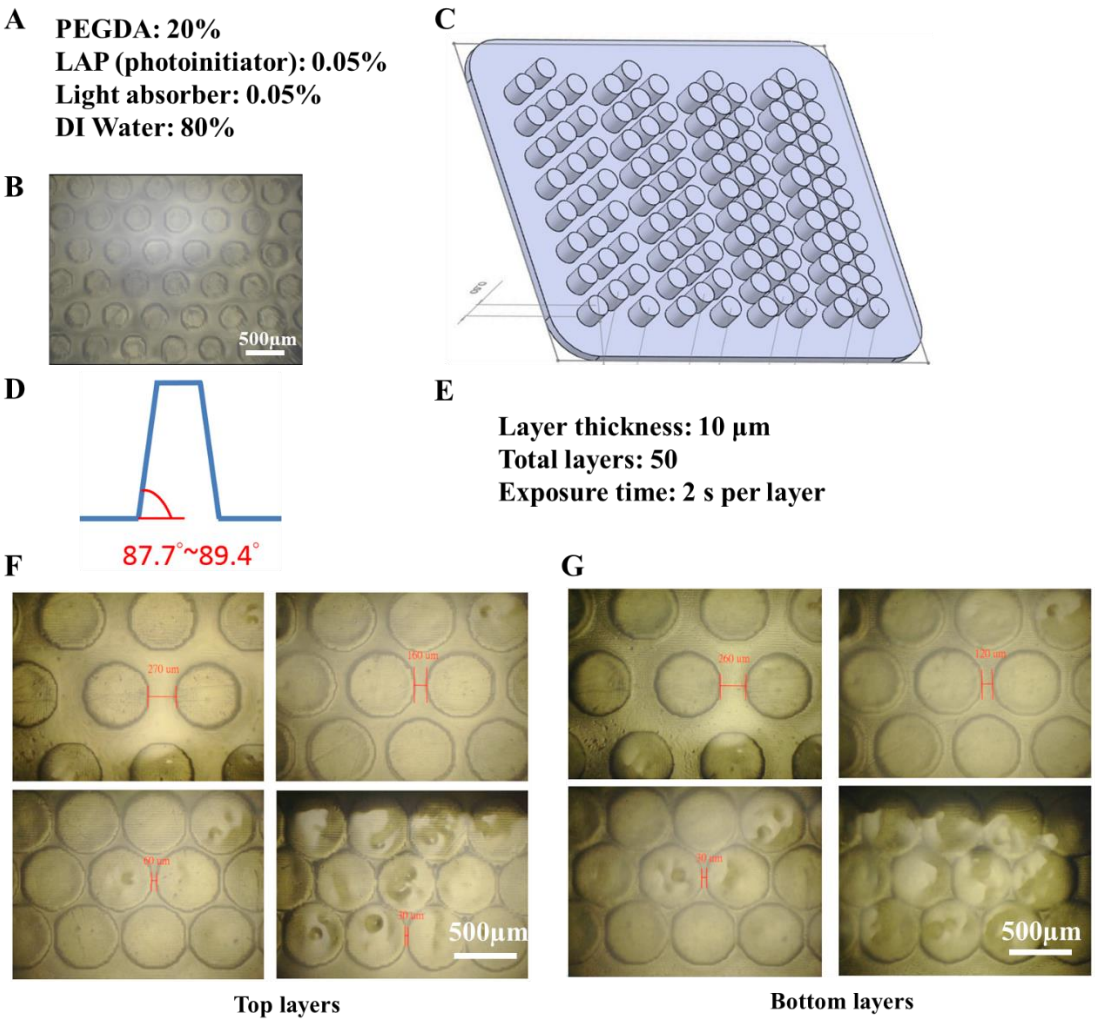

Figure 3.20 Shape fidelity studies of PEGDA hydrogel pattern printed layer-by-layer by DLP 3D printer A: Formula of ink used in this test; B: 3D-printed convex rod pattern with appropriate aspect ratio (2:5); C: 3D design of the convex pattern test model; D: The calculated angle of inclination of the convex pattern after 3D printing; E: Key parameters of 3D printing setup. F: Images of 3D-printed convex pattern test model when focusing on the top layer; G: Images of 3D-printed convex pattern test model when focusing on the bottom layer. Scale bars are 500 µm. (Images were adapted with permission from Mr. Wu of NTHU.)

3.3.5 Patterned PEGDA hydrogel with appropriate aspect ratio and the self-assembly scaffold

From previous studies [23-25], the minimal distance for sufficient mass diffusions between cells and the nearest capillary is around 100-200 µm. Based on this, pattern arrays were designed, in which the diameter of the inscribed circle of the pattern or space interval is around and no more

than 200 μm. From results of above test models, the aspect ratio (width or diameter of the inscribed circle over the thickness or height) of convex pattern printed by this DLP 3D printer is about 1:5 (Figure 3.20 B), and that of concave pattern would be around 3:5. A few PEGDA hydrogels with convex patterns under appropriate aspect ratio (2:5) and space intervals, were printed successfully (Figure 3.21), including rod cylinder (Figure 3.21 A, D), hexagonal cylinder (Figure 3.21 B, E) and squared cylinder (Figure 3.21 C, F). Based on these, self-assembly scaffold was also designed and printed, which sizes and printing parameters were further optimised to improve the quality and resolution (Figure 3.22).

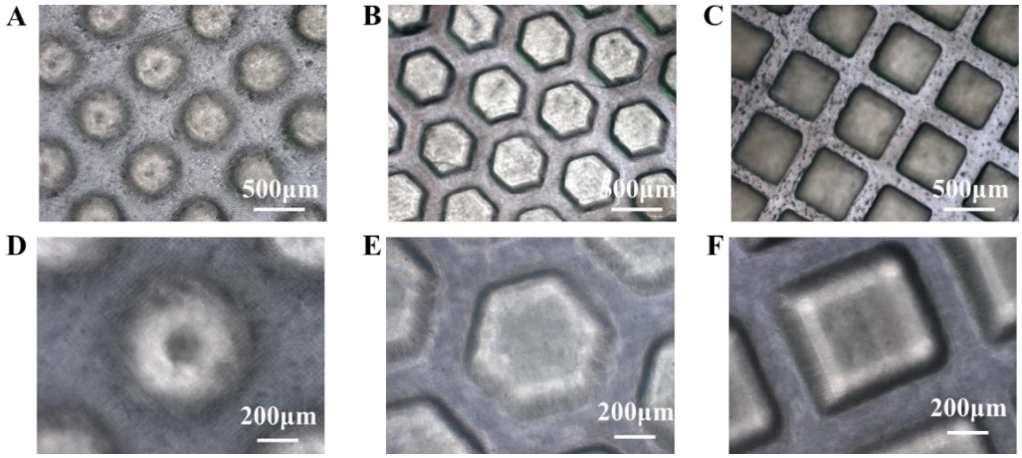

Figure 3.21 3D-printed PEGDA patterns with appropriate aspect ratio and space interval

A: 3D-printed PEGDA hydrogel with rod cylinder pattern with 300 μm in the diameter of the inscribed circle. B: 3D-printed PEGDA hydrogel with hexagonal cylinder pattern with 300 μm in the diameter of the inscribed circle. C: 3D-printed PEGDA hydrogel with squared cylinder pattern with 300 μm in the diameter of the inscribed circle. D, E, F: Images of the rod cylinder, hexagonal cylinder and squared cylinder patterns with higher magnifications. The scale bars are 500 μm in A-C, and 200 μm in D-F.

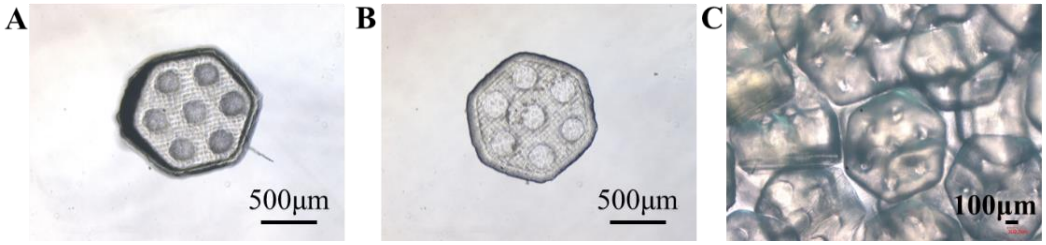

Figure 3.22 The 3D-printed self-assembly PEGDA scaffolds

A, B: 3D-printed self-assembly PEGDA scaffold with different qualities. C: 3D-printed self-assembly PEGDA scaffolds kept in DDW. The scale bars are 500 μm in A and B, and 100 μm in C.

3.3.6 Leaching test of the 3D-printed PEGDA hydrogel scaffold

Based on the instruction of ISO 10993 documents, the 3D-printed PEGDA scaffolds were tested for leaching by MTT assay. NIH3t3 fibroblast was applied and the test was repeated three times, although different patterns of the 3D-printed PEGDA hydrogels were involved. From results (Figure 3.23), comparing to the control groups, conditional medium after soaking the 3D-printed products immediately displayed toxic effect on the living cells after 1-, 4- and 7-days treatment. Most experimental groups generally showed less than 70% cell viabilities after treatment (Figure 3.23 A, B, C). However, the conditional medium from the second soaking, presented almost no toxic effect on the living cells after one- and four-days treatment (Figure 3.23 D, E, F). Hence, we did not test the effect after 7 days treatment. This result suggested that after DLP 3D printing, the PEGDA products would have non-crosslinked monomer or activated photoinitiators accumulated, leading to the leaching problem if applied to culture cells immediately. To solve this, after printing, the sample could be kept in DDW for 2-3 days to leach out possible toxic compounds left in the scaffold after printing. From the results, after the additional step before using, the toxic effect of the 3D-printed PEGDA hydrogel products could be effectively reduced (Figure 3.23 D, E, F).

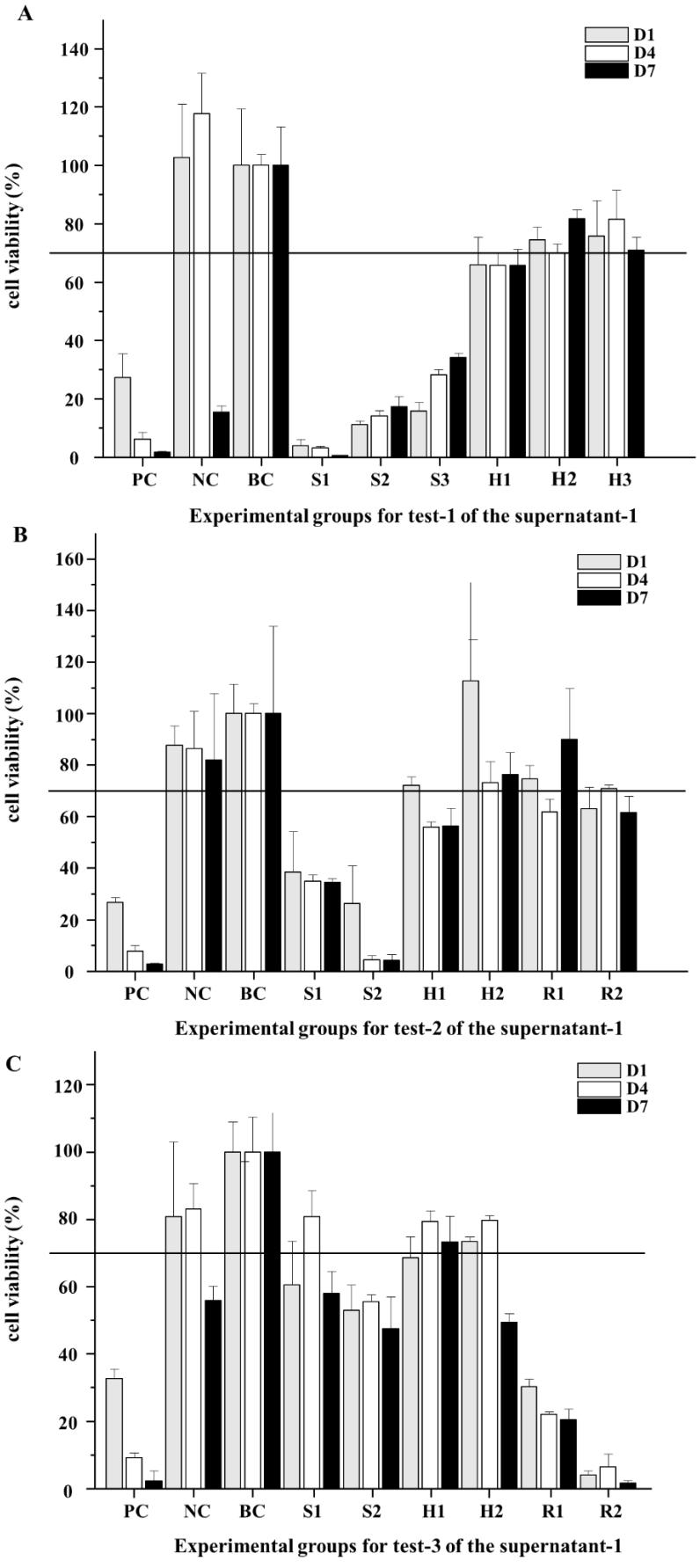
A
D1
D4
D7
cell viability (%)
0
20
40
60
80
100
120
140
PC
NC
BC
S1
S2
S3
H1
H2
H3
Experimental groups for test-1 of the supernatant-1
B
D1
D4
D7
cell viability (%)
0
20
40
60
80
100
120
140
160
PC
NC
BC
S1
S2
H1
H2
R1
R2
Experimental groups for test-2 of the supernatant-1
C
D1
D4
D7
cell viability (%)
0
20
40
60
80
100
120
PC
NC
BC
S1
S2
H1
H2
R1
R2
Experimental groups for test-3 of the supernatant-1

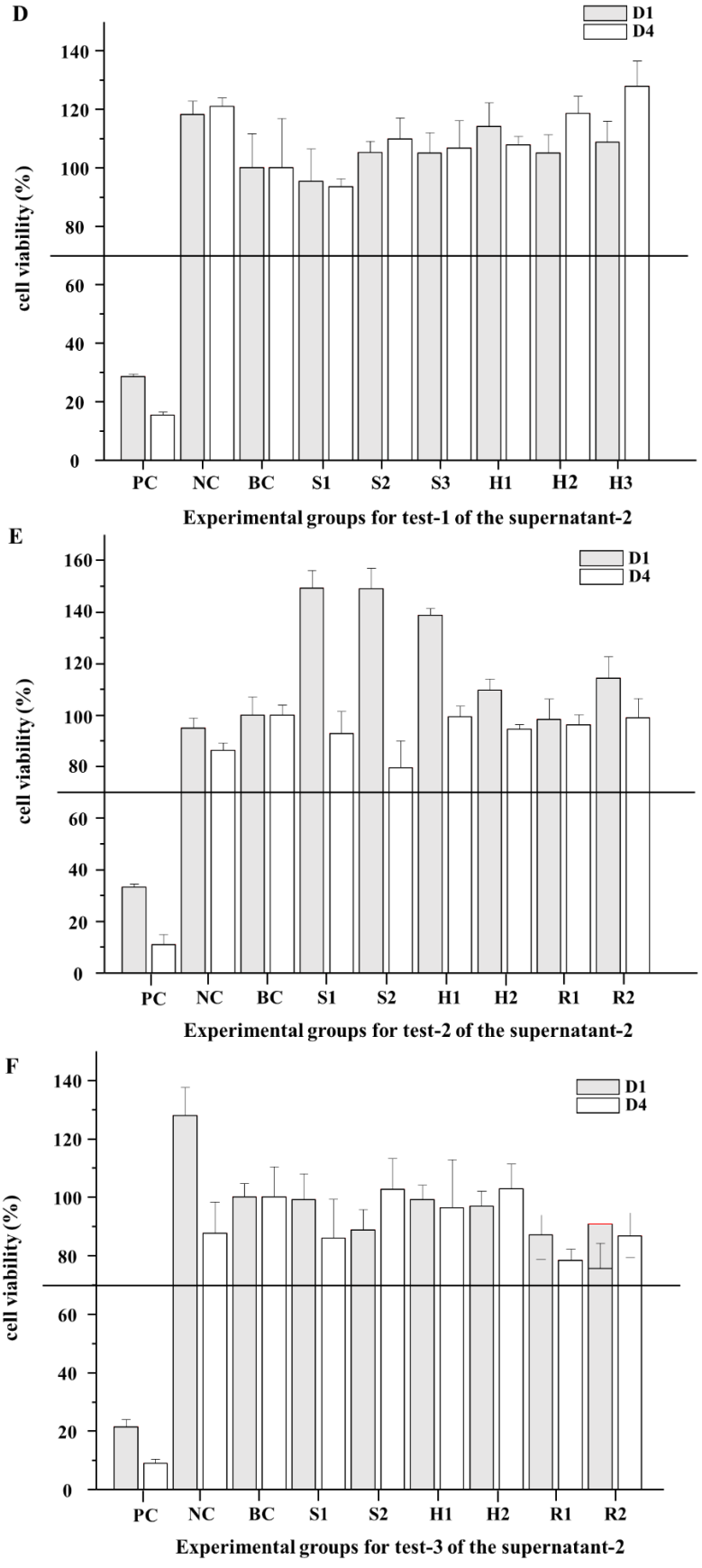

Figure 3.23 Leaching tests of the 3D-printed PEGDA hydrogels by MTT assay

A-C: Effect of the conditional medium prepared from the 3D-printed PEGDA products immediately after printing. D-F: Effect of the conditional medium prepared from the 3D-printed PEGDA products after the first three-day soaking process after printing. PC: positive control; NC: negative control; BC: blank control; S1: conditional medium-1 group from squared pattern-1; S2: conditional medium-2 group from squared pattern-2; H1: conditional medium-1 group from hexagonal pattern-1; H2: conditional medium-1 group from hexagonal pattern-2; R1: conditional medium-1 group from rod pattern-1; R1: conditional medium-2 group from hexagonal pattern-2.

3.3.7 Coverage rate of self-assembly PEGDA scaffolds

To confirm the potential self-assembly property of the designed PEGDA scaffold, coverage rates after injecting the scaffold-suspended solutions were measured.

Firstly, scaffolds with different designs and solutions with different viscosities, were prepared and tested. From results (Figure 3.24), all four sizes scaffolds performed best coverage rate when they were suspended in 7.5 cp viscosity solution, comparing to solution of other viscosities. Scaffolds with the smallest size (0.75mm in width and 0.3mm in thickness), had higher coverage rate after injection, comparing to scaffolds with other sizes in all four types of solutions (Figure 3.24 D).

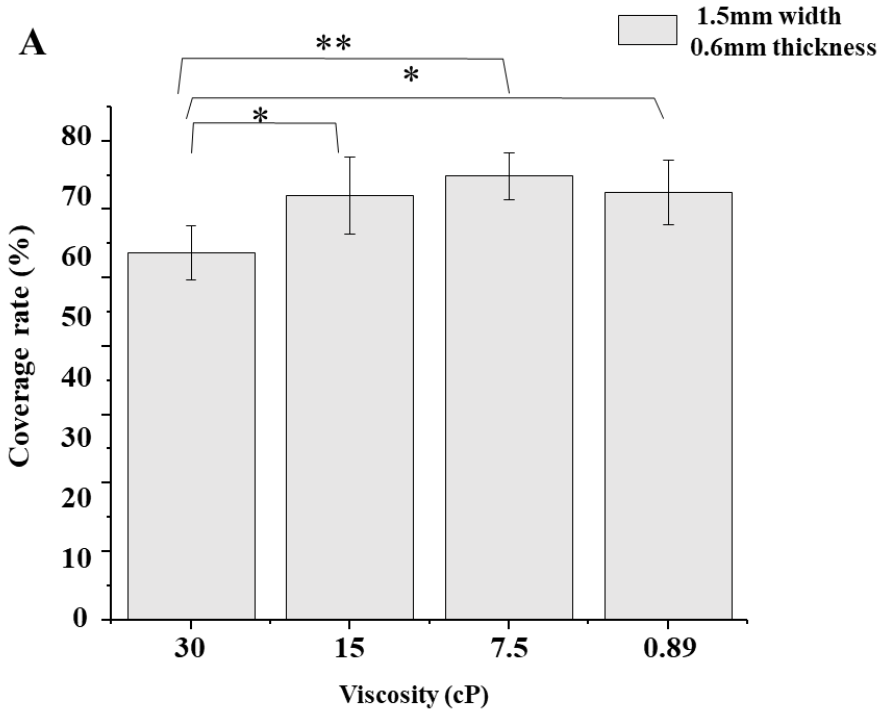

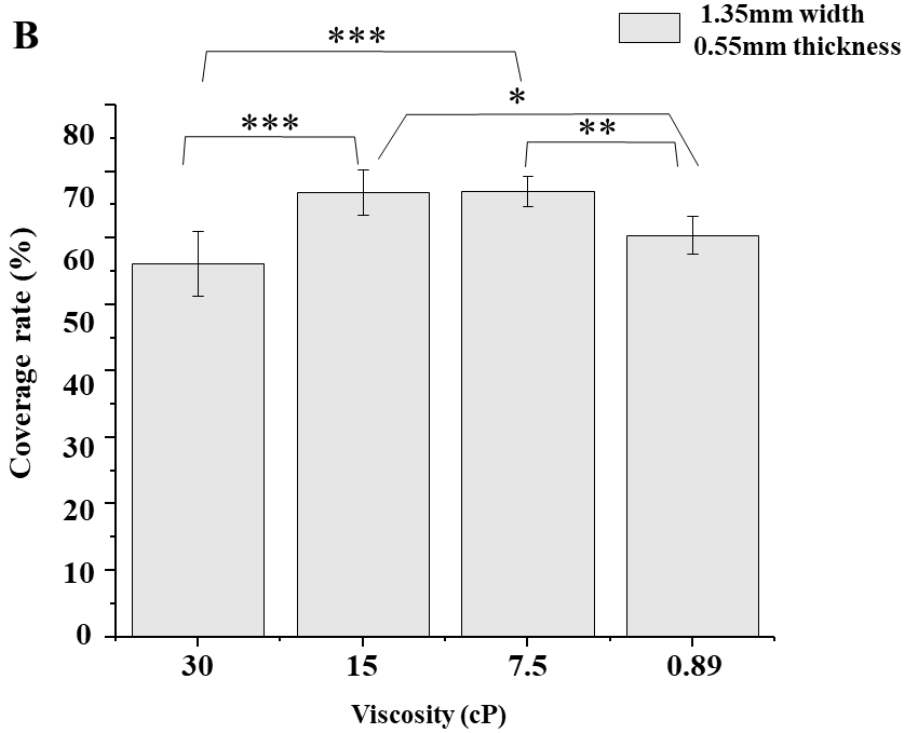
B
1.35mm width
0.55mm thickness
***
*
***
**
Coverage rate (%)
0
10
20
30
40
50
60
70
80
30
15
7.5
0.89
Viscosity (cP)

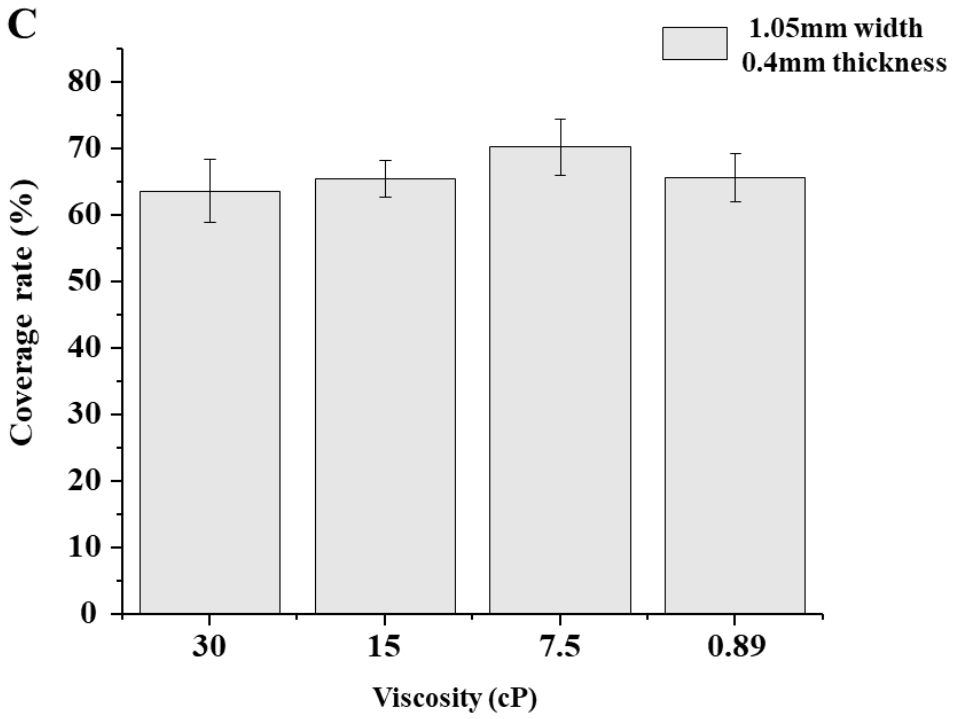
C
1.05mm width
0.4mm thickness
Coverage rate (%)
0
10
20
30
40
50
60
70
80
30
15
7.5
0.89
Viscosity (cP)

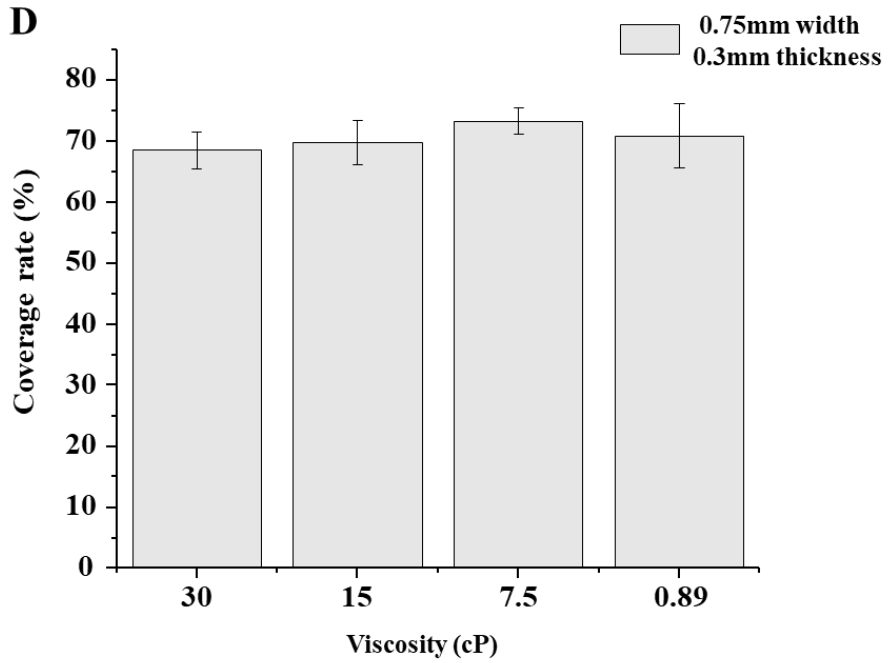

Figure 3.24 Coverage rates of the 3D-printed self-assembly scaffolds with different sizes suspended in solutions with different viscosities

A: Coverage rates after injections of the scaffolds with the size of 1.5 mm in width and 0.6 mm in thickness, suspending in solutions with four different viscosities. B: Coverage rates after injections of the scaffolds with the size of 1.35 mm in width and 0.55 mm in thickness, suspending in solutions with four different viscosities. C: Coverage rates after injections of the scaffolds with the size of 1.05 mm in width and 0.4 mm in thickness, suspending in solutions with four different viscosities. D: Coverage rates after injections of the scaffolds with the size of 0.75 mm in width and 0.3 mm in thickness, suspending in solutions with four different viscosities. Each test was repeated ten times (N=10). Comparisons between experimental group and control group were analysed by ANOVA one way test (Tukey): * P<0.01; * * P<0.001; * * * P<0.0001.

After that, self-assembly scaffolds with the same area but different shape were designed and printed. The scaffolds with three different shapes were all suspended in solutions with 7.5 cp viscosity and to perform the injection. From results (Figure 3.25 A), as expected, the hexagonal shape performed the best coverage rate than the other shapes, confirming our design of the self-assembly scaffold. From Figure 3.25 B, after injection, there were different types of distribution of the scaffolds. Due to the injection was performed from one side of the target area and those scaffolds in solution were moved and diffused to cover the whole area driven by the exuding forces. In the middle of the target area, there was usually some empty spaces and overlapped scaffolds were sometimes happened in the side area. This suggested that the process of the injection required further study

and optimisation.

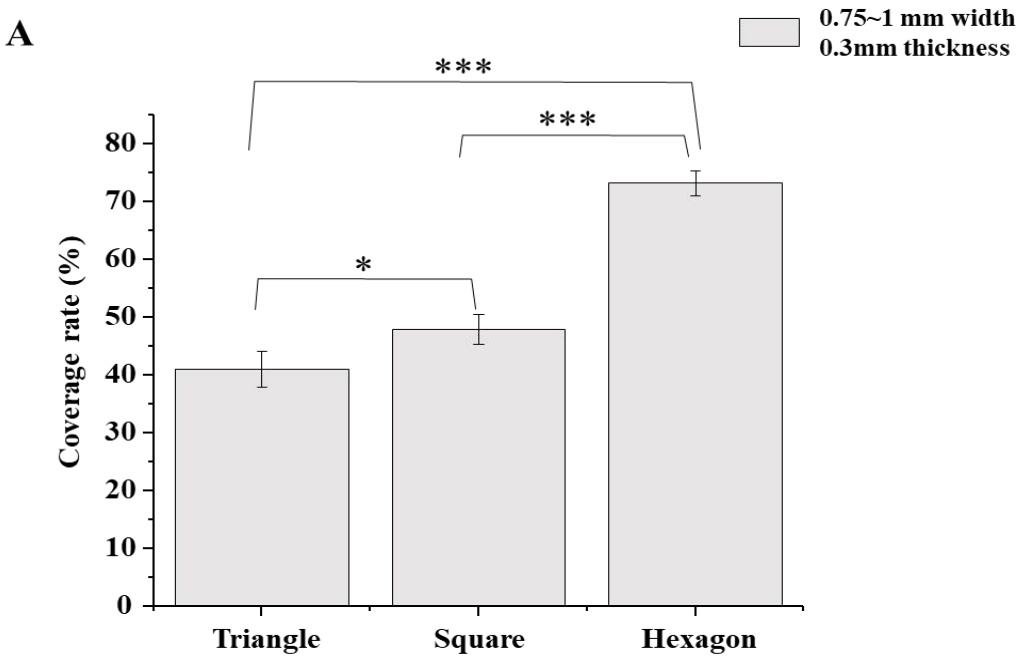

Self-assembly scaffold with different shapes suspending in 7.5cP solution

Figure 3.25 Comparison of the coverage rates of the 3D-rpinted self-assembly scaffolds with different shapes in 7.5cp solutions

A: Comparison of coverage rates after injections of the self-assembly PEGDA scaffolds with different shapes, suspending in the solution with 7.5 cp viscosity. B: Demonstration images of the self-assembly scaffolds after injections. Scale bars are 500 µm. Each test was repeated ten times (N=10). Comparisons between experimental group and control group were analysed by ANOVA one way test (Tukey): * P<0.01; * * P<0.001; * * * P<0.0001. (Images were adapted with permission from Mr. Wu of NTHU.)

3.3.8 Viabilities of cells cultured on 3D-printed PEGDA scaffolds (2.5 D culture)

Fibroblasts were cultured on 3D-printed PEGDA hydrogels with hole patterns about 7 days to

examine the biocompatibility of the scaffold with living cells. From results (Figure 3.26), without coating or surface modification, PEGDA materials are inert to living cells. Cells were mostly aggregated within holes instead of attaching to the materials. But after culturing 7 days, most cells contacting with the 3D-printed PEGDA hydrogels were still alive, suggesting that the pure PEGDA materials had no toxic effect on the cell viabilities. Chondrogenic cell line ATDC5 cells were seeded on the 3D-printed PEGDA hydrogels with hole patterns about 7 days as well. After 7 days incubation, results (Figure 3.27) from chondrocytes confirmed that, without coating or surface modification, biocompatible PEGDA materials are inert to living cells.

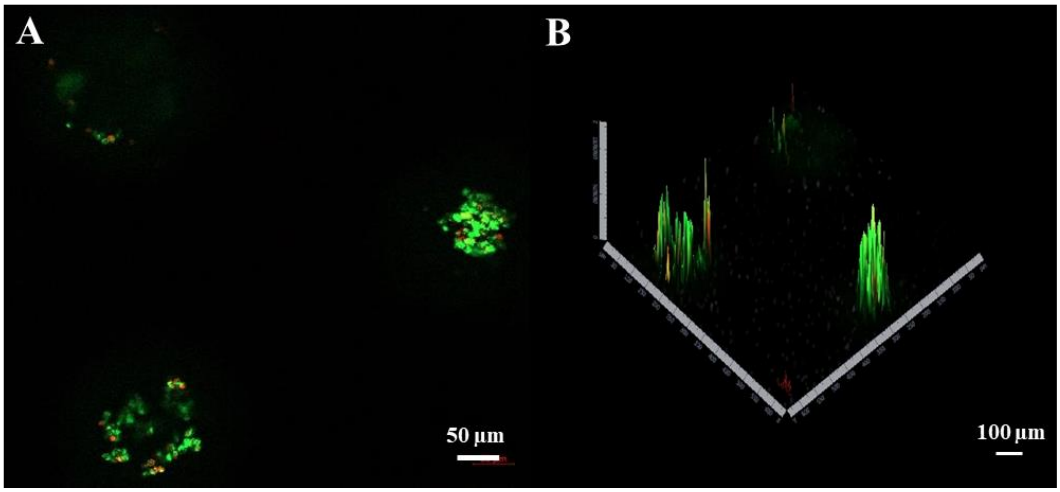

Figure 3.26 Cellular viability of Fibroblasts cultured on 3D-printed PEGDA scaffolds with hole patterns without any coating

Fibroblasts were seeded on the 3D-printed PEGDA scaffold with uniformed hole patterns (100-200 µm) without any coating. After culturing 7 days in an incubator, cells were examined the cellular viability by Live & Dead assay, in which the live cells would be stained in green and dead cells would be stained in red under detection by the fluorescent microscope or LSM 800 confocal microscope. A: Merged 2D image of fibroblasts cultured on the scaffold with hole patterns. The scale bar is 50 µm. B: Merged 2.5 D image of fibroblasts cultured on the scaffold with hole patterns. The scale bar is 100 µm.

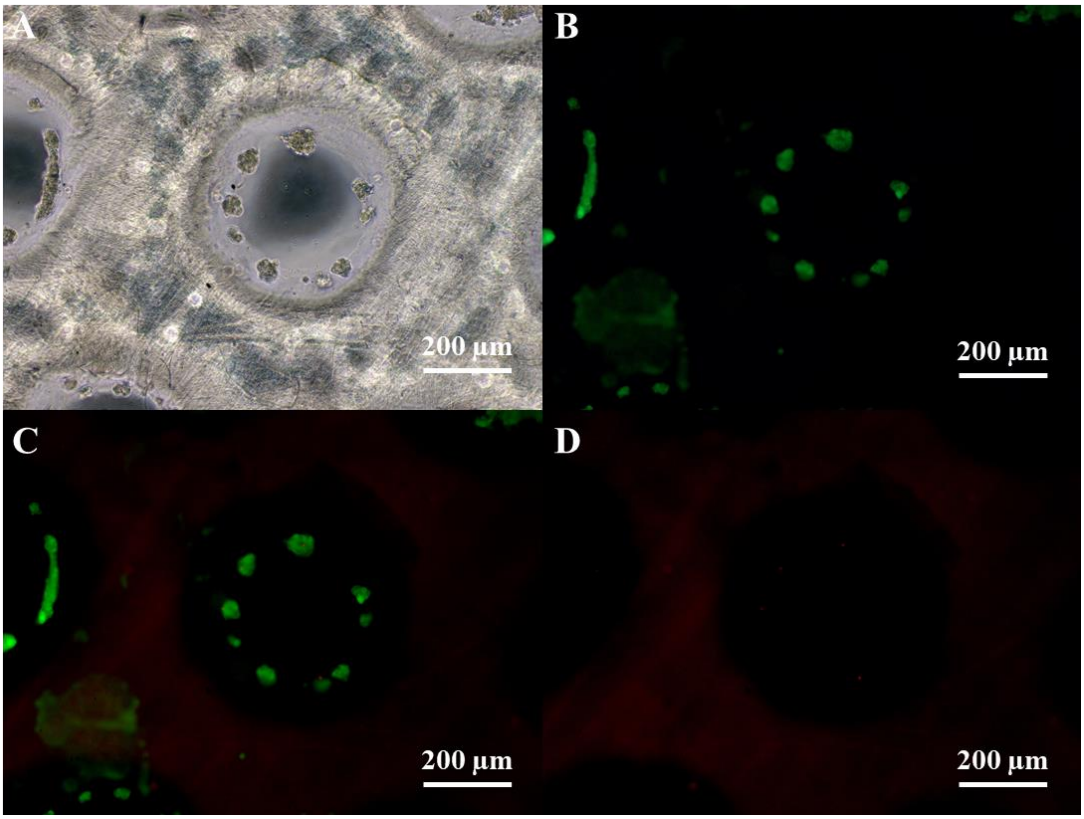

Figure 3.27 Cellular viability of ATDC5 cells cultured on 3D-printed PEGDA scaffolds with hole patterns without any coating

Chondrogenic cell line ATDC5 cells were cultured on the non-coated 3D-printed PEGDA scaffolds with hole patterns (100-200 µm) for about 7 days. Then samples were examined the cellular viability by Live & Dead assay. A: Bright field image of the aggregated cells in the holes of PEGDA scaffolds. B: Living cells in green after staining were displayed under detection by the fluorescent microscope with appropriate filter. C: Merged image of the aggregated cells in the holes of PEGDA scaffolds after staining. D: Dead cells in red after staining were examined under the fluorescent microscope with appropriate filter. Scale bars are 200 µm.

To evaluate whether the additional cellulose fibres in the PEGDA materials would improve the cell attachment, fibroblasts were cultured on the 3D-printed thin sheets with additional nanocellulose fibres (NCFs) in the printing ink (30% PEGDA). After 7 days incubation, cellular viabilities were examined. From results (Figure 3.28), additional nanocellulose fibres improved the cell adherence to the PEGDA materials and had no toxic effect on the cell viability when cultured with cells together. To confirm the results, chondrogenic cell line ATDC5 cells were used. Cells were seeded on the 3D-printed thin sheets with and without additional NCFs in the printing ink (30% PEGDA). After 14 days incubation, cellular viabilities were examined. From results (Figure 3.29), comparing

to the sheets without NCFs (Figure 3.29 E-H), more living cells attached to the thin sheets printed with additional NCFs (Figure 3.29 A-D). Even there were few cells attached to the surface of the thin sheet printed without additional NCFs, they were aggregated, presenting low adherence to the PEGDA materials. This result suggested that the additional NCFs may improve the biocompatibility of PEGDA materials.

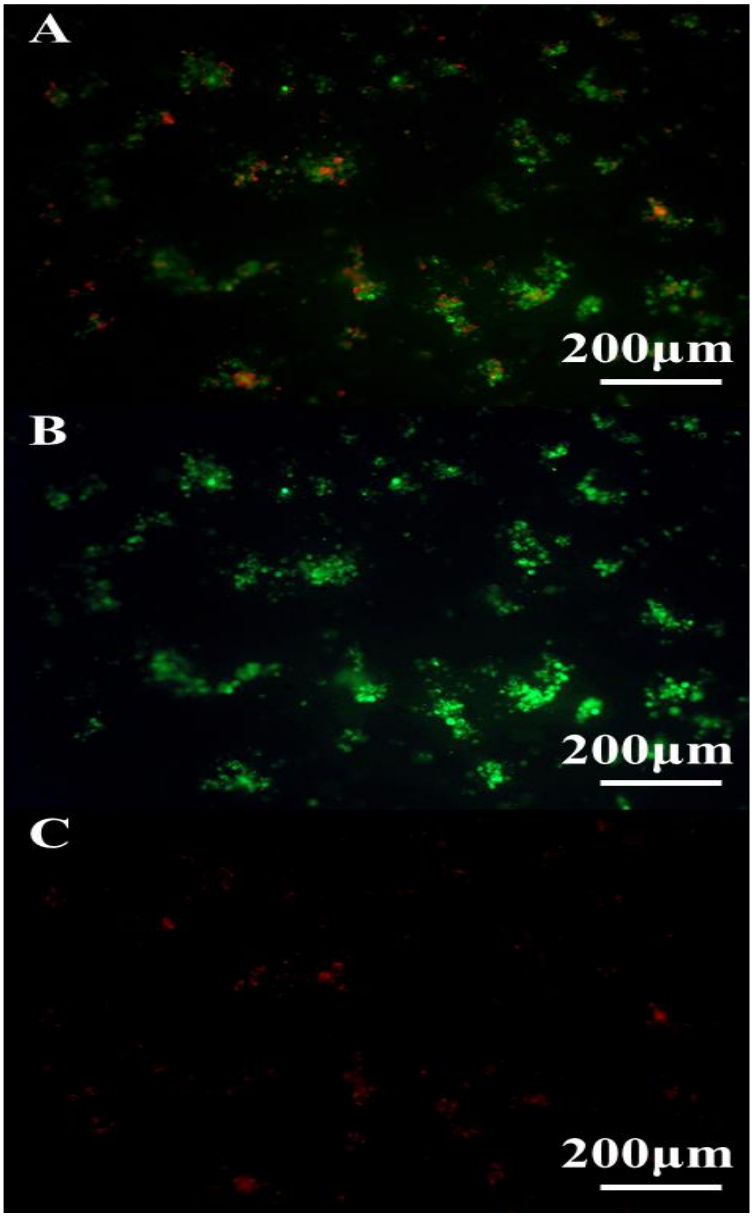

Figure 3.28 Cellular viability of fibroblasts cultured on non-coated 3D-printed PEGDA thin sheets with additional nanocellulose fibres (NCF)

Fibroblasts were seeded on the 3D-printed thin sheet with additional NCFs in the ink and cultured for 7 days to examine the cellular viabilities. A: Merged image of the cells attached to the thin sheet after staining. Living

cells were stained in green and dead cells were stained in red. B: Image of living cells stained in green under the detection by fluorescent microscope with appropriate filter. C: Image of dead cells stained in red under the detection by fluorescent microscope with appropriate filter. Scale bars are 200 µm.

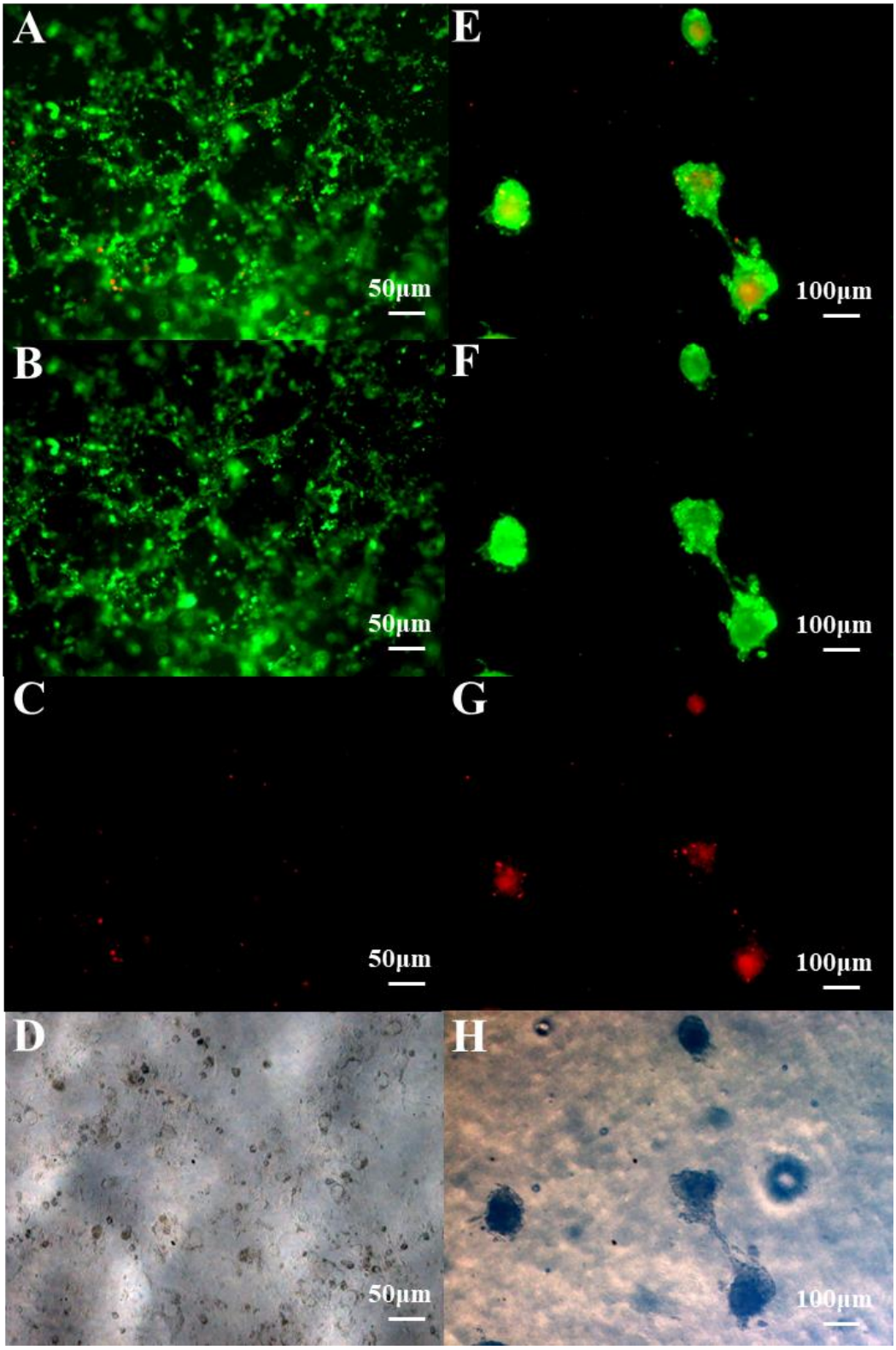

Figure 3.29 Cellular viability of ATDC5 cells cultured on non-coated 3D-printed PEGDA thin sheets with and without additional nanocellulose fibres

ATDC5 cells were seeded on the 3D-printed thin sheets with (A-D) and without (E-H) additional NCFs in the ink (30%PEGDA) and cultured for 14 days to examine the cellular viabilities. A: Merged image of cells attached to the thin sheet with additional NCFs in the ink after staining. Living cells were stained in green and dead cells were stained in red. B: Image of living cells stained in green under the detection by fluorescent microscope with appropriate filter. C: Image of dead cells stained in red under the detection by fluorescent microscope with appropriate filter. D: Image of cells in bright field. E: Merged image of cells attached to the thin sheet without additional NCFs in the ink after staining. Living cells were stained in green and dead cells were stained in red. F: Image of living cells stained in green under the detection by fluorescent microscope with appropriate filter. G: Image of dead cells stained in red under the detection by fluorescent microscope with appropriate filter. H: Image of cells in bright field. Scale bars are 500 μm in A-D, and 100 μm in E-H.

To improve the cellular adherence, type I collage solution was used to coat the 3D-printed PEGDA scaffolds and ATDC5 cells were seeded after coating. From results (Figure 3.30), after coating, more viable cells could be delivered to the 3D-printed PEGDA scaffolds with different patterns, however, the coating skills and process should be optimised and the non-covalent treatment could not support long-term culture *in vitro*, after certain times as the cell proliferation, the type I collagen would be degraded and the coated layer would be detached from the underlying scaffolds. Hence, it is better to use type I collagen to culture cells in 3D. To examine the potential application in further 3D cell culture with the self-assembly PEGDA scaffolds, ATDC5 cells were encapsulated with type I collagen and crosslinked into 3D hydrogels. After incubation 7 days, samples were examined for the cellular viability. Due to the thickness of the 3D gel, without slicing it is difficult to get clear images. But from results (Figure 3.31), it is obvious that more cells were kept alive inside the 3D collagen gel and could spread at some layers., suggesting the possible use in the future 3D experiments.

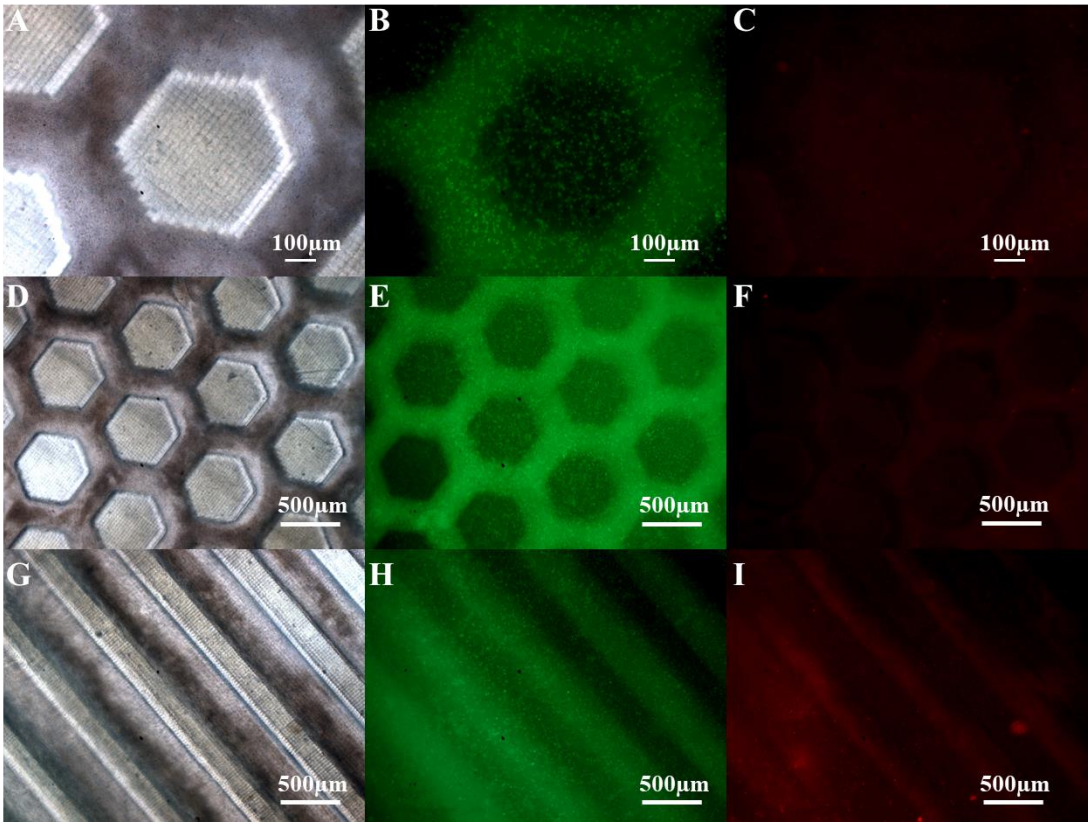

Figure 3.30 Cellular viability of ATDC5 cells cultured on collagen-coated 3D-printed PEGDA scaffolds with patterns

ATDC5 cells cultured on the 3D-printed PEGDA scaffolds with different patterns (honeycomb and groove) after coating with type I collagen for 7 days were examined the cellular viability by Live&Dead assay, by which viable cells were stained in green and dead cells were stained in red. A: Higher magnification image of cells cultured on coated PEGDA scaffold with honeycomb pattern in bright field, in green (B) and red (C) channels by fluorescent microscope with appropriate filters. Scale bars are 100 μm. D: Lower magnification image of cells cultured on coated PEGDA scaffold with honeycomb pattern in bright field, in green (E) and red (F) channels by fluorescent microscope with appropriate filters. Scale bars are 500 μm. G: Image of cells cultured on coated PEGDA scaffold with groove pattern in bright field, in green (H) and red (I) channels by fluorescent microscope with appropriate filters. Scale bars are 500 μm.

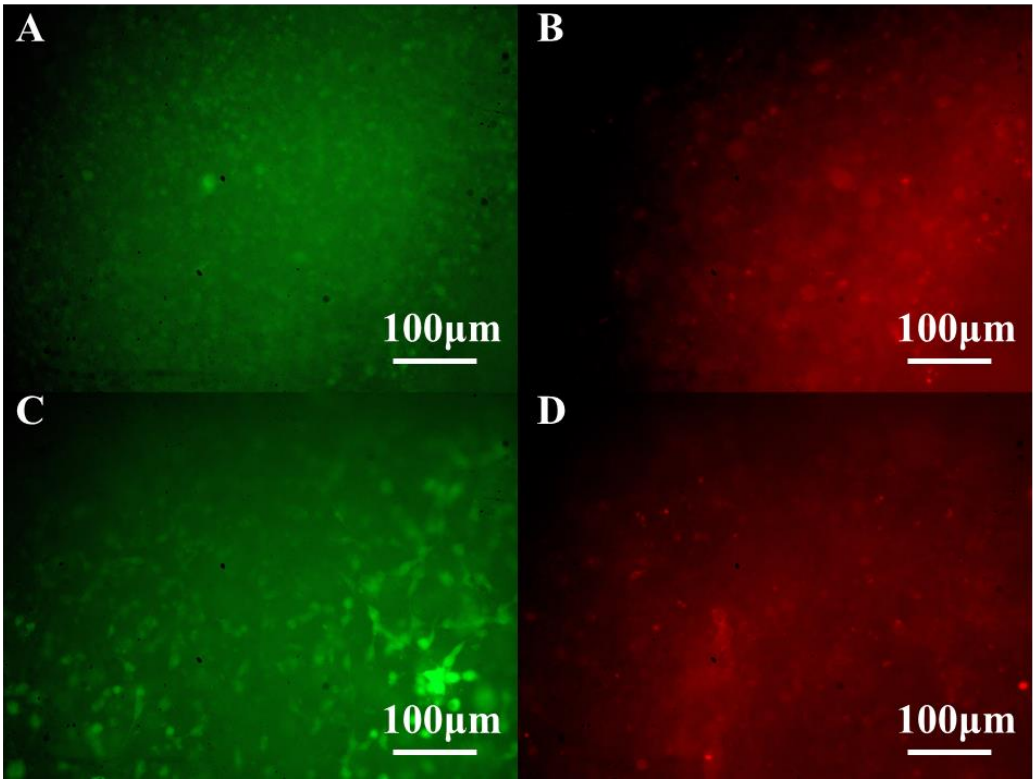

Figure 3.31 Cellular viability of ATDC5 cells cultured within 3D collagen gel

ATDC5 cells were encapsulated in type I collagen and crosslinked into 3D hydrogel. After 7days incubation, cellular viability was examined. A: Image of living cells within one layer of the 3D collagen gel stained in green. B: Image of dead cells within the same layer of A in 3D collagen gel stained in red. C: A: Image of living cells within another layer of the 3D collagen gel stained in green. D: Image of dead cells within the same layer of C in 3D collagen gel stained in red. Scale bars are 100 µm.

3.3.9 Morphologies of cells cultured on 3D-printed PEGDA scaffolds (2.5 D culture)

Cells cultured on coated 3D-printed PEGDA scaffolds with patterns were also visualised by immunostaining the cytoskeletal F-actin protein. From results (Figure 3.32), there were more cells attached to the PEGDA scaffolds displaying a stretched spreading morphology, suggesting that the cell adherence to the PEGDA scaffolds was improved by the coating materials.

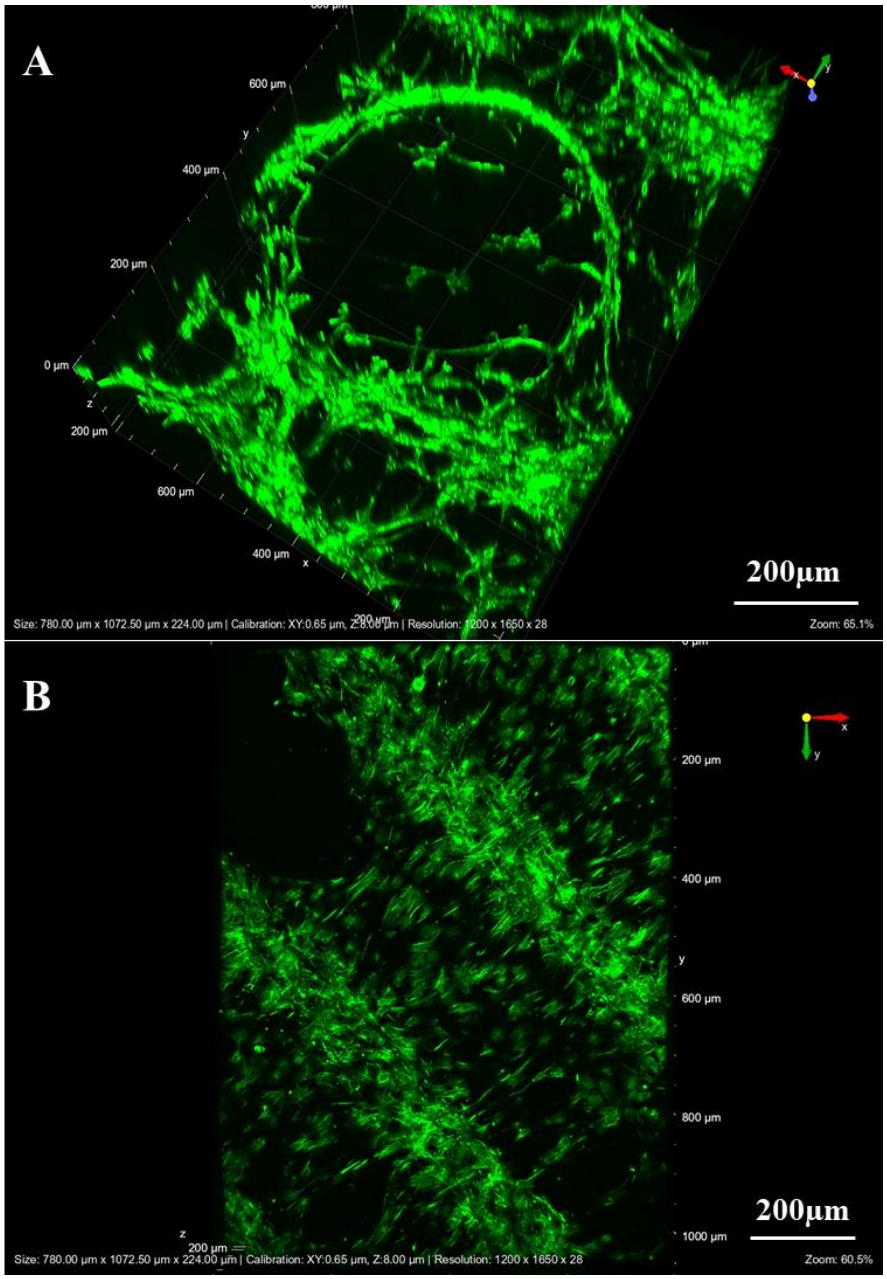

Figure 3.32 Morphologies of fibroblasts cultured on type I collagen coated 3D-printed PEGDA scaffolds with patterns

Fibroblasts were seeded on the 3D-printed scaffolds with rod and groove patterns which were coated with type I collagen before seeding. After 7 days incubation, samples were fixed by 4% formaldehyde solution and stained by the anti-FITC-F-actin. A: Image of the morphology of cells seeded on the 3D-printed PEGDA scaffolds with rod pattern. B: Image of the morphology of cells seeded on the 3D-printed PEGDA scaffolds with groove pattern. Skeletal F-actin protein was stained in green. Scale bars are 200 µm.

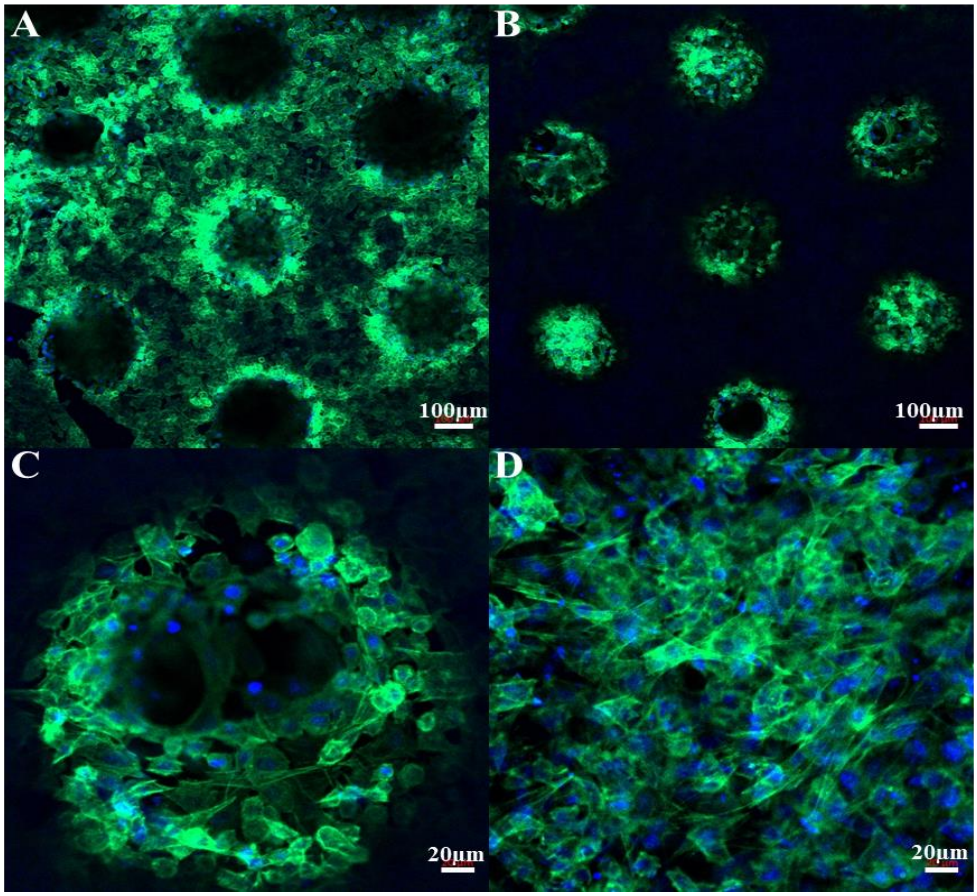

Figure 3.33 Morphologies of the ATDC5 cells cultured in 3D type I collagen with 3D-printed self-assembly PEGDA scaffold patterns

3D-printed PEGDA scaffolds with the designed self-assembly pattern of larger size were prepared and seeded with ATDC5 cells delivered by the type I collagen gel in 3D. After 7 days incubation, cellular morphologies were examined. The skeletal F-actin proteins inside cells were stained in green and the nuclei were stained in blue. A, B: 2D confocal images with different focuses to show the morphologies of cells engrafted on the self-assembly scaffolds. Scale bars are 100 μm. C, D: Higher magnifications of 2D confocal images with different focused areas to show the morphologies of cells engrafted on the self-assembly scaffolds. Scale bars are 20 μm.

Morphology of chondrocytes delivered by type I collagen and cultured with the 3D-printed PEGDA scaffolds with the designed self-assembly pattern in 3D, was also examined. Chondrogenic cell line ATDC5 cells were firstly mixed with the type I collagen solution. Then the mixture was added to cover the 3D-printed PEGDA scaffolds with the designed self-assembly pattern (bigger size) and crosslinked into 3D. After 14 days incubation, samples were fixed and stained by the anti-FITC-F-actin and DAPI. From results (Figure 3.33), within the type I collagen gel in 3D, ATDC5 cells could be engrafted on the 3D-printed PEGDA scaffolds and form the

intercellular connections to support the survival of cells and many other potential cellular behaviours.

3.4 Conclusions limitations and future works

Results presented in this chapter, demonstrated that selected photocurable PEGDA material could be designed and printed with desired pattern by DLP-3D printer to simulate the deep layer of the articular cartilage/OC tissue as hydrogel-based TE scaffold to be applied *in vitro*, proving the hypothesis of this study described in Chapter one. In this section, the outcomes achieved, limitations on current study and potential future works will be discussed.

3.4.1 Conclusions

To conclude outcomes of this study presented in this chapter, firstly, photocurable PEGDA-based biomaterials as candidate printing ink, have been characterised the compressive modulus, swelling capabilities, biocompatibilities, printing resolution and shape fidelity of the associated 3D-printed products by the customised DLP-3D printer in this study. Formula of the PEGDA-based printing ink was selected and the potential of using nanocellulose fibres to reinforce the mechanical property and to improve the bioactivity of PEGDA materials was preliminarily investigated.

Secondly, leaching problem of the 3D-printed PEGDA-based products after printing was observed and evaluated, leading to the optimised process to apply the 3D-printed PEGDA scaffold for subsequent tissue engineering application.

Thirdly, based on the DLP-3D printing technology and the selected printing ink, 3D-printed PEGDA scaffold with hexagonal shape and uniformed hole patterns (100-200 μm in diameter of the hole and space interval) could be successfully fabricated and studied to simulate the

perpendicularly arranged chondrogenic ECM network in the deep zone of the articular cartilage, in which by using type I collagen gel, seeding cells were successfully engrafted and survived in the scaffold, supporting the subsequent scaffold-based 3D cell culture. Hence, a part of the main purpose and objective of this study mentioned in Chapter one, have been achieved.

Finally, to improve the novelty of the designed hydrogel scaffold, miniaturised version of the PEGDA scaffold was successfully developed and confirmed a self-assembly property to be promisingly applied as an injectable scaffold-based TE strategy to facilitate future minimal invasive surgery in dealing with small chondral/osteochondral lesions.

3.4.2 Limitations and future works

Although studies presented in this Chapter, successfully proved the hypothesis and achieved the aim and objective, due to time limitation, current results are insufficient and incomplete in details. Here are some limitations and future works suggested as follows.

The first limitation is the bioactivity of PEGDA material. This study started with a classic photocurable PEGDA material as printing ink, however, it is a kind of biocompatible but bioinert material as introduced in Chapter two. In our results, without bioactive collagen gel as carrier, living cells are less likely engrafted in the scaffold but aggregated around the material. To improve its bioactivity, additional modification or bio-functionalisation on the PEGDA molecules, and use of other photocurable PEG derivatives or higher molecular weight PEGDA, are worth to investigate in future works. Alternatively, composite material containing PEGDA and bioactive materials/compounds could be developed as described in Chapter two, to meet the requirement for biomedical and TE applications. In this study, nanocellulose fibres were added in PEGDA ink to

try to improve the mechanical property and bioactivities of the PEGDA hydrogel, however, due to time limitation, a few concentrations of cellulose material in composites were explored only the compressive modulus and 2D cell viability. In the future, more different concentrations of nanocellulose fibres blended with PEGDA in the composite, other valuable mechanical properties such as the tensile strength and viscoelasticity of the composite ink and 3D-printed products should be considered to further investigate.

The second limitation is about the customised DLP-3D printer and the printing process. As described in this Chapter and Chapter two, the DLP-3D printing technology is managing the light. From our results, there will be the light accumulation issue in the layer-by-layer printing model, having impact on the resolution and design, especially for the convex pattern, the bigger size of a single layer is set, more severe light accumulation issue there will be. Besides, it is difficult to print a precise vertical right angle for the convex pattern. The side of the pattern is not exactly vertical, having a size-dependent tilt while the light incident the printing ink. Those are some potential drawbacks of this customised 3D printer and the DLP-3D printing technology. To improve the configuration and printing quality of this 3D printer, such future works could be suggested, as the fixed flat building platform could be replaced by the one having changeable orientation to improve the photopolymerisation during printing, and additional biocompatible light absorber or components might be developed to be incorporated into the printing ink to improve the resolution and control the photopolymerisation process smoothly.

The third limitation also relates to the photopolymerisation. After photopolymerisation in the DLP-3D printer, there might be potential residues left in the printed hydrogel products, even after performing the post-printing process. From results of leaching test presented in this Chapter, the

potential cytotoxicity of 3D-printed product after photopolymerisation was identified in freshly fabricated PEGDA hydrogel, although an additional cleaning by soaking in water after fabrication, should be sufficient for subsequent biological applications. The time cost by the cleaning step, may be able to be sped up, by applying detergent or organic solvent such as ethanol or isopropanol. However, from experience on chemistry and materials science, considering the potential reaction between the detergent and the photocurable material, to avoid unexpected challenges on changing the physiochemical properties of the final printed product, and on bringing additional toxicants, instead of using chemical detergent, pure water and dialysis should be suggested to explore in future works. This biocompatible issue is important for products fabricated by DLP-3D printing technology, to be applied in biomedical area. Hence, regarding the photopolymerisation and post-printing process, additional cleaning step is worth to study in the future, to reduce the potential cytotoxicity and speed up the fabrication process.

The fourth limitation in this study is about the scaffold-based tissue fabrication results. Seeding cells delivered by collagen gel could be successfully engrafted and survived in the 3D-printed scaffold which has been established in this study. However, Due to the time limitation, the scaffold-based cell proliferation and differentiation and for the self-assembly scaffold, the effect of the self-assembly scaffold-supported tissue culture system on the proliferation and differentiation of seeding cells (chondrocyte and MSCs) *in vitro* in 3D are remained to be further evaluated in future works.

Finally, with regard to the result, previous studies have suggested that chondrogenic components correlate with the mechanical feature of the cartilage, whose function is interdependent to its anatomy in the joint [1]. As a connective tissue in the joint dealing with force and movement, the

collagen fibrous ECM network provides mainly the tensile strength, whereas the interstitially trapped water and proteoglycan in chondrogenic ECM contribute to mitigate the compressive and shear forces. As the chondrogenic tissue development by the proliferation, and differentiation of seeding cells (chondrocyte or MSCs) over time, the mechanical properties of the engineered tissue would be changed as the development of chondrogenic ECM produced by reparative seeding cells. Hence, before and after tissue development, mechanical properties (stiffness and viscoelasticity) of the biomaterial scaffold and time-dependent profile regarding mechanical features of the cell-laden hydrogel scaffold should be extensively and quantitatively investigated. The bioactive function of the additional fibres with the inert PEGDA materials should also be quantitatively examined in 2D and 3D conditions. In addition, a novel oxygen nanosensor (described in Chapter five) is intended to be incorporated in the 3D hydrogel system established in this study, to detect the oxygen concentration during tissue development *in vitro* [26]. All those are suggested to be planned in the future work to not only further confirm the TE function of the developed hydrogel scaffold in both quantitative and qualitative manners, but also to contribute to accomplishing the overall dual project.

References

[1] Mansour JM. Biomechanics of cartilage. Kinesiology: the mechanics and pathomechanics of human movement. 2003;2:66-79.
[2] Shirazi R, Shirazi-Adl A. Deep vertical collagen fibrils play a significant role in mechanics of articular cartilage. Journal of Orthopaedic Research. 2008;26:608-15.
[3] Benninghoff A. Form und Bau der Gelenkknorpel in ihren Beziehungen zur Funktion. Zeitschrift für Zellforschung und mikroskopische Anatomie. 1925;2:783-862.
[4] Nguyen QT, Hwang Y, Chen AC, Varghese S, Sah RL. Cartilage-like mechanical properties of poly (ethylene glycol)-diacrylate hydrogels. Biomaterials. 2012;33:6682-90.
[5] Kaur M, Srivastava A. Photopolymerization: A review. Journal of Macromolecular Science, Part C: Polymer Reviews. 2002;42:481-512.
[6] Hageman H. Photoinitiators for free radical polymerization. Progress in organic coatings. 1985;13:123-50.
[7] Sangermano M. Advances in cationic photopolymerization. Pure and Applied Chemistry. 2012;84:2089-101.
[8] Crivello JV, Liu S. Free radical induced acceleration of cationic photopolymerization. Chemistry of materials. 1998;10:3724-31.
[9] Sangermano M, Malucelli G, Morel F, Decker C, Priola A. Cationic photopolymerization of vinyl ether systems: Influence of the presence of hydrogen donor additives. European polymer journal. 1999;35:639-45.
[10] Crivello JV. Cationic photopolymerization of alkyl glycidyl ethers. Journal of Polymer Science Part A: Polymer Chemistry. 2006;44:3036-52.
[11] Sangermano M. Recent advances in cationic photopolymerization. Journal of Photopolymer Science and Technology. 2019;32:233-6.
[12] Bagheri A, Jin J. Photopolymerization in 3D printing. ACS Applied Polymer Materials. 2019;1:593-611.
[13] Choi JR, Yong KW, Choi JY, Cowie AC. Recent advances in photo-crosslinkable hydrogels for biomedical applications. BioTechniques. 2019;66:40-53.
[14] Taormina G, Sciancalepore C, Messori M, Bondioli F. 3D printing processes for photocurable polymeric materials: technologies, materials, and future trends. Journal of applied biomaterials & functional materials. 2018;16:151-60.
[15] Tang A, Wang Q, Zhao S, Liu W. Fabrication of nanocellulose/PEGDA hydrogel by 3D printing. Rapid Prototyping Journal. 2018;24:1265-71.
[16] Yang W, Yu H, Liang W, Wang Y, Liu L. Rapid fabrication of hydrogel microstructures using UV-induced projection printing. Micromachines. 2015;6:1903-13.
[17] Whitesides GM, Grzybowski B. Self-assembly at all scales. Science. 2002;295:2418-21.
[18] Bowden N, Choi IS, Grzybowski BA, Whitesides GM. Mesoscale self-assembly of hexagonal plates using lateral capillary forces: synthesis using the “capillary bond”. Journal of the American Chemical Society. 1999;121:5373-91.
[19] Oliver SR, Bowden N, Whitesides GM. Self-assembly of hexagonal rod arrays based on capillary forces. Journal of colloid and interface science. 2000;224:425-8.
[20] Rasband WS. ImageJ, US National Institutes of Health, Bethesda, Maryland, USA. http://imagejnihgov/ij/. 2011.

[21] Iso B, STANDARD B. Biological evaluation of medical devices. Part. 2009;1:10993.
[22] Thangaraju P, Varthya SB. ISO 10993: Biological Evaluation of Medical Devices. Medical Device Guidelines and Regulations Handbook: Springer; 2022. p. 163-87.
[23] Jain RK, Au P, Tam J, Duda DG, Fukumura D. Engineering vascularized tissue. Nature biotechnology. 2005;23:821-3.
[24] Rouwkema J, Rivron NC, van Blitterswijk CA. Vascularization in tissue engineering. Trends in biotechnology. 2008;26:434-41.
[25] Lovett M, Lee K, Edwards A, Kaplan DL. Vascularization strategies for tissue engineering. Tissue Engineering Part B: Reviews. 2009;15:353-70.
[26] Koduri MP, S. Goudar V, Shao Y-W, Hunt JA, Henstock JR, Curran J, et al. Fluorescence-based nano-oxygen particles for spatiometric monitoring of cell physiological conditions. ACS applied materials & interfaces. 2018;10:30163-71.

Chapter four: Design and manufacture of alginate-based 3D tissue culture system for reconstructing the middle layer of the articular cartilage/osteochondral tissue *in vitro*

4.1 Introduction

The articular cartilage/osteochondral tissue resents a multi-layered inhomogeneous architecture, in which the middle zone is composed of the randomly-oriented collagenous ECM network and spherical resident chondrocytes (Figure 4.1). Considering the middle zone having no specific architecture, extrusion-based 3D bio-printing and the mould-casting approach would be both suitable to perform the 3D fabrication. The major concern should be the size of the target tissue layer in the engineering point of view.

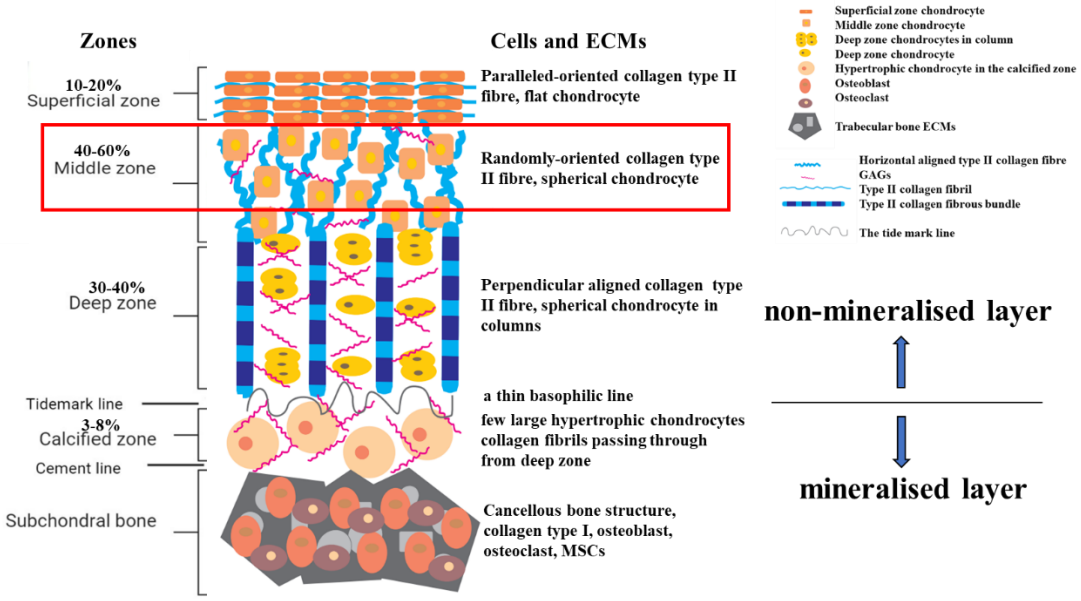

Figure 4.1 Schematic images of the zonal structure of the articular cartilage/osteochondral tissue Zonal structure and the specific components of each zone were displayed. The middle zone was highlighted in the tissue image, to stress the target tissue layer in this Chapter. Image was reproduced from Figure 2.2.

As described in Chapter two, hydrogel polymer material with various categories, polymerisation mechanisms and biocompatible features over other materials, has been extensively used in TE application. As well as its soft, flexible and viscoelastic biomechanical properties and hydrophilic

characters, which make it the best candidate materials to be used in soft tissue fabrication. Hence, hydrogel material and extrusion-based 3D bio-printing were selected to investigate.

In addition, there is a natural hypoxic microenvironment inside the articular cartilage/OC tissue, where mature chondrocytes can survive and endure the low-oxygen condition [1]. Previous studies also found that, neither low nor high oxygen pressures would have positive impacts on the proliferation and anabolism of chondrocytes. There seems a complex relationship between the oxygen consumption of resident chondrocytes and the local oxygen level, involving many potential impact factors such as the thickness of the tissue, cellular density, oxygen levels in both the synovial fluid and the underlying bone and the oxygen consumption rate of resident cells [2]. Throughout the OC tissue, distribution of the diffused oxygen is inhomogeneous and depth-dependent, where from the top superficial layer down to the calcified layer, the oxygen profile has a gradient, relying on the cellular oxygen consumption rate and the local supplying rate of the oxygen inside the tissue [1]. In each layer with specific thickness, cellular density and anatomical depth between synovial fluid and underlying bone, several things remain unclear including the local oxygen concentration, oxygen consumption rate of resident cells, potential impact of the local oxygen level on the local cells, the cellular response to the local oxygen stress and the impact of local oxygen condition on the formation of the specific zone with specific thickness.

To investigate the microenvironment factor in particular the oxygen profile in the articular cartilage/OC tissue, a novel fluorescent oxygen nanosensor was developed in another study of this joint project (as introduced in chapter one), in which the nanosensor was characterised its 3D application in alginate hydrogel crosslinked by strontium chloride [3]. As mentioned in the outline of this joint project in Chapter one, the nanosensor was intended to be applied in the 3D hydrogel-

based tissue culture system developed in this study. To consistent with another study of this joint project, and to achieve the aim and objective of this study mentioned in Chapter one, in this Chapter, alginate material was selected as candidate hydrogel materials and strontium chloride was utilised as ionic crosslinker for crosslinking the alginate-based materials. By extrusion-based 3D printing or mould-casting technology, and alginate-based hydrogel materials, one of the hypotheses described in Chapter one will be investigated in this chapter, where the alginate-based materials would be 3D fabricated to simulate the middle layer of the articular cartilage/OC tissue *in vitro*. It is well-accepted that the mechanical property of hydrogel materials is poor, hence, nanocellulose fibre material was selected to reinforce the alginate hydrogel to improve its mechanical properties for 3D tissue fabrication. The hydrogel-based 3D tissue culture systems established in Chapter three and four, will be incorporated in the novel nanosensor developed in another study of this joint project. Before applying the novel nanosensor, it would be characterised preliminarily in terms of the size and concentration, which study will be described in Chapter five.

TE strategy is aiming to reconstruct the tissue *in vitro* with simulated structure and function. Considering the average size of the middle layer of the articular cartilage/OC tissue, a few moulds with different sizes for fabricating alginate-based hydrogels were designed and applied in this study. On the one hand, thicker moulds, could be used to fabricate bulk hydrogels to characterise the candidate alginate-based materials. On the other hand, 3D chondrocyte culture in the controlled microenvironment to simulate the middle zone tissue development, is within the scope of this study. In the original plan of this study, an extrusion-based 3D printing technology was selected to fabricate the 3D alginate hydrogel system toward the reconstruction of the articular cartilage/OC tissue *in vitro*. To perform the 3D fabrication by the mould-casting way, is the preliminary study.

Besides, for the sake of being printed by an extrusion-based 3D printer, the printability of the alginate-based material was designated to be preliminarily examined and intended to be improved by physically blending with the nanocellulose fibre material in this study. Since the natural articular cartilage tissue is soft, viscoelastic and both of chondrocytes and MSCs have been confirmed sensitivity and responsive to surrounding mechanical microenvironment, especially in 3D tissue culture system, the viscoelasticity of the material to be applied to interact with the viscoelastic cells in 3D has been seen as an important factor having impact on cell fate and behaviours [4-7]. Hence, in this Chapter, mechanical properties of the candidate materials regarding the compressive modulus of the hydrogel and the viscoelasticity of the pre-hydrogel material solution, were both evaluated. Nanocellulose fibre material blended with alginate material to reinforce the alginate hydrogel and to improve the viscoelasticity and so the printability of alginate materials were also investigated. A mould with around 1.5 mm thickness was selected to fabricate the middle zone of the articular cartilage tissue in which the entire thickness of the articular cartilage in human knee is assumed as 3 mm based on previous studies [8-10]. Formulas of alginate-based materials examined in this study and the 3D fabricated alginate-based hydrogels by the mould-casting way intended to be characterised and preliminarily assessed the biocompatibility in both 2D and 3D conditions were listed in Table 4.1. All works described in this Chapter were finished in NTHU in Taiwan. A brief introduction of the ionic crosslinking mechanism regarding the alginate material was provided below, followed by a general description of the nanocellulose material, shear thinning property and the printability involved in this study.

Table 4.1 Formulas, designed sizes and characterisations of candidate materials examined in this study.

Formulas of candidate materials	Designed sizes of 3D fabricated hydrogels	Characterisations
3% Sodium alginate (A3)	10mmx10mmx5mm	Hydrogel morphology by SEM
2% Nanocellulose fibres (NCF)	N/A	Hydrogel morphology by SEM Rheological properties (fluid viscosity, steady state viscosity, amplitude and frequency sweep oscillatory tests)
2% Sodium alginate (A2)	10mmx10mmx 3mm or 5mm	Compressive modulus, Swelling capabilities, Water content, Rheological properties (fluid viscosity, steady state viscosity, amplitude and frequency sweep oscillatory tests)
4% Sodium alginate (A4)		
6% Sodium alginate (A6)		
8% Sodium alginate (A8)		
A2+0.5%NCF		
A4+0.5%NCF		
A2 A4 A2+0.5%NCF A6 A4+0.5%NCF	10mmx10mmx0.6mm	2D viability test (biocompatibility), 2D cellular morphology observation
A2 A4 A2+0.5%NCF A4+0.5%NCF	10mmx10mmx1.5mm	3D viability test (biocompatibility), 3D chondrogenesis
Distilled deionised water	N/A	Fluid viscosity

4.1.1 Ionic crosslinking of alginate materials

The linear polymeric alginic acid molecules in the soluble sodium alginates could be physically crosslinked into insoluble hydrogel in the presence of divalent or multivalent cations which are usually divalent metallic cations such as the magnesium, calcium, strontium, barium ions with different affinities and preferential structure inside alginate molecules to interact with. This process is theoretically reversable due to the crosslinking mechanism. The alginic acid molecules consist of repeating simply-copolymerised β-D-mannuronate (M) and α-L-guluronate (G) blocks forming different compositional structure including homogeneous blocks of M or G, and heterogenous blocks of MG or GM. The ratio of M to G and their arrangement in the alginate materials contributes to determine the physiochemical characters and associated material functions of the alginate solution and alginate hydrogel. Both G and M blocks have free carboxyl and hydroxyl

groups, providing potential physical and chemical functions of the materials, in which the free carboxyl groups in G blocks are usually responsible for interacting with ionic crosslinkers to form the unique 'egg-box structure' (Figure 4.2) [11-13].

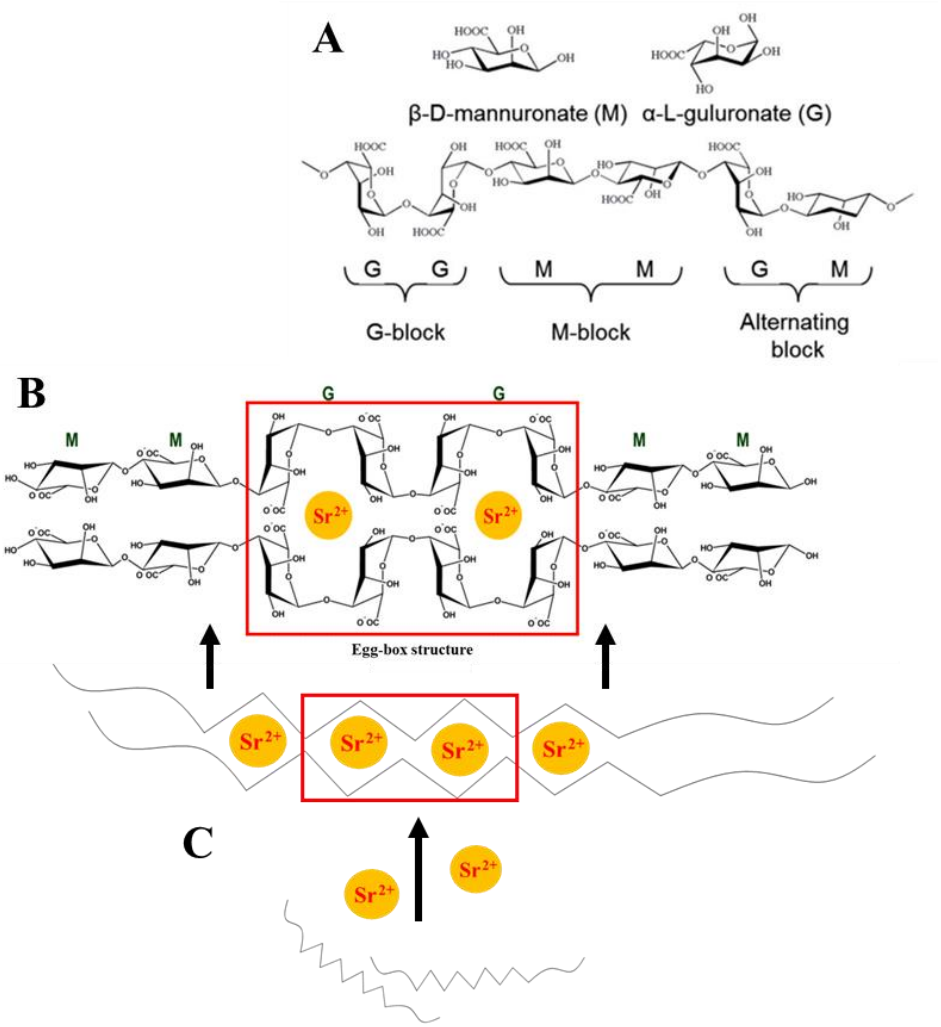

Figure 4.2 Schematic images of the components of alginate molecules and the egg-box structure inside alginate hydrogel crosslinked by strontium ions

A: Chemical structures of the β-D-mannuronate (M), α-L-guluronate (G) and blocks formed by G and M in alginate. B: Schematic image of the egg-box structure inside the strontium ion crosslinked alginate hydrogel. C: Schematic images of the ionic crosslinking process between alginate polymer and strontium ions. Images were adapted from references [13, 14].

Various types of interactions between multiple ions and diversified block sequences in alginate have been reported, for example, the calcium ion could interact with GG or MG but not MM blocks; barium ion could coordinate with GG or MM but not MG blocks; strontium ion could collaborate

with GG, slightly with MG but not with MM blocks, and barium and strontium ions may have stronger affinities than calcium with alginate. To successfully form the 'egg-box' junction during ionic crosslinking, it was also found a required number of consecutive blocks of G in the alginate molecular sequences. As natural abundant biocompatible polysaccharide materials, 3D alginate hydrogel has been widely applied in biomedical areas, in which many important features related to hydrogel functions such as the gel strength, mechanical properties, swelling capabilities, hydrogel stability and degradation of the ion-crosslinked alginate hydrogel are dependent highly on many internal factors including the molecular weight, compositional structure and arrangement, the type and strength of the ionic crosslinker, as well as various external factors, including the competitional factors (monovalent sodium ion, proton, or chelating agent), temperature and the pH value in the surroundings of the materials [11, 12]. Hence, before applying any alginate-related materials, those factors should be considered carefully.

4.1.2 Nanocellulose fibres

Cellulose is another natural abundant polysaccharide which could be isolated from plants or bacteria. With different source, cellulose presents different characters in purity, degree of crystallinity, availability, polymerisation degree and production capability in industry. But they are all renewable, biodegradable, non-toxic biocompatible and environment-friendly materials having similar mechanical tensile strength and capabilities of crystallisation and retaining water, which could be able to interact with bioactive molecules covalently due to the repeating glucose unit within their chemical structure. In the molecular chain of cellulose microfibril, there are carboxyl and hydroxyl groups at two different ends, contributing to the formation, rotation and functionality

of the cellulose structure. Detailed characters of cellulose materials are related to the sample source and preparation process. By different method of extraction, different cellulose with varied types, sizes and aspect ratios could be obtained, such as the microcrystalline cellulose, nanocrystalline cellulose, cellulose microfibril, cellulose nanofibril, micro-cellulose particle, and nano-cellulose particle [15].

Cellulose has hierarchical structures based on the polymeric glucose units, such as cellulose molecules, semi-crystalline filament (cellulose microstructure), cellulose microfibril (cellulose molecule aggregation), cellulose fibres (bundle of cellulose fibrils) (Figure 4.3). Cellulose molecules contain microfibre and nanofibre types, and the cellulose fibrils contain ordered crystalline region and disordered amorphous region [15].

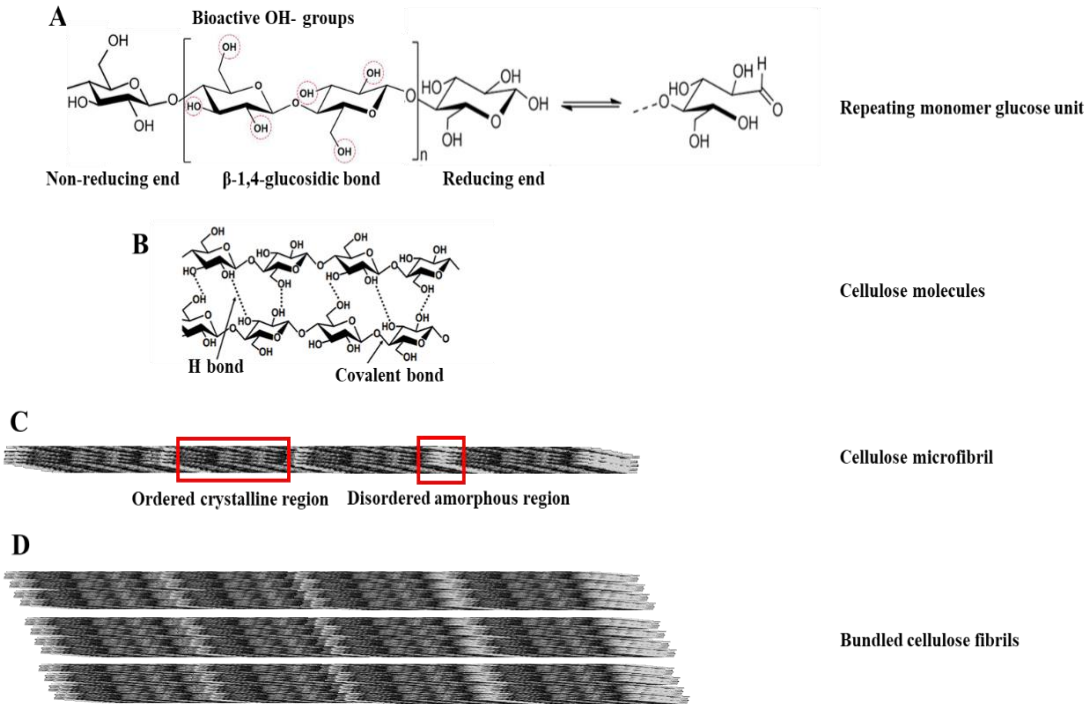

Figure 4.3 Schematic images of four hierarchical structures of cellulose

A: Glucose unit in molecular chain of cellulose. B: Chemical structure of cellulose molecules. C: Schematic image of cellulose microfibril. D: Schematic image of bundled cellulose fibrils. Images were adapted from references [16, 17].

Nanocellulose material contains nano-scaled cellulose object and nano-structured cellulose

material. Cellulose nanocrystal, cellulose nanofibril and cellulose nanoparticle belong to the nano-scaled cellulose object. Cellulose microfibril, bacterial cellulose and micro-fibrillated cellulose belong to the nano-structured cellulose material. Taken advantages of strong mechanical strength and sustainability to the environment, nanocellulose materials have been used to reinforce hydrogel materials. There are three types of nanocellulose materials commonly applied in practice, including the nanocrystal cellulose, nanoparticle cellulose and nano-fibrillated cellulose. They have similar chemical structure but different morphology, size and crystallinity. So far, many studies have found that the nanocellulose fibres having high compressive modulus and strength, low coefficient of thermal expansion and weight, and featuring with renewability and biocompatibility, could be used to fabricate scaffold for biomedical applications. From freeze-drying, gas foaming, electrospinning to various types of rapid prototyping technologies, nanocellulose-involved scaffolds have been designed and fabricated. Details could be found in many good reviews, in particular the physical mixture or polymer blending with cellulose materials to fabricate scaffold have been studied comprehensively from theory to practice, developing the micro/nanocellulose-related binary blends scaffold and ternary blends scaffolds. By blending individual materials to create a physical polymer system, on the one hand, optimised and combined features of both cellulose and other materials could be obtained to satisfy the requirement of tissue engineering scaffold; on the other hand, controlled and adjustable procedure and more economical and faster way than conventional process to develop new materials are offered. Such biocompatible materials as chitosan, polylactic acid, starch, gelatine, collagen, alginate and elastin have been blended with micro/nano-cellulose materials to fabricate scaffold for tissue regeneration applications, providing improvements on mechanical strength, rigidity, flexibility, porosity, and cellular distribution of the scaffold, and

enhancements on the swelling behaviour, hydrophilicity, rheology and many other properties of the composite materials, leading to the advantages of cellulose-based scaffolds to biomedical applications [15-20].

4.1.3 Shear thinning and printability

3D printing technology has become the most promising means to fabricate scaffolds or tissue constructs in TE strategy. An inescapable challenge is to select appropriate materials to be the printing ink (or bio-ink). Hydrogel polymers with great hydrophilicity, water retention ability, relative biocompatibility and able to be bio-functionalised, have been increasingly applied for fabricating substrate matrices or scaffolds for biomedical and TE applications, which are also fascinating for many researchers to exploit advanced printing inks (bio-inks) to enhance vital functions of 3D-printed scaffold, to improve the engineering design in favour of various fabrication (or printing) platforms, and to design and develop stimuli-responsive biomaterials or composites such as the graded shape-memorable polymer materials for 4D printing [21-23]. In this study, extrusion-based 3D printing was planned to apply alginate materials for tissue fabrication *in vitro,* before printing, the printability, in terms of the shear thinning property and viscoelastic behaviours, of the candidate materials were studied to try to select appropriate formula of ink for the subsequent extrusion-based 3D printing.

Shear thinning is one of the common behaviours of non-Newtonian fluid in rheology which is a difficult complex subject to study the flow of matter. At a low shear rate condition, the fluid presents a constant viscosity. At the critical shear rate condition, the viscosity of fluid drops sharply, indicating the beginning of shear thinning. The shear thinning behaviour could be described by

mathematical models, in which the power law model is a simple one to be used for modelling and characterising the non-Newtonian fluid. The power law model or the Ostwald de Waele relationship, could describe the behaviour and fit the viscosity results under a series of shear rates by two fitting constants in the equation and using Microsoft® Excel could be easily analysed. From the two constants, the fluid materials could be preliminary characterised and the injection force for the fluid to be performed by a syringe or a printer could be estimated [24, 25]. Details of this subject could be obtained from many professional literatures [26-28], and the related analysis in this study could be found in the following material and method part.

In TE designs, biomaterial-based tissue scaffold should provide a bioactive microenvironment for cells to interact with, leading to the sustainable tissue development. Mechanical properties of the biomimetic microenvironment are important factors in cell-based tissue engineering practices, where appropriate biomaterials applied to fabricate the scaffold should be able to provide sufficient mechanical support and have fewer negative impacts on the interaction with cells and cell behaviours. Cells have viscoelastic behaviours and are responsive to the mechanical surroundings. Viscoelastic property of living tissue also determines its homeostasis and regeneration, and reflects its physiological and pathological progresses *in vivo* [29]. To be interacted with living cells in both of 2D and 3D conditions, the mechanical features including stiffness, and viscoelasticity of the biomaterials are necessary information to be studied [29-33]. Compressive modulus represents the ability of materials to endure changes when subjected to compressive forces, measuring the stiffness of the material, as mentioned in Chapter three (3.2.5.1). For 2D/3D culture systems, previous studies have confirmed the great influence of the biomechanical microenvironment on seeding cells, in particular, for chondrocytes and MSCs intended to be applied in this study, when

they are cultured *in vitro*, mechanical properties of the material interacting with cells, would be a key factor in cell proliferation, differentiation and the engineered tissue development involving signalling pathways through the mechano-sensing and mechano-transduction processes [4, 5, 34-38]. In terms of the 3D fabrication, the mechanical property also contributes to the stability and shape fidelity of the candidate materials after fabrication, requiring characterisation. In addition, the viscoelasticity demonstrates both the viscous and elastic properties of the material when experiencing deformation. Some metallic materials at high temperature, many polymeric materials, human tissues, several biological fluids, certain biological macromolecule suspensions, and living cells are considered viscoelastic. In the original plan, an extrusion-based 3D printer will be applied, in which the printing ink is suggested to use viscoelastic material, displaying viscoelasticity during and after printing processes. Hence, in this study, apart from characterisations of candidate alginate-based materials regarding compressive moduli, swelling capability and water content, the viscoelasticity along with other rheological parameters of the alginate-based materials was also preliminarily investigated by performing a series of rheological tests including steady state viscosity test, constant viscosity test, and dynamic oscillatory tests.

4.2 Materials and methods

All materials used in experiments presented in this chapter and all experimental methods will be described in this section.

4.2.1 Chemical compounds and solutions

Hydrogel materials, ionic crosslinker and chemicals were purchased from Sigma-Aldrich (Merck, UK) directly or by its agent in Taiwan (Echo Chemical Co. Ltd). They were alginic acid sodium

salt from brown algae (A2033), strontium chloride (CAS No.:10476-85-4), nanocellulose fibre solution (2%), 37% formaldehyde solution (F8775), 25% glutaraldehyde solution (G6257), hydrochloric acid (258148), β-glycerophosphate disodium salt (G9422), Thiazolyl Blue Tetrazolium Bromide (M2128) (CAS No.:298-93-1), trypsin-EDTA solution (T4174), penicillin-streptomycin (PS) (P4333), poly-L-lysine solution (P4707) and albumin bovine serum (BSA, CAS no.: 9048-46-8). VECTASHIELD® Mounting Medium for Fluorescence with DAPI was ordered from Vector Laboratories, Inc. Isopropyl alcohol and ethanol alcohol were ordered from Honeywell (RS components Ltd.).

4.2.2 Medium, agent, assay kit and antibodies

Cell culture medium, balanced salt solutions, growth factors and other additives for cell culture, and differentiations, were purchased from either Corning® or Thermo Scientific Ltd. They are Dulbecco's Modified Eagle medium (DMEM), DMEM and Ham's F-12 medium (DMEM/F12), Phosphate buffered saline (PBS), Dulbecco's phosphate-buffered saline solution (DPBS), 100 mL Penicillin-Streptomycin Solution, 100x (10,000 I.U. Penicillin and 10,000 µg/mL Streptomycin), low viscosity mounting media. Tissue culture serum such as foetal bovine serum (FBS), horse serum (HS), and goat serum (GS), were ordered from Sigma-Aldrich (Merck, UK) and HyClone™ (GE healthcare Life Sciences). Antibodies for immunostaining were ordered from Thermo Scientific Ltd. or Abcam Plc, including anti-collagen type II-FITC, anti-collagen type X, Alexa Fluor® 594 goat anti-rabbit antibody, Alexa Fluor® 488 goat anti-mouse IgG. CyQUANT™ LDH Cytotoxicity Assay (Invitrogen™), ActinGreen™ 488 Ready Probes™ reagent (AlexaFluor™ 488 phalloidin) and LIVE/DEAD™ Viability/Cytotoxicity Kit, for mammalian cells (L3224) were

purchased from Thermo Scientific Ltd.

4.2.3 Consumables and instruments

Ultrapure water (DDW) and distilled water (DW) were produced by lab water purification systems (Merck Millipore Milli-Q™). Three types of centrifuges were used during the study. They are Eppendorf™ 5804 R, Thermo Scientific™ Small Benchtop Centrifuge and Kubota laboratory centrifuges (Japan). Other instruments used in the study, are scanning electron microscopy (SEM) (JSM 7001F FEGSEM; JEOL, Tokyo, Japan), Q150T ES sputter coater, confocal microscope (Zeiss LSM 800), benchtop normal inverted phase contract light microscopes and the rheometer (Anton-Paar's Modular Compact Rheometer 302). Other consumables such as tissue culture flasks, petri dish, microplates, pipette tips, centrifuge tubes, Eppendorf® tubes, beakers, haemocytometer, were provided by suppliers of Thermo Scientific™ (Taiwan), and Bersing Technology Co., Ltd (Taiwan).

4.2.4 Cell lines

Three types of cell lines were used in this chapter. They were NIH 3t3 fibroblasts (American Type Culture Collection (ATCC)), ATDC5 chondrogenic cell line (European Collection of Authenticated Cell Cultures (ECACC)), C2C12 myoblasts (ATCC).

4.2.5 Characterisations of biomaterials

Methods to characterise candidate biomaterials to be used in studies presented in this chapter are described in this section.

4.2.5.1 Compressive modulus

Alginate-based hydrogels were mainly crosslinked in 3D printed moulds to get uniformed sizes. Firstly, sodium alginates were weighed and dissolved in DDW to make alginate solutions of 2%, 4%, 6% and 8% concentrations, and autoclaved to sterilise. For alginate hydrogel with additional nanocellulose fibres, 4% and 8% alginate solutions were mixed with 2% nanocellulose fibre (NCF) solution to make two alginate-cellulose hybrid materials containing 2% alginate 0.5% NCF (A2N0.5) and 4% alginate 0.5% NCF (A4N0.5) respectively. To crosslink (Figure 4.4), alginate-based solutions (with/without NCF) were pippetted into the 3D-printed moulds inside microwells of microplates, and covered by coverslips before being pressed by a deadweight (another mould). Then 100mM strontium chloride solution ($SrCl_2$) was added into microwells containing moulds filled with alginate-based materials to fully crosslink the material at room temperature for about 24 hrs. After 24hrs, the crosslinked hydrogel was gently demoulded from the mould by a tweezer and was put into another microplate containing 50mM $SrCl_2$ for another 24 hrs to reach equilibrium at room temperature.

Alginate-based hydrogels (2%, 4%, 6% and 8% alginate, 2%alginate with 0.5%NCF, 4%alginate with 0.5%NCF) with uniformed sizes (e.g.,12mm X 12mm X 5 mm) were tested for plotting the stress-strain curve under the unconfined uniaxial compressive forces by the universal testing machine (ElectroForce 3100, TA instrument). Each condition of the hydrogel has three samples to test and each measurement was repeated three times before statistical analysis. Compressive force was loaded at a ramp rate of 0.05 mm/s (based on preliminary experiments to adjust the rate from 1mm/min) and the compressive modulus (Young's modulus) representing the stiffness of the crosslinked hydrogel was analysed as mentioned in chapter 3 (3.2.5.1).

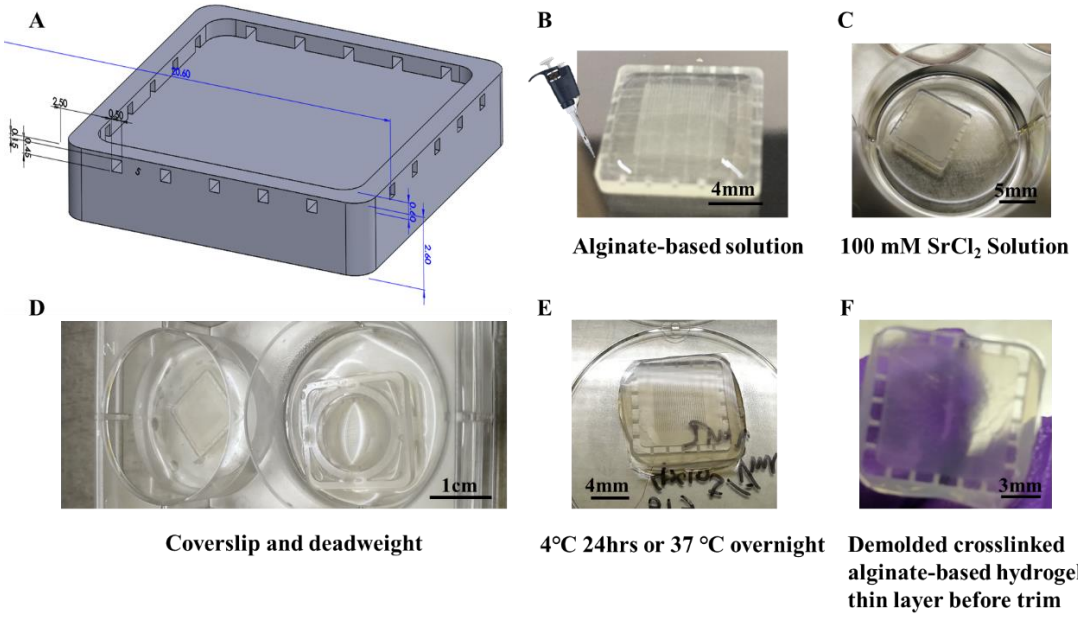

Figure 4.4 Schematic images of 3D fabrication of alginate-based hydrogels by mould-casting method A: Schematic image to show the 3D design of the mould for 3D alginate-based hydrogel fabrication; B: Alginate-based materials were pippetted into the mould; C: 100mM $SrCl_2$ solution (ionic crosslinker for alginate materials) was added into the well after the material-filled mould was covered by glass coverslip and deadweight on the top of the coverslip; D: Images to show the coverslip and deadweight on top the material-filled mould in the well containing $SrCl_2$ solution; E: After 24 hours crosslinking at room temperature (when cells were not encapsulated in the hydrogel materials) or 37°C (when cells were encapsulated in the hydrogel material) in an incubator overnight, the alginate-based materials were crosslinked; F: After removal of the deadweight and coverslip, the crosslinked alginate-based hydrogel could be demoulded and trimmed. (Images were adapted with permission from Mr. Wu of NTHU.)

4.2.5.2 Swelling capabilities

Hydrogel-based materials were crosslinked as mentioned in 4.2.5.1. Crosslinked bulk materials were gently wiped the water on the surface and measured the weight by a weighing machine (Sartorius ED2201-CW). After recording the weight (wet weight), samples were freeze-dried overnight by a freeze-drying machine (FD-12N, LAWSON. Co. Ltd). After freeze-drying, each sample was measured the weight again. After recording the weight (dry weight), samples were soaked into DW or growth medium to reswell. After soaking into DW or growth medium for about 0.5-1 hrs, 2-24hrs, 24hrs, 48hrs, 72hrs and 96hrs, the weight of reswelled hydrogels were measured

respectively again. Before being weighed at the next time point, the sample was gently wiped to dry the surface. After being weighted, samples were put back in DDW or growth medium and kept at room temperature till the next measurement. Each group of hydrogel contains three samples and each measurement was repeated three times for statistical analysis. To calculate the weight degree of swelling, water content, and reswelling of the alginate-based hydrogels, equations mentioned in chapter 3 (3.2.5.2) were used, and experimental groups were normalised with the weight of the wet sample of the associated group.

4.2.5.3 Morphology of alginate-based hydrogel materials

Alginate-based hydrogel materials were crosslinked uniformly as mentioned in 4.2.5.1, and freeze-dried. Before being scanned by the SEM, freeze-dried hydrogel samples were coated with a thin layer of conductive metals such as gold by a sputter coating machine in a vacuumed chamber. The process was same as that mentioned in chapter 3 (3.2.2.3).

4.2.5.4 Rheological properties

Alginate-based materials of a series of concentrations and with/without additional nanocellulose fibres were prepared in DDW and kept in 4°C before testing. All samples were prepared at the same time in the same batch to avoid differences due to different preparation processes. Anton-Paar's Modular Compact Rheometer (MCR) 302 (cone plate 50 platform) was used to test all the rheological parameters of the alginate-based samples at room temperature, including the constant shear viscosity, static state viscosity, amplitude sweep and frequency sweep. Each sample was tested three times and statistically analysed. Flow curves and viscosity of each sample were plotted under constant shear rate (shear stress). Shear thinning property and power law fitting were

calculated by results from steady state viscosity curve. From amplitude sweep curve, linear viscosity region, yield point and flow point of each sample could be observed. By frequency sweep test, the storage modulus and loss modulus of each sample were monitored.

Regime setup for constant shear rate test was: 100 points per test, constant duration, 10s per point and 1000s interval. Constant shear rate value was set at 50 (1/s). Regime setup for the steady state viscosity curve test was: 120 points per test, duration was by steady state and 1s timeout. Shear rate was performed at ramp logarithmic profile from 0.01 to 10000 (1/s). Regime setup for the amplitude sweep test was: 120 points per test and duration was set by the device. Oscillating shear strain was performed at ramp logarithmic profile from 0.01% to 100%. Shear frequency was set constant at value of 1 Hz. Regime setup for the frequency sweep test was: 120 points per test, and duration was set by the device. Oscillating shear strain is constant at 1%. Shear frequency was performed at ramp logarithmic profile from 100 to 0.1 Hz. All tests were set at room temperature around 20°C.

Power law fluid model (1) was applied to fit the steady state viscosity data across shear rates of all tested samples, which were seen as non-Newtonian fluids.

$$\boldsymbol{\eta = K\dot{\gamma}^{n-1}} \qquad \textbf{(1)}$$

Where η represents the viscosity (mPa.s), n is the power law constant (unitless), K is the flow consistency index (mPa.s) and $\dot{\gamma}$ is the shear rate (1/s).

$$\boldsymbol{\log_{10}\eta = (n-1)\log_{10}\dot{\gamma} + \log_{10}K} \qquad \textbf{(2)}$$

Taking the logarithm base 10 of the power law equation (1) will get the linear equation (2) and Microsoft® Excel (Microsoft Corporation, USA) is used to analyse the data and power law equation linear fitting, to get the flow consistency index and power law constant of each sample tested.

$$tan\theta = \frac{\log_{10} loss\ modulus}{\log_{10} storage\ modulus} \qquad (3)$$

The phase angle θ is used to relatively measure the viscosity and elasticity features of the viscoelastic materials [39], which is defined by the equation (3).

4.2.6 Cell culture and cytotoxicity of the ionic crosslinker

Methods regarding cell culture and cell-based assays presented in this chapter are described below.

4.2.6.1 General cell expansion and passaging process *in vitro*

General cell expansion and passaging process *in vitro* in this chapter are same as those mentioned in chapter three (3.2.6.1).

4.2.6.2 Biocompatibility and cytotoxicity of alginate-based hydrogel materials

Investigations on the biocompatibility of the material and cytotoxicity of the ion crosslinker in this study are described in this section.

4.2.6.2.1 Series number test for appropriate seeding density

Appropriate seeding density of specific type of cell was examined by series cell number test before any cell-involved experiment. Cells cultured in flasks were detached and calculated the total number in the way as mentioned above (3.2.6.1). Then cells were seeded and tested in the same process as those mentioned in Chapter three (3.2.6.2.1).

4.2.6.2.2 Cytotoxicity of the ionic crosslinker $SrCl_2$ on living cells by LDH essay

To examine the cytotoxicity of the ionic crosslinker $SrCl_2$ to be applied for fabricating alginate-

based hydrogels, three cell lines were used to evaluate the effect of different concentrations of $SrCl_2$ (0.05M,0.1M,0.15M) dissolved in growth medium on the viability and proliferation of three types of living cells cultured in 2D monolayer *in vitro*, including NIH3t3 fibroblast, C2C12 myoblast and chondrogenic cell line ATDC5.

Cells were cultured and seeded in 24-well microplates at their appropriate density by the same way as mentioned (4.2.6.1 and 4.2.6.2.1). After seeding 24 hrs in an incubator, cells in plates were checked for cellular states under an inverted phase contrast microscope. Then growth medium for cells were replaced by conditional medium (growth medium containing different concentrations of crosslinkers) and examined their effect on the cell viability and proliferation by LDH assay after 1-, 4-, and 7-days treatments, respectively. Cultural medium of each well was replaced every two or three days. The concentrations of $SrCl_2$ used were 0.05M, 0.1M and 0.15M, which would be freshly diluted in growth medium from the stock solutions of 1M $SrCl_2$ prepared in DDW and sterilised by passing through the 0.22 μm filter. Growth medium containing 5% DMSO was prepared to treat cells as the positive control.

4.2.6.2.3 LDH assay

The process of LDH assay to screen the viability and proliferation of cells was performed according to the instruction of the CyQUANT™ LDH kit from the manufacturer. Detailed process was same as that mentioned in Chapter three (3.2.6.2.2).

4.2.7 Phrozen™ Sonic XL 4K 3D printer and 3D mould design

A commercial 3D printer (Phrozen™ Sonic XL 4K, Phrozen Tech Co., Ltd. Taiwan) used in this study and the 3D mould designed for fabricating alginate materials are described in this section.

4.2.7.1 Phrozen™ 3D printer and moulds designed for alginate-based hydrogel fabrication

The Phrozen™ Sonic XL 4K is a commercial 3D printer made specially for the dental industry. It has a spacious area (8.9,") for printing larger models. The printing speed could reach up to 90mm per hour and the printer is controlled by the Formware Slicer Software to support editing and designing of models. And the Phrozen™ Aqua Resin Grey 4K is a special resin material designed for printing high-resolution models, with the special formula to provide many advantages such as low shrinkage, low viscosity and odour, for fast, precise and high-resolution printing. 3D moulds with different thickness but fixed size of central area (10mm x10mm), were designed by Solidwork® software and printed by Phrozen™ Sonic XL 4K 3D printer (Figure 4.5), using the commercial resin material (a safe material for printing dental model without toxicity described by the Phrozen™ Aqua Resin Grey), for alginate-based hydrogel fabrication.

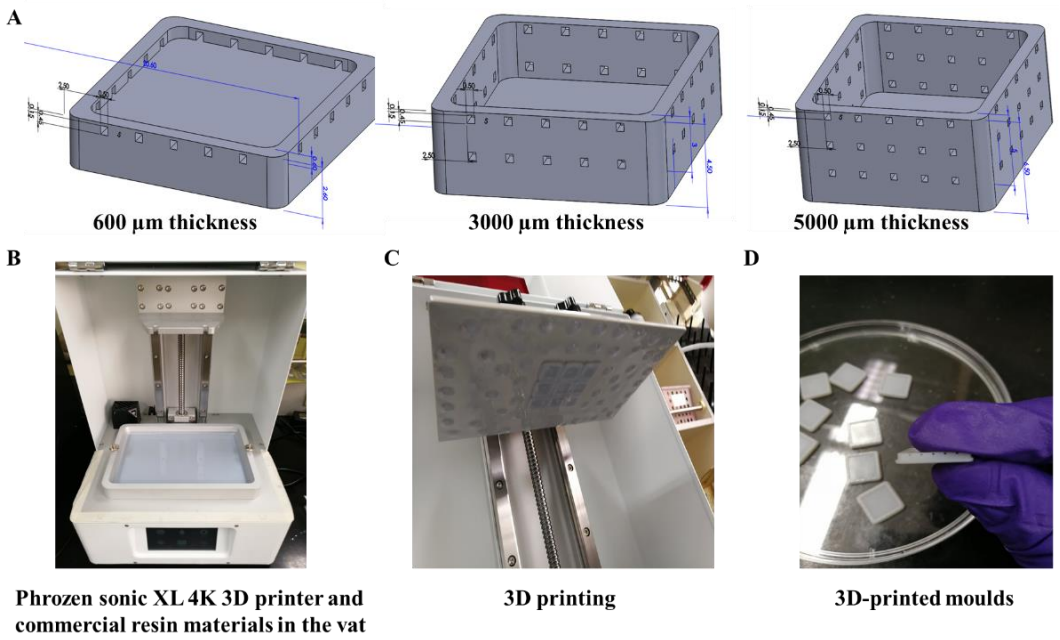

Figure 4.5 Images of the 3D designs of mould with different thickness for fabricating alginate-based hydrogels A: Schematic images showing 3D design of moulds with different thickness (600, 3000, 5000 µm). (Images were adapted with permission from Mr. Wu of NTHU.) B: Image to show the commercial 3D printer and resin materials in the vat (Phrozen™ sonic XL 4K 3D printer, Aqua Resin Grey 4K Special resin for highest resolution); C: Image to show 3D printed moulds on the building platform after printing; D: Image to display 3D printed moulds after post-printing UV exposure.

4.2.7.2 3D fabrication of the alginate-based hydrogel encapsulated with living cells

The process of fabricating alginate-based hdyrogels without cells was mentioned in 4.2.7.1. The process of 3D fabrication cell-laden alginate hydrogels was generally same as that demonstrated by the shematic images in Figure 4.4. In brief, after being printed by 3D printer and washed thoroughly by ethanol, the mould was sterilised by 75% alcohol solution and dried in a biosafety cabinet before UV light exposure for further sterilisation at least 2 hrs. The coverslip and deadweight were also sterilised by the same way. After preparation of the sterilised mould, coverslip, and deadweight, alginate-based materials (sterilised by autoclave) were added into moulds within a six-well microplate. Then the material-filled mould was covered by a glass coverslip and a deadweight on top of the coverslip. 100mM $SrCl_2$ solution (sterilised) was filled in the well containing the mateiral-filled mould until the whole mould was covered by the solution. Finally the casting material-filled mould within the microplate was put into an incubator to crosslink overnight. After crosslinking, the solution was removed before demoulding the crosslinked hydrogel gently by a sterilised tweezer. Demoulded hydrogels were put into another new six-well microplate containing sterilised 50 mM $SrCl_2$ solution for further equilibrium at least 24 hours in an incubator (37℃).

4.2.8 Biocompatibility of alginate-based hydrogels on 2D and 3D cell culture

In this section, the biocompatibility of alginate-based hydrogel on living cells, will be evaluated in 2D and 3D cell culture conditions.

4.2.8.1 Biocompatibility of alginate-based hydrogels on 2D cell culture

Alginate-based thin layers without cell encapsulation, were fabricated by the mould-casting method as mentioned in 4.2.7.1, and punched in the middle area by a sterilised biopsy punch (8mm in diameter) to get the alginate thin sheet with uniformed size, shape and thickness to be put into wells of the 48-well microplate for 2D cell culture.

Alginate thin sheets were kept in 50 mM $SrCl_2$ solution at 4°C after fabrication. Before using, thin sheet was sterilised by 1x sterilised PBS and UV light exposure in a biosafety cabinet for at least 20 mins at both sides. Then the sterilised thin sheet was coated with 0.01% poly-L-Lysine solution (sterilised) and dried in a biosafety cabinet at room temperature. Prepared thin sheets were all put in the well of 48-well microplates and then cells were seeded on the coated thin sheet at appropriate density. Culture medium was gently replaced every two to three days. After 1-, 4- and 7-days incubation, 2D cultured cells were examined by Live & Dead assay for viability. In this experiment, chondrogenic cell line ATDC5 cells were used, and thin sheets with 8mm in diameter and 0.6mm thickness were fabricated by 2% and 4% alginate with/without additional 0.5% NCF respectively. The experimental design was displayed in Figure 4.6.

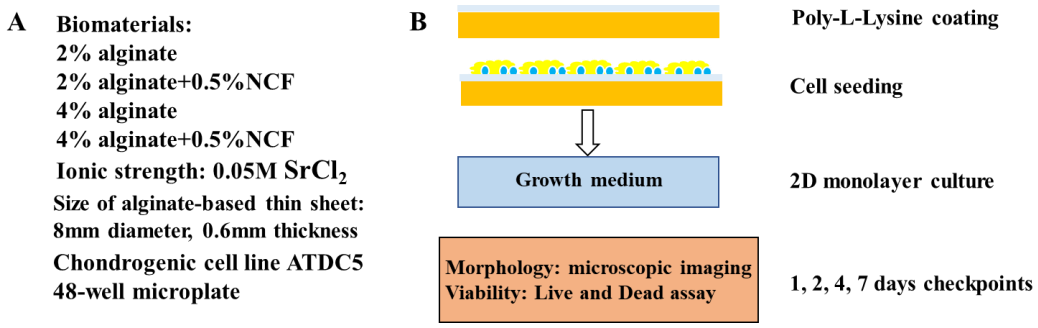

Figure 4.6 Schematic images of the experimental design of the cell viability examination on 2D alginate-based thin sheets

A: Materials and cells used in this examination; B: Schematic images showing the steps of the examination.

4.2.8.2 Biocompatibility of alginate-based hydrogels on 3D chondrocyte differentiation

Chondrocytes at density of one million cells per ml were mixed with alginate-based biomaterials and 3D fabricated by the mould-casting method as mentioned in 4.2.7.2. In this experiment (Figure 4.7), the cell-encapsulated biomaterials were crosslinked in an incubator overnight and the whole process of fabrication was carefully maintained in a sterile condition. After fabrication, 3D hydrogel products were put into the well of 6-well microplates with growth medium supplemented with 50mM $SrCl_2$. Culture medium was replaced every two to three days. After 2-3 days incubation, growth medium was replaced by differentiation medium to culture for at least 28 days. Differentiation medium supplemented with 50mM $SrCl_2$ was replaced every two to three days. 50mM $SrCl_2$ were supplemented in both growth medium and differentiation medium during 3D culture and differentiation. The 3D products were cultured in an incubator for 14, 28 and 45 days and examined the viability by Live and Dead assay. And the chondrogenic differentiation was examined by immunofluorescent staining the anti-type II collagen-FITC antibody for confocal microscopic observation.

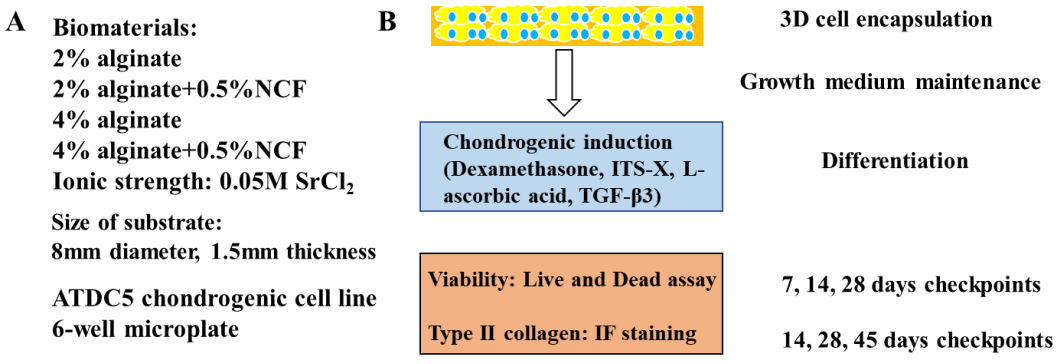

Figure 4.7 Schematic images of the experimental design of the cell viability and differentiation examinations in 3D alginate-based hydrogel system

A: Materials and cells used in this examination; B: Schematic images showing the steps of examinations.

4.2.8.3 Live & Dead assay for cell viability evaluation

To evaluate the cell viability after culture, Live and Dead assay was applied. The process was performed in line with the instruction of the manufacturer (LIVE/DEAD™ Viability/Cytotoxicity Kit, for mammalian cells (L3224). In brief, samples were taken out of the incubator and checked under a normal inverted microscope. Then cultural medium was gently replaced with staining solution containing green-fluorescent calcein-AM (2μM working solution) and red-fluorescent ethidium homodimer-1 (4 μM working solution) diluted in growth medium. Samples in staining were kept in dark at room temperature for about 30-45 mins and then carefully washed twice with PBS. For cells cultured in 2D, after washing, samples in plate could be checked directly by the fluorescent microscope. For cells cultured in 3D, after washing, 3D samples were gentle transferred to the 35-mm confocal dish (glass-bottom petri-dish) and examined by the fluorescent microscope.

4.2.8.4 Immunofluorescent staining

For immunofluorescent (IF) staining the 3D hydrogels encapsulated with chondrocytes, samples were carefully washed twice with PBS and fixed by 4% formaldehyde solutions at room temperature for about 6-8 hrs. Before staining, samples were treated with blocking solution containing 5% BSA, PBS and 0.25% Triton X-100, at room temperature for about 6-8 hrs and washed with washing solution containing PBS and 0.1% TritonX-100, twice gently. Then samples were treated with the fluorescence-conjugated antibody (FITC-conjugated anti-type II collagen) at room temperature for about 2-4 hrs in dark, and washed carefully with washing solution. Stained samples were transferred gently to the 35-mm confocal dish (glass-bottom petri-dish) with mounting agent and kept in dark before being examined by confocal microscope.

For IF staining the cytoskeletal F-actin of cells cultured in 2D or 3D alginate-based hydrogel systems, samples were gently washed once and fixed by 4% formaldehyde solutions at room temperature for about 4-6 hrs. Then samples were washed with DDW twice gently before adding the staining solution containing the FITC-anti-F-actin antibodies and PBS. Samples in staining were kept in dark at room temperature for about 30-45 mins and then carefully washed twice with PBS. For cells cultured in 2D, after washing, samples in plate could be checked directly by the fluorescent microscope. For cells cultured in 3D, after washing, 3D samples were gentle transferred to the 35-mm confocal dish (glass-bottom petri-dish) and examined by the fluorescent microscope.

4.2.9 Statistical analyses

Methods to statistically analyse the experimental data will be described in this section.

4.2.9.1 Compressive modulus

The fabricated alginate-based materials in customised moulds with fixed sizes, including area of the cross section and the length, were recorded and analysed by the Microsoft® Excel (Microsoft Corporation, USA) to calculate the Young's modulus of the 3D alginate-based hydrogels. Mean value and standard deviation of samples were used to plot the diagram.

4.2.9.2 Swelling capabilities and water content

Measurements of the weights of the alginate-based hydrogels, before and after drying, and after reswelling were all analysed by Microsoft® Excel (Microsoft Corporation, USA). Mean value and standard deviation of samples were used to plot the diagram.

4.2.9.3 LDH assay

Absorption data measured by the plate reader (BioTek, Agilent Technologies, Inc., USA) were exposed to Microsoft® Excel (Microsoft Corporation, USA) to compile and were analysed statistically by Origin2018 (OriginLab®, USA), where the differences between groups were analysed by one-way analysis of variance ANOVA (Tukey post hoc test) and linear fitting of the cell numbers were also performed. The p value less than 0.05 was considered as statistically significant.

4.2.9.4 Rheological properties

All experimental data of the viscosity test under constant shear rate, the steady state viscosity test, the amplitude sweep and frequency sweep oscillation tests were exported to Microsoft® Excel (Microsoft Corporation, USA) to re-plot curves and to analyse. The power law constant (unitless) n and flow consistency index K (mPa.s), of each sample were calculated, by fitting the Power law fluid model as mentioned in 4.2.5.4. The storage curve, loss curve and the phase angle of samples under oscillation tests were analysed as mentioned in 4.2.5.4 and plotted curves by using Microsoft® Excel (Microsoft Corporation, USA).

4.3 Results and discussions

Results of experiments investigated in this chapter will be presented and discussed in this section.

4.3.1 Morphologies of the alginate-based biomaterials

3% alginate solution was prepared and crosslinked in the customised mould. After crosslinking and

equilibrium, the alginate hydrogel was freeze-dried and spun coated with a layer of gold before scanned by the SEM to observe the morphology (Figure 4.8 A). 2% nanocellulose fibres (NCF) were diluted and dried in an oven on a small piece of silicon wafer. Dried NCF samples (Figure 4.8 B) were spun coated with a layer of gold before scanned by the SEM together with alginate samples. From images, the multiple porous structure of the alginate hydrogel and fibrous cellulose in nanoscale were both observed. It was known that the hydrogel material has poor mechanical strength which could be improved by additional fibres. Hence in this study biocompatible nanocellulose fibres were applied to blend with alginate materials to try to improve its mechanical properties.

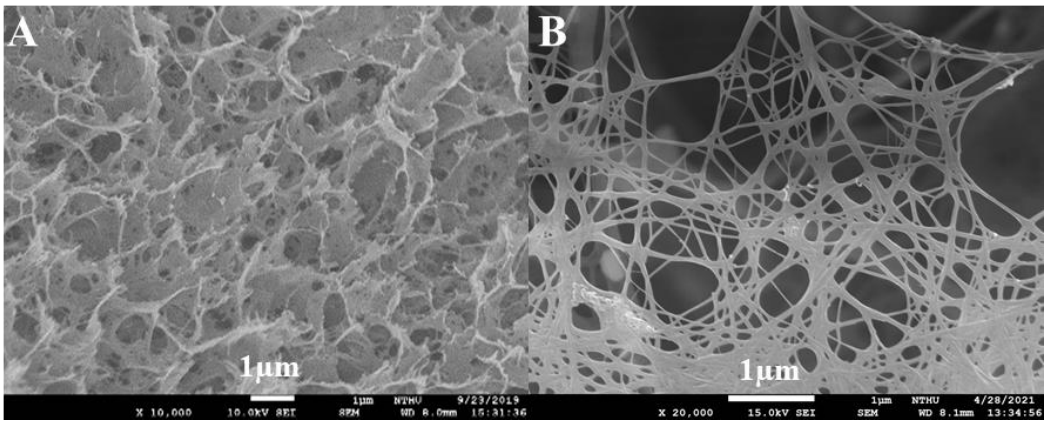

Figure 4.8 Morphologies of the alginate material and cellulose nanofibers by SEM
A: SEM image of the 3% alginate hydrogel crosslinked in the customised mould by 0.1M $SrCl_2$. B: SEM image of the dried nanocellulose fibres. Scale bars were 1 μm.

4.3.2 Mechanical properties of alginate-based hydrogels

By using the mould-casting methods, a series of uniformed alginate-based hydrogels including the 2%, 4%, 6%, 8% alginate, 2% alginate with 0.5% NCF, and 4% alginate with 0.5% NCF, were fabricated and tested the compressive modulus by the represented stress-strain curves. From results (Figure 4.9), there is a concentration-dependent increase in the compressive modulus in pure

alginate materials in which as the concentration of alginate increases, the compressive modulus of the hydrogel will increase. The schematic image of the comparison of the stress-strain curves of the alginate-based hydrogels demonstrated the concentration-related phenomenon. On average, the compressive property of the alginate hydrogel was in KPa level, and comparing to the pure alginate hydrogels, with additional nanocellulose fibres, could slightly improve the mechanical property of the alginate-based hydrogel, comparable to that of the high concentration pure alginate hydrogel, suggesting the possibilities of applying NCF to reinforce the alginate hydrogels.

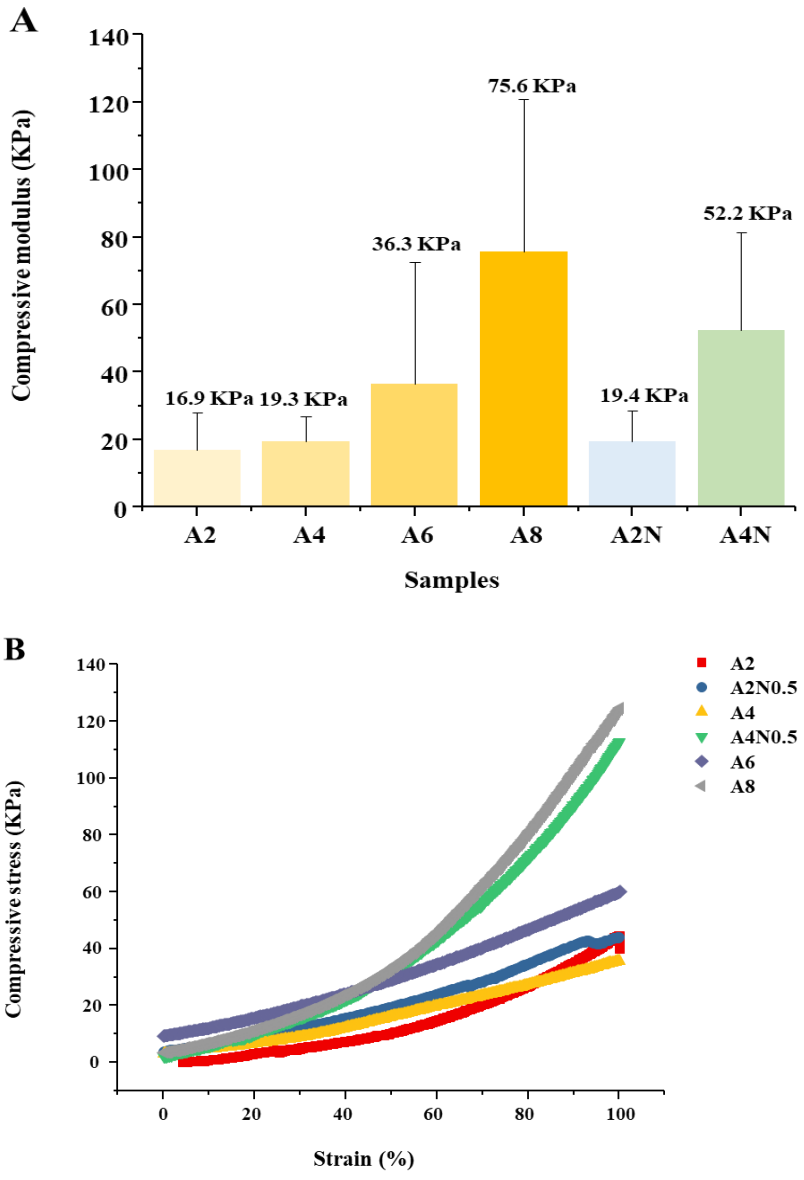

Figure 4.9 Compressive modulus and the stress-strain curve of the alginate-based hydrogels

Different formulations of alginate-based materials were crosslinked in the 3D-printed customised moulds (10x10x5 mm) under the same ionic strength (0.1M $SrCl_2$), and measured the compressive modulus. A: Comparison of the stress-strain curve of the alginate-based hydrogels with different formula. A2:2% alginate; A4:4%alginate; A6: 6% alginate; A8: 8% alginate; A2N0.5: 2%alginate+0.5%NCF; A4N0.5: 4%alginate+0.5%NCF. N=3, n=9. B: Schematic image of the stress-strain curve of different alginate-based hydrogel groups.

4.3.3 Swelling capabilities of alginate-based hydrogels

Equilibrium swelling capability is an important physical character reflecting the network structure and crosslink density of the hydrogel polymer. Crosslinked alginate-based hydrogels were examined the weight degree of swelling (Figure 4.10 A) and water content (Figure 4.10 B) by measuring the weight of hydrogel before and after drying. From results, alginate-based hydrogels have similar weight degree of swelling, except the high concentration (8%) alginate that has a lower weight degree of swelling. Comparing to the pure alginate hydrogel, additional nanocellulose fibres, did not change the weight degree of swelling of alginate-based hydrogel. Alginate-based hydrogels all have relatively more water content (more than 90%).

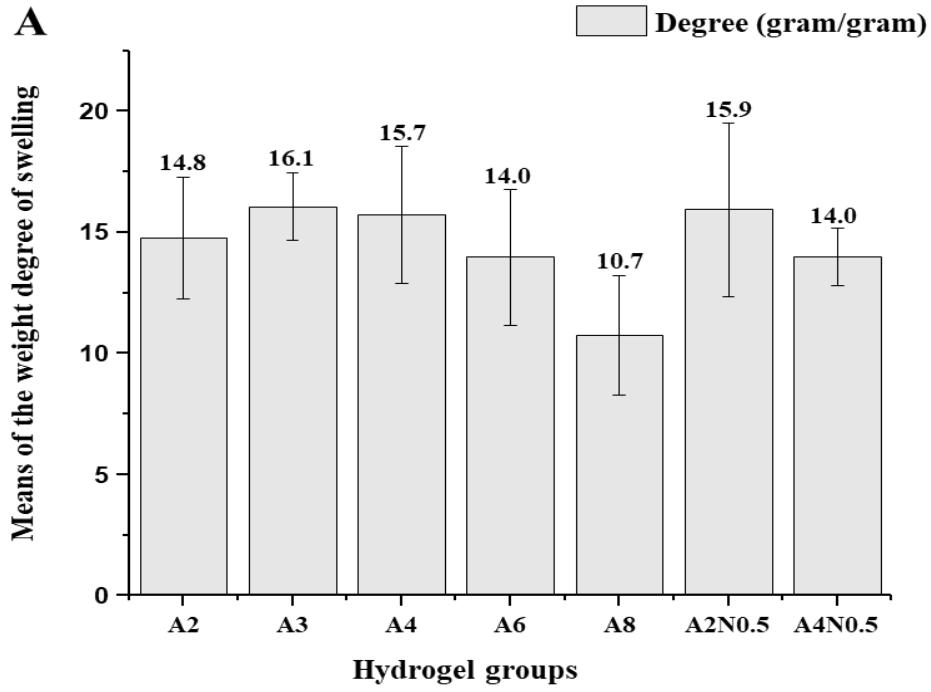

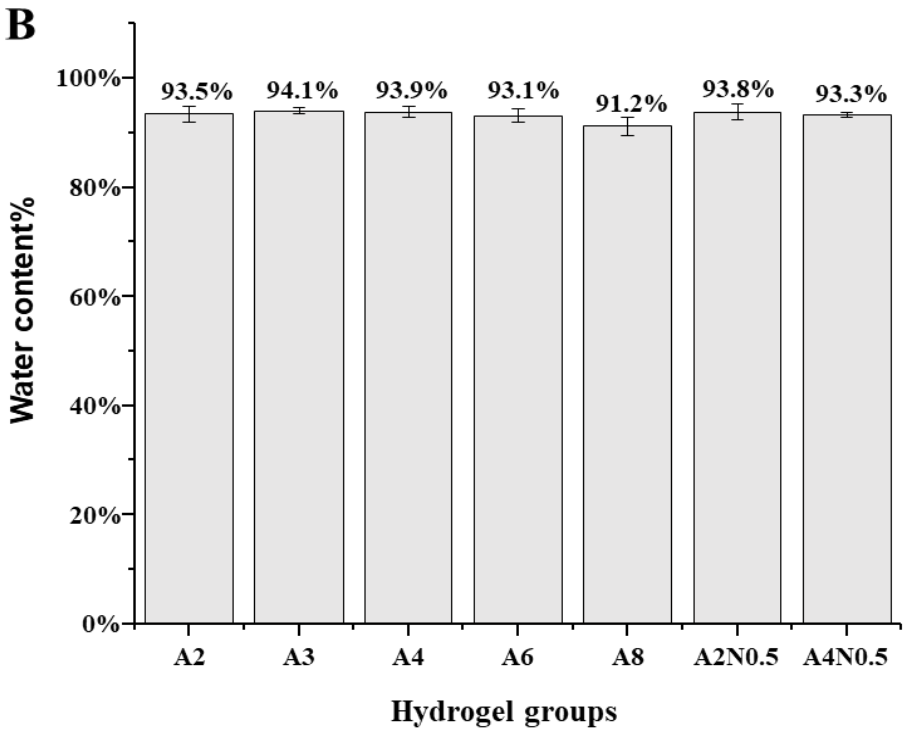

Figure 4.10 Comparison of the degree of swelling and water content of the alginate-based hydrogels A: Comparison of the degree of sweeling of the alginate-based hydrogels. A2: 2%algiante; A3: 3%alginate; A4: 4% alginate; A6: 6%alginate; A8: 8%alginate; A2N0.5: 2%algiante with 0.5%NCF; A4N0.5: 4%alginate with 0.5%NCF. NCF: nanocellulose fibres. B: Comparison of the water content of the alginate-based hydrogels. Alginate-based materials were crosslinked in the customised mould in 4°C overnight and demoulded. Demoulded alginate-based hydrogels were measured the weight before and after freeze-drying. After 48hr reswelling in 4°C, the weight of each sample was measured again. Each test was repeated twice. N=2, n=8.

To compare the reswelling capability (Figure 4.11) of alginate-based hydrogel, freeze-dried hydrogels were soaked in DDW and growth medium respectively, and weight after reswelling at different time points during reswelling was also measured. From results, most freeze-dried hydrogels were reswelled and equilibrium after 24 hours soaking in either DDW or growth medium. Comparing to the results of samples soaked in DDW which on average regained 40% of the original weight before drying, alginate-based hydrogels soaked in growth medium have better reswelling capabilities, which on average could regain 60% of the original weight before drying, suggesting the absorption of things such as the growth factor and protein from growth medium.

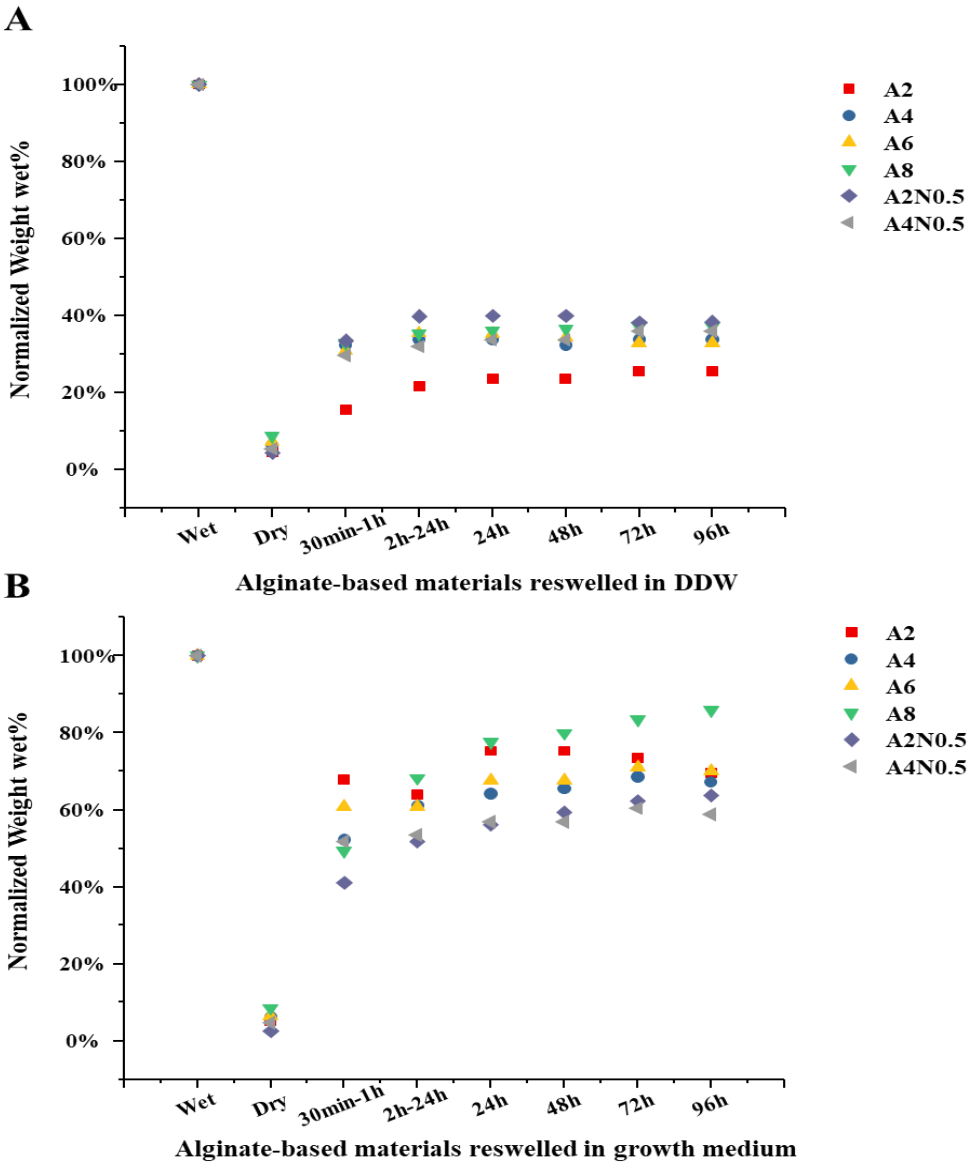

Figure 4.11 Comparison of the reswelling capability of the alginate-based hydrogels reswelled in water and in growth medium

A: Comparison of the reswelling capability of the alginate-based hydrogels reswelled in water; A2: 2%algiante; A4: 4% alginate; A6: 6%alginate; A8: 8%alginate; A2N0.5: 2%algiante with 0.5%NCF; A4N0.5: 4%alginate with 0.5%NCF. NCF: nanocellulose fibres. B: Comparison of the reswelling capability of the alginate-based hydrogels reswelled in growth medium. Alginate-based hydrogels were crosslinked in the customised mould in 4°C overnight and demoulded. Demoulded alginate-based hydrogels were measured the weight before and after freeze-drying. Then the freeze-dried samples were soaked in DDW or growth medium to reswell. After 30min-1hr, 2hr-24hr, 24hr, 48hr, 72hr and 96hr reswelling, the weight of each sample was measured again respectively. Each measurement was repeated three times and each group contains two samples. N=3, n=6.

4.3.4 Effect of the ionic crosslinker $SrCl_2$ on the cell viability and proliferation *in vitro*

Fibroblast NIH 3t3, myoblast C2C12 and chondrogenic cell line ATDC5 cells were tested

individually in this study. From results of the seeding cell density test (Figure 4.12 G-I), cell number between 5K to 10K per well in 24-well microplate would be the appropriate seeding density for fibroblasts and around 10K per well would be suitable for myoblasts and chondrocytes. Based on these, cells were seeded at their appropriate density in 24-well microplates and treated with conditional medium with different concentrations of $SrCl_2$, to examine the cytotoxic effect of $SrCl_2$ on living cells *in vitro*. After incubation 1, 4 and 7 days, samples were checked by performing LDH assay. From results (Figure 4.12 A-C), there was a time-dependent and concentration-related toxic effect of $SrCl_2$ on living cells, especially for chondrogenic cell line ATDC5 cells (Figure 4.12 C). Generally, longer time treatment and higher concentration of $SrCl_2$ have more toxic effect on cells in culture. Variations of results of the 7-day treatment were observed in all three cell lines, in which after 7 days treatments, the cell viabilities were sometimes higher than those of 4 days treatment. This could be explained by the fact that every two to three days, cell medium was replaced with fresh growth medium without $SrCl_2$ in this test. $SrCl_2$ is soluble in water but would be reduced the solubility in conditional medium. The reason could be due to the potential interaction between Sr^{2+} with some proteins or compounds in serum and medium. Precipitation of the salt was observed and the interaction between the precipitated salt with living cells would contribute to the cytotoxic effect of the $SrCl_2$ on cell viability and proliferation. Results suggested that the lowest concentration of $SrCl_2$ in medium in this test would be appropriate for cell culture and this concentration of $SrCl_2$ was selected to be the ionic strength to crosslink the alginate-based materials for cell culture in 2D and 3D. Supplement of $SrCl_2$ in growth medium was also applied this concentration and the conditional medium or supplemented medium were freshly made before administration in cell culture, to avoid the precipitation of the salt in medium with serum.

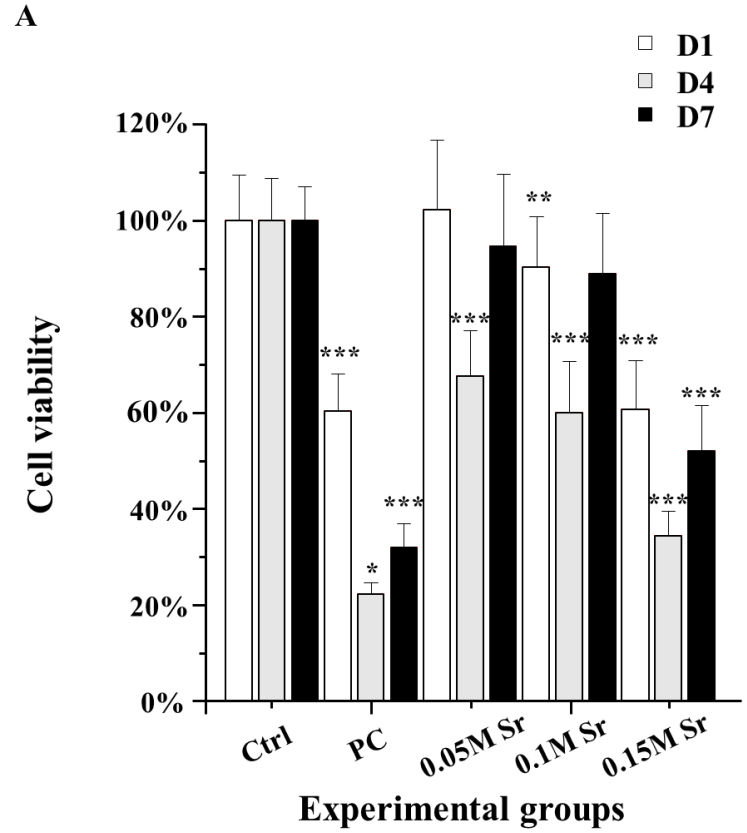
A
D1
D4
D7
120%
100%
80%
60%
40%
20%
0%
Cell viability
***
*
***
***
**
***
***
***
***
***
Ctrl
PC
0.05M Sr
0.1M Sr
0.15M Sr
Experimental groups

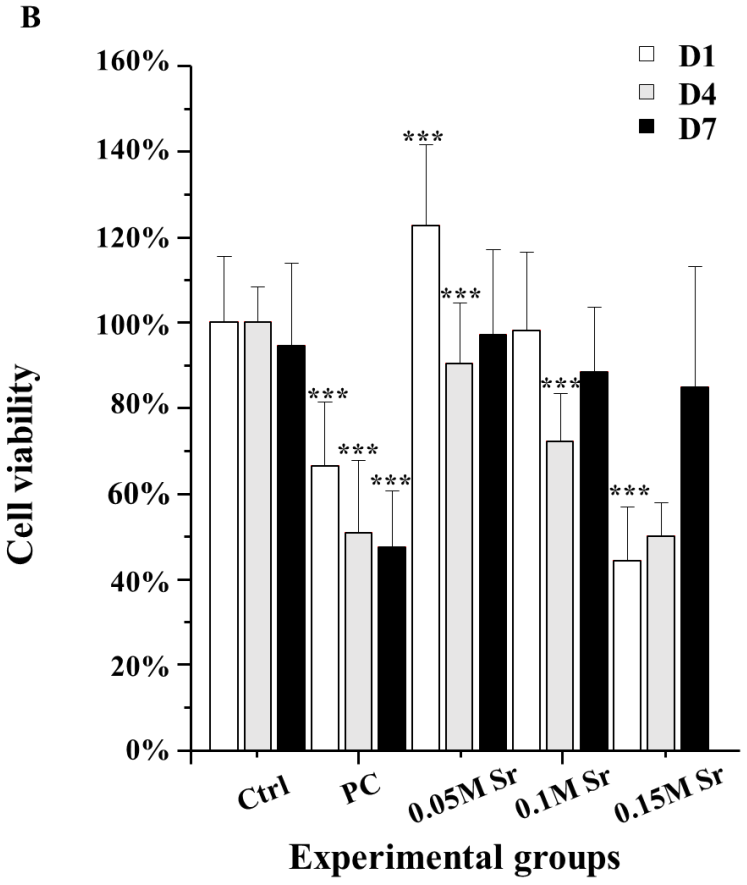
B
D1
D4
D7
160%
140%
120%
100%
80%
60%
40%
20%
0%
Cell viability
***
***
***
***
***
***
***
***
Ctrl
PC
0.05M Sr
0.1M Sr
0.15M Sr
Experimental groups

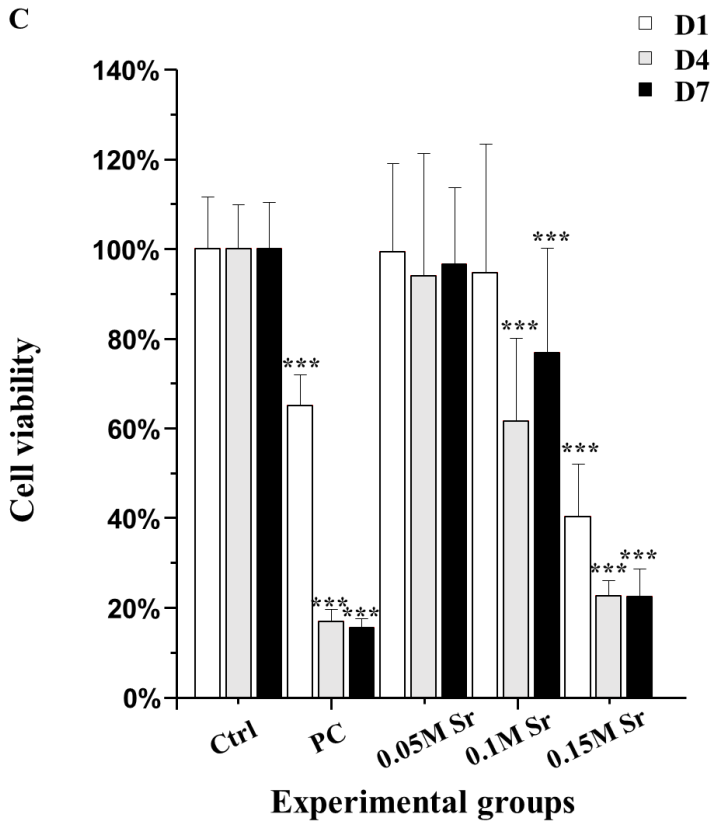
C
D1
D4
D7
140%
120%
100%
80%
60%
40%
20%
0%
Cell viability
***
Ctrl
PC
0.05M Sr
0.1M Sr
0.15M Sr
Experimental groups

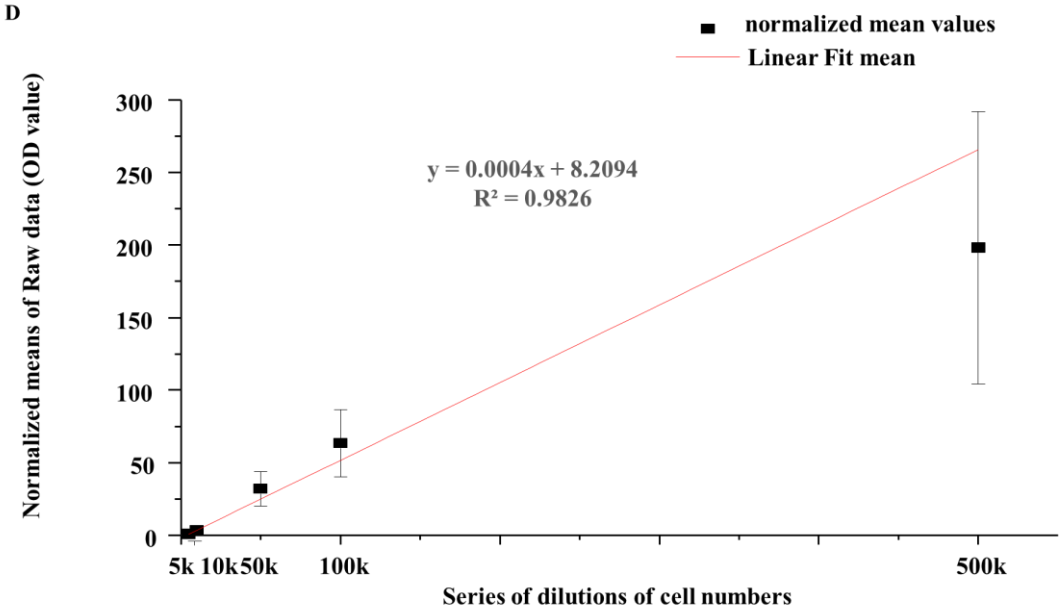
D
normalized mean values
Linear Fit mean
y = 0.0004x + 8.2094
R² = 0.9826
300
250
200
150
100
50
0
Normalized means of Raw data (OD value)
5k
10k
50k
100k
500k
Series of dilutions of cell numbers

E

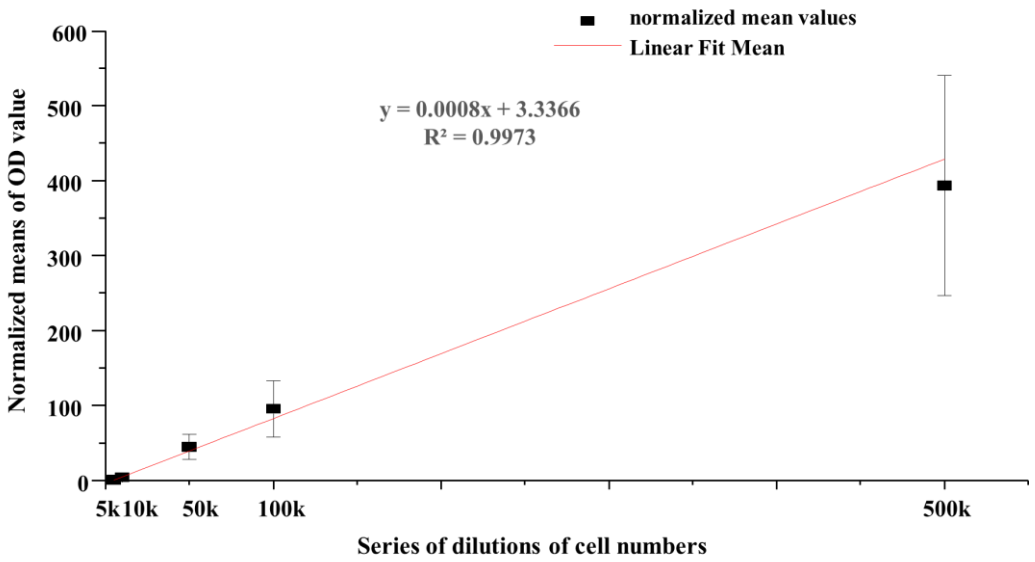
normalized mean values
Linear Fit Mean
y = 0.0008x + 3.3366
R² = 0.9973
Normalized means of OD value
600
500
400
300
200
100
0
5k
10k
50k
100k
500k
Series of dilutions of cell numbers

F

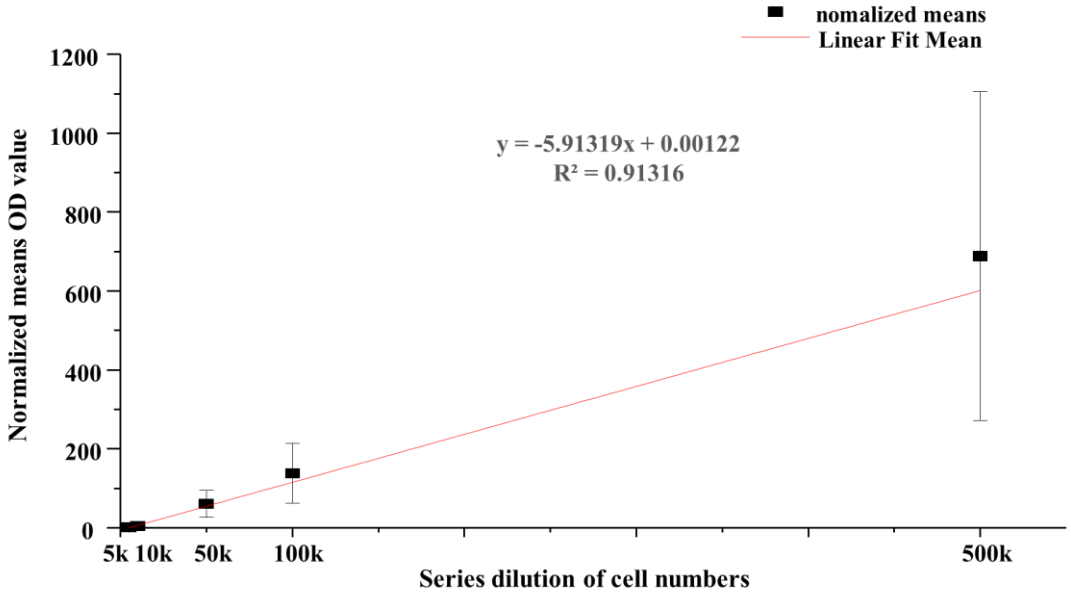
nomalized means
Linear Fit Mean
y = -5.91319x + 0.00122
R² = 0.91316
Normalized means OD value
1200
1000
800
600
400
200
0
5k
10k
50k
100k
500k
Series dilution of cell numbers

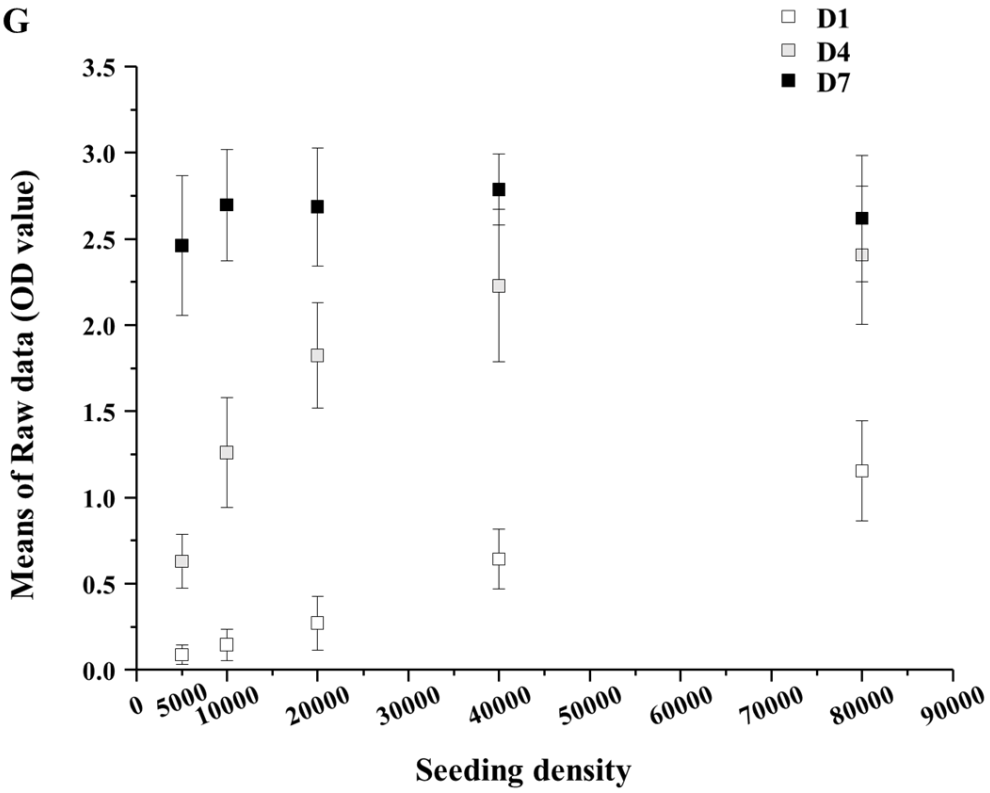
G
D1
D4
D7
Means of Raw data (OD value)
3.5
3.0
2.5
2.0
1.5
1.0
0.5
0.0
0
5000
10000
20000
30000
40000
50000
60000
70000
80000
90000
Seeding density

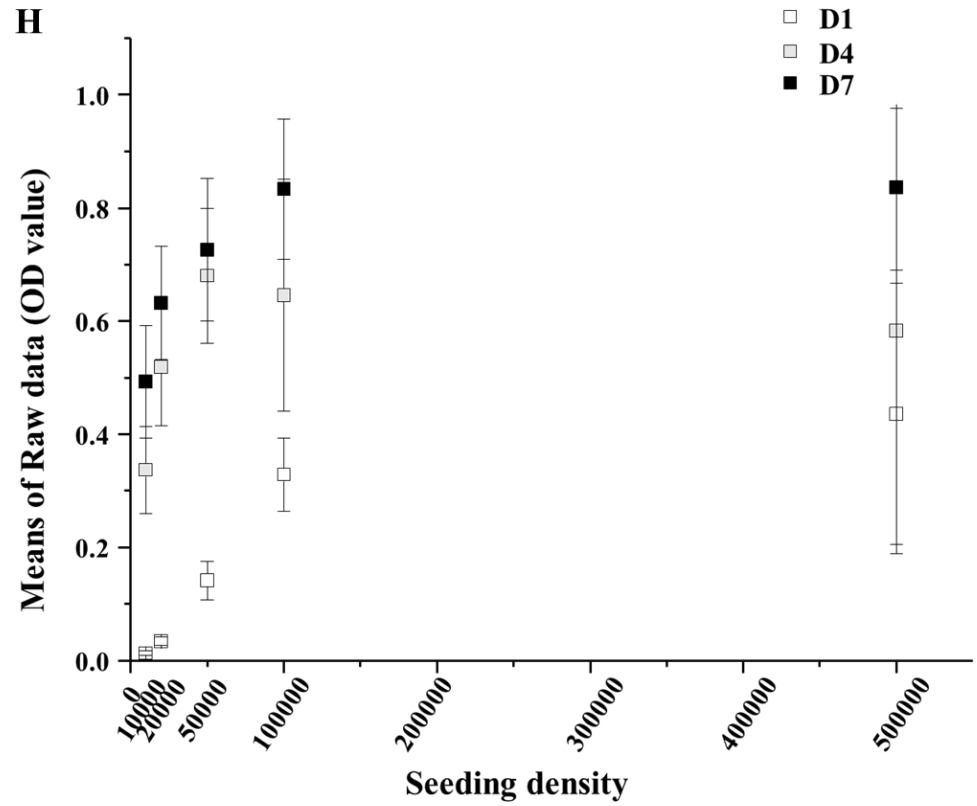
H
D1
D4
D7
Means of Raw data (OD value)
1.0
0.8
0.6
0.4
0.2
0.0
0
10000
20000
50000
100000
200000
300000
400000
500000
Seeding density

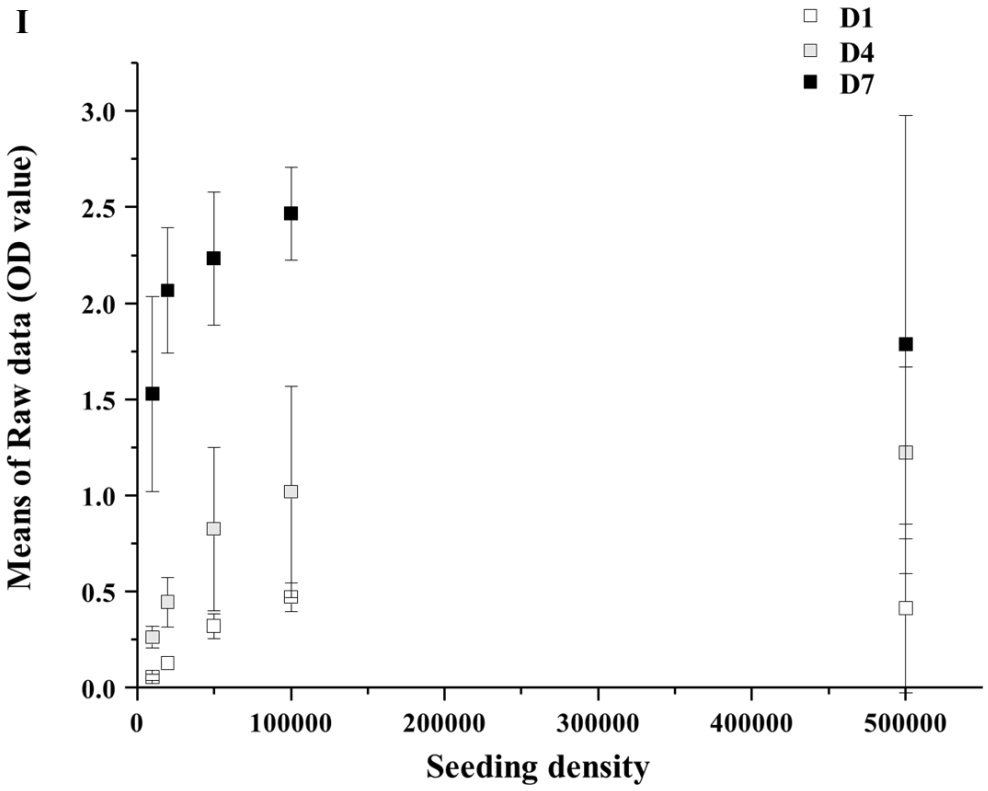

Figure 4.12 Cytotoxic effect of different concentration of $SrCl_2$ on the viability and proliferation of living cells in vitro

Three cell lines were involved in this test, including NIH3t3 fibroblasts (A, D, G), myoblasts C2C12 (B, E, H) and chondrogenic cell line ATDC5 (C, F, I). Before viability tests (A, B, C), cells were examined the seeding density test (G, H, I). Standard curve (D, E, F) for the cell seeding process was performed accompanying with the cell viability test. Series of cell number tests and cell viability tests of $SrCl_2$ on living cells in vitro were both examined by CyQUANT™ LDH Cytotoxicity Assay. Comparisons between experimental group and control group were analysed by ANOVA one way test (Tukey): * P<0.05; * * P<0.01; * * * P<0.001. For series number test of fibroblasts, seeding densities were 5K, 10K, 20K, 40K and 80K per well, and N=4, n=12; for series number test of myoblasts, seeding densities were 10K, 20K, 50K, 100K and 500K per well, and N=3, n=9; for series number test of chondrocytes, seeding densities were 10K, 20K, 50K, 100K and 500K per well, and N=3, n=9. For cell viability test of fibroblasts, seeding density was 5K cells per well and N=4, n=12; for cell viability test of myoblasts, seeding density was 5K cells per well and N=3, n=9; for cell viability test of chondrocytes, seeding density was 5K cells per well and N=3, n=9.

4.3.5 Rheological properties of alginate-based materials

Results of the evaluated rheological parameters of the alginate-based materials will be presented in this section.

4.3.5.1 Viscosities of alginate-based materials under constant shear rate

Samples were first measured the viscosity under the constant shear rate (shear stress) at room temperature (Figure 4.13). From results, all alginate-based materials performed constant viscosities (Figure 4.13 A) except the 6% and 8% alginate materials which displayed a slightly increase as the time increased. Comparing to 6% alginate, the viscosity of 8% alginate material increased more pronouncedly (Figure 4.13 B). Different from alginate-based materials, viscosity of the solution of 1% nanocellulose fibres (NCF) decreased as time increased (Figure 4.13 A), demonstrating the differences between nanocellulose fibre material and alginate materials. From the mean value of the viscosity of samples (Figure 4.13 C), as concentrations of pure alginate materials increased, their viscosities increased. Comparing to corresponding pure alginate materials, additional nanocellulose fibres within alginate, would increase the viscosity of the alginate materials, suggesting that the supplement of fibrous material to alginate material would alter the viscosity of materials.

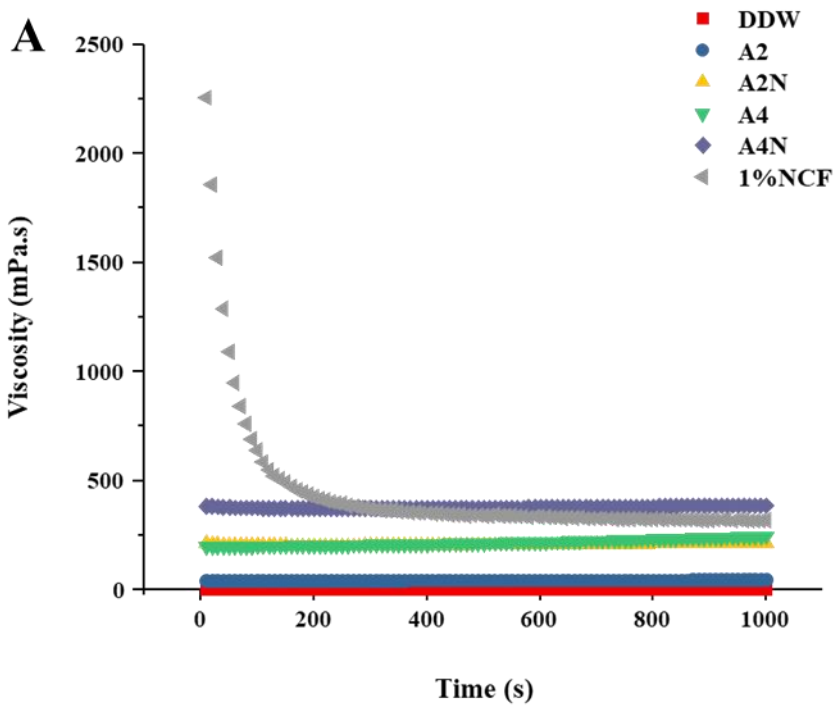

B

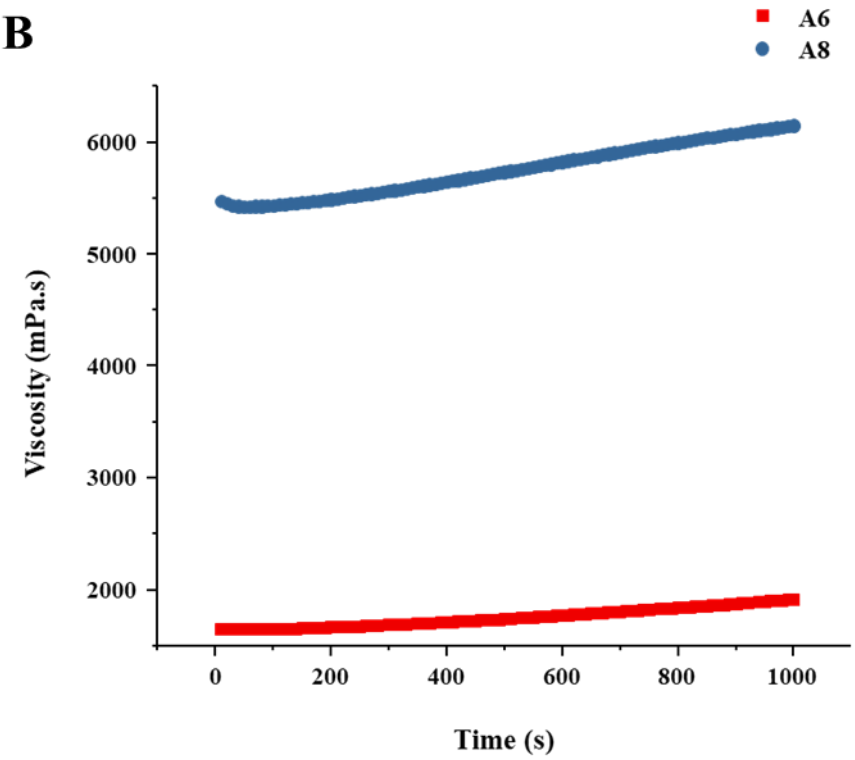

C

Samples (at 20°C)	N total	Mean	Standard Deviation	Minimum	Median	Maximum
2%Alginate (A2)	100	42.51492	1.808583	40.13	42.155	46.301
2%Alginate with 0.5%NCF (A2N)	100	207.0002	4.555693	202.07	205.925	219.97
4%Alginate (A4)	100	217.6107	14.46976	198.02	215.2933	246.2133
4%Alginate with 0.5%NCF (A4N)	100	378.4431	5.9404	371.5167	377.16	393.88
6%Alginate (A6)	100	1752.105	83.77739	1642.567	1740.033	1912.933
8%Alginate (A8)	100	5748.727	234.5875	5423.667	5735.833	6146.033
1% nanocellulose fibres (NCF)	100	441.638	304.8854	315.5067	341.7033	2256.333
Pure water (DDW)	100	0.8529	0.03408	0.77067	0.85382	0.92808

Figure 4.13 Comparison of the viscosities of the alginate-based materials and nanocellulose fibres at room temperature under constant shear rate

A-B: Viscosities of pure water, alginate-based materials and 1% nanocellulose fibres under the constant shear rate at room temperature plotted by the time graph. C: Table of the mean values of the viscosities of pure water, alginate-based materials and 1% nanocellulose fibres, measured by the rheometer under the constant shear rate at room temperature. A2:2% alginate; A2N: 2% alginate with 0.5%NCF; A4:4% alginate; A4N: 4% alginate with 0.5% NCF; A6; 6% alginate; A8: 8% alginate; NCF: nanocellulose fibres.

4.3.5.2 Steady state viscosity flow curves and shear-thinning properties of alginate-based materials

Steady state viscosity flow curve of each sample was measured under a constant shear rate condition and fitted by the power-law model to examine the shear thinning property of the tested liquid samples. The unitless parameter n was used to characterise the fluid. From results (Figure 4.14), all samples have the n values less than 1, indicating the pseudoplastic feature of these samples (non-Newtonian liquid). The lower the n value is, the greater the degree of shear-thinning would be. Hence, as the concentration of alginate materials increases, the shear thinning property of alginate materials become stronger. Additional fibrous material enhanced the shear thinning character of the alginate-based materials. From the information of the flow (K, n), computational fluid dynamic simulation could be applied and the injection force of these fluids from syringes could be estimated before further extrusion-based biomedical applications such as the extrusion-based 3D printing.

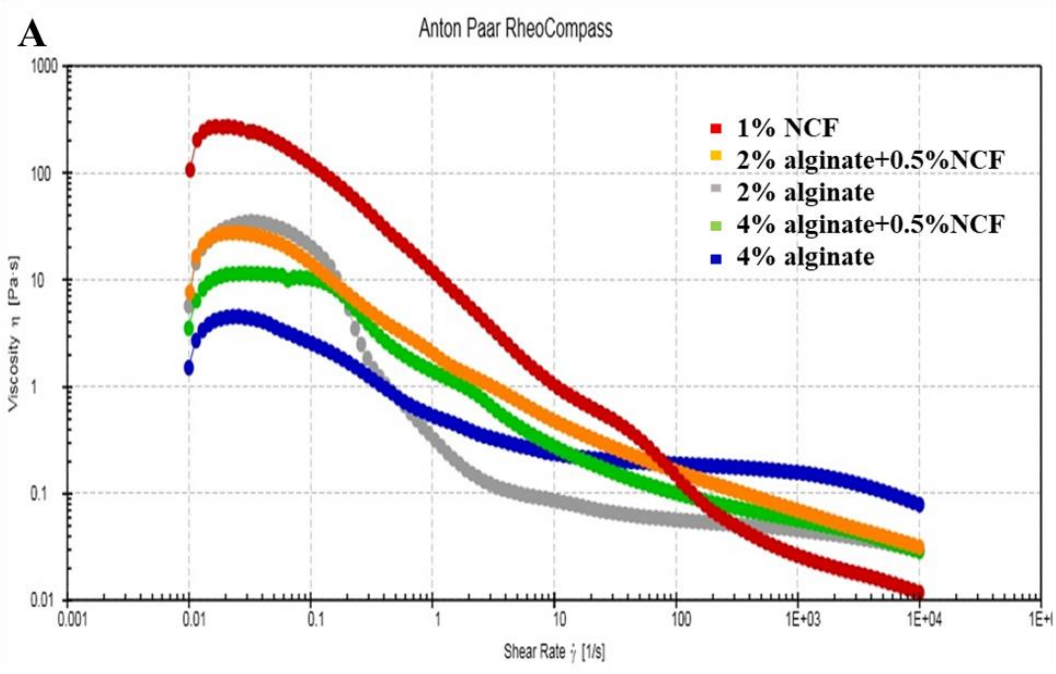

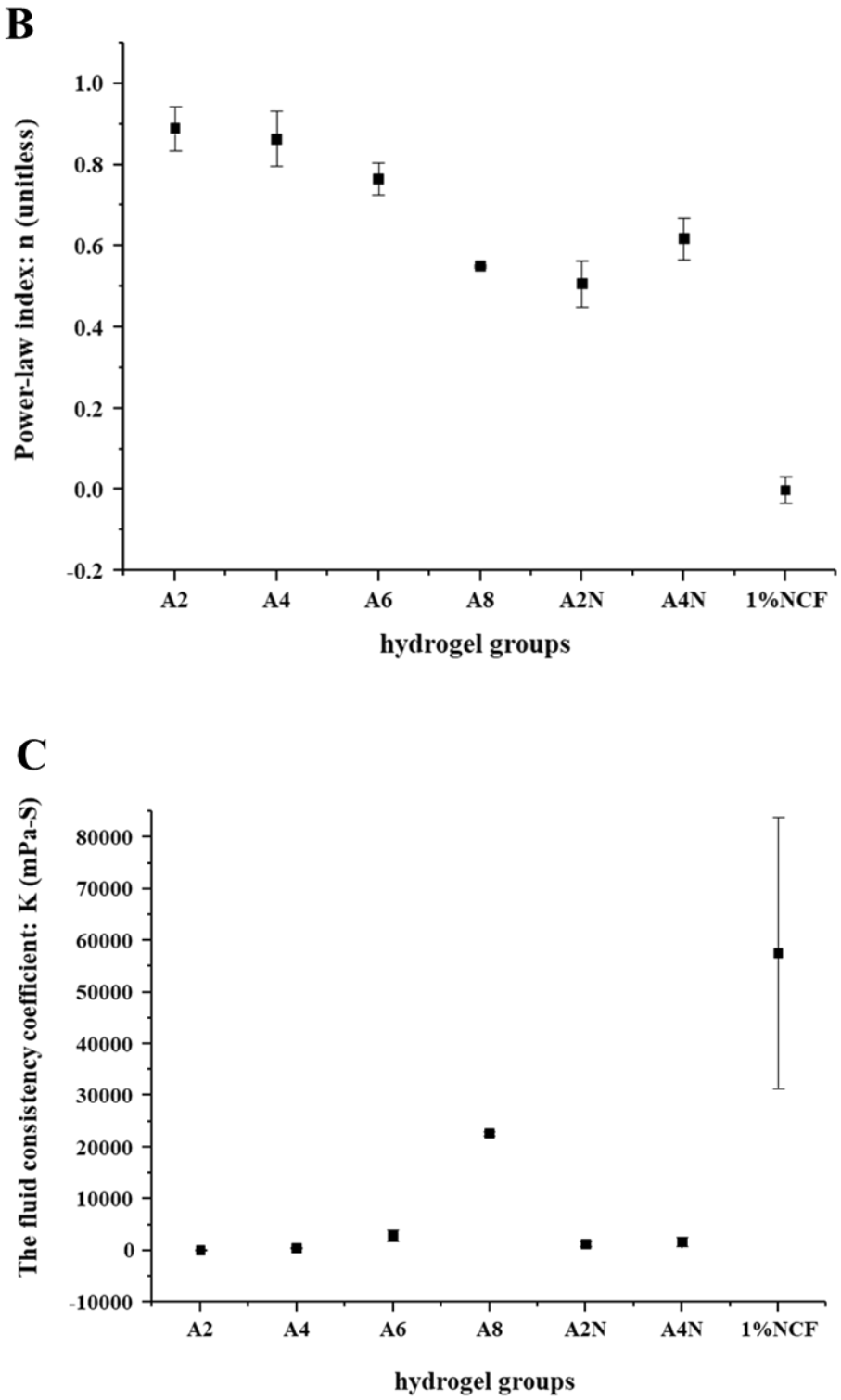

Figure 4.14 The steady state viscosity flow curves, power law index and the fluid consistency coefficients of the alginate-based materials

A: Steady state viscosity flow curves of the alginate-based materials and 1% nanocellulose fibres, measured by rheometer at room temperature. B: Power-law index of the alginate-based materials and 1% nanocellulose fibres calculated by the steady state viscosity flow curves. C: The fluid consistency coefficients of the alginate-based materials and 1% nanocellulose fibres calculated by the steady state viscosity flow curves. D: Table to show the

power-law index and the fluid consistency coefficients of the alginate-based materials and 1% nanocellulose fibres calculated by the steady state viscosity flow curves. A2:2% alginate; A2N: 2% alginate with 0.5%NCF; A4:4% alginate; A4N: 4% alginate with 0.5% NCF; A6; 6% alginate; A8: 8% alginate; NCF: nanocellulose fibres.

4.3.5.3 Amplitude sweep oscillatory test and the limit of the linear viscoelastic region of alginate-based materials

Amplitude sweep oscillatory test was performed to detect the limit of the linear viscoelastic region (LVER) indicating the viscoelastic property of the sample. If the storage modulus of the sample is greater than its loss modulus, the sample displays a solid or gel-like structure (viscoelastic solid material) under the condition of measurement. If the loss modulus is greater than its storage modulus, the sample presents a fluid structure (viscoelastic liquid), under the condition of measurement.

By an increasing energy from amplitude, the stability of the sample could be determined, and oscillation within the LVER will not have big impact on the structure of sample. The value of storage modulus usually represents the stiffness of the sample or the strength of the gel. From results of the storage curves, all pure alginate samples have longer LVER in the logarithmic plot of storage modulus vs shear strain (Figure 4.15 A), indicating more stabilities of their physical structures. Comparing to pure alginate samples, additional fibres to alginate and the 1%NCF materials, had shorter LVER, suggesting the less stabilities of their physical structures. Approximately 3% shear strain was the limit of the LVER of all tested samples which was returned by the analysis of the program of the rheometer after measurement. To compromise the differences of the end of the LVER of alginate materials with/without NCF and the NCF materials, within 1% shear strain would be used for all samples in the subsequent frequency oscillatory test.

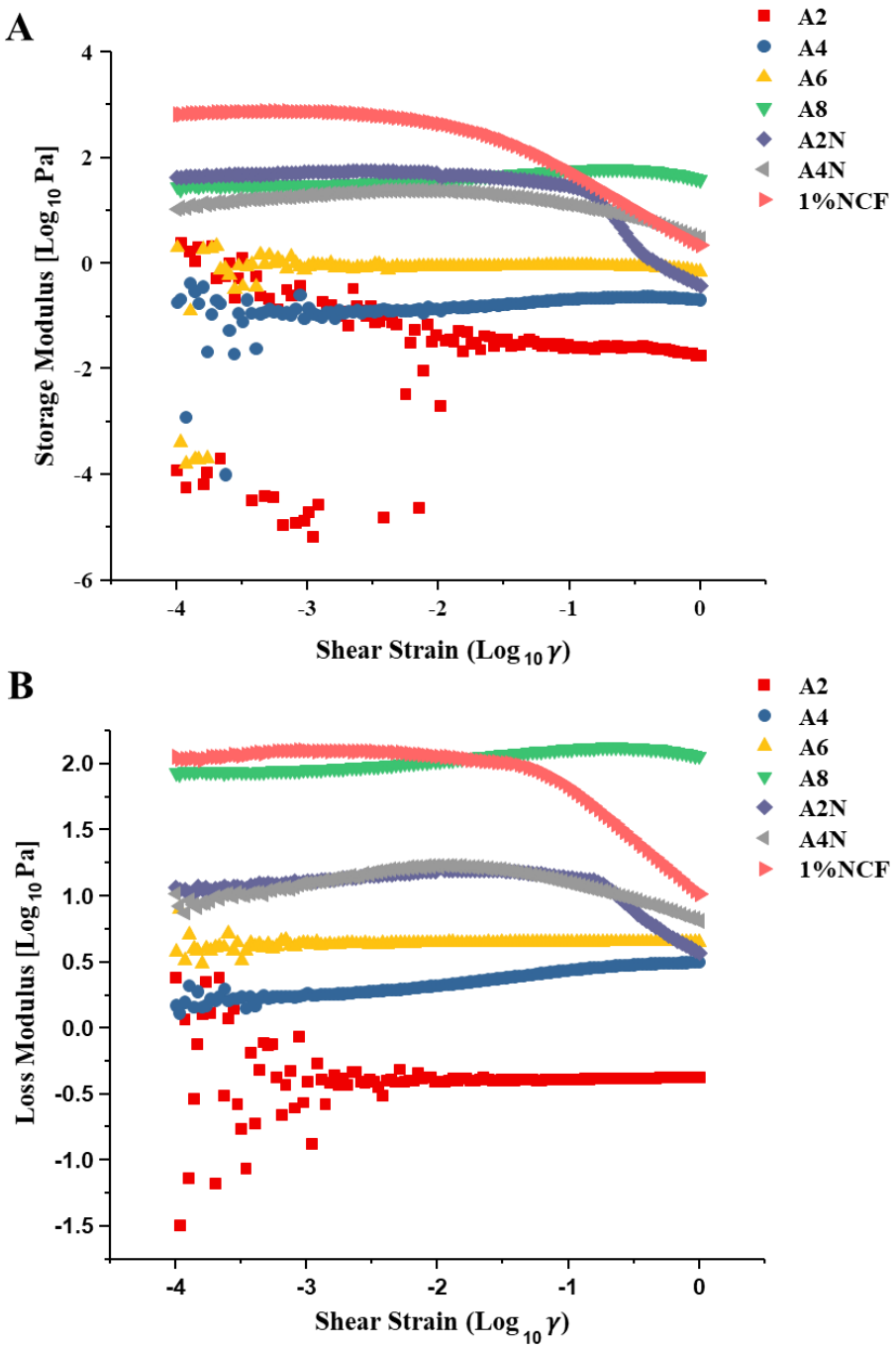

Figure 4.15 Storage modulus and loss modulus of the alginate-based materials and 1% cellulose fibres examined by the amplitude sweep test, were presented by the modulus vs shear strain in logarithmic graph A: Storage modulus of the alginate-based materials and 1% nanocellulose fibres plotted by the shear strain in logarithmic graph. B: Loss modulus of the alginate-based materials and 1% nanocellulose fibres plotted by the shear strain in logarithmic graph. A2:2% alginate; A2N: 2% alginate with 0.5%NCF; A4:4% alginate; A4N: 4% alginate with 0.5% NCF; A6; 6% alginate; A8: 8% alginate; NCF: nanocellulose fibres.

The value of loss modulus usually displays the lost portion of energy due to internal friction generated from shearing. Before sample starts to flow, storage modulus is still dominating the

structure. Once the energy from deformation is greatly lost, to generate more movable pieces of small fragments, the inner structure of sample could not be kept as an integrated network and starts showing the internal viscosity. As the increase in the amount of the movable pieces inside the sample, the viscous behaviour would finally dominate the physical structure and the material begins to flow. The point where the loss modulus is greater than the storage modulus (exceeding the crossover point where the value of loss modulus equals the value of storage modulus), is termed the yield point. The yield point (τy) could also be termed yield stress in practice, which is determined by the value of the shear stress at the limit of the LVER.

The maximal value of the loss modulus is often close or at the same point of the crossover point. The shape of the part of loss curve leaving the LVER, could be used to determine the behaviour of the gel. From results of the loss curves, all pure alginate samples have mild curve without a pronounced change and the LVER, in the logarithmic plot of loss modulus vs shear strain (Figure 4.15 B), indicating that the dominant structures of the samples were liquid and the inner structure of these samples would not be broken during the shearing. Comparing to the curves of pure alginate materials, the curves of 1%NCF and alginate materials with additional NCF, presented consistent and mild portions of curves with the less pronounced maximal values of both of the loss and storage modulus before the LVER. Their curves contain the LVER, in which the values of storage modulus are greater than that of the loss modulus and in the loss curve there were distinctly maximal values of the modulus at higher strain values. After the LVER the portions of the curves of both of the loss and storage modulus were sharply decreased, where the values of loss modulus were greater than that of the storage modulus. In these samples, their internal superstructures formed the consistent 3D networks at the initial part of the test. Small internal cracks were formed and grown as the

breakdown of the internal superstructures of the samples started and increased. The whole process of the breakdown of the structure was delayed but as the increase in the strain, the whole structure would be eventually destroyed presenting the viscous feature of the viscoelastic behaviours.

4.3.5.4 Amplitude sweep test and the flow point (τf) of alginate-based materials

From results of the amplitude sweep oscillatory test, the flow point of the samples could also be determined from the representational graph of shear stress vs complex modulus (the storage and loss modulus). The flow point is another important parameter to dynamically characterise the viscoelastic materials, which could also be termed flow stress. It is the value of the shear stress at the crossover point where the value of the storage modulus equals to that of the loss modulus. From results (Figure 4.16), as the shear increased, only 1% NCF and alginate materials with additional NCF displayed the LVER in the curves, indicating the viscous behaviours after the breakdown of the internal superstructures of these samples. Comparing to that, there were no distinct changes of curves of the pure alginate materials (Figure 4.16 D-G), where there were no flow points, yield points and LVER, their values of the loss modulus were consistently greater than that of the storage modulus, suggesting their consistent internal structures in the liquid form during shearing. For those samples with flow points (τy), yield points (τf) and the LVER on the curves (Figure 4.16 A-C), in the region between the yield point and flow point on the curves, their values of the storage modulus are greater than that of the loss modulus. Samples still presented the solid or gel-like features at this period of time, although the internal structures of these samples had already started breaking accompanying with the decreasing strengths of the sample structures. These results suggested that the additional NCF would enhance the viscoelastic properties of the alginate

materials, probably by forming additional internal superstructures.

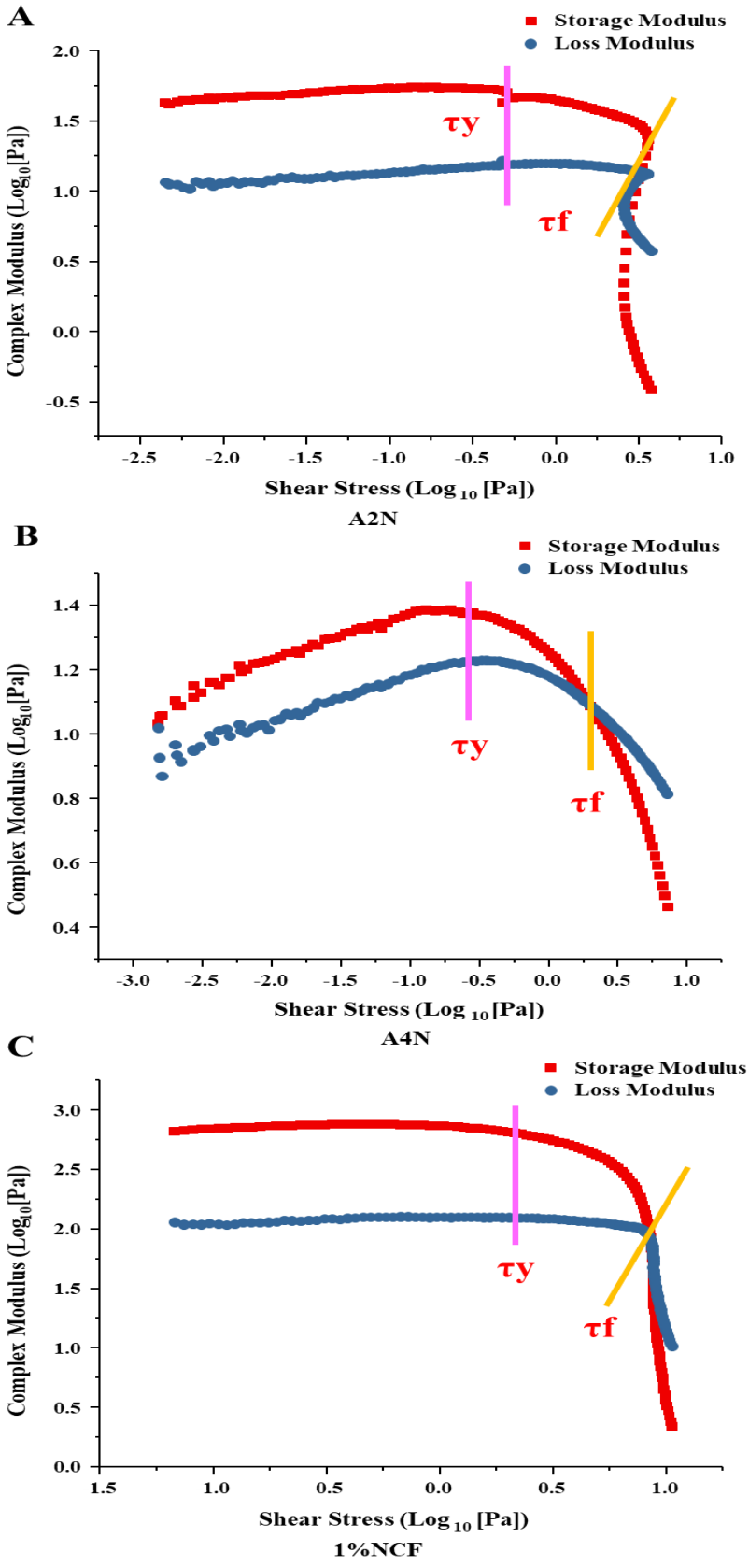

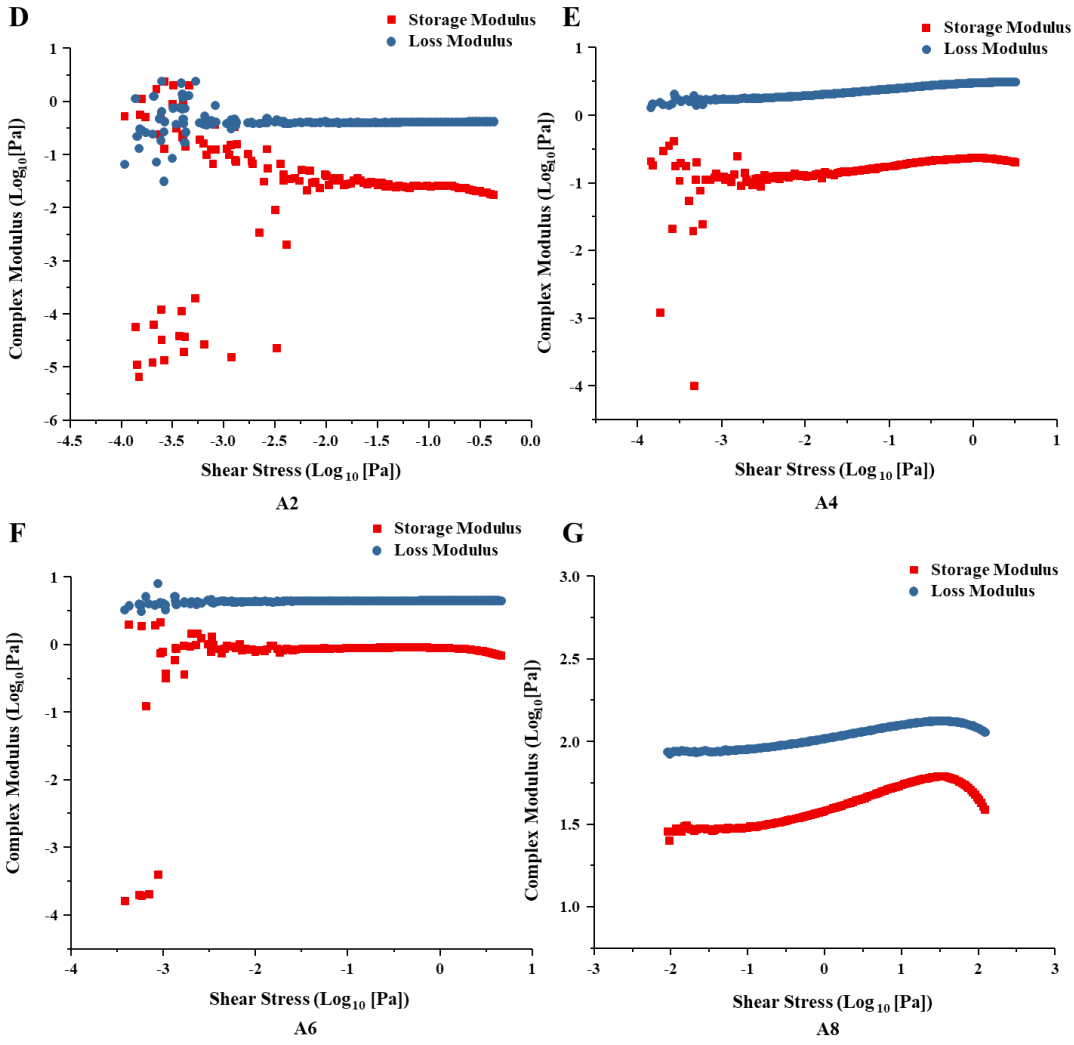

Figure 4.16 Storage modulus and loss modulus of the alginate-based materials and 1% nanocellulose fibres examined by the amplitude sweep test were presented by the shear stress vs storage modulus and loss modulus in logarithmic graph

A: Storage modulus and loss modulus of 2%alginate with 0.5% nanocellulose fibres by the amplitude sweep test were presented by the shear stress vs storage modulus and loss modulus in logarithmic graph. B: Storage modulus and loss modulus of 4%alginate with 0.5% nanocellulose fibres by the amplitude sweep test were presented by the shear stress vs storage modulus and loss modulus in logarithmic graph. C: Storage modulus and loss modulus of 1% nanocellulose fibres by the amplitude sweep test were presented by the shear stress vs storage modulus and loss modulus in logarithmic graph. D: Storage modulus and loss modulus of 8%alginate material by the amplitude sweep test were presented by the shear stress vs storage modulus and loss modulus in logarithmic graph. E: Storage modulus and loss modulus of 2%alginate material by the amplitude sweep test were presented by the shear stress vs storage modulus and loss modulus in logarithmic graph. F: Storage modulus and loss modulus of 4%alginate material by the amplitude sweep test were presented by the shear stress vs storage modulus and loss modulus in logarithmic graph. G: Storage modulus and loss modulus of 6%alginate materials by the amplitude sweep test were presented by the shear stress vs storage modulus and loss modulus in logarithmic graph. The yield point τy and flow point τf of each material were estimated and labelled on the associated graph if any. A2:2% alginate; A2N: 2% alginate with 0.5%NCF; A4:4% alginate; A4N: 4% alginate with 0.5% NCF; A6; 6% alginate; A8: 8% alginate; NCF: nanocellulose fibres.

4.3.5.5 Frequency sweep oscillatory test of alginate-based materials

Frequency sweep oscillatory test was performed to investigate the behaviours of samples at room temperature. From results (Figure 4.17), all samples were performed as typical solutions of polymers. However, on the details, due to the additional NCF to the alginate materials (Figure 4.19), the viscoelastic properties of alginate materials were altered. Comparing to the pure alginate materials (2% and 4%) (Figure 4.19 A, C), samples of alginate with additional NCF (2% alginate with 0.5%NCF, 4% alginate with 0.5% NCF) presented more like the viscoelastic solid materials (Figure 4.19 B, D), in which the value of storage modulus was greater than the loss modulus in the area of the curve before the crossover point (flow point) and after the point, the value of loss modulus was greater than the storage modulus (Figure 4.18). The trend of the pure alginate materials, was almost a constant value similar to that of the gel-like materials. While the trend of phase angles of alginate materials with additional NCF was increased similar to that of the viscoelastic solid materials (Figure 4.18 B). These results indicated that the additional NCF materials enhanced the viscoelastic property of the alginate materials.

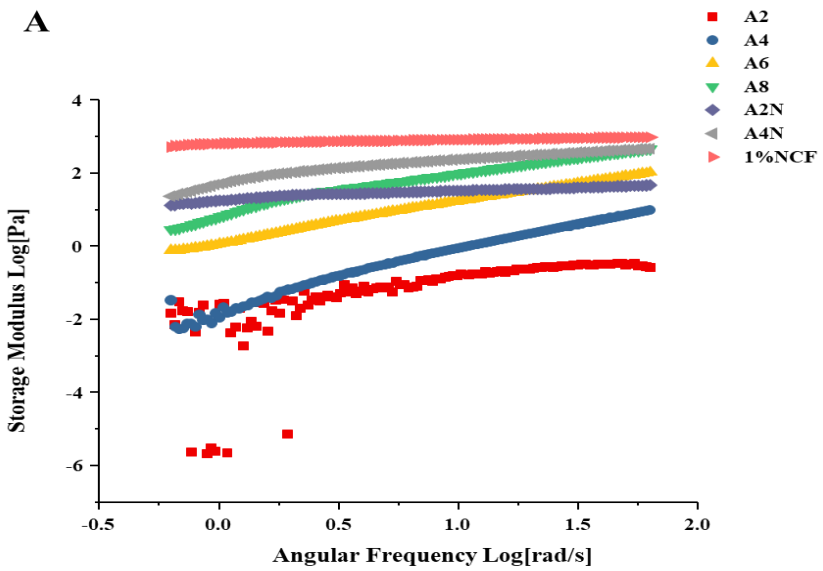

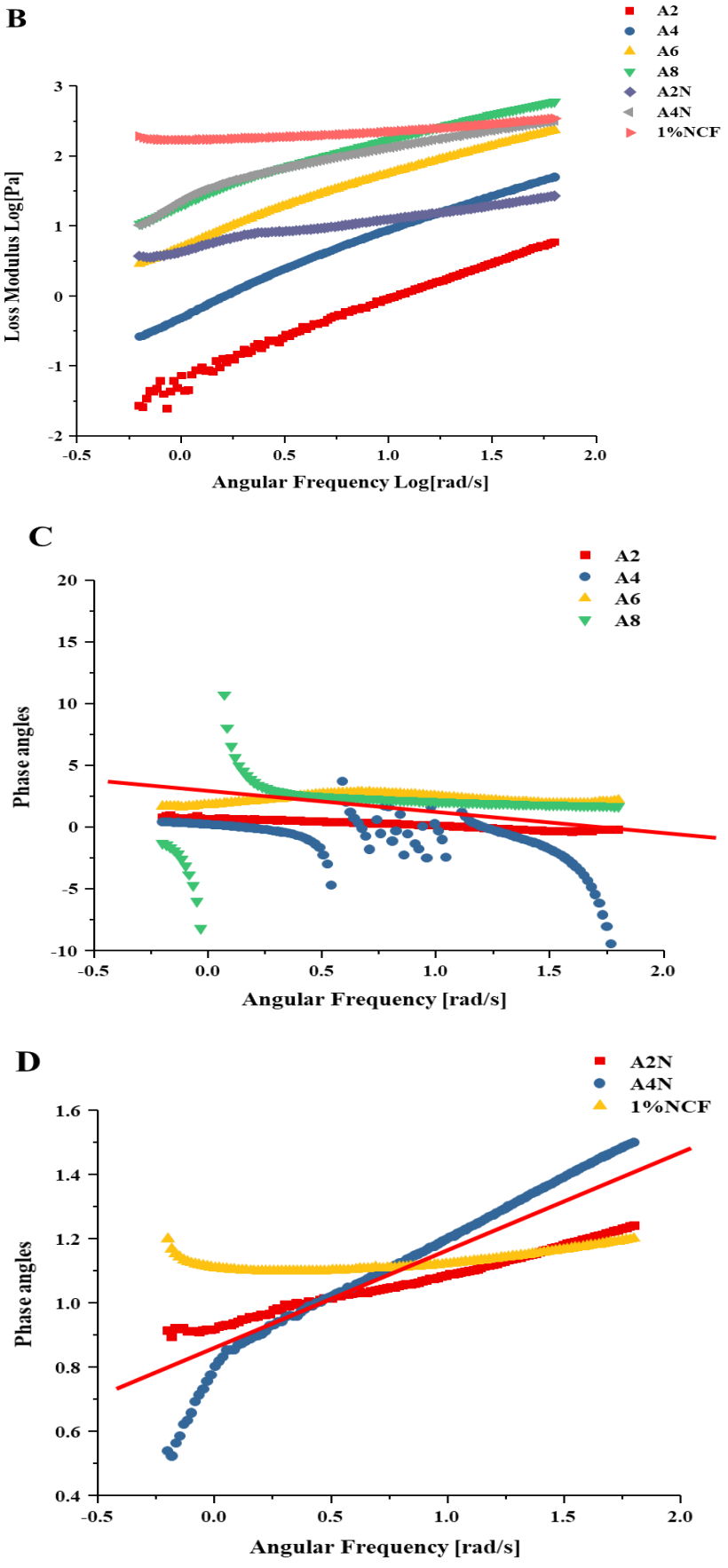

Figure 4.17 Storage modulus and loss modulus of the alginate-based materials and 1% cellulose fibres

examined by the frequency sweep oscillatory test were presented by the modulus vs angular frequency in logarithmic graph respectively and the schematic images of the trend of corresponding phase angles during test

A: Comparison of the logarithmic graphs of the storage modulus vs angular frequency of the alginate-based materials and 1% nanocellulose fibres measured by the frequency sweep oscillatory test. B: Comparison of the logarithmic graphs of the loss modulus vs angular frequency of the alginate-based materials and 1% nanocellulose fibres measured by the frequency sweep oscillatory test. C: Schematic image of the trend of the phase angles of pure alginate materials during test. Schematic linear fitting line is in red. D: Schematic image of the trend of the phase angles of the alginate materials with additional cellulose fibres and the 1% cellulose fibres, during test. Schematic linear fitting line is in red. A2:2% alginate; A2N: 2% alginate with 0.5%NCF; A4:4% alginate; A4N: 4% alginate with 0.5% NCF; A6; 6% alginate; A8: 8% alginate; NCF: nanocellulose fibres.

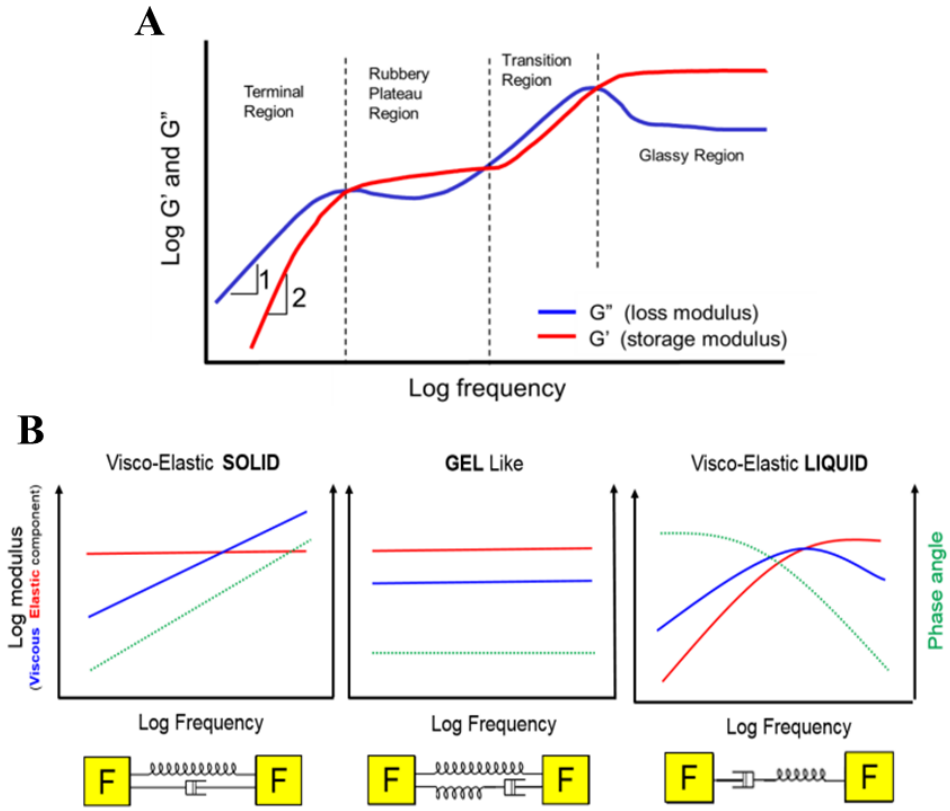

Figure 4.18 Schematic images of a typical viscoelastic spectrum for an entangled polymer system spanning a range of frequencies, and a typical frequency response for a viscoelastic solid, viscoelastic liquid and a gel in oscillatory testing [39].

A: A schematic image of a typical viscoelastic spectrum from polymers. B: A schematic image of atypical frequency response for polymers with different viscoelasticity [15].

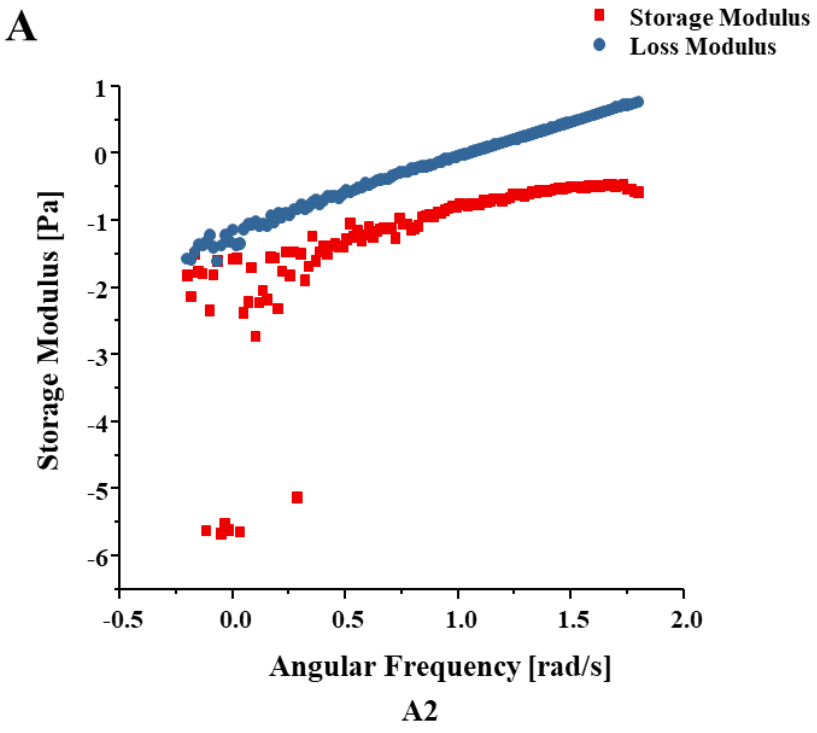
A
Storage Modulus
Loss Modulus
Storage Modulus [Pa]
1
0
-1
-2
-3
-4
-5
-6
-0.5
0.0
0.5
1.0
1.5
2.0
Angular Frequency [rad/s]

A2

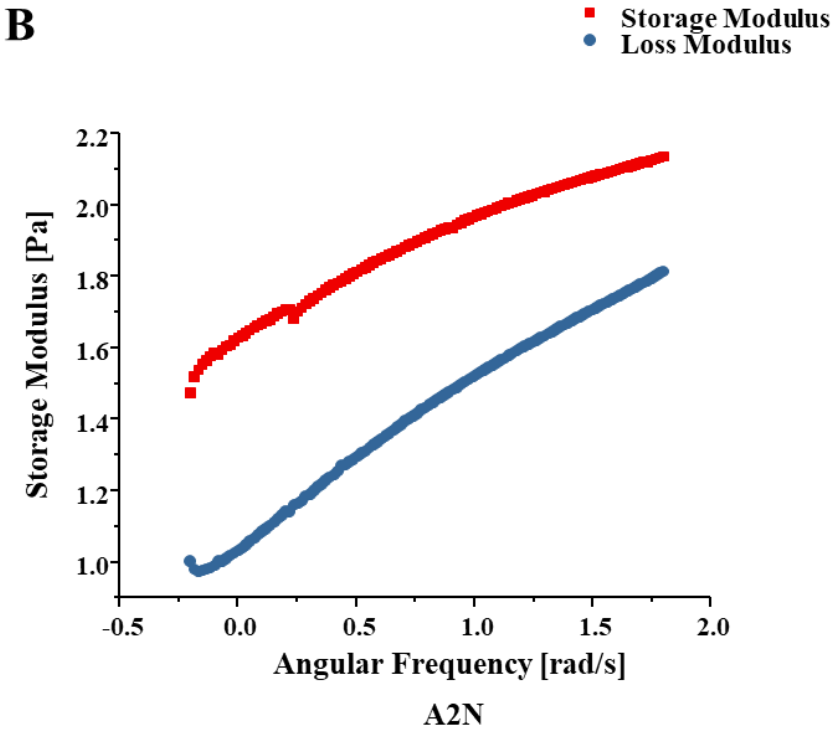
B
Storage Modulus
Loss Modulus
Storage Modulus [Pa]
2.2
2.0
1.8
1.6
1.4
1.2
1.0
-0.5
0.0
0.5
1.0
1.5
2.0
Angular Frequency [rad/s]

A2N

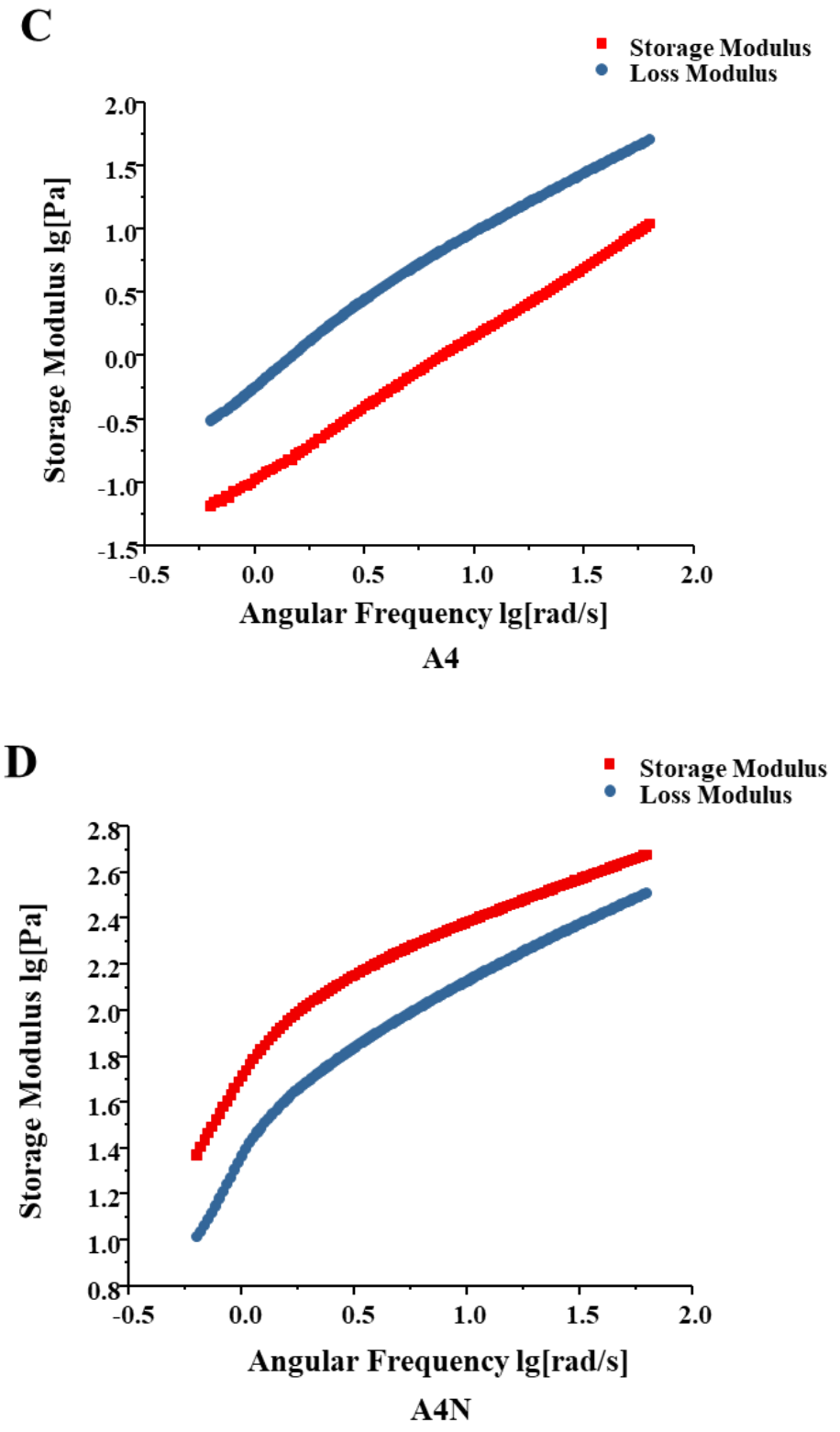

Figure 4.19 Comparison of the frequency sweep of 2% and 4% alginate materials with/without nanocellulose fibres, presented with angular frequency vs storage modulus and loss modulus in logarithmic graph

A: Logarithmic graph of the storage modulus and loss modulus vs angular frequency of the 2% alginate material examined by the frequency sweep at room temperature. B: Logarithmic graph of the storage modulus and loss modulus vs angular frequency of the 2% alginate with 0.5% nanocellulose fibres examined by the frequency

sweep at room temperature. C: L logarithmic graph of the storage modulus and loss modulus vs angular frequency of the 4% alginate material examined by the frequency sweep at room temperature. D: L logarithmic graph of the storage modulus and loss modulus vs angular frequency of the 4% alginate with 0.5% nanocellulose fibres examined by the frequency sweep at room temperature. A2:2% alginate; A2N: 2% alginate with 0.5%NCF; A4:4% alginate; A4N: 4% alginate with 0.5% NCF; NCF: nanocellulose fibres.

4.3.6 Biocompatibilities of the alginate-based materials for 2D cell culture

Biocompatibility of the alginate-based materials on cells cultured in 2D condition regarding the cell viability and cellular morphology will be described in this section.

4.3.6.1 Viabilities of ATDC5 cells cultured on PLL-coated alginate-based hydrogel thin sheets

To validate the biocompatibility of the alginate-based materials to be used in tissue engineering fabrication, the viability of cells cultured on the 2D materials was examined by Live and dead assay. Due to the inert feature of alginate materials with insufficient bioactive groups for cell to adhere to, surface modification by physically coating poly-L-lysine molecules on the thin layer of alginate-based materials was applied before seeding cells. General viability of cells was examined after 1-, 2-, 4- and 7-days incubation by normal inverted phase-contract microscope and the Live and dead assay was performed after 7 days incubation. From results (Figure 4.20), after coating, cells were successfully attached to the alginate-based materials after one day, however, from day 2 to day 7, cells were aggregated on the materials, suggesting the lack of bioactive factors on the materials for cells to migrate. From results of staining after 7 days incubation, most cells in aggregate were alive, suggesting that these materials and the cultural system did not have toxic effect on the cell viability.

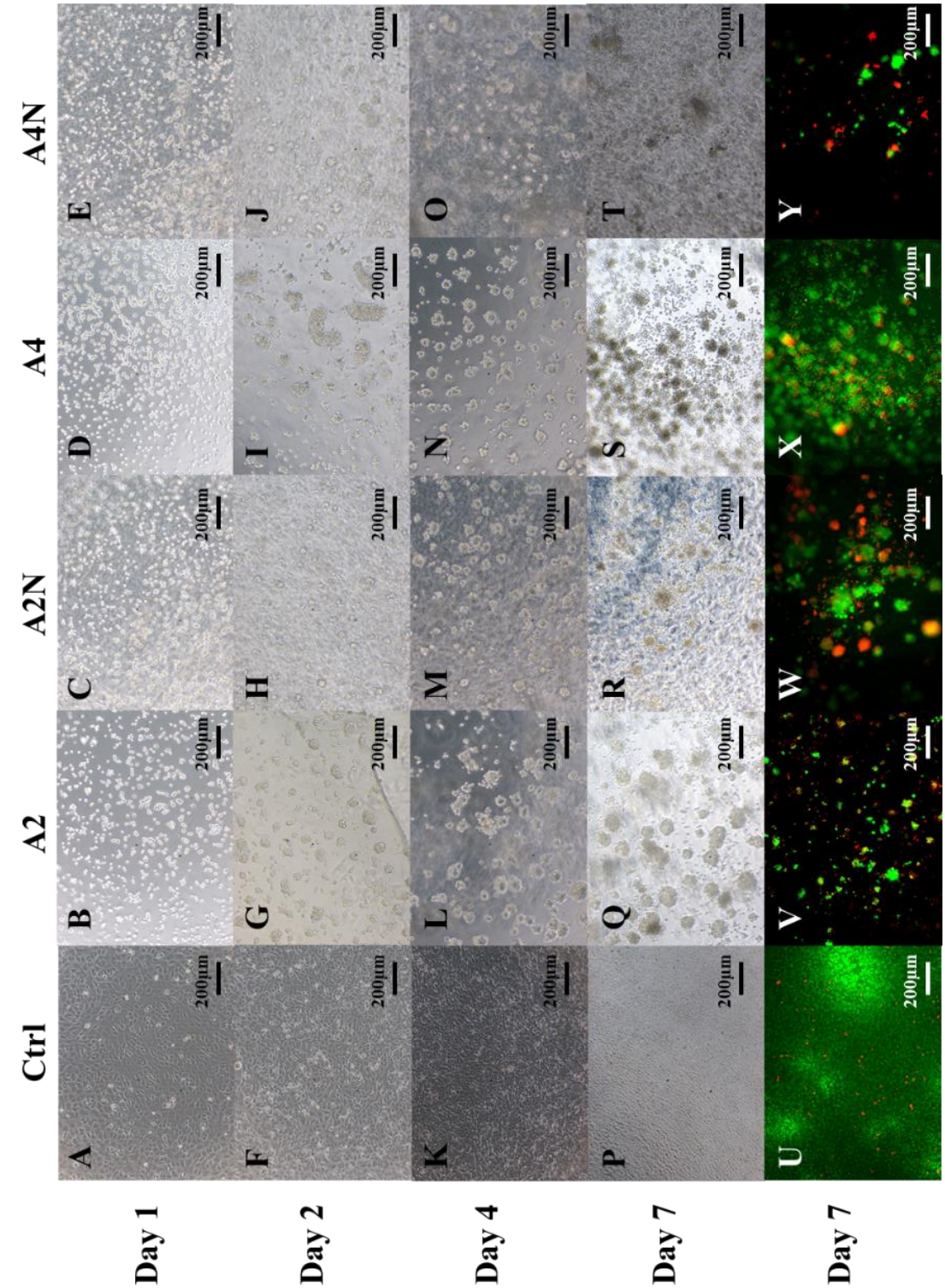

Figure 4.20 Viabilities of ATDC5 cells seeded on PLL-coated single layer of the alginate-based thin sheet (0.6mm thickness) at day 1, 2, 4 and 7 days

A-F-K-P: Images of cells cultured on the tissue culture plate without alginate sheet or coating after 1-, 2-, 4-, and 7-days incubation, taken by the normal inverted phase-contrast light microscope. B-G-L-Q: Images of cells cultured on the PLL-coated hydrogel sheets made up of 2% alginate after 1-, 2-, 4-, and 7-days incubation, taken by the normal inverted phase-contrast light microscope. C-H-M-R: Images of cells cultured on the PLL-coated hydrogel sheets made up of 2% alginate with 0.5% nanocellulose fibre after 1-, 2-, 4-, and 7-days incubation,

taken by the normal inverted phase-contrast light microscope. D-I-N-S: Images of cells cultured on the PLL-coated hydrogel sheets made up of 4% alginate after 1-, 2-, 4-, and 7-days incubation, taken by the normal inverted phase-contrast light microscope. E-J-O-T: Images of cells cultured on the PLL-coated hydrogel sheets made up of 4% alginate with 0.5% nanocellulose fibre after 1-, 2-, 4-, and 7-days incubation, taken by the normal inverted phase-contrast light microscope. U-V-W-X-Y: Merged fluorescent images of the viability of cells after 7 days culture on tissue culture plate and on the alginate-based thin sheets examined by Live and Dead assay, in which the green colour shows the live cells and red colour shows the dead cells. The scale bar is 200 µm. Ctrl: control group; A2:2% alginate; A2N: 2% alginate with 0.5%NCF; A4:4% alginate; A4N: 4% alginate with 0.5% NCF; NCF: nanocellulose fibres.

4.3.6.2 Morphologies of cells cultured on PLL-coated alginate-based hydrogel thin sheets

To confirm the results, morphologies of cells cultured on the coated materials were also examined by immunofluorescent staining the cytoskeletal F-actin molecules of cells. Two cell lines were used in this study, and they were reported the similar results. From images (Figure 4.21), after one day incubation, cells could attach to the 2D alginate-based materials and spread but not fully stretched, even they were cultured on the alginate with highest concentration (indicating highest mechanical property), comparing to cells cultured on normal tissue culture plate. In chondrocytes (Figure 4.22), this phenomenon was more pronounced, suggesting the more sensitivity of chondrocytes than fibroblasts on the microenvironments.

From 2D results, the biocompatibility of alginate-based materials tested in this study could be confirmed, although the cellular adherence of the materials was not satisfied and this could not be addressed by physical coating, especially for long-term culture purposes.

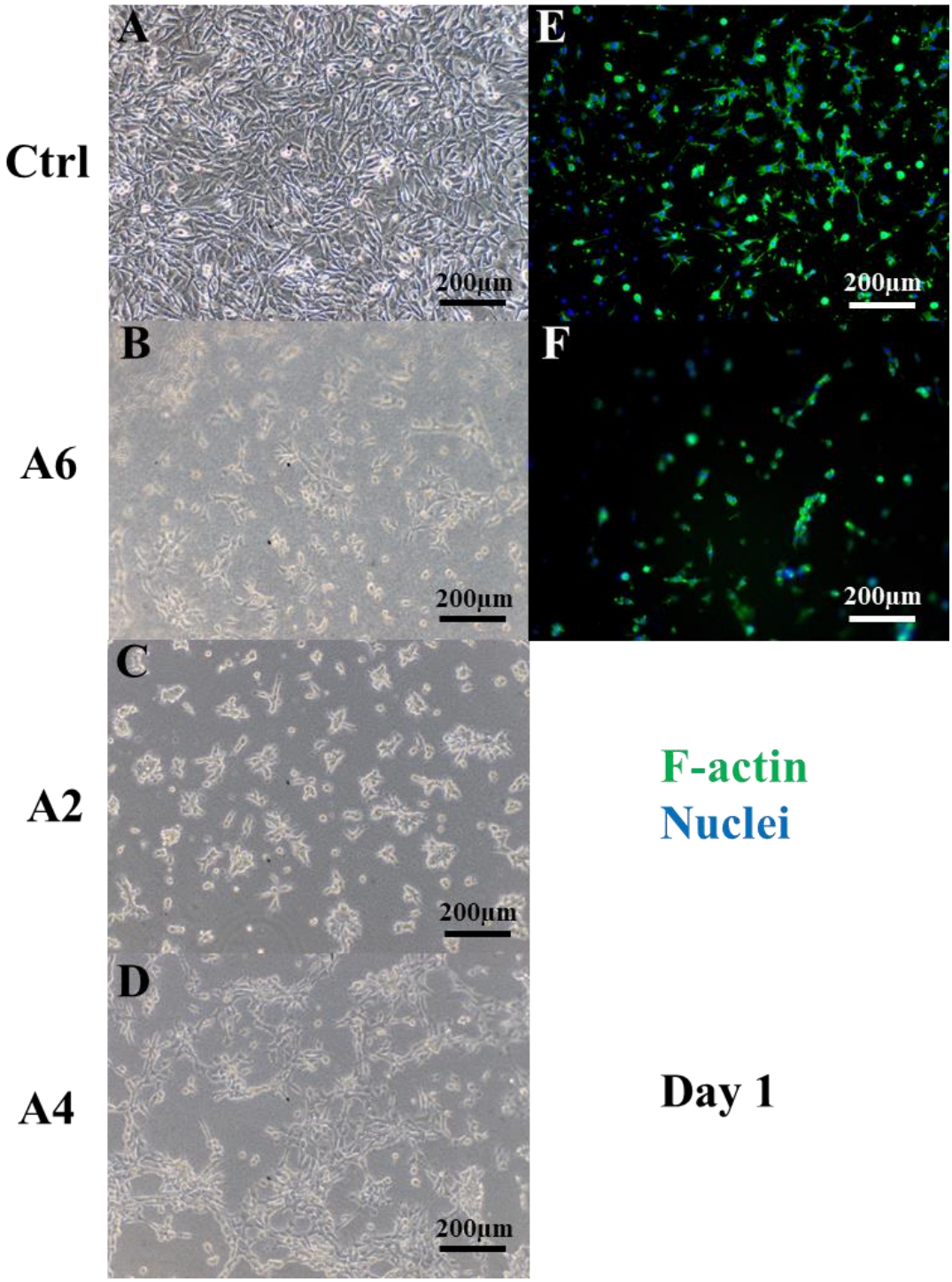

Figure 4.21 Morphologies of NIH3t3 fibroblasts seeded on PLL-coated single layer of alginate-based thin sheets (0.6mm thickness) at day one

A-D: Images of fibroblasts seeded on tissue culture plate without any alginate hydrogel sheet and coating, 6%, 2% and 4% alginate hydrogel thin sheets respectively, after one day incubation, taken by the normal inverted phase-contrast light microscope. E-F: Immunofluorescent images of the cytoskeletal F-actin of the cells cultured on the tissue culture plate and 6% alginate hydrogel thin sheet after one day incubation, in which the green colour shows the cytoskeletal F-actin of cells and blue colour represents the nuclei of cells. The scale bar is 200 μm.

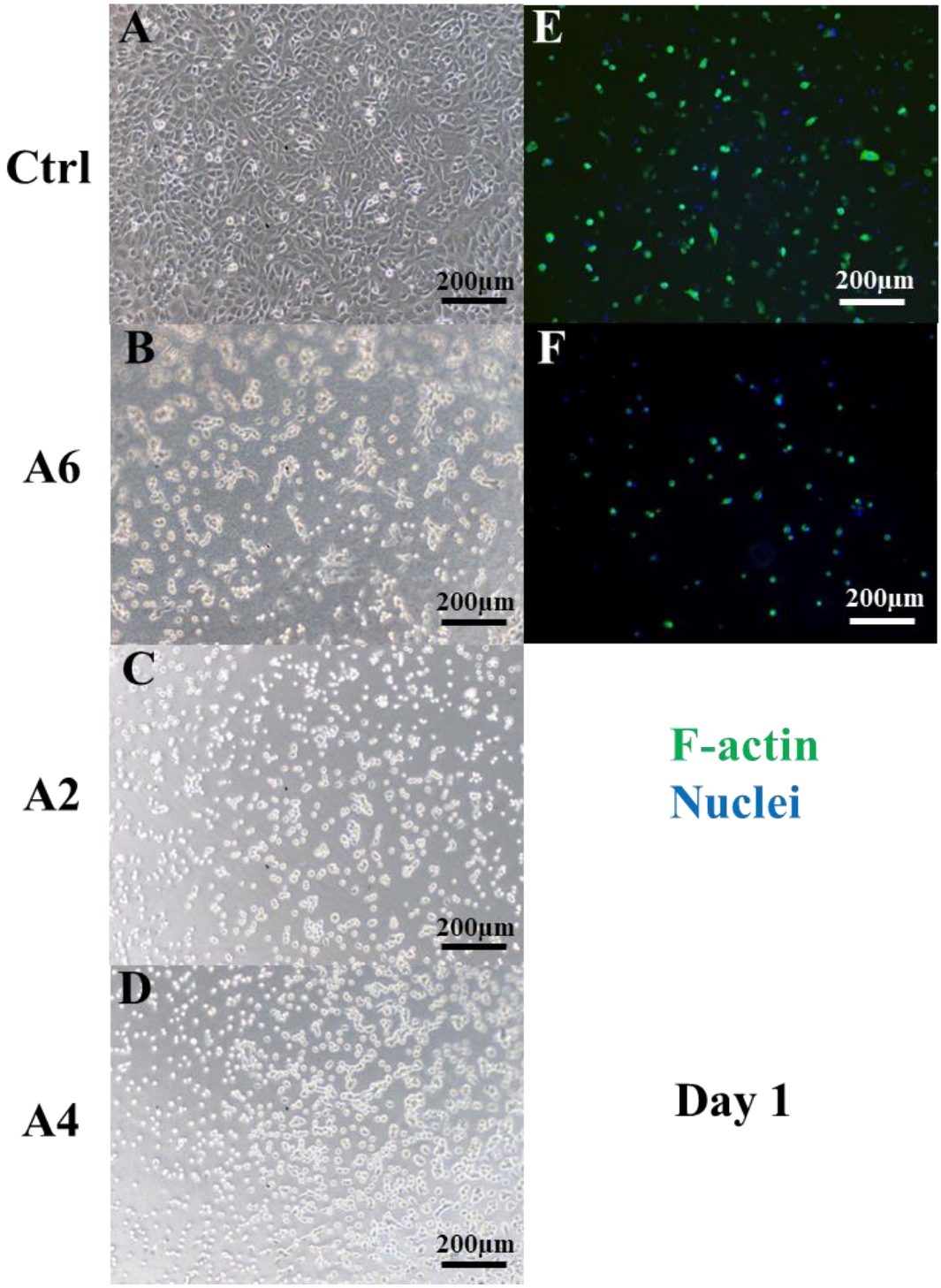

Figure 4.22 Morphologies of ATDC5 cells seeded on PLL-coated single layer alginate thin sheet (0.6mm thickness) at day one

A-D: Images of ATCD5 cells seeded on tissue culture plate without any alginate hydrogel sheet and coating, 6%, 2% and 4% alginate hydrogel thin sheets respectively, after one day incubation, taken by the normal inverted phase-contrast light microscope. E-F: Immunofluorescent images of the cytoskeletal F-actin of the cells cultured on the tissue culture plate and 6% alginate hydrogel thin sheet after one day incubation, in which the green colour shows the cytoskeletal F-actin of cells and blue colour represents the nuclei of cells. The scale bar is 200 µm.

4.3.7 Biocompatibilities of alginate-based hydrogels for 3D cell culture

To validate the biocompatibility of the alginate-based hydrogels to be used in tissue engineering fabrication, the viability of cells cultured inside 3D hydrogels was also examined by Live and dead assay. From results (Figure 4.23), after 7 days 3D culture *in vitro*, most cells were alive and distributed inside the alginate-based hydrogels. In pure alginate hydrogels, some aggregated cells were observed (Figure 4.24).

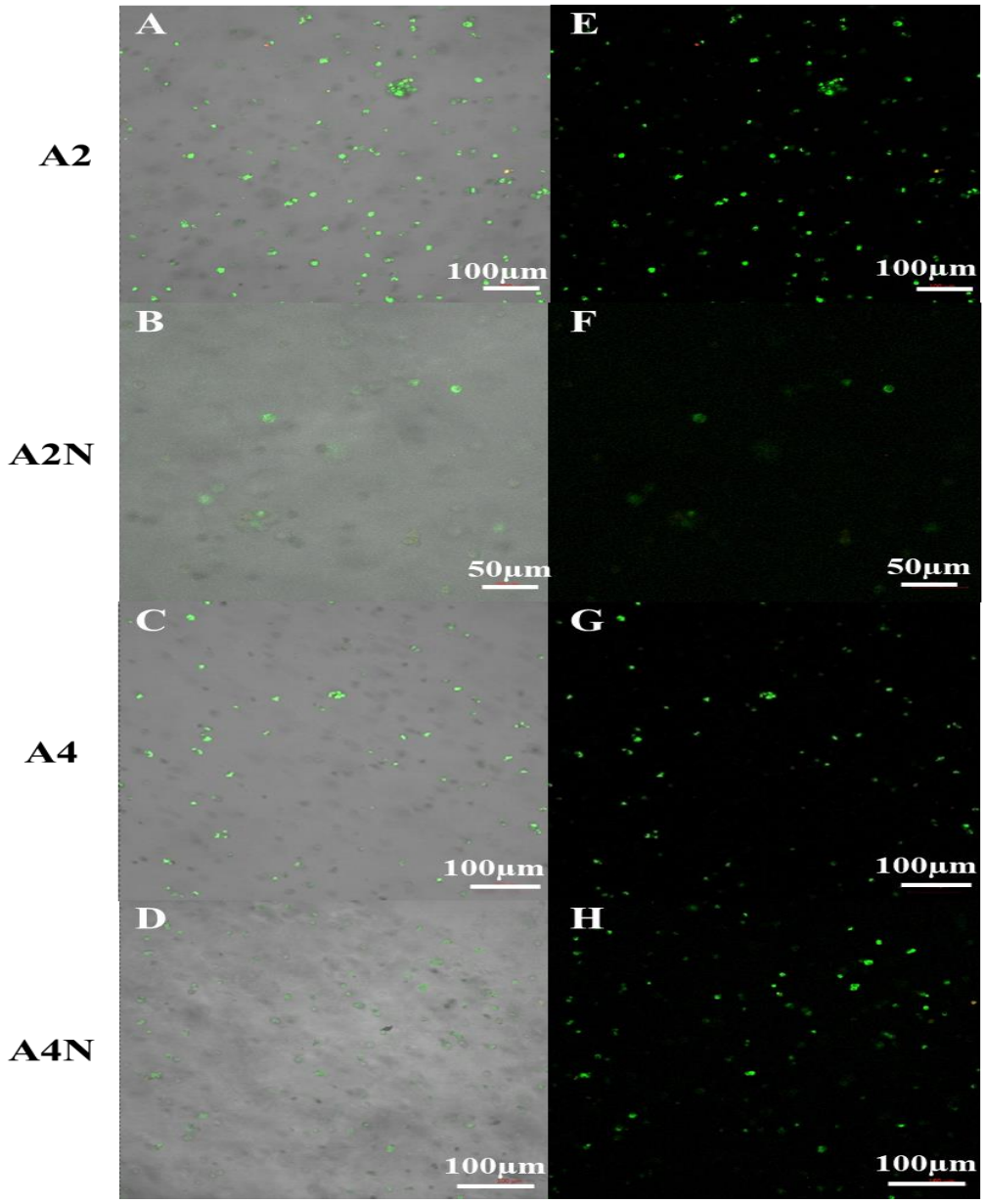

Figure 4.23 Viabilities of ATDC5 cells during 3D chondrogenesis inside the alginate-based hydrogels for 7

days

A-D: Merged confocal images (bright field, green and red channels) of the viability of ATDC5 cells 3D cultured in 2% alginate, 2% alginate with 0.5% NCF, 4% alginate and 4% alginate with 0.5% NCF hydrogels and differentiation for 7 days. E-H: Merged fluorescent images (green and red channels) of the viability of ATDC5 cells 3D cultured in 2% alginate, 2% alginate with 0.5% NCF, 4% alginate and 4% alginate with 0.5% NCF hydrogels and differentiation for 7 days. Green colours display the viable cells and red colours show the dead cells. The scale bar is 100 µm.

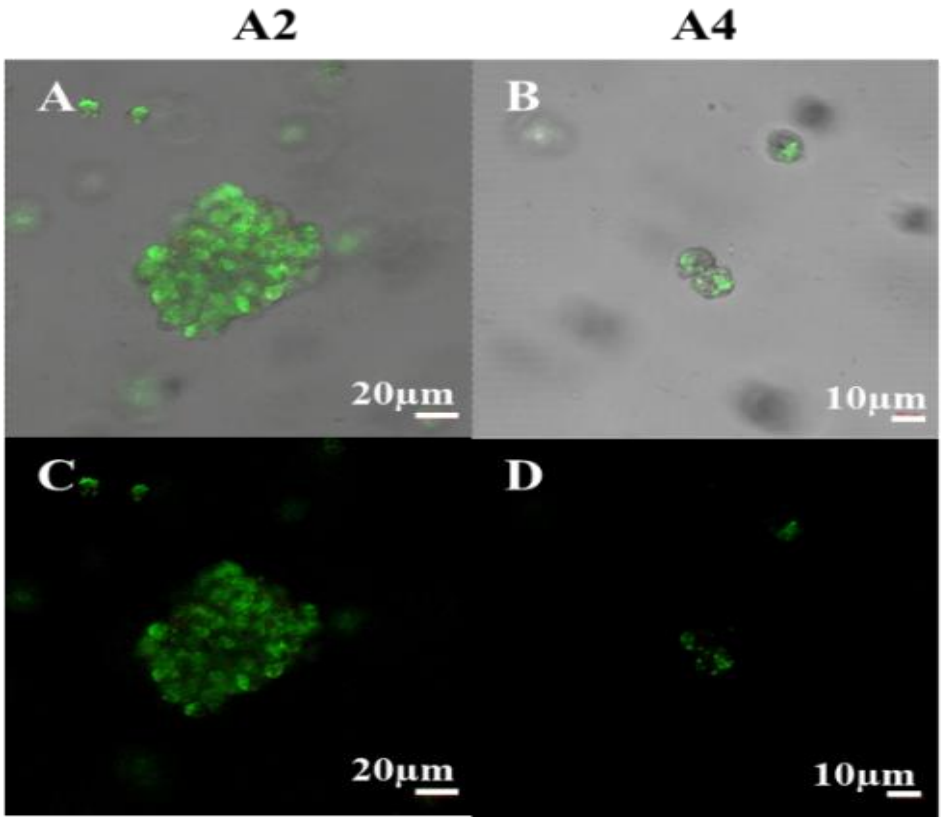

Figure 4.24 Viabilities of ATDC5 cells during 3D chondrogenesis inside the 2% and 4% alginate hydrogels for 7 days

A-B: Merged confocal images (bright field, green and red channels) of the viability of ATDC5 cells 3D cultured in 2% and 4% alginate hydrogels respectively. C-D: Merged fluorescent images (green and red channels) of the viability of ATDC5 cells 3D cultured in 2% alginate and 4% alginate hydrogels respectively. Green colours display the live cells and red colours show the dead cells. Scale bars are 20 µm in A, C, and 10 µm in B, D.

The biocompatibility of alginate-based hydrogels for longer time culture and differentiation was also investigated. Cells were encapsulated with materials and crosslinked to culture in 3D under chondrogenic inducing medium for up to 45 days. From results, most cells were alive inside the 3D alginate-based hydrogels under the chondrogenic inducing medium after 14 days and 28 days incubation *in vitro* (Figure 4.25), and type II collagens secreted by chondrocytes in 3D hydrogels

were detected after 14, 28 (Figure 4.26) and 45 days (Figure 4.27) chondrogenesis *in vitro*, suggesting that there were no toxic impact on the cell viability and differentiation when cells were cultured in 3D alginate-based hydrogel systems *in vitro* in long time culture.

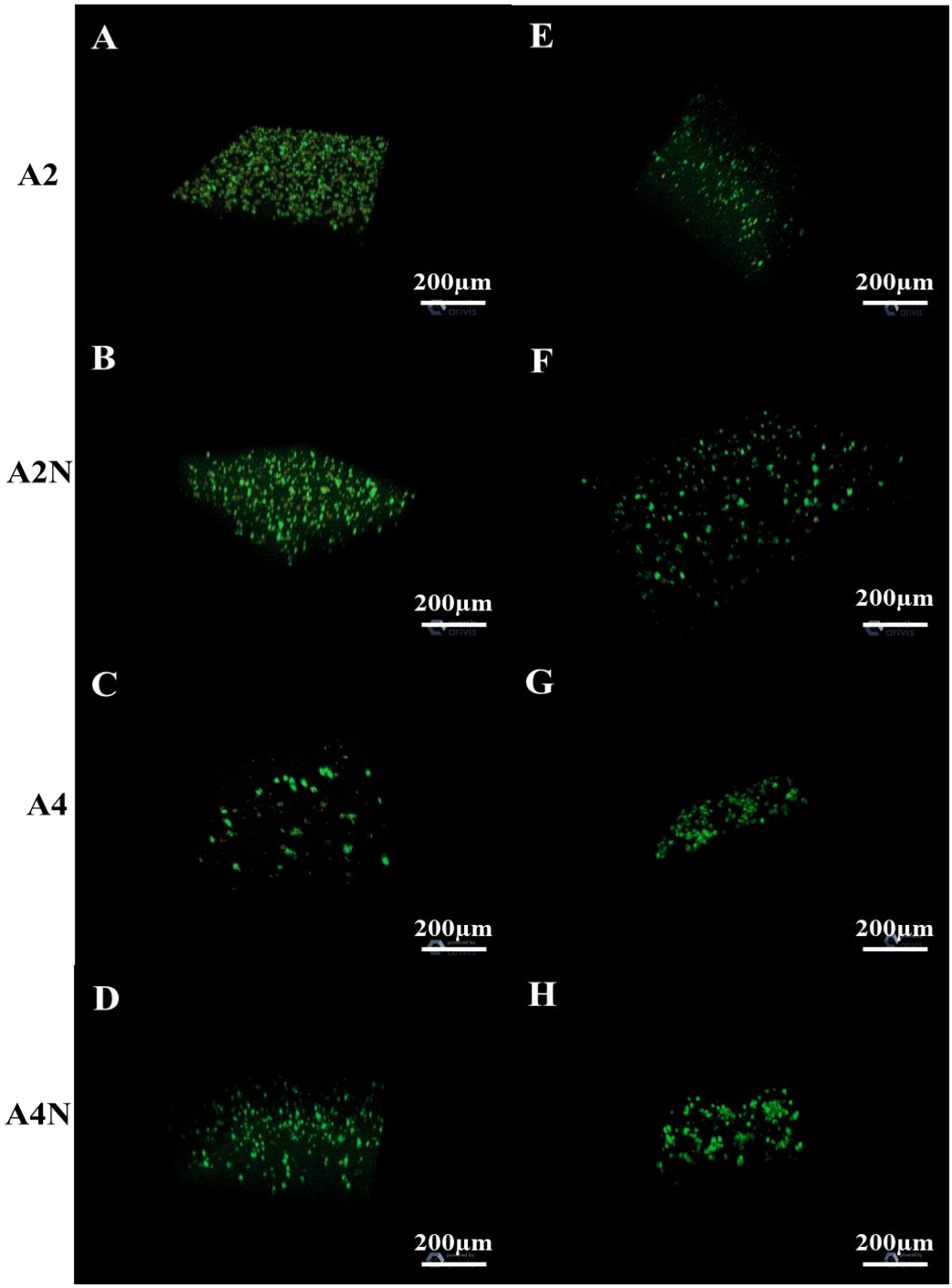

Figure 4.25 Viabilities of ATDC5 cells during 3D chondrogenesis inside the alginate-based hydrogels for 14 and 28 days

A-D: Screenshot images of the z-stack 3D images of the viabilities of cells seeded and differentiated inside the 2% alginate, 2%alginate with 0.5%NCF, 4% alginate and 4% alginate with 0.5% NCF hydrogels for about 14

days. E-H: Screenshot images of the z-stack 3D images of the viabilities of cells seeded and differentiated inside the 2% alginate, 2%alginate with 0.5%NCF, 4% alginate and 4% alginate with 0.5% NCF hydrogels for about 28 days. Green colours display the live cells and red colours show the dead cells. Scale bars are 200 µm.

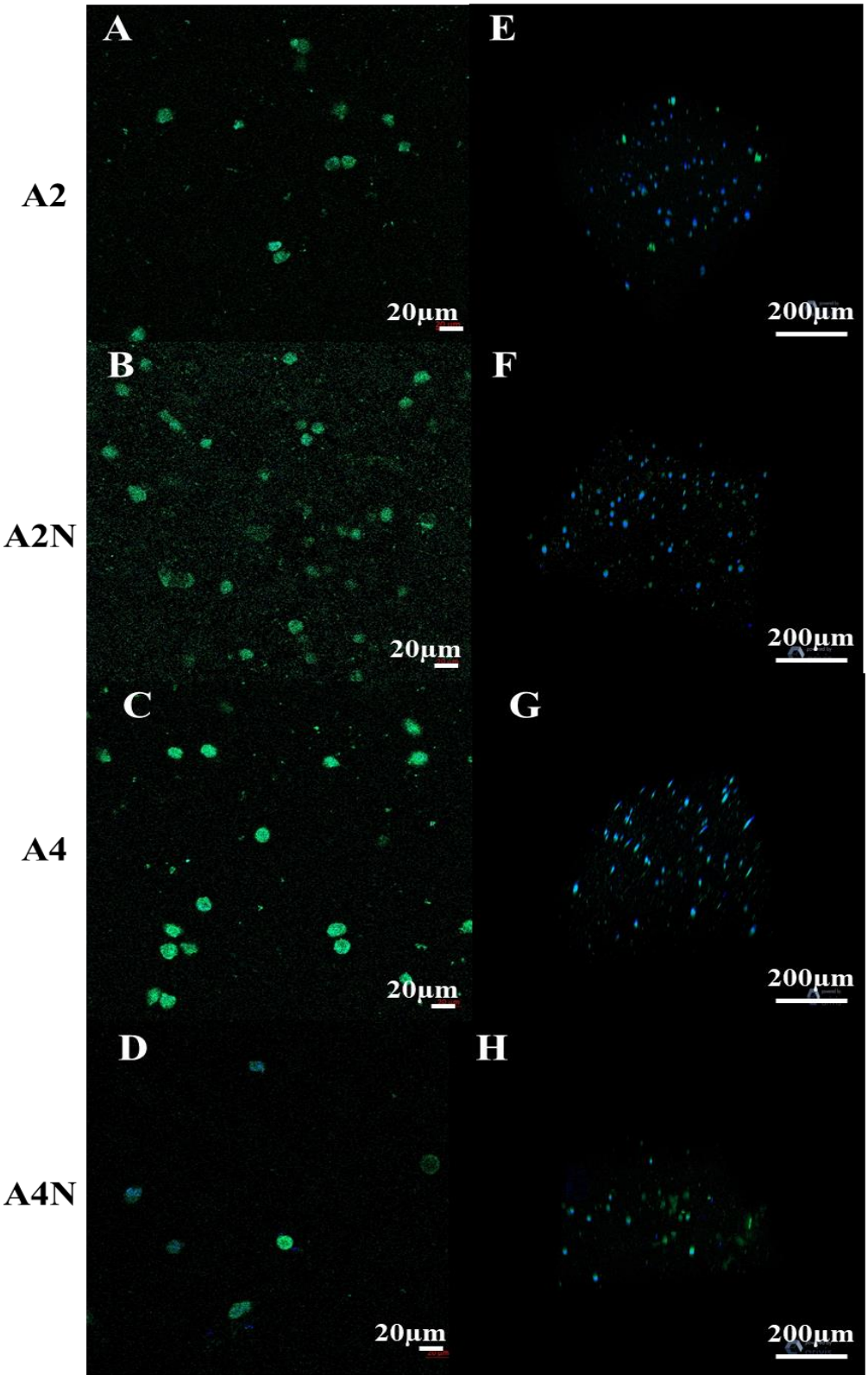

Figure 4.26 3D chondrogenesis of ATDC5 cells inside the alginate-based hydrogels for 14 and 28 days A-D: Merged fluorescent images (green and blue channels) of the type II collagen expression after cells

differentiated inside the 2% alginate, 2%alginate with 0.5%NCF, 4% alginate and 4% alginate with 0.5% NCF hydrogels for about 14 days. E-F: Screenshot images of the z-stack 3D images of the type II collagen expression after cells differentiated inside the 2% alginate, 2%alginate with 0.5%NCF, 4% alginate and 4% alginate with 0.5% NCF hydrogels for about 28 days. Green colours display the type II collagen and blue colours show the nuclei of cells. Scale bars are 20 µm in A-D, and 200 µm in E-H.

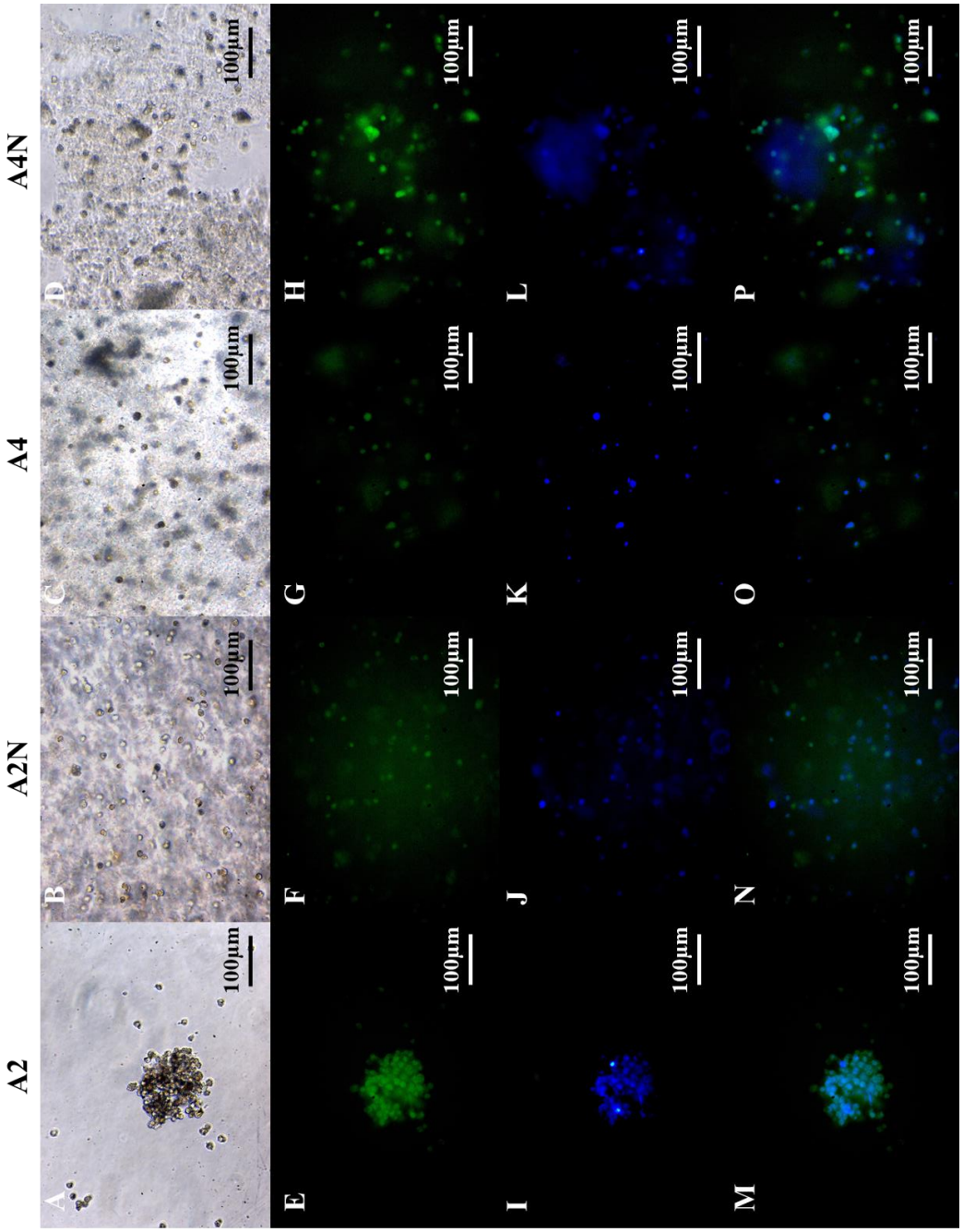

Figure 4.27 3D chondrogenesis of ATDC5 cells inside the alginate-based hydrogels for 45days

A-D: Bright field images of cells seeded and differentiated inside the 2% alginate, 2%alginate with 0.5%NCF, 4% alginate and 4% alginate with 0.5% NCF hydrogels for about 45 days. E-H: Fluorescent images of the type II collagen expression after cells differentiated inside the 2% alginate, 2%alginate with 0.5%NCF, 4% alginate and 4% alginate with 0.5% NCF hydrogels for about 45 days. I-L: Fluorescent images of the nuclei of cells differentiated inside the 2% alginate, 2%alginate with 0.5%NCF, 4% alginate and 4% alginate with 0.5% NCF

hydrogels for about 45 days. M-P: Merged fluorescent images (green and blue channels) of cells differentiated inside the 2% alginate, 2%alginate with 0.5%NCF, 4% alginate and 4% alginate with 0.5% NCF hydrogels for about 45 days. Green colours indicate the type II collagen expression and the blue colours represent the nuclei of cells. Scale bars are 100 μm.

4.4 Conclusions limitations and future works

Results presented in this chapter, demonstrated that assisted by 3D-printed mould, cell-laden alginate-based materials could be fabricated into thin layers with desired size to simulate the middle layer of the articular cartilage/OC tissue *in vitro*, proving the hypothesis of this study described in Chapter one. In this section, the outcomes achieved, limitations on current study and potential future works will be described.

4.4.1 Conclusions

To conclude outcomes of this study presented in this chapter, firstly, alginate-based biomaterials as candidate printing ink for extrusion-based 3D printing to fabricate the articular cartilage/OC tissue *in vitro*, have been investigated the compressive modulus, swelling capability, printability and biocompatibilities of the pre-hydrogel materials and crosslinked hydrogels. Current results revealed that, ion-crosslinked alginate-based hydrogels displayed multiple porous morphology, relatively soft feature, massive water preservation, especially low-concentration alginate materials possessed such appropriate features as higher weight degree of swelling but lower compressive modulus, to be used to fabricate soft tissue.

Secondly, to reinforce and improve the printability of alginate materials, nanocellulose fibre materials were added to the formula. Additional nanocellulose fibres to the alginate materials did not change too much of their swelling capabilities, but relatively increased their compressive modulus, and improve the printability of alginate materials in terms of the shear thinning property

of the flow and viscoelastic behaviours of the pre-gel alginate materials against the dynamic shear stress.

Thirdly, the biocompatible ionic strength to crosslink alginate-based materials for biological application was identified, and by means of 3D-printed moulds designed with different sizes, alginate hydrogel-based 3D cell-laden thin layer to simulate the middle zone of the target tissue could be successfully fabricated *in vitro*. Under the biocompatible condition of the ionic strength, alginate-based hydrogel thin layers fabricated by the mould-casting approach, have no toxic effect on the cell viability and proliferation in 2D condition, and on the chondrogenic differentiation in 3D condition, demonstrating the achievements of the aim and objective of this study mentioned in Chapter one.

4.4.2 Limitations and future works

Firstly, although additional nanocellulose fibres to reinforce and improve the printability of alginate materials have been confirmed in this Chapter, due to the time limitation, only a few formulas of the composite were investigated. In the future, more compositions of alginate and nanocellulose fibre materials are worth further study to find a best formula.

Secondly, before applying the developed alginate-based material for subsequent extrusion-based printing to fabricate 3D scaffold (without cell encapsulation in the ink) or 3D tissue construct (with cell encapsulation in the ink) toward reconstruction of the articular cartilage tissue layer *in vitro*, more viscoelastic behaviours of the printing ink such as stress-relaxation and creep-recovery performances should be further investigated, which results could be used to adjust the formula of printing ink to meet requirements for different seeding cell to be applied (different response and

interaction between biomaterials and different seeding cells), and for the spatiotemporal differences of the dynamic 3D microenvironment around cells during tissue developments.

Thirdly, current results demonstrated that the cell adherence to the 2D alginate-based hydrogel thin sheet was limited due to insufficient anchoring points in alginate materials, suggesting that bioactive modification or bio-functionalisation of the bioinert alginate material are required in future works. In addition, it was also observed that after soaking in growth medium, alginate-based hydrogel might interact with certain components in the serum-containing tissue culture medium, requiring further studies to verify. Because this potential interaction between alginate and other compounds in general growth medium might provide information for improving the biocompatibility of alginate material by encapsulating biochemical compounds and on biofouling issues regarding the subsequent biomedical and tissue engineering applications.

Finally, this study found that, the alginate-based hydrogel formed by the selected ion-crosslinking strength, was biocompatible for chondrocytes to survive and differentiate, in which alginate materials at lower concentrations such as 2 or 4%, and with additional fibre reinforcement might be suitable to perform extrusion-based 3D (bio) printing for 3D tissue fabrications. However, due to the time limitation, effects of the alginate-based 3D tissue culture system on the proliferation and chondrogenesis of seeding cells (chondrocytes or MSCs) *in vitro* in 3D remain further quantitative validations in future works, along with incorporation of a novel oxygen nanosensor [3] in the established 3D hydrogel system to investigate the oxygen level during 3D tissue development over time, the overall dual project would be finally accomplished.

References

[1] Stockwell R. Chondrocytes. Journal of Clinical Pathology Supplement (Royal College of Pathologists). 1978;12:7-13.
[2] Zhou S, Cui Z, Urban JP. Factors influencing the oxygen concentration gradient from the synovial surface of articular cartilage to the cartilage–bone interface: a modeling study. Arthritis & Rheumatism. 2004;50:3915-24.
[3] Koduri MP, S. Goudar V, Shao Y-W, Hunt JA, Henstock JR, Curran J, et al. Fluorescence-based nano-oxygen particles for spatiometric monitoring of cell physiological conditions. ACS applied materials & interfaces. 2018;10:30163-71.
[4] Chaudhuri O, Mooney DJ. Anchoring cell-fate cues. Nature materials. 2012;11:568-9.
[5] Chaudhuri O, Cooper-White J, Janmey PA, Mooney DJ, Shenoy VB. Effects of extracellular matrix viscoelasticity on cellular behaviour. Nature. 2020;584:535-46.
[6] Elosegui-Artola A. The extracellular matrix viscoelasticity as a regulator of cell and tissue dynamics. Current Opinion in Cell Biology. 2021;72:10-8.
[7] Tan SC, Pan WX, Ma G, Cai N, Leong KW, Liao K. Viscoelastic behaviour of human mesenchymal stem cells. BMC cell biology. 2008;9:1-7.
[8] Shepherd D, Seedhom B. Thickness of human articular cartilage in joints of the lower limb. Annals of the rheumatic diseases. 1999;58:27-34.
[9] Van Rossom S, Smith CR, Zevenbergen L, Thelen DG, Vanwanseele B, Van Assche D, et al. Knee cartilage thickness, T1ρ and T2 relaxation time are related to articular cartilage loading in healthy adults. PloS one. 2017;12:e0170002.
[10] Shah RF, Martinez AM, Pedoia V, Majumdar S, Vail TP, Bini SA. Variation in the thickness of knee cartilage. The use of a novel machine learning algorithm for cartilage segmentation of magnetic resonance images. The Journal of arthroplasty. 2019;34:2210-5.
[11] Kakita H, Kamishima H. Some properties of alginate gels derived from algal sodium alginate. Nineteenth International Seaweed Symposium: Springer; 2008. p. 93-9.
[12] Neves MI, Moroni L, Barrias CC. Modulating alginate hydrogels for improved biological performance as cellular 3D microenvironments. Frontiers in bioengineering and biotechnology. 2020;8:665.
[13] Higham AK, Bonino CA, Raghavan SR, Khan SA. Photo-activated ionic gelation of alginate hydrogel: real-time rheological monitoring of the two-step crosslinking mechanism. Soft Matter. 2014;10:4990-5002.
[14] Lee H-R, Jung SM, Yoon S, Yoon WH, Park TH, Kim S, et al. Immobilization of planktonic algal spores by inkjet printing. Scientific reports. 2019;9:1-7.
[15] Khalil H, Jummaat F, Yahya EB, Olaiya N, Adnan A, Abdat M, et al. A review on micro-to nanocellulose biopolymer scaffold forming for tissue engineering applications. Polymers. 2020;12:2043.
[16] Owonubi SJ, Agwuncha SC, Malima NM, Shombe GB, Makhatha EM, Revaprasadu N. Non-woody Biomass as Sources of Nanocellulose Particles: A Review of Extraction Procedures. Frontiers in Energy Research. 2021;9:608825.
[17] Habibi Y. Key advances in the chemical modification of nanocelluloses. Chemical Society Reviews. 2014;43:1519-42.
[18] Li G, Yu J, Zhou Z, Li R, Xiang Z, Cao Q, et al. N-doped Mo2C nanobelts/graphene nanosheets bonded with hydroxy nanocellulose as flexible and editable electrode for hydrogen evolution reaction.

Iscience. 2019;19:1090-100.
[19] Hubbe MA, Ferrer A, Tyagi P, Yin Y, Salas C, Pal L, et al. Nanocellulose in thin films, coatings, and plies for packaging applications: A review. BioResources. 2017;12:2143-233.
[20] Michelin M, Gomes DG, Romaní A, Polizeli MdL, Teixeira JA. Nanocellulose production: exploring the enzymatic route and residues of pulp and paper industry. Molecules. 2020;25:3411.
[21] Chimene D, Lennox KK, Kaunas RR, Gaharwar AK. Advanced bioinks for 3D printing: a materials science perspective. Annals of biomedical engineering. 2016;44:2090-102.
[22] Langford T, Mohammed A, Essa K, Elshaer A, Hassanin H. 4D printing of origami structures for minimally invasive surgeries using functional scaffold. Applied Sciences. 2021;11:332.
[23] Ding A, Lee SJ, Ayyagari S, Tang R, Huynh CT, Alsberg E. 4D biofabrication via instantly generated graded hydrogel scaffolds. Bioactive materials. 2022;7:324-32.
[24] Zandi N, Sani ES, Mostafavi E, Ibrahim DM, Saleh B, Shokrgozar MA, et al. Nanoengineered shear-thinning and bioprintable hydrogel as a versatile platform for biomedical applications. Biomaterials. 2021;267:120476.
[25] Barnes H. Hutton. JF and Walters, K., An Introduction to Rheology. Rheology Series. 1989;3.
[26] Osswald T, Rudolph N. Polymer rheology-Fundamentals and Applications. Cincinnati: Carl Hanser, München. 2015:221.
[27] Polychronopoulos ND, Vlachopoulos J. 'Polymer processing and rheology', in Jafar Mazumder, M., Sheardown, H., Al-Ahmed, A., (Eds). Functional Polymers Polymers and Polymeric Composites: A Reference Series; Springer, Cham. 2018:133-80.
[28] Sunthar P. Polymer rheology. Rheology of complex fluids: Springer; 2010. p. 171-91.
[29] Huang D, Huang Y, Xiao Y, Yang X, Lin H, Feng G, et al. Viscoelasticity in natural tissues and engineered scaffolds for tissue reconstruction. Acta biomaterialia. 2019;97:74-92.
[30] Kucharova M, Doubal S, Klemera P, Rejchrt P, Navrátil M. Viscoelasticity of biological materials-measurement and practical impact on biomedicine. Physiological research. 2007;56:S33.
[31] Bas O, De-Juan-Pardo EM, Meinert C, D'Angella D, Baldwin JG, Bray LJ, et al. Biofabricated soft network composites for cartilage tissue engineering. Biofabrication. 2017;9:025014.
[32] Guimarães CF, Gasperini L, Marques AP, Reis RL. The stiffness of living tissues and its implications for tissue engineering. Nature Reviews Materials. 2020;5:351-70.
[33] Butler DL, Goldstein SA, Guilak F. Functional tissue engineering: the role of biomechanics. J Biomech Eng. 2000;122:570-5.
[34] Brusatin G, Panciera T, Gandin A, Citron A, Piccolo S. Biomaterials and engineered microenvironments to control YAP/TAZ-dependent cell behaviour. Nature materials. 2018;17:1063-75.
[35] Schuman L, Buma P, Versleyen D, de Man B, van der Kraan PM, van den Berg WB, et al. Chondrocyte behaviour within different types of collagen gel in vitro. Biomaterials. 1995;16:809-14.
[36] Knight M, Ross J, Sherwin A, Lee D, Bader D, Poole C. Chondrocyte deformation within mechanically and enzymatically extracted chondrons compressed in agarose. Biochimica et Biophysica Acta (BBA)-General Subjects. 2001;1526:141-6.
[37] Kumar S. Stiffness does matter. Nature materials. 2014;13:918-20.
[38] Vining KH, Mooney DJ. Mechanical forces direct stem cell behaviour in development and regeneration. Nature reviews Molecular cell biology. 2017;18:728-42.
[39] Worldwide MI. Malvern Instruments White Paper-A Basic Introduction to Rheology Shear Flow. 2016:1-20.

Chapter five: Characterisations of a novel fluorescent oxygen nanosensor for cell-based tissue culture *in vitro*

5.1 Introduction

Tissue engineering (TE) is an interdisciplinary subject aiming at developing the functionally bio-active substitute to repair replace and regenerate the diseased or failed tissue or organ [1]. TE strategies stress on manipulating materials, engineering technologies and living cells to reconstruct the prototype of 3D microenvironment for reparative cells to regenerate the tissue or organ. To date, although a few of the engineered tissue constructs such as the artificial skin, cartilage and engineered bladder tissue, have been developed, applied clinically and even commercialised [2-6], complicated challenges and limitations remain to address, such as vascularisation, complex tissue substrate with larger size, and the real functionally and structurally simulated artificial tissue models [7]. To overcome these, comprehensive knowledge on the natural dynamic 3D microenvironment of cells in culture, the potential impact of the microenvironmental factors on cell behaviours and the mutual effects resulting from the interaction between living cells and surroundings during development are necessary [8].

It is well-accepted that the microenvironment of living cells contains many external factors regulating cell behaviours and the cell fate [9, 10]. A biomimetic 3D tissue culture system plays an important role in cell-based TE strategy. To investigate the tissue culture microenvironment and finally simulate it for TE applications fit in with motivations of this study described in Chapter one. For the complex articular cartilage/osteochondral tissue, as extensively introduced in Chapter two, with multiple thin layers and inhomogeneous 3D architecture, it is more difficult to thoroughly understand and entirely simulate its natural microenvironment containing various impact factors,

such as the oxygen profile.

Oxygen is an important element for most living organism and cells, therefore specific signalling pathways have evolved to deal with the sensation and consumption of oxygen both inside and around cells. Previous studies have confirmed the hypoxic conditions inside the cartilage tissue which is adapted by resident chondrocytes in 3D, and could have positive impact on the chondrogenesis of MSCs in 3D culture [11-15]. Results from many studies also demonstrated that the oxygen level around chondrocytes contributed to the transcription and expression of certain zonal markers, especially the production of ECM components, the differentiation status and functions of chondrocytes. Chondrocytes derived from different layers of the articular cartilage tissue, have different requirement for the oxygen concentrations in surroundings to retain their specific phenotypes which are also depth-related and varied, consistent with the depth-dependence of the oxygen profile and consumption within the avascular inhomogeneous tissue [16-19]. In addition, different oxygen pressure has different regulation mechanisms for different types of cells such as MSCs derived from different sources, and articular chondrocytes, individually or synergically working with other impact factors such as the growth factors and mechanical signals, which involves various signalling pathways and cytoplasmic organelles such as the mitochondria [20-26]. However, little details are clear about the balanced oxygen profiles inside the inhomogeneous articular cartilage tissue, specific correlations of the oxygen profiles with the formation, development, maturation and degeneration of this tissue, and the underlying mechanisms individually and synergically with other factors. Especially as an important cue in the cellular microenvironment, how to monitor and quantify this parameter in real time in the long time, still remain challenges. To investigate these topics fits in with motivations of this study

mentioned in Chapter one, and nanotechnology and nanomaterials bring hopes and tools.

Nanotechnology is defined as the technology managing matters at nanoscale which denotes an atomic and molecular level in a size ranging from 1 to 100nm [27]. Nanotechnology consists of the nanomanufacturing, nanomaterials and nanoapplications. Nanomaterial, based on dimension and morphology, consists of discrete nanomaterial (one dimension), nanoscale device material (two dimensions) and bulk nanomaterial (three dimensions), in which nanoparticles and nanowire belong to the discrete nanomaterial [28]. Nanoparticles (NPs) have the scale about 0.2 to 1000 nm with one dimension usually consisting of the amorphous form and crystalline form. There are various types of NPs, ranging from organic, inorganic, metallic to polymeric, such as liposomes, quantum dots and carbon nanotubes [29]. Based on unique properties of having larger surface area and higher ratio of particle number to particle mass which could play significant impacts on the optical, electric, magnetic, mechanical and chemical characteristics, NPs have become an important tool [30], being studied and applied into many fields including mechanical and electronic engineering, transportation and telecommunication, imaging and biomedical sciences, food cosmetics and environmental applications, coating and materials science [29]. Specifically, in stem cell-based biomedical and TE area, NPs have been developed to study intracellular drug delivery, biomedical imaging, and to control and monitor stem cell differentiation [31] and tissue development [32]. Various NP-based nanosensors have also been developed and applied to sense or image intracellular or intercellular chemicals, various biological molecules [33] and metabolic analytes, such as the pH [34], dissolved oxygen content [35], growth factors [36] and the concentration of glucose [37] during tissue development in 2D monolayer or 3D scaffold-supported engineered tissue construct in bioreactors [38, 39]. Nanoparticle sensing as an emerging technology,

is being exploited to optimise the conditions associated with bioreactor development for TE applications and to enhance the efficiency of culturing *de novo* tissue. In addition, by modifying or conjugating with other active materials or agents such as chitosan [40], amino acid [41], polymers [42, 43] or dendrimer [44], electrode [45, 46], and other NPs like quantum dots [47], nanoparticle-based nanosensors have now been utilised to develop complicated hybrid nanomaterials with either improved electrical, biochemical or optical sensitivities, or enhanced competences of sensing various types of chemicals, biochemical molecules in not only artificial tissue construct, but also real samples and animal models. Therefore, the use of NP sensing technologies to monitor the environmental conditions, to optimise the performance of TE scaffolds-based tissue culture system and to incorporate into bioreactor design, becomes a real possibility.

On these grounds, a novel fluorescence-sensitive nanoparticle-based oxygen sensor (FNOP) has been designed and developed to monitor the physiological condition of cells in another study of this joint project in Taiwan [48]. The oxygen nanosensors basically contain the modified polystyrene nanobeads (PS) with carboxyl groups, the amphipathic polymer Pluronic F127 as the linker, and the oxygen sensitive dyes with fluorophores. By physical interactions between hydrophilic and hydrophobic groups of those components, the nanosensor could be synthesised and calibrated, displaying good performances on resolution, accuracy and dynamic range, in a 3D spherical alginate hydrogel system *in vitro* for a short time [48].

As described in Chapter one, this novel nanosensor is intended to be applied to the hydrogel-based 3D tissue culture system (e.g., the one established in chapter three and four) fabricated in this study. However, it was found that the unique properties of nanomaterial on physical, chemical, electrical and magnetic aspects could be finely tuned [49] by engineering process on their constitution such

as atomic composition, surface chemistry and dimension, which increase the possibility of designing and developing novel multifunctional nanomaterials and extend the field of application [50]. The engineered nanoparticles with more complicated structures and functions may have different biocompatibilities regarding the particle features including size, morphology, surface charge and chemistry, physiochemical character, crystal phase, functionalisation and modification, and dynamic interactions of nanoparticles with living entities such as cells, tissues and circulating body systems, from those of the original raw nanoparticles [50-53]. In addition, different types of cells may present different sensitivity and response to nanomaterials, in particular the stem cells which are commonly used in biomedical and TE area, having extreme sensitivity to the extracellular microenvironment in culture *in vitro*. Hence, the cytotoxicity and biocompatibility of nanomaterials are often the top priority to be considered before further applications in biomedical field.

To accomplish the final biomedical application of the nanosensor to stem cell-based 3D tissue culture system, it is necessary to characterise the effect of the engineered nanoparticle-based sensor on the viability and proliferation of normal cells before administrating it to stem cells, and it is also important to clarify the effect of the nanosensor on the morphology, proliferation and differentiation of stem cells in simple and basic culture condition before incorporating it into hydrogel scaffold-based 3D culture platform where the microenvironment is more complicated.

The work presented in this chapter was started in the University of Liverpool (UK), at that time, there were different sizes (390, 520 and 890nm) of nanosensors manufactured in the lab. As mentioned, this novel nanosensor is planned to be used in 3D stem cell-based tissue culture system in a long term to measure the oxygen profile during tissue development *in vitro*. Therefore, in this

study, the biocompatibility of the nanomaterial, in terms of the effects of the size and concentration of the novel nanosensor on the viability and proliferation of living cells (fibroblast first and then stem cells) *in vitro*, the related performance of the fluorescent signal of the nanosensor applied with cells in culture and the optimised regime of the nanosensor for stem cell-based applications, were preliminarily investigated. As described in chapter three, the ISO documents compiled several detailed biocompatibility tests in which the MTT assay was one of the suggested screening assays for *in vitro* cytotoxicity study. Another colorimetric assay the LDH assay, confirmed by many previous studies as a simple and reliable method, was also considered. Hence, in this study, the MTT assay and LDH assay, were both investigated to evaluate the impacts of nanosensor on the cell viability, proliferation, morphology and differentiation in related simple cell culture conditions *in vitro*, along with the fluorescent intensity detection, to characterise the nanosensor, regarding the size and concentration to be administrated to stem cells *in vitro*, which is also a hypothesis of this study mentioned in chapter one. Nanosensors and nanoparticles characterised in this study were listed in table 5.1 and 5.2. All works described in this Chapter were finished in the University of Liverpool in UK.

Table 5.1 Nanosensors characterised in this study.

Size	Concentrations of oxygen nanosensors	Cell line	Seeding density	Characterisation	Time point
390nm 520nm 890nm	25, 50,100,200,500,1000,2000 μg/mL	L929 fibroblasts	10,000 cells/well in 96 well microplate	Viability and proliferation screening by MTT assay, Fluorescent intensity	24hrs, 7days
	25, 500,1000 μg/mL		2,500 cells/well in 96 well microplate		
390nm	25, 500,1000 μg/mL		15,000 cells per well in 24 well microplate	Viability and proliferation screening by LDH assay, Fluorescent intensity	
520nm					
520nm	25, 500,1000 μg/mL	BM-MSCs	5,000 cells/cm² in 24 well microplate	Viability and proliferation screening by LDH assay, Fluorescent intensity	24hrs, 7days
	500 μg/mL			2D Osteogenesis by Anti-Osteocalcin IF staining, von Kossa staining	28 days
				2D monolayer and 3D pellet Chondrogenesis by Anti-Collagen type II IF staining, Alcian blue staining	21 days

Notes: The selected regime of nanosensor was labelled in red. L929 fibroblasts: L929 murine fibroblast cell

line. BM-MSCs: Bone marrow-derived MSC. IF staining: Immunofluorescent staining. MTT: 3-(4,5-dimethylthiazol-2-yl)-2,5-diphenyl tetrazolium bromide. LDH: lactate dehydrogenase.

Table 5.2 Nanoparticles evaluated in this study.

Size	Concentrations of polystyrene beads	Cell line	Seeding density	Cell viability and proliferation screening test	Time point
390nm 520nm 890nm	25, 500,1000,2000 μg/mL	L929 fibroblasts	10,000 cells/well in 96 well microplate	MTT assay	24hrs, 7days
			2500 cells/well in 96 well microplate		1, 4, 24hrs and 7 days

5.2 Material and methods

All materials used in experiments presented in this chapter and all experimental methods will be described in this section.

5.2.1 Chemical compounds and nanoparticles

Most chemicals and polystyrene nanobeads were purchased from Sigma-Aldrich (Merck, UK) directly or by its agent in Taiwan (Echo Chemical Co. Ltd). They were 37% formaldehyde solution (F8775), 25% glutaraldehyde solution (G6257), hydrochloric acid (258148), Thiazolyl Blue Tetrazolium Bromide (M2128) (CAS No.:298-93-1), nuclear fast red (N8002), sodium thiosulphate (CAS No.:7772-98-7), Alcian Blue 8GX (A3157), Aluminium sulphate (202614), silver nitrate (205052), Formic acid (HCOOH, CAS No.:64-18-6), trypsin-EDTA solution (T4174), penicillin-streptomycin (PS) (P4333), L-proline (81709), dexamethasone (D4902), latex beads (carboxylate-modified polystyrene and fluorescent yellow-green-conjugated polystyrene). Tris (4,7-diphenyl-1,10-phenanthroline) ruthenium (II) dichloride (44123) dye was ordered from Alfa Aesar® (Thermo Fisher Scientific). VECTASHIELD® Mounting Medium for Fluorescence with DAPI was ordered from Vector Laboratories, Inc. Isopropyl alcohol and ethanol alcohol were

ordered from Honeywell® (RS components Ltd.).

5.2.2 Medium, agent, assay kit and antibodies

Cell culture medium, balanced salt solutions, growth factors and other additives for cell culture, and differentiations, were purchased from Corning®. They are Dulbecco's Modified Eagle medium (DMEM), Phosphate buffered saline (PBS), 100 mL Penicillin-Streptomycin Solution, 100x (10,000 I.U. Penicillin and 10,000 μg/mL Streptomycin), low viscosity mounting media, ITS (insulin-transferrin-Selenium), Transforming growth factor beta-3 (TGF-β3), sodium β-glycerophosphate (β-GP). Tissue culture serum such as foetal bovine serum (FBS), horse serum (HS), and goat serum (GS), were ordered from Sigma-Aldrich (Merck, UK) and HyClone™ (GE healthcare Life Sciences). CyQUANT™ LDH Cytotoxicity Assay (Invitrogen™) was purchased from Thermo Scientific Ltd. Antibodies for immunostaining were ordered from Thermo Scientific Ltd. or Abcam Plc, including Alexa Fluor® 594 goat anti-rabbit antibody, Alexa Fluor® 488 goat anti-mouse IgG, ActinGreen™ 488 Ready Probes™ reagent (AlexaFluor™ 488 phalloidin), anti-osteocalcin antibody (ab13418), anti-collagen II antibody (ab150771), and albumin bovine serum (BSA, CAS no.: 9048-46-8).

5.2.3 Consumables and instruments

Ultrapure water (deionised distilled water, DDW) and distilled water (DW) were produced by lab water purification systems (Merck Millipore Milli-Q™). Two types of centrifuges were used during the study. They are Eppendorf™ 5804 R and Thermo Scientific™ Small Benchtop Centrifuge. Other instruments used in the study, are scanning electron microscopy (SEM) (JSM 7001F FEGSEM; JEOL, Tokyo, Japan), Q150T ES sputter coater, the energy dispersive X-ray

spectroscopy (EDX), confocal microscope (Zeiss LSM 510), and benchtop normal inverted phase contract light microscopes. Other consumables such as tissue culture flasks, petri dish, microplates, pipette tips, centrifuge tubes, Eppendorf® tubes, beakers, haemocytometer, were provided by suppliers such as the (SLS) Scientific Laboratory Supplies Ltd. (UK) and Thermo Scientific™ (UK).

5.2.4 Cell lines

L929 fibroblasts (ECACC catalogue number 85011425) and human BM-MSCs (Lonza, UK) were mainly used in this study. Human articular chondrocyte (HAC) and osteoblast (OB) were used for the immunohistochemical staining (IHC) control of MSC chondrogenesis and osteogenesis in 2D culture *in vitro*. Chicken chondrocytes (CHO) were used as control of 3D MSC chondrogenesis in pellet culture.

5.2.5 General cell culture process and cytotoxicity evaluations *in vitro*

Methods regarding cell culture and cell-based assays presented in this chapter are described below.

5.2.5.1 General cell expansion and passaging process *in vitro*

In this part, experimental processes for general cell expansion and passaging process *in vitro* are same as those mentioned in chapter three (3.2.6).

5.2.5.2 Cytotoxicity of polystyrene nanobeads and nanosensor on living cells in 2D culture condition *in vitro*

Cytotoxicity of the polystyrene (PS) nanobeads and PS nanobeads-based fluorescent nanosensors

were both evaluated on living cells by the same method described in this section.

5.2.5.2.1 Series number test for appropriate seeding density

General cell expansion process was same as mentioned in Chapter three (3.2.6). Appropriate seeding density was examined by series cell number test before any cell-involved experiment, in the process as mentioned in Chapter three (3.2.6.2.1).

For L929 fibroblast, cells were seeded in 96-well microplate for 1 and 7 days and examined by MTT essay and LDH essay respectively. Appropriate seeding density in 24-well microplate was calculated by considering the differences of the seeding area between the well of 96-well microplate and that of the 24-well microplate, according to the instruction of manufacturer. Seeding density groups were set at 7.5K, 15K, 30K, 60K and 120K cells per well in 96-well microplate for L929 fibroblast. For BM-MSCs used in this study, they were tested in 24-well microplate and the seeding density of BM-MSCs in this test were set at 0, 1K, 2.5K, 5K and 10K cells per well. After 1 and 7days culture *in vitro*, cells were examined by LDH assay.

5.2.5.2.2 Effects of nanosensors on the viability (24 hrs) and proliferation (7days) of cells in 2D culture condition *in vitro*

In this study, at first, there were three sizes of nanosensors and associated polystyrene (PS) nanobeads involved (390, 520 and 890 nm) and a series of concentrations of nanosensors and PS nanobeads suspended in culture medium respectively (ranging from 25 to 2000 μg/mL), were prepared for further optimisation and selection.

For nanosensors/PS nanobeads involved tests, L929 cells were adjusted into low (2500 cells per well) and high density (10K cells per well) in total of 100 μL cell suspension per well to seed in

96-well microplates respectively. After seeding 24 hrs in an incubator, cells in plates were checked the cellular states under a normal inverted phase contrast microscope. Then, cell culture medium in microplate were replaced by conditional medium (growth medium containing different concentrations of three sizes (390, 520 and 890 nm) of nanosensors (25,50,100,200,500,1000,2000 μg/mL) or PS nanobeads (25,500,1000,2000 μg/mL)) to treat for another 24hrs or 7 days in an incubator in dark. Cultural medium of each well was replaced every two to three days.

Firstly, MTT assay was applied to examine the effect of nanoparticles (PS nanobeads and nanosensor) on the viability (24hrs) and proliferation (7 days) of cells in 2D culture system. The process was same as that mentioned in Chapter three (3.2.6.2.2).

Secondly, based on results from L929 cells, appropriate size and density of nanosensors were selected and applied to treat MSCs which results were examined by LDH assay. MSCs were seeded at appropriate density in 24-well microplate and treated with the selected 520 nm nanosensor for another 24 hrs and 7 days culture in an incubator. Culture medium of each well was replaced every two to three days. After treatment, LDH assay to examine cell viability and proliferation was performed according to the instruction of the CyQUANT™ LDH kit from the manufacturer, which was same as mentioned in Chapter three (3.2.6.2.2). All results about the cytotoxicity were shown as the cell viability in percentage (the normalised viable cells of experimental group over that of control groups).

5.2.5.3 Fluorescent intensity of the nanosensor in 2D cell culture system

L929 fibroblast cells were seeded in 96-well microplate at low (2500 cells per well) and high density (10K cells per well) respectively as mentioned above (5.2.5.2.2) and treated with

nanosensors (three sizes at a series of concentrations) in dark in an incubator. After 1- and 7-days treatments, fluorescent intensity of the nanosensor in culture was measured by a plate reader (BioTek, Agilent Technologies, Inc., USA) with appropriate filter at the excitation wavelength of 470-490 nm and the emission wavelength of 610 nm. Each group of test contains at least three wells, and each test was repeated at least three times for further statistical analysis.

5.2.6 BM-MSC differentiations

The MSC differentiations and inducing medium regarding the BM-MSCs differentiations *in vitro* will be described in details in this section.

5.2.6.1 BM-MSC 2D Differentiations

Differentiations of BM-MSCs in 2D was performed in 24-well microplate. In brief, BM-MSCs were detached and resuspended in growth medium. After calculating numbers by a haemocytometer, cells were seeded into 24-well microplate and put into an incubator to culture for 24 hrs. For visualising the morphology and differentiation by immunostaining, sterilised glass coverslips were added into each well before cell seeding, and for visualising the differentiated morphologies of MSCs by SEM, sterilised silicon wafer pieces were added into each well before cell seeding.

Cells in plates were checked the cellular status by a normal inverted phase contrast microscope every day. Once the cell density in each well was reached to 80 to 90% confluence, growth medium in experimental groups would be replaced by differentiation inducing medium. The growth medium and inducing medium were both replaced every two to three days. For osteogenesis, BM-MSCs were induced by osteogenic inducing medium, containing growth medium, 150 μg/ml

ascorbic acid, 2mM sodium β-glycerophosphate, and 10^{-7} M dexamethasone. For chondrogenesis, BM-MSCs were induced by chondrogenic inducing medium, containing growth medium, 10ng/ml TGF-β3, 50μg/ml L-proline, 50μM ITS (insulin-transferrin-Selenium), 100nM dexamethasone and 150 μg/ml ascorbic acid. BM-MSCs were cultured in osteogenic inducing medium for 28 days to perform osteogenesis and cultured in chondrogenic inducing medium for 21 days to perform chondrogenesis *in vitro*.

5.2.6.2 Effects of 520nm nanosensor on 2D differentiations of BM-MSCs *in vitro*

Differentiations of BM-MSCs were performed in 2D monolayer culture system in this study. BM-MSCs were seeded and differentiated as mentioned above in 5.2.5.1. To examine the effect of nanosensor on BM-MSC differentiations, the selected 520 nm nanosensors were suspended in inducing medium at 500 μg/ml and treated with cells in dark during differentiations. Inducing medium was replaced every two to three days. After 28 days induction, samples were examined by immunofluorescent (IF) staining and immunohistochemical staining (IHC), respectively.

To examine the BM-MSC osteogenesis, IF staining by using anti-osteocalcin antibody and von Kossa staining were applied. To examine the BM-MSC chondrogenesis in 2D monolayer culture system, after 21 days induction, IF staining by using anti-collagen type II antibody and Alcian blue staining were applied. Fluorescent signal from the nanosensors applied in culture after differentiations was also examined by confocal microscope with appropriate filter.

5.2.6.3 BM-MSC chondrogenesis by 3D pellet culture *in vitro*

For comparison, 3D pellet culture for BM-MSC chondrogenesis was also performed.

Around 10^6 numbers of BM-MSCs were put in a 15ml conical centrifuge tube to centrifugate at

1500 rpm to deposit. Then the tube with cell pellet was put into an incubator for about two to three days, before replacing the growth medium with chondrogenic medium. For nanosensor-involved experiments growth medium containing the selected 520 nm nanosensors were added into the centrifuge tube to centrifugate with cells and form the cell pellet together. After 21 days chondrogenic induction, cell pellets were examined by IF staining (anti-collagen type II antibody) and Alcian blue staining respectively to validate the 3D chondrogenesis of BM-MSCs with and without nanosensor. Chicken chondrocytes were applied to form cell pellets and cultured as 3D positive control. Fibroblast L929 cells were also applied to form cell pellets and cultured, but did not get integrated pellet after 21 days culture.

5.2.7 Immunostaining and immunohistochemical staining examinations

To evaluate the BM-MSC differentiation, immunostaining and immunohistochemical staining were performed. Methods and processes will be described in this section.

5.2.7.1 Immunostaining evaluations on 2D differentiated samples

For immunostaining 2D differentiated BM-MSCs, cells cultured on glass coverslip after differentiation were washed with PBS twice and fixed by 4% formaldehyde solutions at room temperature for about 4 hrs or overnight at 4°C. Before adding the primary antibody, samples in plate were washed by DW twice and treated with blocking solution containing 5% normal goat/horse serum or 2% BSA, PBS and 0.25% Triton X-100. After 1-2 hrs incubation with primary antibody (anti-osteocalcin for osteogenesis, anti-collagen type II for chondrogenesis) diluted in blocking solution (1:20 or 1:50 used in this study) at room temperature, or overnight at 4°C, samples were washed twice by washing solution containing PBS and 0.1% Triton X-100. Then

samples were treated with secondary antibody diluted in blocking solution at appropriate times (1:1000 used in this study) at room temperature for about 0.5-1 hrs in dark, before being rinsed by washing solution three times. Finally, samples were rinsed again by DW three times and dried before being transferring to the glass slides with mounting agent containing DAPI. Prepared samples were sealed the edge by mineral oil and kept until examination by confocal microscope. Morphology of differentiated cells was examined by treating samples with anti-F-actin antibodies (ActinGreen™ 488) after differentiation, and washed thoroughly by washing solution before being prepared for confocal investigation.

5.2.7.2 Immunostaining evaluations on 3D differentiated samples

For immunostaining 3D cell pellets after differentiation, before and after performing washing or staining steps, samples should be centrifugated to deposit the pellet. Then the other steps of staining were similar as those for 2D samples (5.2.7.1) and with more careful manipulation. Due to the time limitation and facilities, entire 3D samples were examined instead of sliced samples.

5.2.7.3 Immunohistochemical staining

For immunohistochemical staining, including Alcian blue staining and von Kossa staining, samples were processed according to the following protocols. Due to the time limitation and facilities, the whole 3D samples, instead of sliced samples, were evaluated

5.2.7.3.1 Alcian blue staining

Differentiated BM-MSCs cultured on the coverslip in 24 well microplate, were washed with DW three times, before adding Alcian blue solution (1% Alcian blue dissolved in 3% acetic acid, with

pH=0.2) for about 15 mins at room temperature. Then samples were washed thoroughly with DW to remove extra dyes and counterstained with nuclear fast red solution for about 1 min at room temperature. Finally, samples were washed thoroughly with DW again and dried at room temperature.

For staining 3D chondrocyte pellets, before and after performing washing or staining steps, samples were centrifugated to deposit the pellet. The other steps of staining were similar as those for 2D samples.

5.2.7.3.2 von Kossa staining

Differentiated BM-MSCs cultured on the coverslip in 24-well microplate, were washed with DW three times, before adding 1% silver nitrate solution at room temperature. Then samples with silver nitrate solution were put into UV light to expose for about 60 mins at room temperature. After UV exposure, samples were washed with DW thoroughly and treated with 5% sodium thiosulphate solution to remove extra silver, at room temperature for about 5-10 mins. Then samples were washed with DW again thoroughly and counterstained with nuclear fast red solution for about 5 mins at room temperature. Finally, samples were washed with DW again and dried at room temperature. For negative control, samples would be treated with 10% formic acid (HCOOH) about 10 mins, before adding silver nitrate solution, the rest steps are same as those for experimental groups.

5.2.8 Morphology observations by scanning electron microscopy (SEM)

Differentiated BM-MSCs cultured on sterilised silicon wafer pieces were also examined the differentiated morphology by SEM. After differentiation, cells cultured on small pieces of wafers

were washed by PBS and fixed by 4% formaldehyde solution for about 2-4 hrs. After fixation, samples were further performed gradient dehydration by soaking into a series of ethanol alcohol solutions from 25%, 50%, 75% to 100%, before being spinning coated with conductive metals for SEM scanning. Mineral deposition of differentiated BM-MSCs was examined by the energy dispersive X-ray spectroscopy (EDX) accompanying with the SEM instrument.

5.2.9 Statistical analysis

For results from MTT assay, LDH assay and fluorescent intensity of nanosensor, absorption data measured by the plate reader (BioTek, Agilent Technologies, Inc., USA) were exposed to Microsoft® Excel (Microsoft Corporation, USA) to compile and analysed statistically by Origin2018 (OriginLab®, USA), where the differences between groups were calculated by one-way analysis of variance ANOVA (Tukey post hoc test) and linear fitting of the cell numbers were also performed. The p value less than 0.05 was considered as statistically significant.

5.3 Results and discussions

All results in this chapter and discussions will be presented in this section.

5.3.1 Characterisations of nanosensors in normal cell culture condition *in vitro* by MTT assay

At the beginning of this study, the polystyrene (PS) nanobeads based fluorescent sensor was designed and developed with three sizes (390, 520 and 890 nm). To characterise the appropriate size and concentration, for further stem cell application, a series of concentrations of nanosensors (25,500,1000,2000μg/mL) and corresponding nanobeads (25,50,100,200,500,1000,2000 μg/mL) were prepared and evaluated the biocompatibilities in terms of the effect on the cell viability and

proliferation for fibroblast in 2D normal cell culture condition *in vitro*.

5.3.1.1 Effects of nanobeads and nanosensors on the viability and proliferation of L929 cells *in vitro* in 2D by MTT assay

Polystyrene nanobeads and nanosensors were both evaluated on L929 fibroblasts at both high and low seeding density, respectively, by MTT assay.

5.3.1.1.1 Effects of the nanosensors on L929 cells at high seeding density and the fluorescent intensity of nanosensors in culture

Based on the cell number test (Figure 5.1 A), high seeding density (10K cells per well in 96-well microplate) was firstly selected for the following evaluations. From results (Figure 5.1 B, C), there were no toxic effect of three sizes nanosensors on the cell viability (24 hours) and proliferation (7 days), except the 890nm sizes sensor with the highest concentration (2000 μg/mL). In addition, there were concentration-dependent fluorescent intensity of the nanosensors and during 7 days within the 2D cell culture system, the fluorescent intensity of the nanosensor was relatively stable (Figure 5.1 D, E).

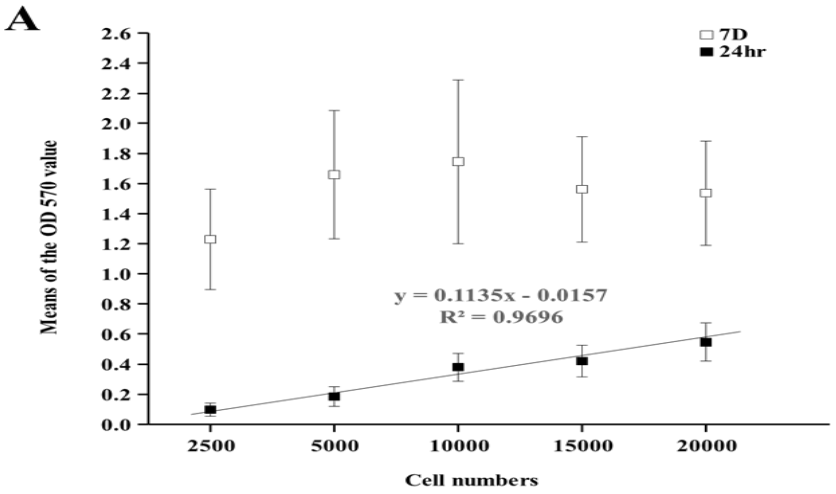

B

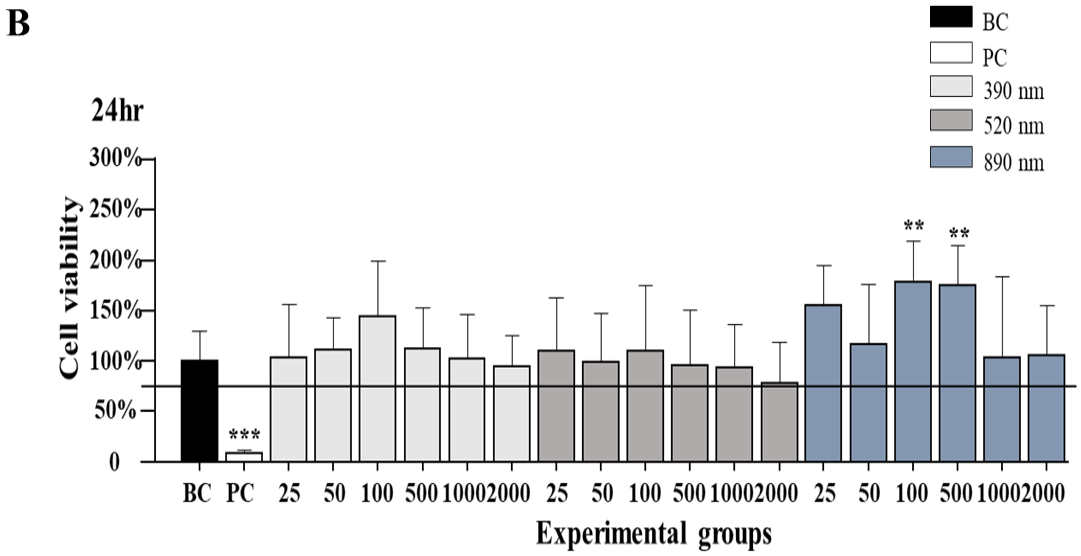
24hr
BC
PC
390 nm
520 nm
890 nm
Cell viability
300%
250%
200%
150%
100%
50%
0
BC PC 25 50 100 500 1000 2000 25 50 100 500 1000 2000 25 50 100 500 1000 2000
Experimental groups

C

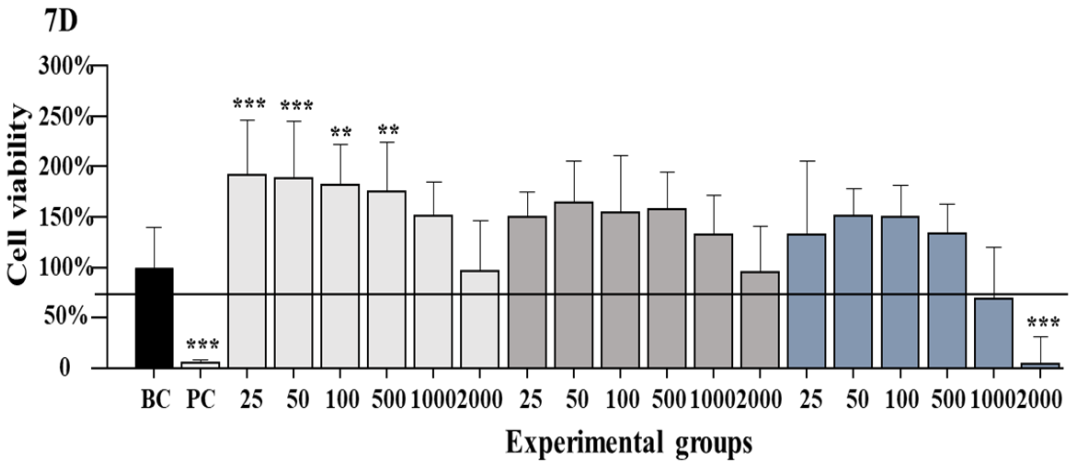
7D
Cell viability
300%
250%
200%
150%
100%
50%
0
BC PC 25 50 100 500 1000 2000 25 50 100 500 1000 2000 25 50 100 500 1000 2000
Experimental groups

D

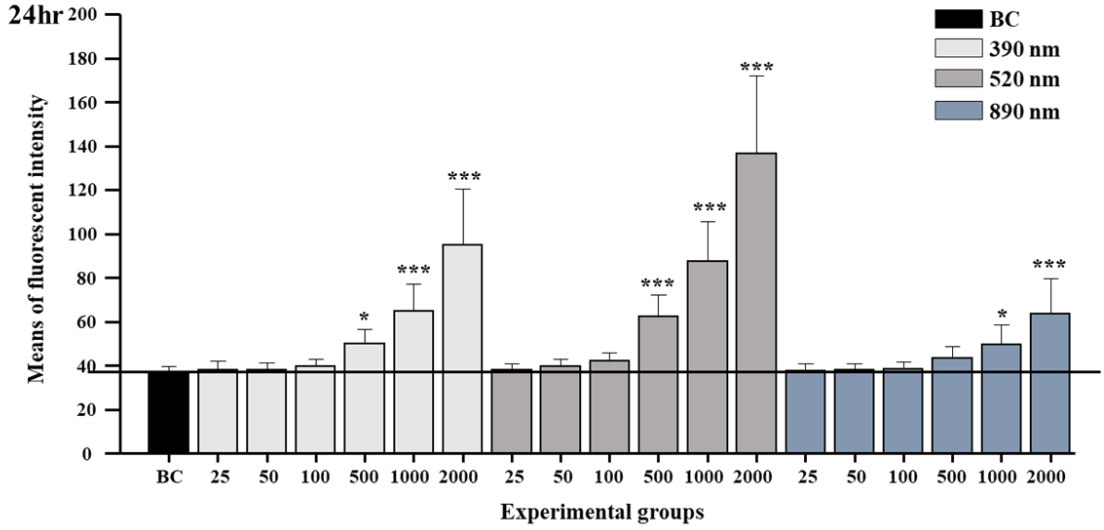
24hr
BC
390 nm
520 nm
890 nm
Means of fluorescent intensity
200
180
160
140
120
100
80
60
40
20
0
BC 25 50 100 500 1000 2000 25 50 100 500 1000 2000 25 50 100 500 1000 2000
Experimental groups

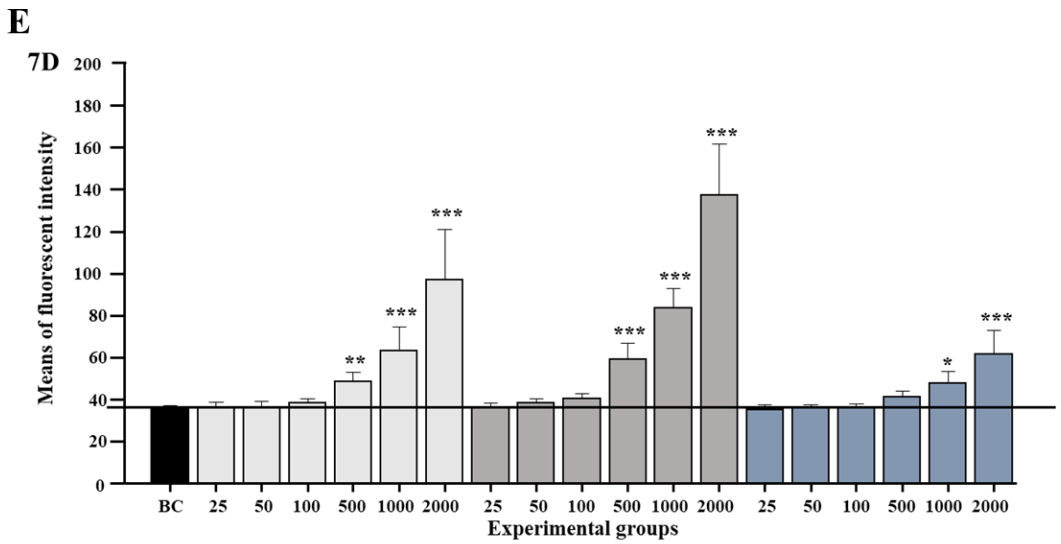

Figure 5.1: Effects of nanosensors with different sizes and concentrations on the viability of L929 cells and the fluorescent intensity of nanosensors culture with cells in vitro in 2D by MTT assay

A: Series cell number test by MTT assay. L929 cells were plated at 2500, 5000, 10,000 15,000 and 20,000 numbers of cells per 100µl per well in a 96 well-plate respectively. For 24 hours test: N=4 n=16; For 7D test: N=4 n=20. B-C: Effects of nanosensors on the viability (24hrs, B) and proliferation (7days, C) of L929 cells measured by MTT essay. Cells were plated at 10,000 cells each well in a 96 well-plate and each well contained 100 µl solution in total. Blank Control (BC) groups are cells threated with growth medium only. Positive Control (PC) groups are cells treated with 1% Triton X100 dissolved in growth medium. Different concentrations of nanosensors at 25, 50,100,200,500,1000,2000 µg/ml were suspended in growth medium respectively and each well was treated with 100 µl particle suspension in total. For 24 hr test, N=3 n=12; for 7 days test, N=3, n=12. All results were normalised by the means of BC groups per individual experiment. Comparisons between experimental group and BC group were analysed by ANOVA one way test (Tukey): * p<0.05 ** p<0.01 *** p<0.001. D-E: Fluorescent intensity of nanosensors cultured with cells after 24 hrs (D) and 7 days (E).

5.3.1.1.2 Effects of the nanobeads on L929 cells at both high and low seeding density

From the preliminary results of nanosensor (Figure 5.1 B, C), cell numbers were greatly increased after 7 days treatment with nanosensor. To study the potential reason, the polystyrene nanobeads, used to fabricate the nanosensor, were further examined its effect on L929 cells at both low and high seeding density. From results of tests with low seeding density (Figure 5.2), generally, there was no toxic effect of the nanobeads on the cell viability and proliferation, especially for short-time treatments, consistent with its instruction from manufacturer. Except for 520 and 890 nm beads at higher concentrations (Figure 5.2 A, C, D) or for long-time culture (Figure 5.2 B, C, D).

From results of tests with high seeding density (Figure 5.3), generally, no pronounced toxic effect of these PS nanobeads on the cell viability and proliferation except the 520 nm beads with the highest concentration (2000 μg/mL) after 7 days treatment (Figure 5.3 B). The greatly improved number of viable cells was again observed (Figure 5.3 A), suggesting further validation by other types of screening methods. In addition, this phenomenon regarding the effect of nanoparticles on the cell proliferation would be worth to study in future work. To summary, low seeding density might be suggested for using L929 cells, whose proliferation rate seems relatively high. The PS nanobeads have less toxic effect on the cell viability and proliferation, however, the bigger size (890nm) and higher concentration (2000 μg/mL) nanobeads would not be suggested for further fabrication of this nanosensor in this project.

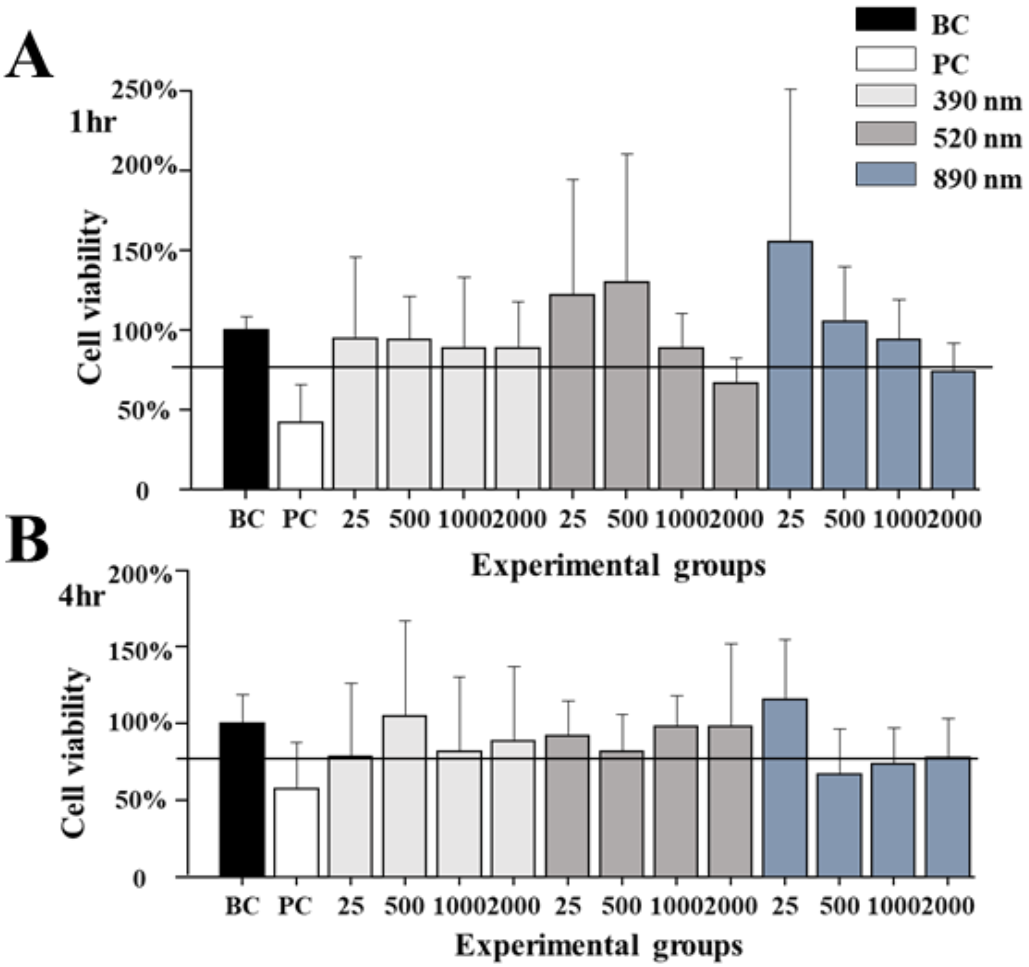

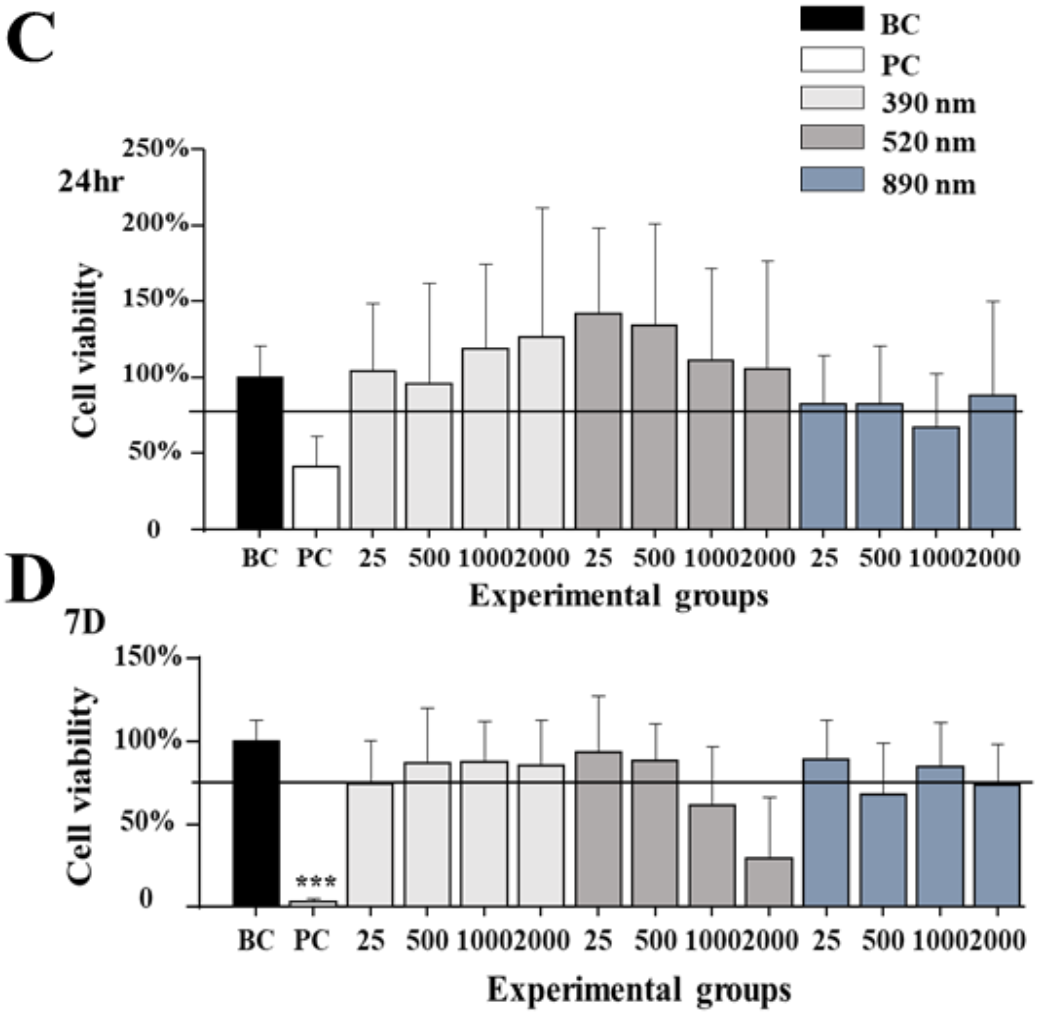

Figure 5.2 Effects of polystyrene (PS) nanobeads with different sizes and concentrations on the viability and proliferation of L929 cells at low seeding densities in vitro in 2D by MTT assay

***A:** Effect of polystyrene nanobeads with different sizes and concentrations on the viability of L929 cells at low seeding density after 1 hours in 2D and in vitro. **B:** Effect of polystyrene nanobeads with different sizes and concentrations on the viability of L929 cells at low seeding density after 4 hours in 2D and in vitro. **C:** Effect of polystyrene nanobeads with different sizes and concentrations on the viability of L929 cells at low seeding density after 24 hours in 2D and in vitro. **D:** Effect of polystyrene nanobeads with different sizes and concentrations on the viability of L929 cells at low seeding density after 7 days in 2D and in vitro. L929 cells were plated in a 96 well plate at 2500 cells per well. After 24h incubation, cells were treated with three sizes of polystyrene nanoparticles with carboxyl groups (PS-NPs) at different concentrations (25, 500, 1000 and 2000 μg/ml) respectively. BC (blank control) groups are cells treated with growth medium. PC (positive control) groups are cells treated with growth medium containing 1% Triton X100. All results were normalised by the means of BC per individual experiment. For 1 hrs test, N=3 n=9; for 4 hrs test, N=3, n=9. For 24 hrs test, N=5 n=17; for 7 days test, N=4, n=14. Comparisons between experimental group and BC group were analysed by ANOVA one way test (Tukey): * p<0.05 ** p<0.01 *** p<0.001.*

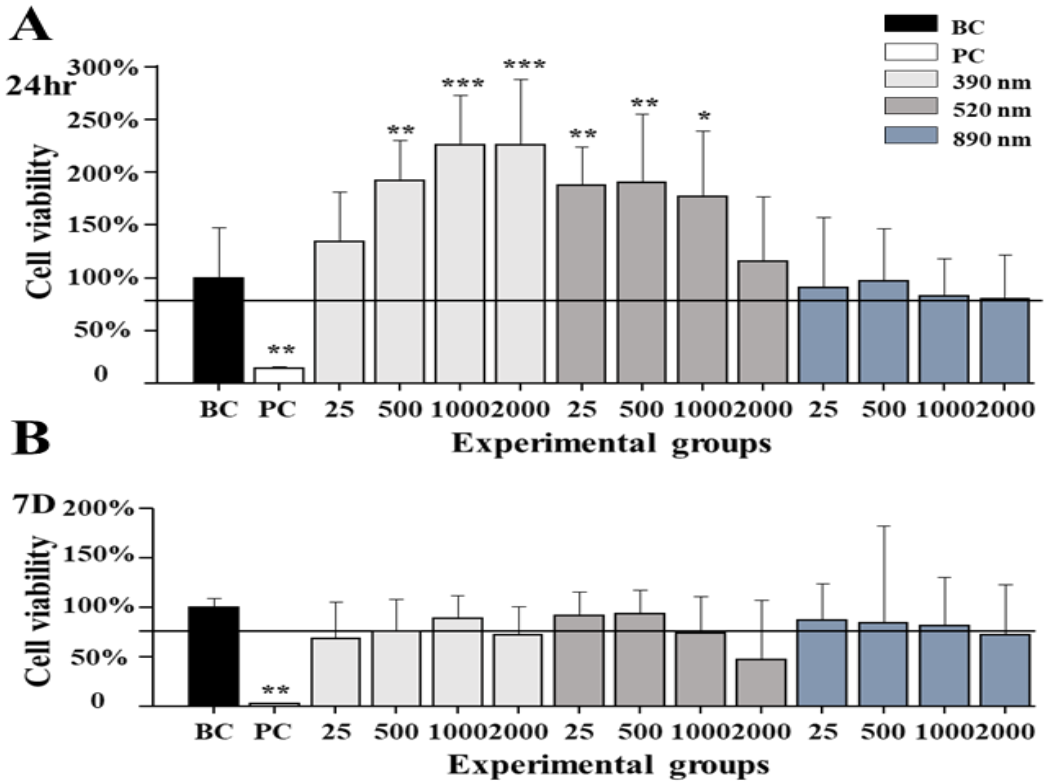

Figure 5.3 Effects of polystyrene (PS) nanobeads with different sizes and concentrations on the viability and proliferation of L929 cells at high seeding density in vitro in 2D by MTT assay

*A: Effect of polystyrene nanobeads with different sizes and concentrations on the viability of L929 cells at high seeding density after 24 hours in 2D and in vitro. B: Effect of polystyrene nanobeads with different sizes and concentrations on the viability of L929 cells at low seeding density after 7 days in 2D and in vitro. Cells were plated at 10,000 cells each well in a 96 well-plate and each well contained 100 µl solution in total. Blank Control (BC) groups are cells threated with growth medium only. Positive Control (PC) groups are cells treated with growth medium containing 1% Triton X100. PS nanobeads were suspended in growth medium at different concentrations of 25, 500,1000,2000 µg/ml respectively and each well was treated with 100 µl particle suspension in total. All results were normalised by the means of BC per individual experiment. For 24 hrs test, N=3 n=12; for 7 days test, N=2, n=8. Comparisons between experimental group and BC group were analysed by ANOVA one way test (Tukey): * p<0.05 ** p<0.01 *** p<0.001.*

5.3.1.1.3 Effects of the nanosensors on L929 cells at low seeding density and the fluorescent intensity of nanosensors in culture

Since the great proliferation rate of the L929 cell in culture and the low cytotoxicity assumed, based on results from nanobeads, effects of the nanosensor on L929 cells with low seeding density was evaluated. From results (Figure 5.4), 390nm nanosensor at 25µg/mL and 890nm nanosensors at

1000µg/mL, had pronounced toxic effects on the viability of L929 cells at low seeding density after 24 hours treatment (Figure 5.4 A). 520 nm nanosensor at 1000µg/mL and 890nm nanosensors with all three concentrations had pronounced toxic effects on the proliferation of L929 cells at low seeding density after 7 days treatment, in which, the concentration-dependent effect on cell proliferation of all three sizes nanosensors was observed (Figure 5.4 B). Results from the fluorescent intensity of nanosensors (Figure 5.4 C, D) were consistent with previous results (Figure 5.1 D, E), suggesting the stability of nanosensor in general cell culture condition *in vitro*. To conclude results by MTT assay, the 890nm size and higher concentration of nanosensor than 1000 µg/mL would not be suggested for further fabrication of this nanosensor in this project.

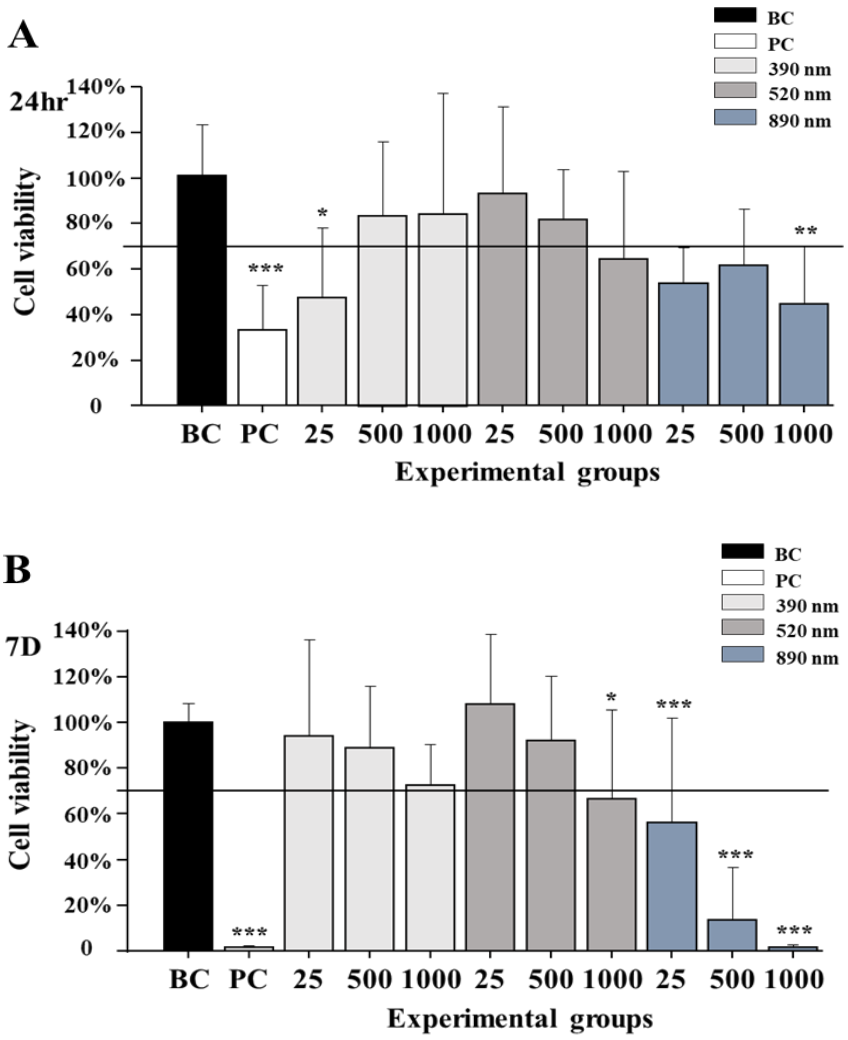

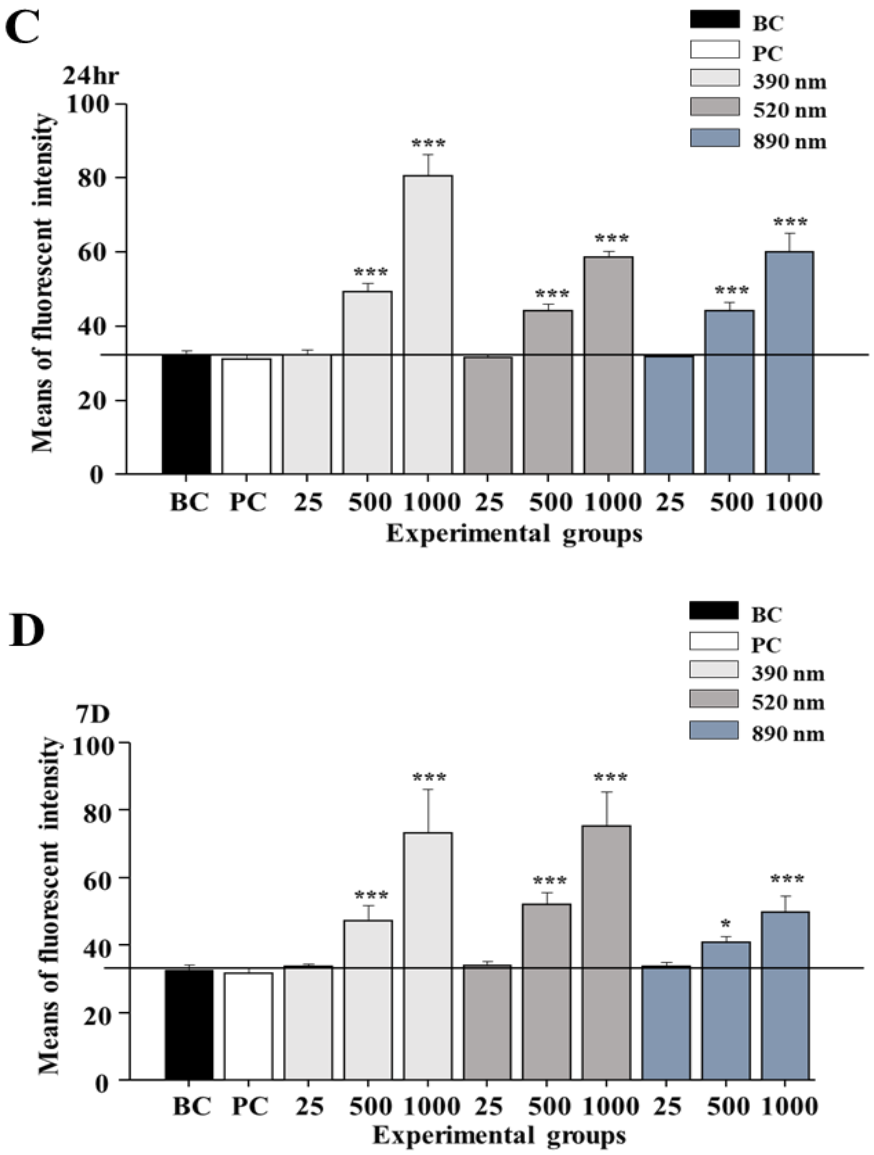

Figure 5.4 Effects of nanosensors with different sizes and concentrations on the viability and proliferation of L929 cells at low seeding density in vitro in 2D by MTT assay and the fluorescent intensity of nanosensor cultured with cells in vitro in 2D

A-B: Effect of nanosensor with different sizes and concentrations on the viability (24hrs, A) and proliferation (7days, B) of L929 cells at low seeding density in vitro in 2D by MTT assay. C-D: Fluorescent intensity of nanosensors cultured with cells after 24 hours (C) and 7 days (D) in vitro in 2D. The effect of nanosensors on the viability and proliferation of L929 was measured by MTT assay. Cells were plated at 2500 cells each well in a 96 well-plate and each well contained 100 µl solution in total. Blank Control (BC) groups are cells threated with growth medium only. Positive Control (PC) groups are cells treated with 1% Triton X100 dissolved in growth medium. Different concentrations of nanosensors at 25,500,1000 µg/ml were suspended in growth medium respectively and each well was treated with 100 µl particle suspension in total. All results were normalised by the means of BC groups per individual experiment. For 24 hr test, N=3 n=9; for 7 days test, N=5, n=20. Comparisons between experimental group and BC group were analysed by ANOVA one way test (Tukey): * p<0.05 ** p<0.01 *** p<0.001.

5.3.1.2 Morphology of L929 cells cultured with and without nanosensor in 2D *in vitro*

In this section, morphology of L929 cells, visualised by both light microscope and fluorescent microscope, when they were cultured with and without nanosensor in 2D, will be presented.

5.3.1.2.1 Morphology of L929 cells at high and low seeding densities after 7 days incubation by inverted phase contract light microscope

Morphologies of L929 cells seeded at high (10K cells per well in 96-well microplate) and low densities (2500 cells per well in 96-well microplate), with and without nanosensors for viability test, were examined under light microscope during culture. From representative images (Figure 5.5), nanoparticles with large size (890nm) at high concentration (2000 µg/ml) were aggregated and interacted with cells. Interactions between nanoparticles and cells in culture might be happened inside or outside cells, requiring further studies. The toxic effect of high concentration of nanosensors/nanoparticles may be due to the physical interaction of the aggregated NPs with cells and more pronounced when cells were seeded at low density.

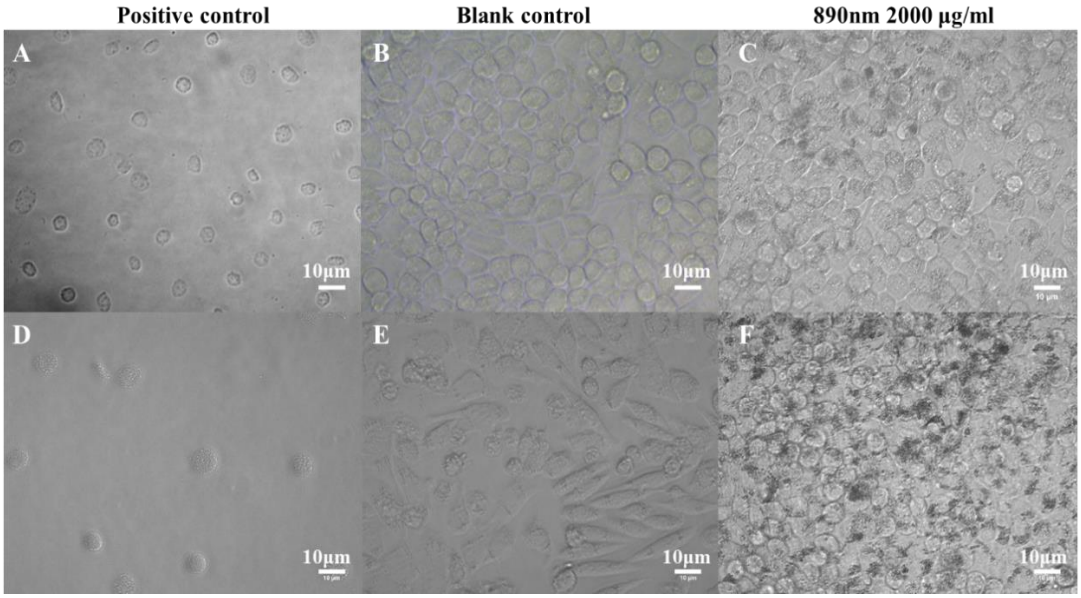

Figure 5.5 Representative images of cellular morphologies of L929 cells at high and low seeding densities,

cultured with and without nanosensors in vitro in 2D for 7 days

A: Positive control of L929 cells seeded at high density (10K cells per well in 96 well microplate) for 7 days, where the culture medium was growth medium with 1% Triton X100 dissolved. B: Blank control group of L929 cells seeded at high density and treated without nanosensors in growth medium for 7 days. C: L929 cells seeded at high density and treated with conditional medium containing growth medium and 890nm nanosensors at 2000 µg/ml for 7 days. D: Positive control of L929 cells seeded at low density (2500 cells per well in 96 well microplate) for 7 days. E: Blank control group of L929 cells seeded at low density and treated without nanosensors in growth medium for 7 days. F: L929 cells seeded at low density and treated with conditional medium containing growth medium and 890nm nanosensors at 2000 µg/ml for 7 days.

5.3.1.2.2 Morphology of L929 cells cultured with and without nanosensor after 24 hours in 2D *in vitro* by immunostaining

To investigate the interaction of nanosensor with living cells *in vitro* in 2D, cellular morphology was examined by immunostaining the cytoskeletal F-actin. From results (Figure 5.6), comparing to cells cultured without nanosensors, the morphology of cells was no pronounced difference, although the cell-cell connection was a little bit sparse. By confocal image (Figure 5.6 D, E), the nanosensor was possibly accumulated around the nuclei of cells, however, the internalisation of nanoparticle by the living cells in this study was remained to further validations by such advanced technologies as higher resolution microscope and transmission electron microscopy (TEM).

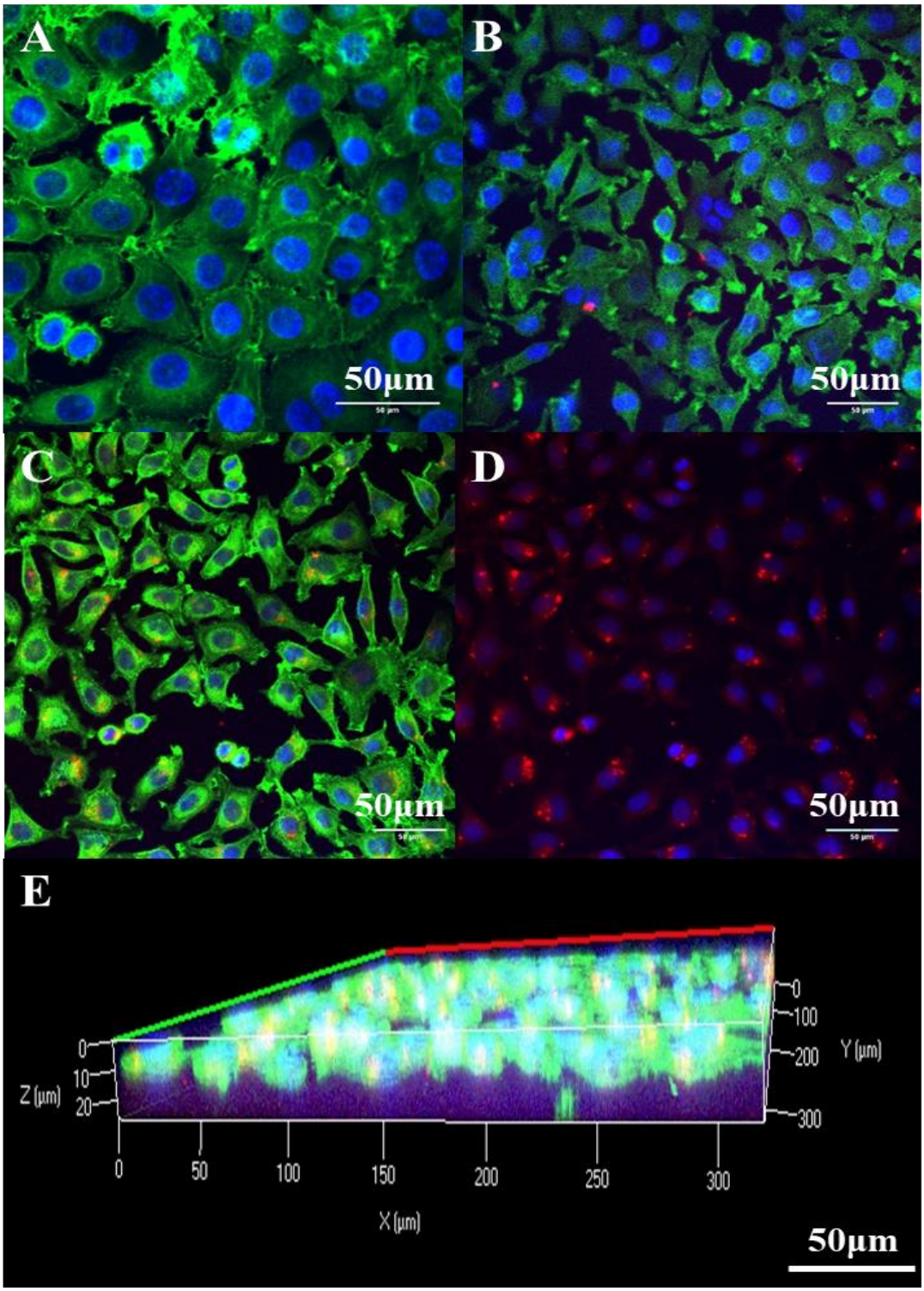

Figure 5.6 Confocal images of the cellular morphology of L929 cells cultured with and without nanosensor in vitro in 2D

A: Cellular morphology of L929 cells cultured without nanosensor. B, C: Merged images of the cellular morphologies of L929 cells cultured with nanosensor in vitro in 2D after 24 hours. D: Merged images of the nanosensors and nuclei of cells. E: 3D z-stack image of the morphologies of L929 cells cultured with nanosensor in monolayer in vitro in 2D after 24 hours. F-action was stained by AlexaFluor™ 488 phalloidin in green, and the nuclei were stained by DAPI in blue. The fluorescence of the nanosensors was red. Scale bars are 50µm.

5.3.1.2.3 Morphology of L929 cells cultured with and without nanosensor after 24 hours in 2D *in vitro* by SEM

Cellular morphology and the potential interaction of nanosensor with living cells in 2D culture system were also examined by SEM. From results (Figure 5.7), no big effect of the nanosensor on the cellular morphology and the distribution of the nanosensors within cell cultures, was observed, although the exact location of the nanosensor within cells or not, could not be confirmed by SEM, requiring further investigations.

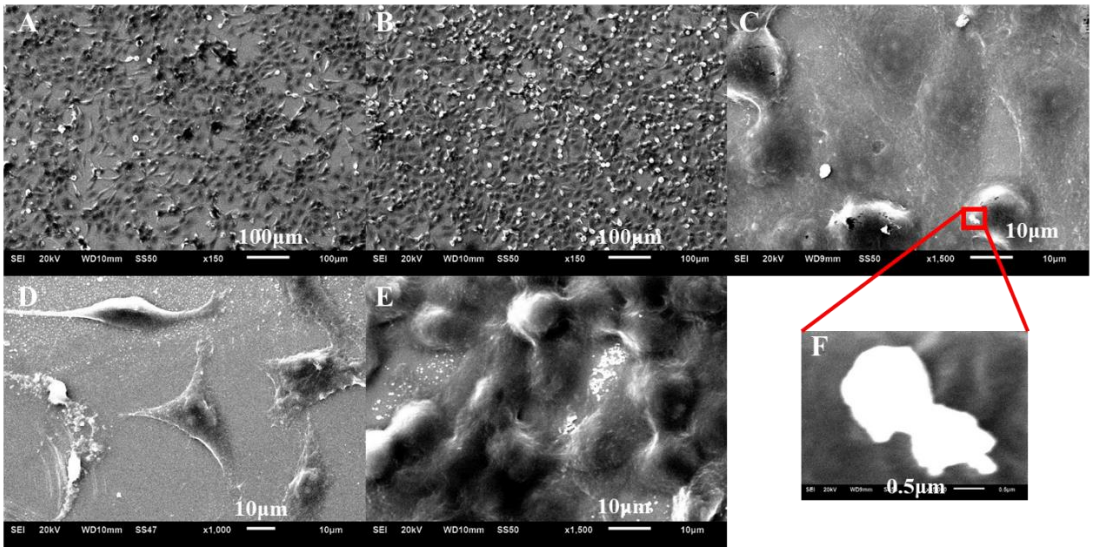

Figure 5.7: SEM images of L929 cells cultured with and without nanosensor after 24 hours in vitro in 2D monolayer

A: L929 cells cultured without nanosensor. B: L929 cells cultured with 520 nm nanosensors. C: High magnification image of L929 cells cultured with 520 nm nanosensors. D: High magnification image of L929 cells cultured without nanosensor. E: High magnification image of L929 cells cultured with nanosensors. F: High magnification image of C to show the potential nanosensors in culture.

5.3.2 Characterisation of nanosensors in cell culture condition *in vitro* by LDH assay

Based on results from 5.3.1, two sizes (390 and 520nm) and three concentrations (25, 500, and 1000 µg/mL) of the nanosensor were preliminarily selected for further evaluations on both L929 cells and MSCs by LDH assay.

5.3.2.1 Effects of the nanosensors on living cells and the fluorescent intensity of nanosensors in culture

Firstly, effects of the selected two sizes and three concentrations of nanosensors on the viability and proliferation of L929 cells in 2D *in vitro* by LDH assay were performed. From results (Figure 5.8 A-C), generally, there was no toxic effect of the nanosensors observed, except the 520nm sensor at 1000µg/mL after 7 days treatment, consistent with previous results from MTT assay (5.3.1). Consistent results of the fluorescent intensity of 520nm nanosensor but the 390nm sensor, were observed, suggesting that the fabrication process of this sensor was not stable in current facilities in this lab. Hence, 520nm nanosensor was selected for subsequent studies on stem cells.

In MSC studies by LDH assay (Figure 5.8 D-F), consistent results with those of L929 cells (Figure 5.8 B, C) were observed, in which, there was generally no toxic effect of the 520nm nanosensor on the viability and proliferation of BM-MSCs cultured *in vitro* in 2D, except the highest concentration of nanosensor (1000µg/mL) after 7 days treatment. Besides, there was a concentration-dependent fluorescent intensity of nanosensor in 2D cell culture system, in which comparing to results from 24 hours treatment, the fluorescent intensity of 520nm nanosensor was stable after 7 days in the cell culture *in vitro*. Nanosensor at 25µg/mL did not present enough fluorescent signal after both 24 hours and 7 days treatments, suggesting that this concentration was inappropriate for further studies.

To conclude, based on these results, 520nm nanosensors at about 500µg/mL concentration, presenting no toxic effects on cell viability and proliferation, consistently stable and enough fluorescent signals in cell culture, would be selected for further BM-MSC differentiation studies.

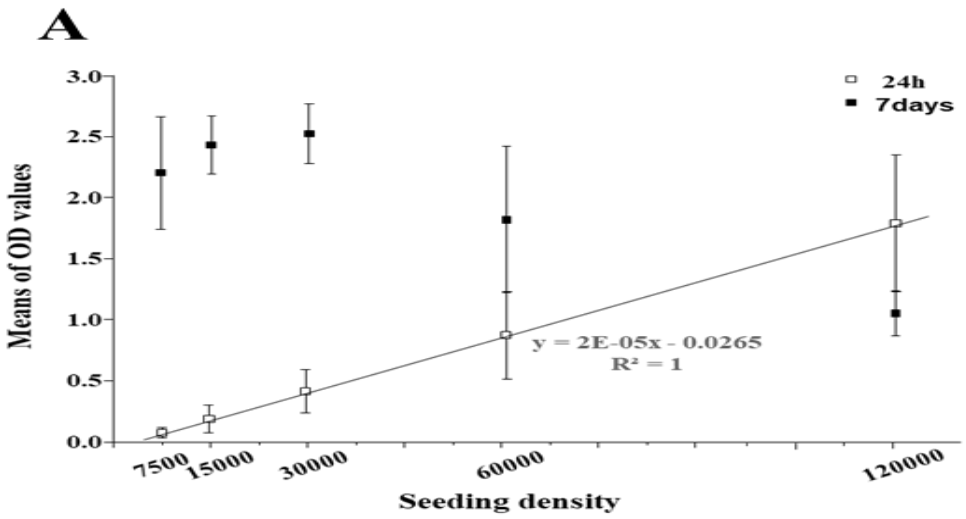
A
24h
7days
Means of OD values
3.0
2.5
2.0
1.5
1.0
0.5
0.0
y = 2E-05x - 0.0265
R² = 1
7500
15000
30000
60000
120000
Seeding density

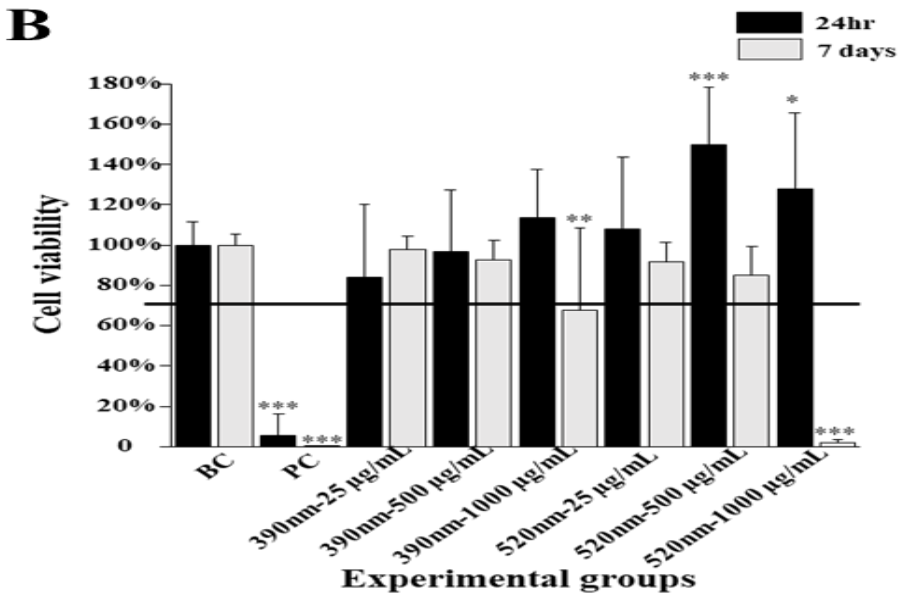
B
24hr
7 days
Cell viability
180%
160%
140%
120%
100%
80%
60%
40%
20%
0
***
**
*
BC
PC
390nm-25 μg/mL
390nm-500 μg/mL
390nm-1000 μg/mL
520nm-25 μg/mL
520nm-500 μg/mL
520nm-1000 μg/mL
Experimental groups

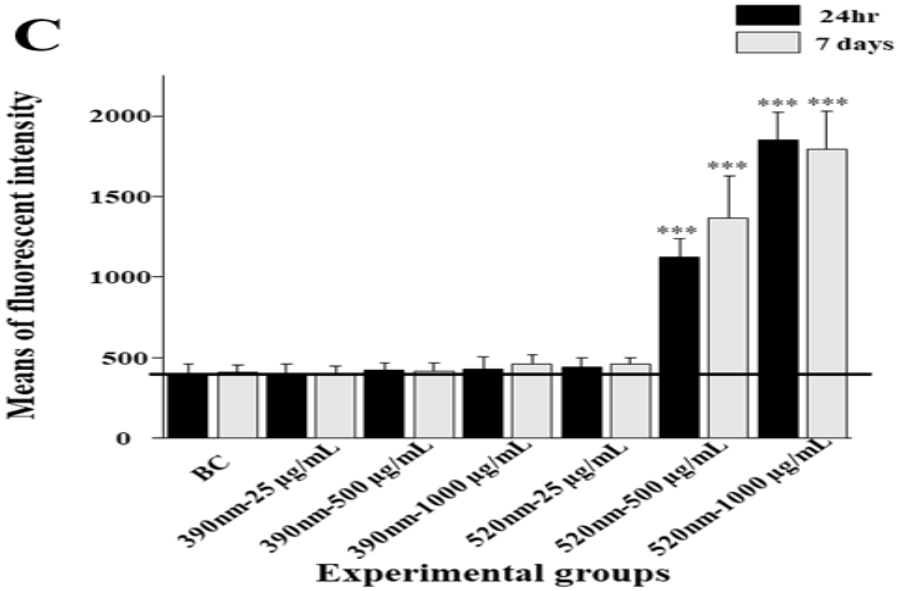
C
24hr
7 days
Means of fluorescent intensity
2000
1500
1000
500
0
***
BC
390nm-25 μg/mL
390nm-500 μg/mL
390nm-1000 μg/mL
520nm-25 μg/mL
520nm-500 μg/mL
520nm-1000 μg/mL
Experimental groups

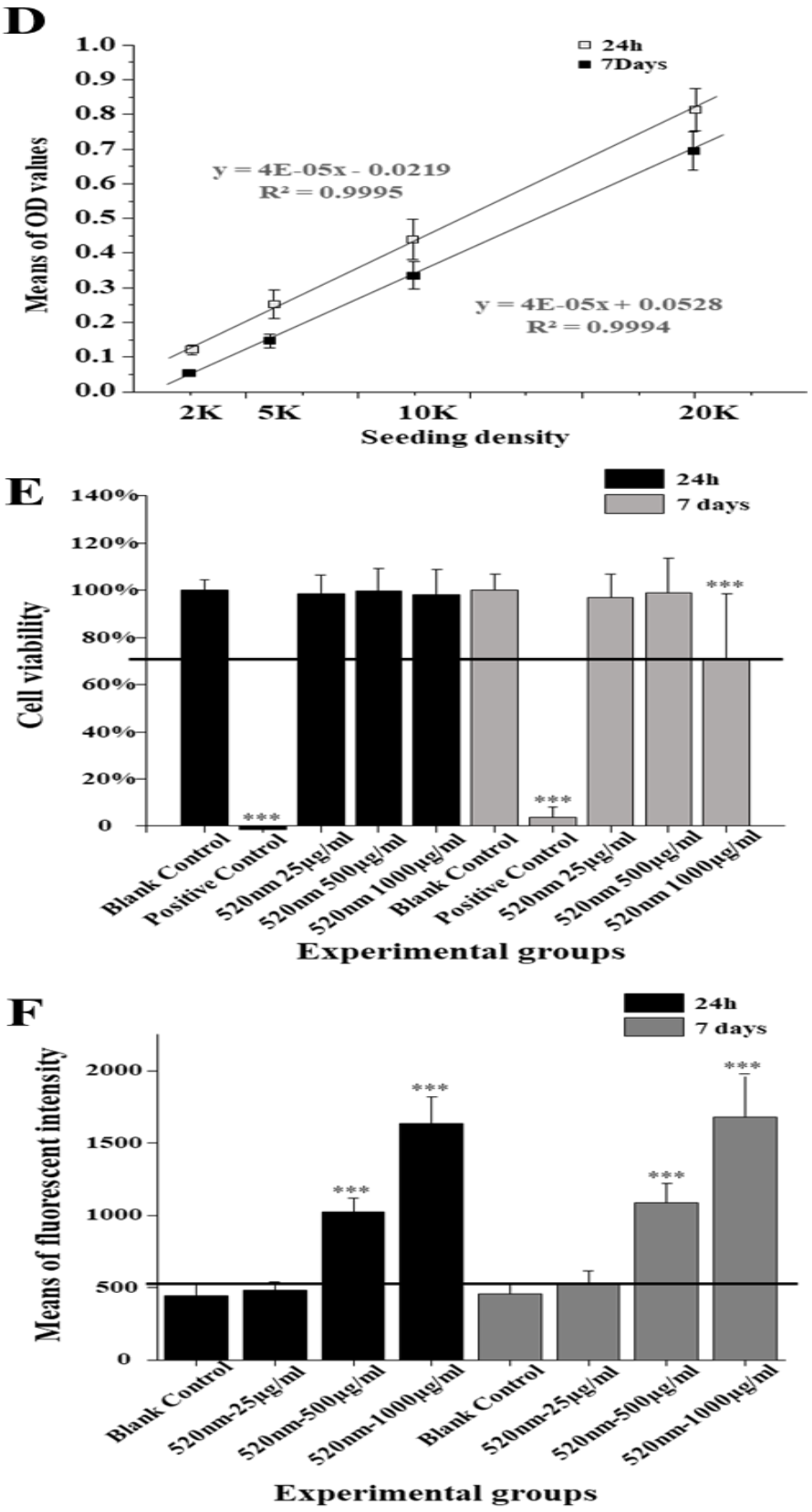

Figure 5.8: Effects of nanosensors with three sizes and three concentrations on the viability and proliferation of L929 cells and MSCs by LDH assay and the fluorescent intensity of nanosensors in cell culture in 2D

A: Series cell number tests of L929 cells by LDH assay. B: Effect of nanosensors on the viability and proliferation of L929 cells. C: Fluorescent intensity of nanosensors cultured with L929 cells in vitro in 2D. D: Series cell number tests of BM-MSCs by LDH assay. E: Effect of nanosensors on the viability and proliferation of BM-MSCs. F: Fluorescent intensity of nanosensors cultured with BM-MSCs in vitro in 2D. For series number tests, L929 cells were seeded at 7500; 15,000; 30,000; 60,000 and 120,000 numbers of cells per 100µl per well in a 96 well-plate respectively. BM-MSCs were seeded at 0, 2000,5000,10000 and 20000 numbers of cells per well (0, 1000, 2500,5000 and 10000 cells /cm^2). For viability tests, L929 cells were plated into a 24-well microplate at the density of 15000 cells per well). BM-MSCs were plated in a 24 well microplate at 5000 cells/cm^2. For 24 hrs and 7 days test of L929, N=3 n=18. For 24 hrs and 7 days test of BM-MSCs. N=3 n=24. Comparisons between different treatment groups and blank control group were analysed by ANOVA one way test (Tukey): * p<0.05; ** p<0.01; *** p<0.001.

5.3.2.2 Effect of the 520nm nanosensor at 500 µg/ml on BM-MSCs differentiations *in vitro*

Based on above mentioned results (5.3.2.1), 520nm nanosensors at 500µg/mL was selected for subsequent evaluations on BM-MSC differentiations *in vitro*. Differentiation results will be presented in this section.

5.3.2.2.1 Effect of the nanosensor on BM-MSCs osteogenesis in 2D *in vitro*

It could be found from results that, there was no negative effect of the nanosensor under the selected regime (520nm at 500µg/mL), on the osteogenesis of BM-MSCs in 2D *in vitro,* in which expressions of the osteogenic marker (osteocalcin) were successfully detected by immunofluorescent staining (Figure 5.9) and specific mineral depositions after MSC osteogenesis were also observed by von Kossa staining (Figure 5.10).

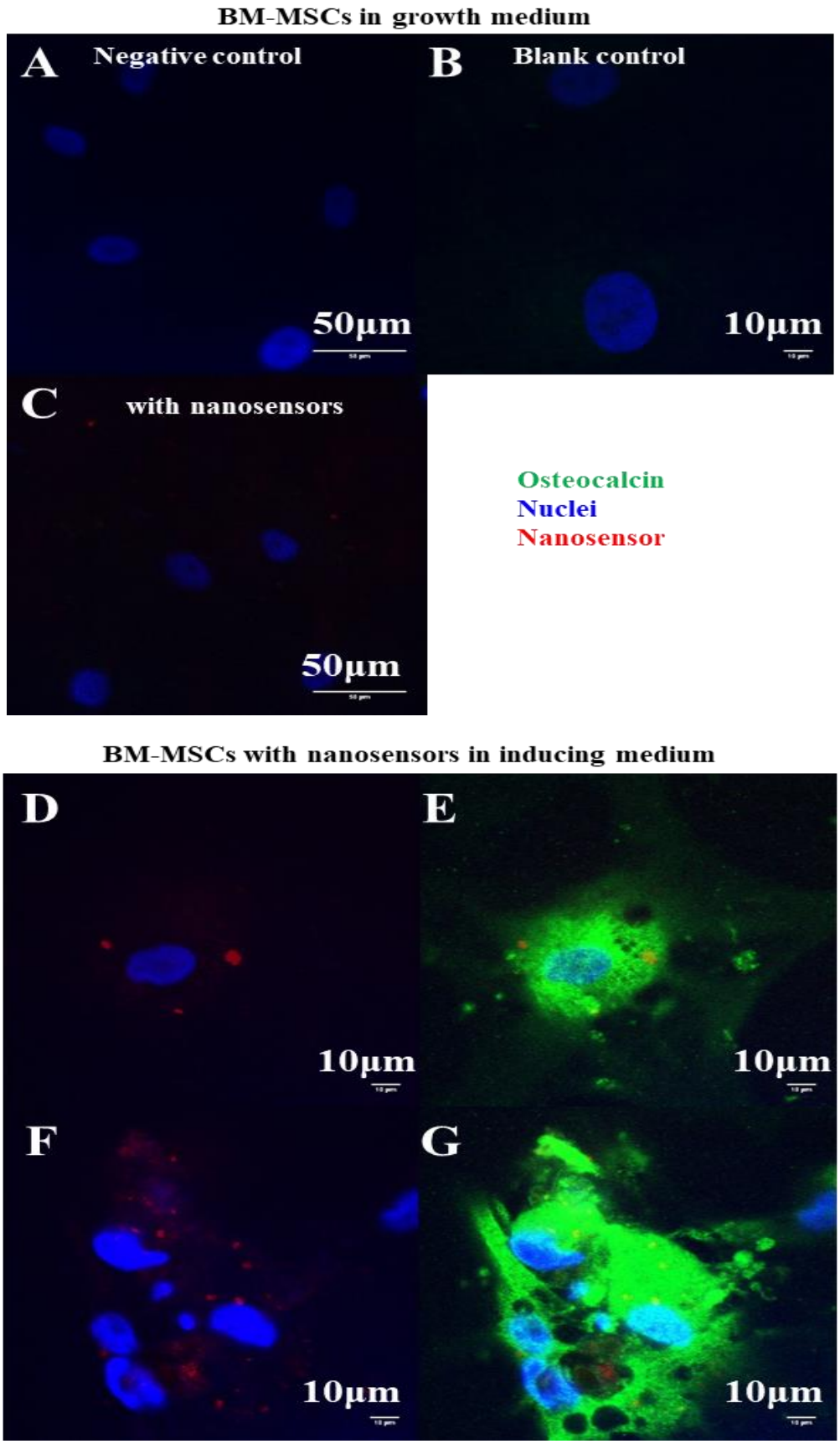

Figure 5.9: Confocal images of BM-MSCs osteogenesis with and without nanosensors in 2D in vitro after 28 days

A: Negative control confocal image of BM-MSCs cultured in growth medium and stained by anti-mouse IgG Alexa Fluor® 488 (secondary antibody only, no primary antibody stained). B: Confocal image of BM-MSCs cultured in growth medium without nanosensors after 28 days. C: Confocal image of BM-MSCs cultured in growth medium with nanosensors after 28 days. D, F: Confocal image of the nanosensors and nuclei of BM-MSCs cultured in osteogenic inducing medium with nanosensor after 28 days. E, G: Confocal image of osteocalcin, nuclei and nanosensor of BM-MSCs cultured in osteogenic inducing medium with nanosensor after 28 days. The osteocalcin secreted by differentiated BM-MSCs was stained by anti-osteocalcin and secondary antibody in green, and the nuclei of cells were stained by DAPI in blue. The fluorescence of nanosensor was red.

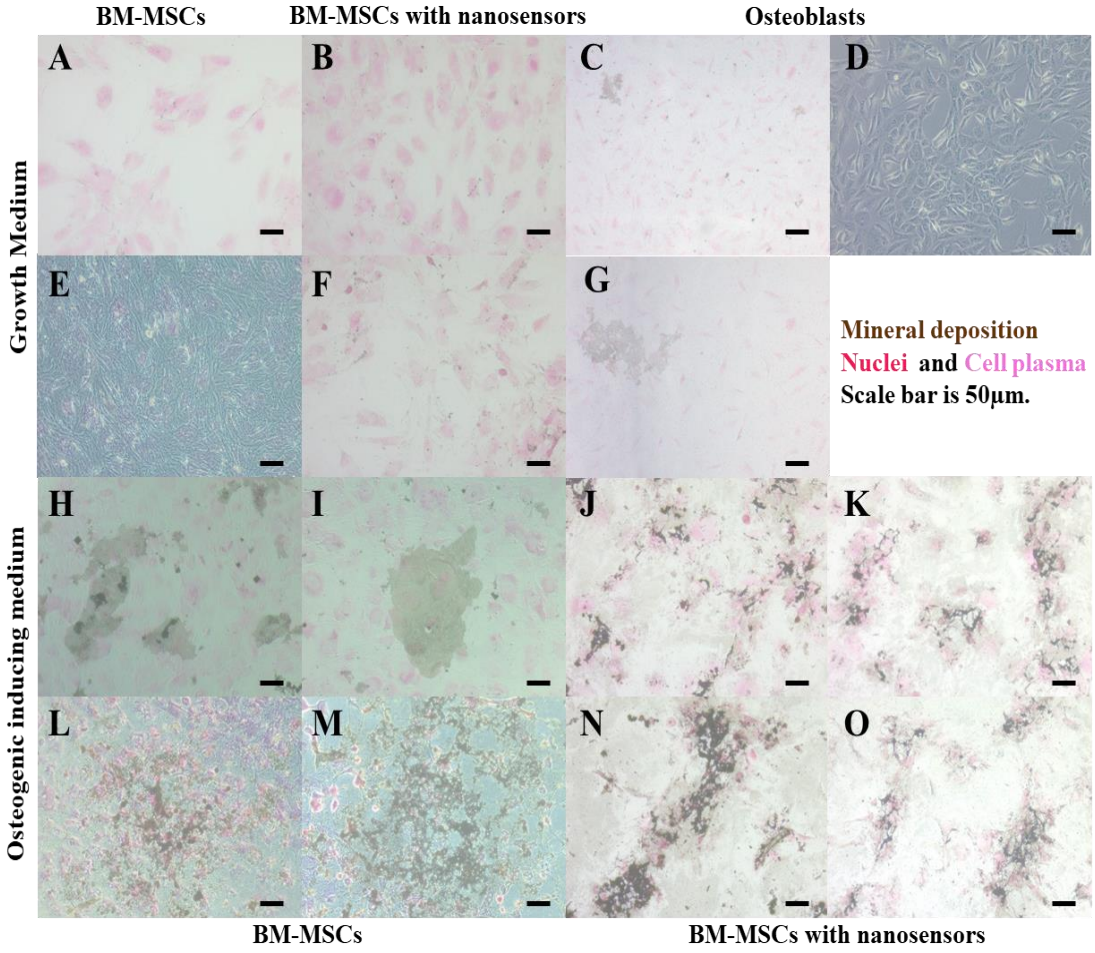

Figure 5.10: Images of BM-MSCs osteogenesis with and without nanosensors in 2D in vitro after 28 days by von Kossa staining

A, E: BM-MSCs cultured in growth medium without nanosensors in vitro in 2D after 28 days by von Kossa staining. B, F: BM-MSCs cultured in growth medium with nanosensors in vitro in 2D after 28 days by von Kossa staining. C, G: Osteoblasts cultured in growth medium without nanosensors in vitro in 2D after 28 days by von Kossa staining. D: Osteoblasts cultured in growth medium without nanosensors in vitro in 2D after 28 days without staining. H, I, L, M: BM-MSCs cultured in osteogenic inducing medium without nanosensors in vitro in 2D after 28 days by von Kossa staining. J, K, N, O: BM-MSCs cultured in osteogenic inducing medium with nanosensors in vitro in 2D after 28 days by von Kossa staining. Nuclei were stained in deep pink after counterstaining. Cell plasma were stained in light pink after counterstaining. The mineral depositions were in dark brown after von Kossa staining. Scale bars are 50μm.

5.3.2.2.2 Effect of the nanosensor on BM-MSCs chondrogenesis in 2D monolayer culture *in vitro*

Effect of nanosensor on BM-MSCs chondrogenesis in 2D monolayer *in vitro* was studied at first. However, from literatures, chondrogenesis of MSCs was difficult in 2D culture system. Consistent results in this study were observed (Figure 5.11 and 5.12), in which after chondrogenic induction, cell numbers were greatly reduced, and after 21 days incubation, very little cells were differentiated in monolayer, being confirmed by poor expressions of type II collagen (Figure 5.11). Even human chondrocytes presented poor differentiation markers (Figure 5.12 D, H, L) in 2D culture system, suggesting that 3D culture system for chondrogenesis would be necessary to be selected in further studies.

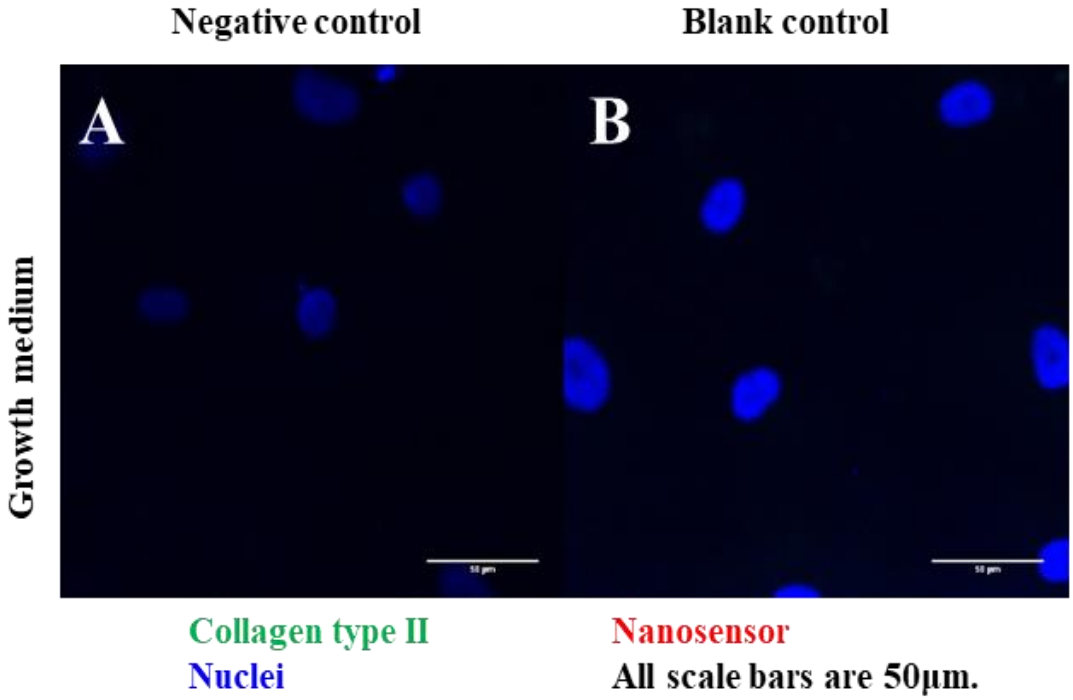

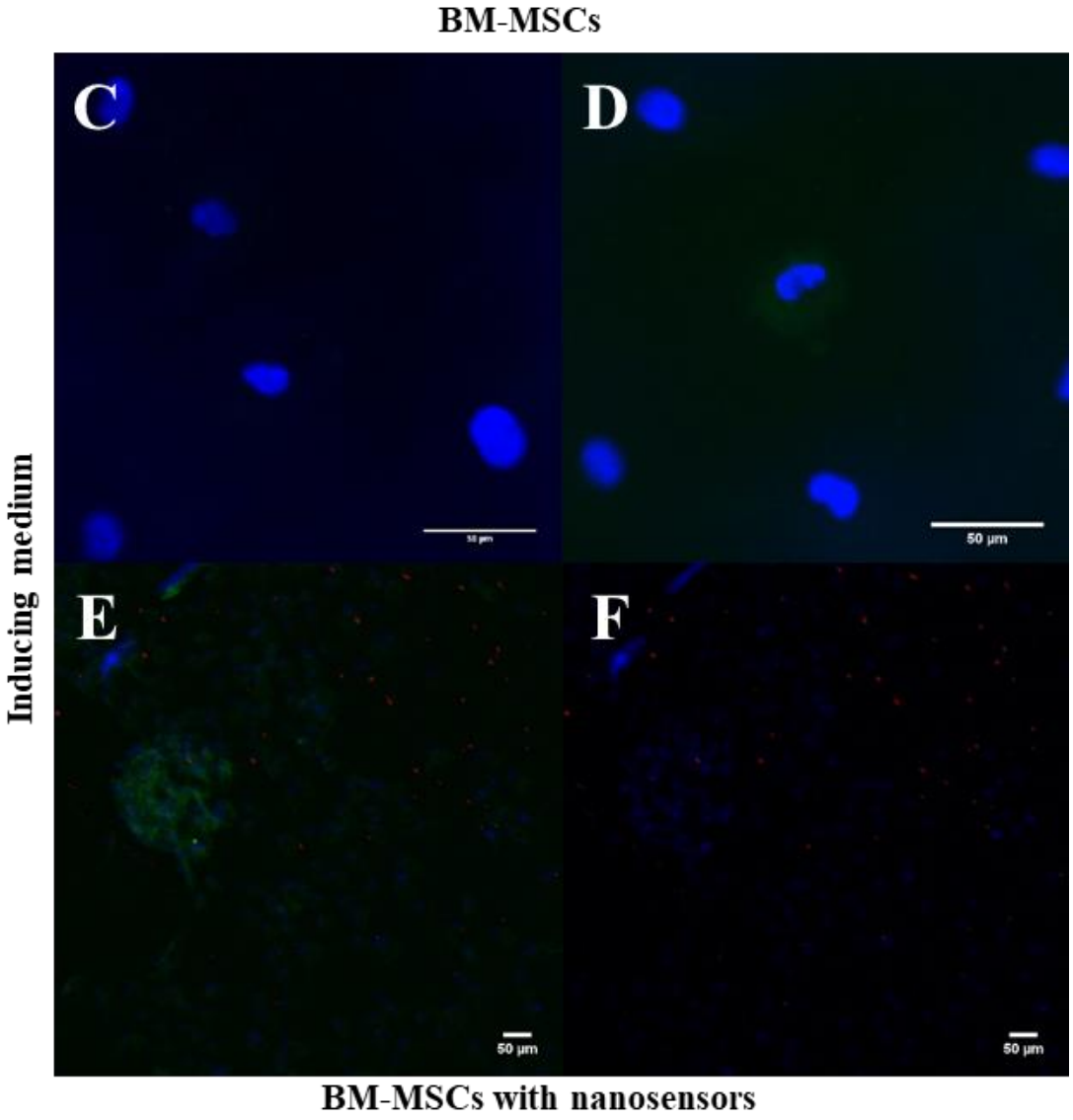

Figure 5.11: Confocal images of BM-MSCs chondrogenesis with and without nanosensors in 2D in vitro after 21 days

A: Negative control confocal image of BM-MSCs cultured in growth medium and stained by anti-mouse IgG Alexa Fluor®488 (secondary antibody only, no primary antibody stained). B: Confocal image of BM-MSCs cultured in growth medium without nanosensors after 21 days. C, D: Confocal images of BM-MSCs cultured in chondrogenic inducing medium without nanosensors after 21 days. E, F: Confocal images of BM-MSCs cultured in chondrogenic inducing medium with nanosensors after 21 days. The type II collagen secreted by differentiated BM-MSCs was stained by anti-type II collagen and secondary antibody in green, and the nuclei of cells were stained by DAPI in blue. The fluorescence of nanosensor was red. Scale bars are 50µm.

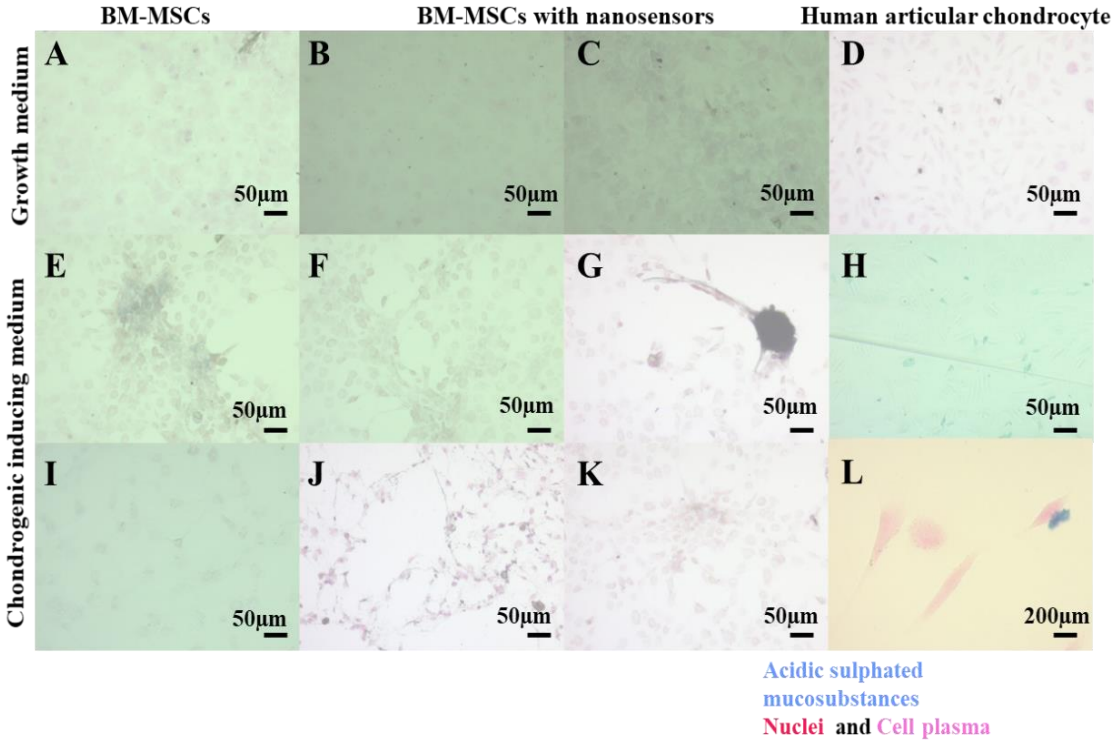

Figure 5.12: Images of BM-MSCs chondrogenesis with and without nanosensors in 2D in vitro after 21 days by Alcian blue staining

A: BM-MSCs cultured in growth medium without nanosensors in vitro in 2D after 21 days by Alcian blue staining. B, C: BM-MSCs cultured in growth medium with nanosensors in vitro in 2D after 21 days by Alcian blue staining. D, H, L: Human articular chondrocytes cultured in growth medium without nanosensors in vitro in 2D after 21 days by Alcian blue staining. E, I: BM-MSCs cultured in chondrogenic inducing medium without nanosensors in vitro in 2D after 21 days by Alcian blue staining. F, G, J, K: BM-MSCs cultured in chondrogenic inducing medium with nanosensors in vitro in 2D after 21 days by Alcian blue staining. Nuclei were stained in deep pink after counterstaining. Cell plasma were stained in light pink after counterstaining. The acidic sulphated mucosubstances were stained in blue after Alcian blue staining. Scale bars are 50μm.

5.3.2.2.3 Effect of the nanosensor on BM-MSCs chondrogenesis in 3D pellet culture *in vitro*

To further evaluate the effect of the selected nanosensor on BM-MSC chondrogenesis *in vitro*, 3D pellet culture was applied. But due to the limitations on the time and facilities, 3D samples were not shaped and sliced to stain. From current results (Figure 5.13), both BM-MSCs and chondrocytes with and without nanosensor could form cell pellets successfully and differentiate for a long time (up to 21 days) *in vitro*. Without using mould to shape the structure, cell pellets formed by different batch of cells were not uniform. Although further validations might be worth

to do, from current results, there was no negative effect of the nanosensor on both chondrocytes and BM-MSCs chondrogenesis in 3D pellet culture *in vitro*, being confirmed by the expressions of type II collagen (Figure 5.13) from immunofluorescent staining and the detections of mucopolysaccharides (Figure 5.14) from Alcian blue staining, respectively.

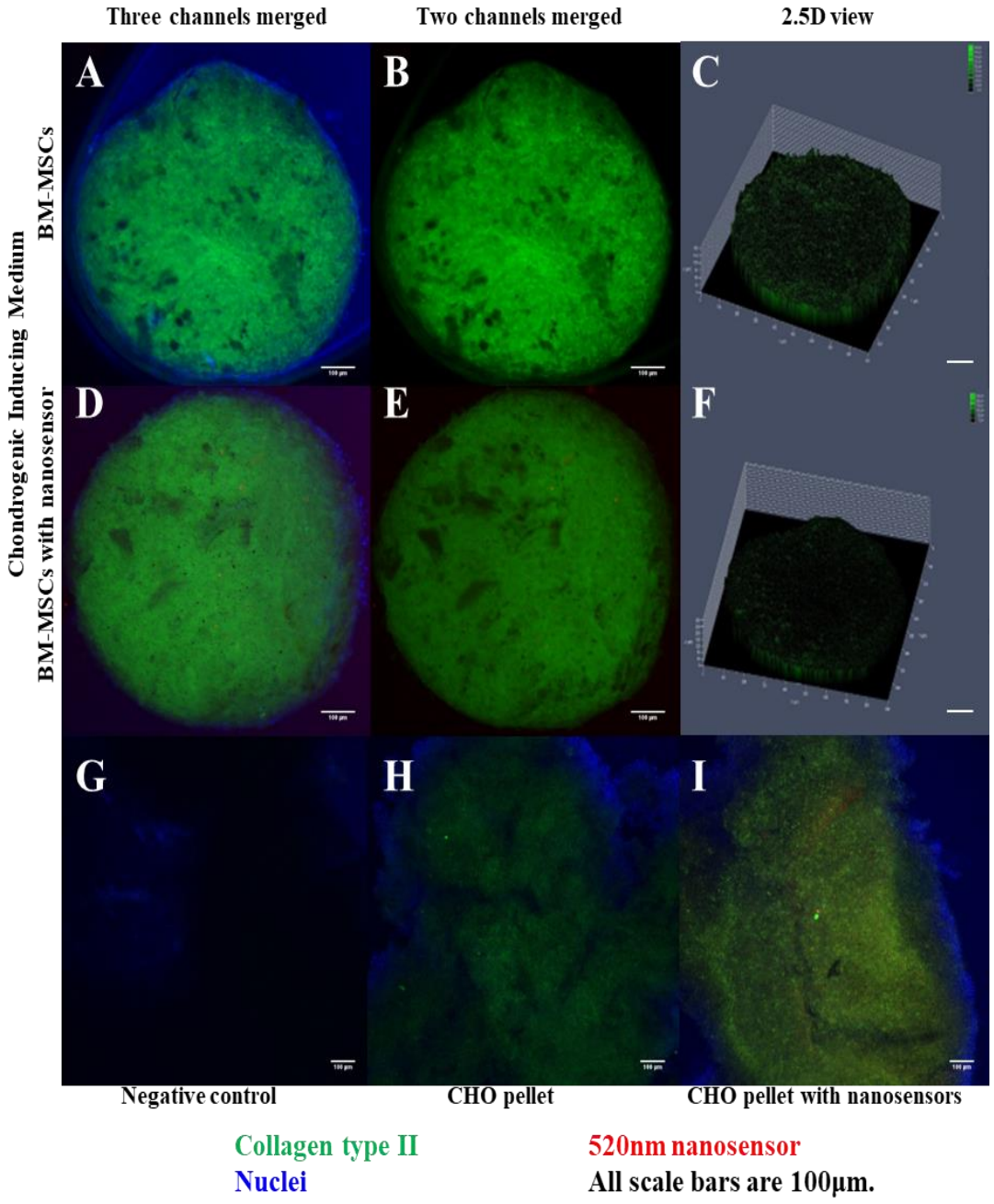

Figure 5.13: Confocal images of BM-MSCs chondrogenesis in 3D pellet by immunofluorescent staining A, B: Confocal images of BM-MSCs chondrogenesis in 3D pellet without nanosensors. C: 2.5D view of the 3D z-stack confocal image of BM-MSCs chondrogenesis in 3D pellet without nanosensors. D, E: Confocal images

of BM-MSCs chondrogenesis in 3D pellet with nanosensors. F: 2.5D view of the 3D z-stack confocal image of BM-MSCs chondrogenesis in 3D pellet with nanosensors. G: Negative confocal image of chicken chondrocytes (CHO) cultured in 3D pellet and stained by anti-mouse IgG Alexa Fluor®488 (secondary antibody only, no primary antibody stained). H, I: Confocal images of chicken chondrocytes (CHO) cultured in 3D pellet with and without nanosensors. The type II collagen secreted by differentiated BM-MSCs and CH were stained by anti-type II collagen and secondary antibody in green, and the nuclei of cells were stained by DAPI in blue. The fluorescence of nanosensor was red. Scale bars are 100µm.

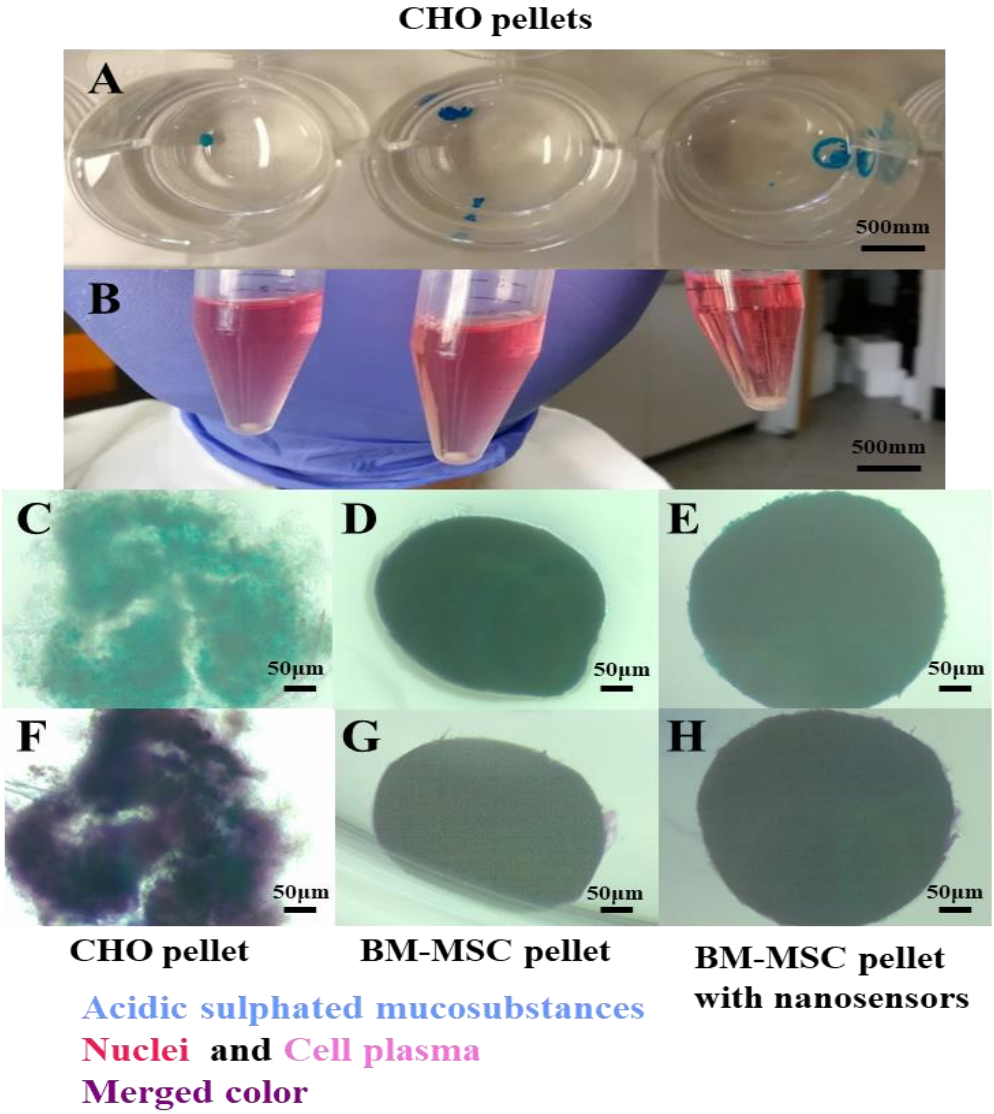

Figure 5.14: Images of differentiated 3D pellets formed by chondrocytes and BM-MSCs with and without Alcian blue staining

A: Image of pellets formed by chicken chondrocytes (CHO) after 21 days culture in vitro by Alcian blue staining. B: Image of 3D pellets formed by chicken chondrocytes. C, D, E: Images of 3D pellets after Alcian blue staining without counterstaining, formed by chicken chondrocytes, BM-MSCs without nanosensors, and BM-MSCs with nanosensors after 3D pellet culture and differentiation in vitro for about 21 days. F, G, H: Images of 3D pellets after Alcian blue staining and counterstaining, formed by chicken chondrocytes, BM-MSCs without nanosensors, and BM-MSCs with nanosensors after 3D pellet culture and differentiation in vitro for about 21 days. Nuclei were stained in deep pink after counterstaining. Cell plasma were stained in light pink after

counterstaining. The acidic sulphated mucosubstances were stained in blue after Alcian blue staining. And the purple was the merged colours of blue and pink after both Alcian blue staining and counterstaining. Scale bars are 50μm.

5.3.3 Morphologies of BM-MSCs with and without nanosensor after osteogenesis in 2D

Cellular morphologies of BM-MSCs after 2D differentiation, were also examine by inverted microscope (Figure 5.15), immunofluorescent staining (Figure 5.16) and SEM (Figure 5.17). From observations, after osteogenesis, cell numbers were greatly reduced, along with greatly changed cellular morphology, due to the cell behaviour was altered from proliferation to differentiation after induction *in vitro*. Cell metabolism was altered, with increased secretion of specific products regarding the specific induction. More pronounced cellular morphology of differentiated BM-MSCs was observed by immunofluorescent staining, in which multiple pores of the intracellular connection rather the stretched fibrous cytoskeleton, were very impressive, suggesting the change of cellular behaviour and the important impact of the cytoskeleton on cell behaviours. There was no negative effect of the novel nanosensor on the cell morphology, viability, proliferation and differentiation observed in this study, although the interaction between nanoparticles and living cells, in particular the potential internalisation of nanoparticles by cells, were remained further studies.

From the SEM image and the EDX analysis, mineral depositions by the differentiated BM-MSCs after osteogenesis, could be evaluated, further confirming the osteogenesis of BM-MSCs applied in this study *in vitro* in 2D culture system. And no negative effect of the nanosensor on the osteogenesis and mineral deposition of the BM-MSCs, was observed, suggesting the biocompatibility of this novel nanosensor under the selected regime to be applied in MSC-based studies.

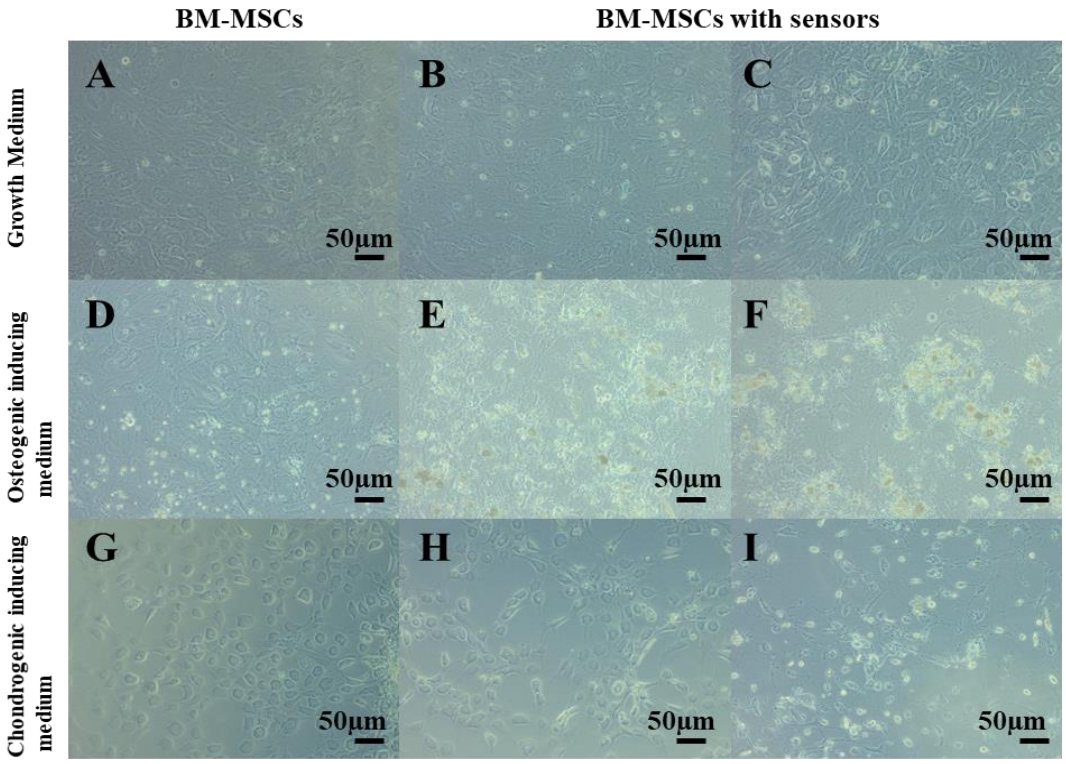

Figure 5.15: Cellular morphologies of BM-MSCs in growth medium and inducing medium after differentiations with and without sensors by normal inverted microscope

A: Morphologies of BM-MSCs cultured in growth medium after 28 days without nanosensors. B, C: Morphologies of BM-MSCs cultured in growth medium after 28 days with nanosensors. D: Morphologies of BM-MSCs cultured in osteogenic inducing medium after 28 days without nanosensors. D, F: Morphologies of BM-MSCs cultured in osteogenic inducing medium after 28 days with nanosensors. G: Morphologies of BM-MSCs cultured in chondrogenic inducing medium after 21 days without nanosensors. H, I: Morphologies of BM-MSCs cultured in chondrogenic inducing medium after 2 days with nanosensors. Scale bars are 50µm.

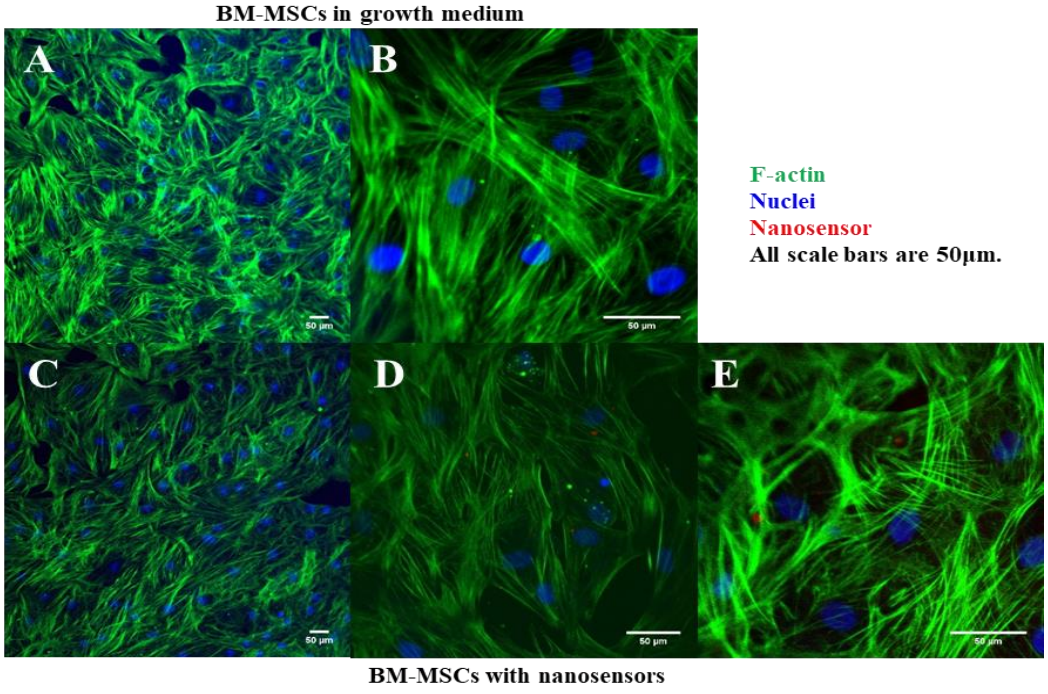

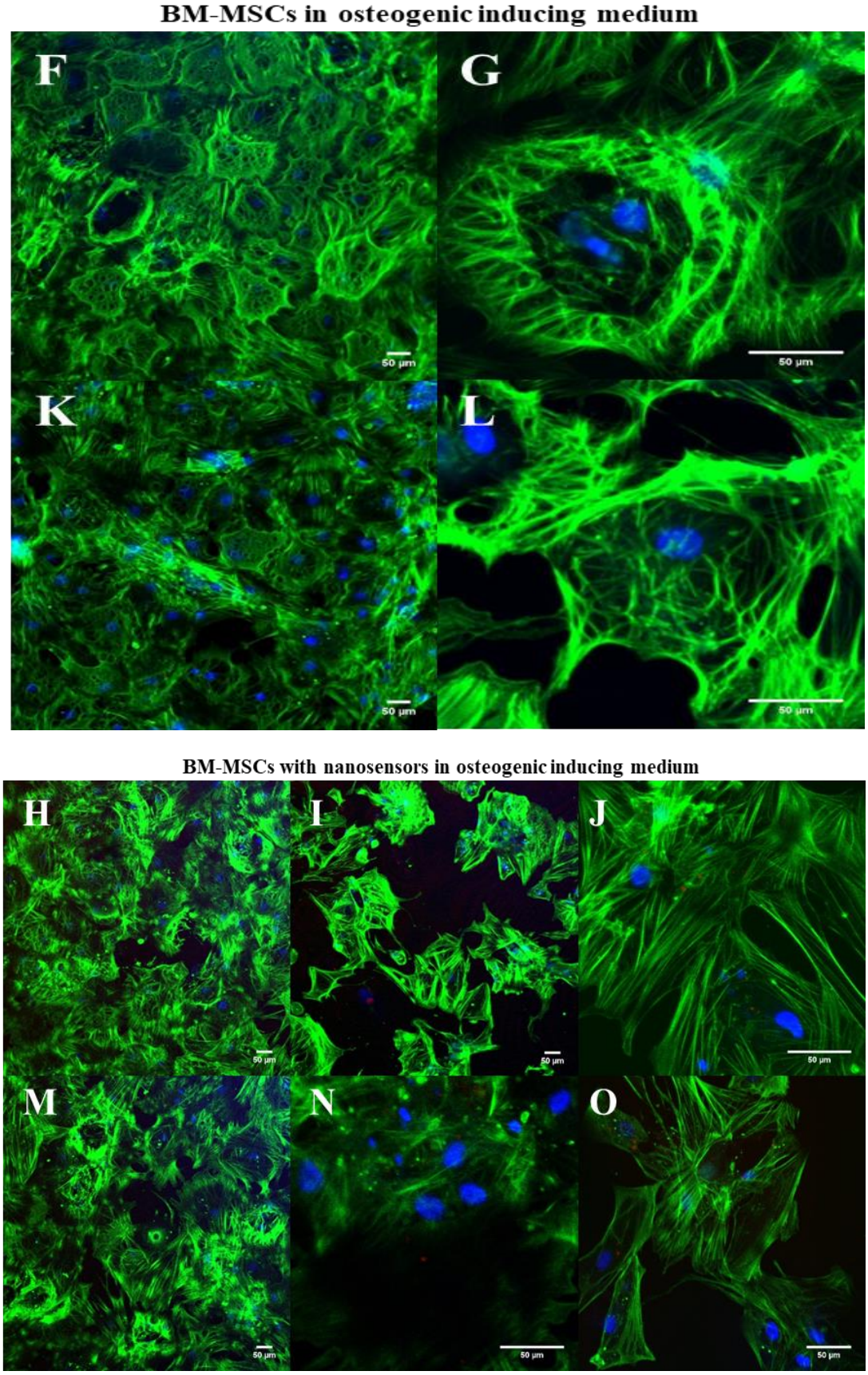

Figure 5.16: Confocal images of the cellular morphologies of BM-MSCs cultured in growth medium and osteogenic inducing medium with and without nanosensors in 2D after 28 days in vitro

A, B: Confocal images of the cellular morphologies of BM-MSCs cultured in growth medium without nanosensors in vitro in 2D after 28 days. C-E: Confocal images of the cellular morphologies of BM-MSCs cultured in growth medium with nanosensors in vitro in 2D after 28 days. F, G, K, L: Confocal images of the cellular morphologies of BM-MSCs cultured in osteogenic inducing medium without nanosensors in vitro in 2D after 28 days. H-J, M-O: Confocal images of the cellular morphologies of BM-MSCs cultured in osteogenic inducing medium with nanosensors in vitro in 2D after 28 days. Cytoskeletal F-actin of cells was stained by AlexaFluor™ 488 phalloidin in green and nuclei were stained by DAPI in blue. Fluorescence of nanosensor was red. Scale bars are 50µm.

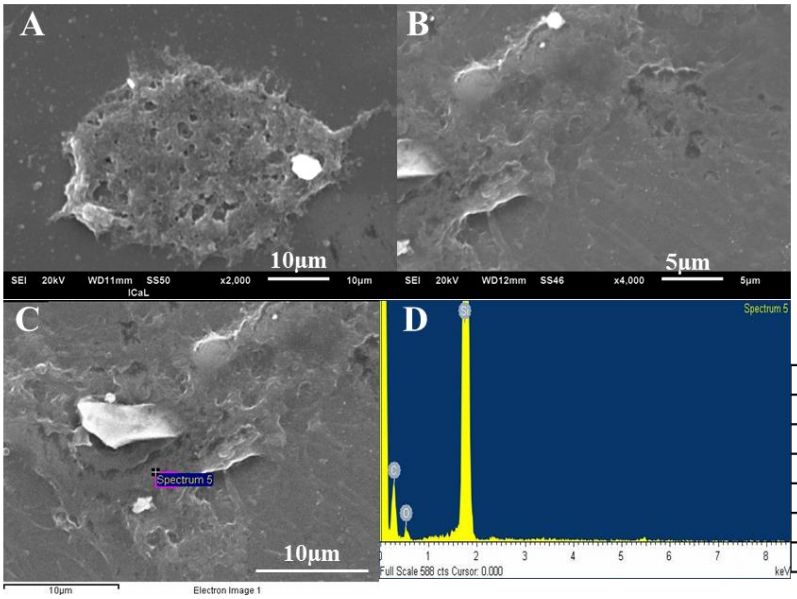

BM-MSCs in growth Medium

E

Element	Weight%	Atomic%
C K	56.32	73.15
O K	6.17	6.02
Si K	37.51	20.83
Totals	100	

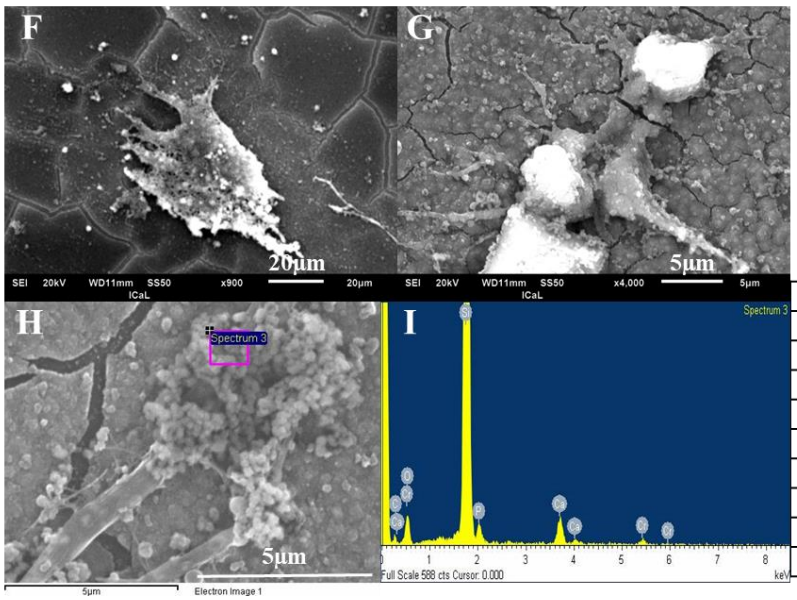

BM-MSCs in Osteogenic inducing medium

J

Element	Weight%	Atomic%
C K	20.65	34.64
O K	17.92	22.57
Si K	54.1	38.82
P K	2.68	1.75
Ca K	3.62	1.82
Cr K	1.03	0.4
Totals	100	

Figure5.17: SEM images of BM-MSCs cultured in growth medium and osteogenic inducing medium with nanosensors after 28 days in vitro in 2D

A-C: BM-MSCs cultured in growth medium with nanosensors after 28 days in vitro in 2D. D, E: EDX analysis of the target in image C. F-H: BM-MSCs cultured in osteogenic inducing medium with nanosensors after 28 days in vitro in 2D. I, J: EDX analysis of the target in image H.

5.4 Conclusions limitations and future works

Results presented in this chapter, demonstrated that by applying cytotoxicity screening tests such as the MTT assay and LDH assay, the biocompatibility of the nanosensor, in terms of the effects on the viability and proliferation of living cells *in vitro*, could be successfully evaluated. Along with the assessment of the fluorescent intensity of the nanosensor in cell culture system, the appropriate regime to further apply the novel nanosensor in MSC studies, regarding the size and concentration, could be characterised, proving the hypothesis of this study described in Chapter one. In this section, the outcomes achieved, limitations on current study and potential future works will be discussed.

5.4.1 Conclusions

To conclude outcomes of this study presented in this chapter, firstly, a novel oxygen nanosensor [48] developed from another study of this joint project was characterised in fibroblast by the cell viability and proliferation screening assays (MTT assay and LDH assay), in terms of the sizes and concentrations to be applied in the following MSC studies. Secondly, a regime of the nanosensor (520nm, 500μg/ml) with biocompatible size, concentration and stable fluorescent intensity in MSC culture system, was selected by means of the LDH assay. Finally, the selected regime of nanosensor was successfully applied in the MSC-based differentiation systems *in vitro*, confirming that the nanoparticle-based sensing technology in combination with fluorescent probes could be used to monitor the selected aspects in the *in vitro* microenvironment over a prolonged culture period, without having negative impacts on the MSC viability, proliferation and differentiations. Current results also offered a valuable information for future applications of the oxygen nanosensor in

monitoring the oxygen concentrations in stem cell-based tissue-engineered construct and hydrogel-based 3D tissue culture systems designed and developed in this study (described in Chapter three and four), toward the multi-layered inhomogeneous articular cartilage/osteochondral tissue reconstruction *in vitro*. Thus, the aim and objective, mentioned in Chapter one, have been achieved in this Chapter.

5.4.2 Limitations and future works

Firstly, there are limitations on the screening assays. Based on current results of fibroblasts and MSCs, there was generally no severe cytotoxicity of the nanosensor and the polystyrene nanobeads with 390, 520 and 890 nm sizes and a series of low concentrations, in 2D cell culture system *in vitro*, consistent with the biocompatible instruction of the commercial polystyrene nanobeads from the manufacturer and some previous studies in which extract from polystyrene nanobeads was applied as negative control in cytotoxicity tests [54]. But considering the specific physiochemical properties of nanoparticle (nanomaterial), the sensitivity of seeding cells, and the potential interaction between nanoparticle and seeding cells, the possible cellular effects of nanoparticles might be relevant to the seeding cell density, cell type, size, concentration and surface chemistry of the nanoparticle, and the evaluation methods [55]. There are a variety of cell viability assays available, in which the MTT assay and LDH assay are classified into the colorimetric assays. MTT assay is simple, classic and well-known as a homogeneous cell viability assay designed for microplate-based high-throughput screening. It is also recommended and described in the ISO (the International Organisation for Standardisation) document for biological evaluation of medical devices [56, 57]. Hence, MTT assay was performed as cell viability and proliferation screening

assays in this study. However, accumulated studies reported limitations, malfunctions and artificial results by using this assay, especially in nanoparticle-involved measurements [55, 58-61]. To avoid those potential risks and to validate results by MTT assay, LDH assay was also employed in this study. Comparing to other *in vitro* cytotoxicity assays, LDH assay might not be the most sensitive one, but by indirectly analysing the number of viable cells left rather directly calculating the number of dead cells after treatments, this measurement could provide stable results and avoid some unexpected interferences between the assessing method and nanoparticles [62]. Certainly, this assay also has limitations and suitability for specific samples [63]. Therefore, more relevant background studies on the sample and test systems, performance of control investigation on the potential interference between sample and specific assay, and selection of more and different assays to assess samples and verify results each other, are often suggested to be considered in experimental plan [63, 64]. In this study, for the future works in terms of the screening assays, other types of assays than the colorimetric assay for cell viability such as dye exclusion assay, luminometric assays and flow cytometric assays, are worth incorporating into the experimental plan to examine more different sizes and concentrations of the nanosensor and related nanobeads, on more different types of cells, to get more accurate results and comprehensive information on this issue.

Secondly, the nanosized particle might be internalised by living cells during interactions which would have further impacts on the proliferation of cells. In this study, the aggregation and possible internalisation of nanosensor might have been observed in the presented results, but due to the time limitation, the validation for the potential interaction between nanosensor and seeding cells was not investigated, in particular, correlations of different sizes and surface modifications of the nanoparticles with the type of seeding cells and the related cellular behaviours, the potential

internalisation of nanosensor by seeding cells in culture and the underlying mechanism, should be worth to be deeply studied in future works.

Thirdly, in this study, the 520 nm size and around 500μg/ml were the selected regime for further fabrication and application of the novel nanosensor, based on evaluations on cell viability, proliferation and differentiations described in this Chapter. Even if there was no pronounced cytotoxicity of the selected nanosensor observed in this study, this nanosensor is designed on the basis of polystyrene nanobeads, in which the polystyrene nanoparticle has been considered as a type of life-threatening pollutant for both environment and living things during interactions in the long term [65-67]. Considering the intended application of this nanosensor with biological cells for tissue development, to improve its biocompatibility and environmentally friendly feature, other types of material such as the biocompatible and biodegradable hydrogel polymer, and certain types of metallic materials, should be considered to develop this kind of nanosensor for the biomedical and TE applications in the future work.

Finally, in line with the overall outcome of this dual project described in Chapter one, this nanosensor will be applied into the hydrogel-based 3D tissue culture system developed in this study (described in Chapter three and four). Based on the optimised regime of nanosensor for MSC culture in 2D, the performance and potential effect of the nanosensor on the established 3D hydrogel-based tissue culture systems should be planned in future investigations, such as the stability and fluorescent intensity of the nanosensor incorporated in the 3D-printed PEGDA-scaffold based tissue culture system (described in Chapter three), and in the nanocellulose blended alginate hydrogel system (described in Chapter four) in longer term *in vitro*, the potential effect of the nanosensor on 3D-cultured seeding cells (chondrocytes, BM-MSCs) during tissue development

in vitro, and the final application and performance of the nanosensor during multi-layered complex tissue development in longer time *in vitro*.

In addition, depending on the type of material, novel design and modification on the nanosensor to improve its biocompatibility, and to be developed into multifunctional nanosensors with enhanced and improved functions, to measure more environmental factors together, such as the oxygen-pH sensor, oxygen-glucose sensor, or oxygen-temperature sensor, would be expected in future works [68-74].

References

[1] Nerem RM, Sambanis A. Tissue engineering: from biology to biological substitutes. Tissue engineering. 1995;1:3-13.
[2] Bello YM, Falabella AF, Eaglstein WH. Tissue-engineered skin. Current status in wound healing. Am J Clin Dermatol. 2001;2:305-13.
[3] Stone KR, Steadman JR, Rodkey WG, Li S-T. Regeneration of meniscal cartilage with use of a collagen scaffold. Analysis of preliminary data. JBJS. 1997;79:1770.
[4] Atala A, Bauer SB, Soker S, Yoo JJ, Retik AB. Tissue-engineered autologous bladders for patients needing cystoplasty. The lancet. 2006;367:1241-6.
[5] Macchiarini P, Jungebluth P, Go T, Asnaghi MA, Rees LE, Cogan TA, et al. Clinical transplantation of a tissue-engineered airway. The Lancet. 2008;372:2023-30.
[6] Gonfiotti A, Jaus MO, Barale D, Baiguera S, Comin C, Lavorini F, et al. The first tissue-engineered airway transplantation: 5-year follow-up results. The Lancet. 2014;383:238-44.
[7] Lovett M, Lee K, Edwards A, Kaplan DL. Vascularization strategies for tissue engineering. Tissue Engineering Part B: Reviews. 2009;15:353-70.
[8] Sisakhtnezhad S, Alimoradi E, Akrami H. External factors influencing mesenchymal stem cell fate in vitro. European journal of cell biology. 2017;96:13-33.
[9] Discher DE, Janmey P, Wang Y-l. Tissue cells feel and respond to the stiffness of their substrate. Science. 2005;310:1139-43.
[10] Sands RW, Mooney DJ. Polymers to direct cell fate by controlling the microenvironment. Current opinion in biotechnology. 2007;18:448-53.
[11] Caron MM, Emans PJ, Coolsen MM, Voss L, Surtel DA, Cremers A, et al. Redifferentiation of dedifferentiated human articular chondrocytes: comparison of 2D and 3D cultures. Osteoarthritis and cartilage. 2012;20:1170-8.
[12] Zscharnack M, Poesel C, Galle J, Bader A. Low oxygen expansion improves subsequent chondrogenesis of ovine bone-marrow-derived mesenchymal stem cells in collagen type I hydrogel. Cells Tissues Organs. 2009;190:81-93.
[13] Tan S, Fang W, Vangsness Jr CT, Han B. Influence of Cellular Microenvironment on Human Articular Chondrocyte Cell Signaling. Cartilage. 2021;13:935S-46S.
[14] Murphy CL, Sambanis A. Effect of oxygen tension and alginate encapsulation on restoration of the differentiated phenotype of passaged chondrocytes. Tissue engineering. 2001;7:791-803.
[15] Buckley CT, Vinardell T, Kelly DJ. Oxygen tension differentially regulates the functional properties of cartilaginous tissues engineered from infrapatellar fat pad derived MSCs and articular chondrocytes. Osteoarthritis and Cartilage. 2010;18:1345-54.
[16] Schrobback K, Malda J, Crawford RW, Upton Z, Leavesley DI, Klein TJ. Effects of oxygen on zonal marker expression in human articular chondrocytes. Tissue Engineering Part A. 2012;18:920-33.
[17] Qu C, Lindeberg H, Ylärinne JH, Lammi MJ. Five percent oxygen tension is not beneficial for neocartilage formation in scaffold-free cell cultures. Cell and tissue research. 2012;348:109-17.
[18] Daly AC, Sathy BN, Kelly DJ. Engineering large cartilage tissues using dynamic bioreactor culture at defined oxygen conditions. Journal of tissue engineering. 2018;9:1-12.
[19] Sieber S, Michaelis M, Gühring H, Lindemann S, Gigout A. Importance of osmolarity and oxygen tension for cartilage tissue engineering. BioResearch Open Access. 2020;9:106-15.
[20] Fermor B, Christensen S, Youn I, Cernanec J, Davies C, Weinberg J. Oxygen, nitric oxide and

articular cartilage. Eur Cell Mater. 2007;13:56-65.
[21] Xu X, Duan S, Yi F, Ocampo A, Liu G-H, Belmonte JCI. Mitochondrial regulation in pluripotent stem cells. Cell metabolism. 2013;18:325-32.
[22] Folmes CD, Dzeja PP, Nelson TJ, Terzic A. Metabolic plasticity in stem cell homeostasis and differentiation. Cell stem cell. 2012;11:596-606.
[23] Zhou S, Cui Z, Urban JP. Factors influencing the oxygen concentration gradient from the synovial surface of articular cartilage to the cartilage–bone interface: a modeling study. Arthritis & Rheumatism. 2004;50:3915-24.
[24] Blanco FJ, Rego I, Ruiz-Romero C. The role of mitochondria in osteoarthritis. Nature Reviews Rheumatology. 2011;7:161-9.
[25] Li J, Dong S. The Signaling Pathways Involved in Chondrocyte Differentiation and Hypertrophic Differentiation. Stem Cells International. 2016;2016:1-12.
[26] Robins JC, Akeno N, Mukherjee A, Dalal RR, Aronow BJ, Koopman P, et al. Hypoxia induces chondrocyte-specific gene expression in mesenchymal cells in association with transcriptional activation of Sox9. Bone. 2005;37:313-22.
[27] Srinivas PR, Philbert M, Vu TQ, Huang Q, Kokini JL, Saos E, et al. Nanotechnology research: applications in nutritional sciences. The journal of nutrition. 2010;140:119-24.
[28] Ramesh KT. Nanomaterials. Nanomaterials: Springer; 2009. p. 1-20.
[29] Buzea C, Pacheco II, Robbie K. Nanomaterials and nanoparticles: sources and toxicity. Biointerphases. 2007;2:MR17-MR71.
[30] Ferreira L. Nanoparticles as tools to study and control stem cells. Journal of cellular biochemistry. 2009;108:746-52.
[31] Wiraja C, Yeo DC, Chong MS, Xu C. Nanosensors for continuous and noninvasive monitoring of mesenchymal stem cell osteogenic differentiation. Small. 2016;12:1342-50.
[32] Starly B, Choubey A. Enabling sensor technologies for the quantitative evaluation of engineered tissue. Annals of biomedical engineering. 2008;36:30-40.
[33] Wilson DR, Routkevitch D, Rui Y, Mosenia A, Wahlin KJ, Quinones-Hinojosa A, et al. A triple-fluorophore-labeled nucleic acid pH nanosensor to investigate non-viral gene delivery. Molecular Therapy. 2017;25:1697-709.
[34] Kneipp J, Kneipp H, Wittig B, Kneipp K. Following the dynamics of pH in endosomes of live cells with SERS nanosensors. The Journal of Physical Chemistry C. 2010;114:7421-6.
[35] Kellner K, Liebsch G, Klimant I, Wolfbeis OS, Blunk T, Schulz MB, et al. Determination of oxygen gradients in engineered tissue using a fluorescent sensor. Biotechnology and bioengineering. 2002;80:73-83.
[36] Yeo DC, Wiraja C, Mantalaris AS, Xu C. Nanosensors for regenerative medicine. Journal of biomedical nanotechnology. 2014;10:2722-46.
[37] Bauer LA, Birenbaum NS, Meyer GJ. Biological applications of high aspect ratio nanoparticles. Journal of Materials Chemistry. 2004;14:517-26.
[38] De M, Ghosh PS, Rotello VM. Applications of nanoparticles in biology. Advanced Materials. 2008;20:4225-41.
[39] Malda J, Brink PVD, Meeuwse P, Grojec M, Martens D, Tramper J, et al. Effect of oxygen tension on adult articular chondrocytes in microcarrier bioreactor culture. Tissue engineering. 2004;10:987-94.
[40] Baranwal A, Kumar A, Priyadharshini A, Oggu GS, Bhatnagar I, Srivastava A, et al. Chitosan: an undisputed bio-fabrication material for tissue engineering and bio-sensing applications. International

journal of biological macromolecules. 2018;110:110-23.
[41] Yang X, Dang Y, Lou J, Shao H, Jiang X. D-alanyl-D-alanine-modified gold nanoparticles form a broad-spectrum sensor for bacteria. Theranostics. 2018;8:1449-57.
[42] Rahim S, Khalid S, Bhanger MI, Shah MR, Malik MI. Polystyrene-block-poly (2-vinylpyridine)-conjugated silver nanoparticles as colorimetric sensor for quantitative determination of Cartap in aqueous media and blood plasma. Sensors and Actuators B: Chemical. 2018;259:878-87.
[43] Gomez D, Morgan SP, Hayes-Gill BR, Correia RG, Korposh S. Polymeric optical fibre sensor coated by SiO2 nanoparticles for humidity sensing in the skin microenvironment. Sensors and Actuators B: Chemical. 2018;254:887-95.
[44] Barman SR, Nain A, Jain S, Punjabi N, Mukherji S, Satija J. Dendrimer as a multifunctional capping agent for metal nanoparticles for use in bioimaging, drug delivery and sensor applications. Journal of Materials Chemistry B. 2018;6:2368-84.
[45] Chen K-C, Li Y-L, Wu C-W, Chiang C-C. Glucose sensor using U-shaped optical fiber probe with gold nanoparticles and glucose oxidase. Sensors. 2018;18:1217.
[46] Bahrani S, Razmi Z, Ghaedi M, Asfaram A, Javadian H. Ultrasound-accelerated synthesis of gold nanoparticles modified choline chloride functionalized graphene oxide as a novel sensitive bioelectrochemical sensor: Optimized meloxicam detection using CCD-RSM design and application for human plasma sample. Ultrasonics Sonochemistry. 2018;42:776-86.
[47] Zhang Z, Zhang Z, Liu H, Mao X, Liu W, Zhang S, et al. Ultratrace and robust visual sensor of Cd2+ ions based on the size-dependent optical properties of Au@ g-CNQDs nanoparticles in mice models. Biosensors and Bioelectronics. 2018;103:87-93.
[48] Koduri MP, S. Goudar V, Shao Y-W, Hunt JA, Henstock JR, Curran J, et al. Fluorescence-based nano-oxygen particles for spatiometric monitoring of cell physiological conditions. ACS applied materials & interfaces. 2018;10:30163-71.
[49] Dahoumane SA, Jeffryes C, Mechouet M, Agathos SN. Biosynthesis of inorganic nanoparticles: A fresh look at the control of shape, size and composition. Bioengineering. 2017;4:14.
[50] Raliya R, Singh Chadha T, Haddad K, Biswas P. Perspective on nanoparticle technology for biomedical use. Current pharmaceutical design. 2016;22:2481-90.
[51] Kunzmann A, Andersson B, Thurnherr T, Krug H, Scheynius A, Fadeel B. Toxicology of engineered nanomaterials: focus on biocompatibility, biodistribution and biodegradation. Biochimica et Biophysica Acta (BBA)-general subjects. 2011;1810:361-73.
[52] Panessa-Warren BJ, Warrren JB, Maye MM, Schiffer W. Nanoparticle interactions with living systems: in vivo and in vitro biocompatibility. Nanoparticles and Nanodevices in Biological Applications: Springer; 2009. p. 1-45.
[53] Monti DM, Guarnieri D, Napolitano G, Piccoli R, Netti P, Fusco S, et al. Biocompatibility, uptake and endocytosis pathways of polystyrene nanoparticles in primary human renal epithelial cells. Journal of biotechnology. 2015;193:3-10.
[54] Scelza MZ, Caldas IP, Mattos JMd, Oliveira F, Carvalho W, Alves GG. In Vitro Analysis of the Cytotoxicity of Indirect Restorative Materials. Brazilian Dental Journal. 2018;29:507-12.
[55] Kroll A, Pillukat MH, Hahn D, Schnekenburger J. Interference of engineered nanoparticles with in vitro toxicity assays. Archives of toxicology. 2012;86:1123-36.
[56] Iso B, STANDARD B. Biological evaluation of medical devices. Part. 2009;1:10993.
[57] Thangaraju P, Varthya SB. ISO 10993: Biological Evaluation of Medical Devices. Medical Device Guidelines and Regulations Handbook: Springer; 2022. p. 163-87.

[58] Jaszczyszyn A, Gąsiorowski K. Limitations of the MTT assay in cell viability testing. Advances in clinical and experimental medicine. 2008;17:525-9.
[59] Olivier V, Rivière C, Hindié M, Duval J-L, Bomila-Koradjim G, Nagel M-D. Uptake of polystyrene beads bearing functional groups by macrophages and fibroblasts. Colloids and Surfaces B: Biointerfaces. 2004;33:23-31.
[60] Holder AL, Goth-Goldstein R, Lucas D, Koshland CP. Particle-induced artifacts in the MTT and LDH viability assays. Chemical research in toxicology. 2012;25:1885-92.
[61] Almutary A, Sanderson B. The MTT and crystal violet assays: potential confounders in nanoparticle toxicity testing. International journal of toxicology. 2016;35:454-62.
[62] Fotakis G, Timbrell JA. In vitro cytotoxicity assays: comparison of LDH, neutral red, MTT and protein assay in hepatoma cell lines following exposure to cadmium chloride. Toxicology letters. 2006;160:171-7.
[63] Han X, Gelein R, Corson N, Wade-Mercer P, Jiang J, Biswas P, et al. Validation of an LDH assay for assessing nanoparticle toxicity. Toxicology. 2011;287:99-104.
[64] Kamiloglu S, Sari G, Ozdal T, Capanoglu E. Guidelines for cell viability assays. Food Frontiers. 2020;1:332-49.
[65] Kik K, Bukowska B, Sicińska P. Polystyrene nanoparticles: Sources, occurrence in the environment, distribution in tissues, accumulation and toxicity to various organisms. Environmental Pollution. 2020;262:114297.
[66] Hwang J, Choi D, Han S, Jung SY, Choi J, Hong J. Potential toxicity of polystyrene microplastic particles. Scientific reports. 2020;10:1-12.
[67] Libralato G, Galdiero E, Falanga A, Carotenuto R, De Alteriis E, Guida M. Toxicity effects of functionalized quantum dots, gold and polystyrene nanoparticles on target aquatic biological models: a review. Molecules. 2017;22:1439.
[68] Deng M, Qiao Y, Liu C, Wang Z, Shi J, Pan T, et al. Tricolor core/shell polymeric ratiometric nanosensors for intracellular glucose and oxygen dual sensing. Sensors and Actuators B: Chemical. 2019;286:437-44.
[69] Dmitriev RI, Borisov SM, Düssmann H, Sun S, Müller BJ, Prehn J, et al. Versatile conjugated polymer nanoparticles for high-resolution O2 imaging in cells and 3D tissue models. ACS nano. 2015;9:5275-88.
[70] Qu F, Guo X, Liu D, Chen G, You J. Dual-emission carbon nanodots as a ratiometric nanosensor for the detection of glucose and glucose oxidase. Sensors and Actuators B: Chemical. 2016;233:320-7.
[71] Wang X-d, Stolwijk JA, Lang T, Sperber M, Meier RJ, Wegener J, et al. Ultra-small, highly stable, and sensitive dual nanosensors for imaging intracellular oxygen and pH in cytosol. Journal of the American Chemical Society. 2012;134:17011-4.
[72] Brasuel M, Kopelman R, Aylott JW, Clark H, Xu H, Hoyer M, et al. Production, characteristics and applications of fluorescent PEBBLE nanosensors: potassium, oxygen, calcium and pH imaging inside live cells. Sensors Mater. 2002;14:309-38.
[73] Zhang X-a, Zhang W, Wang Q, Wang J, Ren G, Wang X-d. Quadruply-labeled serum albumin as a biodegradable nanosensor for simultaneous fluorescence imaging of intracellular pH values, oxygen and temperature. Microchimica Acta. 2019;186:1-11.
[74] Zhang W, El-Reash A, Ding L, Lin Z, Lian Y, Song B, et al. A lysosome-targeting nanosensor for simultaneous fluorometric imaging of intracellular pH values and temperature. Microchimica Acta. 2018;185:1-9.

Chapter six: Conclusions and future works suggested for this project

6.1 Conclusions

The first aim of this study is to develop hydrogel-based tissue culture system for multi-layered articular cartilage/OC tissue reconstruction *in vitro*. At present, there are still challenges and limitations to reconstruct the multi-layered inhomogeneous articular cartilage/OC tissue *in vitro* for a long term, even if the commercialised products are designed and developed to mainly support the tissue regeneration *in vivo* for the purpose of clinical auxiliaries laying more stress on recovering physiological functions than anatomical structures. This study belongs to a joint project in which the 3D tissue culture system is required for applying a novel (oxygen) nanosensor [1] to study and control the external impact factors (e.g. the oxygen profile) in the 3D microenvironment during tissue development *in vitro*. Instead of fabricating the entire inhomogeneous target tissue simultaneously, this study planned to build distinctive layers of the multi-layered inhomogeneous target tissue individually, in the light of their specific characteristics. 3D printing technique enables the controlled fabrication process as a platform to faithfully produce complex architectures of the 3D product based on the sophisticated design. Therefore, assisted by 3D printing techniques, objectives regarding the design and manufacture of hydrogel-based two distinctive layers of the multi-layered articular cartilage/OC tissue were achieved, which details have been described in chapter three and four.

In **chapter three**, with a selected formula containing 20-30% PEGDA and 0.05% LAP (photoinitiator), and the optimised setup of the customised DLP 3D printer, PEGDA-hydrogel scaffold with biomimetic patterns were designed and 3D-printed in a layer-by-layer model, where best resolution at 3:5 aspect ratio (ratio of the width over height) for the concave (having light

accumulation phenomena) and 1:5 for convex structures could be reached. To simulate the perpendicular arrangement of the solid ECM network of the deep zone of the inhomogeneous articular cartilage/OC tissue, a scaffold with hexagonal shape and uniformed hole patterns was selected. Associated characterisations of the biomaterial and 3D-printed product, such as the mechanical property, swelling capability, resolution and shape fidelity of the hydrogel-applied DLP 3D printing, as well as the biocompatibilities, were evaluated. To reinforce the hydrogel-based product, nanocellulose fibre materials were incorporated into the printing ink to make composite ink which was also characterised preliminarily. Due to the time limitation, regarding the nanofibre-reinforced PEGDA scaffold there are still more works remained to be accomplished in the future. By using bioactive carrier materials such as the type I collagen gel, chondrocytes were delivered to engraft in the 3D-printed PEGDA scaffold. Survival and growth of seeding cells were confirmed, but further quantitative validation is still required in the future work. In addition, to improve the novelty of the designed scaffold, miniaturised microscale scaffold was fabricated and examined preliminarily. The miniaturised microscale scaffold with the designed pattern displayed a self-assembly property after being injected by a syringe to an area with the size mimicking the chondral/osteochondral defect, when suspended in aqueous solution with appropriate viscosity, providing a hope to be developed into an injectable scaffold to facilitate the third generation of scaffold-assisted ACI techniques in surgical applications in the future.

In **chapter four**, alginate materials were selected to fabricate the 3D thin layer designed to simulate the middle zone of the multi-layered articular cartilage/OC tissue. The original plan was to use extrusion-based 3D printing to fabricate, however, due to limitations of the time and facilities, 3D-printed mould was alternatively designed and successfully applied to fabricate the thin layer in the

mould-casting manner in current study to perform preliminary examinations for the future extrusion-based 3D printing work. Among a series of concentrations of the ionic crosslinker ($SrCl_2$) evaluated in cytotoxicity test, 0.05M $SrCl_2$ having the least toxic impact on the viability and proliferation of three different cell lines (fibroblast, myoblast and chondrogenic cell line) *in vitro*, was selected as the ionic strength to crosslink the alginate-based materials in this study. Nanocellulose fibre material was blended with alginate to form composite hydrogel and a series of composite materials and crosslinked composite hydrogels by 3D-printed moulds were assessed such characteristics as the mechanical property, swelling capability, printability, viscoelasticity and biocompatibility. Composite material of alginate blended with additional nanocellulose fibres displayed improved compressive modulus, viscoelasticity and printability in terms of the shear thinning property. Composite alginate-based hydrogels (2% and 4%, with and without nanocellulose fibre) were biocompatible in both 2D and 3D culture condition, although bioactive modification was required to improve the cellular attachment and bioactivity of alginate materials. Regarding the improved printability, viscoelasticity and biocompatibility, alginate at lower concentration such as the 2 or 4%, with additional nanocellulose fibre material were suggested for extrusion-based 3D (bio) printing in the future work.

Another aim of this study is to characterise a novel oxygen nanosensor [1] designed for *in vitro* 3D tissue culture. As the advancement of nanotechnology, nanoparticle-based sensors have been developed to sense various types of chemical compounds and biomolecules *in vitro* and *in vivo*, however with improved and tuneable properties in physical, chemical, electrical and magnetic aspects, the biocompatibility of the nanoparticle materials might be varied after fabrication. Living cells could sense and response to surroundings, and different type of cells have different

sensitivities and interactions with nanoparticles. Before applying the nanoparticle-based nanosensor in tissue culture system, the biocompatibility of the nanomaterial, regarding the effects of the engineered nanosensor on the viability, proliferation and differentiations of fibroblast and BM-MSCs were evaluated in this study which was described in chapter five.

In **chapter five**, two sizes (390, 520 nm) and three concentrations (25, 500, 1000μg/mL) of the engineered oxygen nanosensor were preliminarily selected from three sizes (390, 520, 890 nm), to be applied in stem cell culture, after screening their effects on the viability and proliferation of murine fibroblast L929 by MTT assay, along with the assessment on the fluorescent intensity of the nanosensor in culture. After further assessments of the biocompatibility of nanosensor by LDH assay, 520nm and around 500 μg/mL of the oxygen nanosensor were selected for evaluating effects of the nanosensor on differentiations of BM-MSCs *in vitro*. Finally, there was no toxic effect of the selected 520nm oxygen nanosensor on the 2D osteogenesis (monolayer) and 3D chondrogenesis (pellet culture) of BM-MSCs *in vitro*, supporting the further development of the 520nm nanosensor at around 500 μg/mL to be applied for future tissue culture applications in this project.

To conclude the overall outcomes, two distinctive layers of the multi-layered articular cartilage/OC tissue were designed and fabricated by hydrogel materials and 3D printing, presenting biocompatible and biomimetic structure and size of the microenvironment of the targeted tissue layer, respectively. The novel oxygen nanosensor with 520nm at around 500 μg/mL was characterised in cell culture system and suggested for future stem cell-based tissue culture applications in this project. Thus, the aims and objectives, mentioned in chapter one, were all successfully achieved, and hypotheses of this study, were proved by the outcomes described in chapter three, four and five, respectively. Additionally, a miniaturised microscale PEGDA hydrogel

scaffold with designed patterns was also observed a self-assembly property in viscous solution, providing a hope to be developed into injectable scaffolds to facilitate scaffold-assisted ACI techniques in minimally invasive clinical applications in the future.

6.2 Future works suggested for this project

Although this study successfully achieved the aims and objectives, and proved the hypotheses, as mentioned, due to limitations on the time and facilities, here a few works are suggested for future investigations in this project.

6.2.1 For the deep zone fabrication

To improve the mechanical property and bioactivity, fibrous materials such as the nanocellulose fibres could be put into the formula of the printing ink to fabricate the designed scaffold. And essential growth factors for chondrogenesis, such as TGF-β and BMP could be incorporated into the hydrogel material in which the amount and release of these compounds could be controlled and designed to support the biochemical microenvironment during cartilage tissue development in a spatiotemporal manner.

By collagen gel carriers, seeding cells such as the chondrocytes could be delivered and survive in the 3D-printed PEGDA scaffold. To validate the proliferation and differentiation of the PEGDA scaffold-assisted cartilaginous tissue regeneration, further quantification and qualification, such as to evaluate the seeding cell proliferation and differentiation in the 3D scaffold for up to 28 days at a series of time points, to examine the expression profiles of typical chondrogenic markers (type II collagen and aggrecan), and to investigate the mechanical properties of the 3D tissue construct during the 28 days induction, are suggested. Besides, the self-assembly PEGDA scaffold with

chondrocytes and collagen gel to be used as injectable solution for ACI technique in clinical applications are also worth to investigate to improve the injecting process, bioactivity and biocompatibilities of the material to meet clinical requirements.

6.2.2 For the middle zone fabrication

The potential improvement of additional nanocellulose fibre materials on the mechanical properties of alginate materials were observed, especially the viscoelasticity and printability of alginate material was enhanced. In the future, the composite ink could be applied for extrusion-based 3D printing to fabricate the tissue construct and effects of the composite materials on the proliferation and differentiation of chondrocytes cultured in 3D are worth to be further validated quantitatively.

6.2.3 For the superficial zone fabrication

3D printing could also be applied to fabricate patterned scaffolds mimicking the arrangement of collagenous ECMs in the superficial zone of the articular cartilage/OC tissue, and mechanical stimulations such as cyclic or intermittent hydrostatic pressure and shear stress of continuous fluid flow under physiological regimes are worth to employ, to improve the arrangement and differentiation of seeding cells in 3D *in vitro*. Bioreactors designed with these biomechanical stimulations, are suggested for future works.

6.2.4 For the integration of individual layers

Because distinctive layers of the multi-layered articular cartilage/OC tissue were planned to fabricate individually, after fabrication and validation, individual layers could be integrated and cultured to simulate the complex inhomogeneous architecture of the target tissue, to be a complete

3D tissue culture model for further *in vitro* studies. Fibrin glue and photocuring hydrogel materials are suggested to be applied for the integration.

6.2.5 Nanosensor incorporation into the 3D tissue culture system

As mentioned in the outline of this project (chapter one), the oxygen nanosensor [1] developed in this joint project would be incorporated into the established hydrogel-based 3D tissue culture systems to study the potential effect of the nanosensor on the development of each zone *in vitro* individually and combined. Besides, the fluorescent intensity of the nanosensor would be measured to reflect the oxygen profiles in both the individual tissue layer and integrated 3D tissue culture systems during tissue development *in vitro*. Correction and interpretation of the fluorescent signal and standard curve of the applied nanosensor in the 3D hydrogel-based tissue culture system are suggested to be investigated in the future work.

Reference

[1] Koduri MP, S. Goudar V, Shao Y-W, Hunt JA, Henstock JR, Curran J, et al. Fluorescence-based nano-oxygen particles for spatiometric monitoring of cell physiological conditions. ACS applied materials & interfaces. 2018;10:30163-71.

Appendix A

Table A: Advantages and Disadvantages of a few commercialised biomaterial scaffolds to deal with chondral lesion (collected and adapted from references [208-211]).

Cell sources	Biomaterial/Scaffold	Related clinical technique	Advantages	Disadvantages	Products
Autologous chondrocytes	Scaffold-free, Fibrin gel	ACI, M-ACI/MACT	Fully autologous chondrocyte, directly adhere to the subchondral bone without additional scaffold	Inappropriate for treating cartilage damage aassociated with generalised OA	Caticell®(FDA approved), Spherox®(co.don chondrosphere/ACT3D-CS/ARTHROCELL 3D)
Allogeneic juvenile chondrocytes			One-step surgical procedure	Limited cell sources	RevaFlex(DeNovo ET)
Platelet-rich plasma/bone marrow concentrate/autologous reparative cells and factors	PGA/HA,Fibrin/HA, by Freeze-drying	ACI	Biodegradable, adsorbable, synthetic, stable, mechanically resistant, one-step surgical procedure	Limited clinical data, requiring additional growth factors to stimulate the proliferation of chondrocytes	Chondrotissue® Biocart™II
Autologous chondrocytes (minced cartilage or in vitro expansion)	Collage membrane, agarose/alginate, Fibrin glue, collagen I/III, by 3D fabrication technique	C-ACI/M-ACI/MACT/MA-MFX	Biodegradable, safe materials, some were bioresorbable, some no need periosteum/membrane, autologous tissue sources, some can be customised size and shape.	Limited cell sources, donor site morbidity, some are expensive, requiring complex procedure with risks	Catimaix® (mechanically stable and highly resist tangential force, slowly resorbable), Cartipatch®, Chondron™, NeoCart®(3D expansion cells in vitro and used with a bioreactor Tissue Engineering Processor (TEP) having simulated mechanical stimuli and oxygen), ACI-Maix™(MACI®) (FDA approved), CaReS®-1S
Autologous chondrocytes from minced cartilage	PCL/PGA/TPC/PDO mesh by 3D fabrication technique	C-ACI/M-ACI/MACT/MA-MFX	One-step surgical procedure, autologous tissue sources	Limited cell sources, donor site morbidity	Cartilage Autograft Implantation System (CAIS)
Juvenile chondrocytes from minced allogeneic young cartilage	minced juvenile hyaline cartilage pieces with fibrin glue	Debridement	High productivity of proteoglycan production from juvenile chondrocytes, no immunogenic stimulation	About 40 days shelf life, usually two-stage surgery procedure, risk of disease transmission or immunogenicity	DeNovo Natural Tissue (NT)
Allogeneic umbilical cord blood derived stem cells	Sodium hyaluronate/HA	Implantation	One-step surgical procedure, cell number availability	Tumorigenicity	CARTISEM®
Autologous chondrocytes, MSCs	PVA hydrogel, polyethylene glycol diacrylate (PEGDA), denatured fibrinogen	In conjunction with marrow stimulation	Biodegradable hydrogel material mimicking the articular cartilage in water proportion; When use MSCs, having potential to induce chondrogenesis and osteogenesis but no immunogenicity	Inadequate connection to the bone and risk of dislocation, risk in the formation of fibrocartilage and scar in the defect area without filling implant	SaluCartilage™, GelrinC

Appendix B

Table B: Advantages and Disadvantages of a few commercialised biomaterial scaffolds to deal with chondral/osteochondral lesion (collected and adapted from references [208-211]).

Cell sources	Biomaterial/Scaffold	Related clinical technique	Advantages	Disadvantages	Products
MSCs	Benzyl ester of HA(HYAFF®) Chitosan	OC implantation, some requiring to be used in conjunction with with bone marrow stimulation (BMS) techniques	Single layer biodegradable non-woven pad, adaptable size and shape, no need fibrin sealant, can be stacked, large lesion allowable, one-step surgical procedure, no need fixation.		HyaloFast®
	GP/autologous whole blood		Ready to use, easy to prepare during a single-step bone marrow stimulation procedure, to stabilize fibrin clot and retain mesenchymal stem cells.	Requiring to be used in conjunction with with bone marrow stimulation (BMS) techniques	BST-CarGel®
	Type I/III collagen(Porcine)		Minimally-invasive one-step surgical procedure, biocompatible and resorbable, versatile functions (cell carrier, protective cover for neo-tissue, membrane wrap for meniscus.		AMIC®Chondro-Gide®
Allogeneic chondrocytes, MSCs, osteochondral allograft	Growth factor, cellular/molecular components(a cryopreserved, viable osteochondral allograft (CVOCA))	Implant designed to improve healing of bone marrow stimulation procedures	An allograft cartilage implant, easily cut to desired size and shape, 2-year shelf life, one-step surgical procedure, biodegradable, minimally manipulated, four sizes diameter available, full-thickness pores throughout the graft, flexible, biomimicking topography, 2-year shelf life in -80°C	Requiring bioactive factors	Cartiform®
Autologous chondrocytes (may from minced cartilage or in vitro expansion)	Type I collagen (Bovine)/CS (3D biphasic (bilayer sponge with cells and homologous serum) or 3D biphasic matrix membrane)	M-ACI/MACT	Single layer biodegradable non-woven pad, adaptable size and shape, no need fibrin sealant, can be stacked, large lesion allowable, one-step surgical procedure, no need fixation	Requiring bioactivity, risk in using animal collagen	NOVOCART® 3D, Novocart® Basic
Autologous cultured chondrocytes, MSCs	PLA/PDS/fibrin/PLGA	M-ACI/MACT/OC implantation	Biodegradable, slowly absorbable, good mechanical property and adequate structure, autologous tissue sources	Limited cell sources, donor site morbidity risk in attracting reparative cell and factors	Bioseed®-C
	Calcium carbonate/aragonite/ HA	Osteochondral Autograft Transplantation procedure	Biodegradable, possessing a nano-rough surface and porous architecture which permit cells to adhere and proliferate biodegradable, biomimetic structure		Agili-C™
	Collagen/HA/ß-TCP				Collagraft®
	Collagen/GAG/CaP				Chondromimetic™
	Type I collagen/ß-TCP/PLA				OsseoFit®plug
	Calcium sulphate/PLGA/PGA				TruFit™BGS plug (fit for filling osteochondral defect, and integration to native cartilage tissue)
Autologous cultured chondrocytes, MSCs	Acellular scaffold (Type I collagen from equine/magnesium/HA)	Osteochondral Autograft Transplantation procedure, isolated grafts and applied in conjunction with marrow stimulation	Biodegradable, potential effect on subchondral trabecular bone regeneration	Risk in attracting reparative cell and factors	MaioRegen®
	A decellularized osteochondral allograft with hyaline cartilage and cancellous bone		Biodegradable, 2-year shelf life	High failure rate, risk of disease transmission or immunogenicity	Chondrofix®
	Osteochondral allograft disc with viable chondrocytes, matrix, and growth factors		Biodegradable, minimally manipulated, fresh made and can be stored in 4°C, highly viable chondrocytes, matrix, and growth factors, five sizes diameter available	Risk in disease transmission or immunogenicity	ProChondrix

Appendix C

Table C: Advantages of a few commercialised injectable products to deal with chondral lesion and mainly to reduce pain and inflammation (collected and adapted from references [208-211]).

Products	Components	Related clinical technique	Clinical indications	Advantages
Orthokin/Regenokin	Autologous conditioned serum (ACS)	Extraction, manipulation and reintroduction of bloods from patients	Chondral lesion, Osteoarthritis	Derived from platelet-rich plasma therapy with improved efficacy, an injectable agent as a type of regenerative medicine containing autologous serum, growth factors and naturally produced anti-inflammatory protein (the IL-1 receptor antagonist) to deal with joint pain and inflammations, less invasive.
Platelet-rich plasma (PRP)	Platelets, plasma proteins, growth factors	Derived from centrifugation of autologous blood to attain a supraphysiologic concentration of platelet and plasma proteins	Chondral lesion	Can accelerate the repair process by stimulating cartilage matrix synthesis and counteracting the effects of catabolic cytokines.
Autologous and allogeneic MSCs	MSCs	Cell-based therapy, intra-or inter- articular injection	Chondral lesion	MSC product, and anti-inflammatory and immunomodulatory effects.
Sprifermin(rhFGFR-18)	Growth factor	Interaction with fibroblast growth factor receptor 3 (FGFR-3) for chondrogenesis	Chondral lesion	It induces chondrocyte proliferation by increasing ECM production.
Bone marrow aspirate concentrate (BMAC)	Adult bone marrow-derived MSCs (BM-MSCs), platelets, cytokines, and growth factors	Bone marrow aspiration from iliac spine or iliac crest usually.	Chondral lesion, Osteoarthritis	Approved by US-FDA, minimal invasive, non-surgical treatment. It provides a rich cell source of MSC product, MSC-related anti-inflammatory and immunomodulatory effects.
Lipogems®	Autologous adipose tissue containing AD-MSCs	Aspiration or fat suction from abdomen.	Orthopaedic conditions including osteoarthritis	An easy-use patent system, US FDA approved, minimal invasive medical option. For osteoarthritis, significant improvements in pain, functional scores, and cartilage thickness
OP-1 (BMP-7)	Growth factor	Failed to commercialise	Osteoarthritis	For osteoarthritis, showing reparative effects on cartilaginous tissue formation and preventing catabolism
Gel-One®	Crosslinked hyaluronate (HA) hydrogel	A single-use injection, Non-surgical option	Joint inflammation, Knee Osteoarthritis	A type of viscosupplement, approved by US FDA, a natural, sterilised, transparent, viscoelastic HA hydrogel designed as a convenient single-injection treatment for knee.

Appendix D

Table D: Advantages and challenges of applying currently promising seeding cells in cell-based articular cartilage/osteochondral tissue reconstructions (collected and adapted from references [120,121]).

Seeding cells	Advantages	Challenges
Chondrocyte	Economic and clinically safe, approved by FDA to be associated with the ACI related surgical techniques; Direct and restricted source of reparative cells for cartilaginous tissue repair.	Limited cell numbers and sources, usually requiring autologous cartilaginous tissues; Risks in the doner site morbidity, regarding autologous cell harvest; Dedifferentiation and dysfunction in in vitro culture/expansion systems; Multiple steps in the procedure included in clinical interventions (e.g. ACI) and long recovery time after surgery.
MSCs (BM-MSCs, AD-MSCs, synovial MSCs etc.,), Articular cartilage-derived mesenchymal progenitor cells (AC-MPCs), Chondrogenic progenitor cells (CPCs)	Various cell sources, no need autologous sample to obtain, and some were relatively easy to acquire (AD-MSCs); Marrow-stimulation techniques such as microfracture, have been used clinically to recruit autologous BM-MSCs; Comparing to BM-MSCs, some types of MSCs were found higher proliferation rate (e.g. AD-MSCs), chondrogenesis ability (e.g. synovial membrane MSCs) or both (e.g. synovial fluid MSCs); In response to chondral injuries and OA, presenting varied phenotypes and activities regarding the disease status (e.g. CPCs) Usually no immunologic rejection and immunogenicity involved; Immunomodulation and anti-inflammatory ability (AD-MSCs); No ethical issue and could be obtained by non-invasive approaches; Induced chondrogenesis under specific condition; Some types or subpopulations of MSCs could resist cellular senescence in long term expansion *in vitro*.	Risks in the fibrous cartilage generation by marrow-stimulation techniques recruited BM-MSCs; Usually heterogenous chondrogenic potency at single-cell level (e.g. synovial membrane MSCs) , requiring enrichment in subpopulation (e.g. CPCs by platelet lysate); Some MSCs or progenitor cells were difficult to isolate and costly; Donor status/source-dependent biological abilities (chondrogenesis) (synovial fluid MSCs); Risks in hypertrophic differentiation, vascularisation, mineralisation and osteogenesis of some MSCs (BM-MSC), weak chondrogenesis (AD-MSCs), and non-specific differentiations (not chondrogenesis) after MSC inductions; Potential to stimulate tumorigenesis, unwanted colonisation of other tissue after artificial inductions; Risks in infectious diseases transmission regarding the use of allogeneic human or animal serum related substances or agents; Few high quality clinical data regarding synovial MSCs and progenitor cells; Cultured primary MSCs in vitro after long time expansion present cellular senescence, aging-related changes, dysfunctions and problems, relevant to circumstances such as the cell source, cell type, donor status, isolation technique, cell culture system, genetic and epigenetic factors.
Embryonic stem cells (ESCs)	Strong chondrogenesis; Requiring feeder layers in in vitro culture to expand or differentiate; Better differentiation when applied in coculture system.	Ethical issue and regulations, hence difficult to find cell sources legally; Risks in oncogenicity and tumorgenicity, immunologic rejection by host, uncontrolled spontaneous differentiations, and teratoma formation, regarding clinical transplantation; Less and limited valuable clinical studies and data.

Continued

Continued Table D

Induced pluripotent stem cells (iPSCs)	High and unlimited proliferation ability *in vitro*, no need autologous cell sources; Comparable biological functions to ESCs but without ethical issues; Low oncogenicity and tumorgenicity; Controlled inductions of plasticity and potentially reduced cellular senescence during expansion.	Purification required *ex vivo*; Requiring stable and reliable gene modification protocol and reprogramming technique; Host genome is modified and altered, which may have effects on other genes and functions, hence the whole efficacy of chondrogenesis of iPSCs may need to consider and balance; Potential risks in teratogenesis and malformation of tissue *in vivo*; Potential risks in safety and pathogenicity of cells after genetical alterations.
Gene-modified (transgenic) cells	Strongly improved chondrogenesis; Controlled plasticity and desired modifications to meet various clinical requirements;	Requiring stable and reliable gene modification protocol and validation; Host genome is modified and altered, which may have effects on other genes and functions, hence the whole efficacy after transgenic modification may need to consider and balance; Risks in gene modification process and materials applied in transgenic procedures; Potential risks in safety and pathogenicity of cells after gene modification; Limited clinical studies and data.
Co-cultured cells (e.g. chondrocytes+MSCs)	Improved MSC chondrogenesis and cellular activity of chondrocytes such as proliferation and metabolism; Required number of chondrocytes, number-related dedifferentiation, cellular expansion and cost could be all reduced; Anti-inflammatory ability and immunomodulation due to the use MSCs; Improved safety and potential to reduce the use and amount of growth factors and biomaterials.	Limited knowledge on the underlying mechanisms; Inconsistent results depend on the ratio and types of co-cultured cells in practices; Biomaterial scaffolds and devices may have impacts on efficacies of applying co-cultured systems in tissue developments; Limited clinical studies and data.